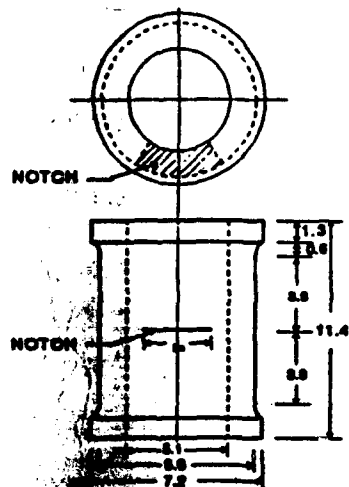




AD-A 250 896

CRACK PROPAGATION AND FABRIC CONTROL ON THE STATIC AND DYNAMIC STRENGTH OF COHESIVE SOILS



Approved for public release;
distribution unlimited.

Adel S. Saada and Gary F. Bianchini

INSTITUTE FOR GEOTECHNICAL RESEARCH (IGR)
THIS REPORT AND APPENDIX TO THIS
REPORT HAVE BEEN REVIEWED AND IS
DISTRIBUTED UNRESTRICTED IN ACCORDANCE IAW AFR 190-12
GL-1. MARCH 1992

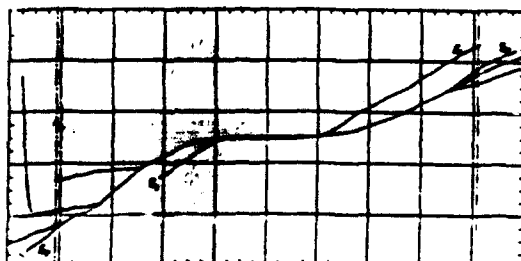
STN#0 00000 ManJaguary, 1992

92-12942

[REDACTED]

Air Force Office of Scientific Research
Bolling Air Force Base
D.C. 20332-6448

Grant No. AFOSR-88-0169



GEOTECHNICAL ENGINEERING LABORATORIES
CASE SCHOOL OF ENGINEERING
Case Western Reserve University

92 5 14 055

AD-A250 896

SECURITY CLS:



REF ID: A250 896

2

ACTION PAGE

Form Approved
OMB No. 0704-0188

1a. REPORT NUMBER UNCLASSIFIED	1b. RESTRICTIVE MARKINGS						
2a. SECURITY CLASSIFICATION AUTHORITY SELECTED	3. DISTRIBUTION/AVAILABILITY OF REPORT Approved for Public Release; Distribution Unlimited						
2b. DECLASSIFICATION/DOWNGRADING SCHEDULE MAY 19 1992							
4. PERFORMING ORGANIZATION REPORT NUMBER(S) AF-SFRAC-1	5. MONITORING ORGANIZATION REPORT NUMBER(S) AFCSR-TW-12-0362						
6a. NAME OF PERFORMING ORGANIZATION Case Western Reserve Univ.	6b. OFFICE SYMBOL (If applicable) N/A	7a. NAME OF MONITORING ORGANIZATION AFOSR/NA					
6c. ADDRESS (City, State, and ZIP Code) Cleveland, OH 44106-7201	7b. ADDRESS (City, State, and ZIP Code) Bldg. 410 Bolling AFB, DC 20332-6448						
8a. NAME OF FUNDING / SPONSORING ORGANIZATION AFOSR	8b. OFFICE SYMBOL (If applicable) N/A	9. PROCUREMENT INSTRUMENT IDENTIFICATION NUMBER AFOSR-88-0169					
8c. ADDRESS (City, State, and ZIP Code) Bldg. 410 Bolling AFB, DC 20332-6448	10. SOURCE OF FUNDING NUMBERS <table border="1"> <tr> <td>PROGRAM ELEMENT NO. 6.1102F</td> <td>PROJECT NO. 2302</td> <td>TASK NO. CS</td> <td>WORK UNIT ACCESSION NO.</td> </tr> </table>			PROGRAM ELEMENT NO. 6.1102F	PROJECT NO. 2302	TASK NO. CS	WORK UNIT ACCESSION NO.
PROGRAM ELEMENT NO. 6.1102F	PROJECT NO. 2302	TASK NO. CS	WORK UNIT ACCESSION NO.				
11. TITLE (Include Security Classification) Crack Propagation and Fabric Control on the Static and Dynamic Strength of Cohesive Soils							
12. PERSONAL AUTHOR(S) Saada, Adel S. and Bianchini, Gary F.							
13a. TYPE OF REPORT FINAL	13b. TIME COVERED FROM 6/1/88 TO 1/31/92	14. DATE OF REPORT (Year, Month, Day) 1992-1-31	15. PAGE COUNT 456				
16. SUPPLEMENTARY NOTATION							

17. COSATI CODES	18. SUBJECT TERMS (Continue on reverse if necessary and identify by block number) Clay, Fracture, Fabric, Anisotropy, Damage, Crack Propagation, Strength		
FIELD	GROUP	SUB-GROUP	

19. ABSTRACT (Continue on reverse if necessary and identify by block number)
--

Discontinuities in the form cracks or fissures and inclusions are often present in natural clays. They serve as stress concentrators when loads are applied to the material. Such concentrations result in the cracks advancing, often surrounded and preceded by a propagating damage zone. As the crack propagates, the damage may be in the form of one or more shear bands, which may play the part of new stress concentrators and blunt the action of the original crack. This report examines some of the phenomena associated with the presence of cracks in overconsolidated clays as well as in the less brittle normally consolidated clays. Differences between isotropic and anisotropic materials, and the level at which serious modifications take place in the fabric of the material are noted. Observations made with a surface analyzer as well as with a transmission electron microscope indicate that the changes in fabric mostly occur at the level of the cluster or flock. The influence of the cracks and of the shear bands on the kinematics and strength of the test specimens is studied and discussed.

20. DISTRIBUTION/AVAILABILITY OF ABSTRACT <input type="checkbox"/> UNCLASSIFIED/UNLIMITED <input type="checkbox"/> SAME AS RPT. <input type="checkbox"/> DTIC USERS	21. ABSTRACT SECURITY CLASSIFICATION	
22a. NAME OF RESPONSIBLE INDIVIDUAL Martin Lewis (previously Col. S. Boyce)	22b. TELEPHONE (Include Area Code) (202) 767-6963	22c. OFFICE SYMBOL AFOSR/NA

UNCLASSIFIED

FINAL REPORT

ON

**CRACK PROPAGATION AND FABRIC CONTROL
ON THE STATIC AND DYNAMIC STRENGTH OF COHESIVE SOILS**

Grant No. AFOSR-88-0169

by

**Adel S. Saada and Gary F. Bianchini
Department of Civil Engineering
Case Western Reserve University
Cleveland, Ohio 44106-7201**

January, 1992

Prepared for

**Air Force Office of Scientific Research
Bolling Air Force Base
D.C. 20332-6448**



Accession For	
NTIS	Serial
Publ	Ref
Unpublished	
Justification	
By	
Distribution/	
Availability Codes	
Dist	Avail and/or Special
A-1	

**CRACK PROPAGATION AND FABRIC CONTROL
ON THE STATIC AND DYNAMIC BEHAVIOR OF COHESIVE SOILS**

by

Adel S. Saada and Gary F. Bianchini

RESEARCH OBJECTIVES AND ACCOMPLISHMENTS

To conduct parallel studies on strength behavior, kinematics of deformation and soil fabric, in saturated clay soils; with particular emphasis being placed on crack and damage propagation, bifurcation, and localization in the form of shear bands. The following questions were asked in the original research proposal:

1. How does the fabric and the strength of a cross anisotropic clay change with the inclination of the principal stresses on the axis of symmetry of the material?
2. What is the effect of a crack or notch and of anisotropy on the dynamic modulii E and G and on the damping ratio , at small strains in fast cyclic tests?
3. How does the fabric change in the vicinity of a crack propagating in Mode II during fast and slow cyclic testing?
4. How does a damage zone propagate under static loading as compared to its propagation under fast loading and cyclic loading? What is the influence of the amplitude and of the number of cycles?
5. What is the nature of the densification strips in the damage zone? What happens to the clay clusters in those strips?
6. How do cracks and damage zones coalesce in case of more than one crack propagating initially in Mode II?
7. How is the fabric modified as the damage zones propagate and coalesce?

All the questions were answered. In addition, the observations and measurements made along the shear bands during their propagation provide the necessary ingredients for the development of the appropriate constitutive equations. Testing with hollow cylindrical specimens allows one to apply a whole spectrum of stress states to a material. This is the first time that initiation and propagation of shear bands were measured in a material subjected to a tri-dimensional system of stress. The fact that we are dealing with a relatively weak material allows us to obtain excellent results while using simple equipment.

STUDENTS PARTICIPATION

Four students were involved of whom three left after spending relatively short periods of time working on this research. Mr. Liqun Liang the fourth student joined the project a year and a half ago and contributed substantially to the conduct of the experiments. The bulk of the work, however was done by the principal investigators. Mr. Liang will be using the results to develop a finite elements code, most probably based on elasto-plasticity, to model the bifurcation and shear banding phenomena in his Ph.D. thesis.

PUBLICATIONS & PRESENTATIONS

Two papers are being prepared for publication. This is a project in which one has to wait to the end in order to reach definite conclusions.

A presentation will be made in Paris in June of 1992 during a Franco-American Workshop on Strain Localization and Interfaces; the workshop being supported and sponsored by the National Science Foundation and the French "Centre National pour la Recherche Scientifique" (CNRS).

In addition, a presentation will be made at the November 1992 ASCE New York Convention during a session on Fracture Mechanics Applied to Soils.

FINAL REPORT

ON

**CRACK PROPAGATION AND FABRIC CONTROL
ON THE STATIC AND DYNAMIC STRENGTH OF COHESIVE SOILS**

Grant No. AFOSR-88-0169

by

**Adel S. Saada and Gary F. Bianchini
Department of Civil Engineering
Case Western Reserve University
Cleveland, Ohio 44106-7201**

January, 1992

Prepared for

**Air Force Office of Scientific Research
Bolling Air Force Base
D.C. 20332-6448**

TABLE OF CONTENTS

ABSTRACT

ACKNOWLEDGMENT

LIST OF TABLES

LIST OF FIGURES

CHAPTER

I. INTRODUCTION AND BRIEF REVIEW OF LITERATURE

II. EXPERIMENTAL PROGRAM

- 2.1 The Hollow Cylinder Testing Cell
- 2.2 Loading Devices
- 2.3 Observation and Recording Devices
- 2.4 Preparation of Clay Specimens Macroscopic Examination
- 2.5 Scope of the Investigation

III. TEST RESULTS AND OBSERVATIONS RELATED TO STRENGTH

- 3.1 Observations Corresponding to the Tests in Tables 2.1, 2.2 and 2.9
- 3.2 Observations Corresponding to the Tests in Table 2.3
- 3.3 Observations Corresponding to the Tests in Table 2.4
- 3.4 Observations Corresponding to the Tests in Table 2.5
- 3.5 Observations Corresponding to the Tests in Tables 2.6 and 2.7
- 3.6 Observations Corresponding to the Tests in Table 2.8

IV. KINEMATICS OF DEFORMATION, CRACK AND DAMAGE PROPAGATION

- 4.1 Specimens Without Cracks Under Static Loading
- 4.2 Specimens With One Crack Under Static Loading
- 4.3 Specimens With One Crack Under Dynamic Loading
- 4.4 Specimens With Two Cracks
- 4.5 Kinematics of Deformation, Crack and Damage Propagation

V. APPLICATION OF FRACTURE MECHANICS AND PLASTICITY THEORY

- 5.1 Stress Concentration Around Crack Tips
- 5.2 Finite Elements Elasto-Plastic Analysis.

VI. FABRIC CHANGE AND MICROMECHANISMS OF DEFORMATION

- 6.1 Macroscopic Observations**
- 6.2 Strip Characterization**
- 6.3 Microscopic Observations**
- 6.4 Conclusions**

VII. CONCLUSIONS

- 7.1 In the Area of Strength**
- 7.2 In the Area of Bifurcation and Shear Band Development**
- 7.3 In the Area of Modelling**
- 7.4 In the Area of Fabric**

REFERENCES

APPENDIX

- I. CONSOLIDATIONS TESTS**
- II. RESONANT COLUMN TEST**
- III. TESTS LISTED IN TABLE 2.1**
- IV. TESTS LISTED IN TABLE 2.2**
- V. TESTS LISTED IN TABLE 2.3**
- VI. TESTS LISTED IN TABLE 2.4**
- VII. TESTS LISTED IN TABLE 2.5**
- VIII. TESTS LISTED IN TABLE 2.8**
- IX. TESTS LISTED IN TABLE 2.9**

ABSTRACT

Discontinuities in the form cracks or fissures and inclusions are often present in natural clays. They serve as stress concentrators when loads are applied to the material. Such concentrations result in the cracks advancing, often surrounded and preceded by a propagating damage zone. As the crack propagates, the damage may be in the form of one or more shear bands, which may play the part of new stress concentrators and blunt the action of the original crack. This report examines some of the phenomena associated with the presence of cracks in overconsolidated clays as well as in the less brittle normally consolidated clays. Differences between isotropic and anisotropic materials, and the level at which serious modifications take place in the fabric of the material are noted. Observations made with a surface analyzer as well as with a transmission electron microscope indicate that the changes in fabric mostly occur at the level of the cluster or flock. The influence of the cracks and of the shear bands on the kinematics and strength of the test specimens is studied and discussed.

ACKNOWLEDGMENT

This research was sponsored by the Air Force Office of Scientific Research with Colonel Steven C. Boyce as Supervising Officer. The Principal Investigators Professor Adel S. Saada and Dr. Gary F. Bianchini, both of Case Western Reserve University, wish to express their gratitude to the sponsoring organization and its representatives, as well as to those who helped in this challenging endeavor. In particular, we wish to thank Dr. Raymond Yong of McGill University for his help in the electron microscopy part of the investigation. Mr. Liqun Liang, a graduate student at Case Western Reserve University, helped conduct many of the experiments; Ms. Kathleen Dangerfield ably typed this report.

LIST OF TABLES

Table

- 2.1 Static Tests on K_o Consolidated EPK, Configuration of Fig. 2.7a, No Crack.
- 2.2 Static Tests on K_o Consolidated EPK, Configuration of Fig. 2.7b, No Crack.
- 2.3 Static Tests on K_o Consolidated EPK, $\sigma_c = 345$ kPa, Configuration of Fig. 2.7b, with Crack.
- 2.4 Static Tests on K_o Overconsolidated EPK, Mean OCR=4, Configuration of Fig. 2.7b, No Crack.
- 2.5 Static Tests on K_o Overconsolidated EPK, Mean OCR=4, Configuration of Fig. 2.7b, with Crack.
- 2.6 Dynamic Tests on K_o Consolidated EPK, $\sigma_c = 345$ kPa, Configuration of Fig. 2.7b, with Crack.
- 2.7 Dynamic Tests on K_o Overconsolidated EPK, Mean OCR=4, Configuration of Fig. 2.7b, with Crack.
- 2.8 Static Tests on K_o Overconsolidated EPK, Mean OCR=4, with Two Cracks, Free Axial Deformation.
- 2.9 Tests on K_o Consolidated H121, $\sigma_c = 345$ kPa.
- 4.1 Inclination of Shear Bands for Various Inclinations of Major Principal Stresses; No Cracks.
- 4.2 Inclination of Shear Bands Emanating from Cracks.
- 4.3 Inclination of Shear Bands and Crack Shear Displacements for Twc Cracks.

- 5.1 Stress Values on Various Contour Lines.**
- 5.2 Equivalent Plastic Strain Values on Various Contour Lines.**

LIST OF FIGURES

Figure

- 2.1 Cell for Axial and Torsional Stresses on Hollow Cylinders
- 2.2 Stress Controlled SPAC and Supporting Equipment
- 2.3 Deformation Controlled SPAC and Supporting Equipment
- 2.4 Notation
- 2.5 Photograph of Image Analysis System
- 2.6 Schematic Set-up for Hollow Cylinder System
- 2.7 Specimen's Geometry
- 2.8 Preparation of a Hollow Cylinder of Clay
- 2.9 Specimens with Square Grid
- 2.10 Impregnation and Sectioning of Clay Specimens
- 2.11 Clay Clusters after Impregnation
- 3.1a Normalized Octahedral Shear Stress vs. Octahedral Shear Strain; EPK; $\beta = 0$
- 3.1b Normalized Octahedral Shear Stress vs. Octahedral Shear Strain; EPK; $\beta = 30^\circ$
- 3.1c Normalized Octahedral Shear Stress vs. Octahedral Shear Strain; EPK; $\beta = 45^\circ$
- 3.1d Normalized Octahedral Shear Stress vs. Octahedral Shear Strain; EPK; $\beta = 60^\circ$
- 3.1e Normalized Octahedral Shear Stress vs. Octahedral Shear Strain; EPK; $\beta = 90^\circ$
- 3.2a Normalized Pore Pressure Developed vs. Octahedral Shear Strain; EPK; $\beta = 0$
- 3.2b Normalized Pore Pressure Developed vs. Octahedral Shear Strain; EPK; $\beta = 30^\circ$
- 3.2c Normalized Pore Pressure Developed vs. Octahedral Shear Strain; EPK; $\beta = 45^\circ$
- 3.2d Normalized Pore Pressure Developed vs. Octahedral Shear Strain; EPK; $\beta = 60^\circ$
- 3.2e Normalized Pore Pressure Developed vs. Octahedral Shear Strain; EPK; $\beta = 90^\circ$

- 3.3a Normalized Octahedral Shear Stress vs. Octahedral Shear Strain; H121
- 3.3b Normalized Pore Pressure Developed vs. Octahedral Shear Strain; H121
- 3.4 Influence of the Inclination of the Major Principal Stress on ϕ'
- 3.5a Comparison of Trimmed and Uniform Specimens
- 3.5b Comparison of Trimmed and Uniform Specimens
- 3.6a Bifurcation and Resulting Shear Bands; $\beta = 30^\circ$
- 3.6az Bifurcation and Resulting Shear Bands; $\beta = 30^\circ$
- 3.6b Bifurcation and Resulting Shear Bands; $\beta = 60^\circ$
- 3.6bz Bifurcation and Resulting Shear Bands; $\beta = 60^\circ$
- 3.7a Comparison Between Notched and Unnotched Specimens
- 3.7b Comparison Between Notched and Unnotched Specimens
- 3.8a Comparison Among Various Modes of Testing
- 3.8b Comparison Among Various Modes of Testing
- 3.9a Effect of the Inclination of the Crack on the Strength
- 3.9b Effect of the Inclination of the Crack on the Pore Water Pressure
- 3.10a Normalized Octahedral Shear Stress vs. Octahedral Shear Strain; Overconsolidated EPK
- 3.10b Normalized Pore Pressure Developed vs. Octahedral Shear Strain; Overconsolidated EPK
- 3.11a Bifurcation and Resulting Shear Bands; $\beta = 30^\circ$
- 3.11az Bifurcation and Resulting Shear Bands; $\beta = 30^\circ$
- 3.11b Bifurcation and Resulting Shear Bands; $\beta = 45^\circ$
- 3.11bz Bifurcation and Resulting Shear Bands; $\beta = 45^\circ$
- 3.11c Bifurcation and Resulting Shear Bands; $\beta = 60^\circ$
- 3.11cz Bifurcation and Resulting Shear Bands; $\beta = 60^\circ$

- 3.12a Comparison Between Notched and Unnotched Specimens
- 3.12b Comparison Between Notched and Unnotched Specimens
- 3.13a Influence of the Size of the Crack on the Strength
- 3.13b Influence of the Size of the Crack on the Pore Water Pressure
- 3.14 Decay of Shear Modulus and Increase in Damping of an Anisotropic EPK with a Horizontal Crack
- 3.15 Decay of Shear Modulus and Increase in Damping of an Isotropic EPK with a Horizontal Crack
- 3.16 Decay of Shear Modulus and Increase in Damping of an Anisotropic EPK with an Inclined Crack
- 3.17a Influence of the Number of Cracks and Their Relative Position on the Strength
- 3.17b Influence of the Number of Cracks and Their Relative Position on the Pore Water Pressure
- 4.1 Morgenstern and Tchalenko's Definitions
- 4.2 Multiple Shear Bands in an H121 Clay in Torsion
- 4.3a Influence of the Filter Paper on the Formation of Shear Bands
- 4.3b Influence of the Filter Paper on the Formation of Shear Bands
- 4.4 Influence of the Filter Paper on the Formation of Shear Bands
- 4.5 Inclination of the Shear Bands
- 4.6a Shear Bands for One Crack and $\beta = 30^\circ$
- 4.6az Shear Bands for One Crack and $\beta = 30^\circ$
- 4.6b Shear Bands for One Crack and $\beta = 45^\circ$
- 4.6bz Shear Bands for One Crack and $\beta = 45^\circ$
- 4.6c Shear Bands for One Crack and $\beta = 60^\circ$
- 4.6cz Shear Bands for One Crack and $\beta = 60^\circ$
- 4.7a Shear Bands for One Crack Under Torsion with Fixed Length

- 4.7az Shear Bands for One Crack Under Torsion with Fixed Length
- 4.7b Shear Bands for One Crack Under Torsion with Fixed Length
- 4.7bz Shear Bands for One Crack Under Torsion with Fixed Length
- 4.8a Shear Bands for an Inclined Crack in the Downstep Position; $\alpha = 45^\circ$
- 4.8az Shear Bands for an Inclined Crack in the Downstep Position; $\alpha = 45^\circ$
- 4.8b Shear Bands for an Inclined Crack in the Upstep Position; $\alpha = 45^\circ$
- 4.8bz Shear Bands for an Inclined Crack in the Upstep Position; $\alpha = 45^\circ$
- 4.8c Shear Bands for an Inclined Crack in the Downstep Position; $\alpha = 22.5^\circ$
- 4.8cz Shear Bands for an Inclined Crack in the Downstep Position; $\alpha = 22.5^\circ$
- 4.9a Shear Bands for One Crack and $\beta = 30^\circ$
- 4.9az Shear Bands for One Crack and $\beta = 30^\circ$
- 4.9b Shear Bands for One Crack and $\beta = 45^\circ$
- 4.9bz Shear Bands for One Crack and $\beta = 45^\circ$
- 4.9c Shear Bands for One Crack and $\beta = 60^\circ$
- 4.9cz Shear Bands for One Crack and $\beta = 60^\circ$
- 4.9d Shear Bands for One Crack Under Torsion with Fixed Length; Isotropic Clay
- 4.9dz Shear Bands for One Crack Under Torsion with Fixed Length; Isotropic Clay
- 4.10a Influence of the Size of the Crack on the Shear Bands; $a/l = 0.0$
- 4.10az Influence of the Size of the Crack on the Shear Bands; $a/l = 0.0$
- 4.10b Influence of the Size of the Crack on the Shear Bands; $a/l = 0.10$
- 4.10bz Influence of the Size of the Crack on the Shear Bands; $a/l = 0.10$
- 4.10c Influence of the Size of the Crack on the Shear Bands; $a/l = 0.18$
- 4.10cz Influence of the Size of the Crack on the Shear Bands; $a/l = 0.18$
- 4.10d Influence of the Size of the Crack on the Shear Bands; $a/l = 0.30$

- 4.10dz Influence of the Size of the Crack on the Shear Bands; $a/l = 0.30$
- 4.10e Influence of the Size of the Crack on the Shear Bands; $a/l = 0.35$
- 4.10ez Influence of the Size of the Crack on the Shear Bands; $a/l = 0.35$
- 4.10f Influence of the Size of the Crack on the Shear Bands; $a/l = 0.4$
- 4.10 fz Influence of the Size of the Crack on the Shear Bands; $a/l = 0.4$
- 4.11a Crack Propagation and Damage Zone for a K_o Normally Consolidated Clay (EPK)
- 4.11b Crack Propagation and Damage Zone for a K_o Overconsolidated Clay (EPK)
- 4.12 Crack Propagation and Damage Zone for a K_o Normally Consolidated Clay (H121)
- 4.13 Crack Propagation and Damage Zone for a K_o Overconsolidated Clay (EPK)
- 4.14 Crack Propagation and Damage Zone for an Isotropic Overconsolidated Clay
- 4.15 Damage Zone for an Inclined Crack
- 4.16 Tensile Failure under Cyclic Torsional Load
- 4.17a Shear Bands and Distortion under Impulse Loading
- 4.17b Displacement Pattern During Impulse Loading
- 4.18 Shear Bands and Interaction of Two Cracks in the Downstep Position; $e = 0$
- 4.18z Shear Bands and Interaction of Two Cracks in the Downstep Position; $e = 0$
- 4.19 Shear Bands and Interaction of Two Cracks in the Upstep Position; $e = 0$
- 4.19z Shear Bands and Interaction of Two Cracks in the Upstep Position; $e = 0$
- 4.20 Shear Bands and Interaction of Two Cracks in the Upstep Position; $e = 0.6\text{cm}$
- 4.20z Shear Bands and Interaction of Two Cracks in the Upstep Position; $e = 0.6\text{cm}$
- 4.21 Shear Bands and Interaction of Two Cracks in the Upstep Position; $e = 1.3\text{cm}$
- 4.21z Shear Bands and Interaction of Two Cracks in the Upstep Position; $e = 1.3\text{cm}$
- 4.22 Shear Bands and Interaction of Two Cracks in the Upstep Position; $e = 2.54\text{cm}$
- 4.22z Shear Bands and Interaction of Two Cracks in the Upstep Position; $e = 2.54\text{cm}$

- 4.23 Length of First Shear Band for Various Levels of Rotation (18-1-15-91)
- 4.24 Amount of Slip Along the First Shear Band (18-1-15-91)
- 4.25 Slip Along the First Shear Band for Various Levels of Rotation (18-1-15-91)
- 4.26 Length of Shear Bands for Various Levels of Rotation (66-5-29-91)
- 4.27 Amount of Slip Along the Shear Bands (66-5-29-91)
- 4.28 Length of Shear Bands for Various Levels of Rotation (16-12-13-90)
- 4.29 Amount of Slip Along the Shear Bands (16-12-13-90)
- 4.30 Length of First Shear Band for Various Levels of Rotation (70-6-14-91)
- 4.31 Slip Along the First Shear Band for Various Levels of Rotation (70-6-14-91)
- 5.1 Influence of the Size of the Crack on the Strength
- 5.2 Torque Energy vs. Rotation
- 5.3 J-Integral vs. Rotation
- 5.4a Notation
- 5.4b Loading Conditions
- 5.5 Superposition Model for Elastic Analysis
- 5.6a Lines of Equal Shear Stress
- 5.6b 3-D Plot of Shear Stress
- 5.6c Lines of Equal Normal Stress
- 5.6d 3-D Plot of Normal Stress
- 5.6e Lines of Equal Normal Stress
- 5.6f 3-D Plot of Normal Stress
- 5.6g Lines of Equal Maximum Principal Stress
- 5.6h 3-D Plot of Maximum Principal Stress
- 5.6i Lines of Equal Minimum Principal Stress

- 5.6j 3-D Plot of Minimum Principal Stress
- 5.6k Lines of Equal Maximum Shear Stress
- 5.6l 3-D Plot of Maximum Shear Stress
- 5.6m Lines of Equal Mean Stress
- 5.6n 3-D Plot of Mean Stress
- 5.6o Principal Stresses and Their Directions
- 5.7a Lines of Equal Shear Stress
- 5.7b 3-D Plot of Shear Stress
- 5.7c Lines of Equal Normal Stress
- 5.7d 3-D Plot of Normal Stress
- 5.7e Lines of Equal Normal Stress
- 5.7f 3-D Plot of Normal Stress
- 5.7g Lines of Equal Maximum Principal Stress
- 5.7h 3-D Plot of Maximum Principal Stress
- 5.7i Lines of Equal Minimum Principal Stress
- 5.7j 3-D Plot of Minimum Principal Stress
- 5.7k Lines of Equal Maximum Shear Stress
- 5.7l 3-D Plot of Maximum Shear Stress
- 5.7m Lines of Equal Mean Stress
- 5.7n 3-D Plot of Mean Stress
- 5.7o Principal Stresses and Their Directions
- 5.8a Lines of Equal Shear Stress
- 5.8b 3-D Plot of Shear Stress
- 5.8c Lines of Equal Normal Stress

- 5.8d 3-D Plot of Normal Stress
- 5.8e Lines of Equal Normal Stress
- 5.8f 3-D Plot of Normal Stress
- 5.8g Lines of Equal Maximum Principal Stress
- 5.8h 3-D Plot of Maximum Principal Stress
- 5.8i Lines of Equal Minimum Principal Stress
- 5.8j 3-D Plot of Minimum Principal Stress
- 5.8k Lines of Equal Maximum Shear Stress
- 5.8l 3-D Plot of Maximum Shear Stress
- 5.8m Lines of Equal Mean Stress
- 5.8n 3-D Plot of Mean Stress
- 5.8o Principal Stresses and Their Directions
- 5.9a Lines of Equal Shear Stress
- 5.9b 3-D Plot of Shear Stress
- 5.9c Lines of Equal Normal Stress
- 5.9d 3-D Plot of Normal Stress
- 5.9e Lines of Equal Normal Stress
- 5.9f 3-D Plot of Normal Stress
- 5.9g Lines of Equal Maximum Principal Stress
- 5.9h 3-D Plot of Maximum Principal Stress
- 5.9i Lines of Equal Minimum Principal Stress
- 5.9j 3-D Plot of Minimum Principal Stress
- 5.9k Lines of Equal Maximum Shear Stress
- 5.9l 3-D Plot of Maximum Shear Stress

- 5.9m Lines of Equal Mean Stress
- 5.9n 3-D Plot of Mean Stress
- 5.9o Principal Stresses and Their Directions
- 5.10 Boundary Conditions for F.E. Analysis
- 5.11 Convention for the Drucker-Prager Criterion
- 5.12 Lines of Equivalent Plastic Strain; Von Mises Model; Pure-Torsion
- 5.13 Lines of Equivalent Plastic Strain; Drucker-Prager Model; Pure-Torsion
- 5.14a Lines of Equal Major Principal Stress; Elastic Solution; Pure-Torsion
- 5.14b Lines of Equal Minor Principal Stress; Elastic Solution; Pure-Torsion
- 5.14c Lines of Equal Principal Stress Difference; Elastic Solution; Pure-Torsion
- 5.15a Lines of Equal Major Principal Stress; Elasto-Plastic Solution; Pure-Torsion
- 5.15b Lines of Equal Minor Principal Stress; Elasto-Plastic Solution; Pure-Torsion
- 5.15c Lines of Equal Principal Stress Difference; Elasto-Plastic Solution; Pure-Torsion
- 5.16a Elastic Stress Distribution along OA
- 5.16b Elasto-Plastic Stress Distribution along OA
- 5.17a Elastic Stress Distribution along OB
- 5.17b Elasto-Plastic Stress Distribution along OB
- 5.18a Spread of the Plastic Zone for a Compression-Torsion Test
- 5.18b Spread of the Plastic Zone for a Pure-Torsion Test
- 5.18c Spread of the Plastic Zone for a Tension-Torsion Test
- 5.19a Lines of Equal Major Principal Stress; DP Model; Compression-Torsion Test
- 5.19b Lines of Equal Minor Principal Stress; DP Model; Compression-Torsion Test
- 5.19c Lines of Equal Principal Stress Difference; DP Model; Compression-Torsion Test
- 5.20a Lines of Equal Major Principal Stress; DP Model; Pure-Torsion Test

- 5.20b Lines of Equal Minor Principal Stress; DP Model; Pure-Torsion Test**
- 5.20c Lines of Equal Principal Stress Difference; DP Model; Pure-Torsion Test**
- 5.21a Lines of Equal Major Principal Stress; DP Model; Tension- Torsion Test**
- 5.21b Lines of Equal Minor Principal Stress; DP Model; Tension- Torsion Test**
- 5.21c Lines of Equal Principal Stress Difference; DP Model; Tension-Torsion Test**
- 6.1 Impregnated specimen of EPK**
- 6.2 Sections of Undamaged and Damaged K_o Overconsolidated EPK**
- 6.3 LSD Measurements Procedure**
- 6.4 LSD Histograms at Various Locations in Front of the Crack Tip.**
- 6.5 3D LSD Densification Plot**
- 6.6 Sections of Undamaged and Damaged Isotropic EPK**
- 6.7 Section of Undamaged and Damaged K_o Consolidated H121**
- 6.8 Clay Fabric Model**
- 6.9 Photomicrograph of Horizontal Section; EPK**
- 6.10 Photomicrograph of Vertical Section; EPK**
- 6.11 Photomicrograph of H121 (Yong & Warkentin)**

CHAPTER I

INTRODUCTION AND SHORT REVIEW OF PAST WORK

The mechanical response of clays is dictated by their fabric as well as by flaws or discontinuities that may exist in the material. These flaws, often in the form of cracks (or notches), result in shear bands that spread from the crack and form a damaged zone in which most of the deformation is localized. Bifurcation theories have been and are being used to predict the occurrence of shear bands based on the pre-localization constitutive relations of the material.

Many branches of mechanics must be brought together to analyze the phenomena at hand. The following briefly summarizes, or better lists, key investigations conducted by various researchers; the hope being that at some time a coherent formulation will be found to express the various observed phenomena.

1.1 In the Area of Shear Band Observation:

Morgenstern and Tchalenko (1967) used thin sections of carbowax impregnated clay to study the behavior of a clay tested in a direct shear device. They defined two types of discontinuities, namely strain and displacement, and bring out the kinematic restraint imposed by the configuration. They also adopt a sequential numbering system in referring to the shear bands. Their detailed examination of the development of kink bands and compression textures lead to the notion of basal plane slip as the basic mechanism in shear induced structures.

Houlsby and Wroth (1980) classify kinematic discontinuities and show that a velocity discontinuity does not necessarily have to be a line of zero extension; whether it is or not depends on the adopted constitutive relation.

Balasubramaniam (1976) working with clays used X-rays to study the pattern of deformation. He found the strains to be uniform up to 75 percent of the peak value.

Arthur and Dunstan (1982) used radiography to show that in granular non-cohesive material rupture layers formed gradually by local layers of higher dilation in pre-failure strain align along pre-failure incremental non-extension directions, axes of stress and strain rate being generally coincident. Rupture layers, formed at failure in homogenous samples of soil sheared slowly under homogeneous stresses with fixed principal stress directions, are oriented at a specific angle according to soil particle size between the limits of $(\pi/4 - \phi'/2)$ and $(\pi/4 - \beta/2)$; the limits being determined by the plane strain values of ϕ' and β the angle of dilation.

Scarpelli and Wood (1982) used radiography to study the orientation of the shear bands in direct shear tests conducted on sand. They suggest that the degree of constraint perceived by the sand will influence the particular bifurcation that it adopts at any particular location. Where the sand sees freedom it may adopt the Vardoulakis-Arthur solutions. Where the imposed constraint is larger, as in the direct shear device the shear band would aim for the Roscoe solution and follow directions of zero extension.

Desrues, J. (1983) used stereophotogrammetry to study localization in granular materials. For sands Desrues accurately measured the direction of shear bands due to plane strain compression of sand samples. He provided local measurements of the

dilatancy angle and showed that, under certain circumstances, the local dilatancy angle within the shear band was twice as large as the global dilatancy angle calculated from the total volume change measurements.

1.2 In the Area of Bifurcation Theories :

Vardoulakis (1982) in his review of the theoretical and experimental work done in the area of stability and bifurcation of soil samples, states that research in this area has been primarily influenced by the work of Hill (see Hill and Hutchinson, 1975). Hill and Hutchinson (1975) based their work on Biot's pioneering studies (1965) and Ariaratnam and Dubey's (1969) studies of diffuse bifurcation modes under plane strain conditions for elasto-plastic incompressible materials. They studied in great detail bifurcation of incompressible materials in the plane-tension tests covering a broad spectrum of constitutive assumptions. They covered both diffuse and localized shearing modes. Plane compression tests were analyzed by Young (1976), and more recently Needleman (1979) extended this work to pressure sensitive incompressible materials.

Rudnicki and Rice (1975) studied localization by comparing an isotropic hardening model with a yield vertex model for a pressure sensitive, dilatant material. They showed that the yield vertex model provides a better description and that non normality permits non uniqueness with positive hardening. Both these features are shown to be destabilizing and to strongly influence the resulting predictions for localization by comparison to predictions based on classical plasticity idealizations, involving normality and smooth yield surfaces.

Rice (1976) discusses the localization of plastic deformation into a shear band as an instability of plastic flow and a precursor to rupture. The material is assumed rate-independent and critical conditions are sought for its constitutive relations to allow a bifurcation from a smoothly varying deformation into a highly-concentrated shear band mode. He essentially explores a bifurcation approach in which concentrated deformation occurs simultaneously (or near simultaneously) at all points of the zone of localization. The results are applied to rigid-plastic, elastic-plastic and plastically dilatant with pressure sensitive yielding materials.

Rice and Rudnicki (1980) make a distinction between continuous and discontinuous bifurcation. In the first further plastic deformation is assumed to occur both inside and outside the zone of localization; while in the second elastic unloading occurs outside the zone of localization while continued elastic-plastic deformation occurs within it. Discontinuous bifurcations become possible at the same time continuous ones occur. The elastic unloading will cause localization to accelerate through the remainder of the specimen.

Vardoulakis et al (1978) discussed the spontaneous formation of shear bands in sand bodies. The formation of such bands is looked upon as a bifurcation problem. They demonstrated theoretically and experimentally that both Coulomb's and Roscoe's solutions for the orientation of the shear bands are possible, namely,

$$\Theta_c = \pi/4 - \phi'/2 \text{ (Coulomb)}$$

$$\Theta_c = \pi/4 - \psi/2 \text{ (Roscoe)}$$

where δ is the dilatancy angle (see Arthur and Dunstan, 1982). They analyze four modes of deformation and find that Coulomb's solution holds for non-rotating stress axes while the Roscoe solution holds for co-rotating stress and strain increment axes during failure.

Vardoulakis (1980) in a continuation of the previous paper gives experimental results obtained in biaxial tests on sand that show that the inclination of the shear bands indeed fall between the two limits of Coulomb and Roscoe. He concludes that because of the failure of the normality rule in sands, localization under those conditions always occur in the hardening regime.

Vardoulakis and Graf (1982) placed wooden inclusions in their biaxial testing device and studied shear band formation as an imperfection sensitivity problem. In 1983, Vardoulakis studied diffuse and localized bifurcation modes in axisymmetric, rectilinear deformations on rigid-granular dilatant material. He found that localizations in the compression test occur in the softening regime and in the extension test they occur in the hardening regime.

Hettler, A. and Vardoulakis, I. (1984) conducted an extensive investigation on sands in a large triaxial apparatus and concluded that when the platens were lubricated bifurcation into diffuse bulging occurred in the hardening regime. Diffuse bulging could be avoided by using flat specimens. However, shear bands inevitably occur in the softening regime of the stress-strain curve.

Vardoulakis (1985) examined the stability and bifurcation of water saturated sands and normally consolidated clay. He described their behavior by means of a two-dimensional flow theory of plasticity with a non-associated flow rule. He concluded that

for dilatant materials the dominant failure mode is shear banding that occurs close to the state of maximum principal effective stress ratio. Whether the shear bands have a thickness or not is a topic that was also studied by Mühlhaus and Vardoulakis (1987). The conclusion was that they do and that this thickness is a small multiple of the mean grain size, and that it grows as one progresses in the strain hardening region.

Having proven that in shear band analysis the difference between the true stress rate and the Jaumann stress rate could be ignored, Vermeer (1982) deduced elegant and simple relations predicting the instant of initiation as well as the direction of the shear bands. His predictions are in line with Mandel's conclusions for material stability. Molenkamp (1985) studied the material behavior under uniform deformation and the occurrence of a shear band as a coupled phenomenon. He attempted to solve the bifurcation problem for a range of popular constitutive models such as Mohr Coulomb's and Lade and Duncan's. He found among those models large variations in the predicted directions and instants of initiation of the shear bands.

Desrues and Chambon (1989) examine the implication of using complex constitutive relations on the development of shear bands. They give expression of the restriction to be imposed for various solutions to be possible.

Kolymbas and Rombach (1989) use a non-linear constitutive equation for sand with fixed material constants to express analytically a necessary criterion for shear band formation. This band is considered to be a shearing zone which may appear spontaneously in the course of a homogeneous plane deformation. Their criterion predicts not only the

stress state at the moment of a shear band formation but also the inclination of the shear band and the angle of initial dilatancy within the shear zone.

Bardet (1991) discusses the scatter in the results obtained by various investigators while emphasizing the observations made by Desrues. He uses an extended Mohr-Coulomb model to get a more accurate analytical expression for the average orientation of the shear bands in soils. The concept of delayed localization together with this model allows him to retrieve the lower and upper bounds of Roscoe and Mohr Coulomb for the orientation of shear bands.

1.3 In the Areas of Strain Localization Using Finite Elements :

There are two main approaches to treat bifurcation problems in the context of finite elements analysis; the direct method and the indirect method. The direct method analyses the bifurcation condition for every time step, for each element. The calculation for the bifurcation branches requires the determination of the eigenvalues and eigenvectors of the tangent stiffness matrix. In the indirect method, the original structure is slightly modified with the help of initial imperfections. No special element is introduced and strain softening is often part of the model.

Prevost and Hughes (1981) demonstrate that elastic-plastic failure states may be captured in finite element models by employing, the elastic-plastic material stiffness to form the global stiffness, selective integration techniques to alleviate mesh locking due to incompressibility, and an imperfection in the form of weak element. Prevost (1984) applied this technique to the classical punch and slope stability problems.

Bardet and Mortazavi (1987), introduced a material imperfection to initiate strain localization in a homogeneously strained clay subjected to plane strain compression.

Hsu, Peters and Saxena (1987) studied the influence of the mesh design on the location of initiation of shear bands. They recommended that a medium size mesh be chosen for capturing shear bands.

Potts, Dounias and Vaughan (1987) used the direct method to study the behavior of frictional materials in the direct shear box. The boundary conditions themselves initiate the shear bands. Highly stressed zones were found to propagate from the edges of the box at early stages of loading. Those zones grow and rotate with further loading. They examined non-strain softening behavior as well as strain softening behavior arising from both dilation of dense soil and particle orientation in clays. In this last case the analysis shows that at the peak a narrow shear zone along the center plane of the sample is just beginning to form; but very shortly after the peak the shear zone is completely formed. The post peak behavior involves plastic straining only within a thin central line of elements with elastic unloading of the material on either side.

Shuttle and Smith (1988) numerically initiated zones of localized shear strain within idealized cohesive and frictional soil specimens by assuming inhomogeneities and imperfect boundaries. For non-strain softening cohesive soil the localization was triggered by material imperfections. For strain softening cohesive soils, the introduction of the softening conditions resulted in a greater or lesser degree of global softening or brittleness. Upon yield major stress redistributions take place as localization proceeds through the weakest point in the specimen. Their use of elastic strain until the peak is reached results

in the storage of much energy which is later used to drive the localization process on. In reality much of the pre-peak strain in soils involves dissipative effects and a smaller amount of energy is available for release. The authors are primarily interested in pore water pressure migration in relation to shear band formation.

Leroy and Ortiz (1989) confirm that in the absence of normality, localization can take place even under hardening conditions. Their numerical simulations suggest that the observed softening is a geometrical effect not attributable to constitutive behavior (see also Drescher and Vardoulakis, 1982). Conventional finite elements techniques are shown to be limited. They propose the use of an enriched displacement field to capture the localization at the point of bifurcation.

Hobbs and Ord (1989) show that the shear band width is sensitive to the finite difference mesh chosen in the solution given by the finite difference code FLAC and is also controlled by the magnitude of both angles of friction and dilation.

1.4 In the Area of Fracture Mechanics Applied to Soils :

Based on the qualitative descriptions of the failure mechanisms responsible for progressive failure, Palmer and Rice (1973) suggested that sliding occurs on concentrated slip surfaces. Using concepts from fracture mechanics (i.e. the J-integral), attempts were made to assess the time dependence governing the propagation rate of a particular shear band. The assumed model used for the shear band was very similar to the cohesive force models. It asserts that there is a fixed linear relationship between the shear stress in the material and the displacement required to produce it. Since displacement is the integral of

the strains over a given region, an immediate consequence is that size effects will occur. Specifically, the size effect appears in the resistive part of the crack driving force equation. In addition, Palmer and Rice give advice for experimentally obtaining the energy release rate in an approximate manner by computing the energy under the unloading portion of the stress-strain curve in a particular shear box test. Their model, however, does not predict the direction of propagation of the shear band (crack growth).

Saada, A.S., Chudnovsky, A. and Kennedy, M.R. (1985) applied concepts of linear fracture mechanics to overconsolidated brittle clays tested in Modes I and II. They used a stability criterion to predict failure of infinite slopes.

Chudnovsky, A., Saada, A.S. and Lesser, A.J. (1988) and Lesser (1989) studied the propagation of cracks and damage zones in stiff clays, in mode II, under cyclic loading. Both macroscopic and microscopic observations led to the conclusion that the deformation in the material primarily occurs at the level of the clusters. Such clusters coalesce along shear bands on both sides of a propagating crack and form the damaged zone. Stress distributions around the tip of the crack were also given by Lesser.

Using a plane stress direct shear apparatus Vallejo (1987) tested brittle kaolinite with pre-existing opened cracks. He found that the cracks propagated from the tip in the direction normal to the direction of the maximum tensile stress. In 1988, he observed the marked differences between the behavior of brittle and ductile clay when subjecting specimens with inclined cracks to compressive loads. For the particular clay used (namely kaolinite) he found that at a water content less than 20 percent the behavior was brittle. Vallejo (1989) also examined the interference between two cracks in a specimen of brittle

clay subjected to compression. Depending on the relative position of the cracks and the direction of the load he noticed the weakening effects due to the superposition of the tensile stresses that develop near the crack tips.

CHAPTER II

EXPERIMENTAL PROGRAM

The following sections describe the testing and recording devices, the specimens preparation, the scope of the investigation and the conduct of the tests.

2.1 The Hollow Cylinder Testing Cell

Used since 1965 to validate failure criteria and constitutive equations, this cell was first used in 1985 by Saada et al. to study fracture and damage propagation in clay soils. It has been discussed at length in two state-of-the-art papers by Saada and Townsend (1981) and Saada (1988). Fig. 2.1 shows the cell used at Case Western Reserve University. All the measurements are made both inside and outside the cell with a variety of transducers. Axial, torsional and spherical stresses can be applied to the specimen through a piston and a confining fluid. To maintain uniformity of the normal stresses, the same pressure, namely the cell pressure, acts inside and outside the hollow cylinder.

Expressions for the average values of the stresses and strains in terms of the measured forces and displacements are given in the two papers previously mentioned.

2.2 Loading Devices

Two types of loading devices were used in this investigation:

The first is a controlled stress device which applies combinations of axial, torsional and spherical stresses at predetermined ratios, thus resulting in radial paths. It is called

SPAC and has been described by Saada and Townsend (1981). With this device one cannot go beyond the peak, and failure is catastrophic in nature. All its controls are pneumatic and use fluidic components. Fig. 2.2 shows a photograph of SPAC.

The second is a controlled rotation device that uses both mechanical and fluidic controls. A motor applies a slow rotation to the base of the hollow cylinder cell whose piston is prevented from rotating. The resulting torque is measured with a transducer and its electrical output is converted to a pneumatic one. This output is operated on by a variety of fluidic components and sent to an actuator which applies to the cell's piston an axial load proportional to the torque. The result is a radial path with the possibility of going beyond the peak when the failure is torsional in nature. This device was used whenever one wanted to observe the slow development of the shear bands and the slow propagation of damaged zones and cracks. Fig. 2.3 shows a photograph of this device.

All the tests conducted were at constant volume. If, in addition, the height of the specimen is fixed, a condition of constant cross section is present. Fig. 2.4 shows the system of stresses and the sign convention adopted in this paper.

2.3 Observation and Recording Devices

Standard and high speed cameras were used to keep the visual record of the cracks and shear bands propagation in the test specimens.

A Bioquant surface analyzer was used to study the fabric of the material on a macroscopic level. This device helps observe and quantify changes in the fabric, specially in the vicinity of the crack, shear bands and damaged zones (Fig. 2.5).

Transmission electron microscopes were used to look inside the macroscopic units examined by the surface analyzer.

A state-of-the-art data acquisition and reduction system was used to obtain, calculate and graphically present the data (Fig. 2.6).

2.4 Preparation of Clay Specimens. Macroscopic Examination

Two kaolinitic types of clay were used in this investigation. The first one is known as Edgar Plastic Kaolin (EPK). It has been extensively used in soil mechanics research. It has a low activity, a liquid limit of 56.3% and a plastic limit of 37.3%. The second one is known as Hydrite 121 (H121). It has been extensively used at McGill University, Canada. Its liquid limit is 49.6% and its plastic limit is 37.9% resulting in a low plasticity index. It is different from EPK in that its particles are quite large and, when dried it easily crumbles. H121 is very difficult to bring to a low water content by consolidation alone and one has to revert to slow drying to obtain stiff specimens: A relatively small loss of water causes this clay to become quite stiff compared to EPK.

The procedure briefly described herein has been presented in detail by Saada (1988). The clay powder was mixed under vacuum with distilled water to form a slurry at approximately twice the liquid limit. The slurry was then consolidated in a large 20 cm diameter consolidometer to yield a block from which solid cylinders were cut. 5cm diameter cores were removed from the center of the cylinders to yield the specimen shown schematically in Fig. 2.7a. While this shape was most satisfactory for routine tests not involving crack propagation studies, it was found necessary to adopt another configuration

whenever careful observation of shear bands formations were needed. The specimens with enlarged ends shown in Fig. 2.7b were made by pressing and coring the configuration shown in Fig. 2.7a using special cutters and moulds. End effects were thus considerably reduced, if not totally eliminated during testing. Fig. 2.8 shows a succession of photographs illustrating the samples preparation.

When studying isotropic clays, the powder was hand mixed and specimens consolidated isotropically.

To study crack propagation radial notches were made in the specimens using a thin vee-shaped brass sheet. The ratio of the circumferential length, a , of the notch to the mean perimeter l of the specimen varied between 0.1 and 0.4. Some of the notches were inclined to the horizontal. The reference ratio was $a/l = 0.18$ (Fig. 2.7b).

To prevent the notch (or crack) from closing during consolidation and shear, two layers of very thin Teflon sheets were inserted in the artificially made notch. Such sheets transmit very little or no shear; but transmit compressive normal stresses across the notch surfaces.

To simplify the recording of the observation a 0.6 cm square grid was stamped on the specimens (Fig. 2.9). Photographs were taken during the tests to study the deformation patterns. Prior to placing the specimens in the oven for moisture content determination, the specimens were rotated in front of a stationary camera and photographs were taken for small increments of rotation. Those photographs were then overlapped with matching grids so that deformations and slip patterns could be examined on the development of the

cylinder. In case of formation of shear bands, a digitizer was used to obtain a line drawing of the bands.

Most of the tests were conducted on K_o consolidated specimens. This kind of consolidation is routinely performed using a pneumatic analog computer that measures the water expelled from the specimen as the pressure in the cell increases and imposes a vertical displacement such that the original cross section remains constant. The value of K_o is continuously given by a transducer during the whole process. At the end of the K_o consolidation process, K_o was 0.44 for the EPK clay and 0.51 for the H121 clay.

All the specimens were rebounded to a condition of spherical state of stress prior to shearing. Any K_o consolidation test in which the piston load is removed, results in a specimen that is normally consolidated in the horizontal direction and that has an overconsolidative ratio (OCR) of nearly 2 in the vertical direction. If one is to think in terms of mean stresses this ratio is 1.3. Because of the size of this ratio the material will be referred to as slightly overconsolidated or normally consolidated. If in addition to removing the piston load one decreases the pressure in the cell by a factor of 3 say, the specimen is at an OCR of 3 laterally and 6 vertically. In terms of mean stresses the OCR is

4. The return to a spherical state of stress allows one to conduct a radial path test.

To examine the clay in the surface analyzer thin sections of wax impregnated specimens are needed. At the end of a test, triaxial specimens are placed in an oven to determine the final water content. Once this is done, a piece of the dried specimen including the zone to be examined is placed in a bath of wax under a vacuum bell. It is kept there for a specific length of time then withdrawn and left to dry. Thin radial sections,

3mm thick are cut, their faces polished, and then placed in the analyzer's microscope. The image that appears on the screen lends itself to a variety of measurements controlled by the Bioquant software.

It is extremely time consuming to find an impregnation technique that yields good resolution, good thin sections and a satisfactory visual demonstration of the changes in the fabric of the clay. Through trial and error a technique to impregnate dry specimens of clay with wax under vacuum was developed. Fig. 2.11 shows a section in an undisturbed part of a clay specimen. The white clusters of clay are surrounded by a dark matrix of wax and are homogeneously distributed. The impregnation technique was adjusted such that clay clusters of about 100 microns are formed and are visible with relatively small magnification.

Electron microscope examinations were made at McGill University, Canada, by Dr. R. Yong.

2.5 Scope of the Investigation

This experimental investigation is aimed at studying the mechanism of deformation and the development of the shear bands in a clay subjected to various systems of stresses. Emphasis is placed on the influence of cracks, the way they propagate together with the shear bands, and the changes that occur in the fabric of the material, in particular in the vicinity of the cracks and the damaged zone.

Series of tests were conducted on specimens with the configurations in Figs. 2.7a and 2.7b. Most of the cracks artificially induced in the specimens were horizontal. Only a

few were inclined. Some specimens had two cracks. The specimens prepared through one dimensional consolidation are cross anisotropic in nature. Some tests were conducted on isotropic materials to examine the influence of anisotropy on the direction of the shear bands. A number of cyclic loading and fast loading tests were also conducted. All the tests were of the consolidated undrained type with pore pressures measurements.

In all, the experimental investigation was quite extensive. Reference tests, i.e., tests without cracks had to be conducted to allow for comparisons. Their number and variety are sufficient to provide a data base to validate any constitutive model for cohesive soils. The tests conducted on specimens with cracks can be used, not only to describe the kinematics of the deformation, but also to test the appropriateness of presently available crack and bifurcation theories. Sections made in the various specimens allow one to observe how the fabric changes.

A large number of backup tests were conducted to insure repeatability. In addition one dimensional as well as triaxial consolidation tests were needed to determine properties and provide a complete description of the clays used. Resonant column tests on specimens with and without cracks were conducted to study the influence of the cracks on shear moduli and damping ratios. All the tests will be referred to in the following discussions and are completely detailed in the appendices.

Tables 2.1 to 2.9 list the tests conducted and have comments giving information on the specific tests. The column labelled DESIGNATION is a combination of a number and a date. Such labels are used to locate the file containing the data. The angle β is the inclination of the principal stresses on the vertical axis of symmetry. In all the tests for

which β is given, the stress path was radial. To each β there corresponds a value for the coefficient b . The tests in which the length is kept constant, have a variable ratio of axial to torsional stresses. The consolidation pressure in the tables is expressed in terms of effective cell pressure $\bar{\sigma}_c$; with the understanding that the specimen has been K_o consolidated at a cell pressure $\bar{\sigma}_c$ and at whatever vertical stress is necessary to keep the cross section constant. A sketch shows the configuration used.

The order of the tables is such the tables listing the static tests on EPK are given first, followed by those listing the dynamic tests. Also, those related to K_o overconsolidated specimens follow those related to K_o normally consolidated specimens. The tests conducted on H121 clay are in the last table.

Table 2.1 lists three series of five tests on EPK, each series corresponding to a different consolidation cell pressure $\bar{\sigma}_c$, namely 241.5 kPa (35 psi), 345 kPa (50 psi) and 552 kPa (80 psi).

Table 2.2 lists three tests on EPK used to examine the shear bands that develop in specimens without cracks. Two tests were conducted under controlled rotation conditions and one under controlled stress condition.

Table 2.3 lists test conducted on EPK on specimens with horizontal cracks under various inclinations of principal stresses, five free to change length and two with fixed length; also listed are three tests with inclined cracks.

Table 2.4 lists tests conducted on K_o overconsolidated EPK where the cell pressure $\bar{\sigma}_c$ dropped from 621 kPa (90 psi) to 207 kPa (30 psi) with corresponding drop in the vertical effective stress as explained in the previous section. There were no initial cracks in

those specimens. They are used as reference, as well as to study shear bands development with the inclination of the principal stresses.

Table 2.5 lists tests similar to the ones appearing in Table 4 but with a horizontal crack whose ratio a/l is equal to 0.18. In addition, it lists tests conducted in torsion on specimens with horizontal cracks with different ratios a/l .

Table 2.6 lists two torsional cyclic tests and one torsional impulse test conducted on EPK with K_o consolidated specimens ($\bar{\sigma}_c = 345$ kPa) and with fixed length. One of the specimens tested under cyclic condition had a 45° inclined crack and the two others had horizontal cracks.

Table 2.7 lists two torsional cyclic tests conducted on EPK with K_o overconsolidated specimens, both with horizontal cracks, one with fixed length and the other free to change length.

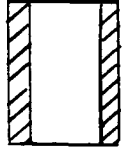
Table 2.8 lists five tests conducted on EPK with K_o overconsolidated specimens and two cracks. The vertical distance between the cracks d is 0.63 cm (0.25 in) and the horizontal distance e varies between zero and 2.54 cm (1.0 in.). Four of the specimens have their cracks in the downstep relative position and one in the upstep relative position. All were free to deform longitudinally.

Table 2.9 lists all the tests conducted on the H121 clay. There are five reference static tests with various inclinations of principal stresses, two torsion tests, and one fixed length torsional cyclic tests.

Not listed in the tables are the limited number of the resonant column tests and the identification triaxial and consolidation tests.

TABLE 2.1 - STATIC TESTS ON K_o CONSOLIDATED EPK

CONFIGURATION OF FIG. 2.7a, NO CRACK

β^o	b	$\bar{\sigma}_c$ kPa			COMMENTS AND CONFIGURATION
		241.5	345	552	
DESIGNATION					
0	0	31-1-29-91	1b-1-10-90	36-2-15-91	<ul style="list-style-type: none"> .Stress Controlled .Radial Stress Path .Free Axial Deformation 
30	.25	32-1-31-91	2-11-15-89	37-2-19-91	
45	.50	33-2-5-91	3b-12-28-89	38-2-21-91	
60	.75	35-2-12-91	5b-11-13-91	40-3-5-91	
90	1.0	34-2-7-91	4b-12-20-89	41-3-7-91	
Average w%		36.20	34.53	32.66	

**TABLE 2.2 - STATIC TESTS ON K_o CONSOLIDATED EPK
CONFIGURATION OF FIG. 2.7b, NO CRACK**

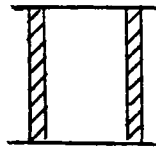
β^o	b	$\bar{\sigma}_c$ kPa	DESIGNATION	CONTROL	COMMENTS AND CONFIGURATION
30	.25	345	62-5-16-91	ROTATION	.Free Axial Deformation
45	.50	345	3t-1-23-90	STRESS	
60	.75	345	61-5-14-91	ROTATION	
60	.75	345	61b-19-11-91	STRESS	
Average w% = 34.42					

TABLE 2.3 - STATIC TESTS ON K_0 CONSOLIDATED EPK, $\bar{\sigma}_c = 345$ kPa

CONFIGURATION OF FIG 2.7b, WITH CRACK

β^o	b	DESIGNATION	CONTROL	CRACK ANGLE	COMMENTS AND CONFIGURATION
0	0	50-4-3-91	STRESS	0	.Free Axial Deformation .a/l = .18
30	.25	51-4-5-91	STRESS	0	
45	.50	6V-9-26-90	ROTATION	0	
60	.75	52-4-9-91	STRESS	0	
90	1.0	53-4-11-91	STRESS	0	
TORSION		3f-2-6-90 6f-6-2190	STRESS ROTATION	0 0	.Fixed Length .a/l = .18
45	.50	56-4-17-91	ROTATION	45°	.Free Axial Deformation
45	.50	57-4-19-91	ROTATION	45°	
45	.50	58-4-23-91	ROTATION	22.5°	
Average w% = 34.60					

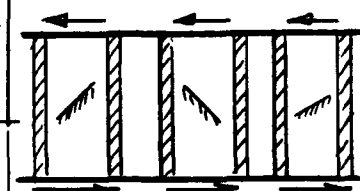
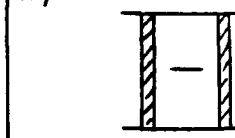


TABLE 2.4 - STATIC TESTS ON K_o OVERCONSOLIDATED EPK

MEAN OCR = 4, CONFIGURATION OF FIG 2.7b, NO CRACK

β^o	b	DESIGNATION	CONTROL	COMMENTS AND CONFIGURATION
0	0	87-7-25-91	STRESS	.Free Axial Deformation
30	.25	89-8-1-91	ROTATION	
45	.50	86-7-23-91	ROTATION	
60	.75	90-8-13-91	ROTATION	
90	1.0	88-7-30-91	STRESS	
Average w% = 33.92				

* One static test on EPK, DESIGNATION 7a-9-6-90 was conducted on an isotropic overconsolidated specimen under controlled deformation conditions, and fixed length under torsion. OCR = 3, w% = 30.20.

TABLE 2.5 - STATIC TESTS ON K_o OVERCONSOLIDATED EPK

MEAN OCR = 4, CONFIGURATION OF FIG. 2.7b, WITH CRACK

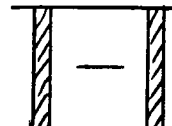
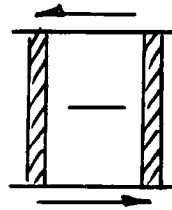
β^o	B	DESIGNATION	CONTROL	a/l	COMMENTS AND CONFIGURATION
0	0	67-5-31-91	STRESS	.18	.Free Axial Deformation 
30	.25	68-6-5-91	ROTATION	.18	
45	.50	66-5-29-91	ROTATION	.18	
60	.75	70-6-14-91	ROTATION	.18	
90	1.0	69-6-7-91	STRESS	.18	
TORSION		19-1-23-91	ROTATION	0	.Fixed Length 
		16-12-13-90	ROTATION	.10	
		18-1-15-91	ROTATION	.18	
		15-11-28-90	ROTATION	.30	
		13-11-7-90	ROTATION	.35	
		14-11-20-90	ROTATION	.40	
Average w% = 32.97					

TABLE 2.6 - DYNAMIC TESTS ON K_0 CONSOLIDATED EPK, $\bar{\sigma}_c = 345$ kPa

CONFIGURATION OF FIG. 2.7b, WITH CRACK

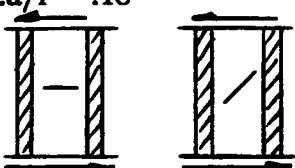
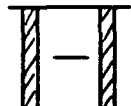
β	b	DESIGNATION	CONTROL	CRACK ANGLE	COMMENTS AND CONFIGURATION
	TORSION	3-1-30-90 3-2-13-90 3-2-22-90	CYCLIC IMPULSE CYCLIC	0 0 45	.Fixed Length .a/l = .18 
Average w% = 33.87					

TABLE 2.7 - DYNAMIC TESTS ON K_o OVERCONSOLIDATED EPK

MEAN OCR = 4, CONFIGURATION OF FIG. 2.7b, WITH CRACK

β	b	DESIGNATION	CONTROL	a/l	COMMENTS AND CONFIGURATION
TORSION 45	.5	17-1-3-91 6vc-10-3-901	CYCLIC CYCLIC	.1 .18	.Fixed Length .Free Axial Deformation
Average w% = 32.03					

* One cyclic loading test on EPK, DESIGNATION 7-6-27-90 was conducted on an isotropic overconsolidated specimen with fixed length under torsion. OCR = 3, w% = 29.91%

TABLE 2.8 - STATIC TESTS ON K_o OVERCONSOLIDATED EPK
 MEAN OCR = 4, WITH TWO CRACKS, FREE AXIAL DEFORMATION

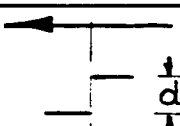
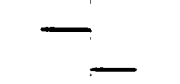
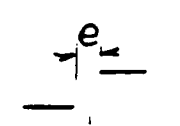
β	b	DESIGNATION	CONTROL	CRACKS POSITION	COMMENTS
45	.5	81-7-3-91	ROTATION		.Downstep e = 0 d = .6cm a/l = .18
45	.5	82-7-9-91	ROTATION		.Upstep e = 0 d = .6cm a/l = .18
45	.5	83-7-11-91	ROTATION		.Downstep e = .6cm d = .6cm a/l = .18
45	.5	84-7-17-91	ROTATION		.Downstep e = 1.3cm d = .6cm a/l = .18
45	.5	85-7-19-91	ROTATION		.Downstep e = 2.54cm d = .6cm a/l = .18
Average w% = 33.62					

TABLE 2.9 - TESTS ON K_o CONSOLIDATED H121, $\bar{\sigma}_c = 345$ kPa

β	b	DESIGNATION	CONTROL	COMMENTS AND CONFIGURATION
0	0	1-5-1-90	STRESS	.Free Axial Deformation
30	.25	2-6-1-90	STRESS	
45	.50	3-5-3-90	STRESS	
60	.75	5-6-8-90	STRESS	
90	1.0	4-6-5-90	STRESS	
TORSION TORSION		3f-5-16-90 6f-9-17-90	STRESS ROTATION	.Fixed Length .Crack a/l = .18
TORSION		3-6-13-90	CYCLIC	
Average w% = 31.14				

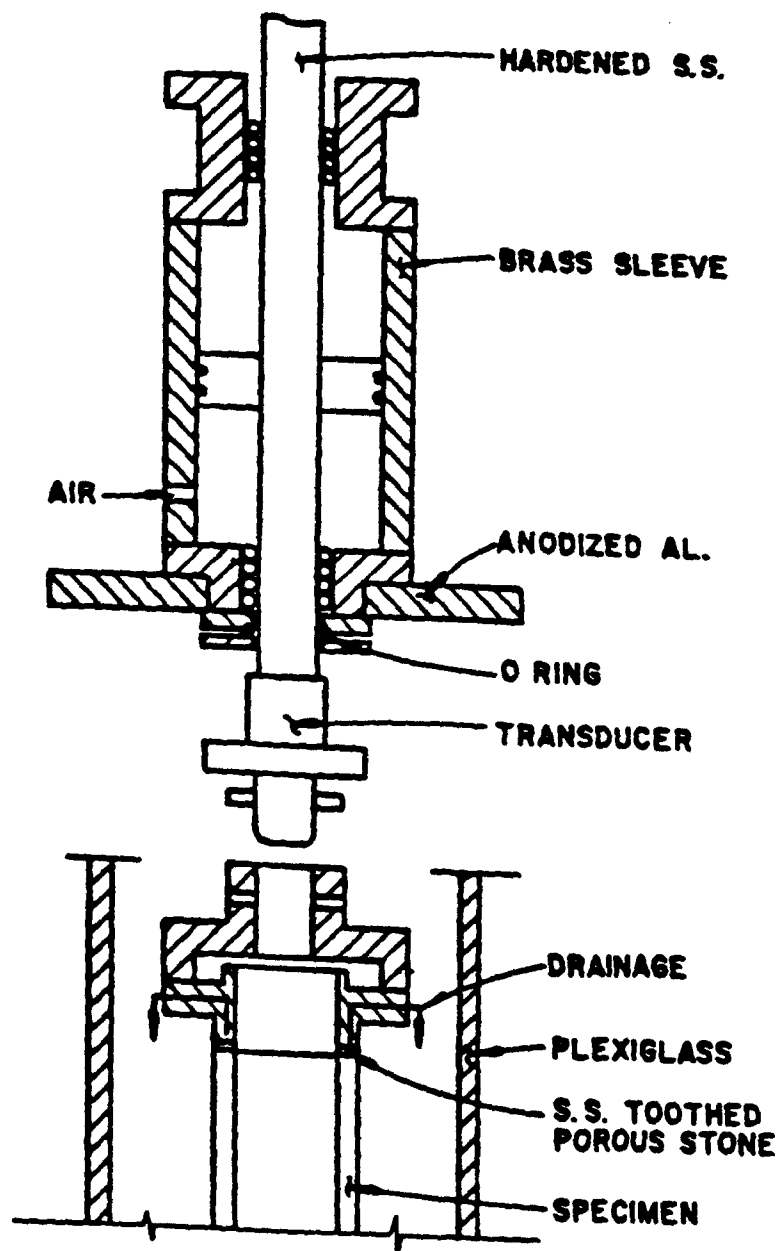


Figure 2.1 Cell for Axial and Torsional Stresses on Hollow Cylinders

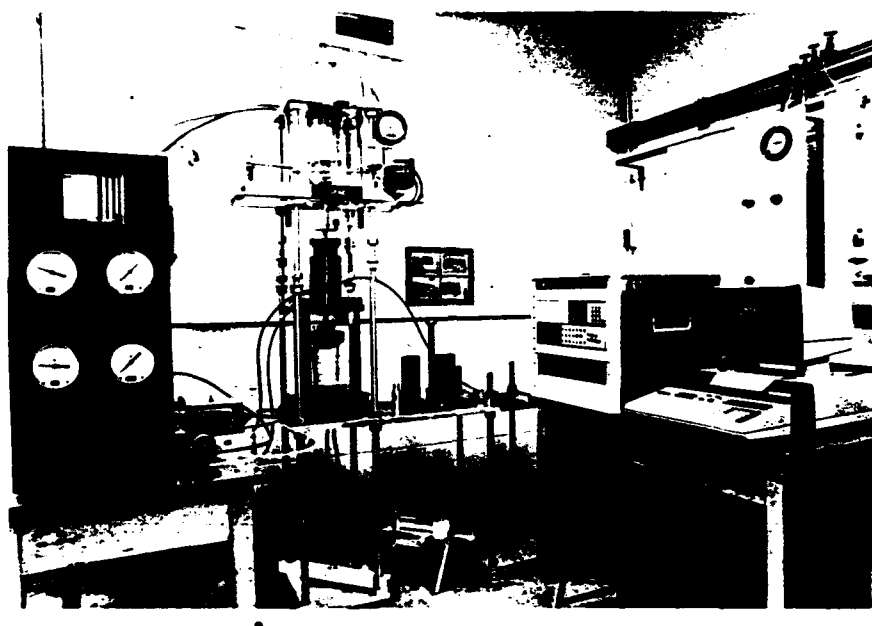


Figure 2.2 Stress Controlled SPAC and Supporting Equipment

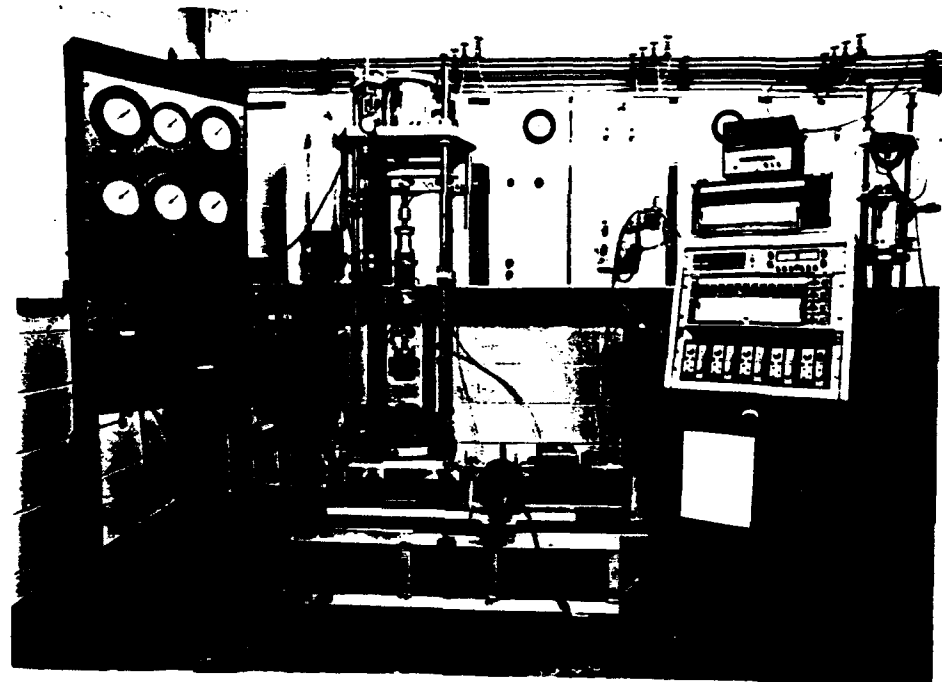


Figure 2.3 Deformation Controlled SPAC and Supporting Equipment

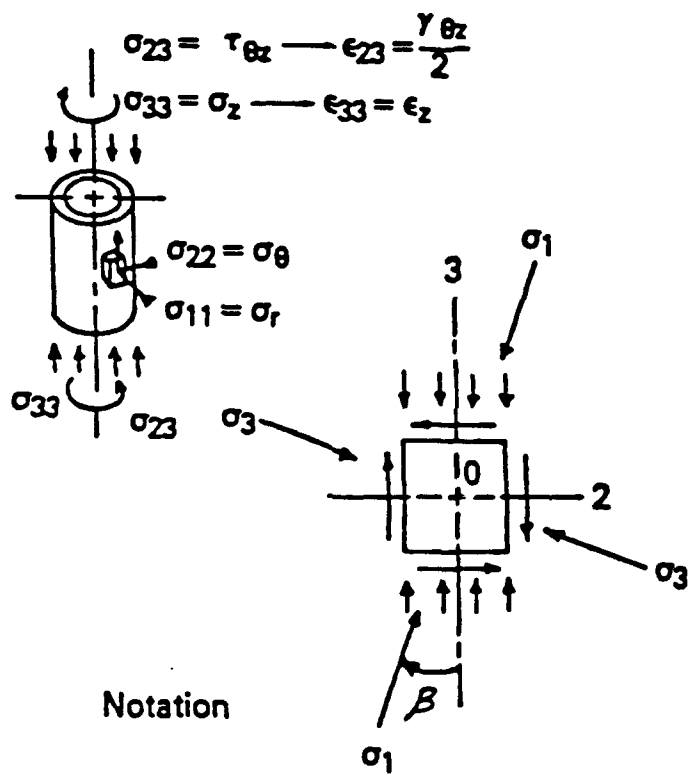


Figure 2.4 Notation

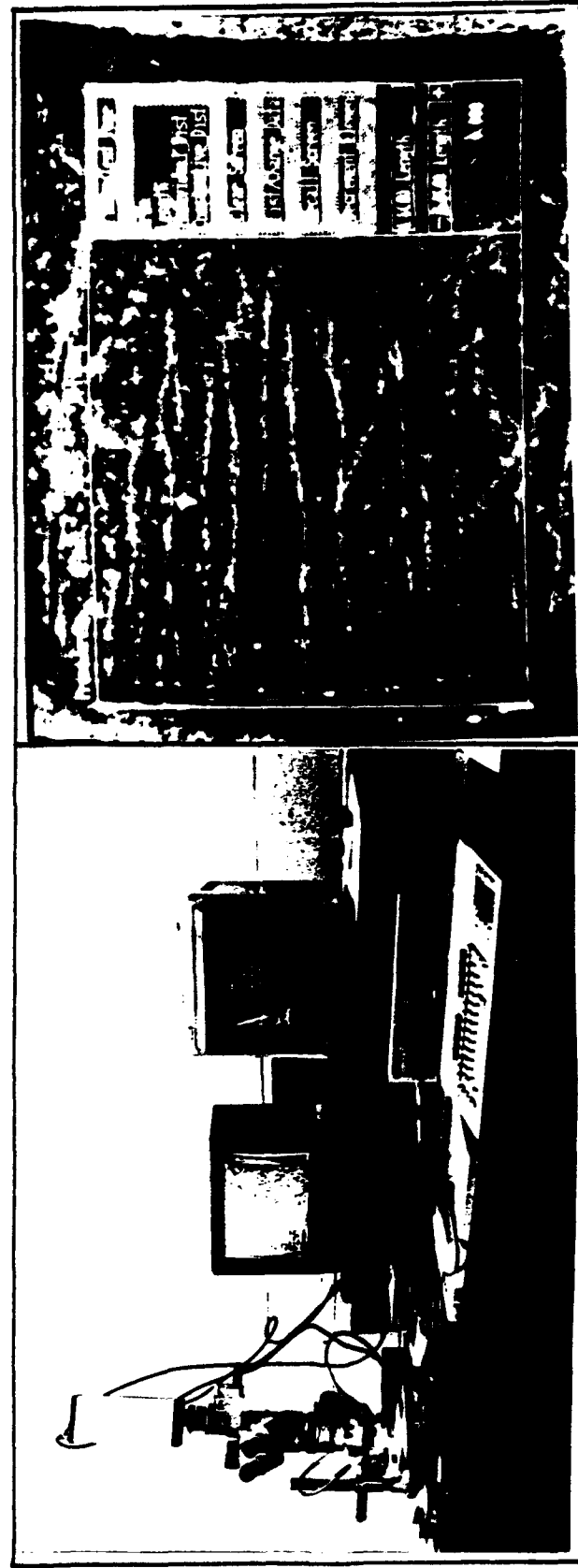


Figure 2.5 Photograph of Image Analysis System

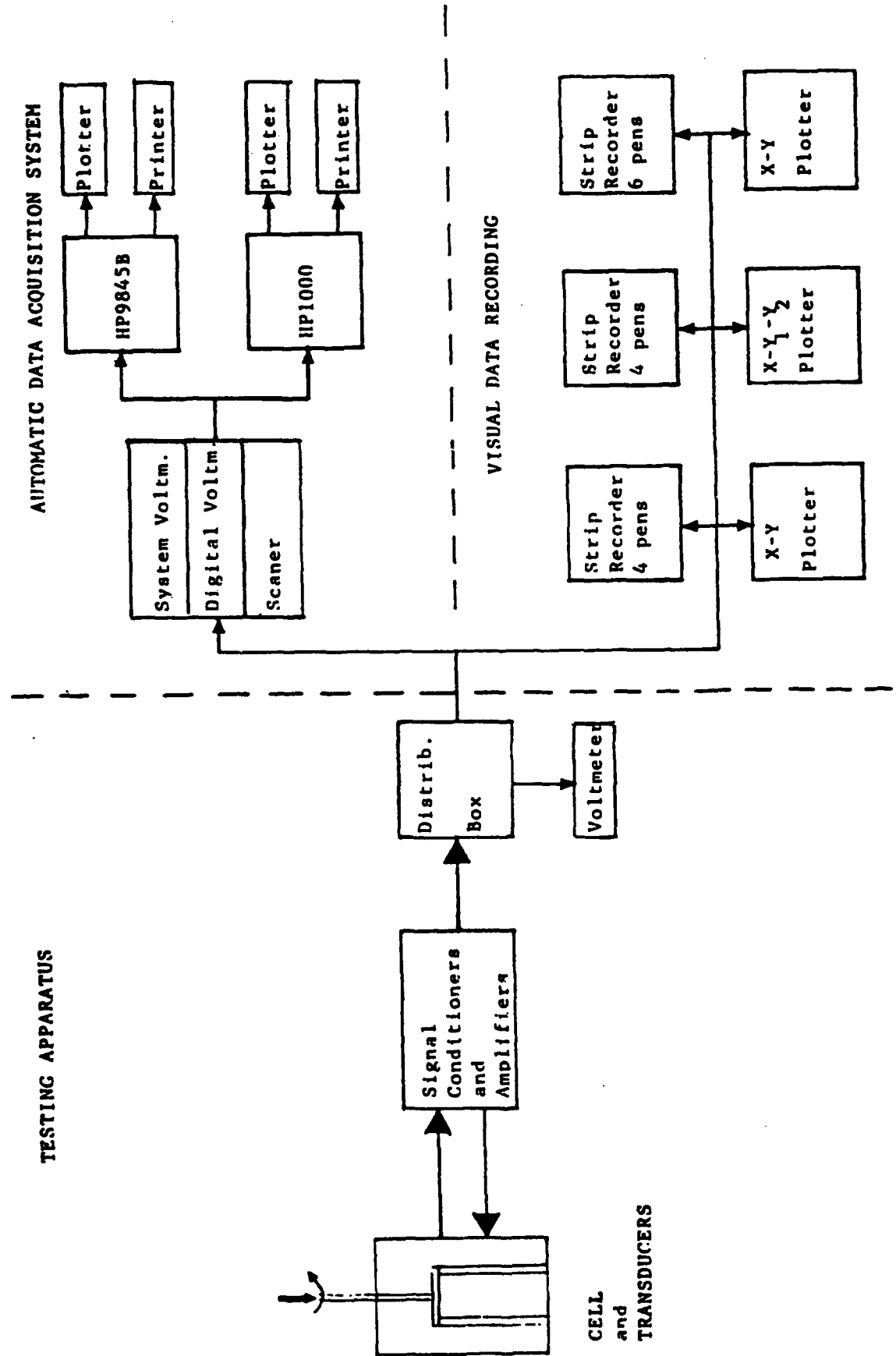


Figure 2.6 Schematic Set-up for Hollow Cylinder System

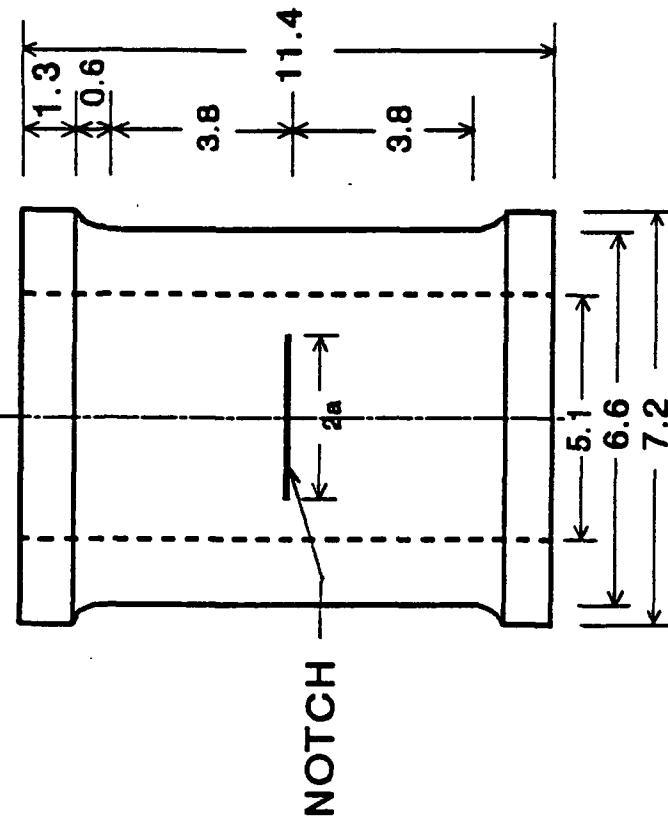
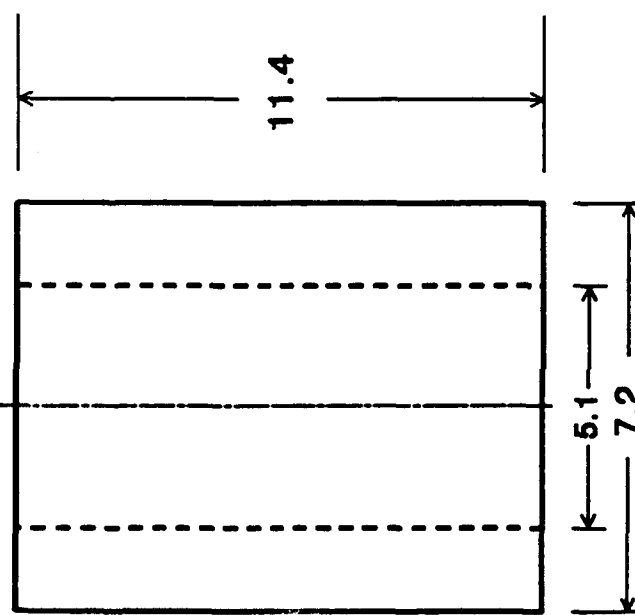
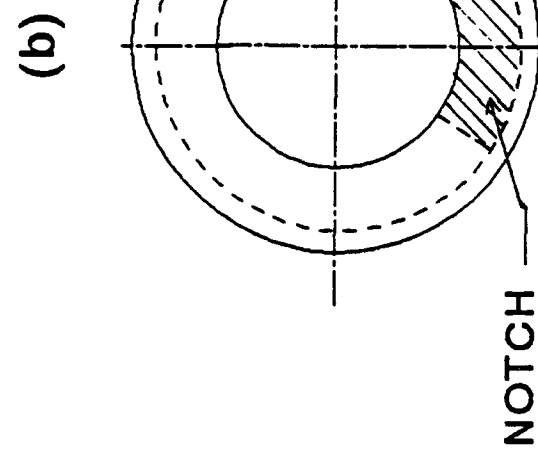
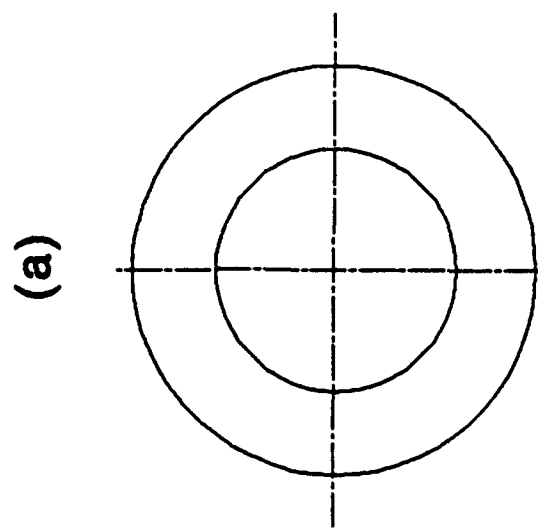


Figure 2.7 Specimen's Geometry

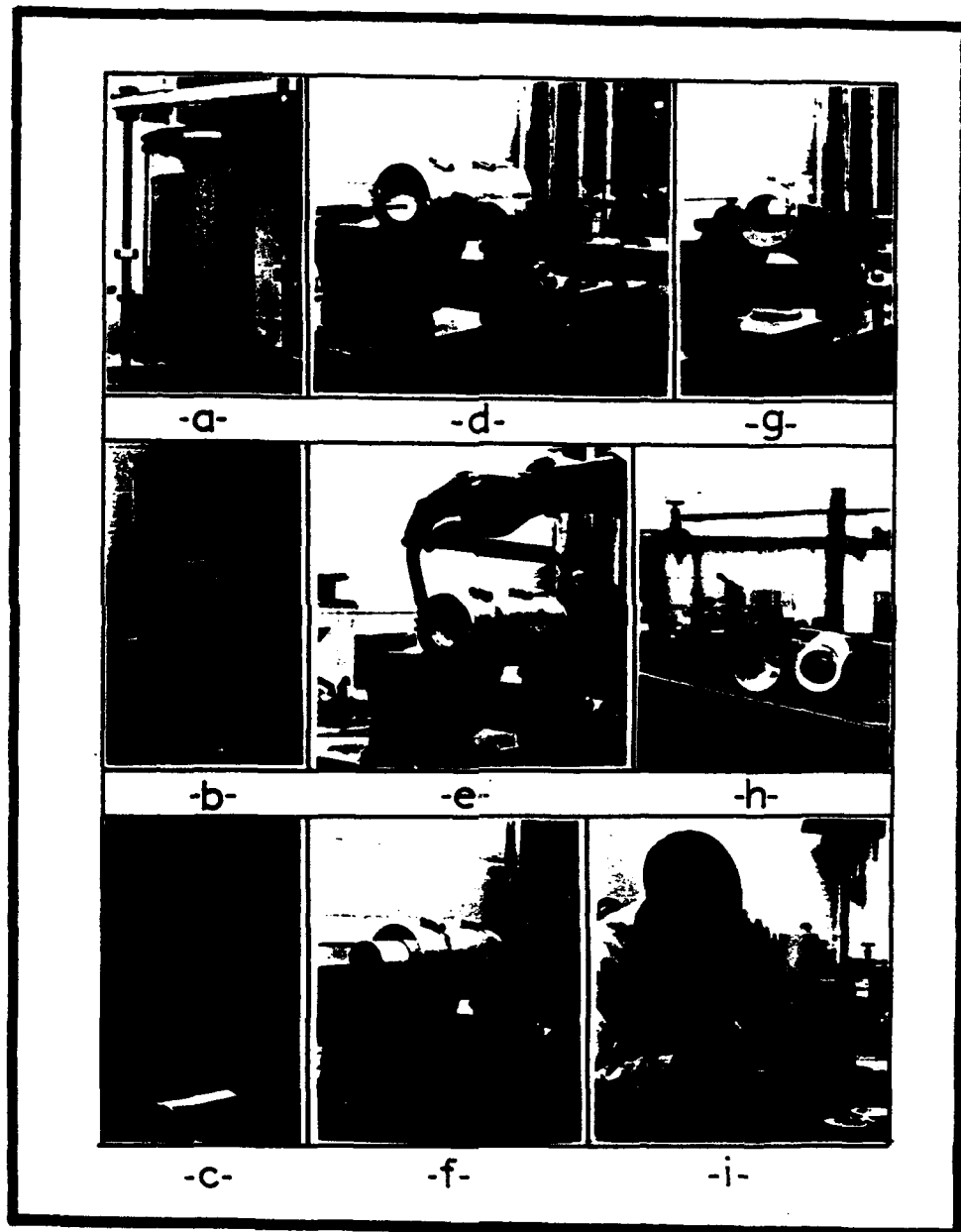


Figure 2.8 Preparation of a Hollow Cylinder of Clay

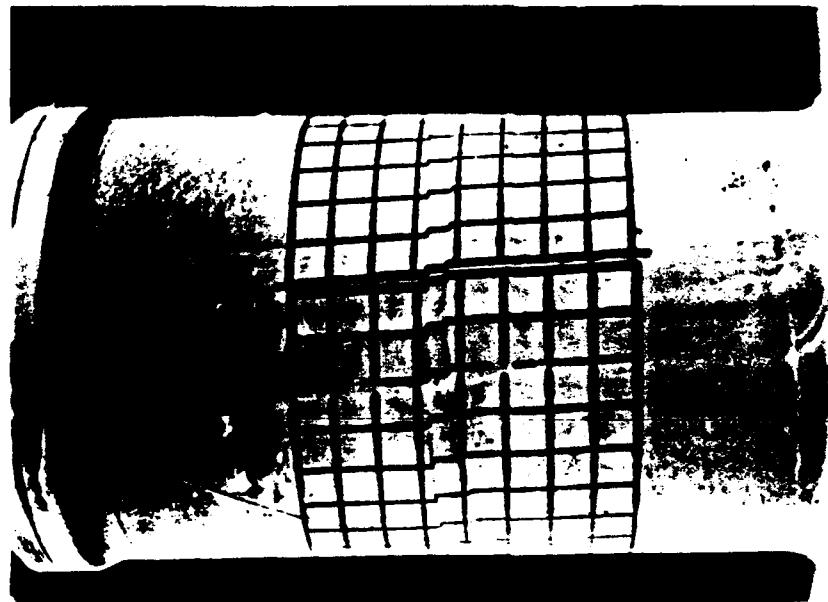
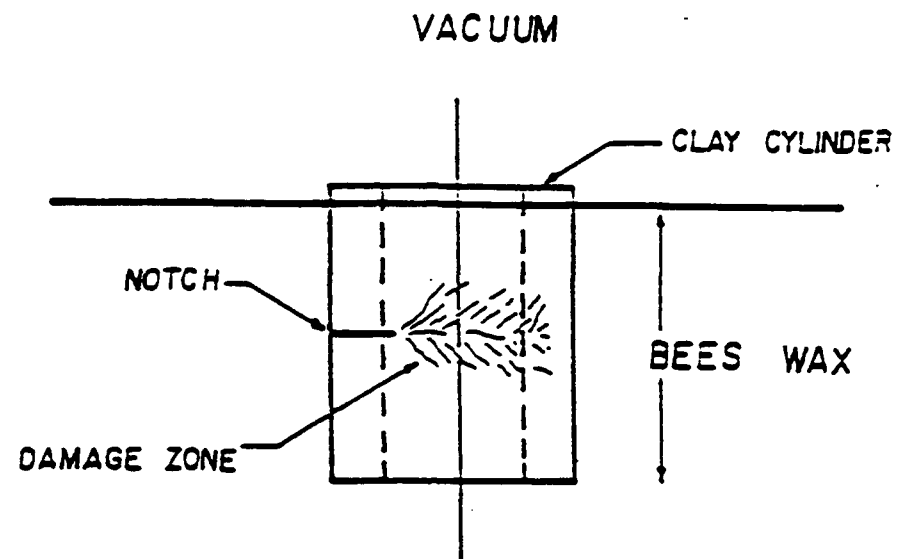


Figure 2.9 Specimens with Square Grid



Schematic for Specimen Impregnation.

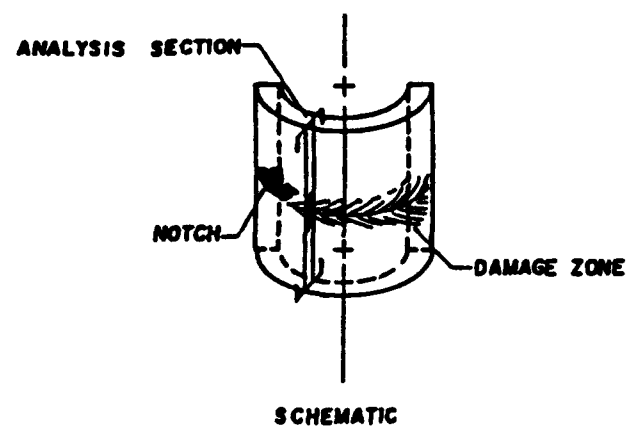


Figure 2.10 Impregnation and Sectioning of Clay Specimens

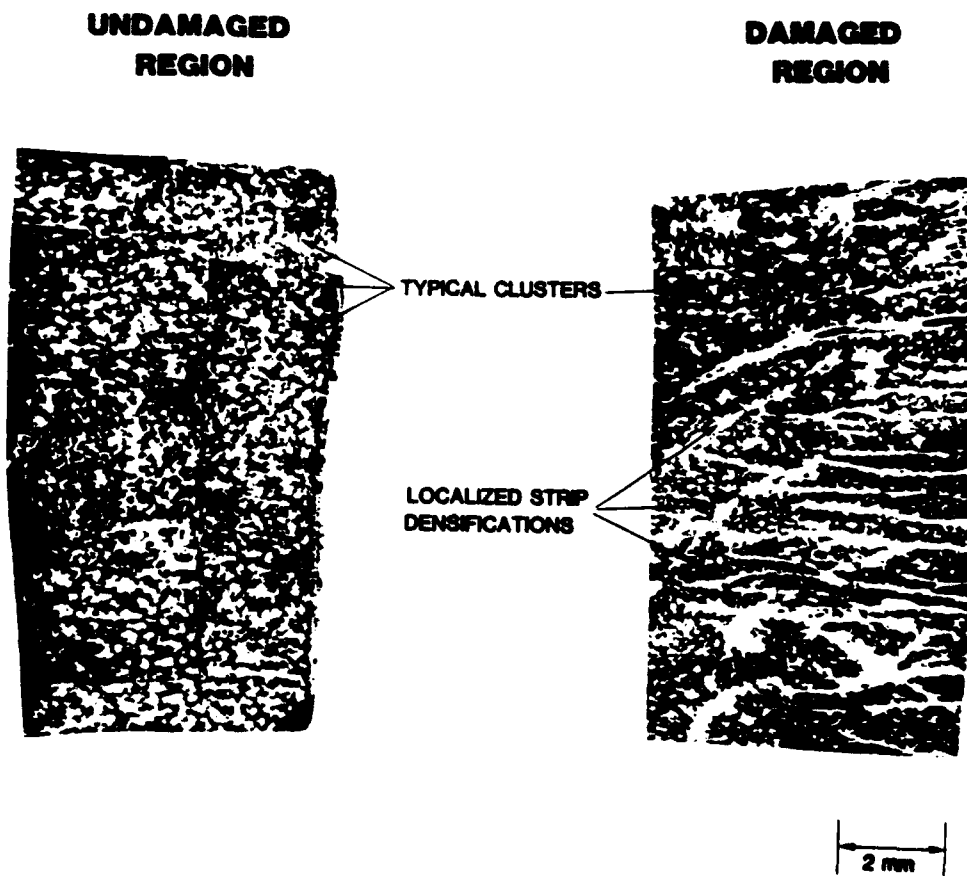


Figure 2.11 Clay Clusters after Impregnation

CHAPTER III

TEST RESULTS AND OBSERVATIONS RELATED TO STRENGTH

3.1 Observations Corresponding to the Tests in Tables 2.1, 2.2 and 2.9.

The test conducted on specimens without cracks serve not only as a reference in the analysis of strength and shear band directions, but also to determine the influence of the cracks on the strength parameters as the system of stresses rotates.

Figs. 3.1a to 3.1e show the normalized octahedral shearing stresses τ_{oct} versus the octahedral shearing strains γ_{oct} for various consolidation pressures and various inclinations β or the principal stresses. Notice that $b = (\sigma_2 - \sigma_3)/(\sigma_1 - \sigma_3) = \sin 2\beta$. The octahedral variables take into account the influence of σ_2 and by comparing the various figures one can see the influence of anisotropy. Regardless of the consolidation pressure the material behaves in a stiffer way when the compressive component of the applied stress is prevalent. This is primarily due to the transverse isotropy resulting from K_o consolidation. As the strain increases the slope of the stress-strain curves decreases far more rapidly when the tensile stresses are the predominant ones. For the same direction of the principal stresses normalization does not lead to a unique curve as can be seen in each of the figures. The situation is made more dramatic when one tries to superimpose all the stress strain curves. Uniqueness is certainly not present. For completeness the pore water pressures are given in Figs. 3.2a to 3.2e. Notice that in those figures the value of the applied mean stress is subtracted from the developed pore pressure and the result normalized with respect to the effective consolidation pressure. Here, too, this normalized pore water pressure due to

shear varies dramatically with the inclination of the principal stresses. The above puts in question the theories based on unique pore water pressure coefficients at failure, be they Skempton's or Henkel's.

Figs. 3.3a and 3.3b gives the results obtained for the H121 clay. Here, again, uniqueness is not obtained.

To assess the validity of various strength theories, it is interesting to study the direction of the shear bands that were observed in the specimens when subjected to various stress paths. There are five different stress paths and, if the Mohr Coulomb theory of failure was perfectly valid, the plane of failure at each point should contain the intermediate principal stress, which, in our case is radial. The tests with paths corresponding to an inclination $\beta = 30, 45$ and 60 degrees show that this is not the case: The surfaces in the three cases are inclined on the radial direction, the most noticeable being the ones corresponding the $\beta = 30^\circ$ tests. In this case, however, the inclination was under ten degrees. Because of symmetry the pure compression and extension tests give the standard conical failure surface. Fig. 3.4 shows the angle of friction ϕ' as defined by $\sin^{-1}(\sigma_1 - \sigma_3)/(\sigma_1 + \sigma_3)$ obtained from the tests conducted on EPK as a function of the inclination β (or b). We see that ϕ' varies drastically with β and loses its meaning as the tensile stresses become predominant. The variations in ϕ' among the various one-dimensional consolidation pressures are primarily due to changes in anisotropy as the K_0 consolidation pressures are increased. Similar results are obtained for H121 illustrating the influence of both b and anisotropy on the friction angle ϕ' . Such observations have

appeared in the literature and commented on by Saada and Bianchini (1975) and Ladd et al. (1977).

It is worthwhile to comment on the tests listed in Table 2.2. These tests were conducted on the same material used in Table 2.1 but with a different geometric configuration and in two cases at a controlled rate of rotation rather than at a controlled rate of stress. Figs. 3.5 shows the superposition of the results on the ones obtained from the tests listed in Table 2.1. The corresponding curves are quite close, the difference being within acceptable experimental error. In addition, it is appropriate to show at this stage the inclination of the shear bands for those three tests. As previously stated, the photographs in Figs. 3.6a and b were made of a succession of single shots taken while rotating the specimen around its axis of symmetry prior to placing it in the oven for moisture content determination. Many photographs were also taken during the test to observe the development of the shear bands. One notices on those photographs that the inclination of the shear bands varies as one moves from compression to extension. Shown on the digitized plots 3.6az and 3.6bz is the direction of shear bands predicted by the Mohr-Coulomb theory. The angle $(45 + \phi')/2$ giving the inclination of the Coulomb slip planes was computed with an average angle of friction of 33 degrees obtained from direct triaxial compression tests (Fig. 3.4). One can see that for the two tests at hand the agreement is remarkable. The grid stamped on the specimens allows us to measure angles with quite a reasonable accuracy. It also visually enhances the shear bands and their directions.

While the observations above are important and are the first of their kind to be obtained under combined stresses, the fact, remains that the reference ϕ' was obtained

from direct compression and Fig. 3.4 is enough of a reminder that the traditionally defined ϕ' is certainly not unique.

3.2 Observations Corresponding to the Tests in Table 2.3.

Seven out of the ten tests listed in Table 2.3 were conducted on specimens with horizontal cracks and a ratio $a/l = 0.18$. The three last tests had inclined cracks 2.5 cm in length. Figs. 3.7a and b show the stress-strain curves for various inclinations of the principal stresses on the axis of symmetry and the pore water pressures respectively. In Figs. 3.7 we have superimposed the curves from Fig. 3.5 to study the influence of the crack. Such influence is seen to be minimal for the size of the crack studied. It will be seen in the chapter reserved to the kinematics of deformation that once the shear band starts in the vicinity of a crack the deformation is completely controlled by the plastic behavior of the material.

In Figs. 3.8a and b the results of three torsion tests on specimens with horizontal cracks are superimposed; two conducted under fixed length conditions and one free to deform axially. In the fixed length cases the principal stresses rotate a little depending on the axial stress that is developed during torsion. The presence of the axial stress necessary to prevent elongation results in higher stresses for the same strain and in differences in the measured pore water pressures.

The influence of the inclination of the crack on the shear strength behavior and the pore water pressure is shown in Figs. 3.9a and b. There, all the specimens are under a state of pure torsion and free to deform axially. Whether the inclination is 45, 22.5 or 0 degrees

the undrained strength is the same; except at very large strains. The pore water pressures are close to each others. Here again, it appears that once the shear bands develop the behavior is plastic and the influence of the crack nearly vanishes. This will be further discussed in the next chapter.

3.3 Observations Corresponding to the Tests in Table 2.4.

This set of tests was conducted on overconsolidated specimens of EPK clay without cracks and a mean overconsolidation ratio of 4. Like their counterparts in Table 2.1, they serve as a reference; this time for the study of strength, crack and damage propagation in a brittle material. Figs 3.10a and b show the strength and pore water pressure relations. Fig. 3.11 a, b and c shows the pattern of slip lines that developed for an angle $\beta = 30^\circ$, $\beta = 45^\circ$ and $\beta = 60^\circ$. In all cases the prediction of the inclinations of the slip lines by Coulomb's Theory (with ϕ' equal to 33 degrees) fits extremely well the measured ones; as shown on the digitized plots 3.11az, 3.11 bz and 3.11cz. The photographs in those figures will be used for comparison purposes when examining the shear bands that develop in the presence of a crack.

3.4 Observations Corresponding to the Tests in Table 2.5.

There are two sets of tests in this table: One set in which the specimens with an $a/l = 0.18$ were subjected to the same radial stress paths listed in Table 2.4, and a second set in which the specimens, with various sizes of cracks, were subjected to torsion under fixed length condition. Figs. 3.12a and b show the shear strength and the pore water pressure as

a function of the strains. In these figures we have superimposed the results shown in Figs. 3.10 to study the influence of the crack. As in the case of Figs. 3.7 such an influence is seen to be minimal in spite of the length of the crack being about twenty percent of the perimeter.

The results above led to a study of the influence of the length of the crack on the strength. Six specimens with various values of a/l were subjected to torsion under fixed length conditions. The relations stress versus strain and pore water pressure versus strain are shown in Figs. 3.13a and b. The ultimate strength drops as the size of the crack increases. This is expected. However the fact that the length remains constant results in higher values of the stresses when comparisons are made with tests in which the specimens are free to elongate.

The photographs taken during the formation of the shear bands in the vicinity of the tip of the crack will be examined in Chapter IV in a comparative study of the kinematics of specimens with and without cracks.

3.5 Observations Corresponding to the Dynamic Tests in Tables 2.6 and 2.7.

The tests in those tables were conducted primarily to examine the pattern of damage propagation when a specimen with a crack is subjected to cyclic and impulse loadings. Photographs were taken as torques of fixed amplitude were cyclically applied to the specimen, and as a step loading was induced. The third test in Table 2.6 was conducted on a specimen with an inclined crack. Table 2.7 lists the dynamic tests conducted on overconsolidated material.

Fig. 3.14 shows the decay of the shear modulus and increase in damping for the first specimen listed Table 2.6. The hysteresis loops increase in size as their inclination on the horizontal axis decreases with the number of cycles. Note the lack of symmetry in Fig. 3.14. On the other hand Fig. 3.15 which corresponds to the isotropically overconsolidated specimen shows a more symmetric pattern. Such hysteresis loops had been noticed and commented on by Macky and Saada (1984) and Saada and Macky (1985) for both laboratory prepared specimens and undisturbed specimens.

Fig. 3.16 indicates that the hysteresis loops for an inclined crack in a K_0 consolidated material are not different from the ones obtained with a horizontal one for an isotropic clay. This shows that the fabric, the inclination of the crack and the direction of the stress, all affect the response.

The two tests in Table 2.7 yield results similar to the ones above. The development of shear bands in all the tests listed in Tables 2.6 and 2.7 was carefully observed and photographed. Crack and damage propagations were not expected in the K_0 normally consolidated specimens; but they did take place, just as they did with overconsolidated specimens. Comparisons will be made in Chapter IV.

3.6 Observations Corresponding to the Tests with Two Cracks in Table 2.8.

Those tests were conducted to answer questions about coalescence of cracks and their damage zone during the shearing process. In the five tests listed in Table 2.8 the two cracks were separated horizontally and vertically as shown. While d was kept constant at 0.6 cm (0.25 in), e varied between 0 and 2.54 cm (1.0 in.). The direction of the torque was

the same for all tests and the specimens free to deform axially leading to the same value of $\beta = 45^\circ$. Notice that the two first tests are identical except that the first has its cracks in the downstep position while the second has them in the upstep position.

Figs. 3.17a and b shows the strength and pore pressure curves for all five tests in Table 2.8. Also, drawn on this figure for comparison purposes is the curves for a specimen with one crack from Fig. 3.12, and the curve for a specimen with no cracks from Fig. 3.10. As expected the strength curves for two cracks fall below the ones with one or no crack. Also, the position of the cracks relative to the direction of the shearing stresses is very important. For the same direction of shear stress the two notches in the upstep position give a result close to the one obtained with one notch; indicating very little coalescence of the damage zones of the two notches. On the other hand such damage zones interfere and coalesce when the cracks are in the downstep position, leading to a weakening of the specimen. In such a case, for a given distance d , e plays an important role in the weakening process. It is obvious that, as d increases, the behavior tends towards that of the single crack specimen. For all specimens however, it seems that the cracks and their position do not affect the behavior until fifty percent of the stresses have been applied. Shear bands become visible to the naked eye shortly after. The corresponding strain is about 0.5 percent. Photograph taken during the tests and showing the shear bands will be discussed in Chapter IV.

3.7 Resonant Column Tests.

A number of resonant column tests of the fixed-free type were conducted on EPK clay specimens with and without notches. Some were conducted on specimens with two

notches. Complete description and results of those tests can be found in the appendix. Young's modulii, shear modulii and damping ratio are listed for each test. They indicate that for the levels of strain involved ($< 10^{-3}$) the cracks have no effect on the response.

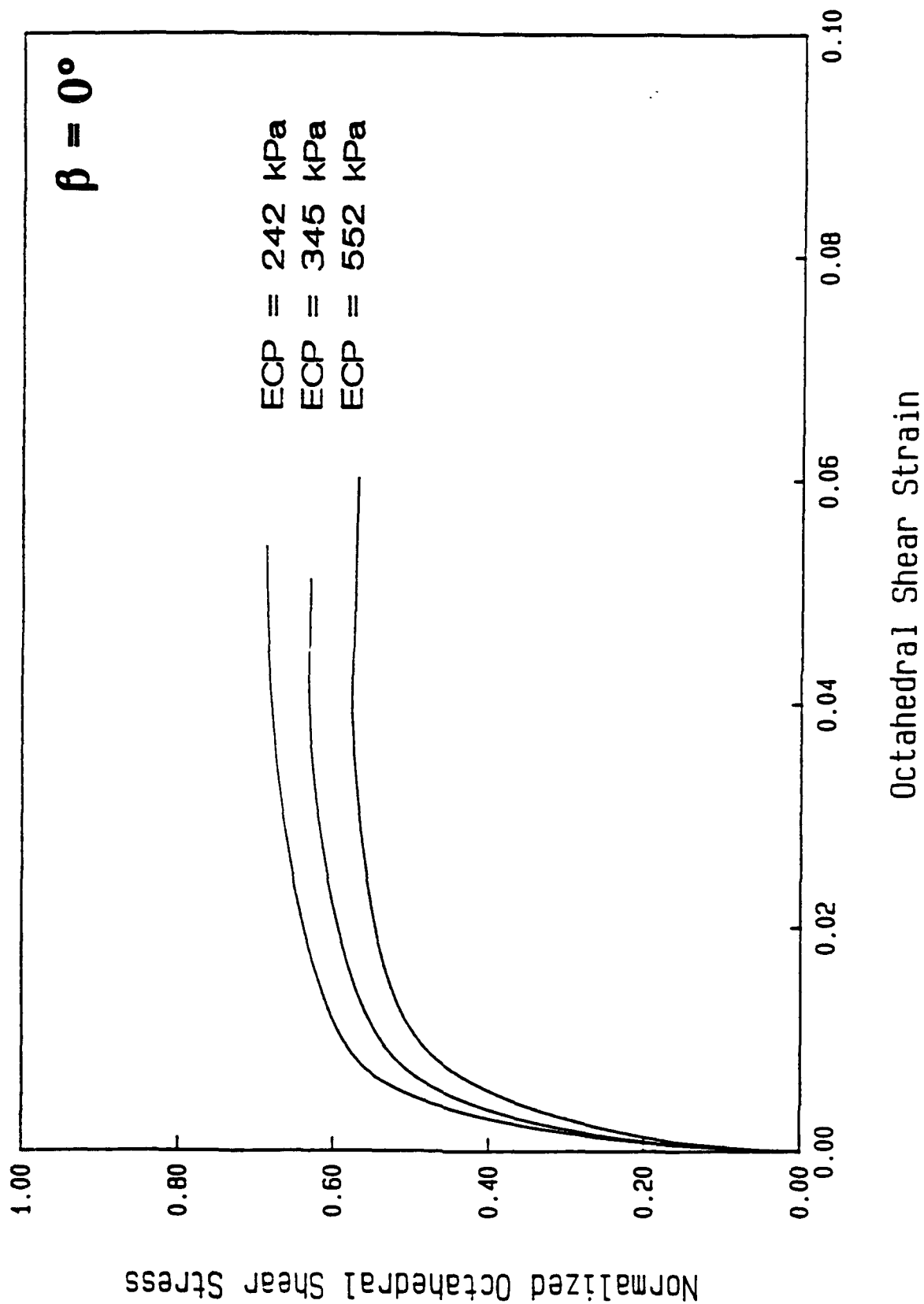


Figure 3.1a Normalized Octahedral Shear Stress vs. Octahedral Shear Strain; EPK; $\beta = 0$

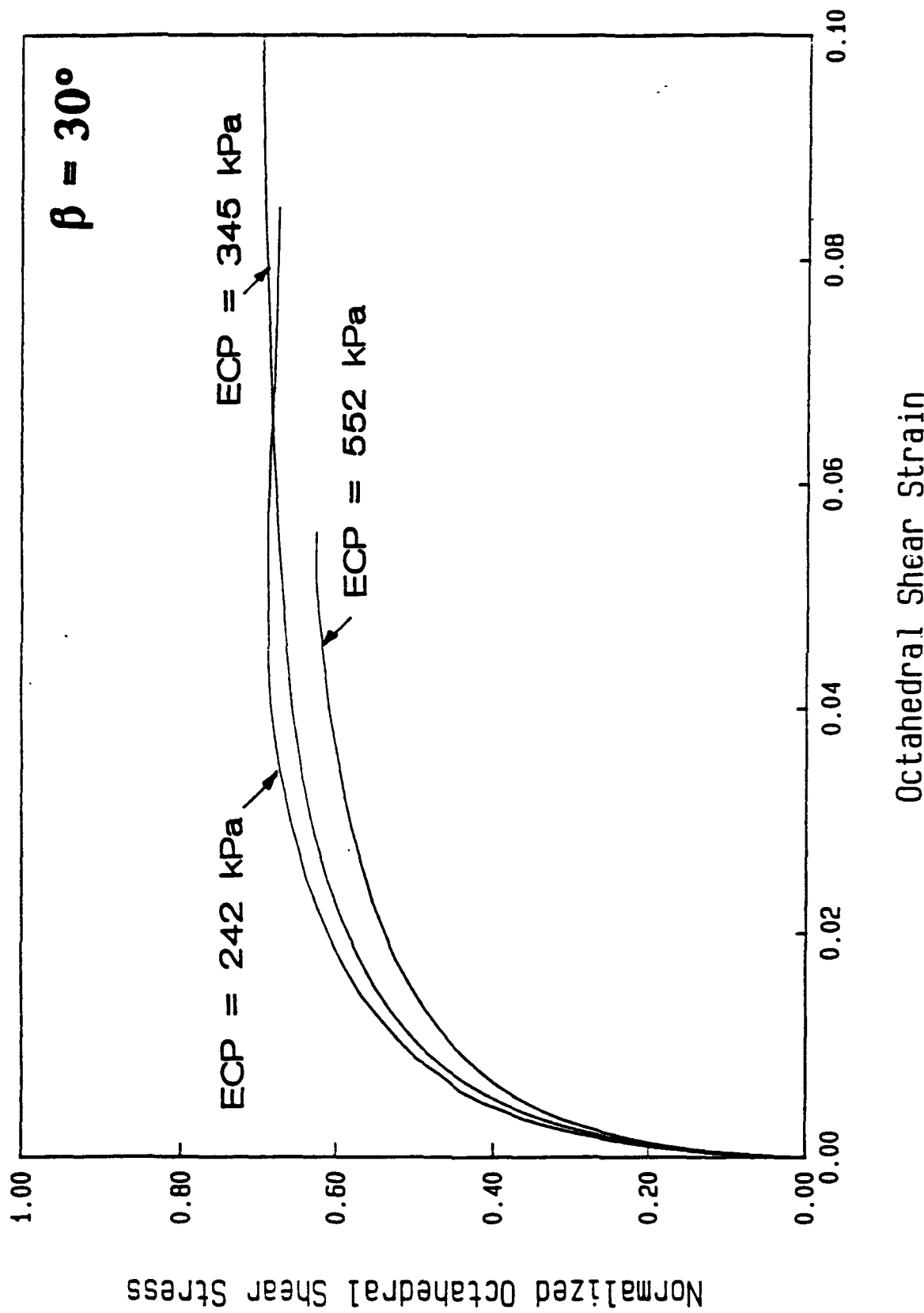


Figure 3.1b Normalized Octahedral Shear Stress vs. Octahedral Shear Strain
EPK; $\beta = 30^\circ$

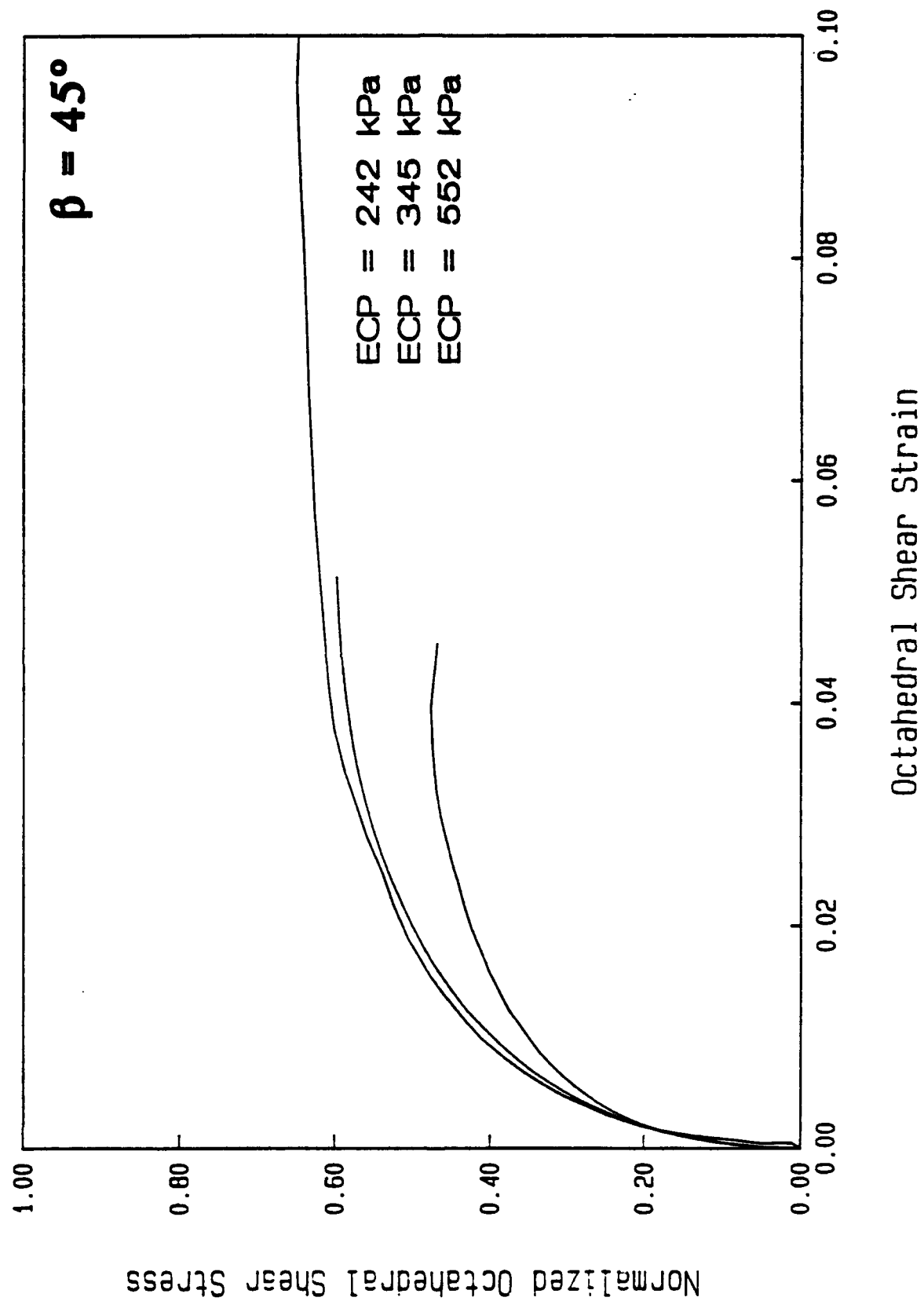


Figure 3.1c Normalized Octahedral Shear Stress vs. Octahedral Shear Strain; EPK; $\beta = 45^\circ$

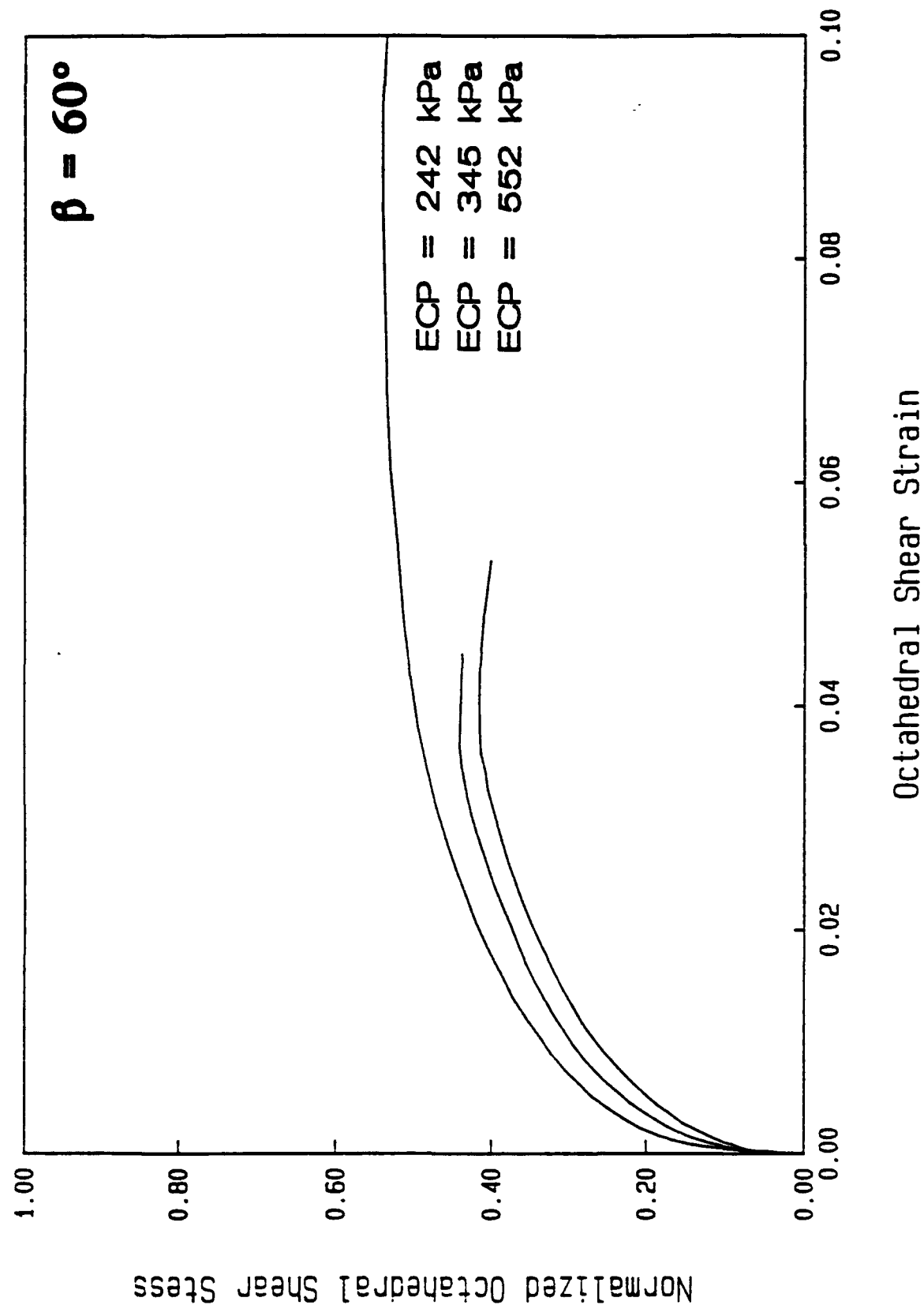


Figure 3.1d Normalized Octahedral Shear Stress vs. Octahedral Shear Strain; EPK; $\beta = 60^\circ$

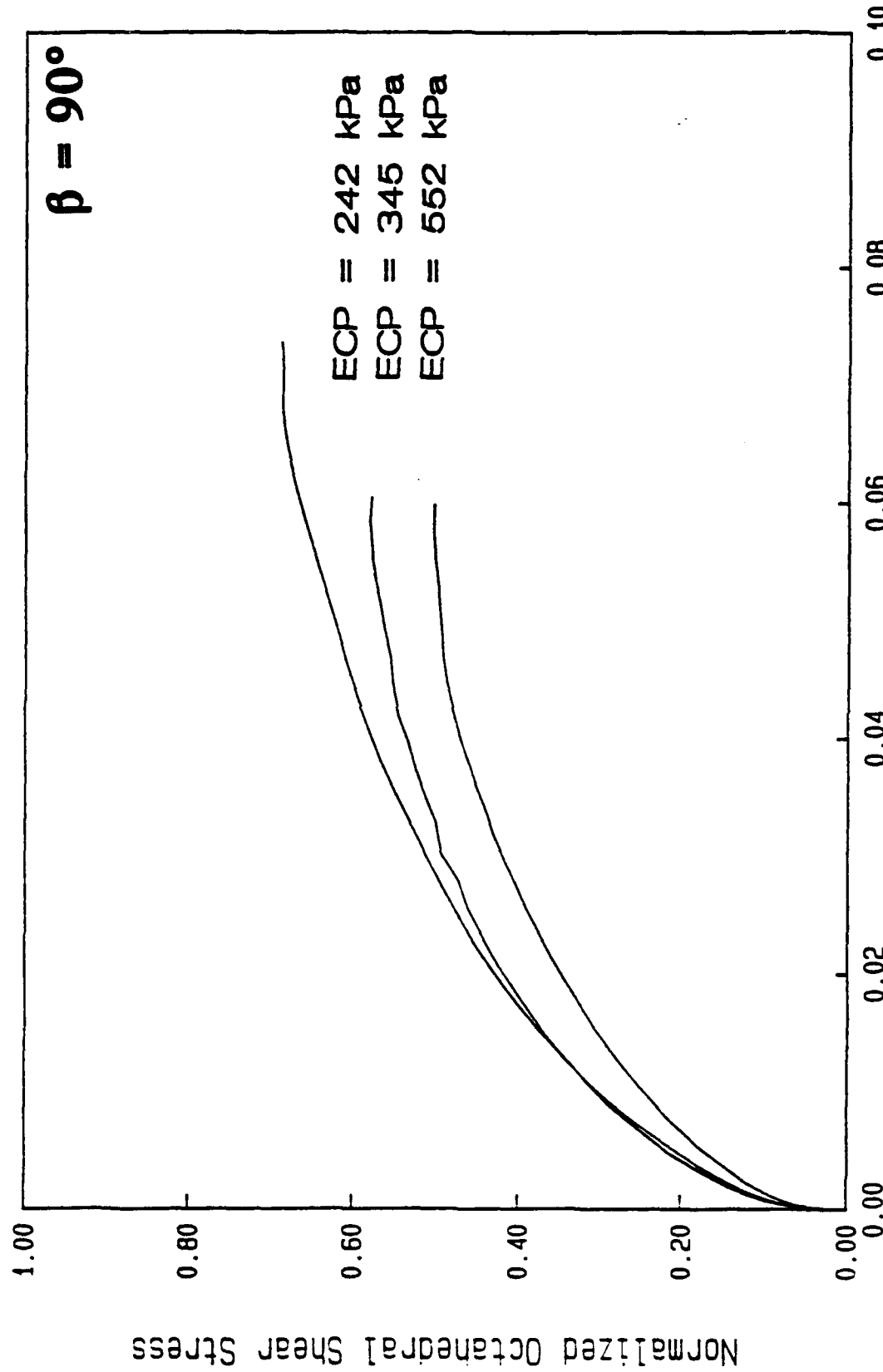


Figure 3.1e Normalized Octahedral Shear Stress vs. Octahedral Shear Strain; EPK; $\beta = 90^\circ$

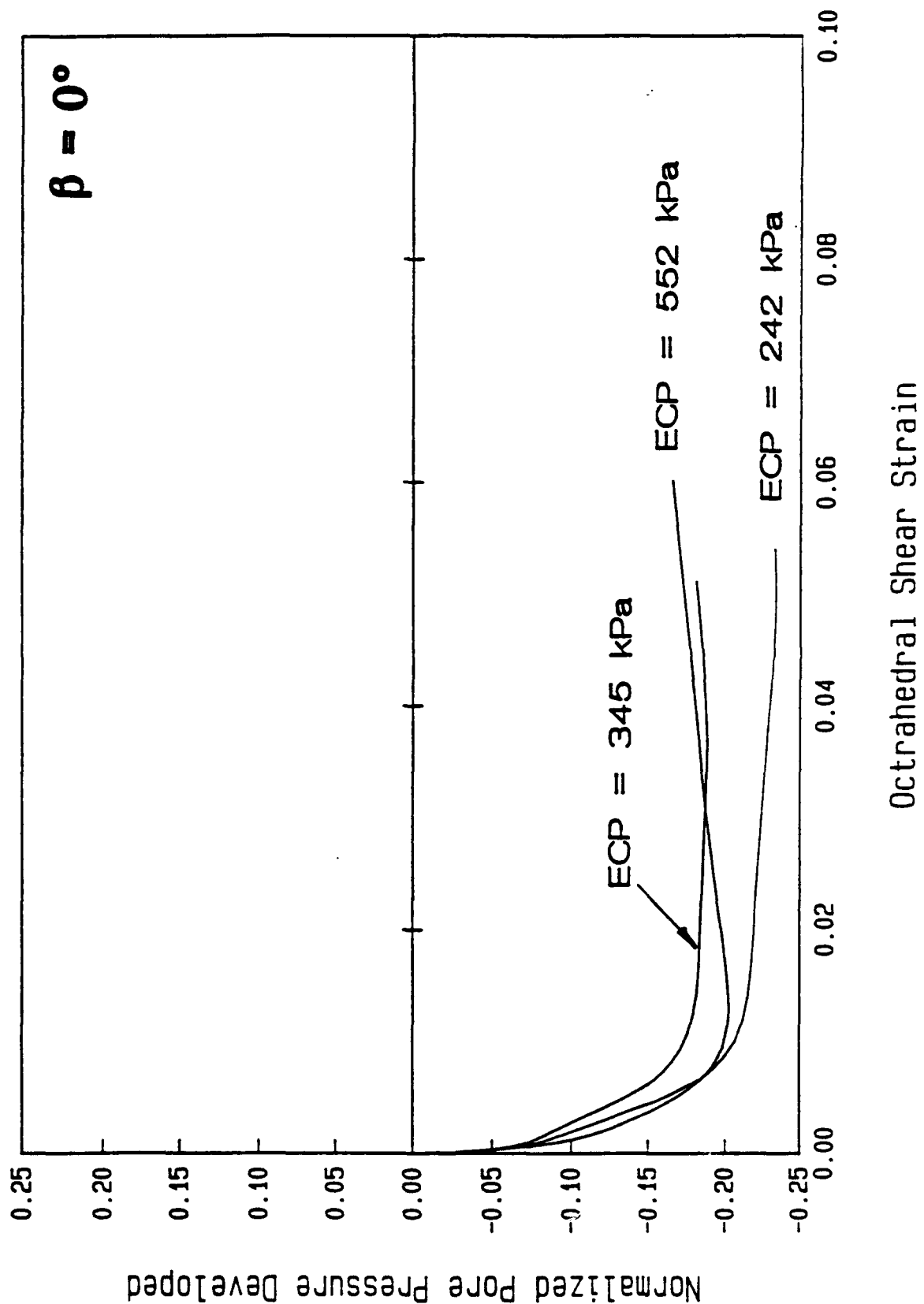


Figure 3.2a Normalized Pore Pressure Developed vs. Octahedral Shear Strain; EPK; $\beta = 0$

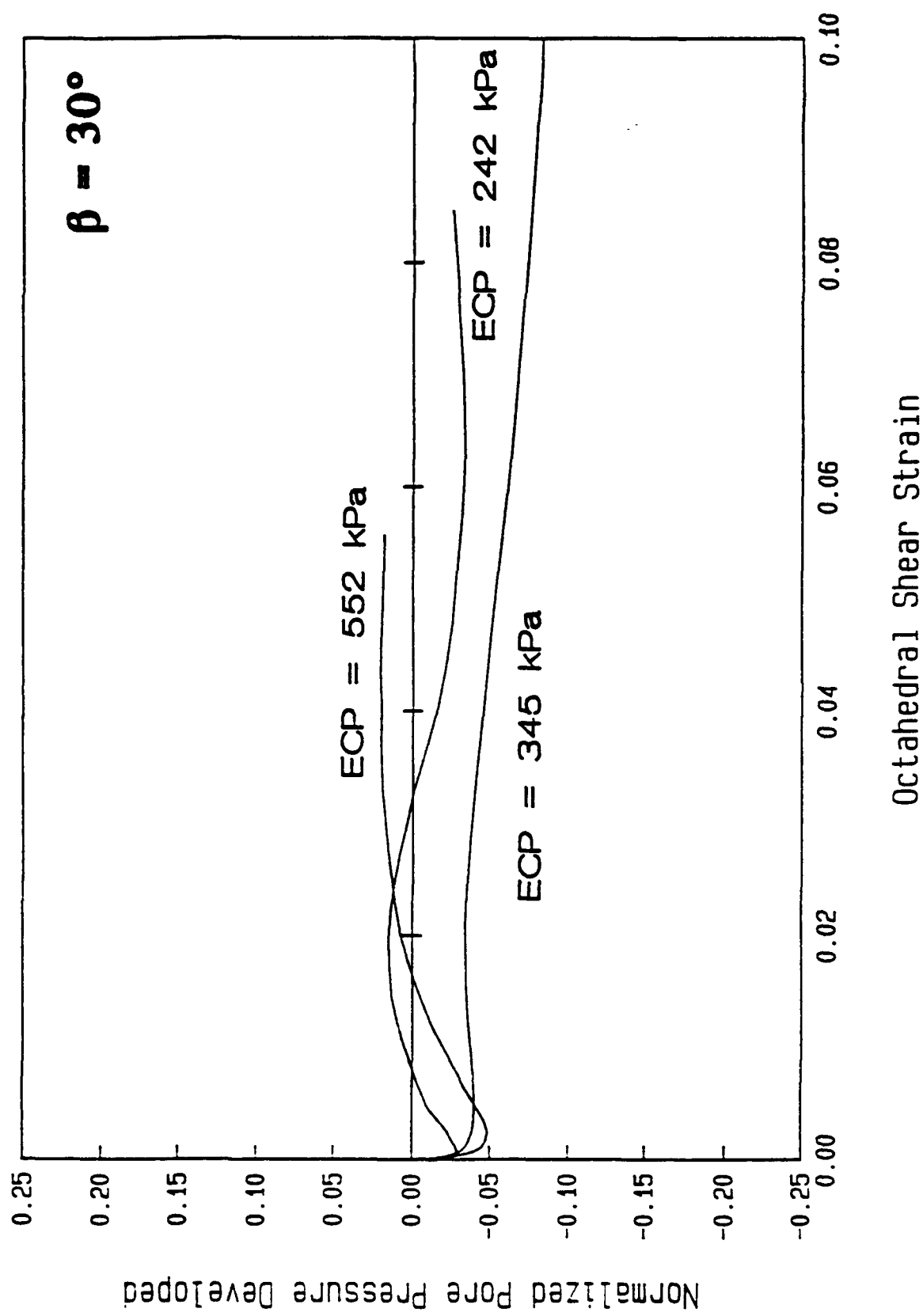


Figure 3.2b Normalized Pore Pressure Developed vs. Octahedral Shear Strain; EPK; $\beta = 30^\circ$

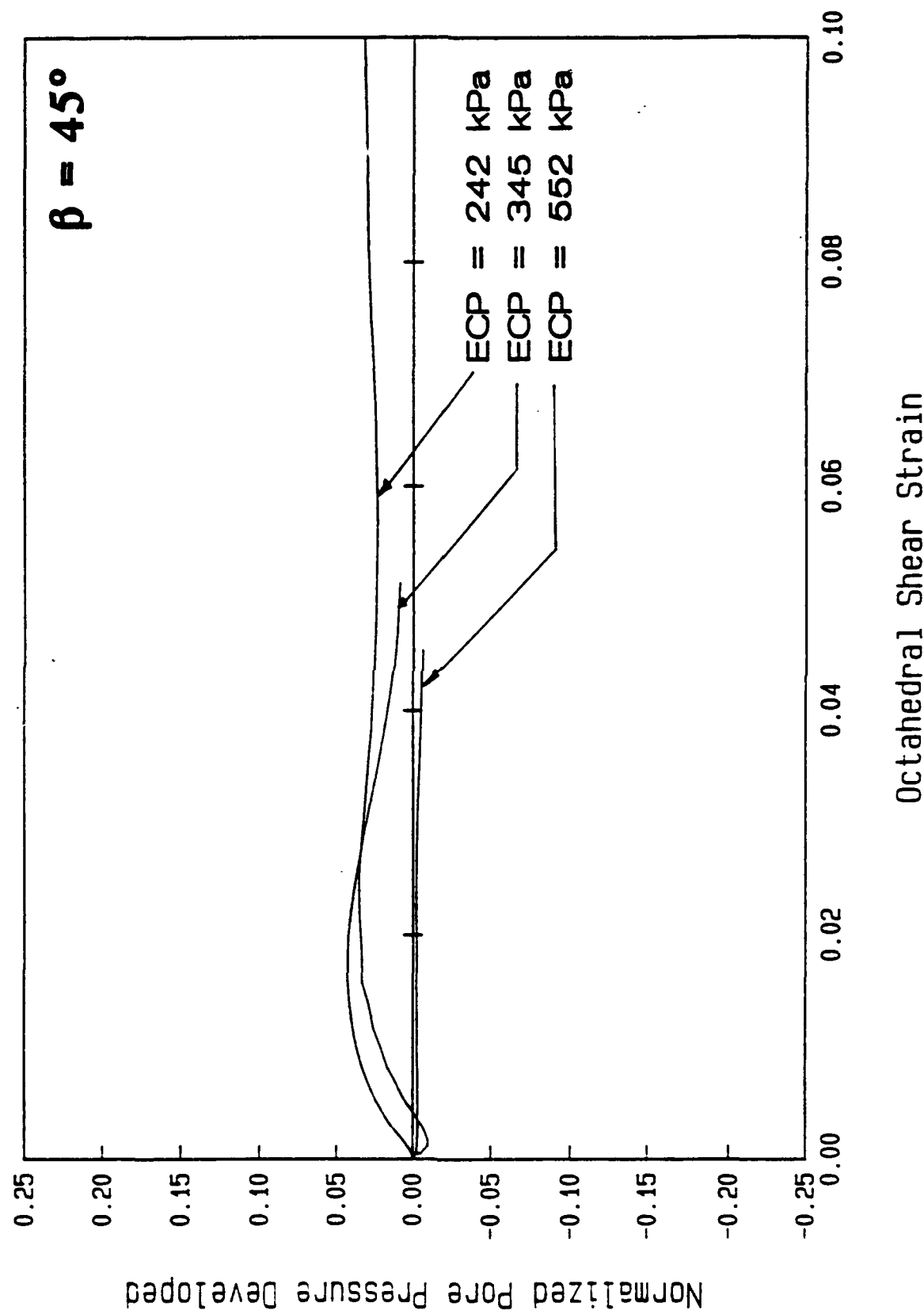


Figure 3.2c Normalized Pore Pressure Developed vs. Octahedral Shear Strain; EPK; $\beta = 45^\circ$

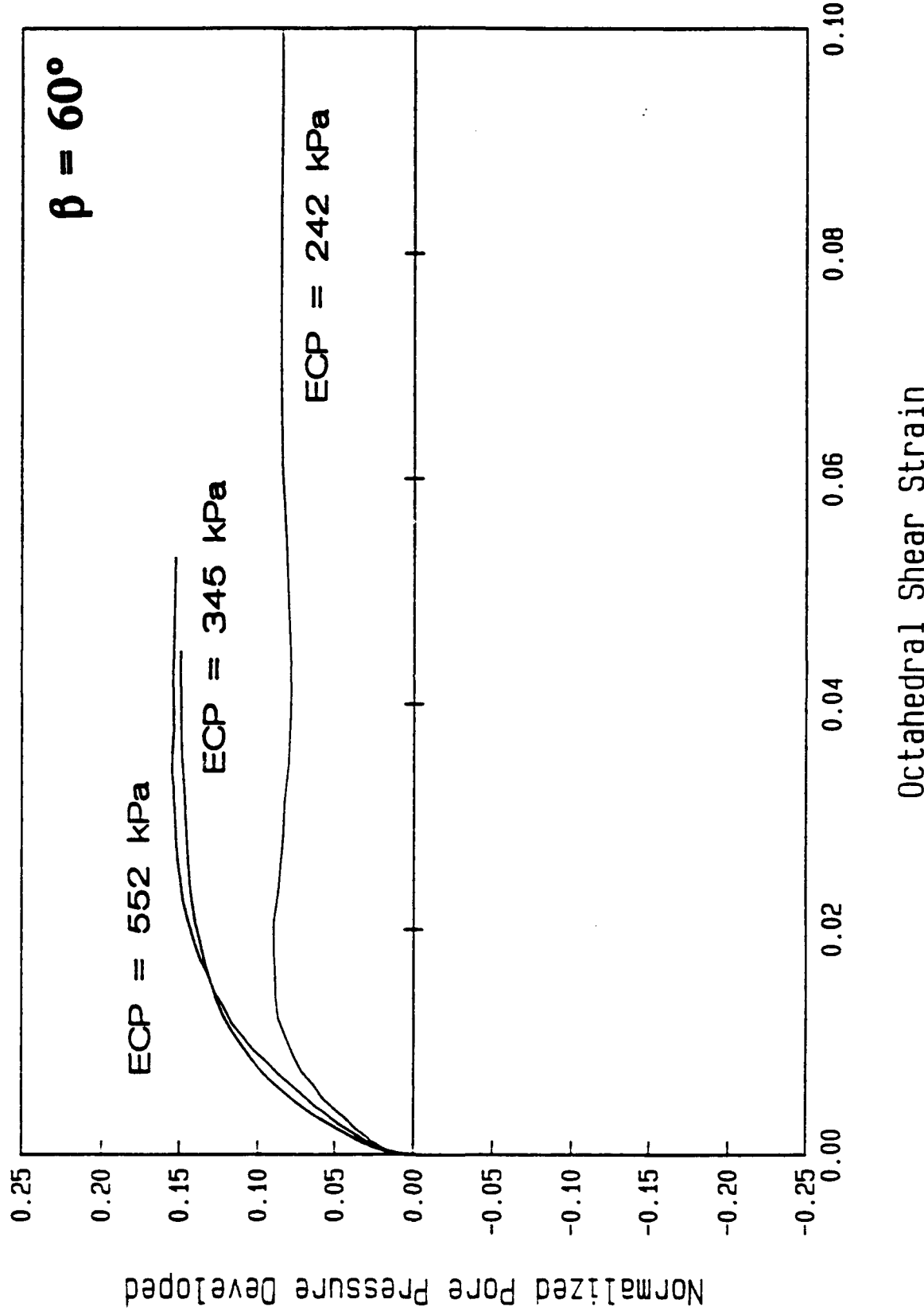


Figure 3.2d Normalized Pore Pressure Developed vs. Octahedral Shear Strain; EPK; $\beta = 60^\circ$

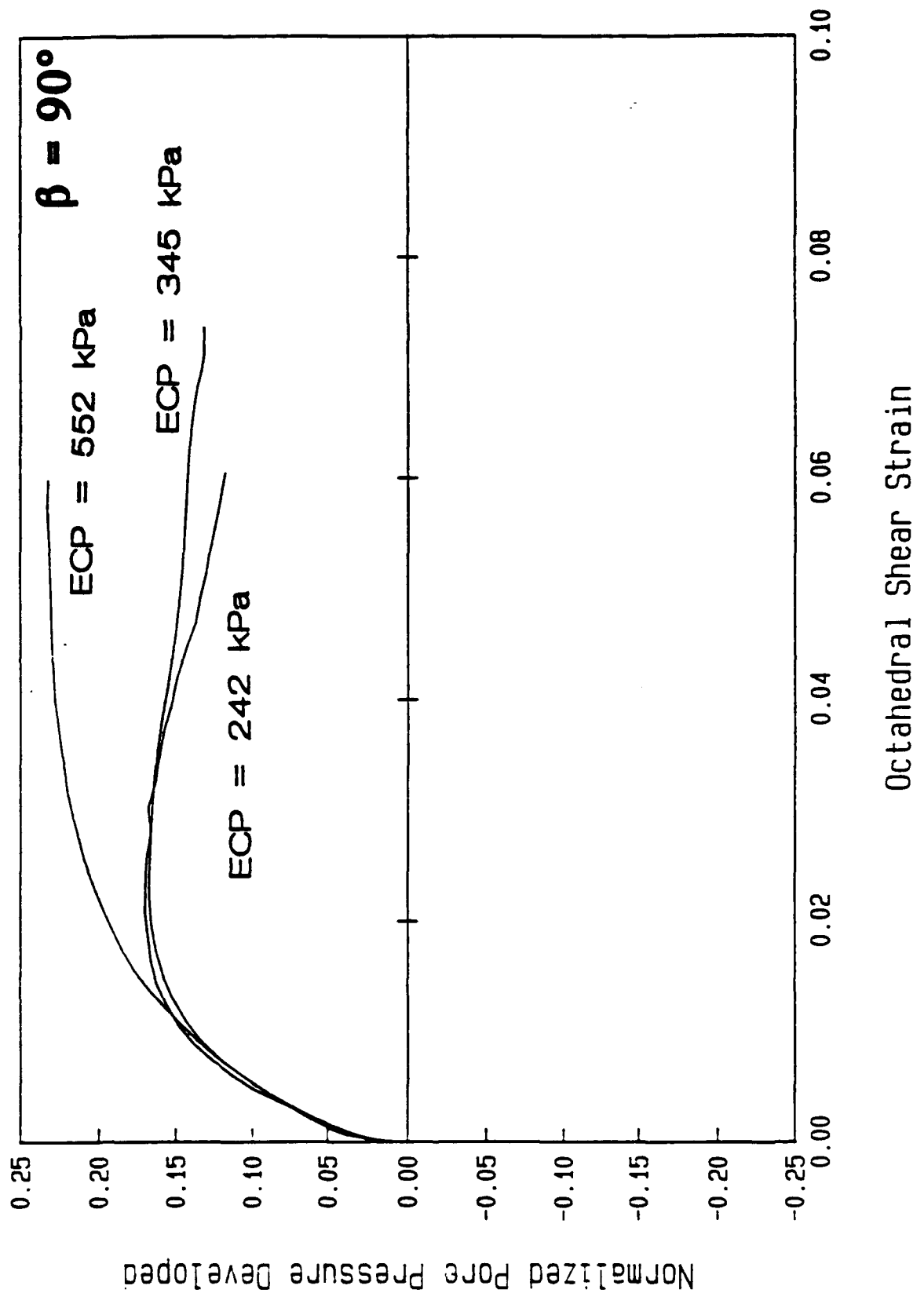


Figure 3.2e Normalized Pore Pressure Developed vs. Octahedral Shear Strain; EPK; $\beta = 90^\circ$

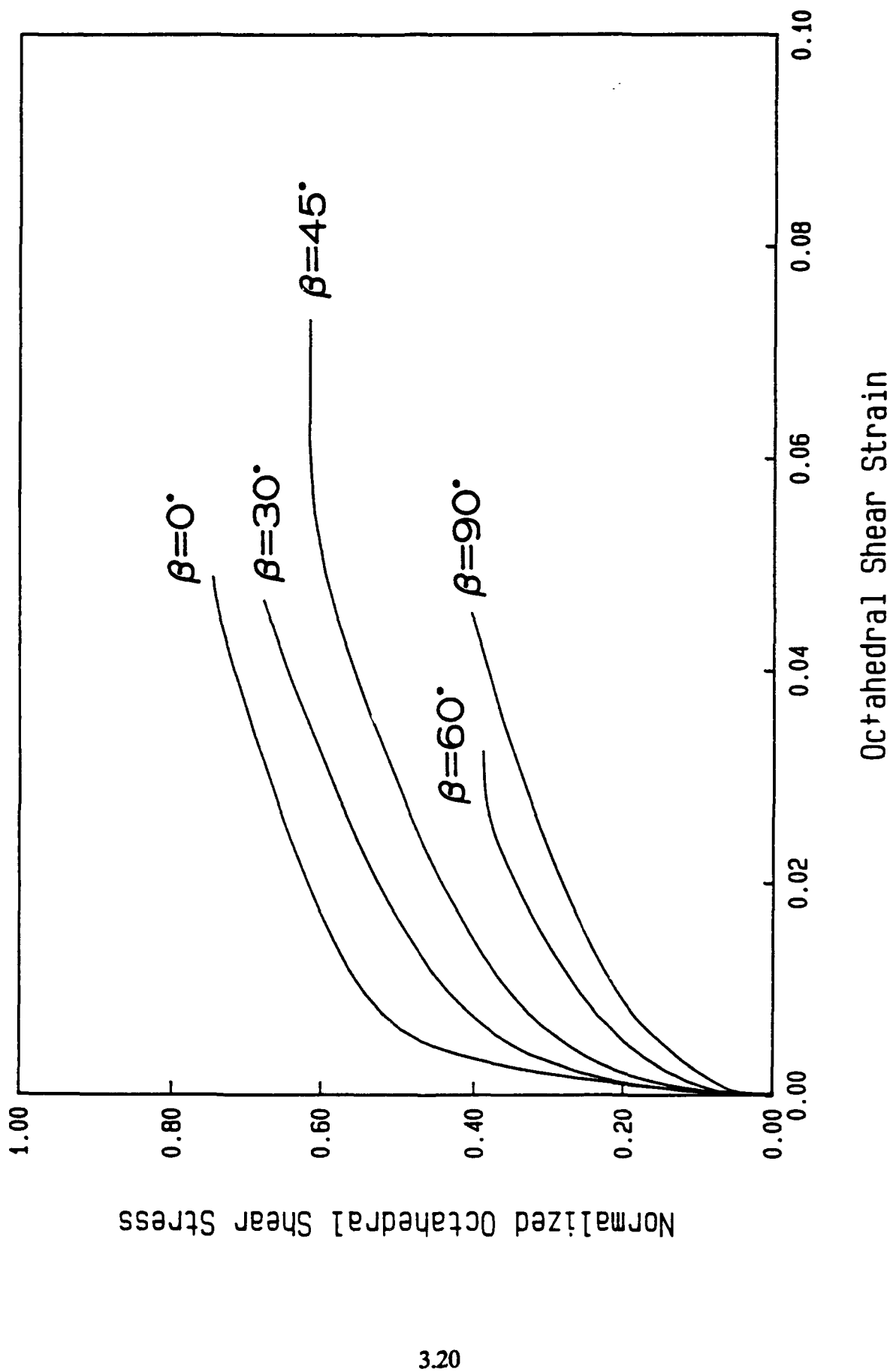


Figure 3.3a Normalized Octahedral Shear Stress vs. Octahedral Shear Strain; H121

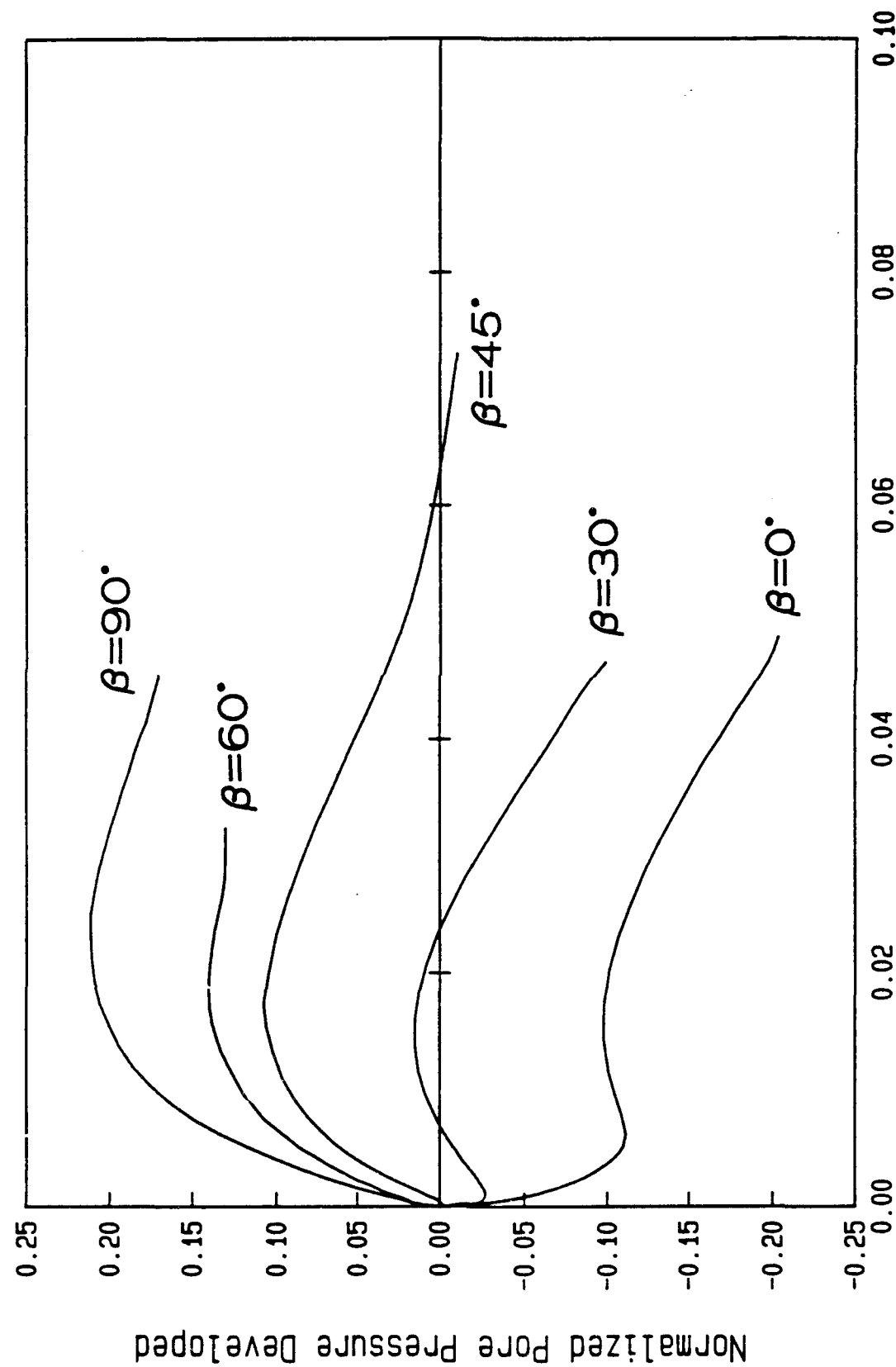


Figure 3.3b Normalized Pore Pressure Developed vs. Octahedral Shear Strain; H121

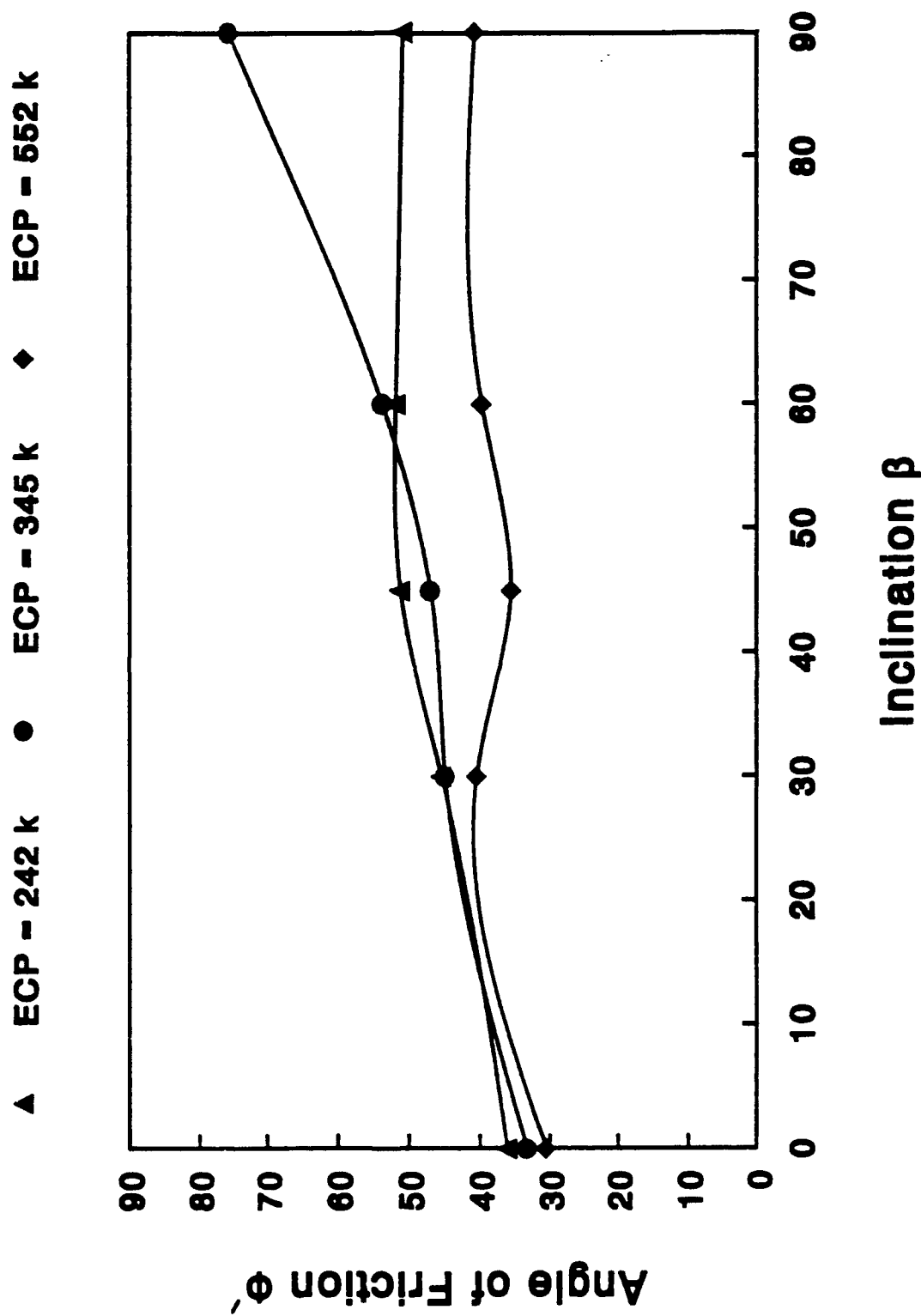


Figure 3.4 Influence of the Inclination of the Major Principal Stress on ϕ'

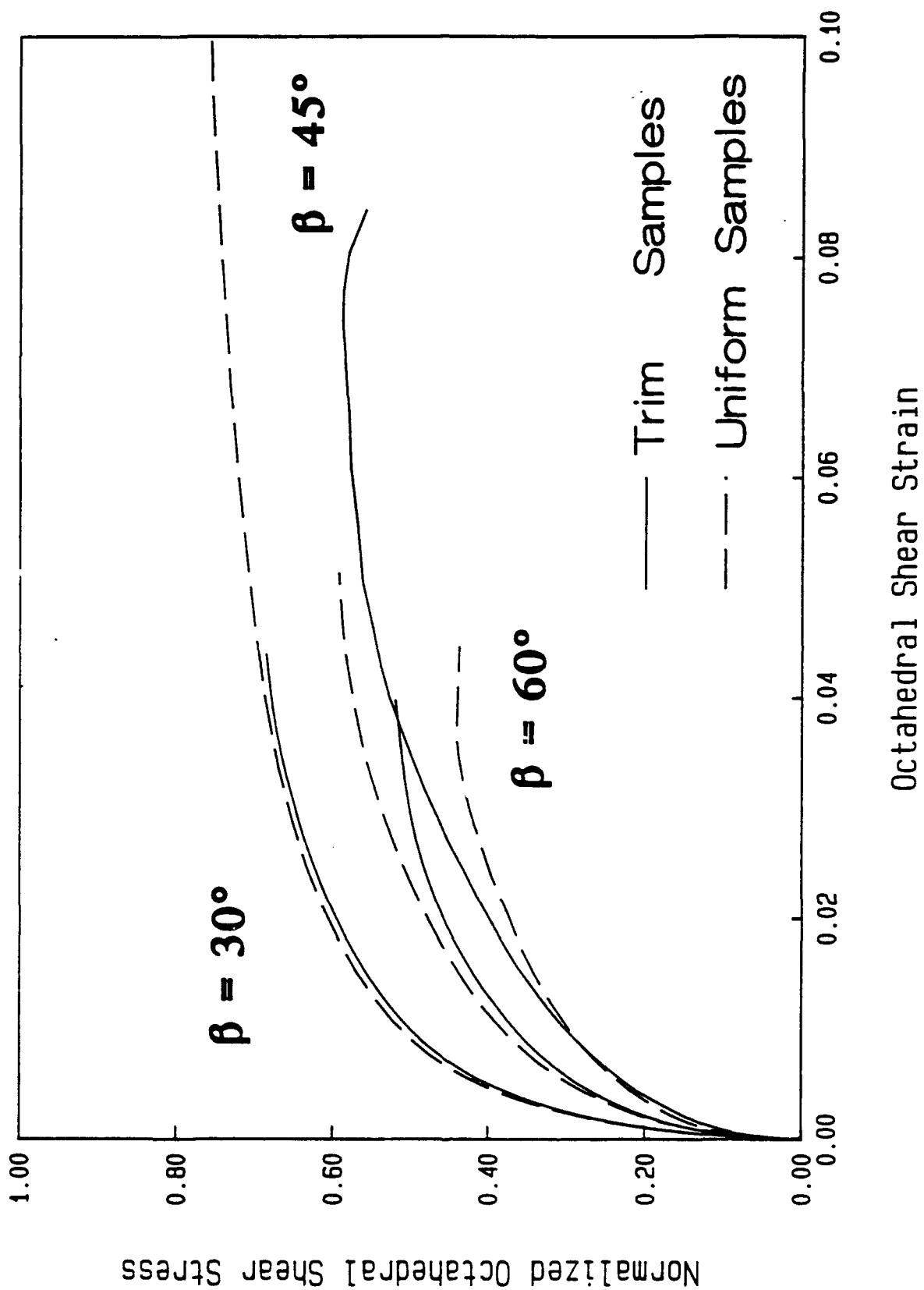


Figure 3.5a Comparison of Trimmed and Uniform Specimens

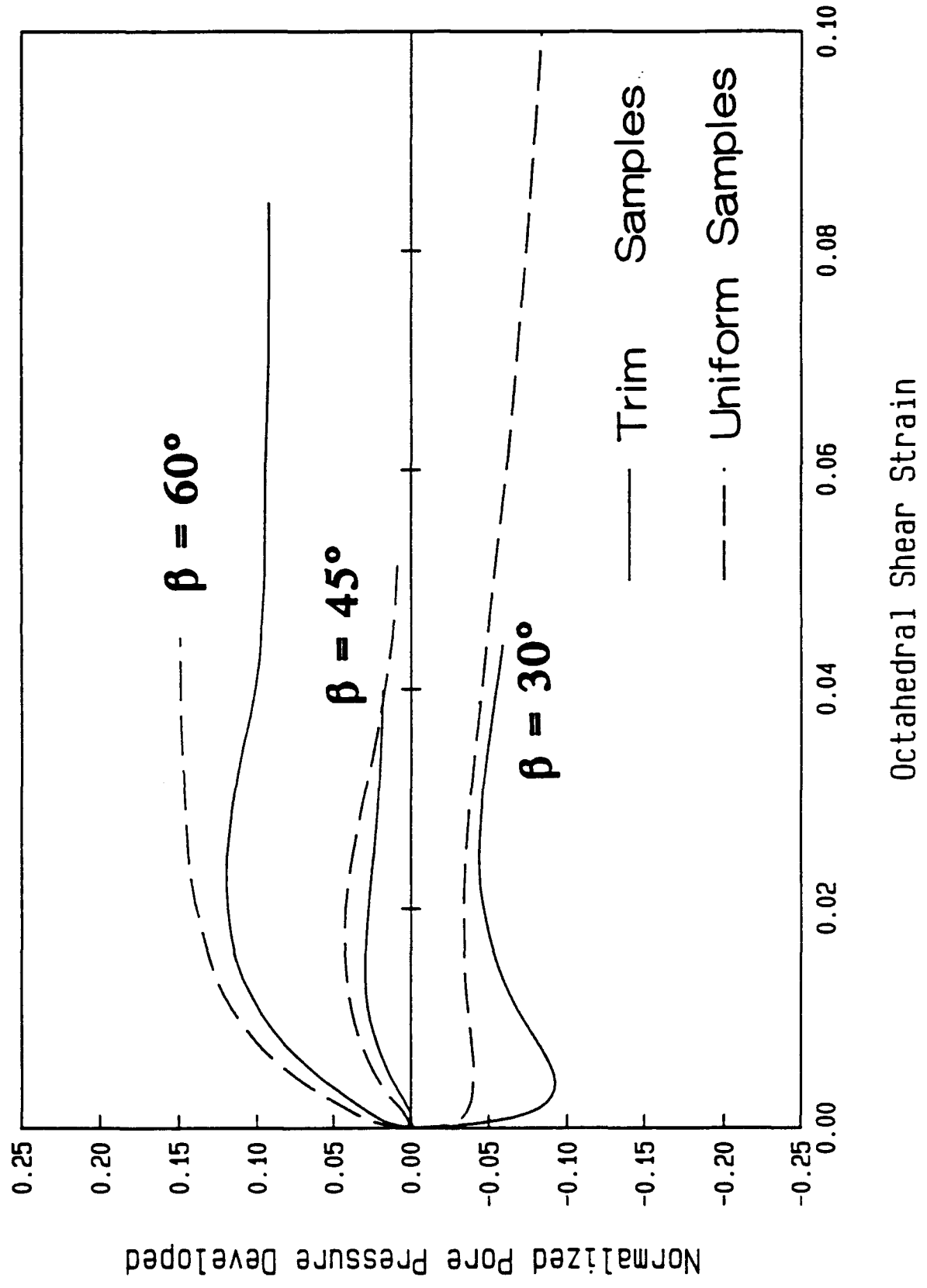


Figure 3.5b Comparison of Trimmed and Uniform Specimens



Test Name: 62_05/16/91 Consol.: Ko NC Beta: 30
Material: EPK 345 kPa Control: Deform.
Height: variable

Figure 3.6a Bifurcation and Resulting Shear Bands; $\beta = 30^\circ$

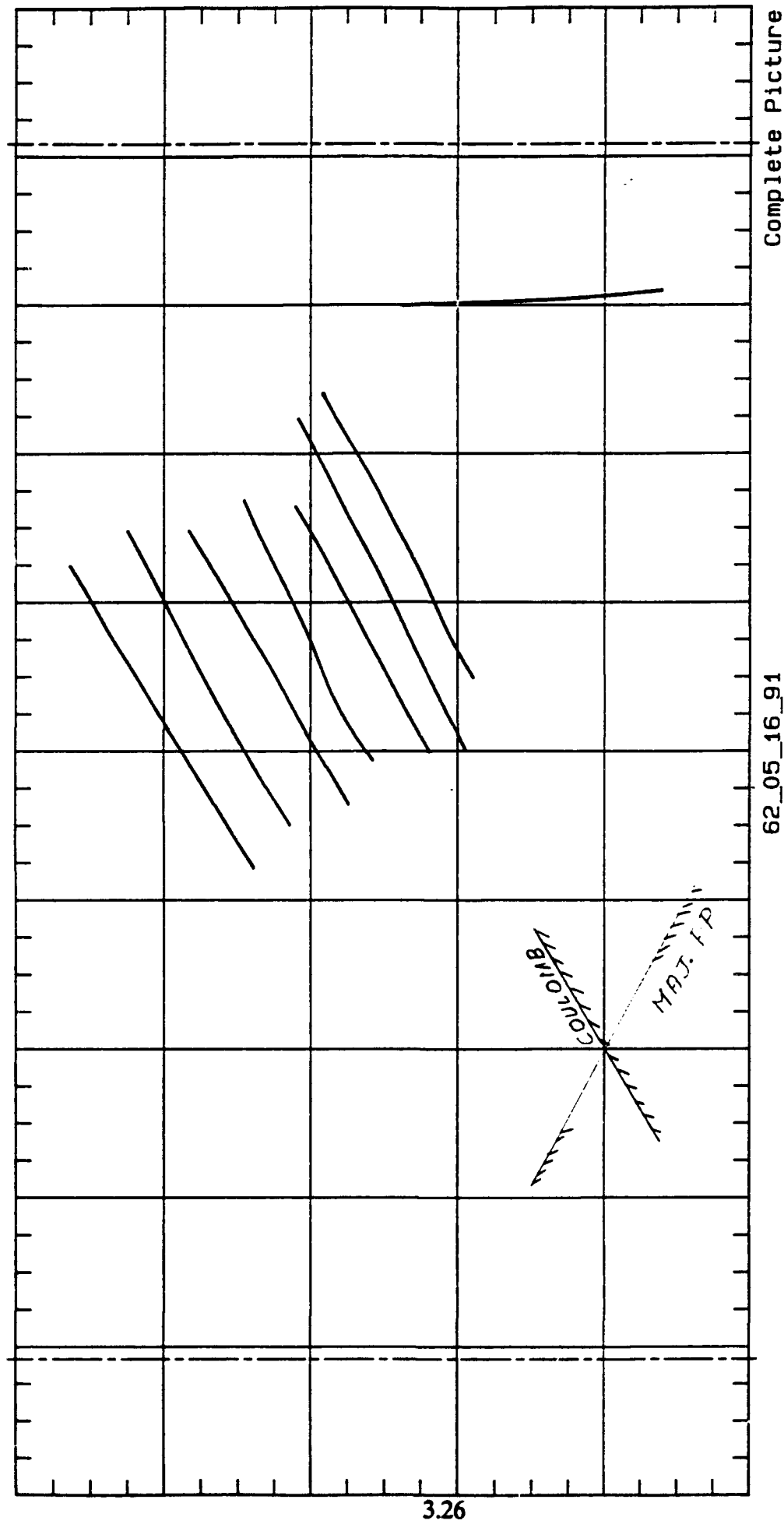
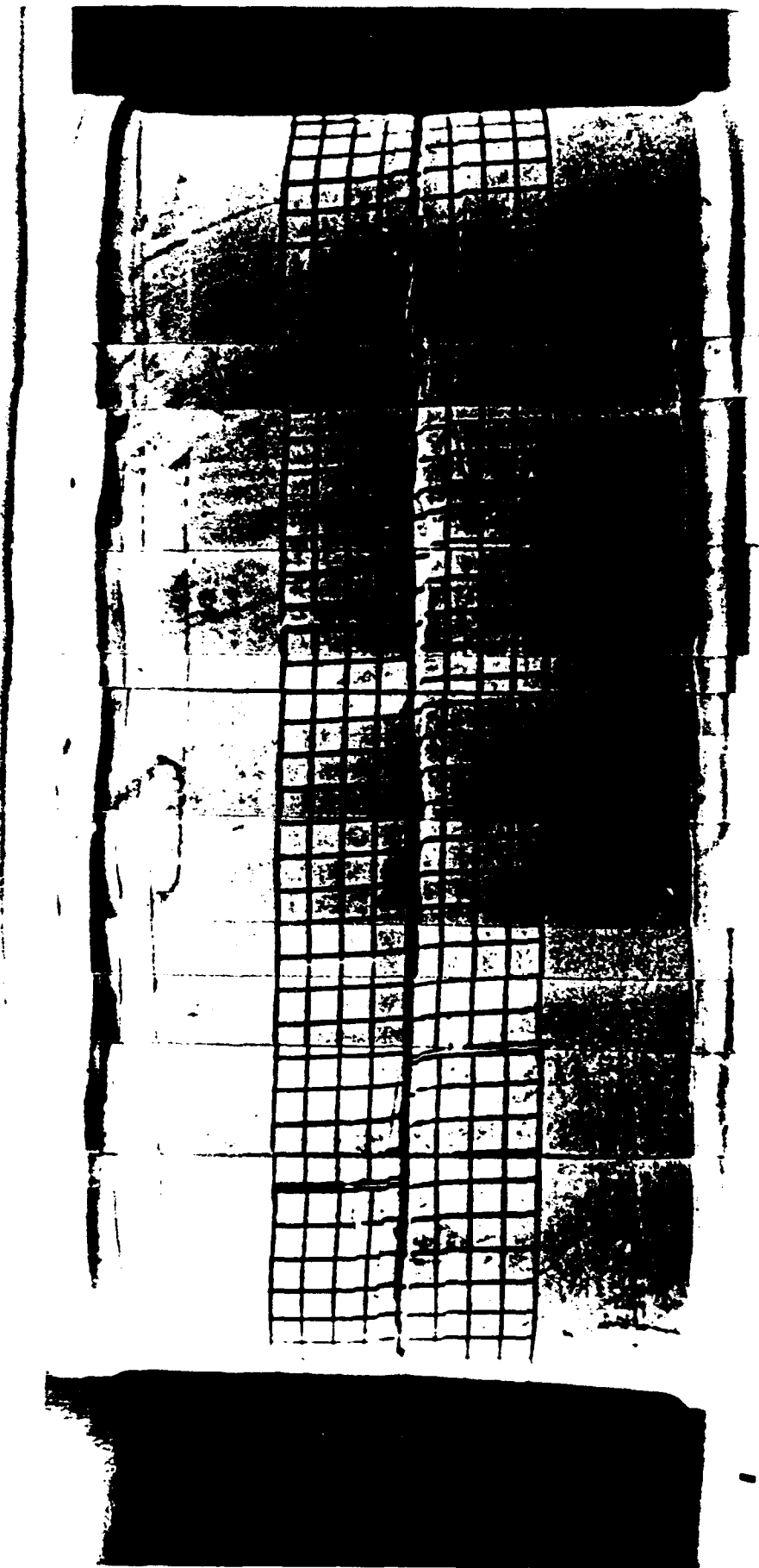


Figure 3.6az Bifurcation and Resulting Shear Bands; $\beta = 30^\circ$



Test Name: 61b_11/19/91 **Consol.:** Ko NC
Material: EPK **Beta:** 60
 345 kPa **Control:** stress

Figure 3.6b Bifurcation and Resulting Shear Bands; $\beta = 60^\circ$

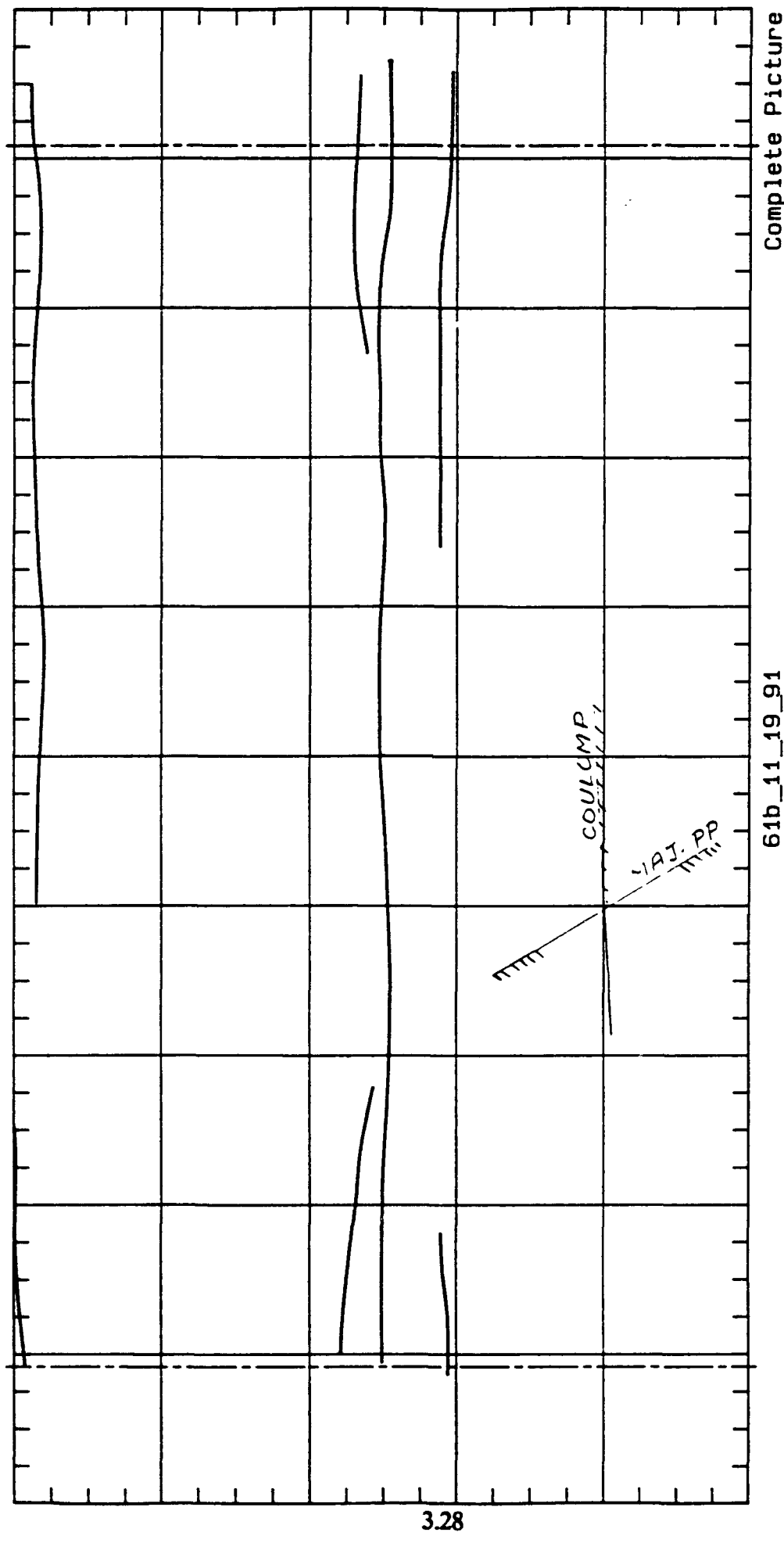


Figure 3.6bz Bifurcation and Resulting Shear Bands; $\rho = 60^\circ$

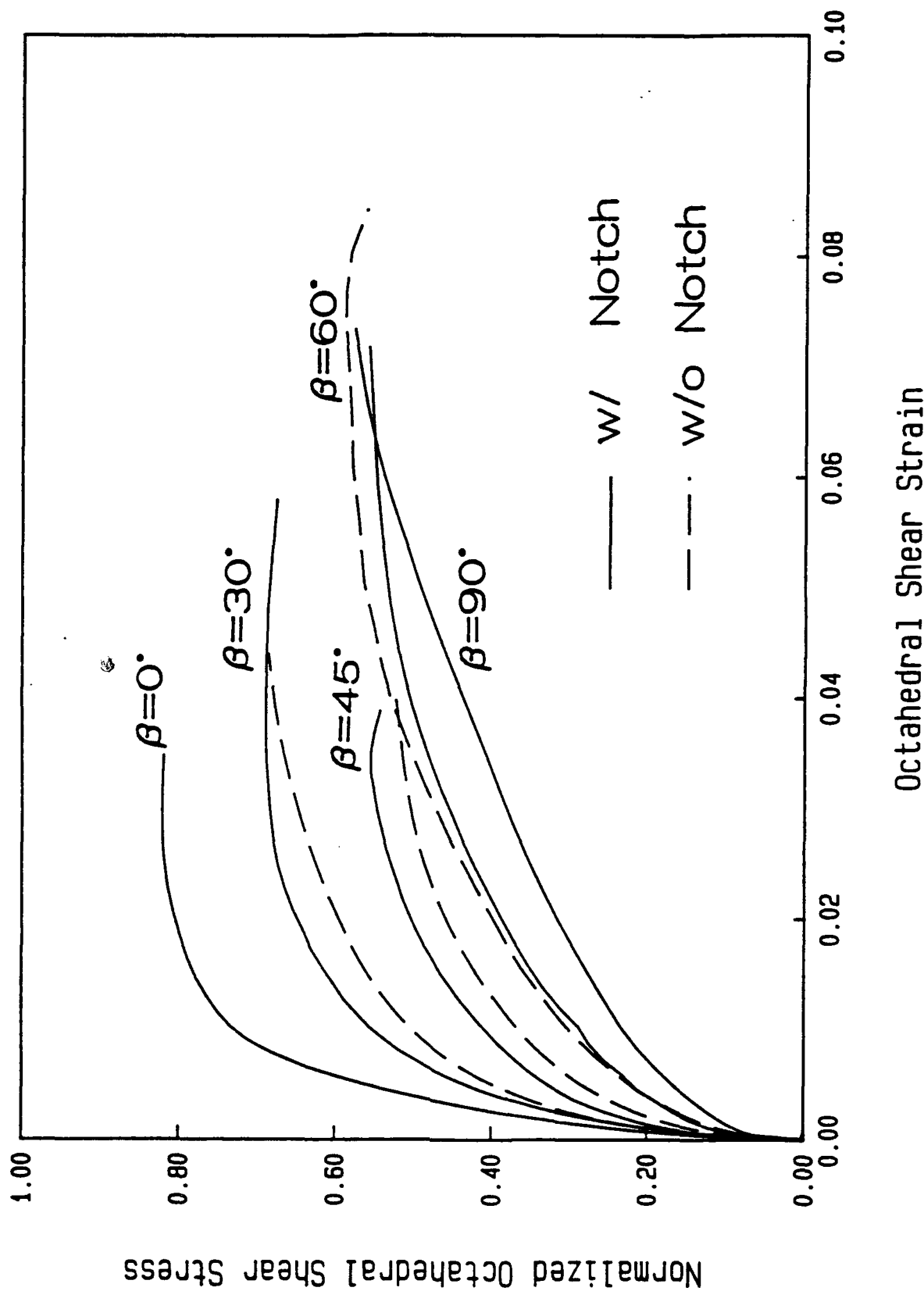


Figure 3.7a Comparison Between Notched and Unnotched Specimens

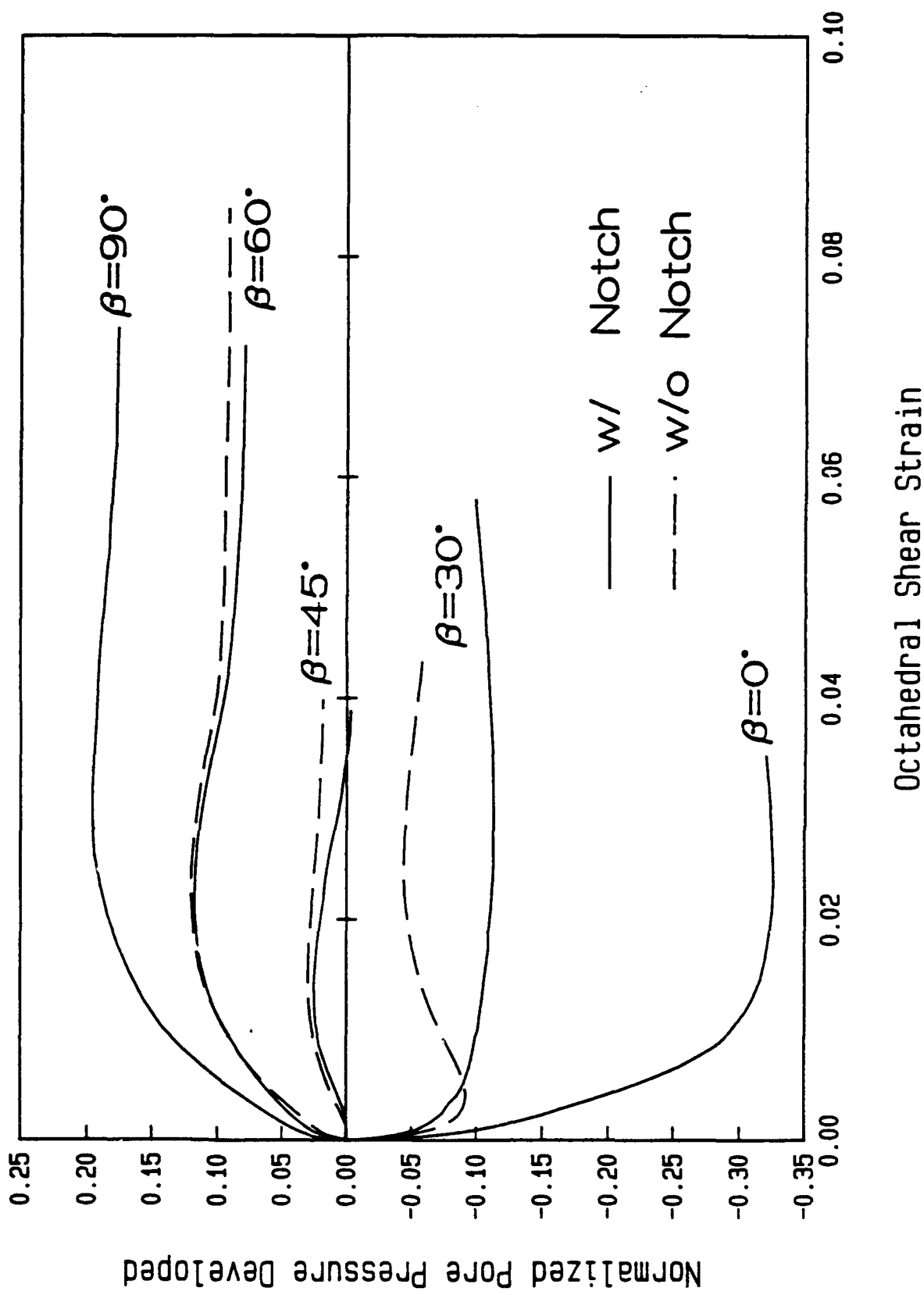


Figure 3.7b Comparison Between Notched and Unnotched Specimens

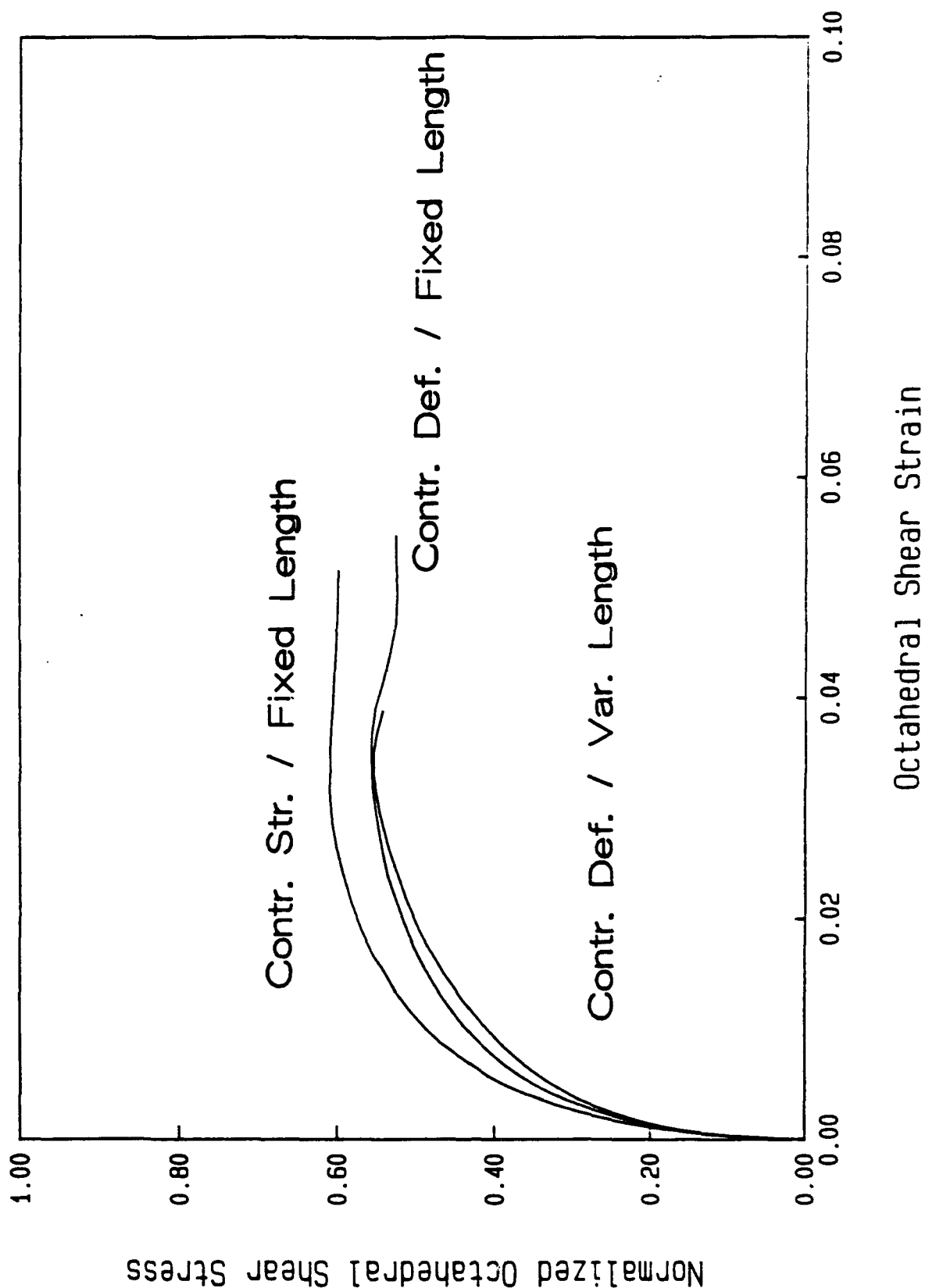


Figure 3.8a Comparison Among Various Modes of Testing

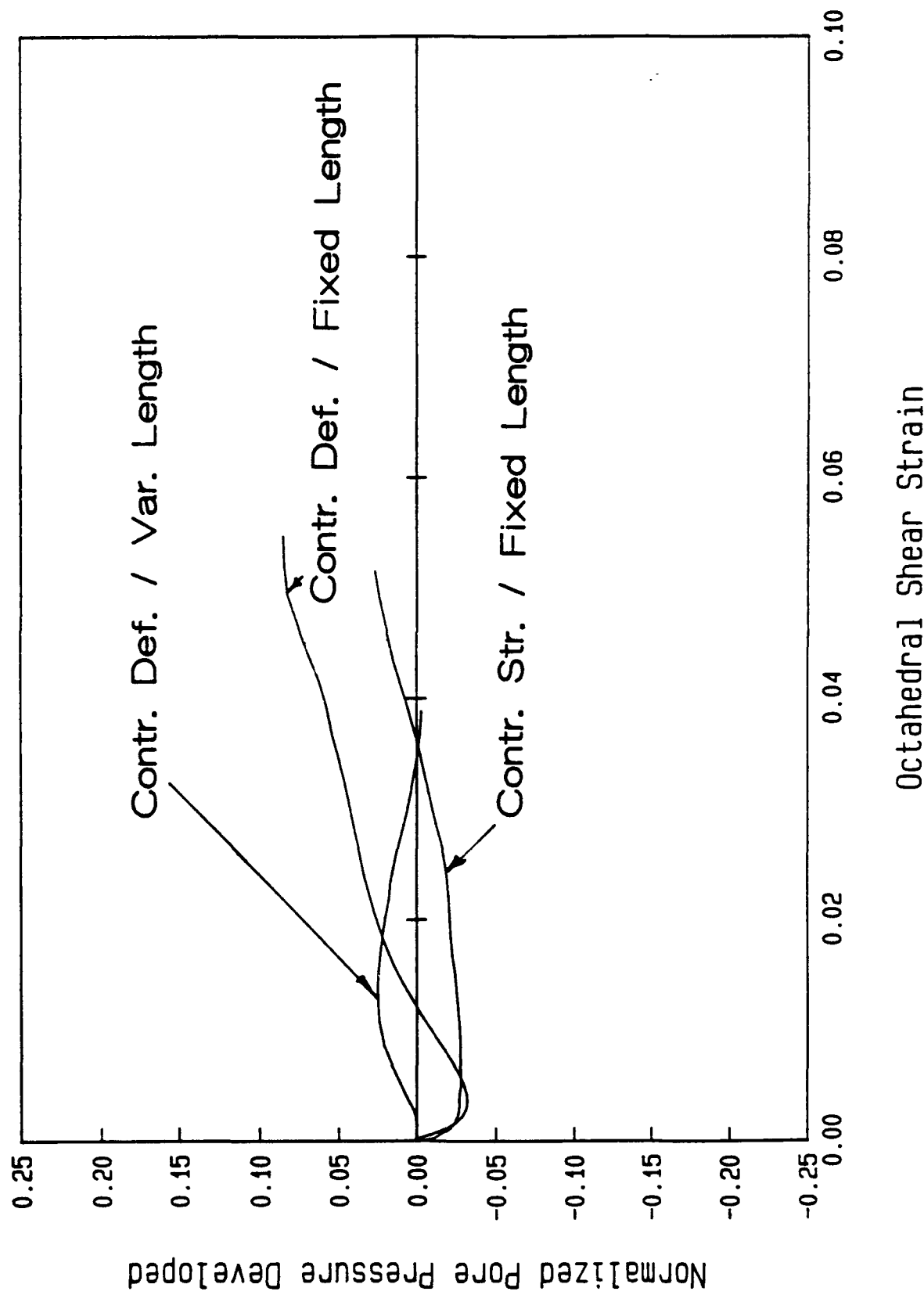


Figure 3.8b Comparison Among Various Modes of Testing

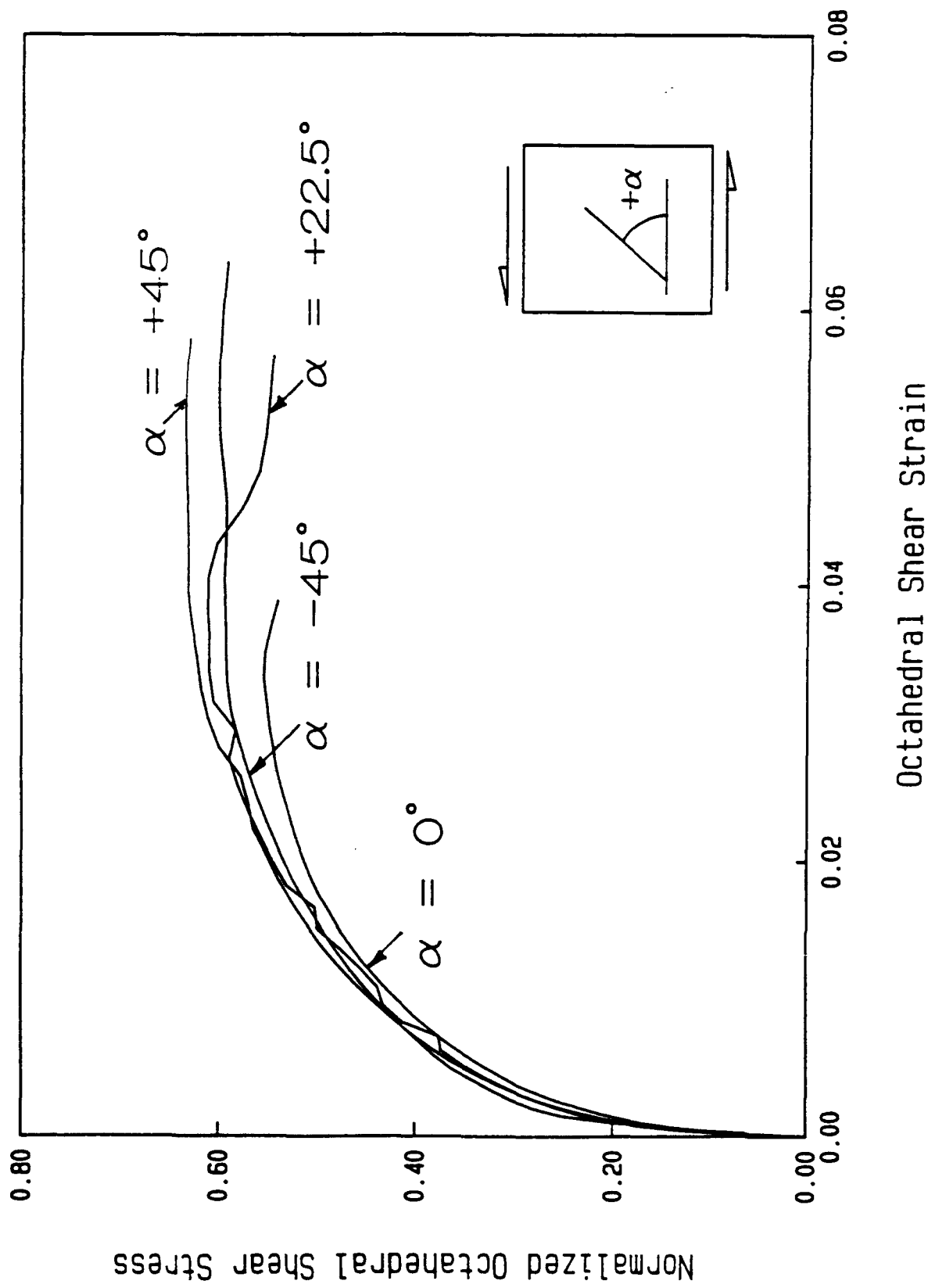


Figure 3.9a Effect of the Inclination of the Crack on the Strength

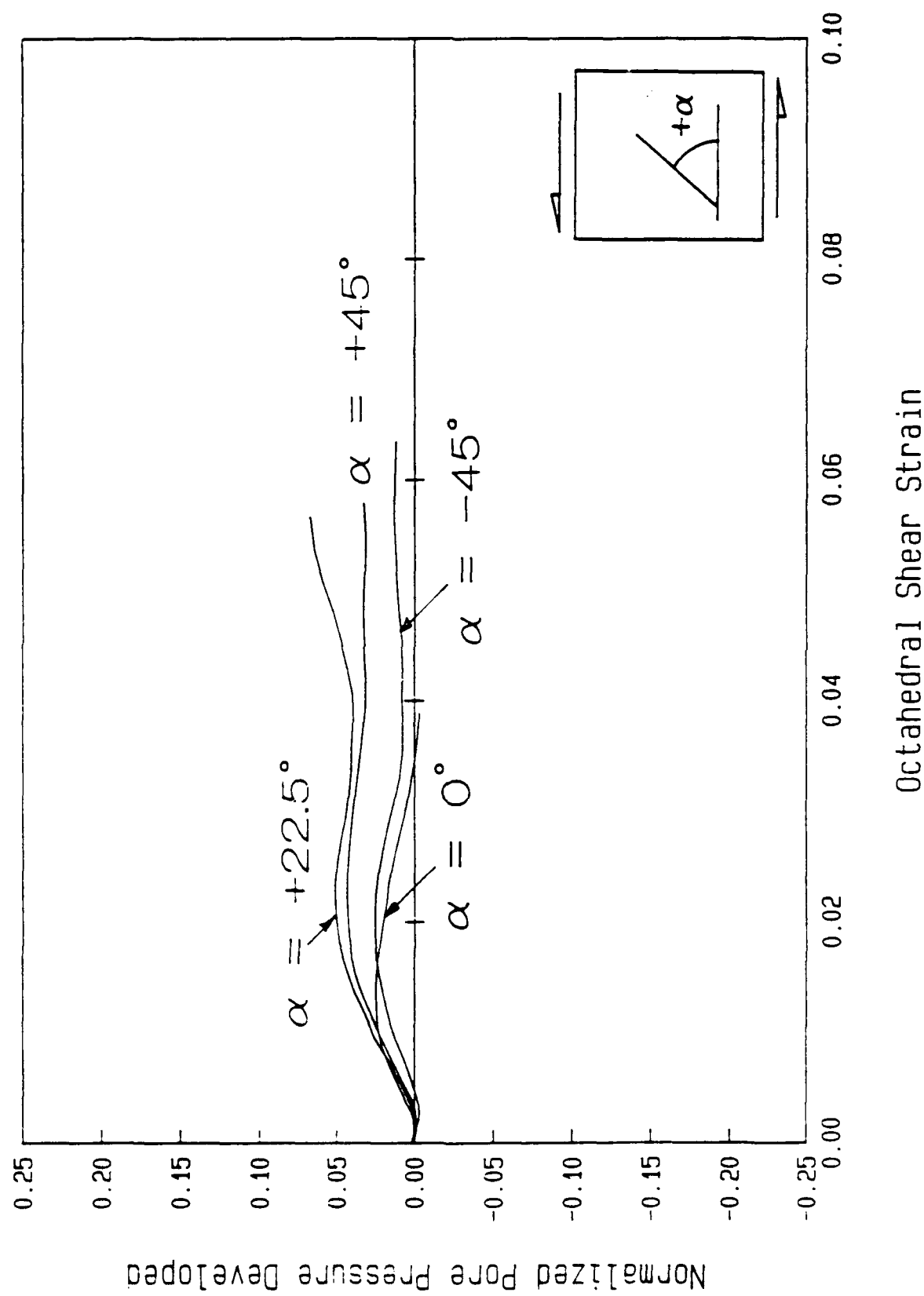


Figure 3.9b Effect of the Inclination of the Crack on the Pore Water Pressure

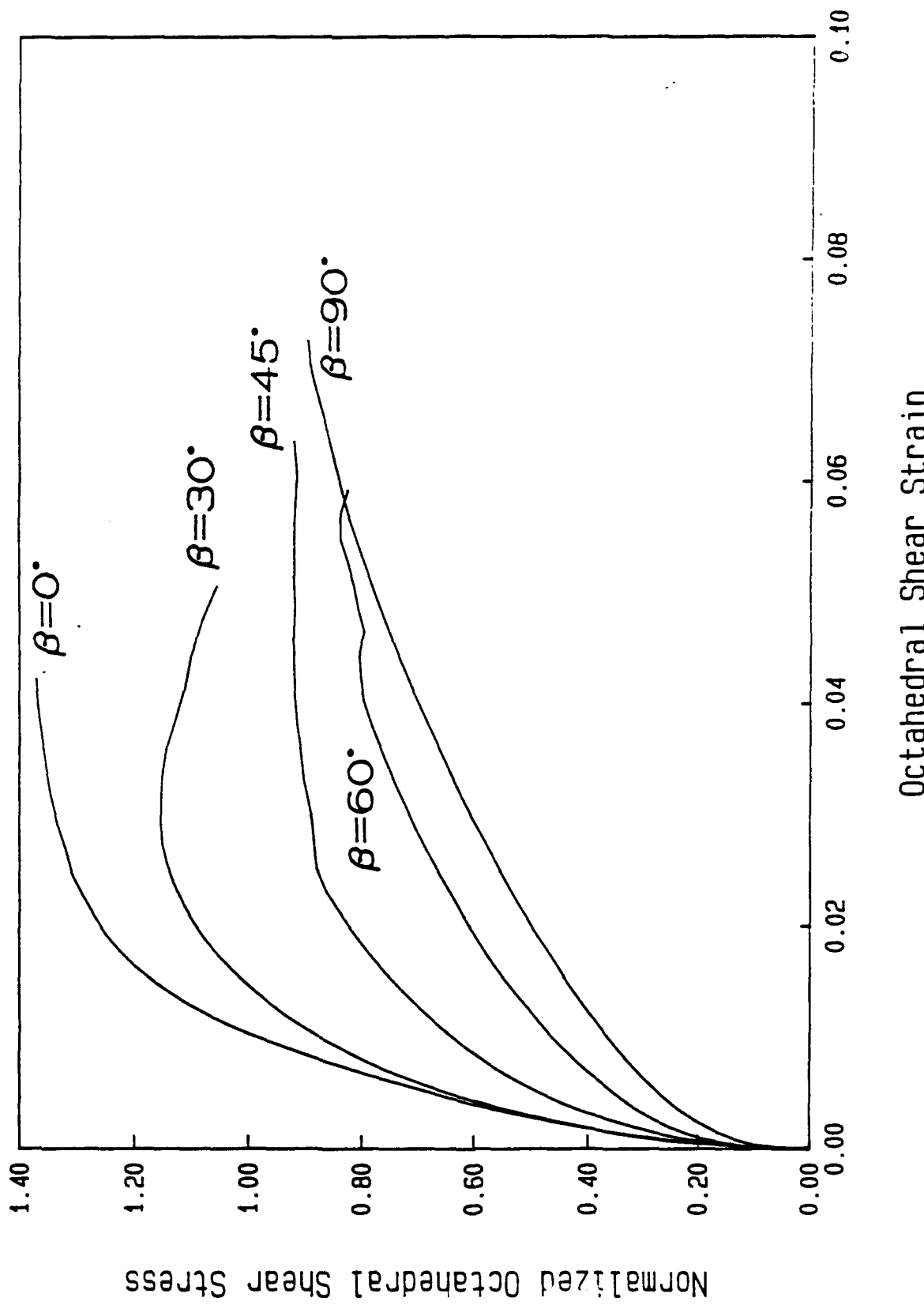


Figure 3.10a Normalized Octahedral Shear Stress vs. Octahedral Shear Strain
Strain; Overconsolidated EPK

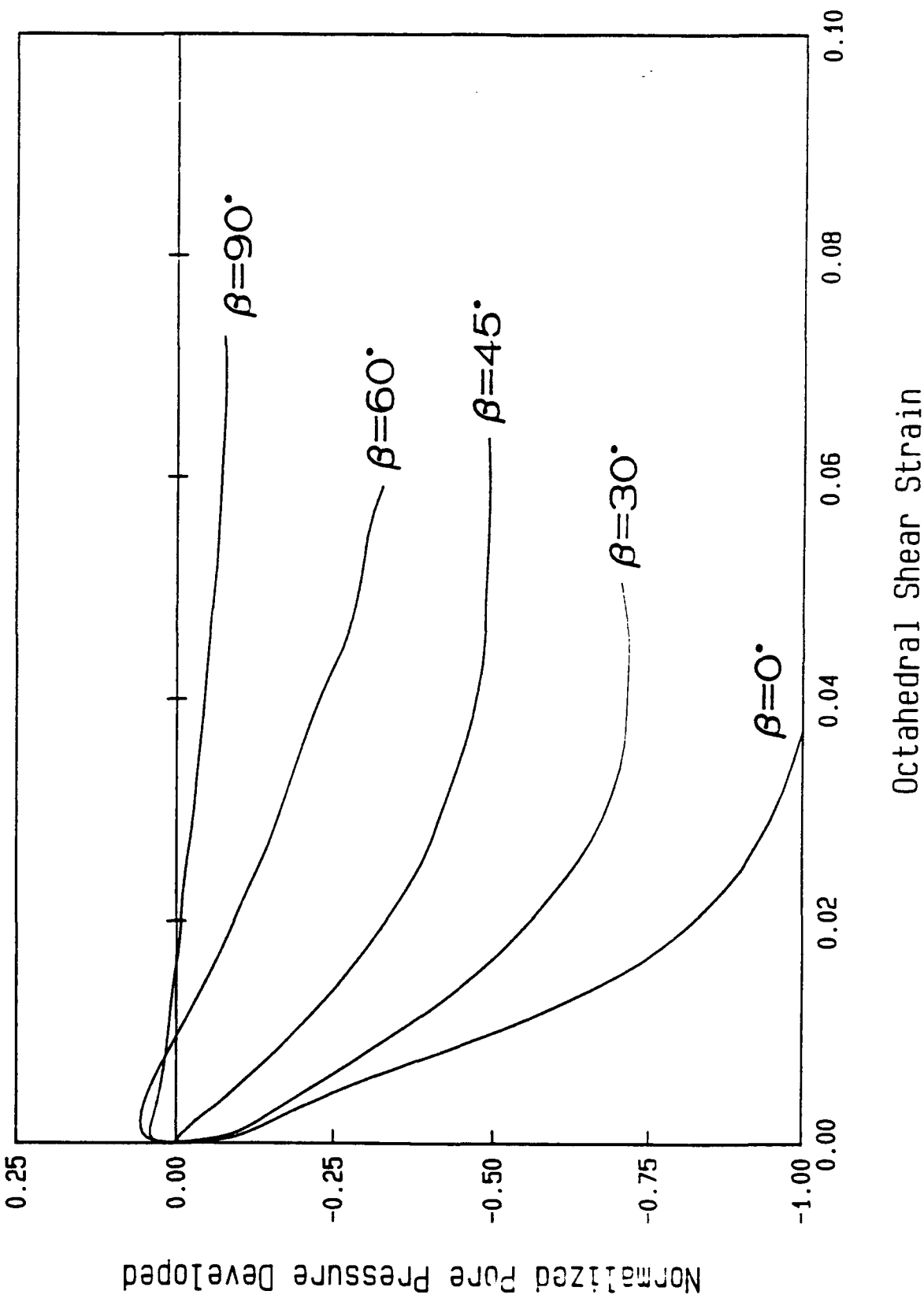
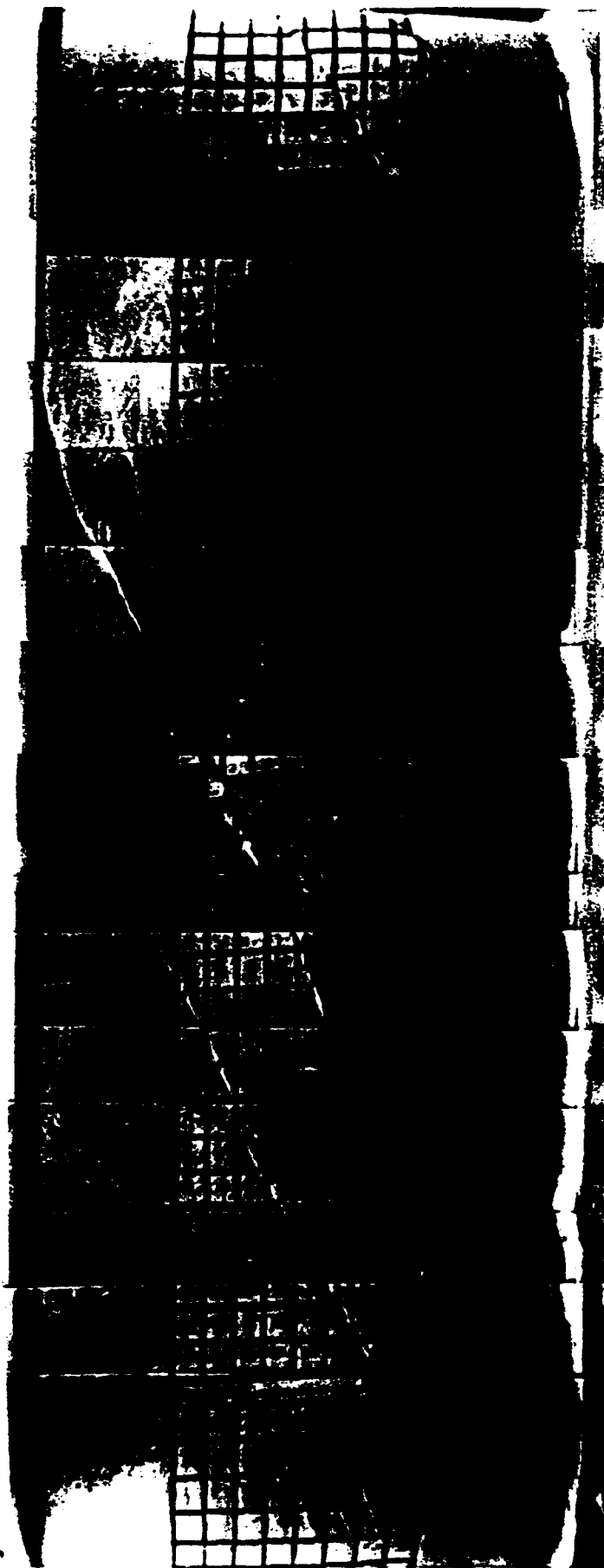


Figure 3.10b Normalized Pore Pressure Developed vs. Octahedral Shear Strain; Overconsolidated EPK



Test Name: 89_08/01/91 Consol.: Ko OC
Material: EPK Control: OCR-4
Beta: 30 Deform.
Height: Variable

Figure 3.11a Bifurcation and Resulting Shear Bands; $\beta = 30^\circ$

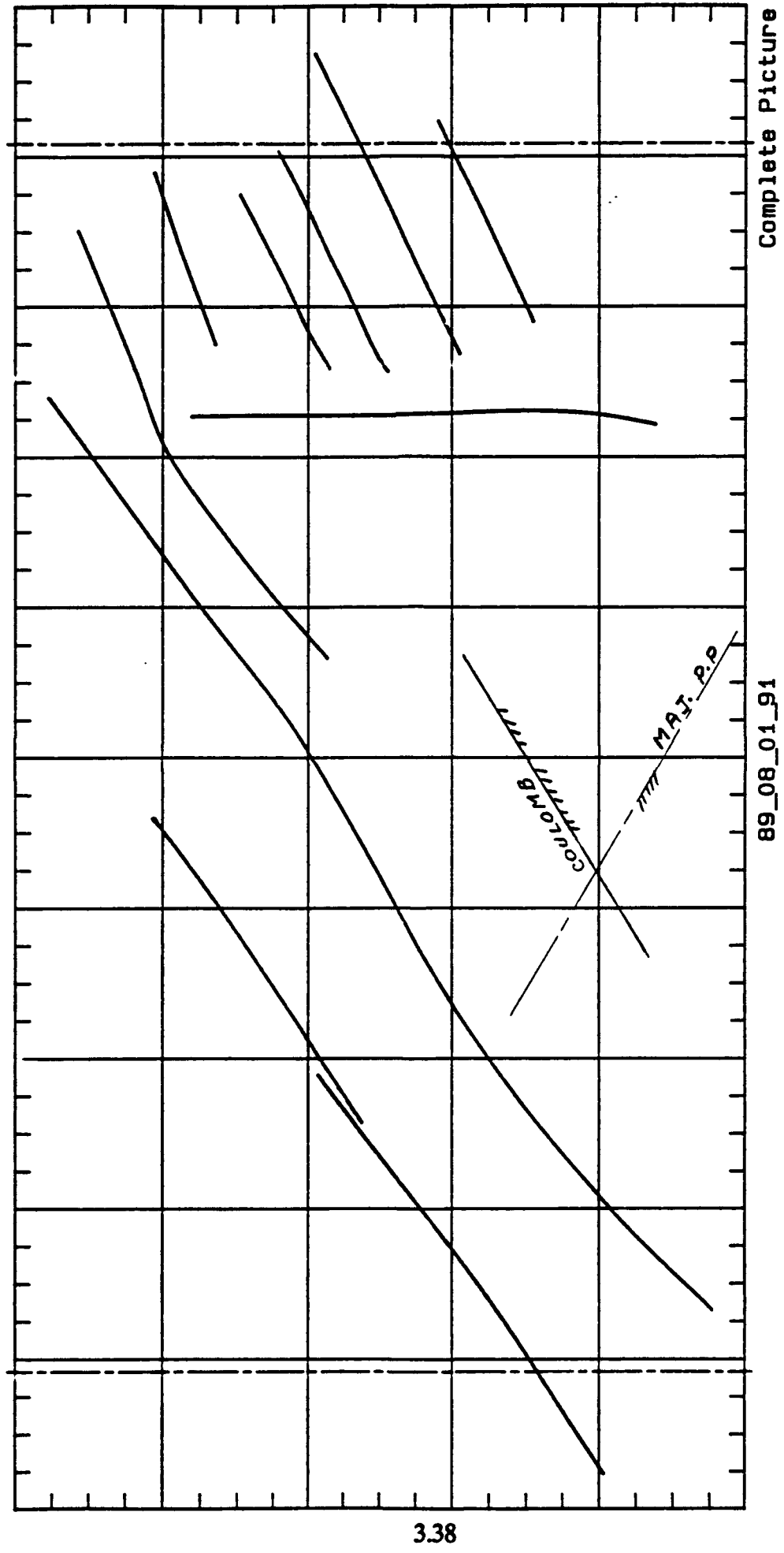


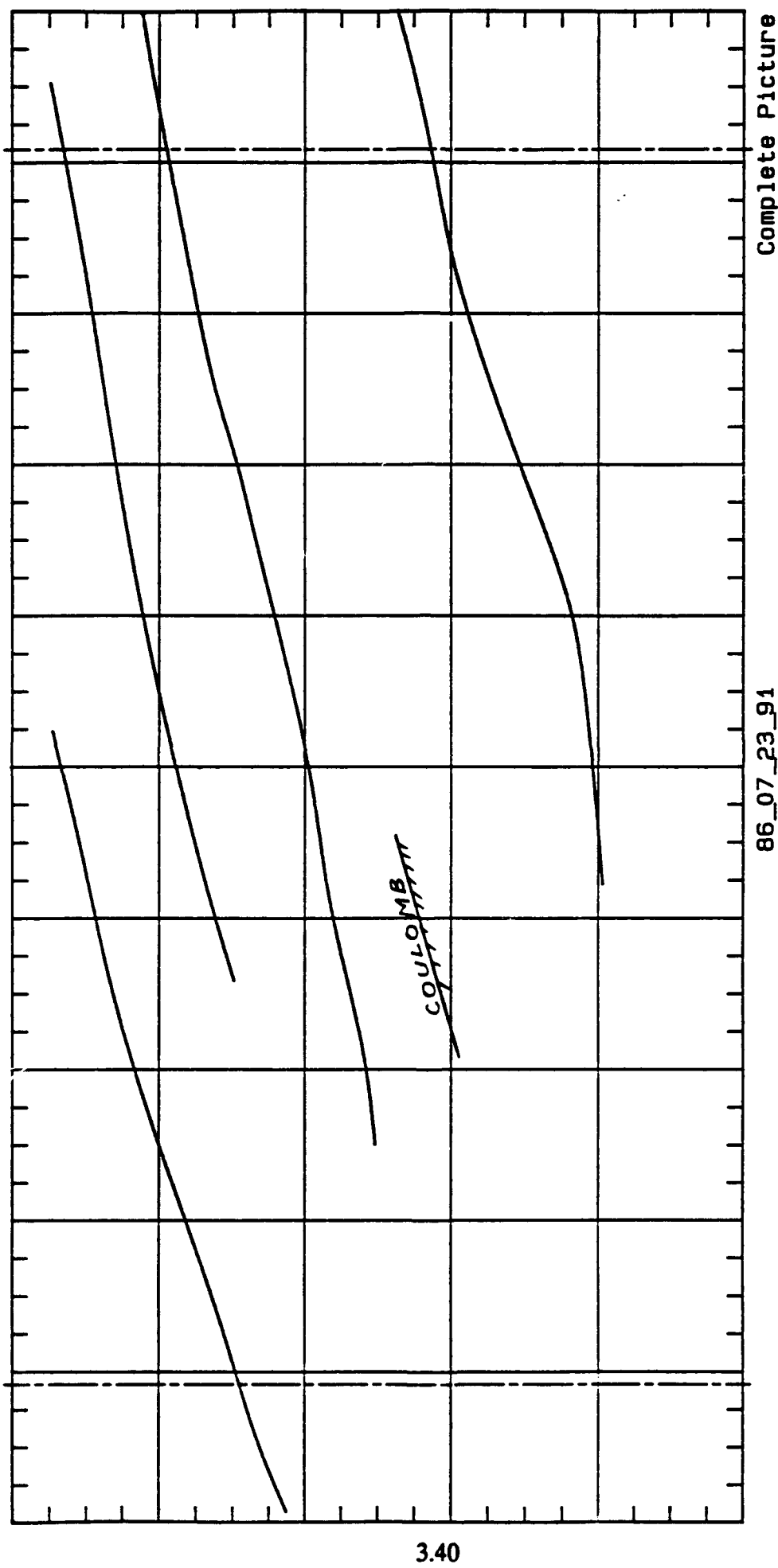
Figure 3.11az Bifurcation and Resulting Shear Bands; $\beta = 30^\circ$

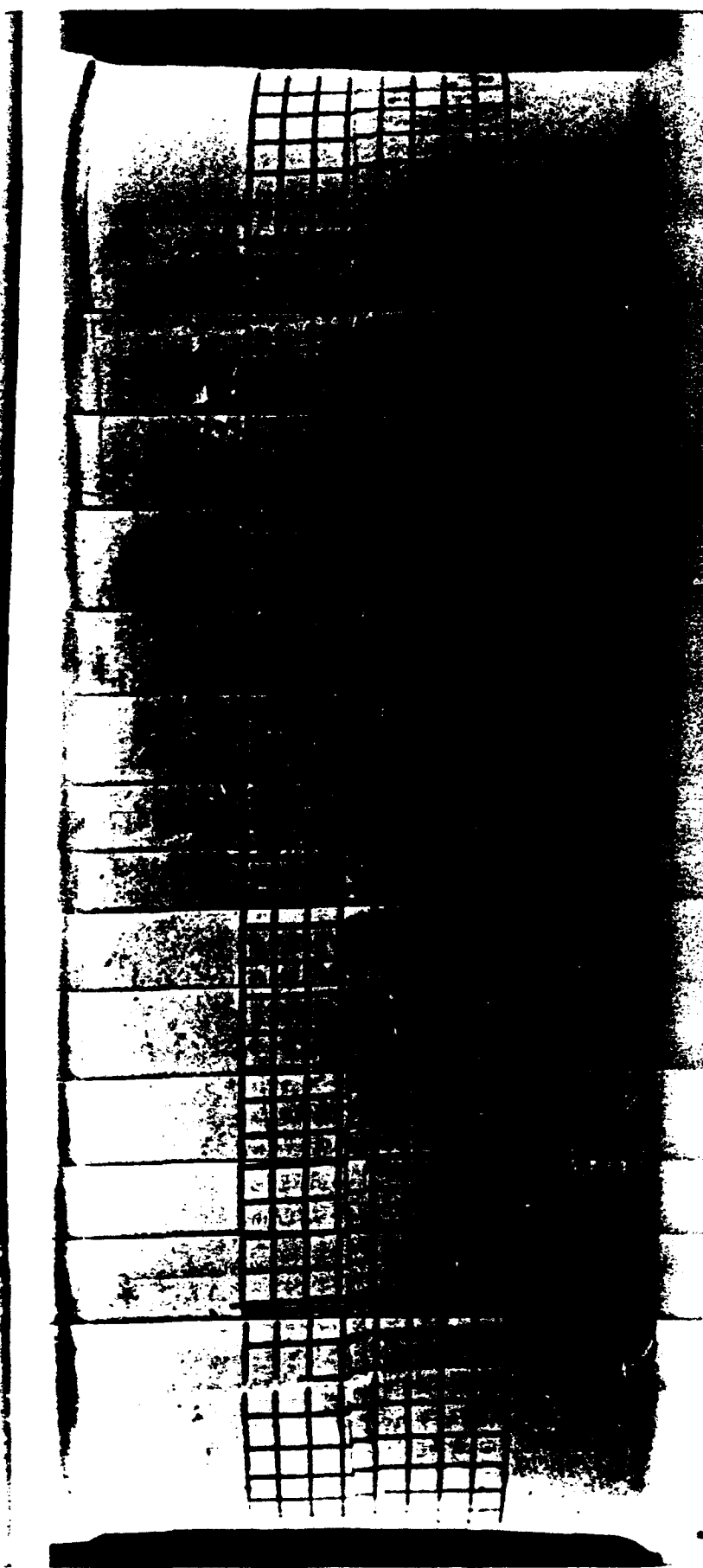


Test Name: 86_07/23/91 **Consol.:** Xo OC
Material: EPK **Beta:** 45
 OCR-4 **Control:** Deform.
 Height: variable

Figure 3.11b Bifurcation and Resulting Shear Bands; $\beta = 45^\circ$

Figure 3.11bz Bifurcation and Resulting Shear Bands; $\beta = 45^\circ$

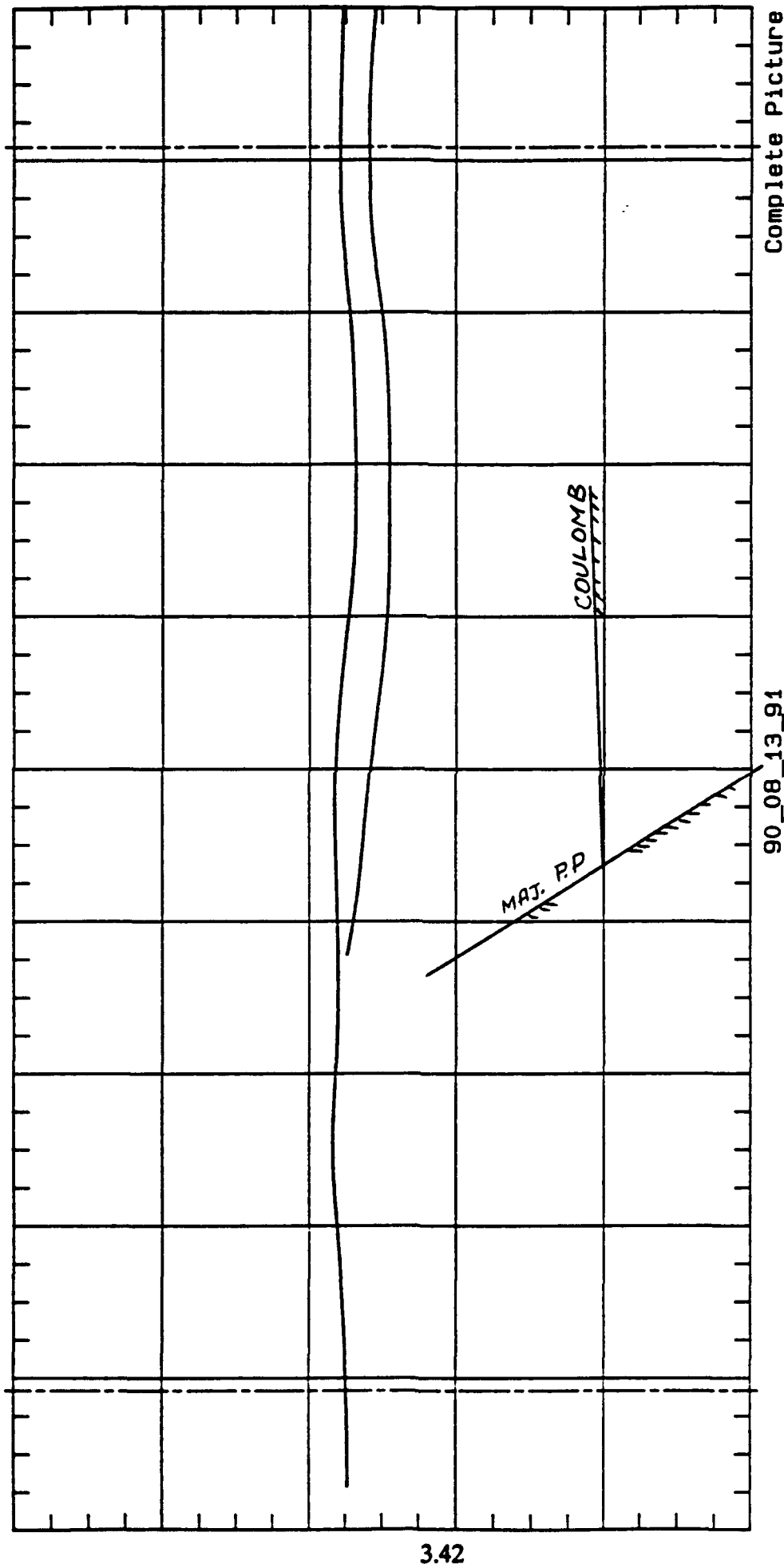




Test Name: 90_08/13/91 Consol.: Ko OC
Material: EPR Control: OCR-4
Beta: 60 Deform.
Height: variable

Figure 3.11c Bifurcation and Resulting Shear Bands; $\beta = 60^\circ$

Figure 3.11cz Bifurcation and Resulting Shear Bands; $\rho = 60^\circ$



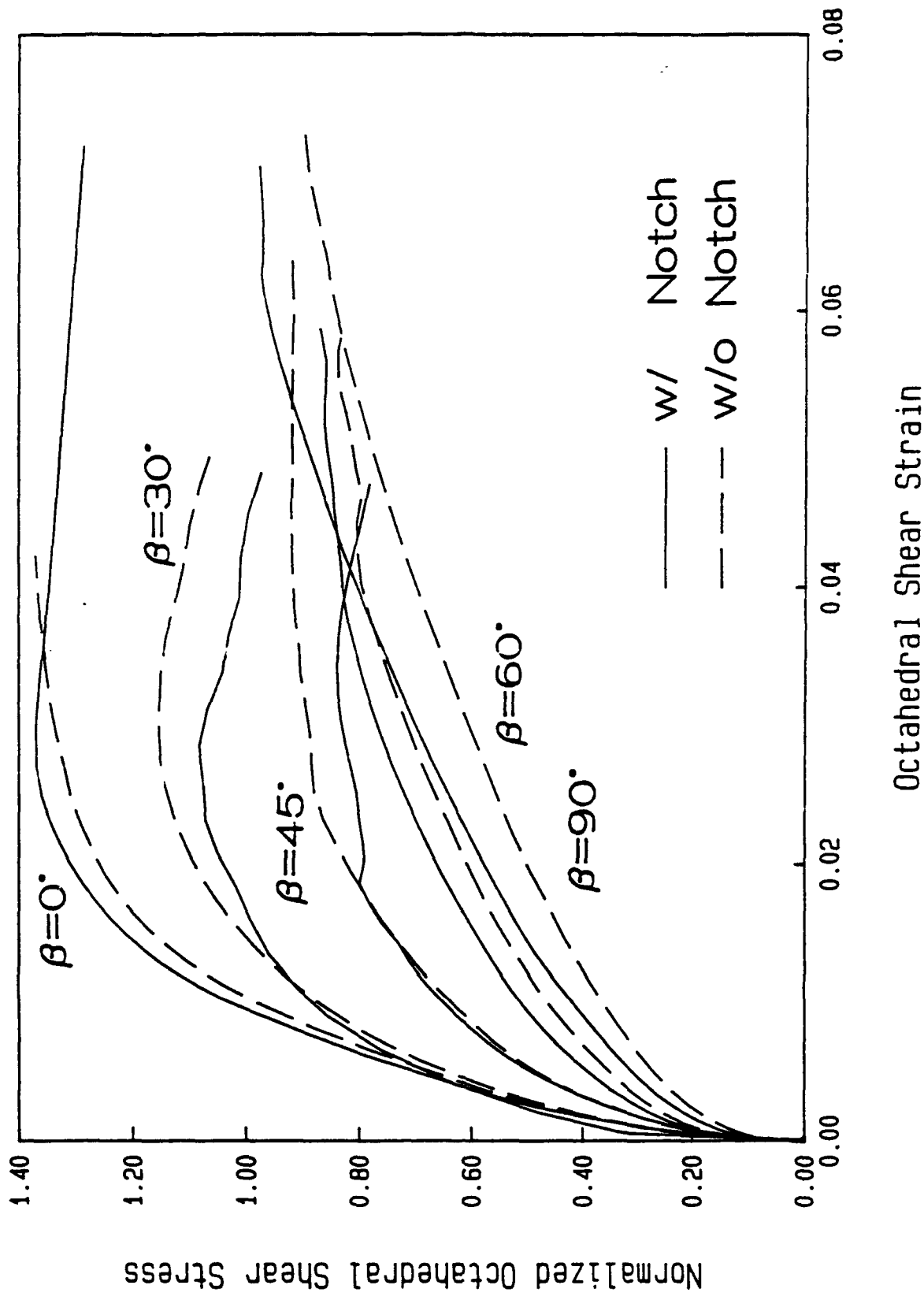


Figure 3.12a Comparison Between Notched and Unnotched Specimens

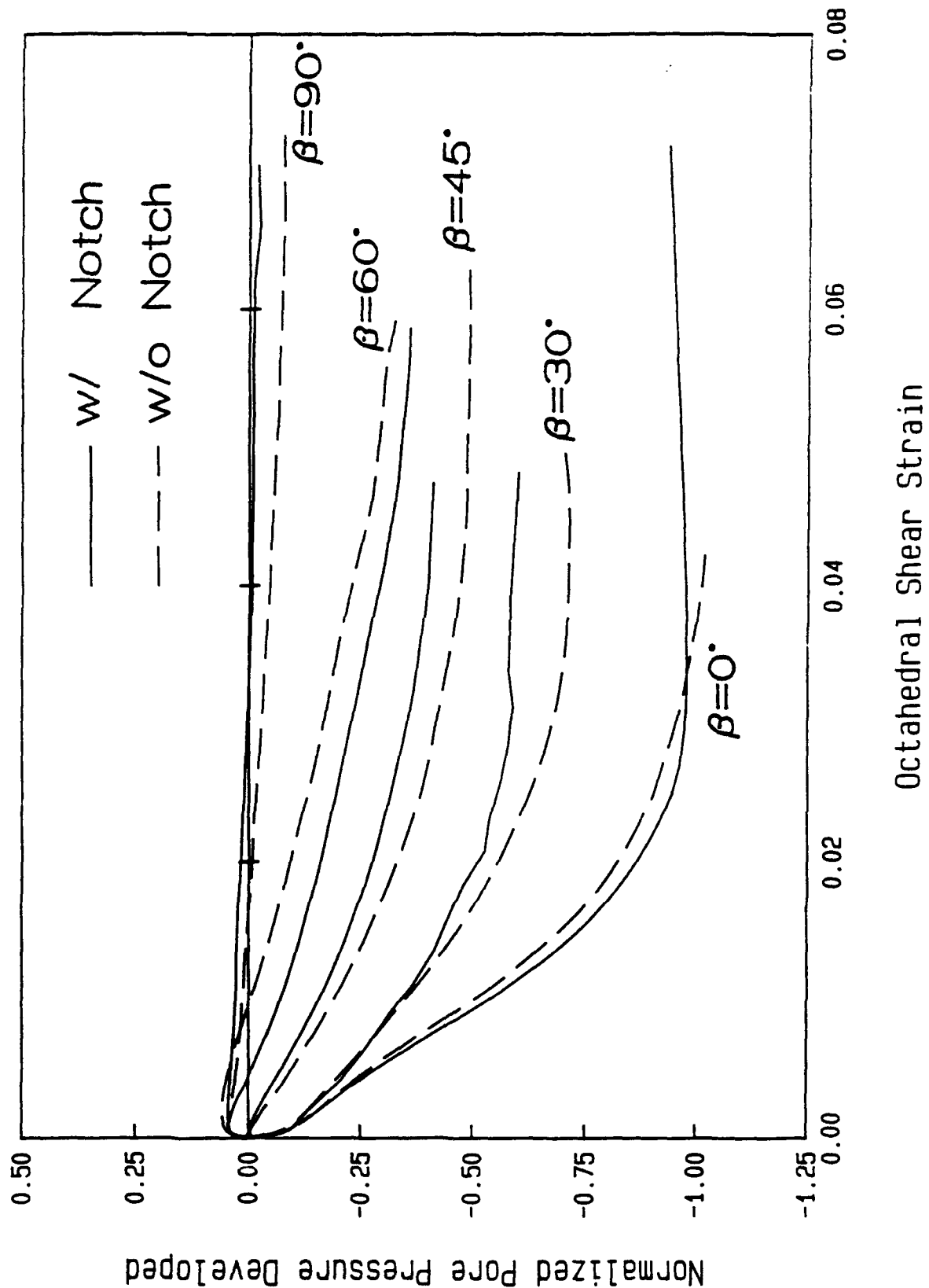


Figure 3.12b Comparison Between Notched and Unnotched Specimens

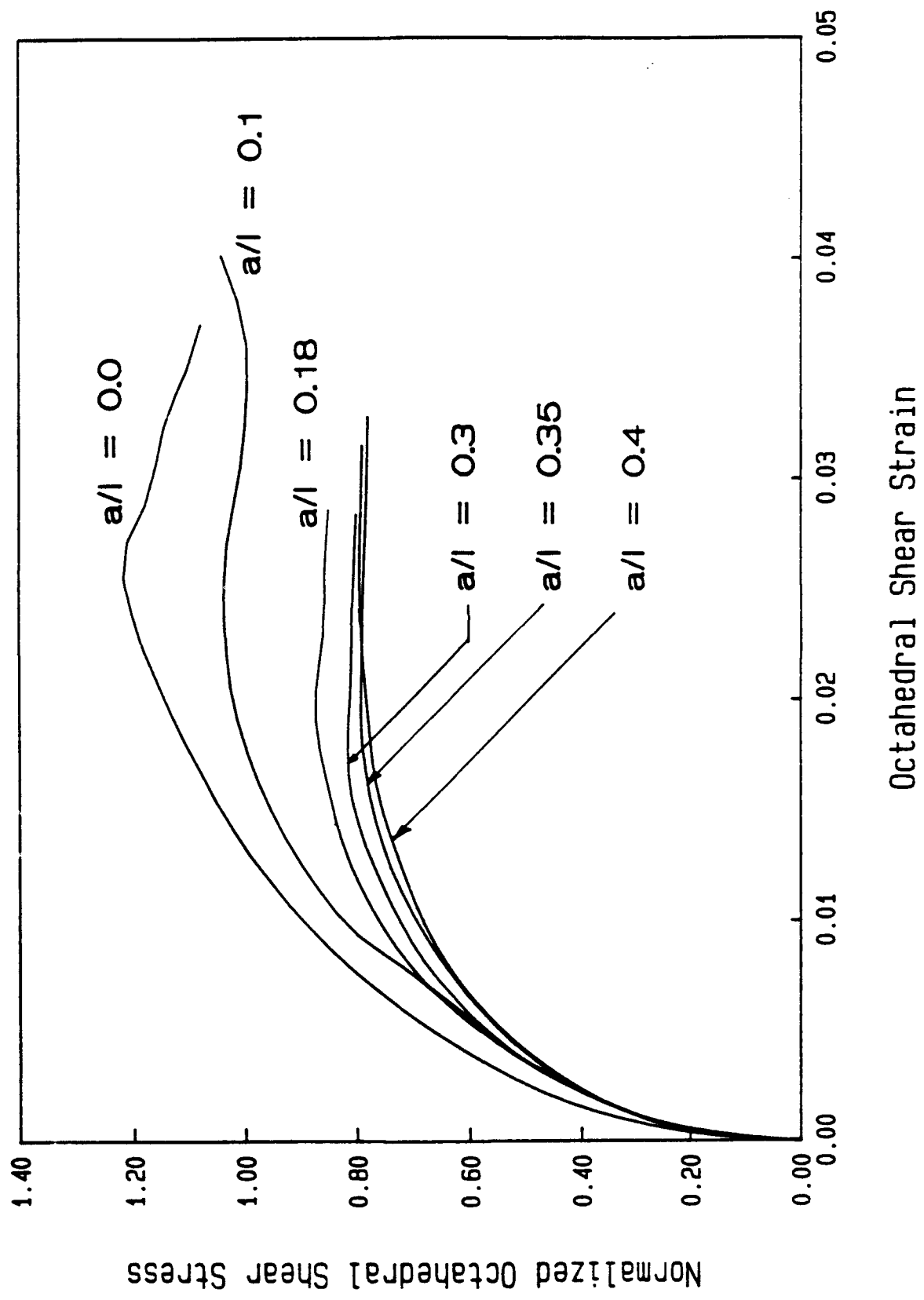


Figure 3.13a Influence of the Size of the Crack on the Strength

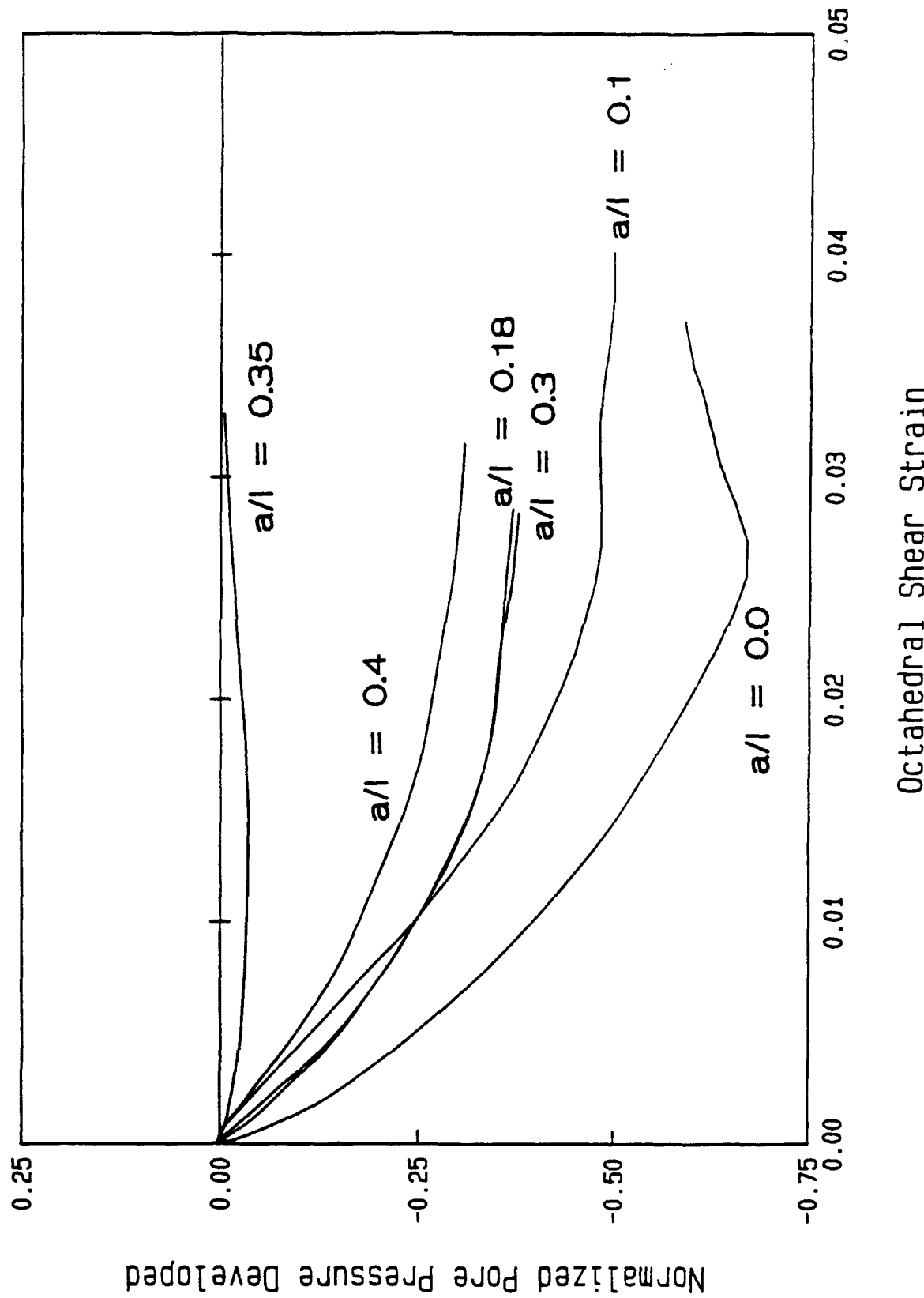
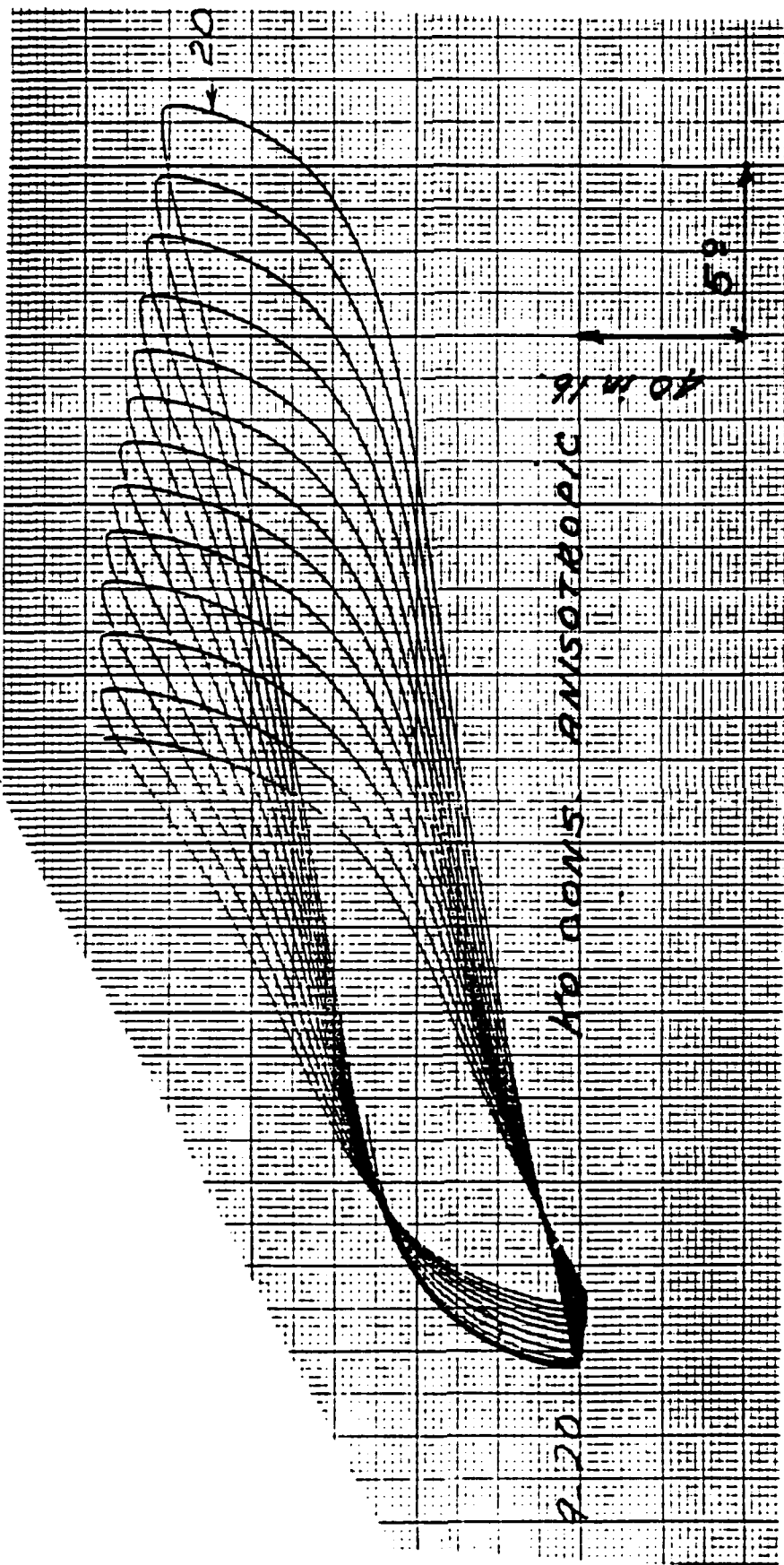


Figure 3.13b Influence of the Size of the Crack on the Pore Water Pressure

Figure 3.14 Decay of Shear Modulus and Increase in Damping of an Anisotropic EPK with a Horizontal Crack



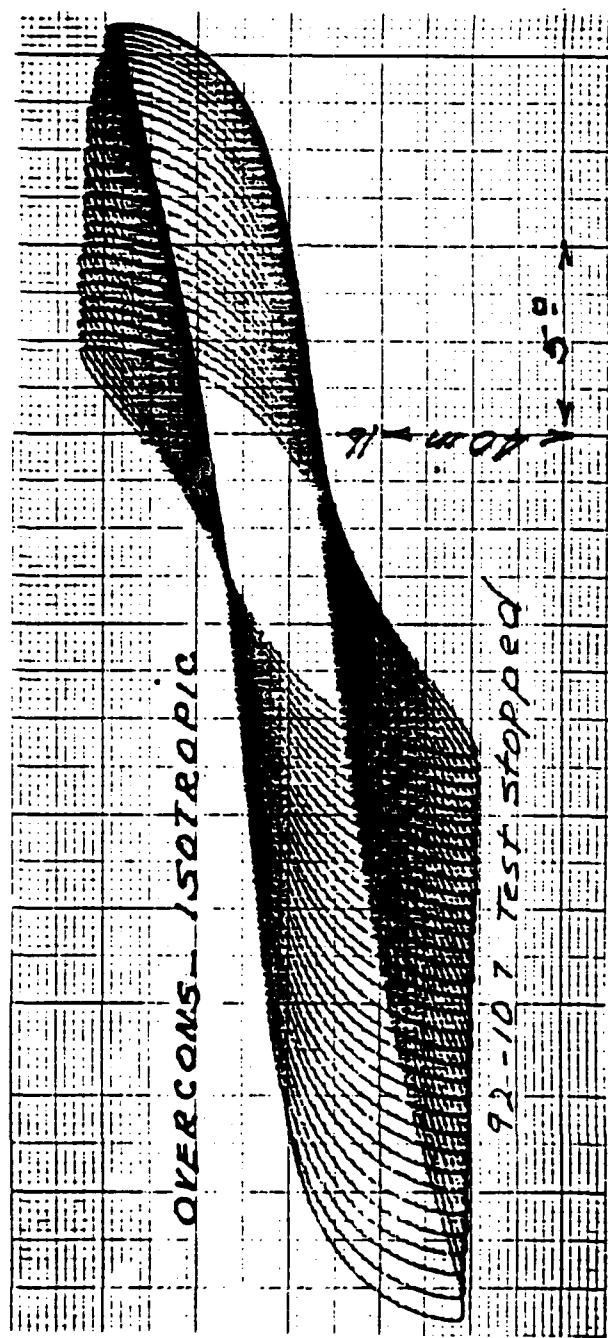


Figure 3.15 Decay of Shear Modulus and Increase in Damping of an Isotropic EPK with a Horizontal Crack

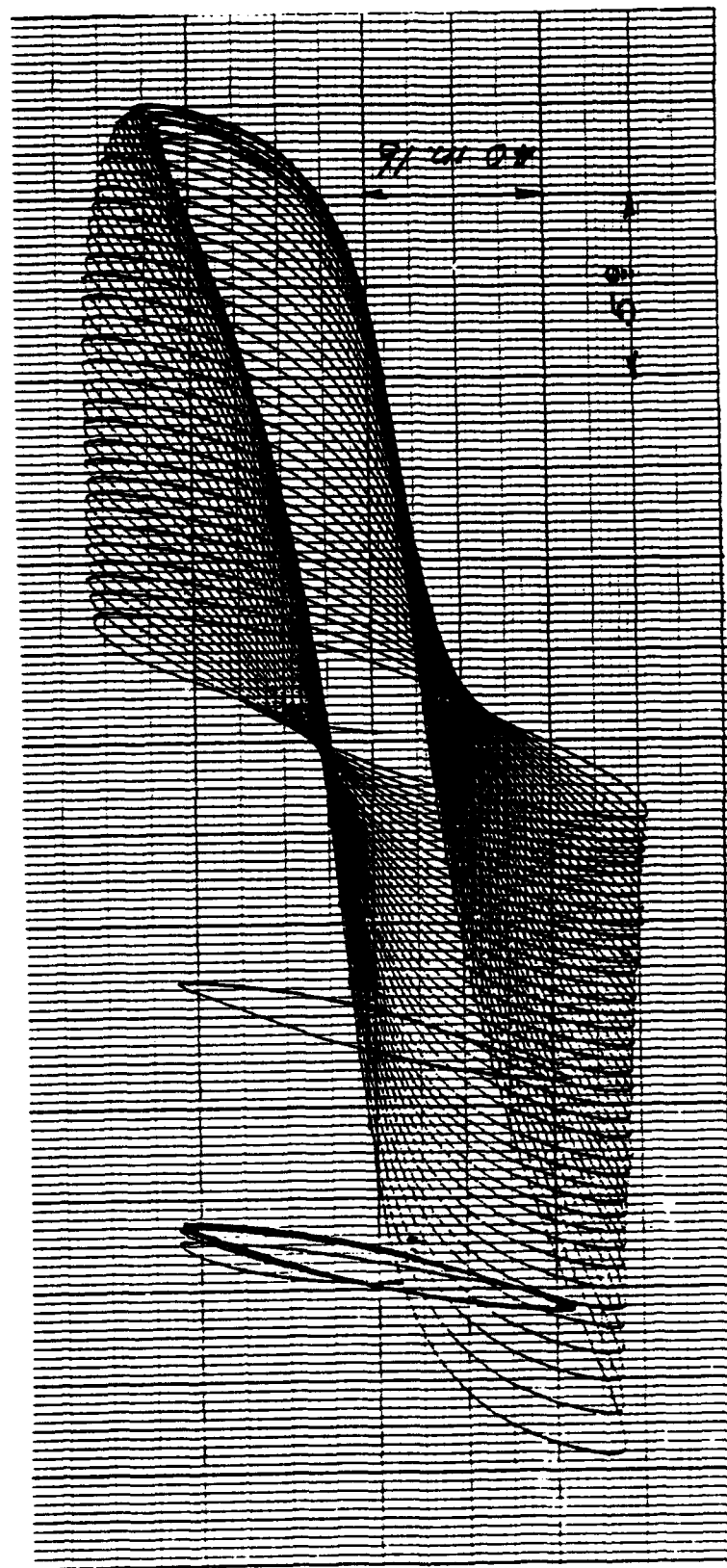


Figure 3.16 Decay of Shear Modulus and Increase in Damping of an Anisotropic EPK with an Inclined Crack

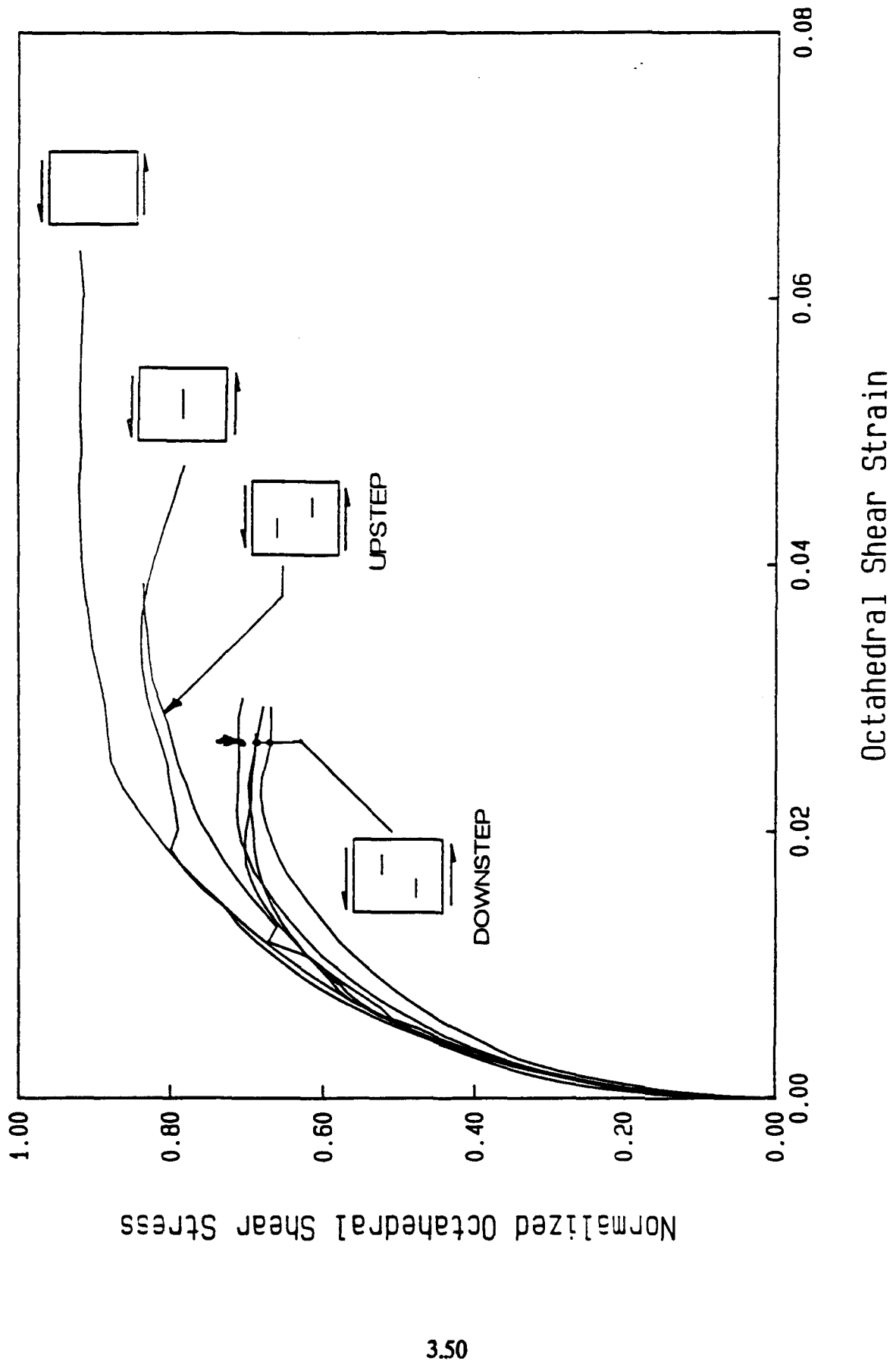


Figure 3.17a Influence of the Number of Cracks and Their Relative Position on the Strength

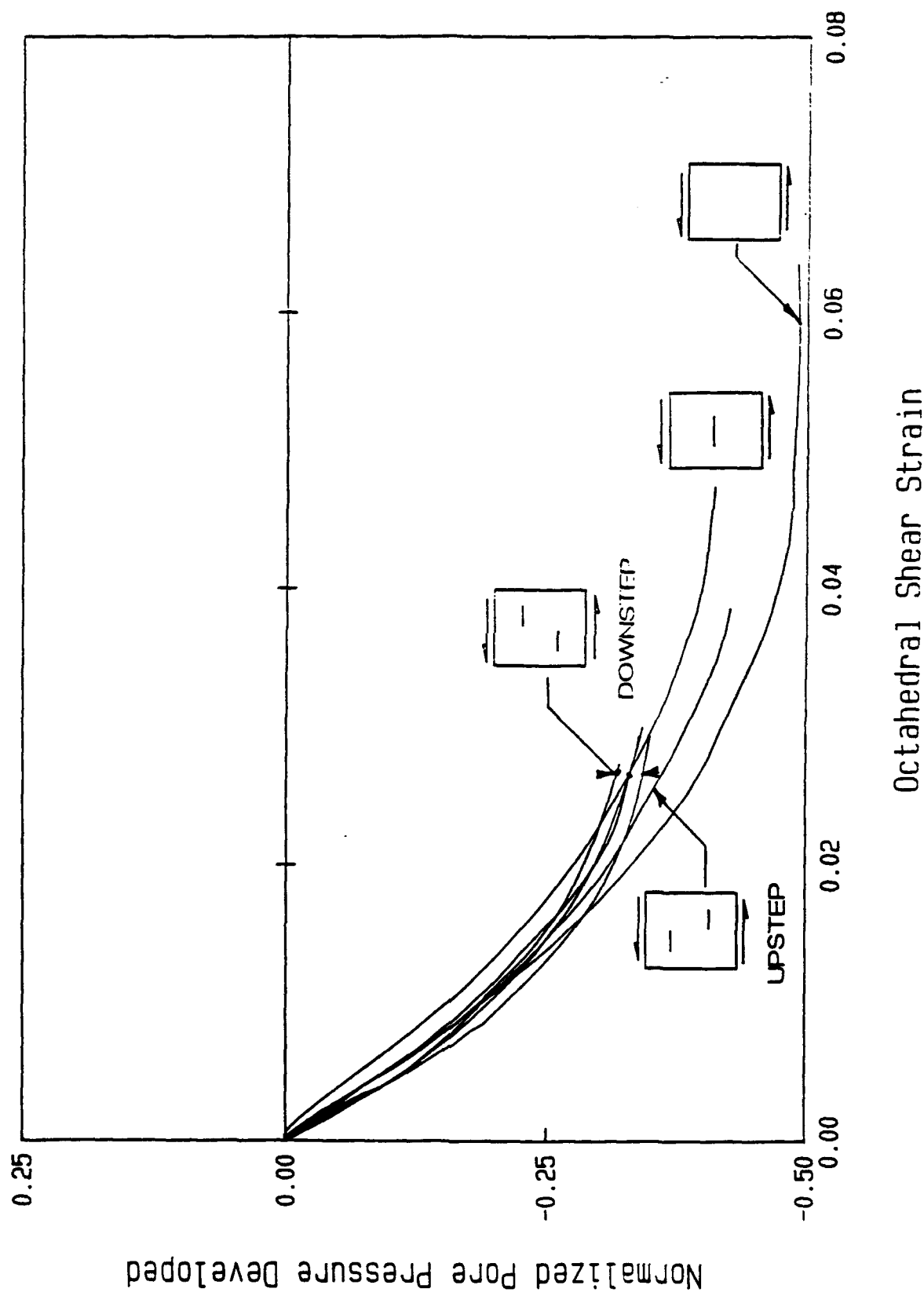


Figure 3.17b Influence of the Number of Cracks and Their Relative Position on the Pore Water Pressure

CHAPTER IV

KINEMATICS OF DEFORMATION, CRACK AND DAMAGE PROPAGATION

Photographs taken during and at the end of many of the tests listed in Tables 2.1 to 2.9 allow one to study the pattern of crack propagation, shear bands development and the relative displacement of the various parts of the specimens. One of the difficulties in developing constitutive equations is in the measurements of strains within the soil specimens. Once a shear line of slip band is formed, whether initiated by the existence of a crack or not, different parts of the specimen under test move as blocks. Bifurcation theories and models have been developed to mathematically describe, indeed predict those phenomena in various materials. The observations described in this chapter are but a first step in developing a model suitable to clay soils.

Discontinuities that occur during deformation have been classified by Morgenstern and Tchalenko (1967), as strain discontinuities and displacement discontinuities (Fig. 4.1). Strain discontinuities generally precede the displacement ones in front of the crack tip as well as in front of the propagating shear bands. The extensive photographic record made during deformation and failure allows us to follow the kinematics of the specimen while relating it to the resistance of the material. As previously stated, this record was digitized and stored in our data base so that a pattern of slip lines can be directly recalled and plotted without referring to the original photograph.

4.1 Specimens without Cracks under Static Loading.

Whether it is under axial loads or under a combination of axial and torsional loads, the maximum stress is reached before slip lines form. Close to the peak the deformations usually occur along a large number of slip surfaces often uniformly distributed along the

length of the cylinder. Such slip surfaces could not be clearly seen in the past because of the presence of filter paper, which inhibited the formation of some while emphasizing others; specially where the paper is slit to decrease its resistance. The photographs in the following figures illustrate those points:

Fig. 4.2 shows the slip lines formed on a specimen of H121 clay subjected to torsion;

Fig. 4.3a shows the slip lines formed on a specimen of EPK clay with which the external filter was made of vertical paper strips. Notice the shear bands between the strips;

Fig. 4.3b shows the vertical shear bands after very large torsional deformations in an EPK clay specimen; the localization being along the once vertical filter strips.

Fig. 4.4 shows the slip bands that develop where the filter paper is slit horizontally to decrease its resistance to torsion.

Figs. 3.6 which were partially commented on in Chapter III show the slip bands for a normally consolidated clay under two different stress paths and Figs. 3.11 show the slip bands for an overconsolidated clay under three different stress paths. No outer filter paper was used and the grid brings out the discontinuities that take place. All stress paths used in those tests resulted in the kind of discontinuities illustrated in Fig. 4.1. The photographs in those two sets of figures were taken at the end of the test; in other words after the release of the stresses acting on the specimens. Some rebound obviously occurred but one would expect that all parts would have suffered some permanent displacement. Figs. 3.6 which correspond to a normally consolidated clay support this expectation. However Figs. 3.11 which correspond to an overconsolidated clay show regions between the slip lines where the vertical grid has very little if no inclination. Also, it has been noticed during the tests that, at the instant of formation of the shear bands, some rebound takes place in the rest of the specimen.

The inclination of the observed shear bands when compared to the inclination of the principal stresses deserves comments. Table 4.1 lists normally consolidated clays from Tables 2.1 and 2.2 and overconsolidated clays from Table 2.4 together with their value of β , the inclination of the shear bands with the horizontal δ , and Θ the inclination of the shear bands on the major principal stress. Θ is seen to be nearly constant. Fig. 4.5 shows δ plotted versus b ($b = \sin\beta$). Similar results were obtained by Arthur and Dunstan (1982) for non-cohesive soils. This observation shows that the dilatation angle can be neglected; which is to be expected globally when the test is undrained.

The formation of the shear bands close to the peak stresses, and the subsequent occurrence of a deformation made of relative motion of blocks along those bands, forces one question the validity of the displacements measurements and the subsequent calculations of the strains. The jumps that one notices in the grids are clear indications of the total lack of uniformity at and beyond the peaks. Measurements during the strain softening period cannot be used to support or discredit many of the constitutive equations attempting to model the behavior of the material during this stage.

Additional photographs of shear bands and their digitized plots can be found in the following sections.

4.2 Specimens with One Crack under Static Loadings.

For an angle $\beta = 0$, i.e. for specimens in triaxial compression, the crack hardly affects the stress-strain behavior. Combination of axial and torsional stresses however, result in a shear band starting at and propagating from the tip of the crack, before the peak is reached. While in the absence of cracks we have a very large number of shear lines all around the specimen, here the number is limited to two or three all starting at the crack or emanating from each other. The first band starts at the crack tip with a slope that is

dictated by the stress concentration and the directions of the principal stresses there. It is the steepest, while the second and third start at a smaller slope. As they propagate however, they tend to run parallel to one another as the influence of the crack vanishes with distance.

Figures 4.6a, b and c show the shear bands for the three K_0 normally consolidated tests in Table 2.3 corresponding to $\beta = 30, 45$ and 60 degrees respectively. Notice the very large displacements in 4.6a and 4.6c. This is due to the fact that this was a stress controlled test where failure occurs in a catastrophic way if left unchecked. Compare now the patterns and directions of the slip lines obtained in Figs. 4.6 to those obtained if Figs. 3.6. While there seems to be an infinite (very large) number of shear bands in Figs. 3.6, the presence of the crack initiates and results in one or two main shear bands which propagate all around the specimen to cause failure. The fact that blocks of specimens move with respect to each others once the shear bands form is very striking when the crack is the initiator. In Figs. 4.6 many of the vertical lines remained nearly vertical after the load was removed and do not show discontinuities. Also, once one moves away from the crack the inclination of the shear bands is nearly the same whether the specimen has a crack or not. This is a clear indication that while the stress concentrations near the tip of the crack control the moment of initiation and the initial direction of the shear band, their influence quickly vanishes leaving the plasticity of the material in command of the kinematics of the specimen.

In Figs. 4.6 the main system of shear bands appears to be made of a primary band which develops first followed by secondary bands. In the figures, we shall use the notation of Morgenstern and Tchalenko (1967), in referring to those bands. The first, or primary, will be called S_1 , followed by $S_2, S_3 \dots$ etc., in the order they were observed to form. Those plots follow each photograph showing shear bands.

Table 4.2 lists the inclination of the shear bands emanating from the cracks. This table is to be read in conjunction with the digitized plots so as to see the level of approximation involved in such numbers. The table also lists the "Crack Sliding Displacement," (C.S.D.) for the various tests.

In Fig. 4.6a, and others corresponding to combinations of compression and torsion, one notices vertical shear bands. It is believed that such shear bands materialize at large deformations as a release mechanism for excessive shearing stresses.

The photographs show the magnitude of the slippage along each of the main shear bands. The slippage varies from band to band and along each band as indicated by the grid. It was often observed that when a primary shear band could not propagate any further because of boundary restrictions, secondary bands would emanate from it. This is seen in Fig. 4.6a and its digitized plot.

The case of Fig. 4.6c is special in that the shear bands form and propagate essentially along the original direction of the crack: Primary and Secondary bands overlap and meet.

Figs. 4.7a and b show the results of the same test conducted under controlled stress and under controlled deformation respectively, but with fixed length. The pattern of deformation is practically identical including the verticality of the grid lines below the crack. One major slip line develops and stops after a while; a second and a third one take over until failure takes place. Notice that the bands are more inclined than those appearing in Fig. 4.6b because of the axial stresses that develop when the specimen is prevented from increasing in length. Once the main shear band and its first or second offshoots propagate, practically all the deformations take place along those bands with the original crack as part of the slip surfaces. The grid shows that hardly any permanent

deformation takes place in the rest of the specimen. Also notice that Fig. 4.7a indicates a crack shear displacement twice as large as that seen on Fig. 4.7b.

Inclined cracks results in shear bands that start at the tip too and again, at a short distance from the crack, take a direction dictated by the plastic behavior of the clay. Fig. 4.8a shows the pattern caused by a downstep crack inclined at 45 degrees when the specimen is subjected to torsion and free to deform axially. Additional shear bands having no physical connection with the crack develop at the peak. This can clearly be seen on the photograph as well as on the digitized plot.

Fig. 4.8b shows the results of a test identical to the one above but with the crack in an upstep position; the slip lines at the front and tail of the cracks have the same inclinations in both cases. In the first case, however, the crack is part of the surface along which the blocks move, while in the second case it is not.

Fig. 4.8c shows a downstep crack inclined at 22.5 degrees. Here, a shear band emanates from the tip and keeps nearly the same direction as that of the crack. Also, there is appreciable crack sliding displacement (C.S.D.) when compared to the two previous cases. Only one shear band passing through the crack was noticed, in other words the specimen became two blocks moving with respect to each other.

The pattern of shear bands in Figs. 4.8 is extremely instructive as to the influence of the inclination of the principal stresses on the direction of the crack. In the case of the downstep crack (Fig. 4.8a) torsion results in a combination of tension across the face of the crack and compression along it. This results in a weak point at the tip of the crack resulting in an initiation of a shear band there. On the other hand, in the case of the upstep crack (Fig. 4.8b) the directions of tension and compression with respect to the crack are reversed resulting in compression across the faces. The specimen reacts as if there was no crack and the normal development of shear bands takes place; one of which is seen to be passing

through the tip (Fig. 4.8b). In both the cases above the magnitude of the Crack Sliding Displacement is negligible. The crack remains closed due to hydrostatic stresses and the shear along the faces are negligible.

For all the specimens with a crack the shear bands show up first before the peak is reached. This, generally causes a more or less pronounced kink in the stress strain curves.

The shear bands observed for overconsolidated clays are in general more sharply defined than the ones obtained for K_o normally consolidated clays. The tests listed in Table 2.5 illustrate this fact specially the ones conducted under controlled rotation conditions:

Figs. 4.9a, b and c show the shear bands for $\beta = 30, 45$ and 60 degrees respectively. The specimens are free to deform axially. Note in Fig. 4.9a the limited number of shear bands starting at the tip of the crack and spreading circumferentially around the specimen. Fig. 3.11a which corresponds to the same conditions without crack has practically the whole specimen covered with slip lines. Similar situations are encountered for the cases of torsion and combinations of tensions and torsion as shown in Figs. 4.9b and c on one hand, and Figs. 3.6a, 3.6b and Figs. 3.11a and 3.11b, and 3.11c on the other hand.

It is also interesting to notice that isotropically overconsolidated specimens result in a diffuse zone of shear bands starting at the tip of the crack, but with limited propagation. There were no displacement discontinuities similar to the ones occurring in the K_o consolidated cases. Fig. 4.9d shows this pattern. It appears that random orientation of clusters and particles impedes the formation of continuous shear bands.

Figs. 4.10a to f show the shear bands when the length of the specimen is kept constant and when the size of the crack varies from $a/l = 0$ to $a/l = 0.4$ (Table 2.5). Fig. 4.10a, for $a/l = 0$, shows only one shear line. On the other hand, Fig. 3.11b which corresponds to the same test but with free axial deformation indicates the presence of a

large number of slip lines. It appears that the compressive forces that are axially generated to prevent the specimen from elongating are sufficient to keep the multitude of slip lines seen on Fig. 3.11b to form and become active. The deformation then amounts to two blocks slipping on each others. The vertical lines of the grid remain continuous except where they cross the slip line. By looking at all of Figures 4.10a to 4.10f one notices that as one moves away from the crack the primary shear bands adopt the inclination of the one seen in 4.10a indicating once more a shear behavior dictated by the plasticity of the material and not by the stress concentration in the close vicinity of the crack. It is to be noticed however that beyond $a/l = 0.2$ the pattern of shear bands is very much influenced by the size of the cracks with respect to the overall size of the sample. It is not known how the stress distribution in the specimen is affected by the fact that we do not really have a hollow solid cylinder subject to pure torsion and that averaging the stresses around the circumference is not a valid approximation.

4.3 Specimens with One Crack under Dynamic Loading.

Slow cyclic loading in torsion results in a horizontal crack propagating horizontally, preceded and surrounded by a damage zone. The slow cyclic loading allows the development of a herringbone type of shear bands that propagate on both sides of the crack as it advances. It is essentially the first band that is formed in the static test that keeps being generated as the crack advances and the stresses are reversed. It is interesting to note that most of the damage and deformation are localized in a strip on both sides of the propagating crack. While it was thought that this kind of damage could only occur in overconsolidated clays, tests conducted on normally consolidated clays show that the same characteristics are present there too; even though the magnitude of the torque was about 60 percent of the peak reached under static loading. (Remember that in the static case the

shear bands appear at about 80 percent of the peak). Figs. 4.11a and b show the results of two tests listed in Table 2.6 and 2.7, both at fixed length, the first on a normally consolidated specimen and the second on an overconsolidated one. Fig. 4.12 shows the results obtained with a normally consolidated H121 clay also subjected to cyclic torsion with fixed length. All cases show a similar herringbone pattern and a crack propagating in the horizontal direction. The pattern obtained when the specimen is free to deform axially while being subjected to cyclic torsion is not any different as indicated by Fig. 4.13. Tests conducted on isotropic overconsolidated clays led to a damage strip significantly narrower than the ones obtained with K_o overconsolidated anisotropic clays. It appears, as previously noticed, that randomly oriented clusters do not result in well defined shear bands. Fig. 4.14 clearly illustrates those conditions.

Cyclic loading on a specimen with an inclined crack resulted in very small herringbone shear bands starting at the tip of the crack and spreading in a horizontal direction; showing again that the shear bands and damage zones are primarily controlled by the system of stresses and the plasticity of the clay (Fig. 4.15).

Sometimes, in the case of a very brittle highly overconsolidated clay under small confining pressure, the specimen fails under a single cycle showing a pattern very much in line with the predictions of classical fracture mechanics. Fig. 4.16 is a photograph of a specimen that failed under those conditions. Notice the symmetry of the fracture lines due to tensile stresses that develop at the tip.

The impulse loading which is a fast monotonic loading does not allow for any shear band to seriously develop. As shown in Fig. 4.17a, which was taken at the end of the test, most of the vertical lines remain continuous and at best the type of discontinuity shown in Fig. 4.1a is present near the crack. Away from the crack the shearing strains are well distributed showing no influence of crack or block relative motion. Fig. 4.17b shows a

series of photographs taken with an SP2000 high speed camera at 0.5m sec intervals during a similar impulse test (Lesser 1989). The material and configuration are the same as the ones used in Fig. 4.17a, but the clay here is overconsolidated.

4.4 Specimens with Two Cracks.

Here the relative position of the cracks plays an important role in the development of the shear bands. The interaction of the cracks depends, not only on their relative position but also on the direction of the applied torsional shear stress. In this investigation the shearing stresses were always applied in one direction and the position of the cracks changed as shown in Table 2.8. The cracks when placed in a downstep position result in a tensile instability (local necking) which is quite localized and allows the specimen to still resist additional loading without failing. This result of the superposition of two zones with high tensile stress was illustrated by Vallejo (1989). Actual calculation of stress distributions will be given in Chapter V. Fig. 4.18 shows the interference of two zones of high tensile stress at the tips of two cracks. This is the first test listed in Table 2.8 and for which $e = 0.0$ and $d = 0.6$ cm. The interference appears as a dark hole in the figures. Indeed, at this location the specimen becomes locally much thinner to the point that the inner and outer membranes touch each other. The very local tensile failure takes place even though the material is under general hydrostatic compression while being subjected to torsion. Fig. 4.19, on the other hand shows two systems of shear bands each developing and spreading on its own without visible interference effects. Here the cracks are in the upstep position.

With the cracks in the downstep position and e increasing there comes a distance at which the superimposed tensile stresses are not large enough to overcome the compressive spherical stresses. Figs. 4.20, 4.21 and 4.22 show the pattern of shear band development as

e takes successive values of 0.6 cm, 1.3 cm and 2.54 cm. At $e = 2.54$ cm the crack tips are far enough from one another so that no tensile instability takes place. In all downstep cases, the shear bands pattern resembles quite closely that observed for large single cracks. Indeed, once the necking takes place the two cracks behave as a single large one.

Table 4.3 lists the inclinations of the shear bands and the C.S.D.'s for the case of two cracks.

While examining the photographs notice that the crack shear displacement is often nearly equal to the unit size of the grid (0.6 cm). There are reference grid lines on each photograph that indicate the size of the displacement.

4.5 Shear Bands Propagation and Their Measurements.

The series of photographs taken at the initiation of a shear band (at the tip of a crack), and during its subsequent propagation allow one to plot relations involving the length of the band, the angle of rotation of the top of the specimen with respect to its fixed bottom, the amount of slip measured along the band, etc.... All the tests for which such graphs were generated are listed in Table. 2.5

Fig. 4.23 shows the length of the shear band versus the angle of rotation for specimen 18-1-15-91. Fig. 4.24 shows the amount of slip measured along the first shear band at the end of the test. This is the kind of displacement discontinuity shown in Fig. 4.1c. Fig. 4.25 shows the amount of slip measured along the first shear band for various angles of rotation.

Figs. 4.26 and 4.27 correspond to specimen 66-05-29-91, tested under variable length conditions. These two figures differ from their counterparts in Figs. 4.23 and 4.24 in that they show the slip along the second shear band.

Figs. 4.28 and 4.29 correspond to specimen 16-12-13-90, tested under fixed length conditions.

Figs. 4.30 and 4.31 correspond to specimen 70-06-14-91, tested under combinations of tension and torsion.

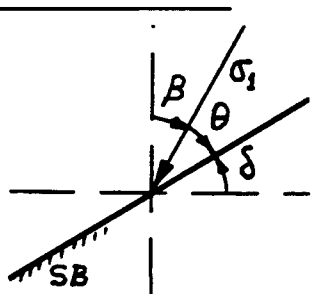
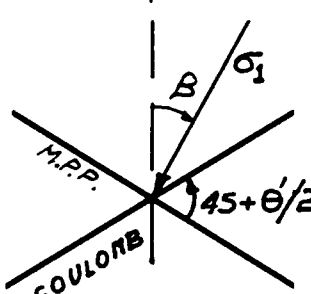
In all the cases observed, the formation and propagation of the shear bands was stable. The length of the shear band varies linearly with the angle of rotation (Figs. 4.23, 4.26, 4.28 and 4.30). The second shear band, after its initiation propagated at a rate faster than that of the first one; it also became the dominant one.

The appearance of additional shear bands beyond the first, depends on the amount of rotation induced in the specimen, the end effects, the presence of the inclusion formed by the teflon strips, and the fact that the first shear band may not be propagating in the direction of the original crack (see Fig. 4.8c)

The slip that takes place along each shear band varies with the distance from the tip of the crack (Figs. 4.24, 4.27, 4.29 and 4.31). While it was possible to approximate this relation with a straight line in Figs. 4.24 and 4.25, this is not the case in Figs. 4.27 and 4.28. The appearance of secondary branches affects the magnitude of the slip and leads to a more complex relation between the two variables. At the point of branching, it was noticed that the magnitude of the slip along the main band is nearly equal to the sum of the magnitudes along each of the branches.

The measurements and observations above are the ingredients needed to test the validity of the various models that have been, or will be proposed for bifurcation and shear banding resulting from localization. The level of accuracy of such measurements, although reasonably limited by the fact that observations are made from outside the cell, is more than sufficient to evaluate the suitability of a behavioral model.

TABLE 4.1 - INCLINATION OF SHEAR BANDS FOR VARIOUS
INCLINATIONS OF MAJOR PRINCIPAL STRESSES; NO CRACK

TABLE	$\bar{\sigma}_c$	DESIGNATION	β°	δ°	θ°	
1	241.5	32-1-31-91	30	32	28	
	241.5	33-2-5-91	45	17	28	
	552	37-2-19-91	30	29	31	
	552	38-2-21-91	45	19	26	
	345	62-5-16-91	30	29	31	
	345	61-5-14-91	60	0	30	
	345	61b-11-19-91	60	0	30	
4	O.C	89-8-1-91	30	31	29	
	O.C	86-7-23-91	45	14	30.5	
	O.C	90-8-13-91	60	-1	31	

**TABLE 4.2 INCLINATION OF THE SHEAR BANDS AND CRACK SLIDING
DISPLACEMENT (C.S.D.); ONE CRACK**

REF. TABLE	DESIGNATION	C.S.D. (cm)	LEFT SIDE		RIGHT SIDE	
			LABEL	ANGLE °	LABEL	ANGLE °
2.3	51-04-5-91	2.20	S_1 S_2	32 35	S_1 S_2	30 26
	6V-09-26-90	0.64	S_1 S_2	30 25	S_1 S_2	28 22
	52-04-09-91	1.27	S_1 S_2	0 3	S_1 S_2	6 5
	3f-02-06-90	1.91	S_1 S_2	25 22	S_1 S_2	35 32
	6f-06-21-90	0.95	S_1 S_2	28 20	S_1 S_2	33 28
	56-04-17-91	0.16	S_1 S_2	20 20	S_2	17
	57-04-19-91	0.8	S_1 S_2	19 17	S_1	20
	58-04-23-91	0.89	S_1	20	S_1	20
2.9	6F-09-17-90	0.64	S_1 S_2	30 24	S_1 S_2	36 32
2.4	71-09-06-90	0.64	S_{1u} S_{1l}	23 8	S_{1u} S_{1l}	23 9

COMMENTS: Specimen 7a-09-06-90 is isotropic and results in a diffuse zone of shear bands. Subscripts u and l refer to upper and lower bounds respectively.

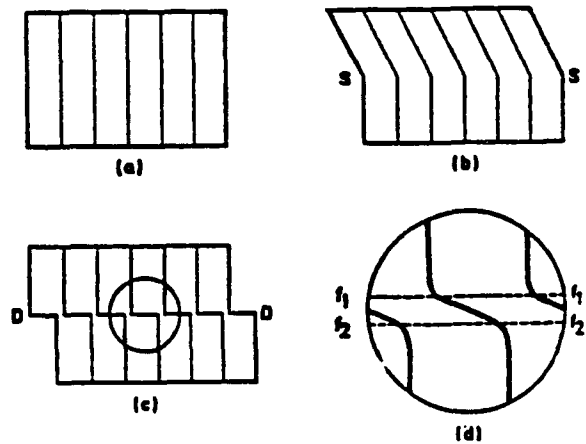
(continued)

TABLE 4.2

REF. TABLE	DESIGNATION	C.S.D. (cm)	LEFT SIDE		RIGHT SIDE	
			LABEL	ANGLE °	LABEL	ANGLE °
2.5	68-06-05-91	0.89	S ₁ S ₂	38 33	S ₁ S ₂	39 33
	66-05-29-91	0.95	S ₁ S ₂	24 25	S ₁ S ₂	30 23
	70-06-14-91	0.36	S ₁ S ₂	6 -8	S ₁ S ₂	4 -7
	16-12-13-90	0.45	S ₁ S ₂	30 21	S ₁ S ₂	28 18
	18-01-15-91	0.43	S ₁ S ₂	29 26	S ₁ S ₂	35 33
	15-11-28-90	0.64	S ₁ S ₂	30 29	S ₁ S ₂	34 34
	13-11-07-90	0.71	S ₁ S ₂	31 27	S ₁ S ₂	37 31
	14-11-20-90	0.76	S ₁ S ₂	27 27	S ₁ S ₂	33 27

**TABLE 4.3 INCLINATION OF THE SHEAR BANDS AND CRACK SLIDING
DISPLACEMENT (C.S.D.); TWO CRACKS**

REF. TABLE	DESIGNATION	C.S.D. (cm)	LEFT SIDE		RIGHT SIDE	
			LABEL	ANGLE °	LABEL	ANGLE °
2.8	81-07-03-91	0.51	S_1 S_2	33 28	S'_1 S'_2	27 24
	82-07-09-91	0.25-0.50	S_1 S_2 S'_1 S'_2	27 14 30 20	S_1 S_2 S'_1 S'_2	26 18 22 19
	83-07-11-91	0.63	S_1	25	S'_1 S'_2	22 20
	84-07-17-91	0.51	S_1 S_2	25 23 17	S'_1 S'_2	26 18
	85-07-19-91	0.63	S_1 S_2	27 17	S'_1 S'_2	26 22



Types of Discontinuity in Deformation [2]

- (a) Unstrained State
- (b) Strain Discontinuity SS
- (c) Displacement Discontinuity DD
- (d) Magnification of Central Portion of DD Showing Two Strain Discontinuities $f_1 f_1'$ and $f_2 f_2'$.

Figure 4.1 Morgenstern and Tchalenko's Definitions

3.2

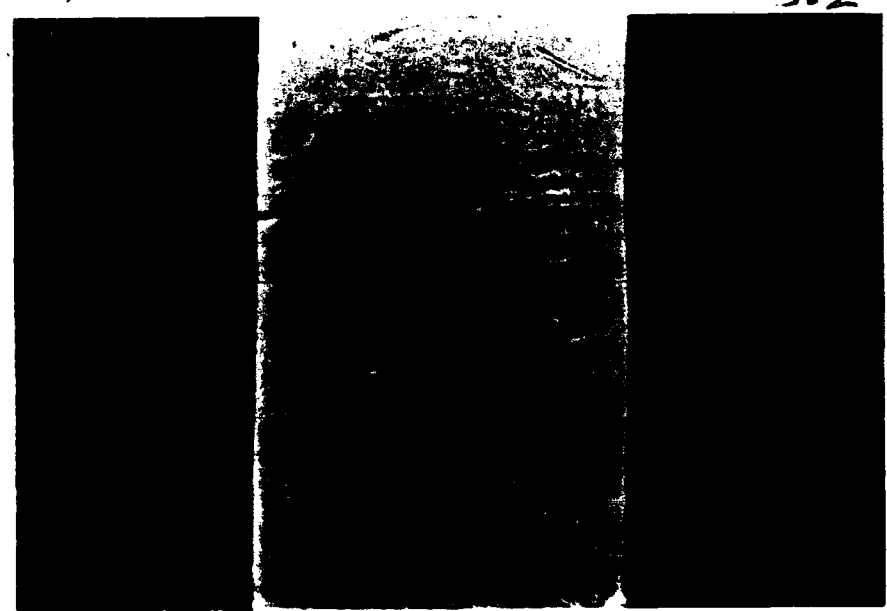


Figure 4.2 Multiple Shear Bands in an H121 Clay in Torsion



Figure 4.3a Influence of the Filter Paper on the Formation of Shear Bands

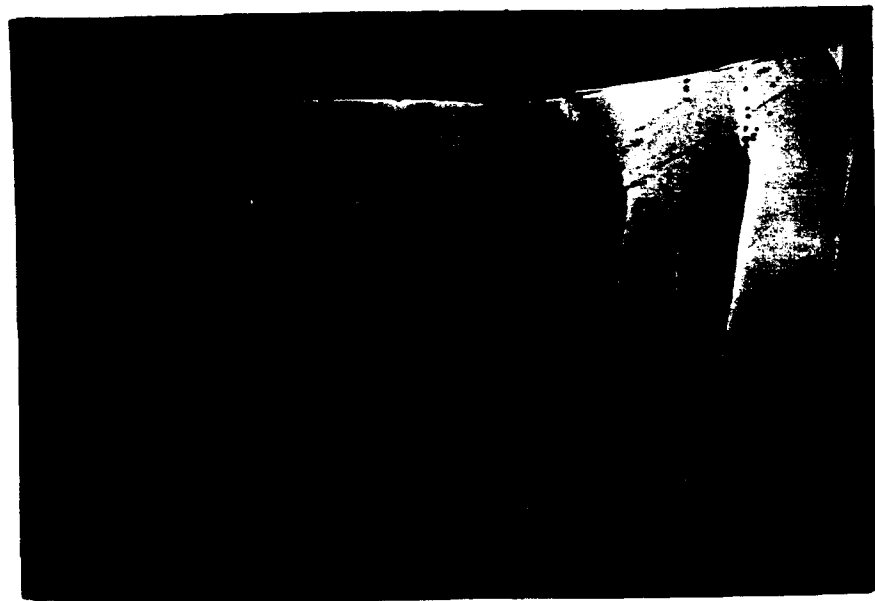


Figure 4.3b Influence of the Filter Paper on the Formation of Shear Bands

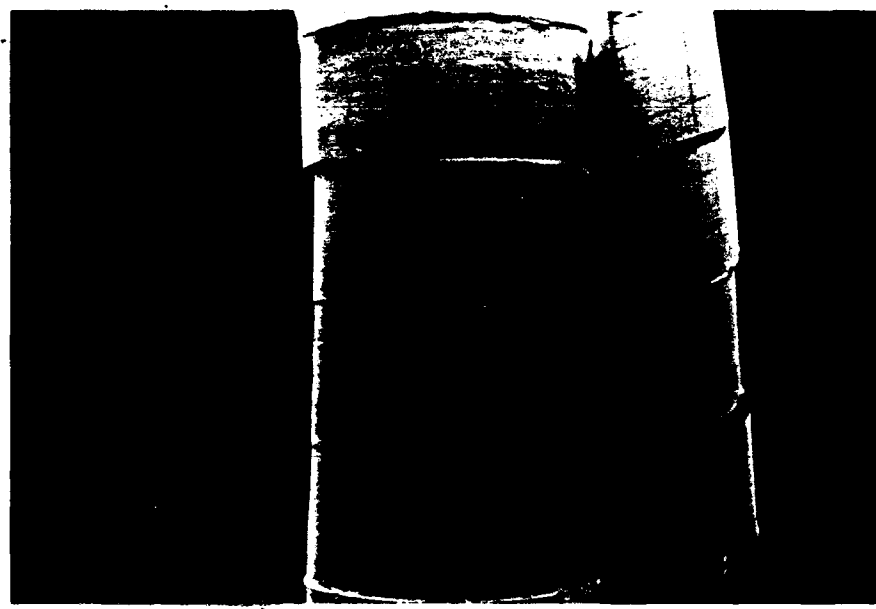
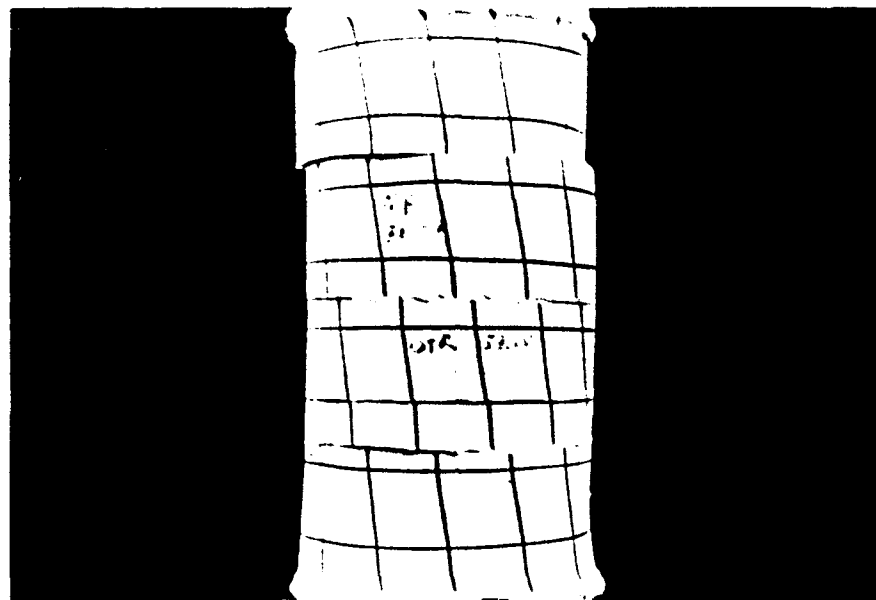


Figure 4.4 Influence of the Filter Paper on the Formation of Shear Bands

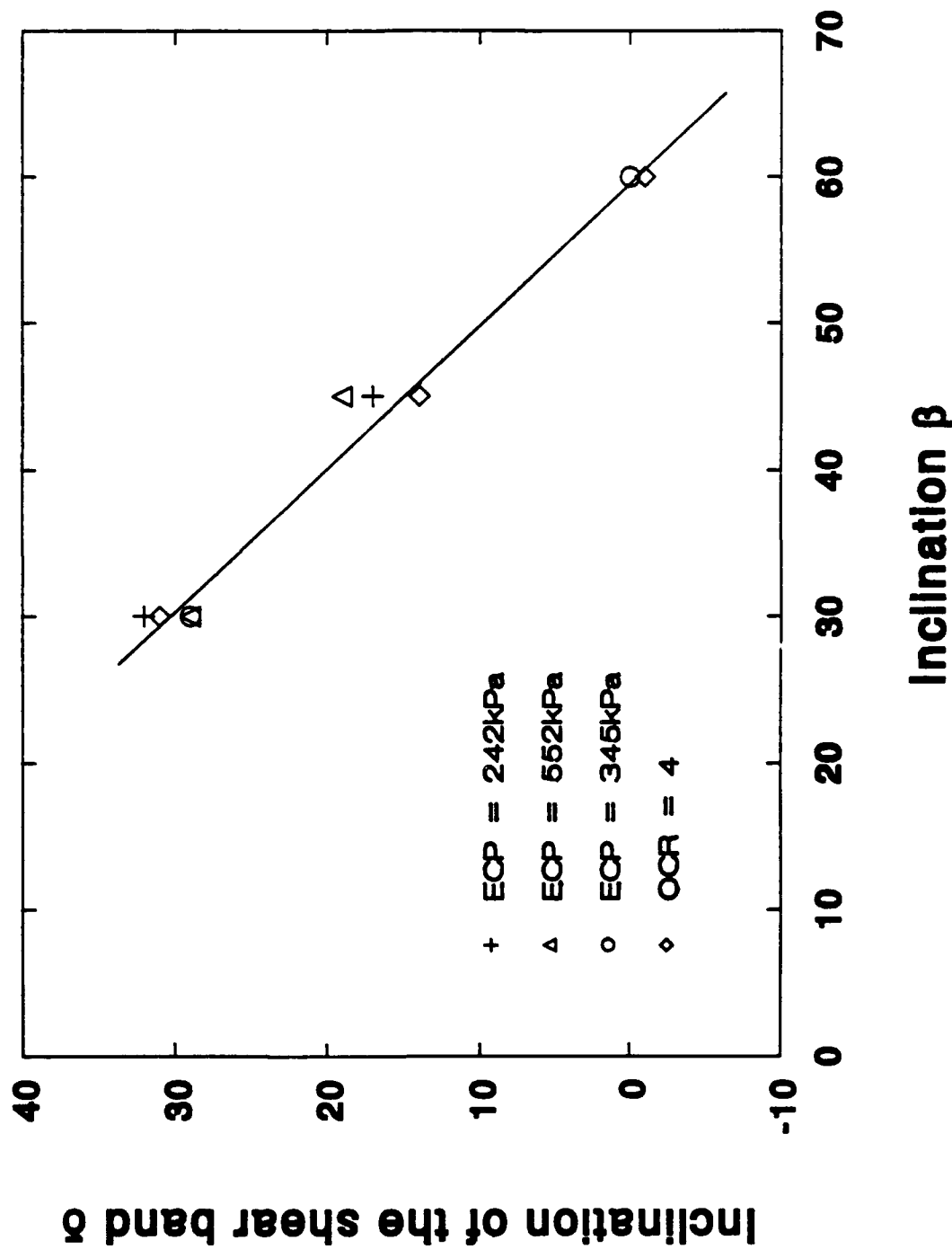


Figure 4.5 Inclination of the Shear Bands



Test Name: 51_04/05/91 Consol.: Ko NC Beta: 30
Material: EPK 345 kPa Control: Stress
Height: Variable

Figure 4.6a Shear Bands for One Crack and $\beta = 30^\circ$

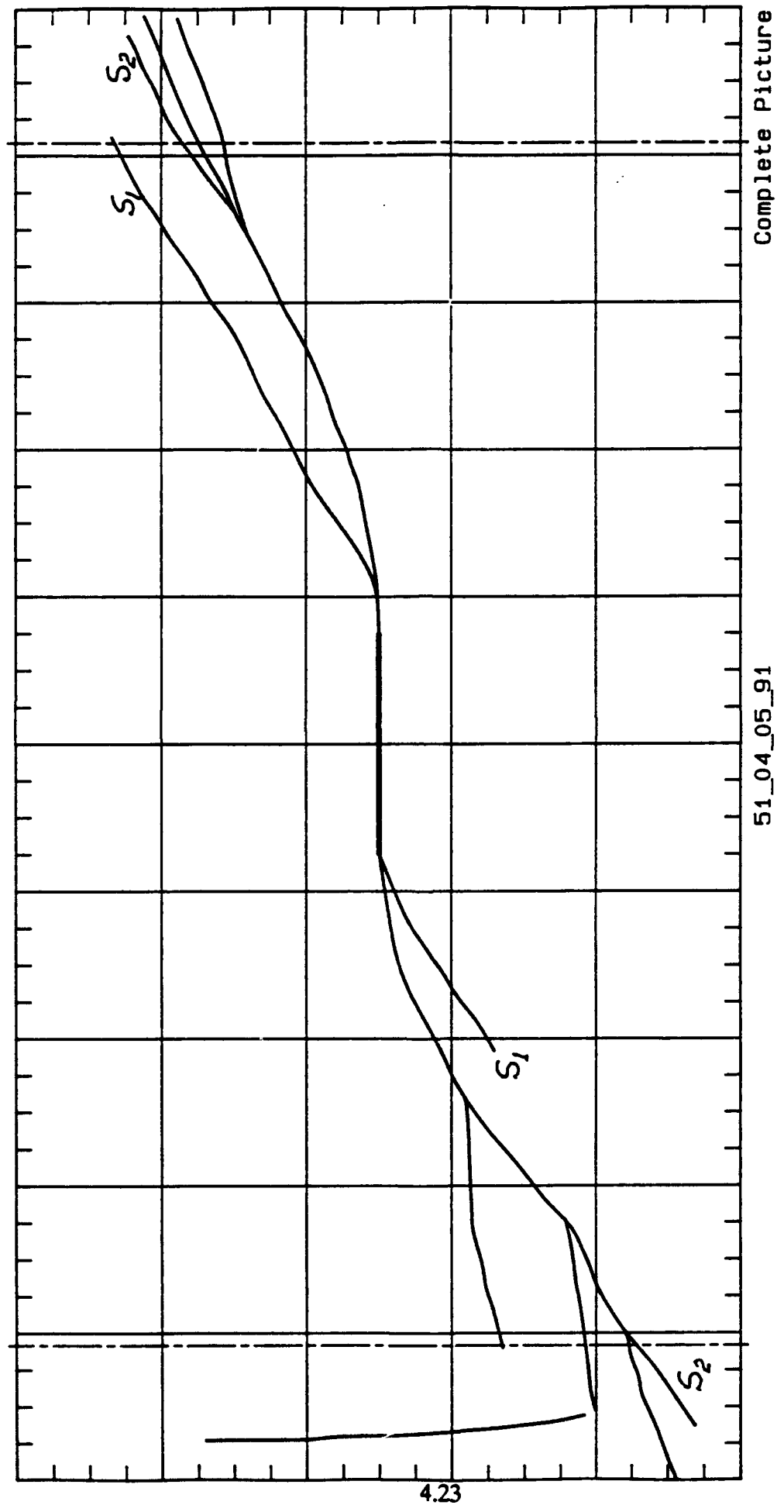
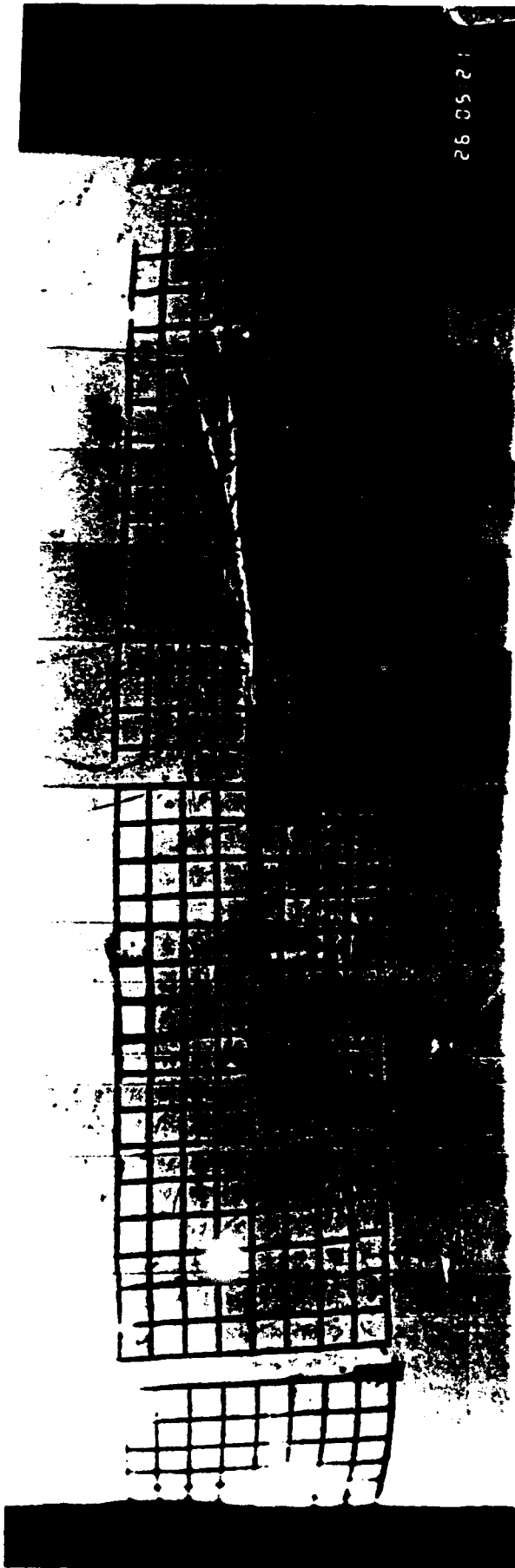


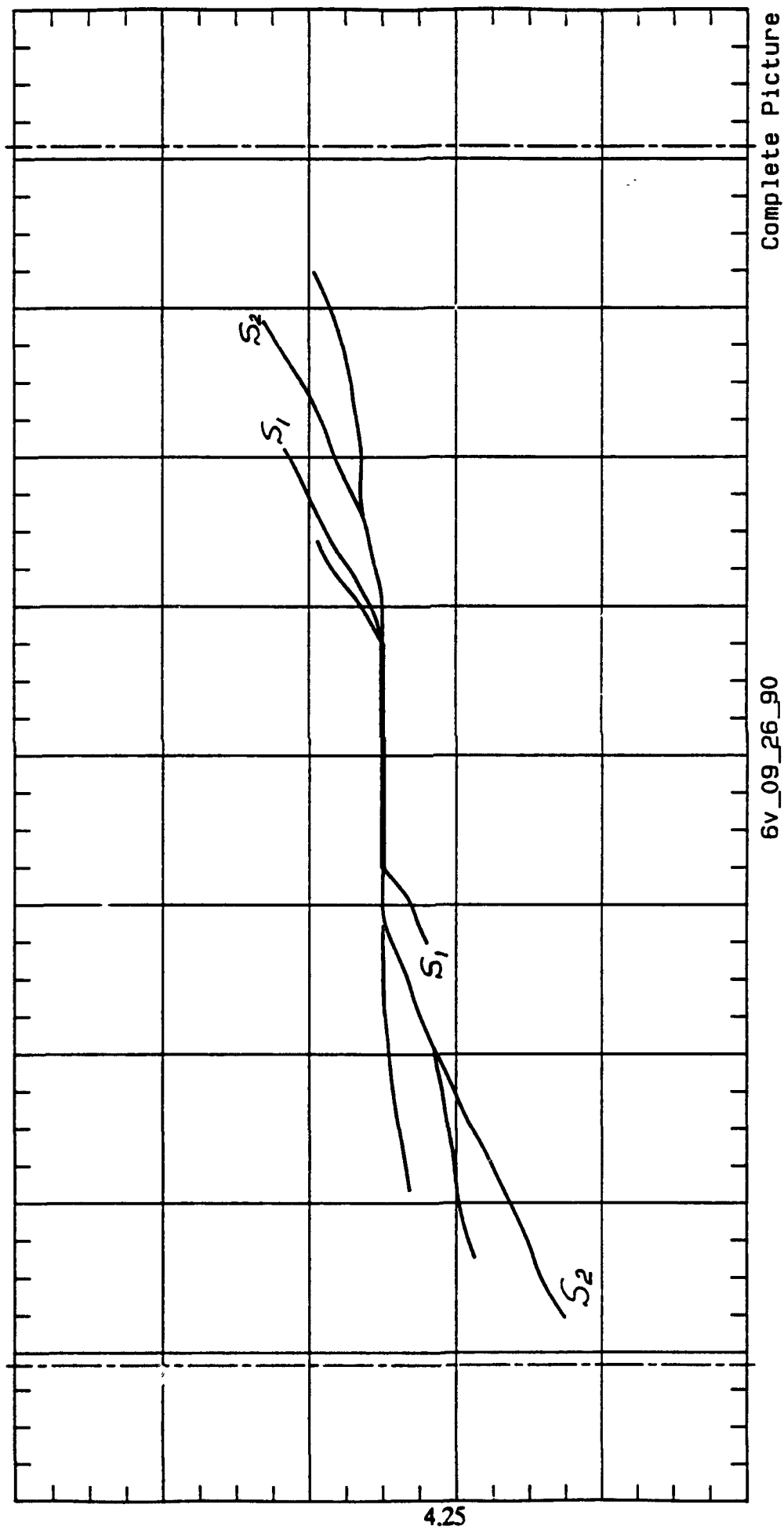
Figure 4.6az Shear Bands for One Crack and $\beta = 30^\circ$

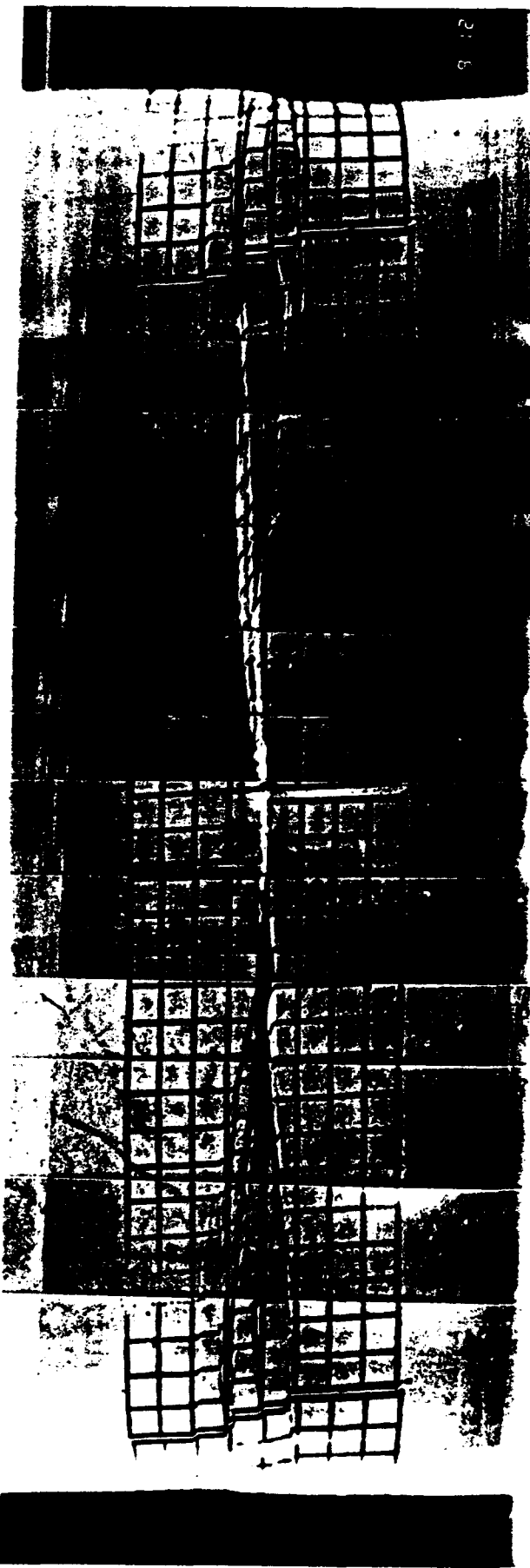


Test Name: 6v_09/26/90 Consol.: K0 NC
Material: EPK Beta: 45
 345 kPa Control: Deform.
 Height: variable

Figure 4.6b Shear Bands for One Crack and $\beta = 45^\circ$

Figure 4.6bz Shear Bands for One Crack and $\beta = 45^\circ$





Test Name: 52_04/09/91 Consol.: Ro NC Beta: 60
Material: EPK 345 kPa Control: stress
Height: variable

Figure 4.6c Shear Bands for One Crack and $\beta = 60^\circ$

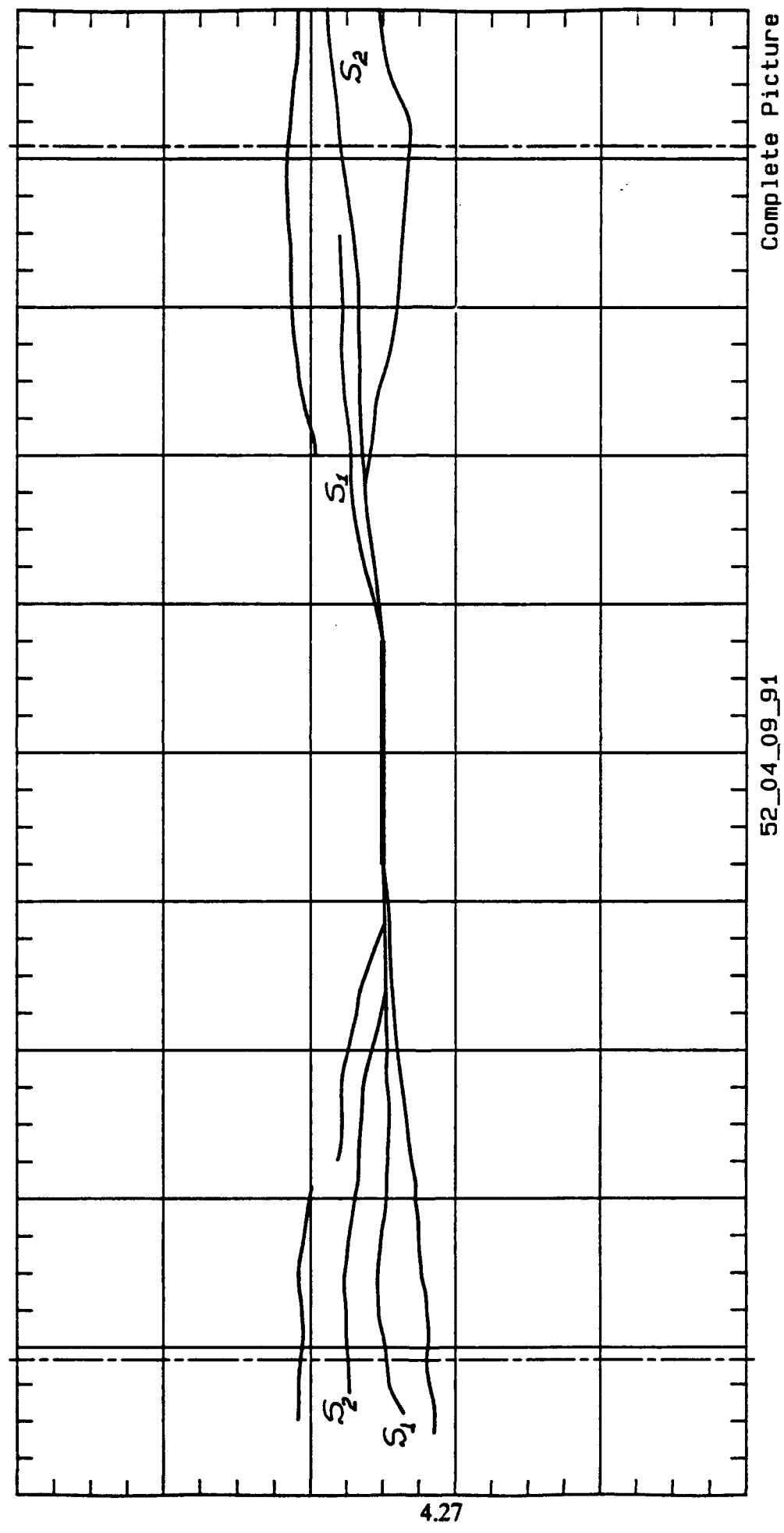


Figure 4.6cz Shear Bands for One Crack and $\beta = 60^\circ$

Figure 4.7a Shear Bands for One Crack Under Torsion with Fixed Length



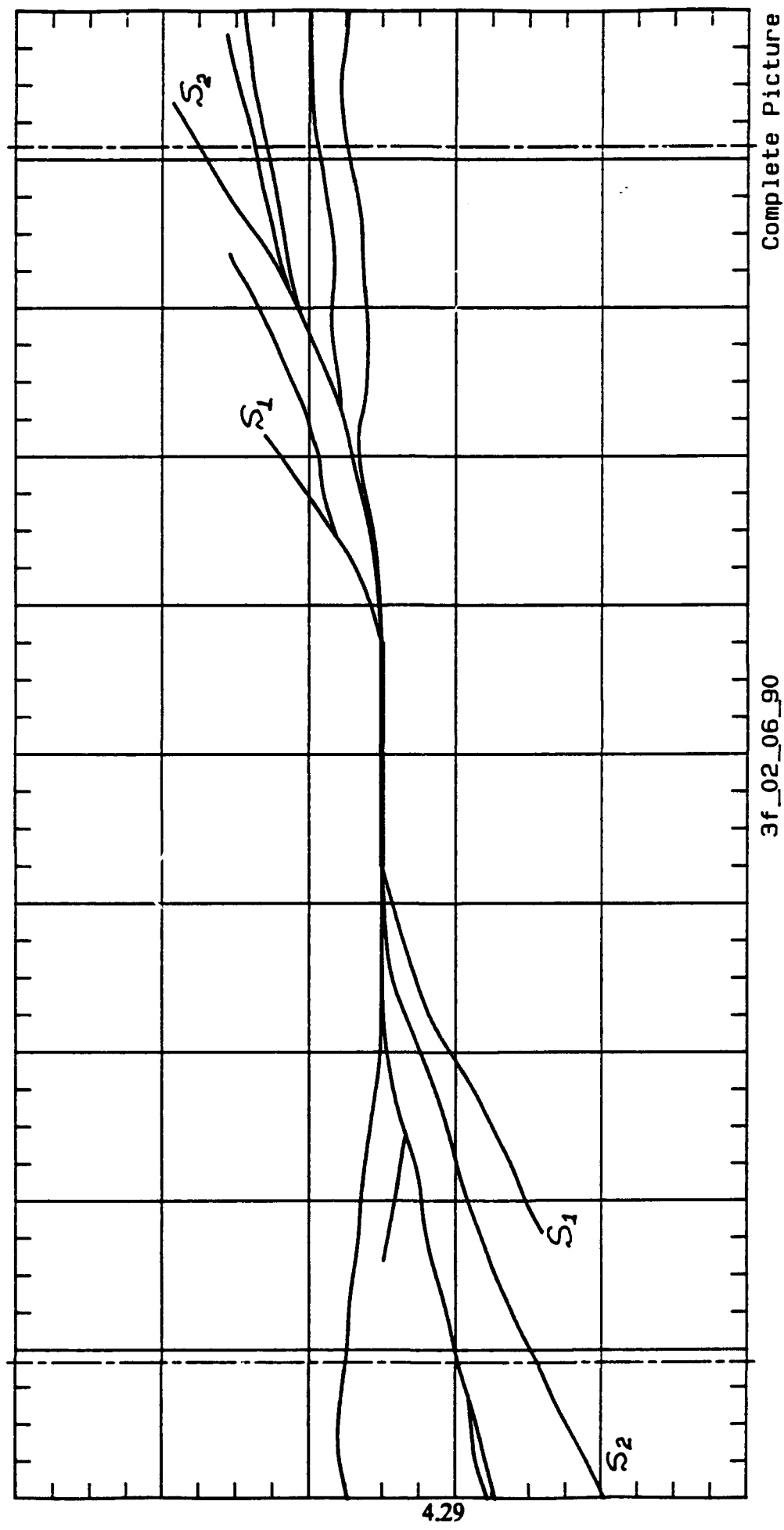
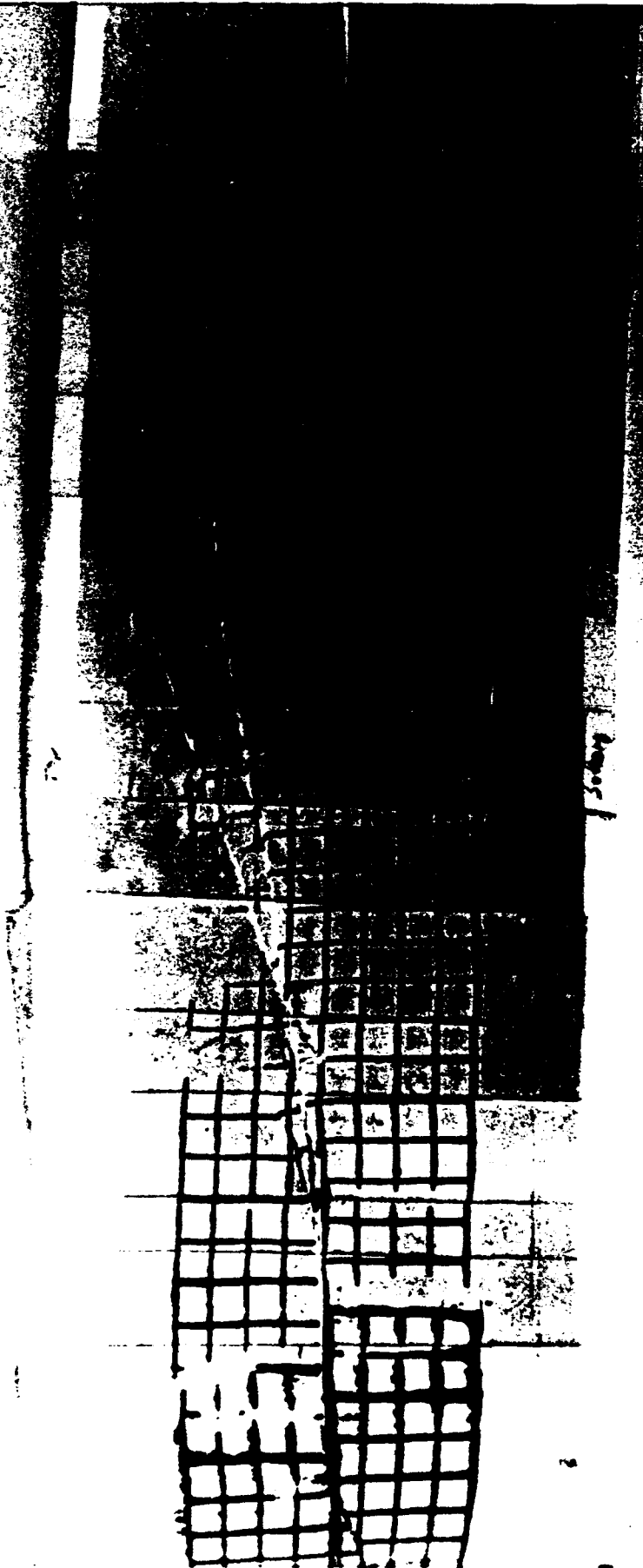


Figure 4.7az Shear Bands for One Crack Under Torsion with Fixed Length

Figure 4.7b Shear Bands for One Crack Under Torsion with Fixed Length

Test Name: 6f_06/21/90 Consol.: No NC
Material: EPK 343 kPa Contact
Length: 3.0 mm



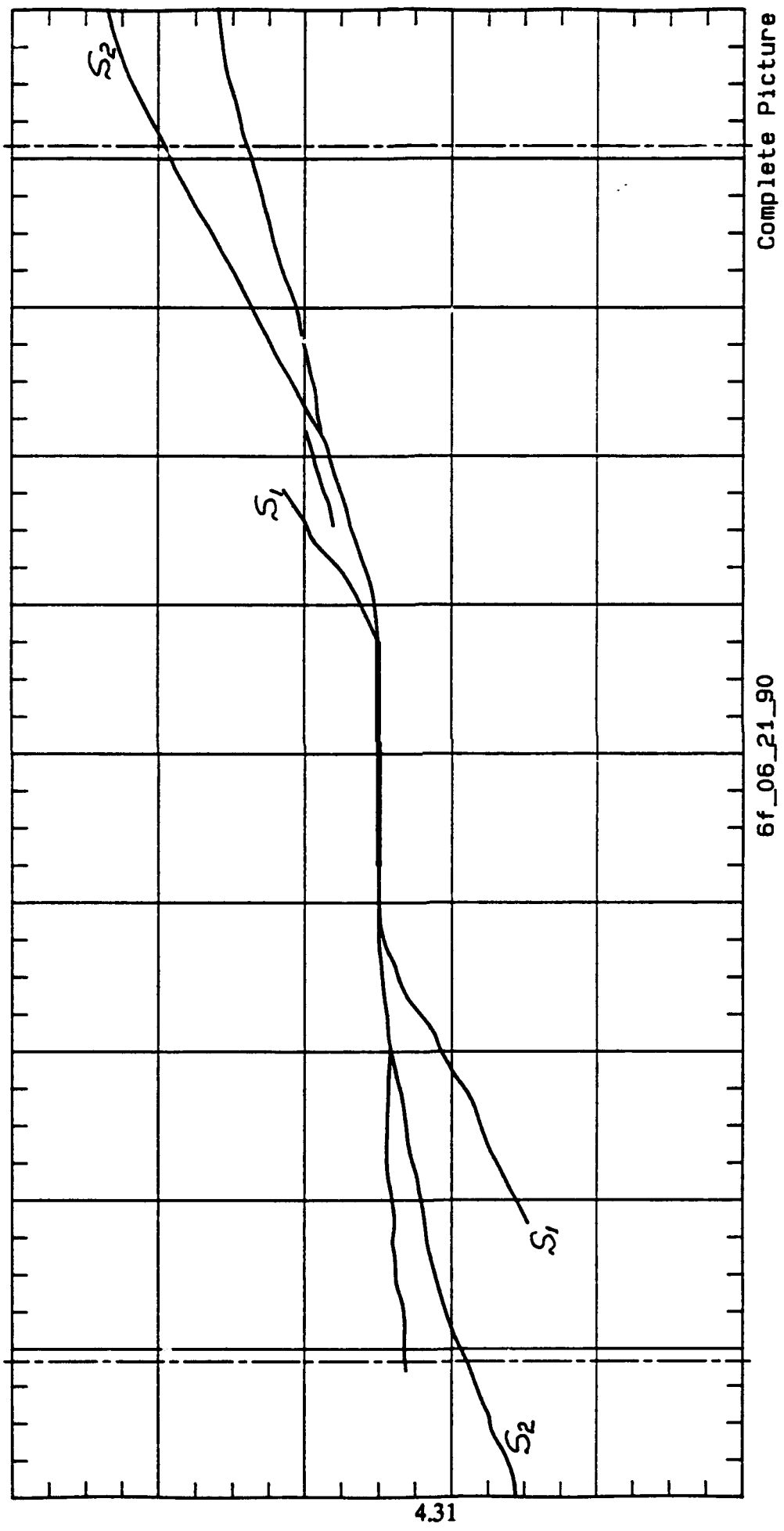


Figure 4.7bz Shear Bands for One Crack Under Torsion with Fixed Length



Test Name: 56_04/17/91 Consol.: Ro NC
Material: EPK Beta: 45
Control: Deform.
Height: variable

Figure 4.8a Shear Bands for an Inclined Crack in the Downstep Position;
 $\alpha = 45^\circ$

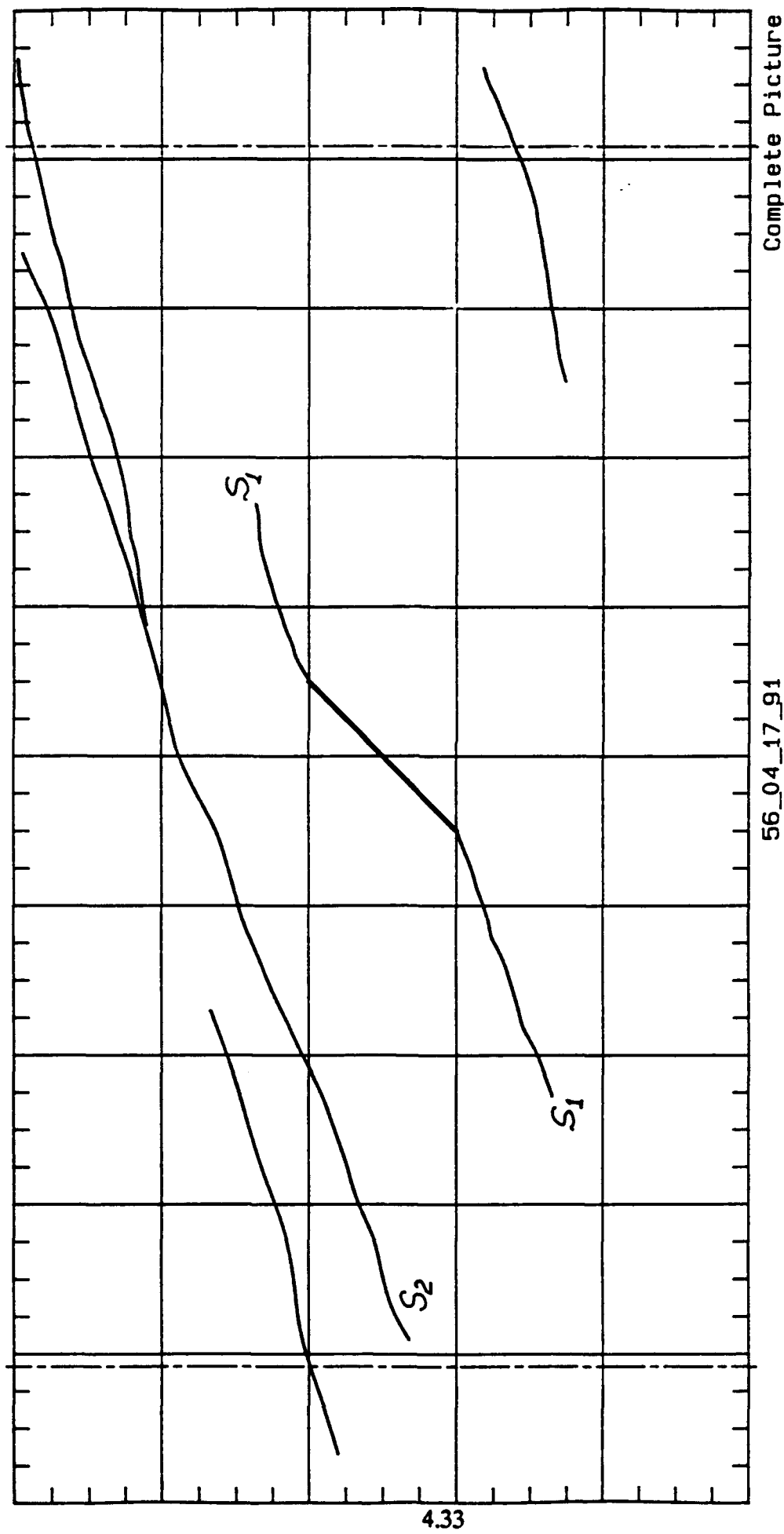
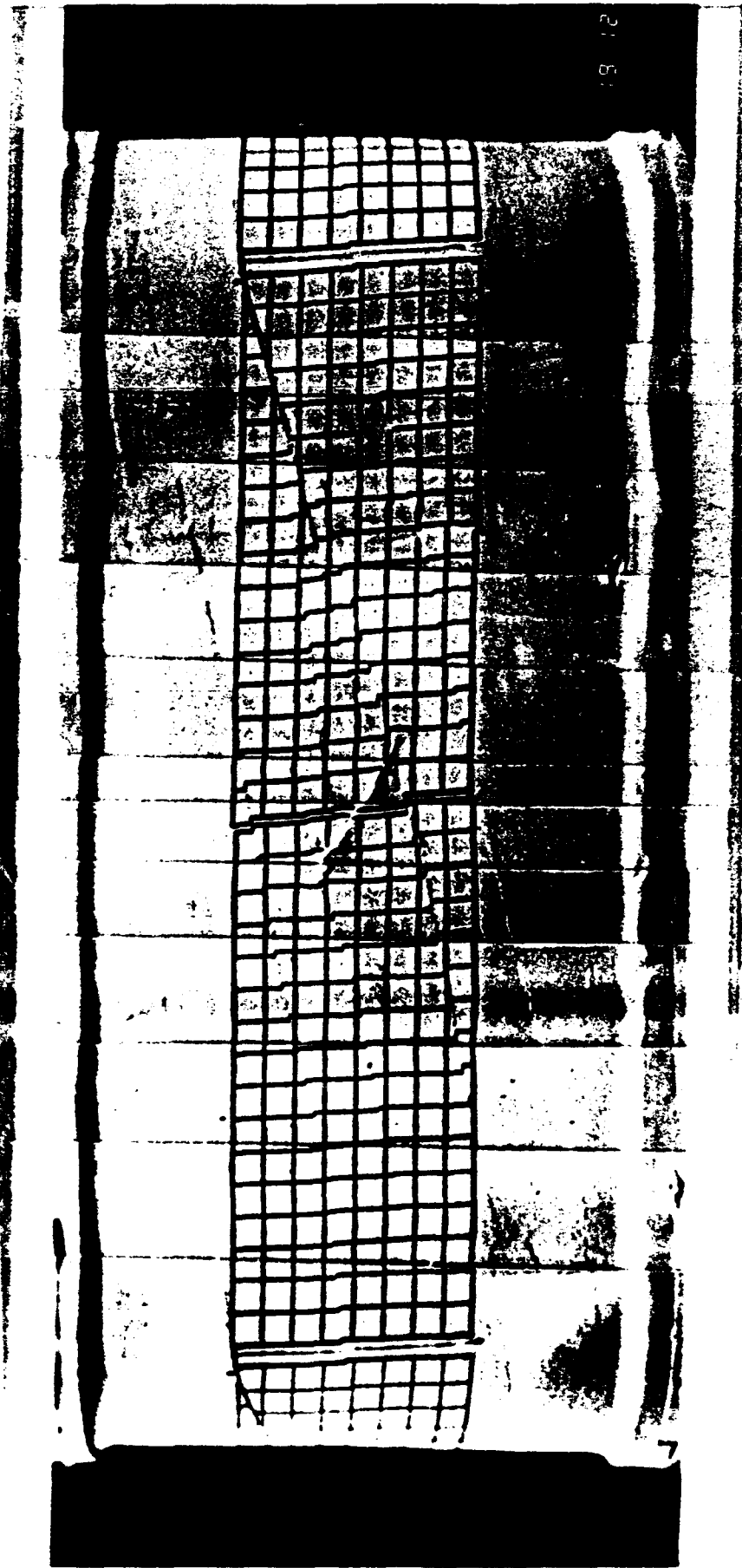


Figure 4.8az Shear Bands for an Inclined Crack in the Downstep Position;
 $\alpha = 45^\circ$



Test Name: 57_04/19/91 **Consol.:** KO NC
Material: EPK **Control:** 45
 345 kPa **Deform.**
 Height: variable

Figure 4.8b Shear Bands for an Inclined Crack in the Upstep Position;
 $\alpha = 45^\circ$

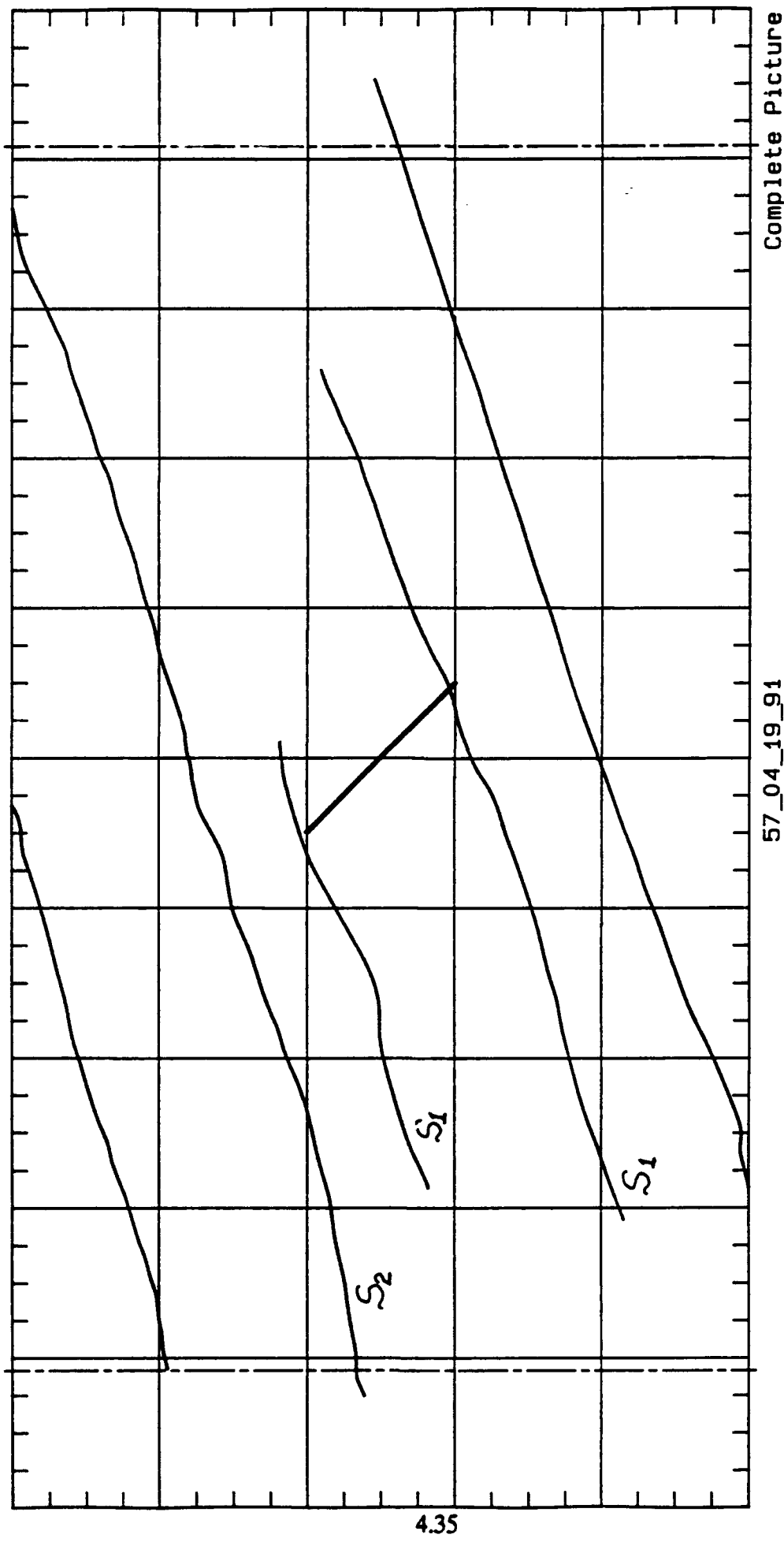
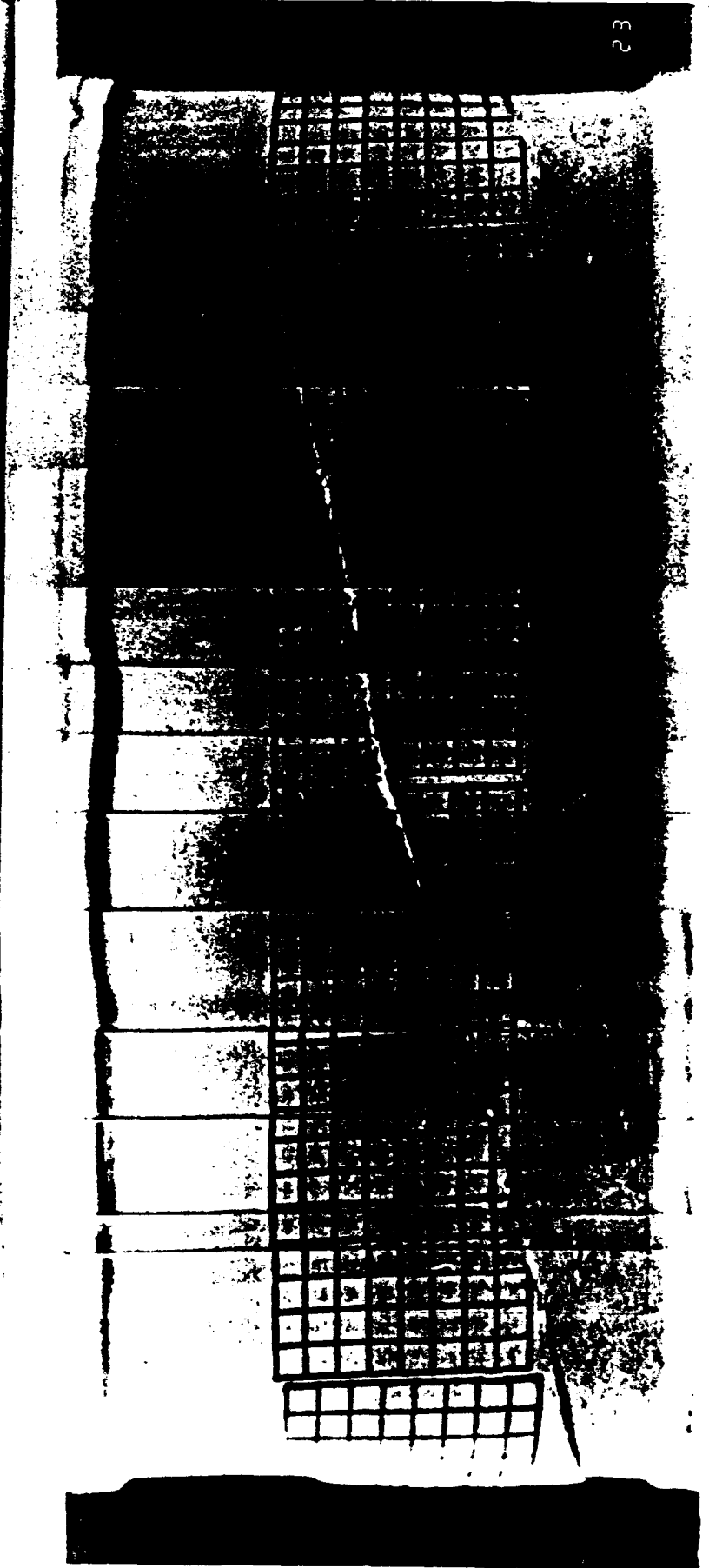


Figure 4.8bz Shear Bands for an Inclined Crack in the Upstep Position;
 $\alpha = 45^\circ$



Test Name: 58_04/23/91 **Consol.:** Ko NC **Beta:** 45
Material: EPK **Control:** Deform.
Height: variable

Figure 4.8c Shear Bands for an Inclined Crack in the Downstep Position;
 $\alpha = 22.5^\circ$

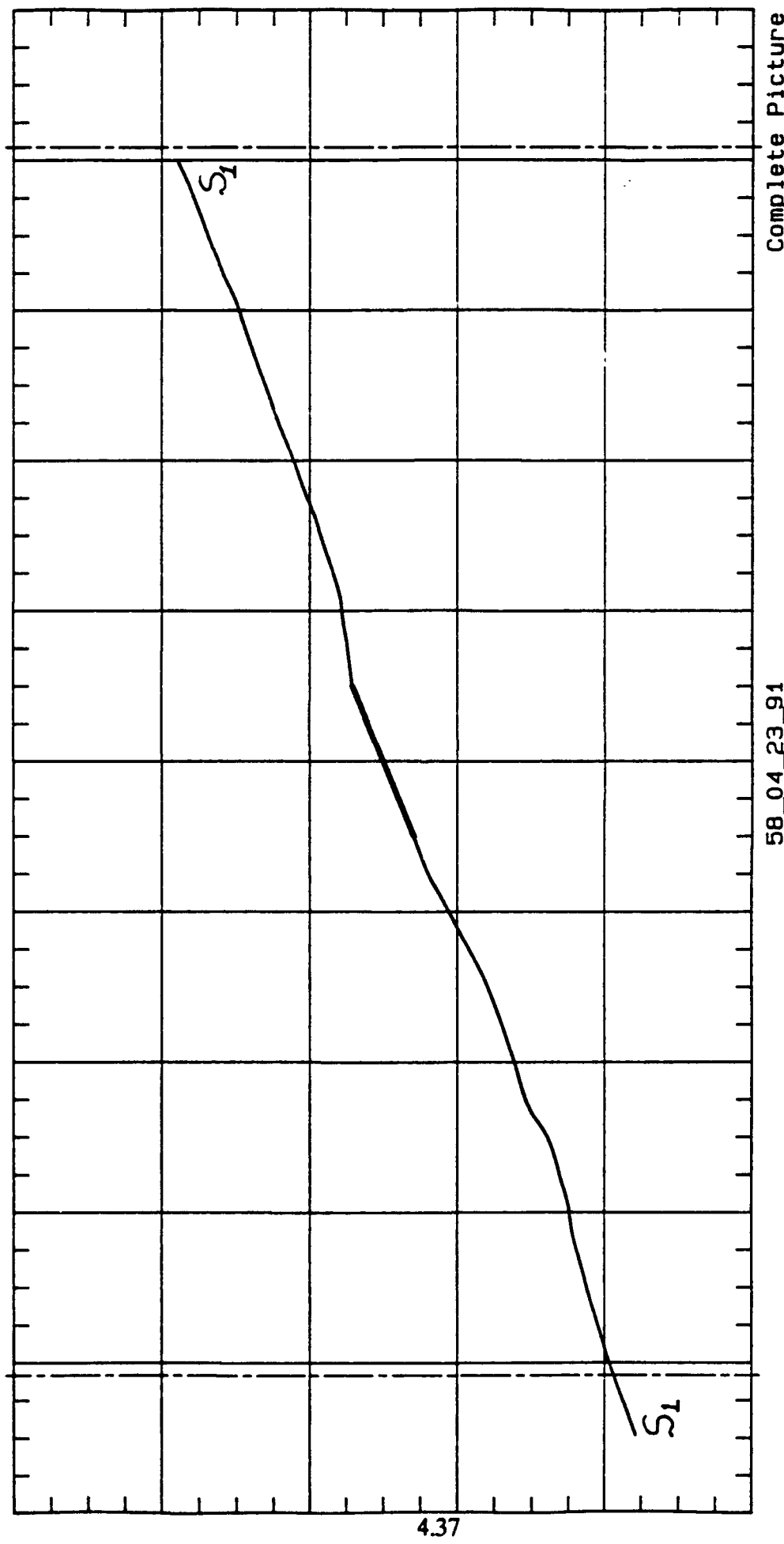


Figure 4.8cz Shear Bands for an Inclined Crack in the Downstep Position;
 $\alpha = 22.5^\circ$



Test Name: 68_06/05/91 Consol.: Ko OC
Material: EPK Control: OCR-4
Height: Deform.
Variable

Figure 4.9a Shear Bands for One Crack and $\beta = 30^\circ$

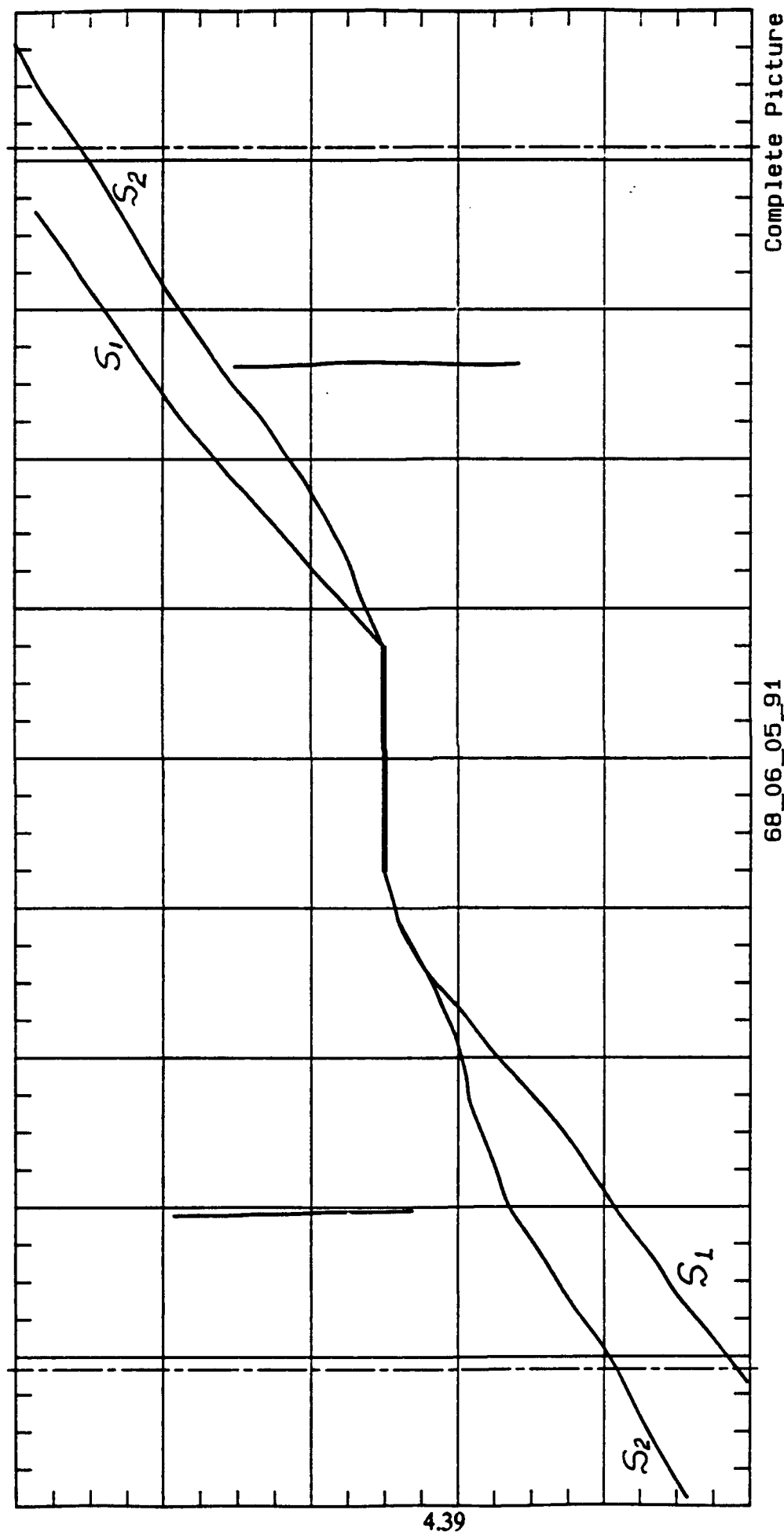


Figure 4.9az Shear Bands for One Crack and $\beta = 30^\circ$



4.40

Test Name: 66_05/29/91 Consol.: Ko OC Beta: 45
Material: EPK OCR-4 Control: Deform.
Height: Variable

Figure 4.9b Shear Bands for One Crack and $\beta = 45^\circ$

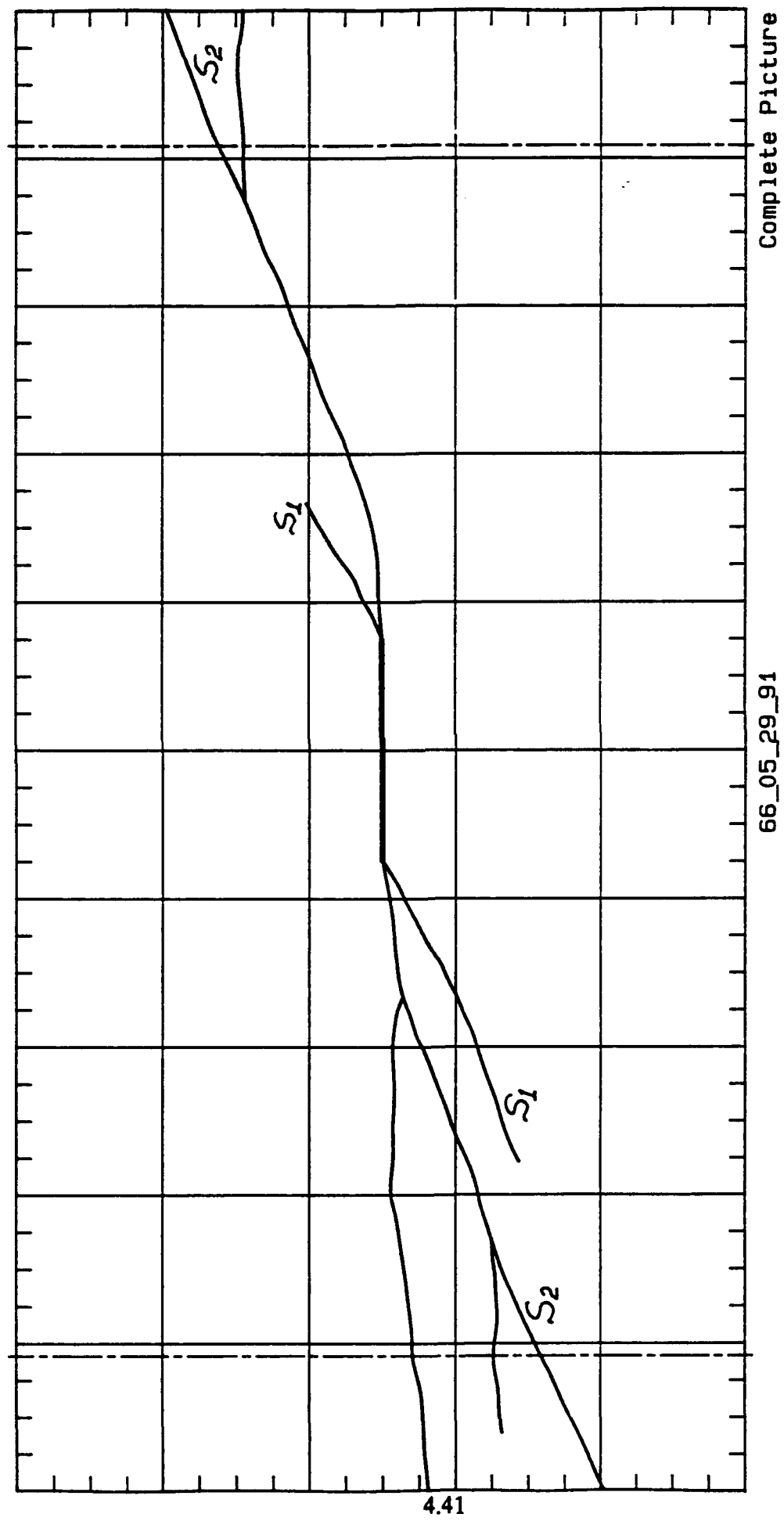
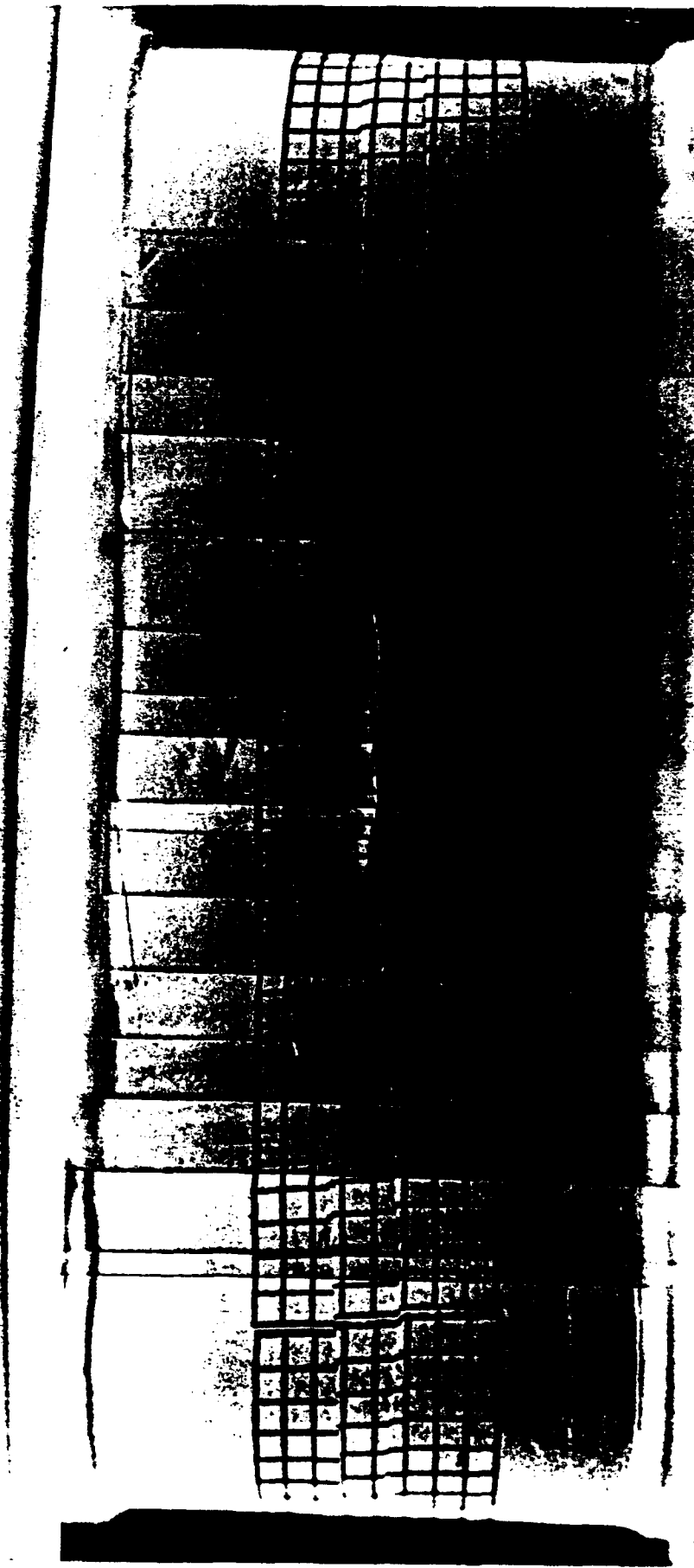


Figure 4.9bz Shear Bands for One Crack and $\beta = 45^\circ$

66_05_29_91

Complete Picture



Test Name: 70_06/14/91 Consol.: Ko oc Beta: 60
Material: EPK Control: Deform.
Height: variable

Figure 4.9c Shear Bands for One Crack and $\beta = 60^\circ$

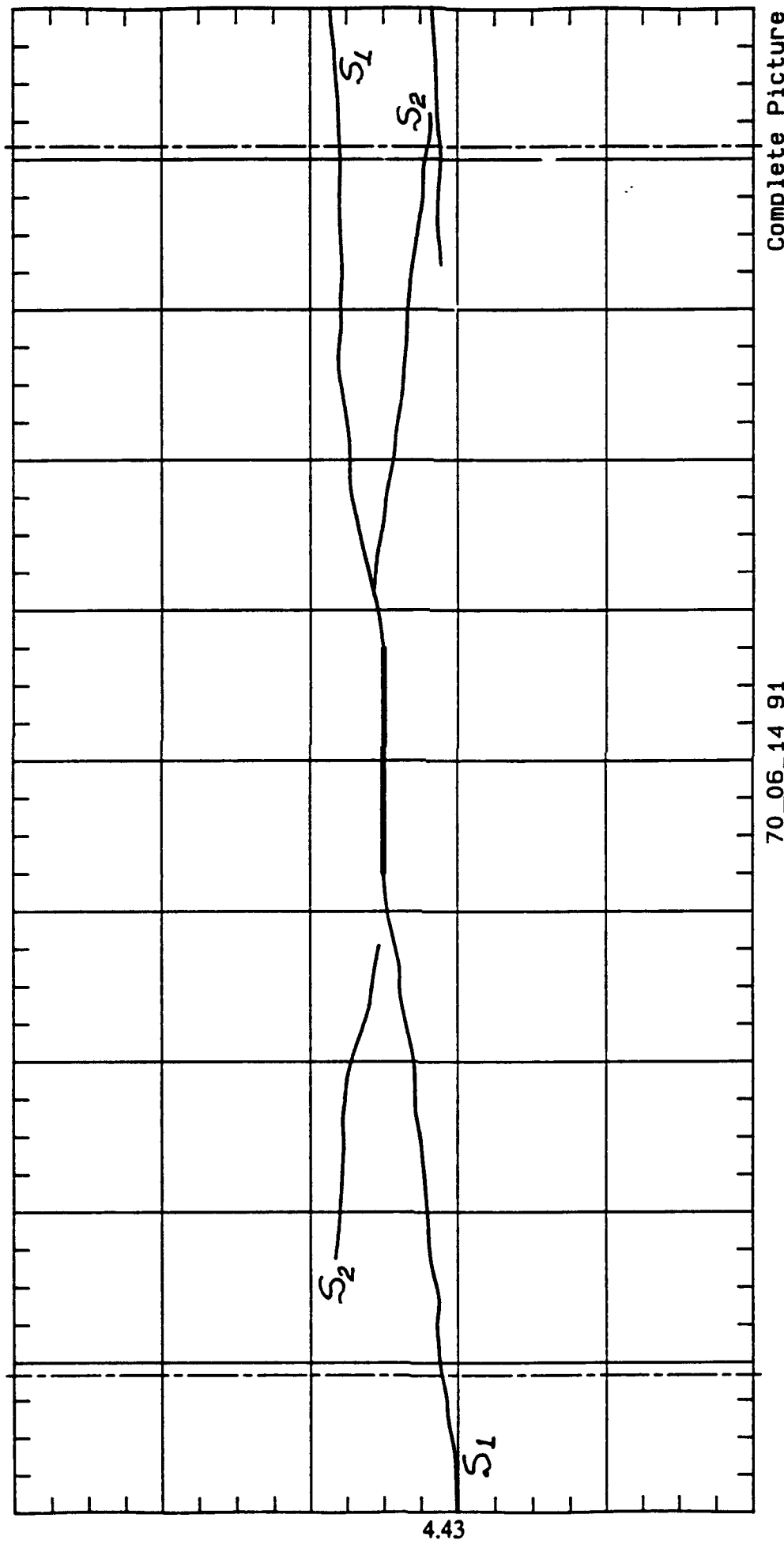
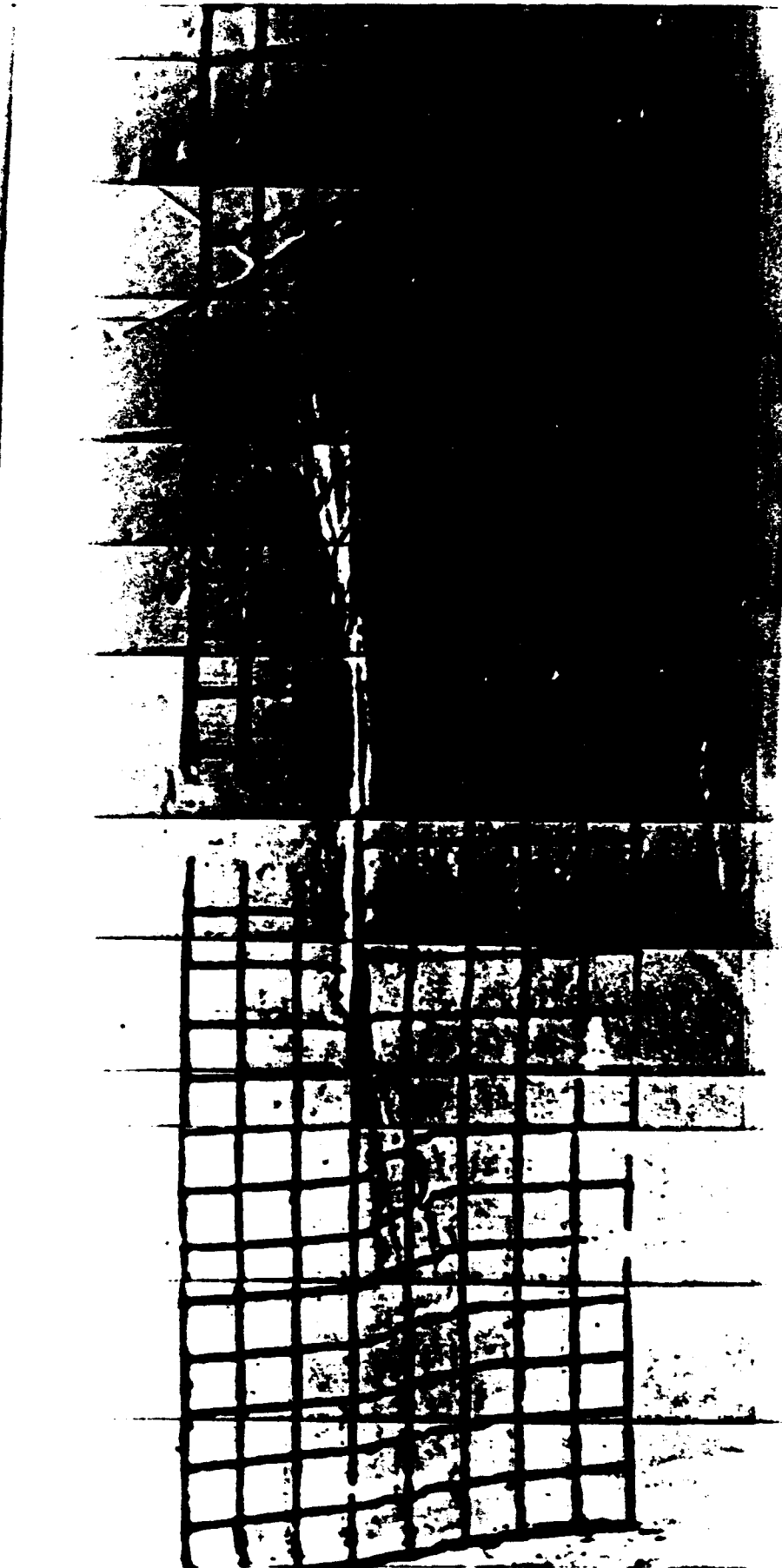


Figure 4.9cz Shear Bands for One Crack and $\beta = 60^\circ$



Test Name: 7a_09/06/90 Consol.: Isotropic Beta: 45
Material: EPK OCR-3 Control: Deform.
Height: Fixed

Figure 4.9d Shear Bands for One Crack Under Torsion with Fixed Length;
Isotropic Clay

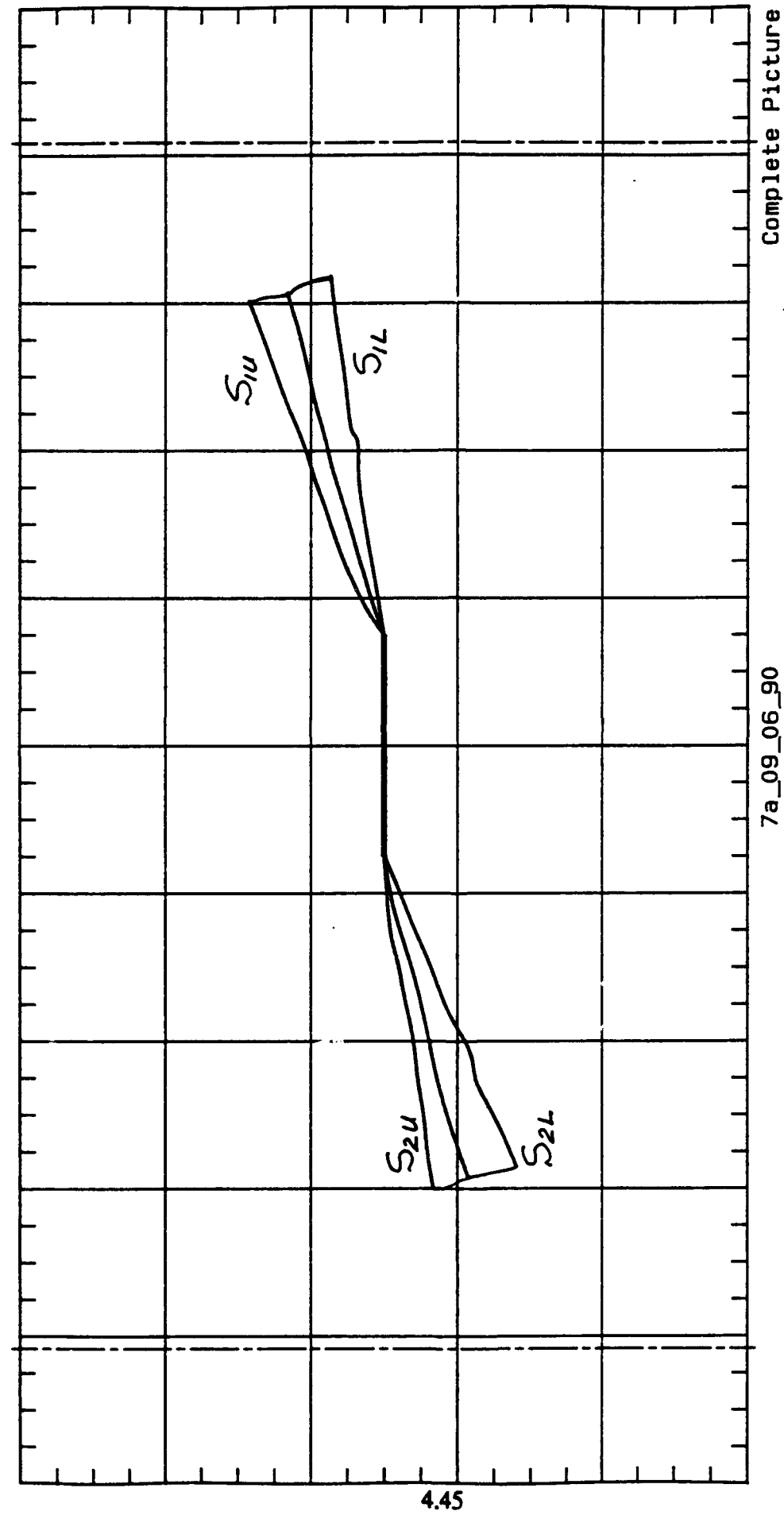
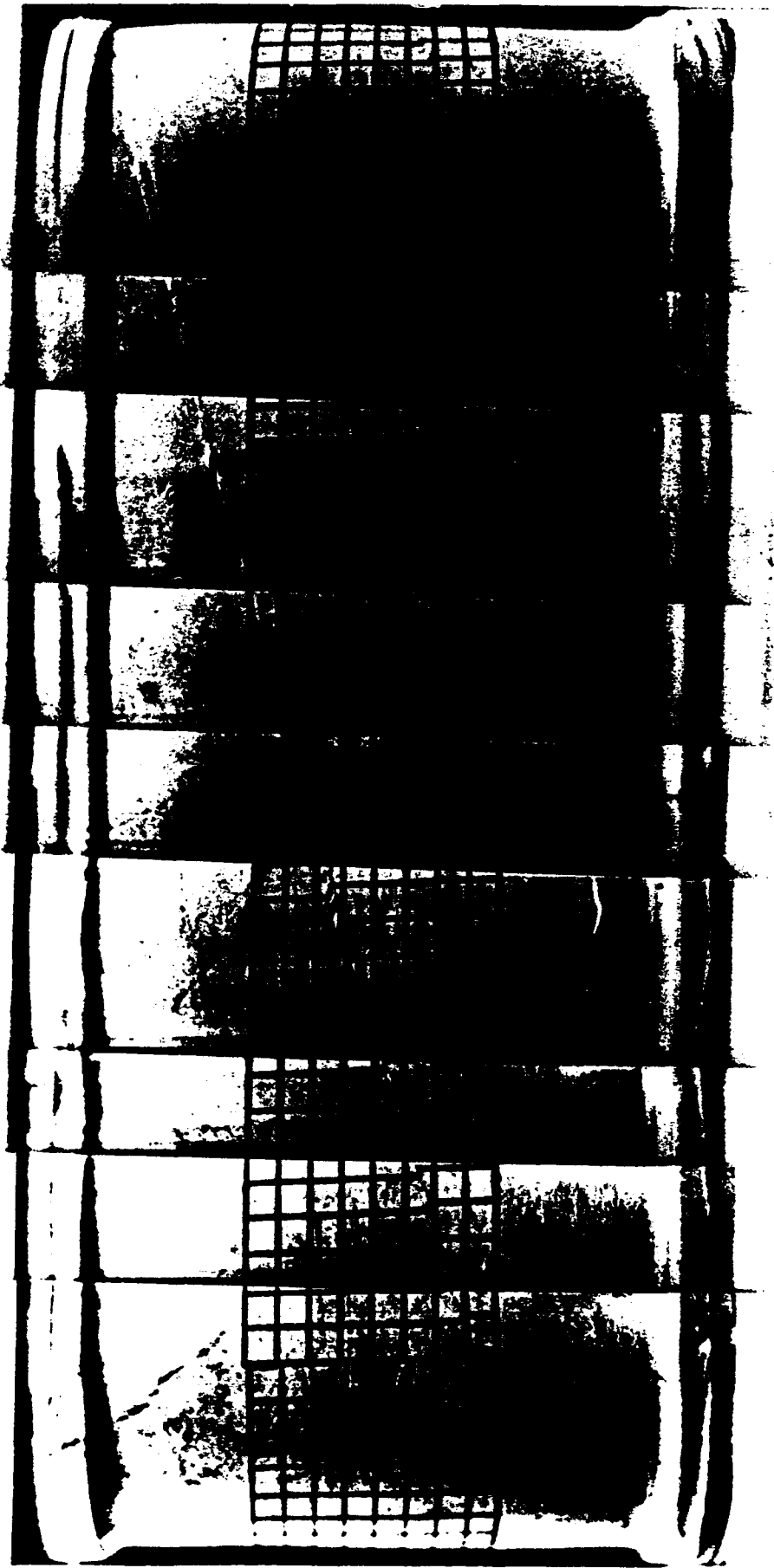


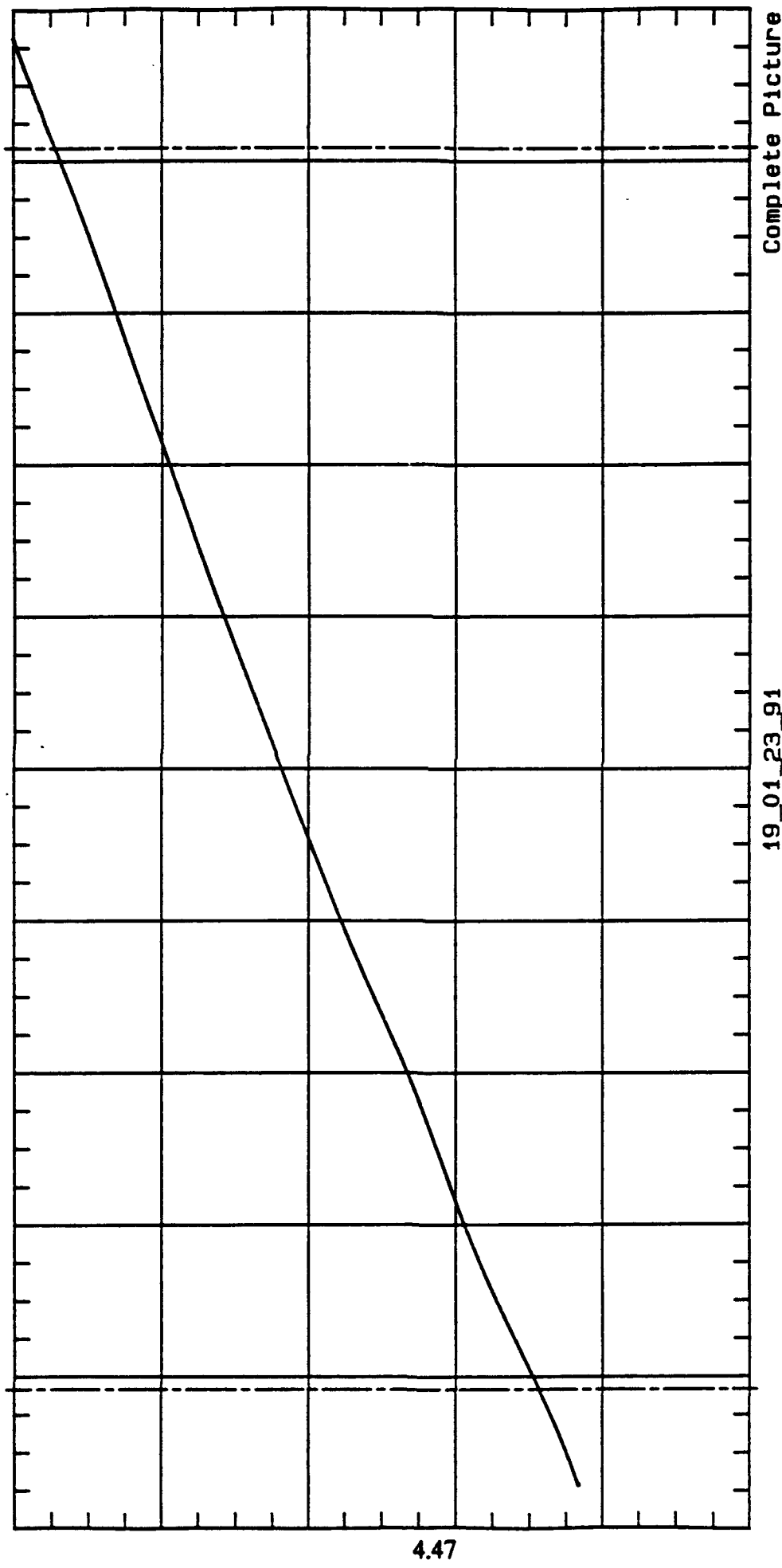
Figure 4.9dz Shear Bands for One Crack Under Torsion with Fixed Length;
Isotropic Clay



Test Name: 19_01/23/91 Consol.: No OC Material: EPK Control: Height: Fixed Deform.

Figure 4.10a Influence of the Size of the Crack on the Shear Bands; $a/l = 0.0$

Figure 4.10az Influence of the Size of the Crack on the Shear Bands; $a/l = 0.0$





Test Name: 16_12/13/90 Consol.: No OC
Material: EPK Beta: 45
Control: Defor Height: Fixed

Figure 4.10b Influence of the Size of the Crack on the Shear Bands;
 $a/l = 0.10$

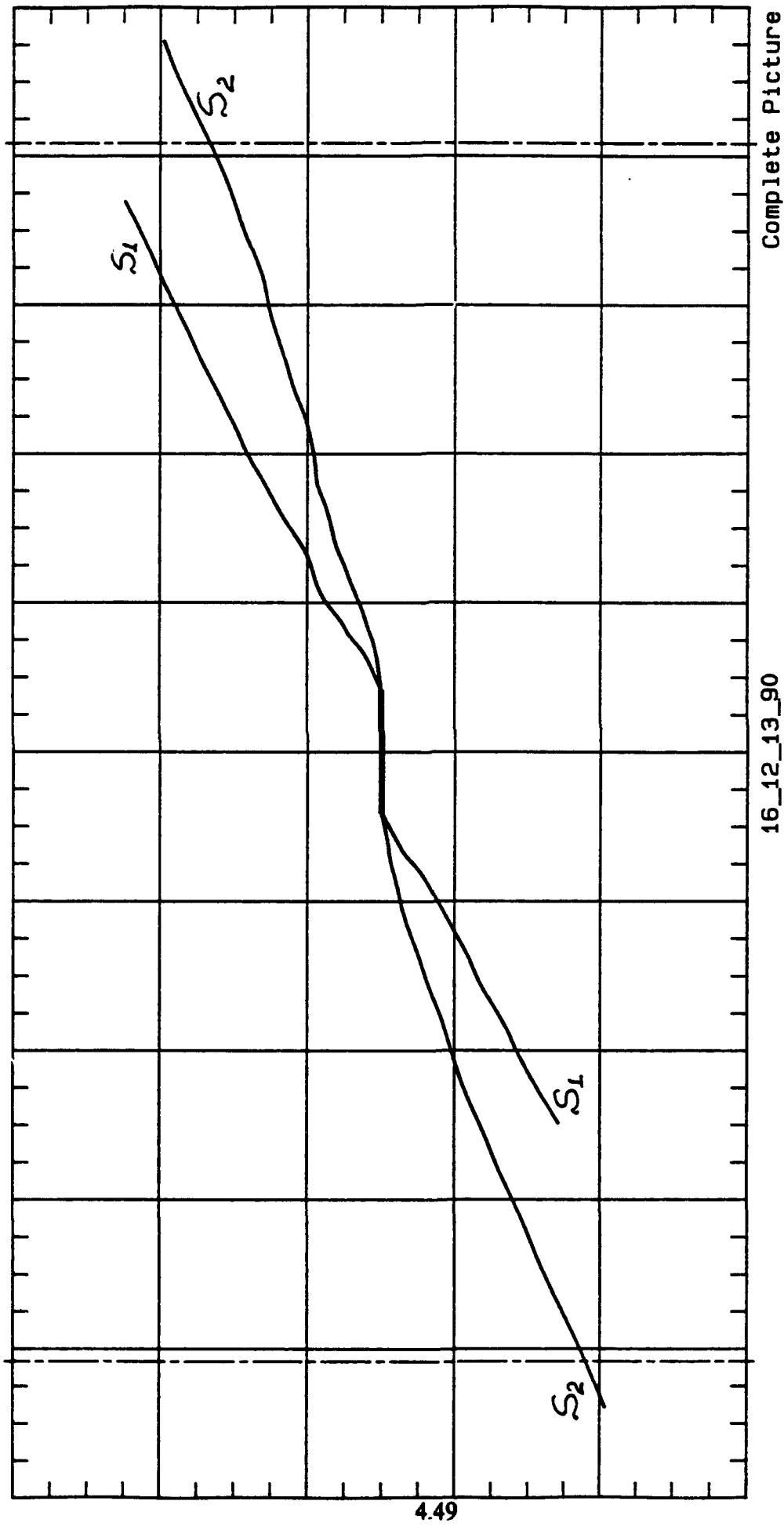
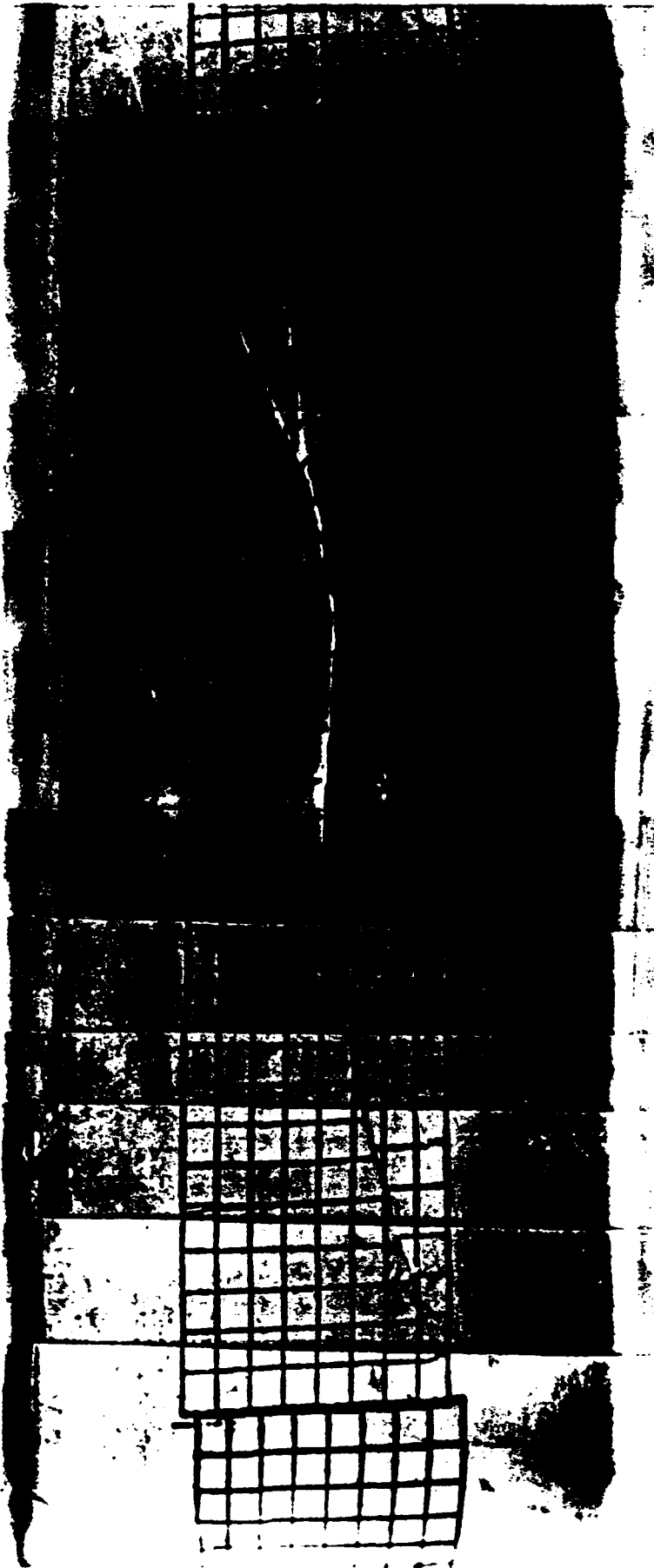


Figure 4.10bz Influence of the Size of the Crack on the Shear Bands;
 $a/l = 0.10$



Test Name: 18_01/15/91 Consol.: No OC
Material: EPK OCR-4
Beta: 45
Control: Deform.
Height: Fixed

Figure 4.10c Influence of the Size of the Crack on the Shear Bands;
 $a/l = 0.18$

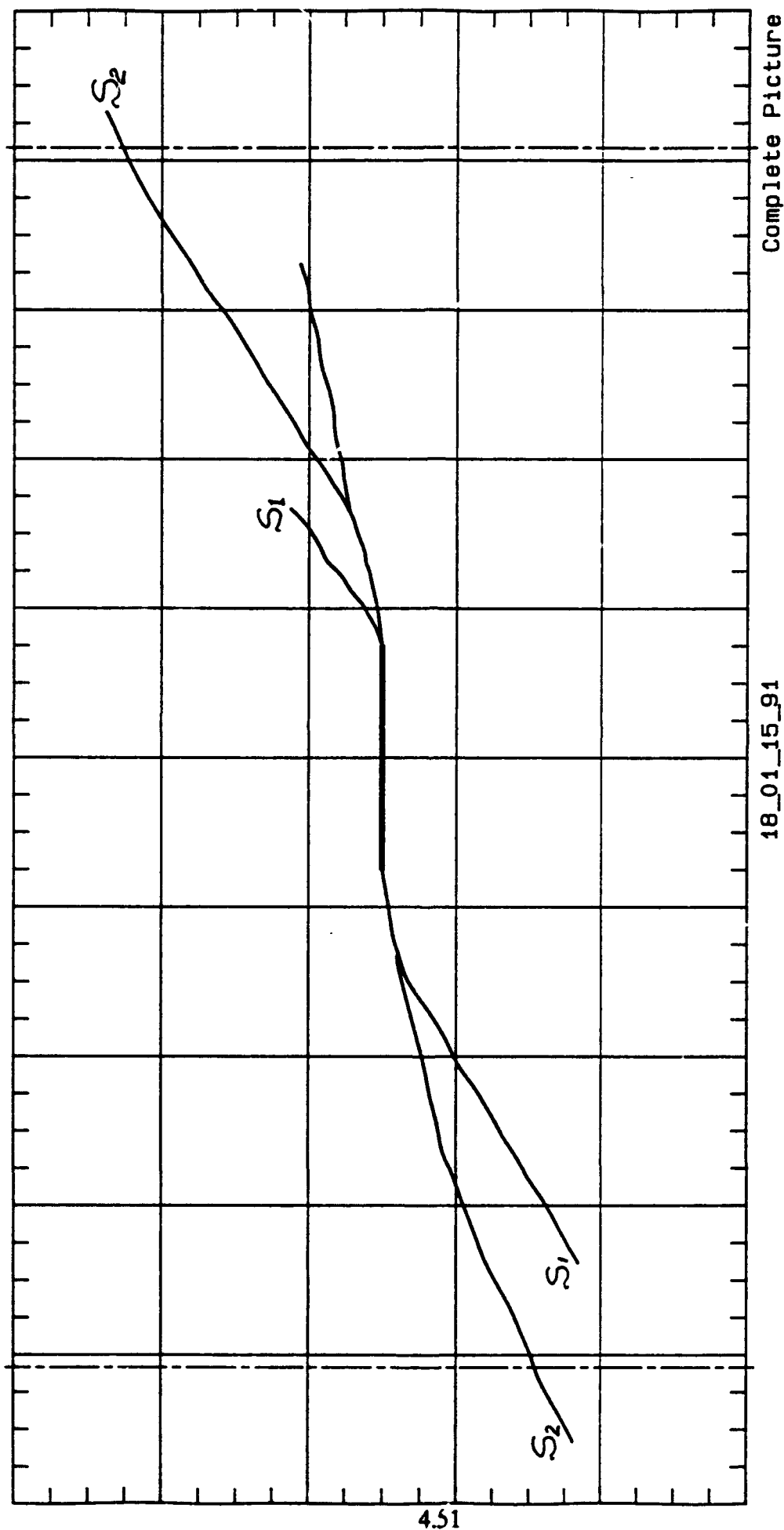
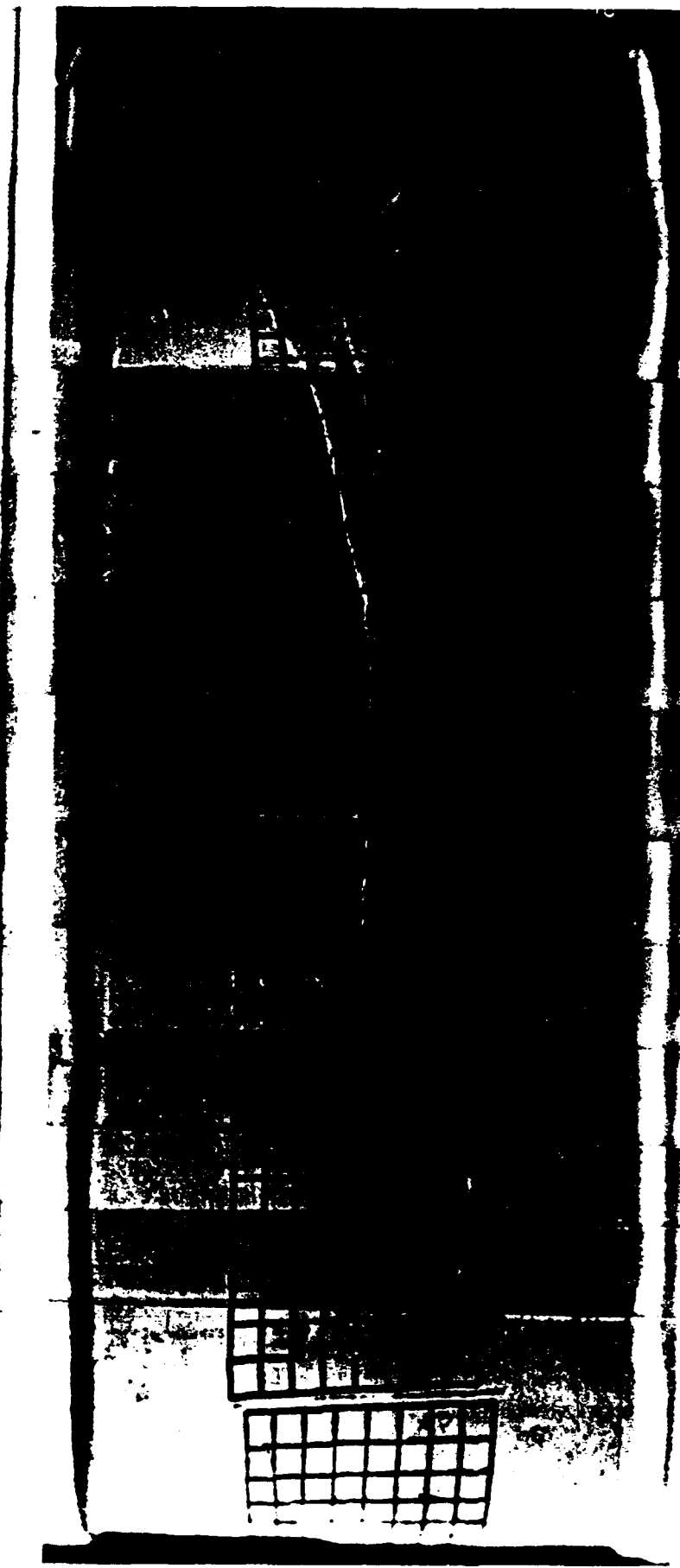


Figure 4.10cz Influence of the Size of the Crack on the Shear Bands;
 $a/l = 0.18$



Test Name: 15_11/27/90 **Consol.:** Ko OC
Material: EPK **Beta:** 45
 Control: Deform.
 Height: Fixed

Figure 4.10d Influence of the Size of the Crack on the Shear Bands;
 $a/l = 0.30$

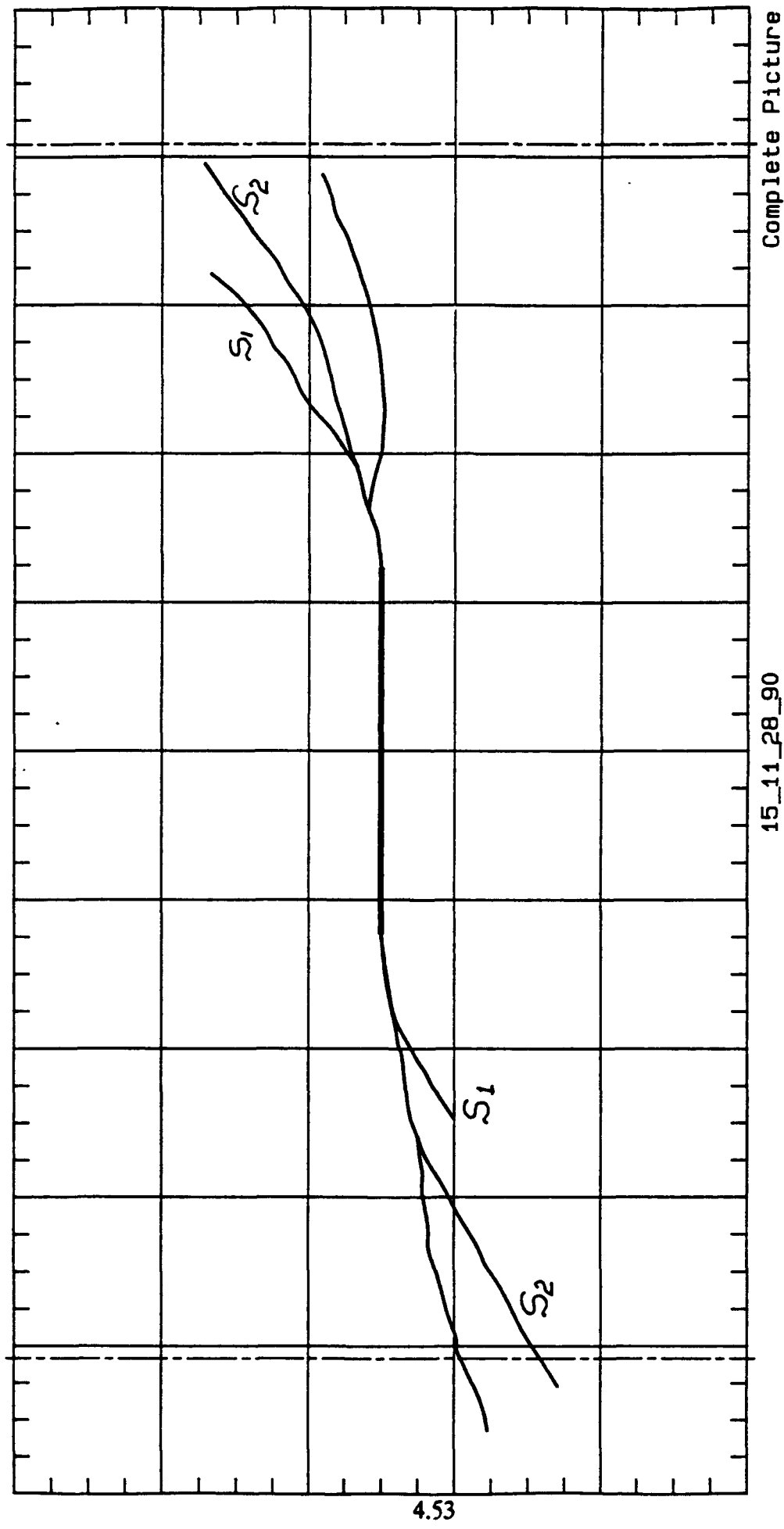
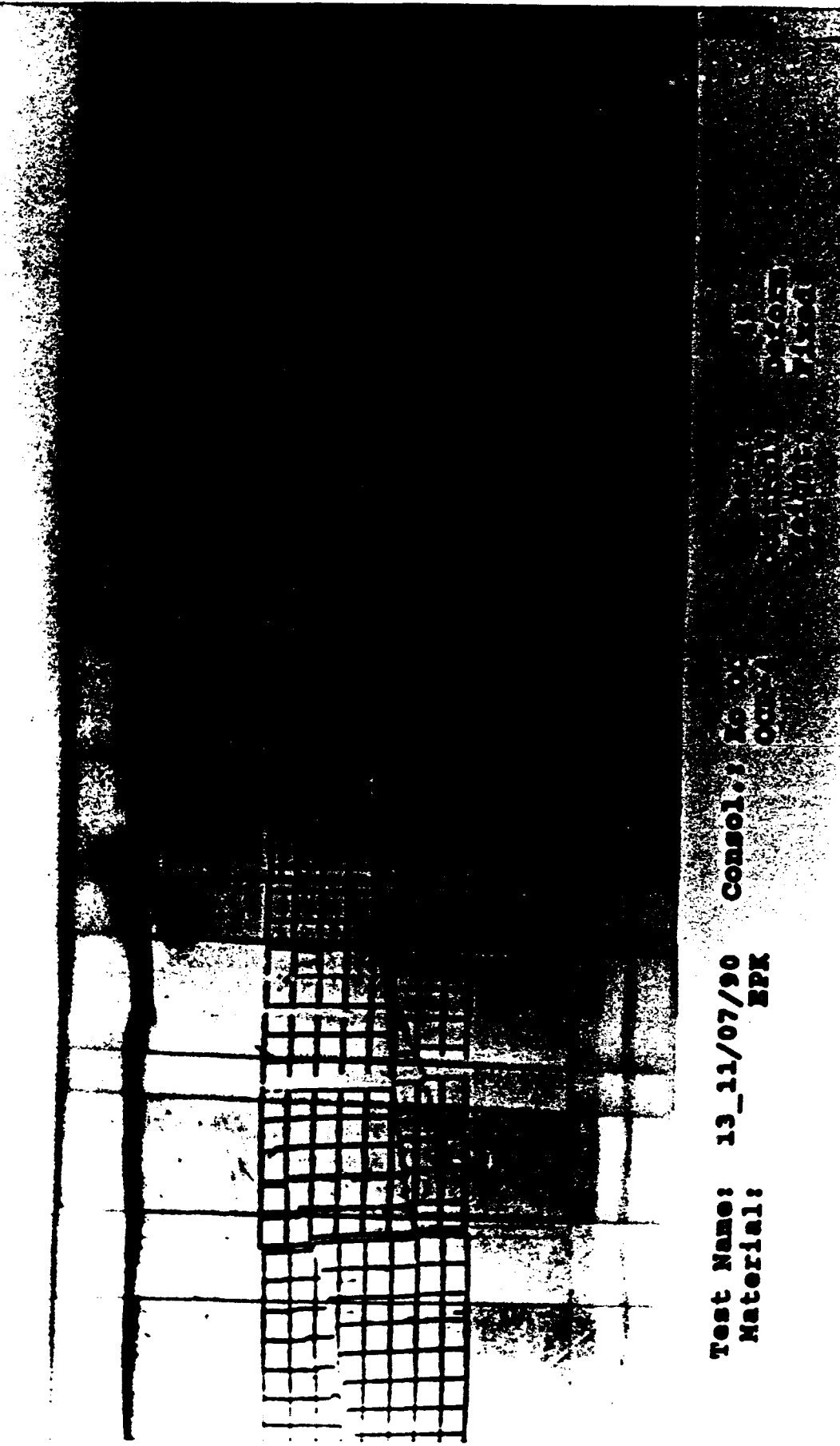


Figure 4.10dz Influence of the Size of the Crack on the Shear Bands;
 $a/l = 0.30$



Test Name: 13_11/07/90 consol. no. 38
Material: EPK occ. no. 1

Figure 4.10e Influence of the Size of the Crack on the Shear Bands;
 $a/l = 0.35$

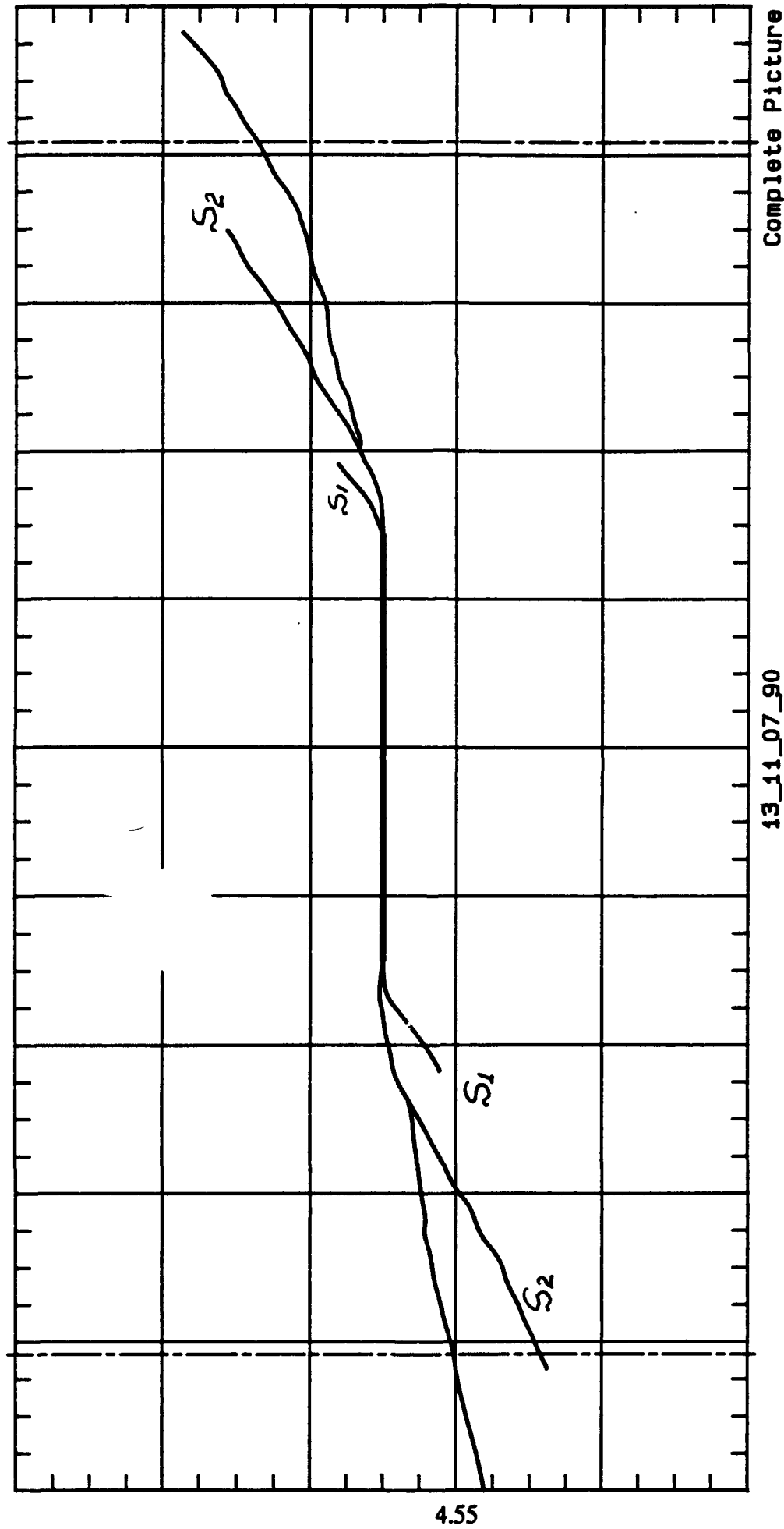
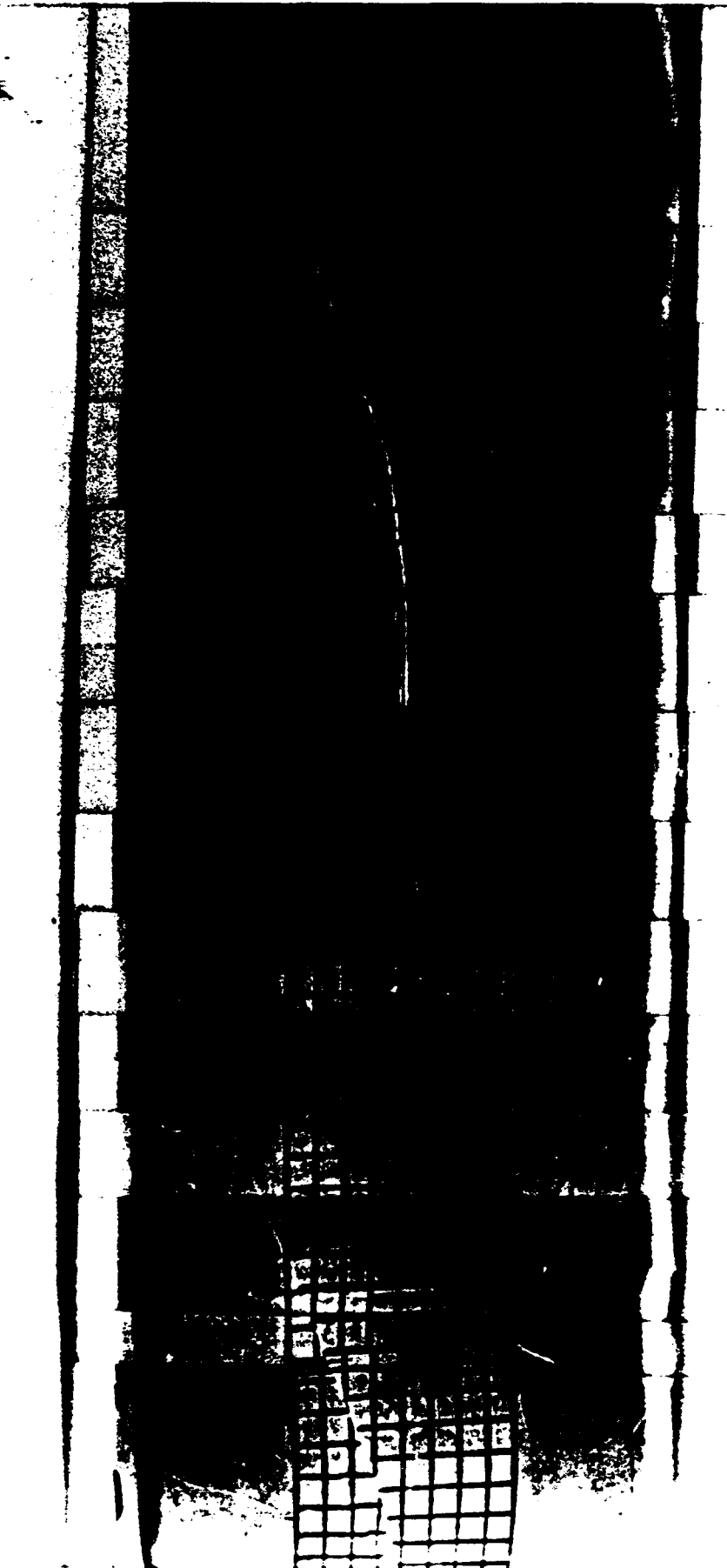


Figure 4.10ez Influence of the Size of the Crack on the Shear Bands;
 $a/l = 0.35$



Test Name: 14_11/20/90 **Consol.:** Ro OC
Material: EPK **Beta:** 45
 Control: Deform.
 Height: Fixed

Figure 4.10f Influence of the Size of the Crack on the Shear Bands; $a/l = 0.4$

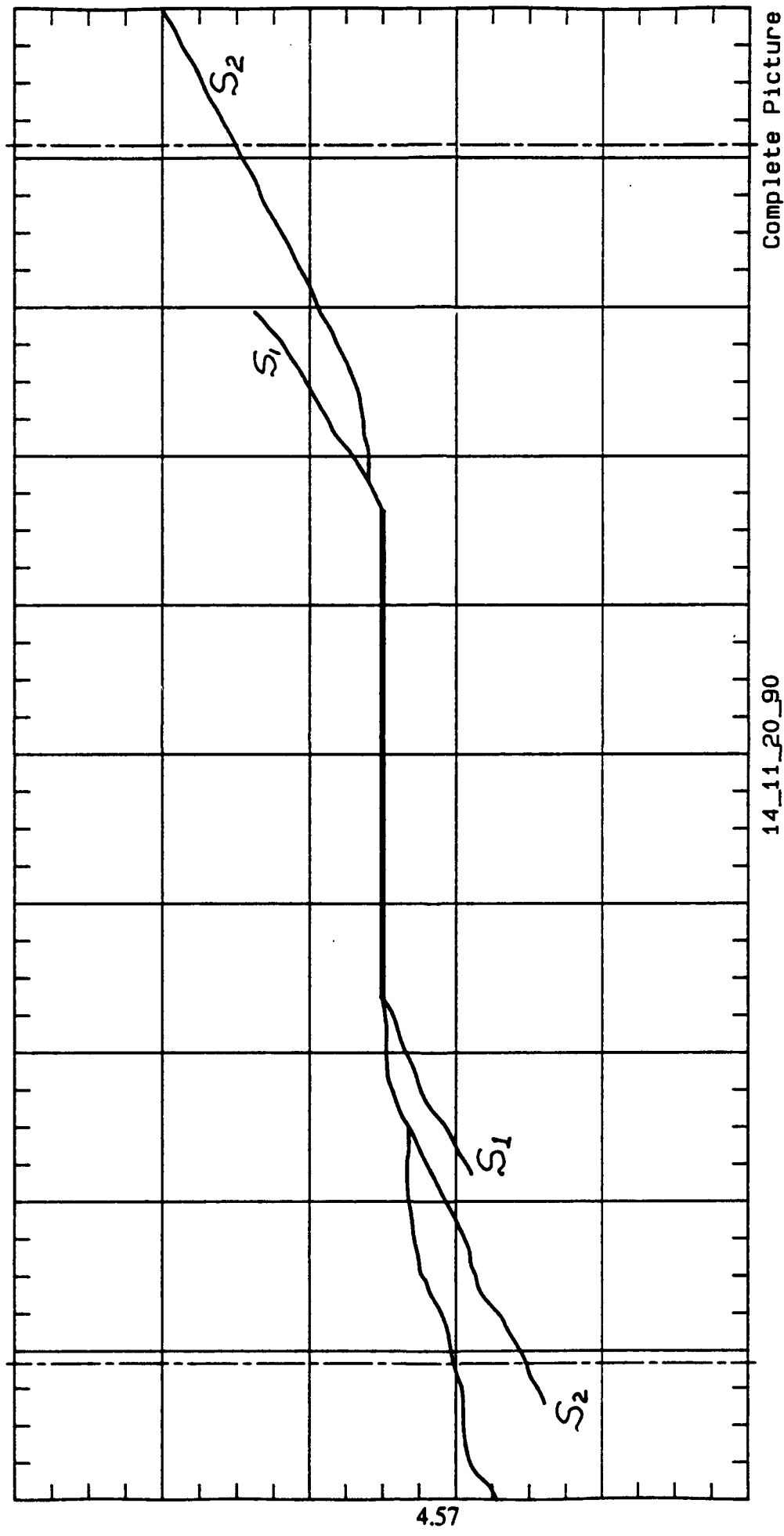
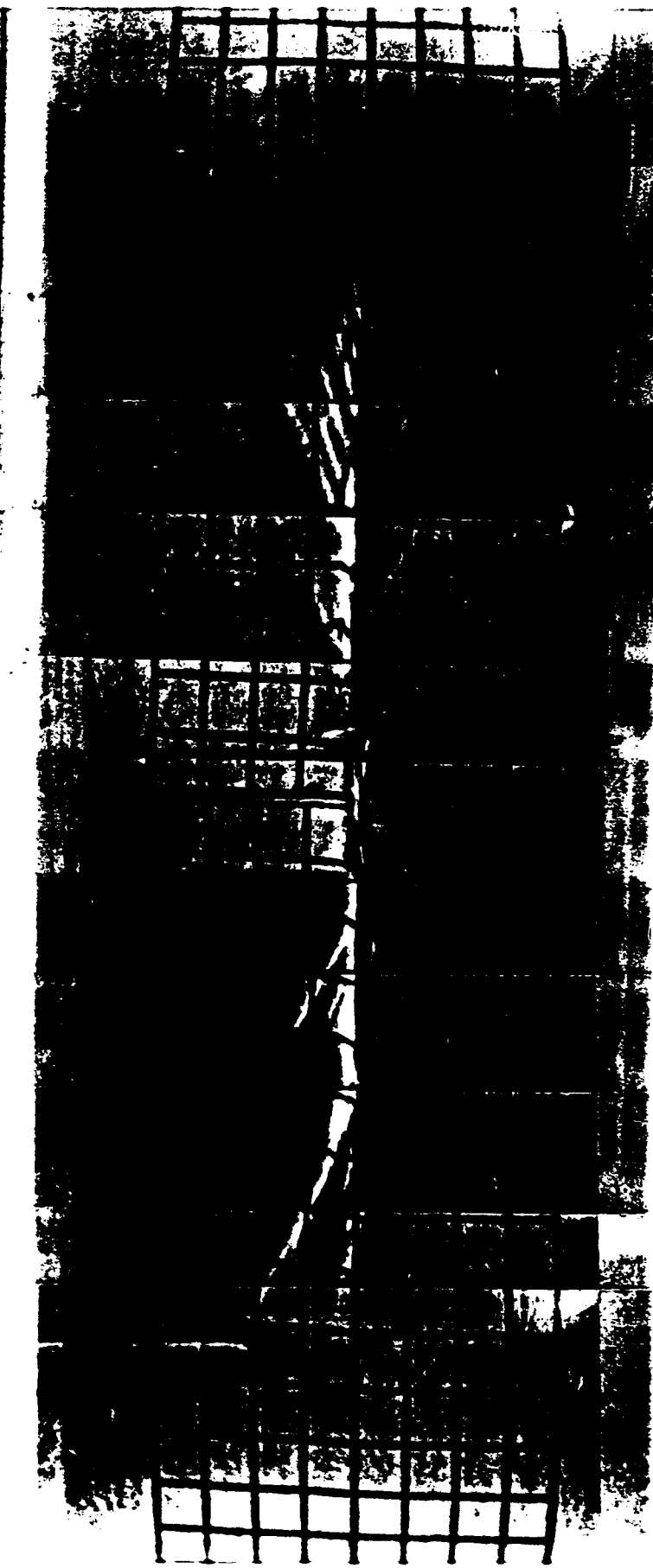


Figure 4.10fz Influence of the Size of the Crack on the Shear Bands; $a/l = 0.4$



Test Name: 3a_01/30/90 consol.: Ko NC Beta: 45
Material: EPK 345 kPa Control: stress
Height: Fixed

Figure 4.11a Crack Propagation and Damage Zone for a K_o Normally Consolidated Clay (EPK)



Test Name: 17_01/03/91 Consol.: K_o OC
Material: EPK OCR-4
Beta: 45
Control: Stress
Height: Fixed

Figure 4.11b Crack Propagation and Damage Zone for a K_o Overconsolidated Clay (EPK)

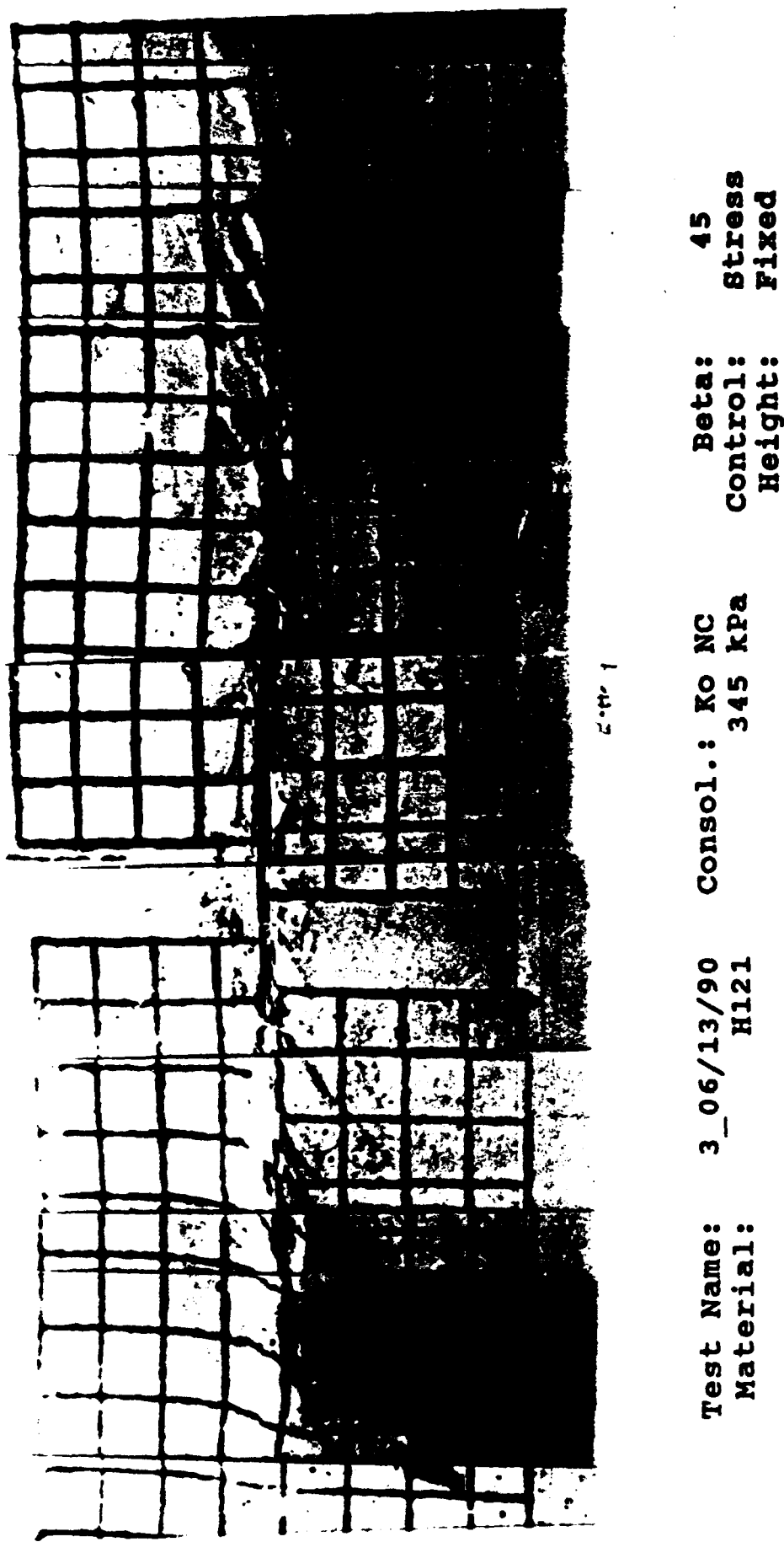
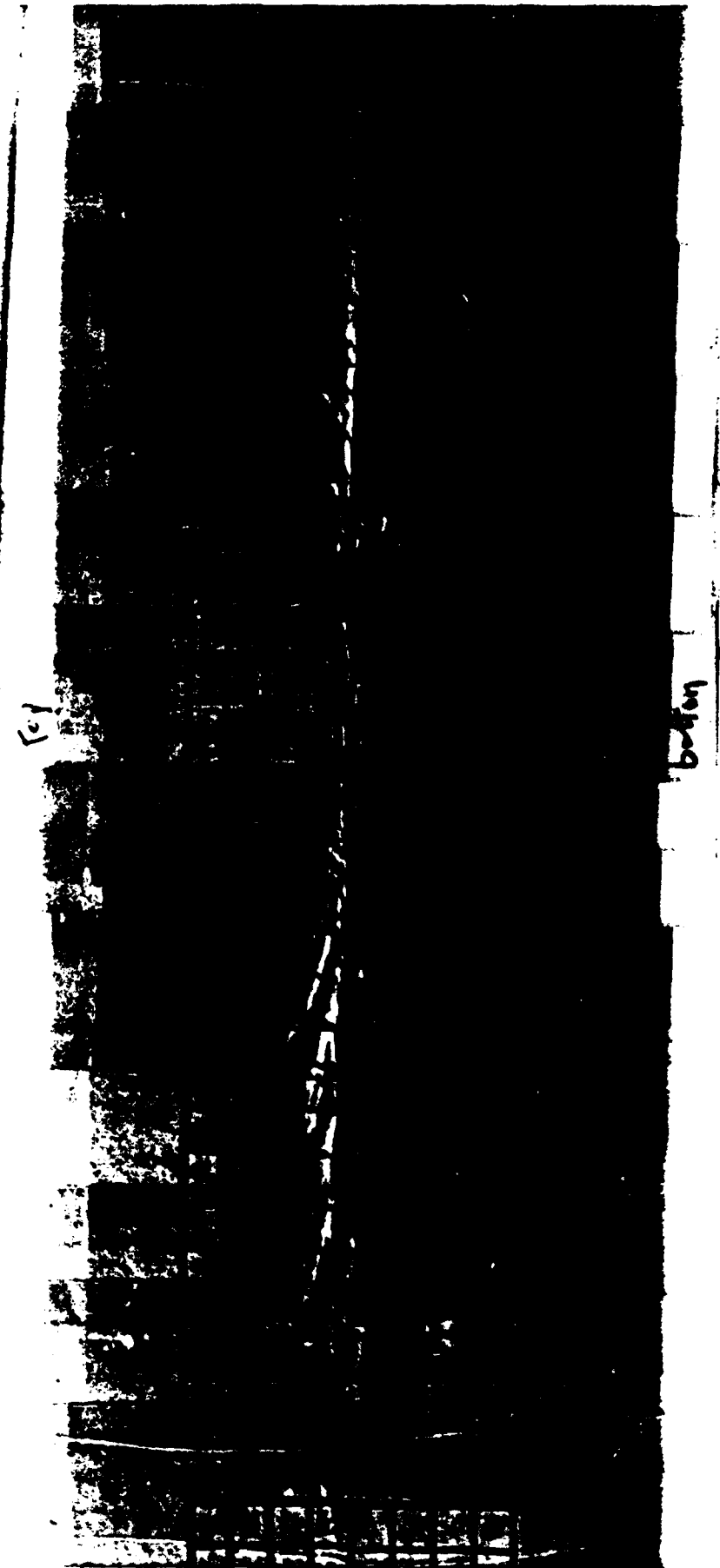
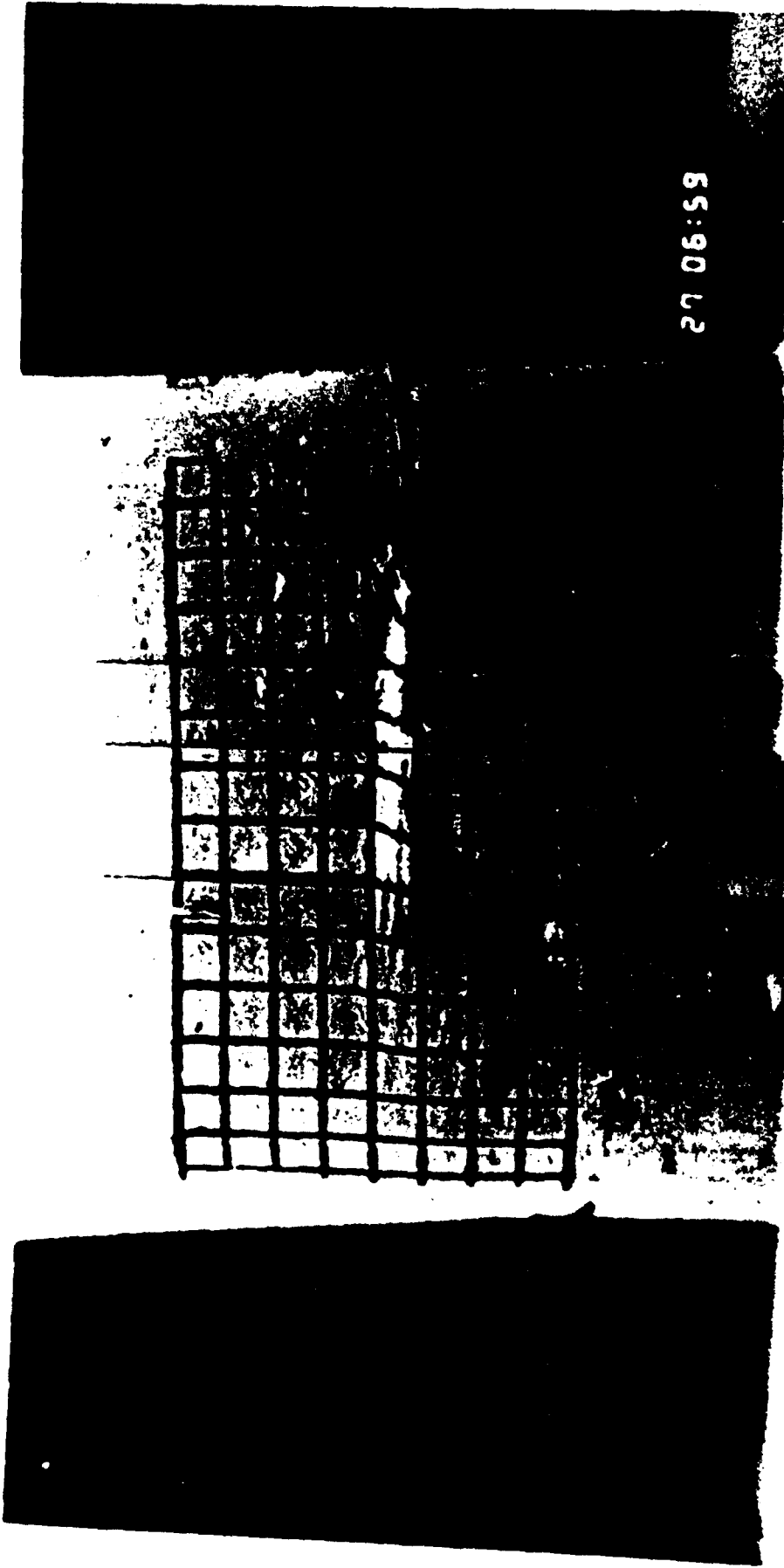


Figure 4.12 Crack Propagation and Damage Zone for a K_o Normally Consolidated Clay (H121)



Test Name: 6vc_10/03/90 Consol.: Ro OC
Material: EPK OCR-4 Beta: 45
Control: Stress
Height: Variable

Figure 4.13 Crack Propagation and Damage Zone for a K_o Overconsolidated Clay (EPK)



Test Name: 7_06/27/90 Consol.: Isotropic Beta: 45
Material: EPK OCR-3 Control: Defor
Height: Fixed

Figure 4.14 Crack Propagation and Damage Zone for an Isotropic Overconsolidated Clay



Test Name: 3c_02/22/90 Consol.: NC
Material: EPK Control: 345 kpa Beta:
Height: 45 stress fixed

Figure 4.15 Damage Zone for an Inclined Crack

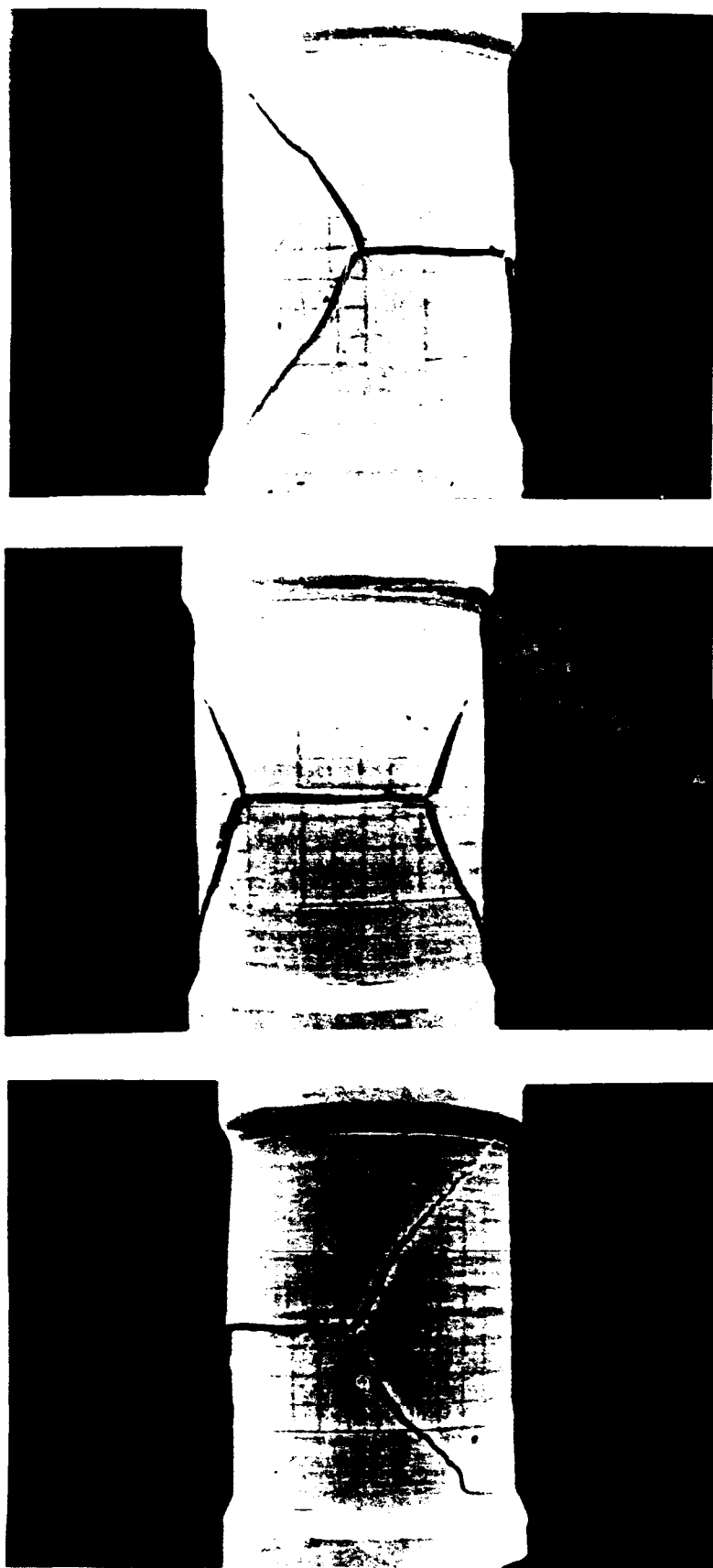


Figure 4.16 Tensile Failure under Cyclic Torsional Load



Test Name: 3b_02/13/90 Consol.: Ko NC Beta: 45
Material: EPK Control: Stress
345 kPa Height: Fixed

Figure 4.17a Shear Bands and Distortion under Impulse Loading

DYNAMIC LOADING RESPONSE

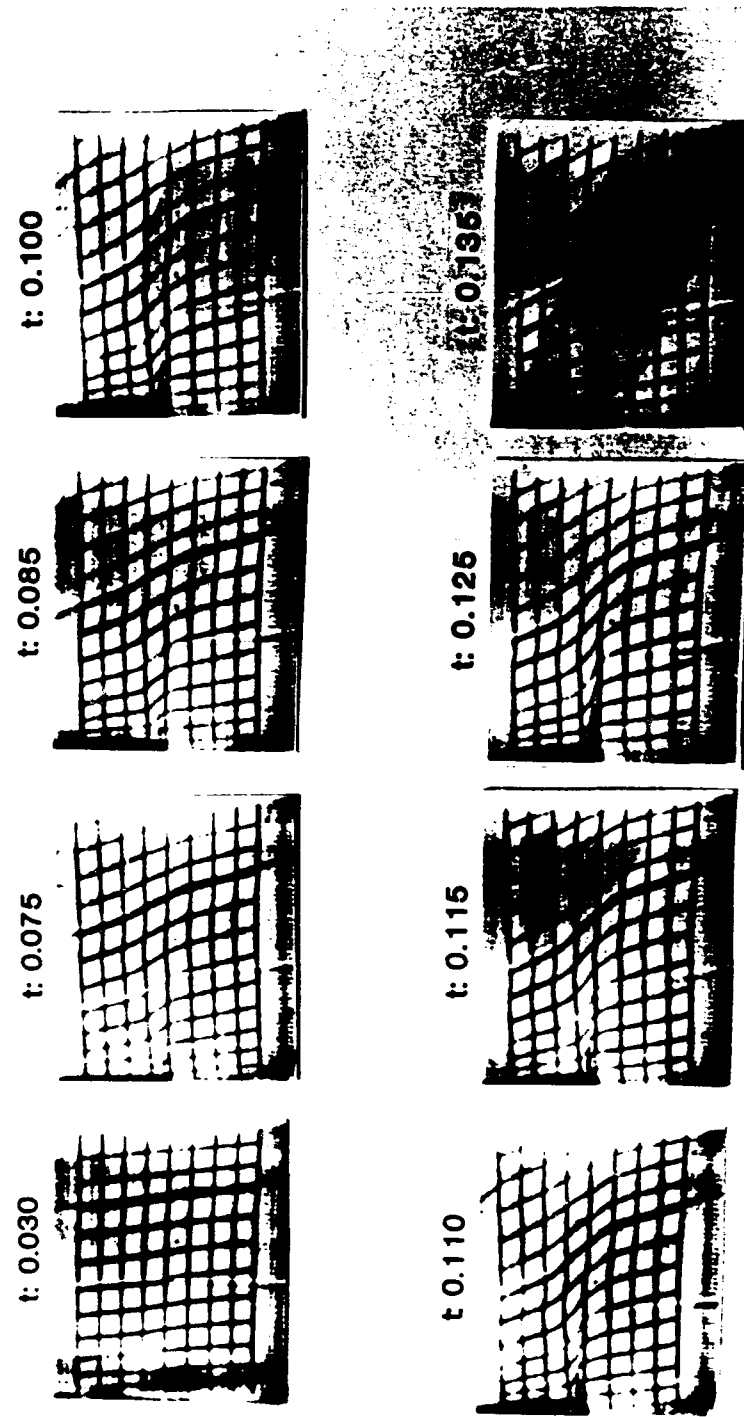
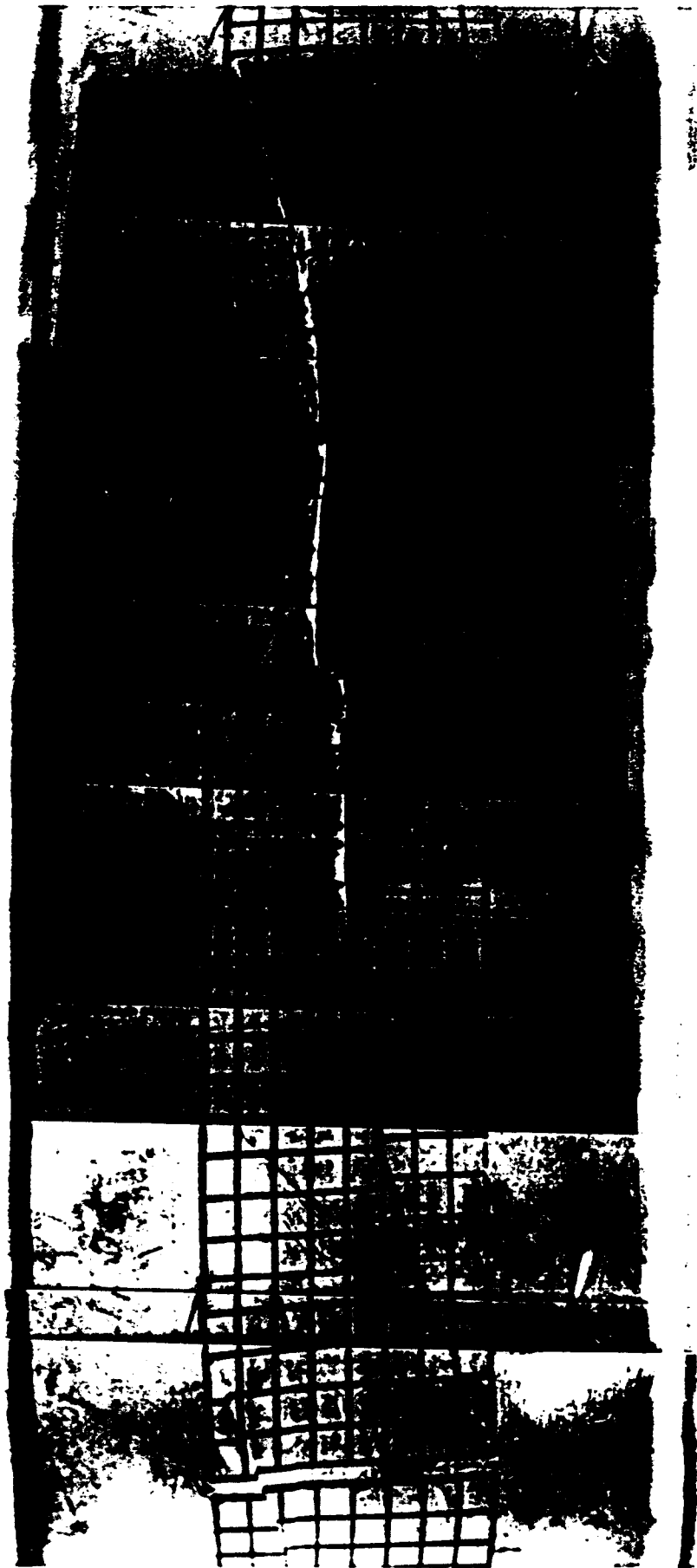


Figure 4.17b Displacement Pattern During Impulse Loading



Test Name: 81_07/03/91 Consol.: Ro OC
Material: EPR-4 Beta: 45
Control: Deform.
Height: variable

Figure 4.18 Shear Bands and Interaction of Two Cracks in the Downstep Position; $e = 0$

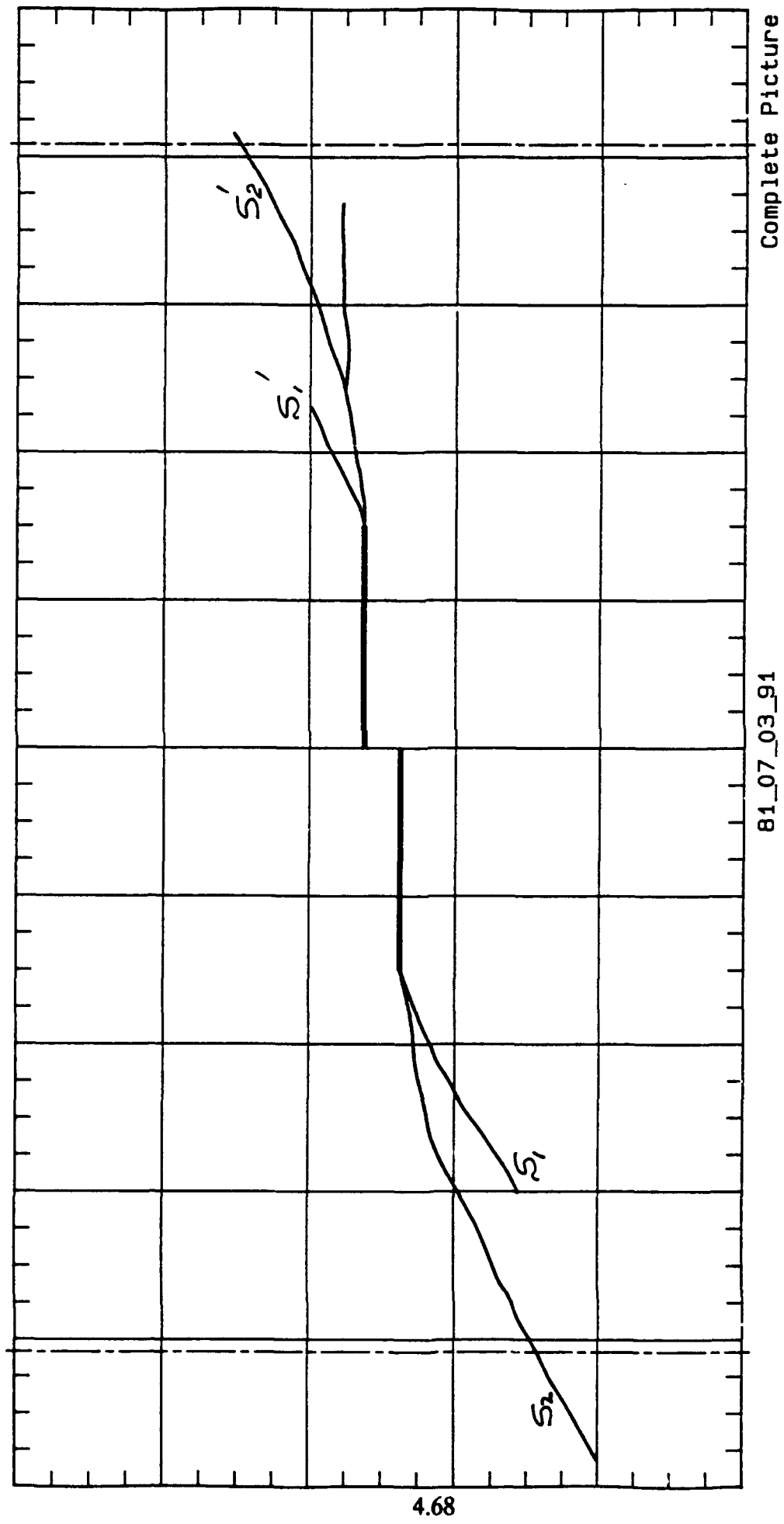
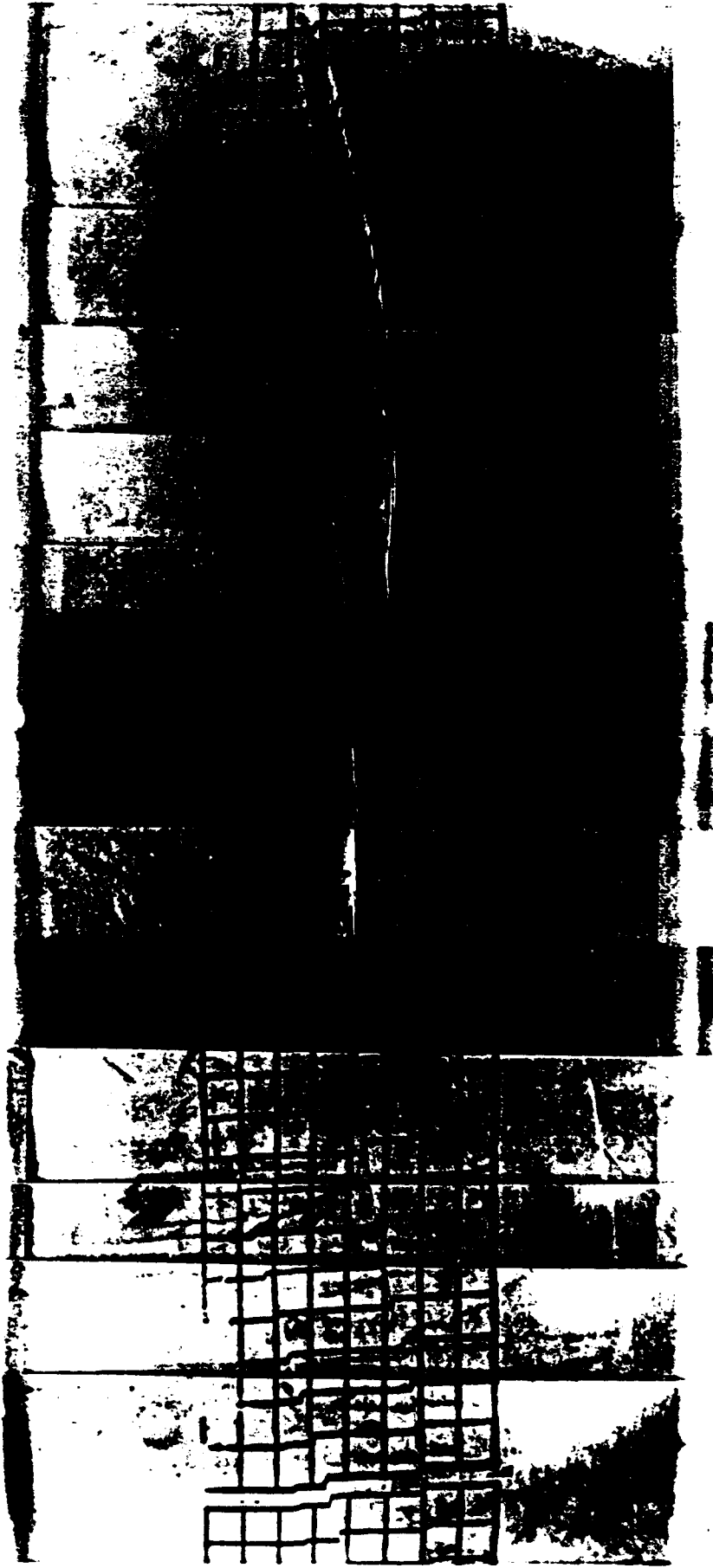


Figure 4.18z Shear Bands and Interaction of Two Cracks in the Downstep Position; $\epsilon = 0$



Test Name: 82_07/09/91 **Consol.:** Ko OC
Material: EPK **Beta:** 45
 Control: Deform.
 Height: variable

Figure 4.19 Shear Bands and Interaction of Two Cracks in the Upstep Position; $e = 0$

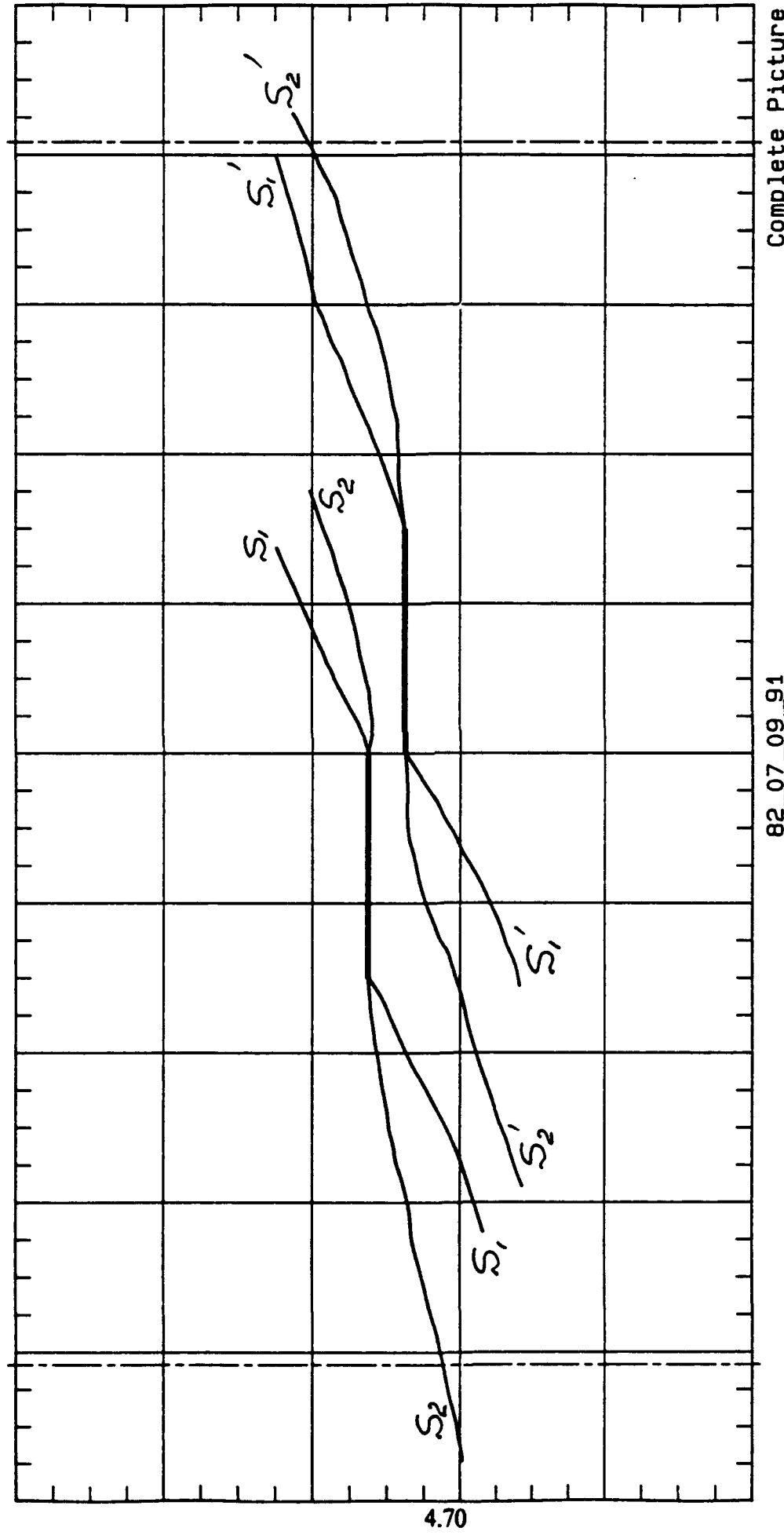
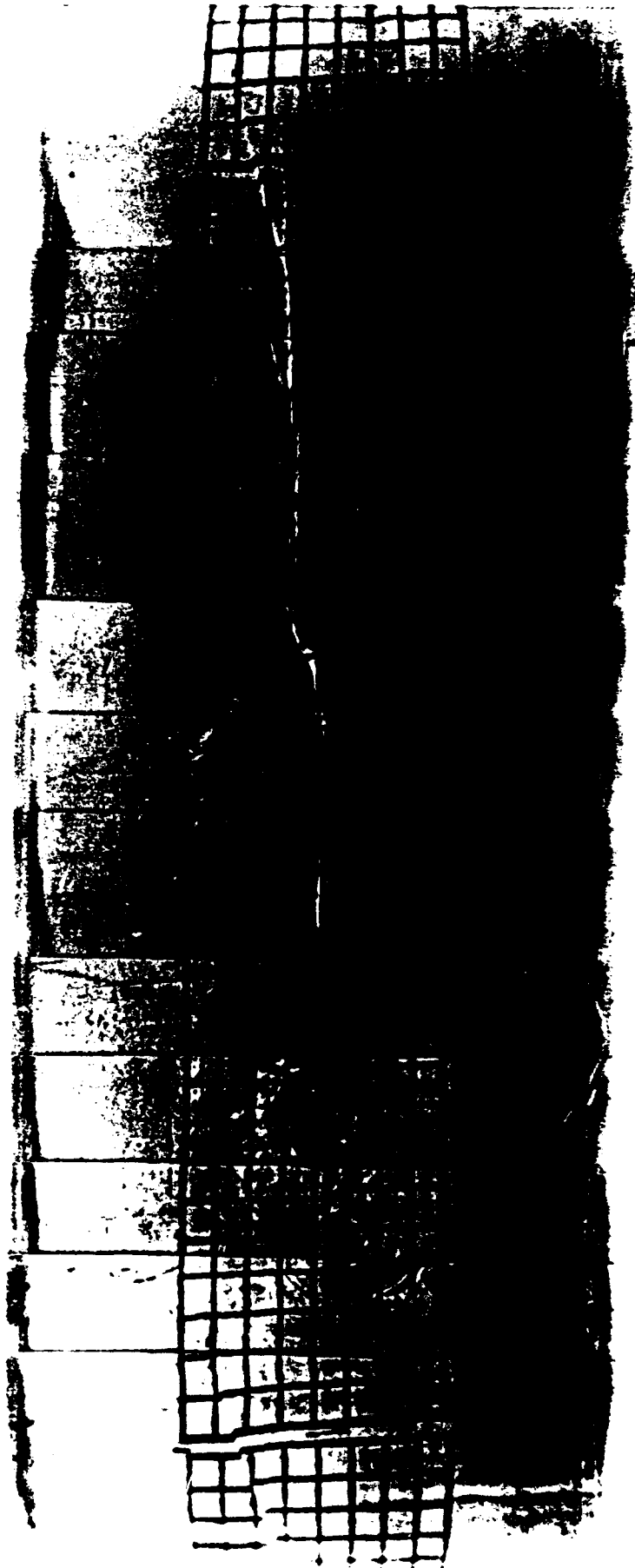


Figure 4.19z Shear Bands and Interaction of Two Cracks in the Upstep Position; $\epsilon = 0$



Test Name: 83_07/11/91 Consol.: Ko OC
Material: EPK Control: OCR-4
Beta: 45
Control: Deform.
Height: Variable

Figure 4.20 Shear Bands and Interaction of Two Cracks in the Upstep Position; $e = 0.6\text{cm}$

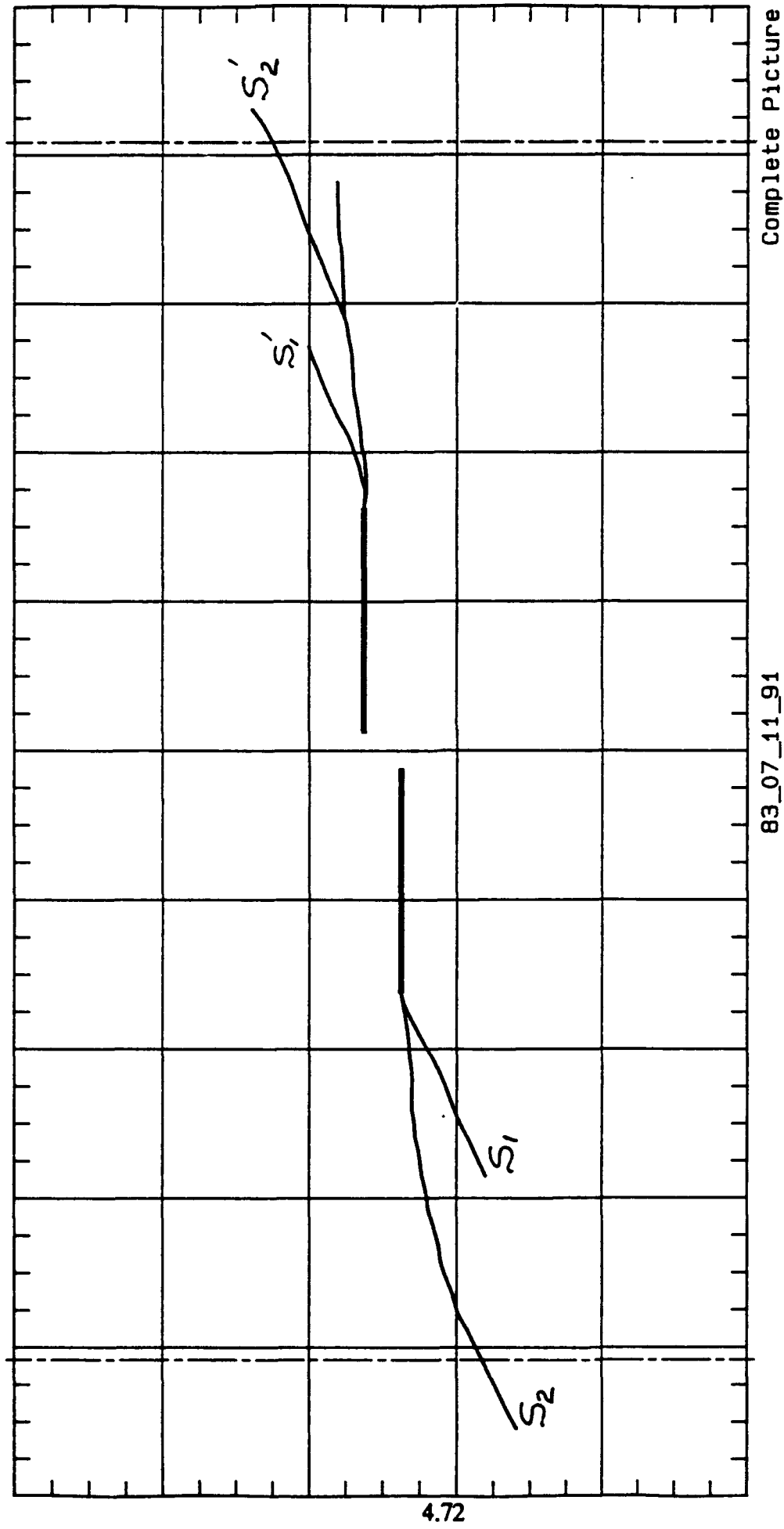
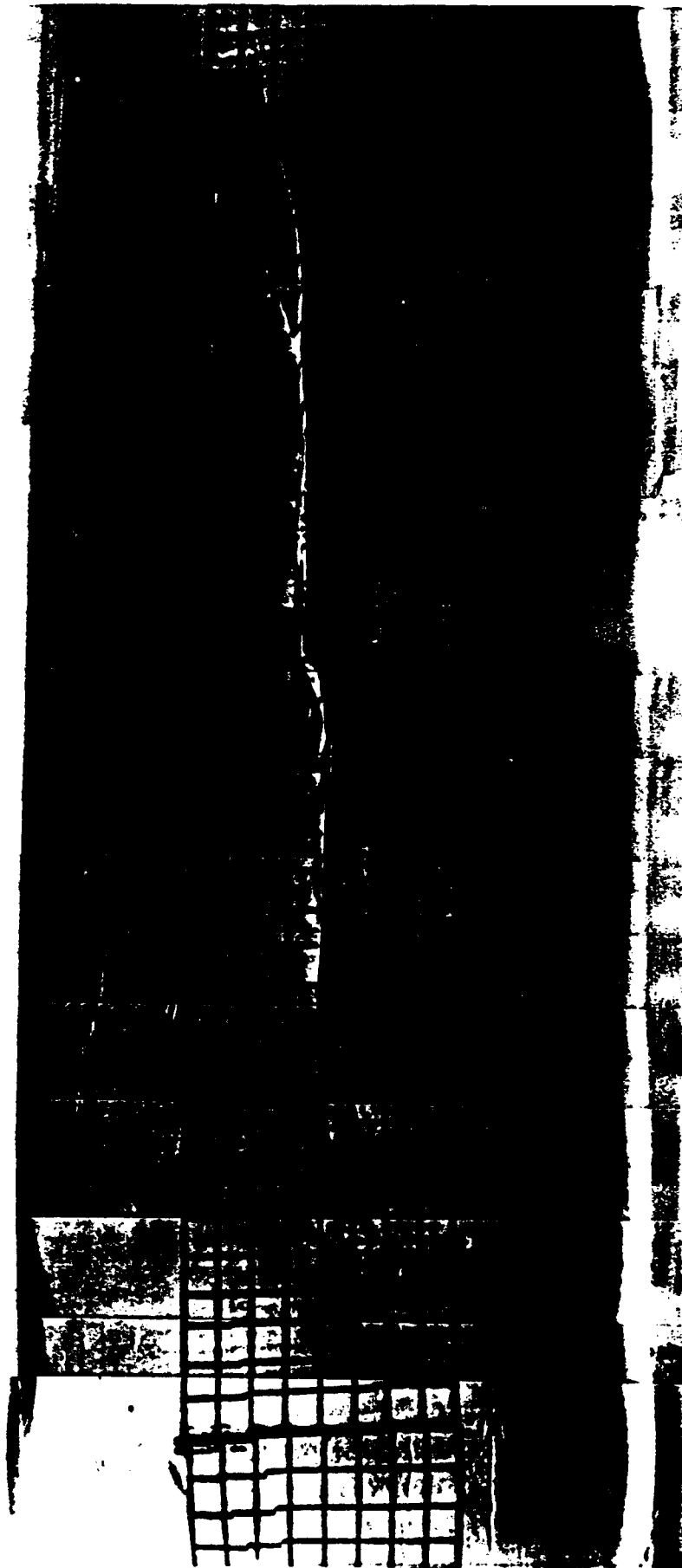


Figure 4.20z Shear Bands and Interaction of Two Cracks in the Upstep Position; $e = 0.6\text{cm}$



Test Name: 84_07/17/91 **Consol.:** Ko OC
Material: EPK **Beta:** 45
 OCR-4 **Control:** Deform.
 Height: variable

Figure 4.21 Shear Bands and Interaction of Two Cracks in the Upstep Position; $e = 1.3\text{cm}$

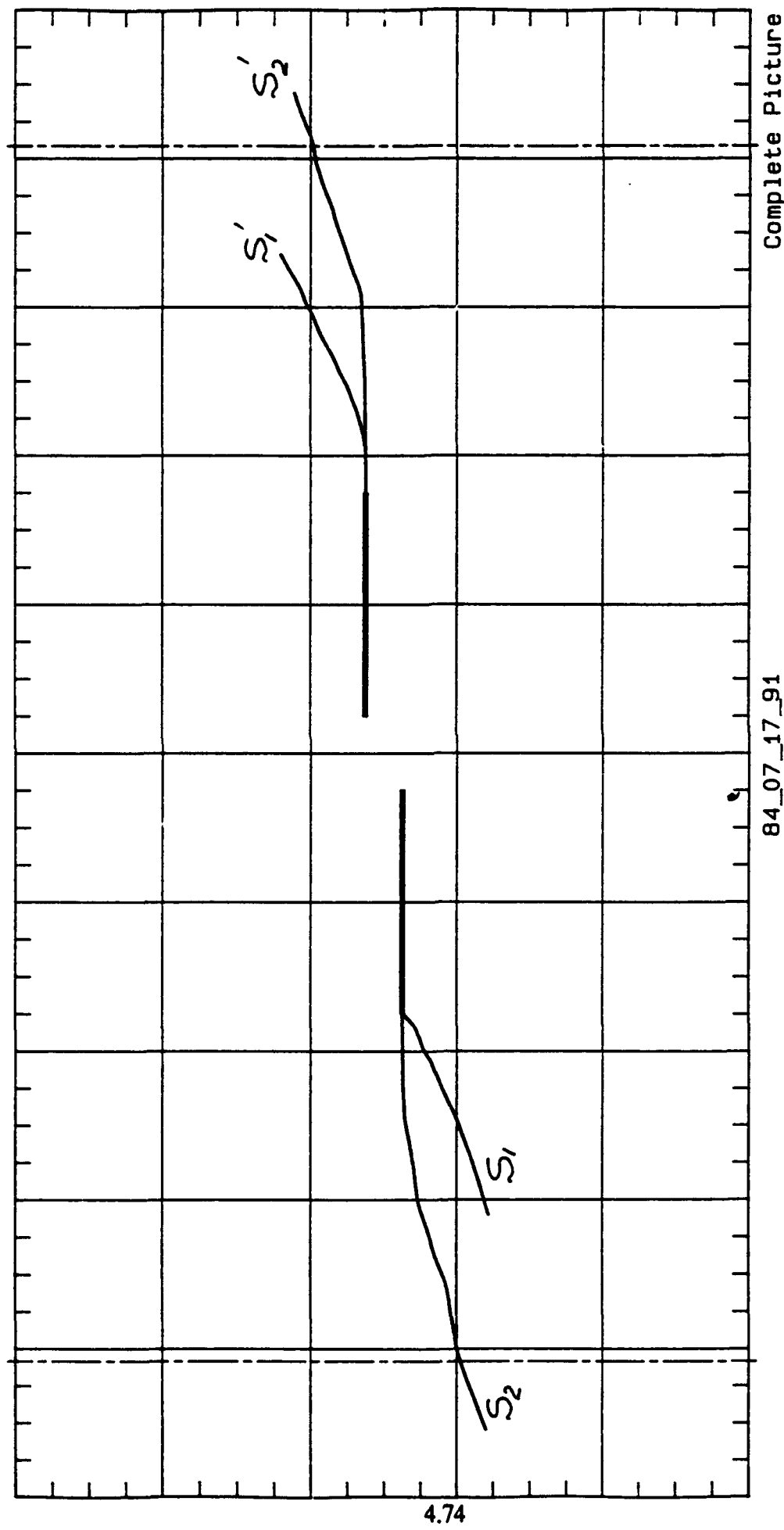
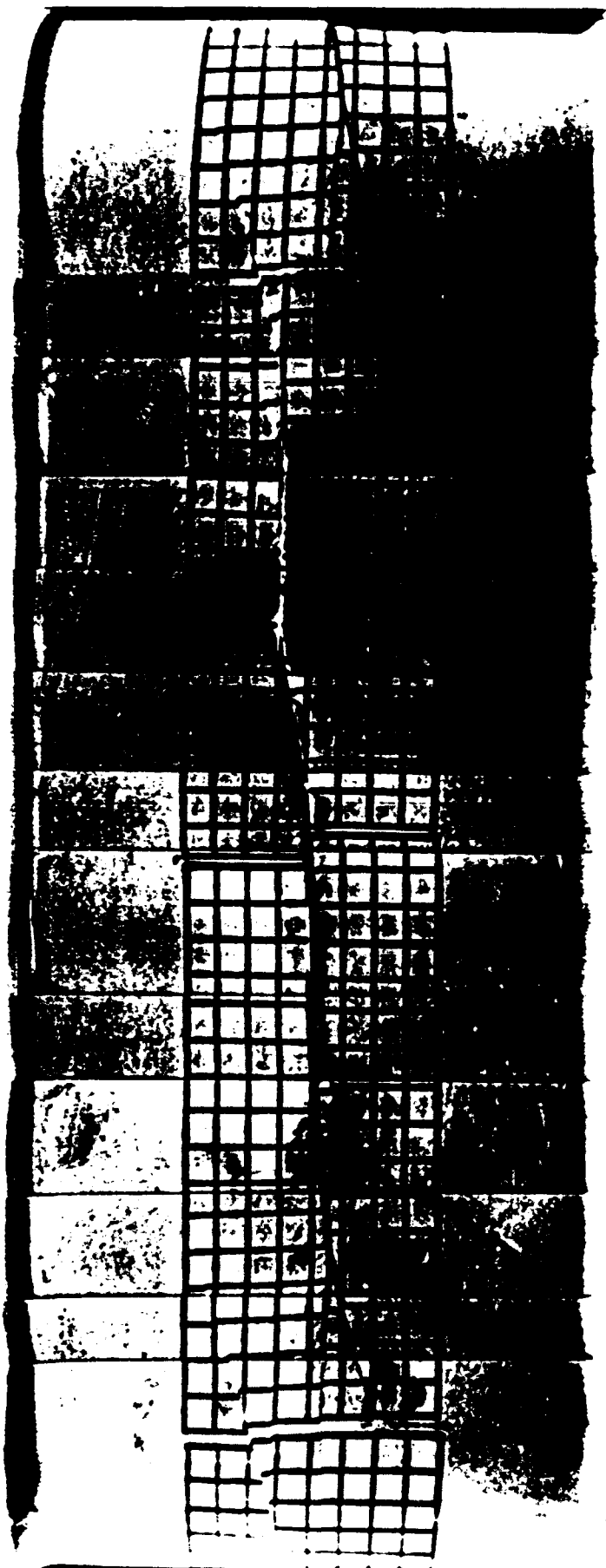


Figure 4.21z Shear Bands and Interaction of Two Cracks in the Upstep Position; $e = 1.3\text{cm}$



Test Name: 85_07/19/91 **Conso1.:** Ro OC
Material: EPK **OCR-4** **Beta:** 45
Position; e = 2.54cm **Control:** Deform.
Height: variable

Figure 4.22 Shear Bands and Interaction of Two Cracks in the Upstep Position; e = 2.54cm

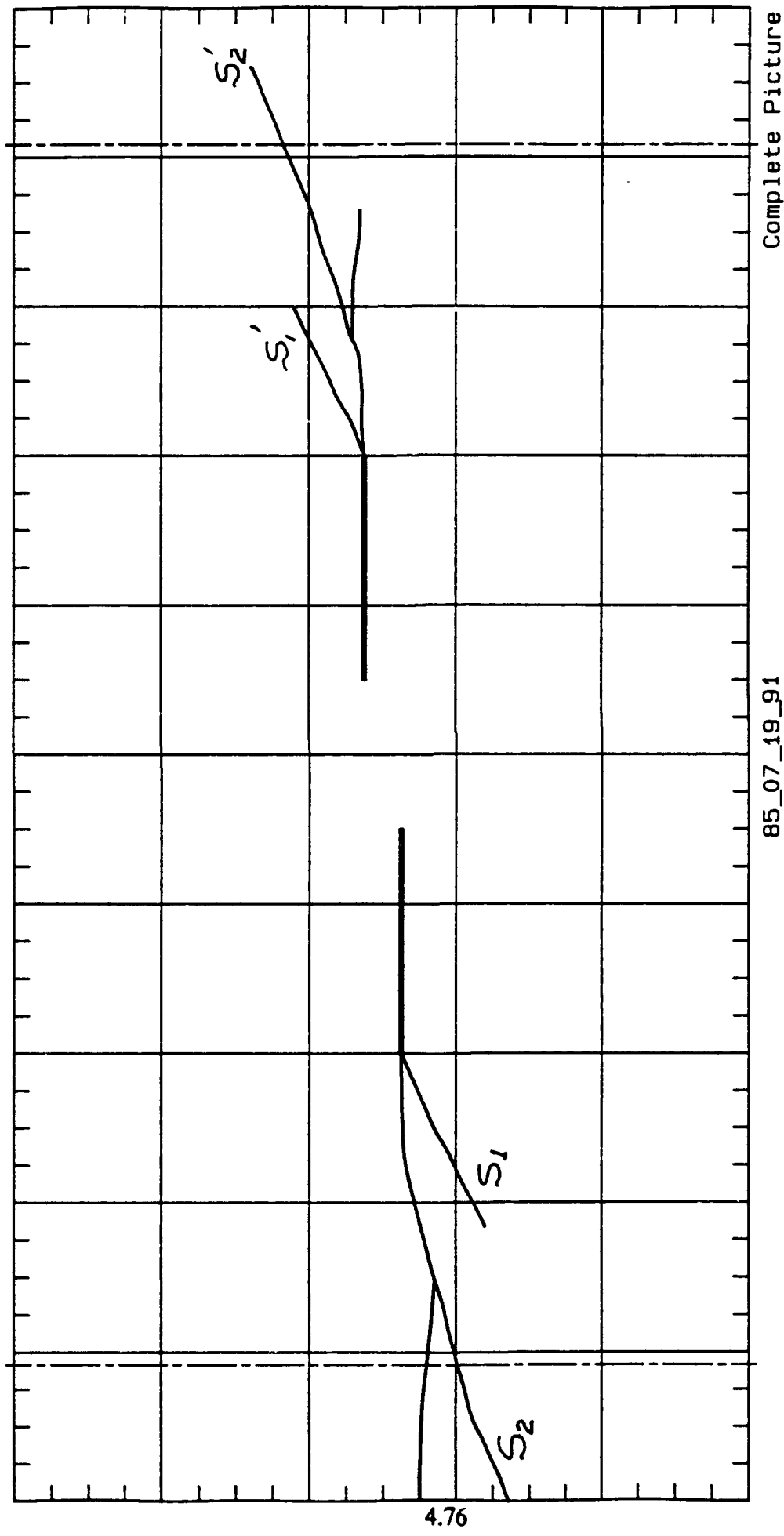


Figure 4.22z Shear Bands and Interaction of Two Cracks in the Upstep Position; $e = 2.54\text{cm}$

Length of first Shear Band for various levels of Rotation

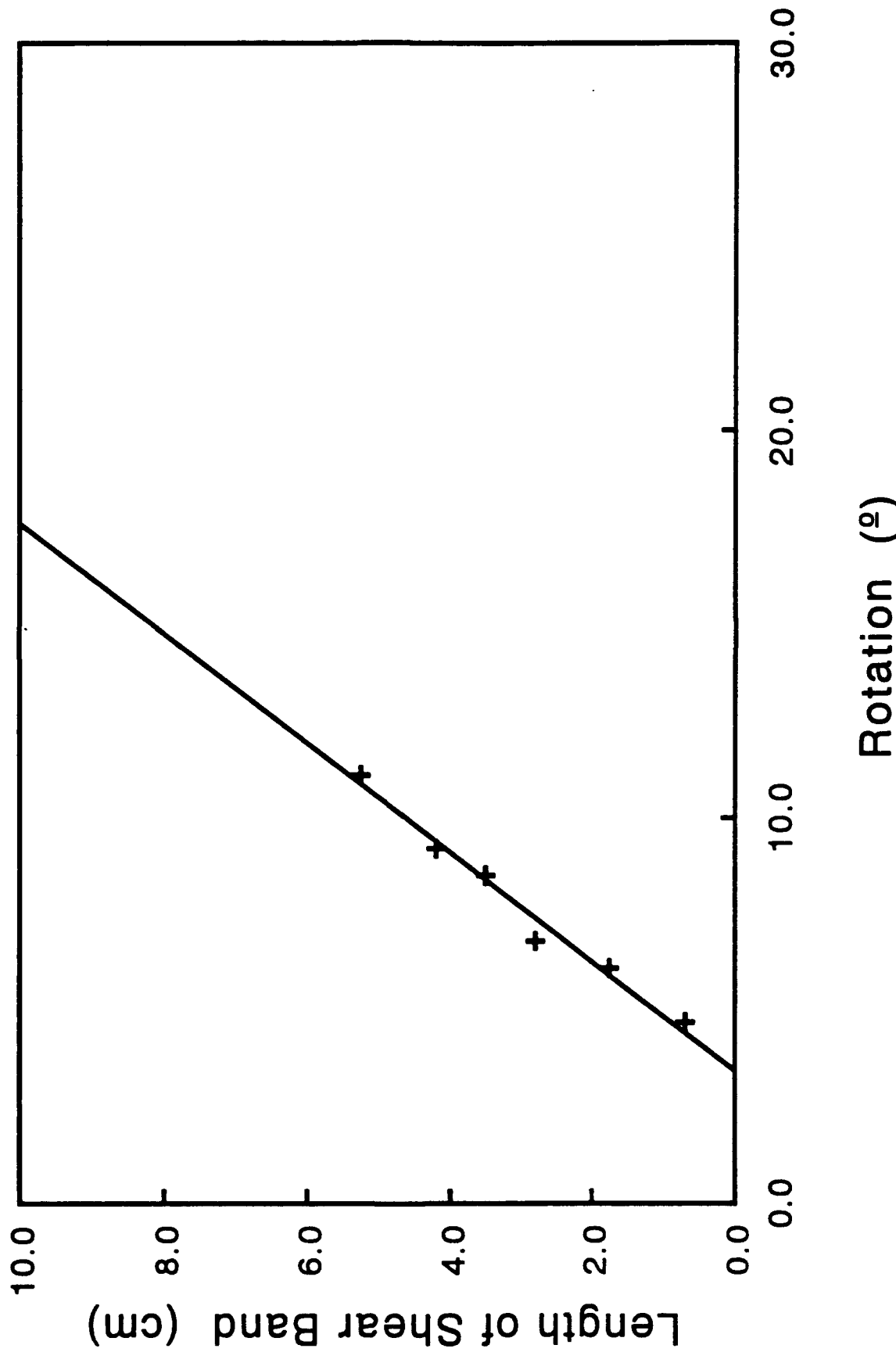


Figure 4.23 Length of First Shear Band for Various Levels of Rotation
(18-1-15-91)

**Slip measured along Shear Band
at the end of the test**

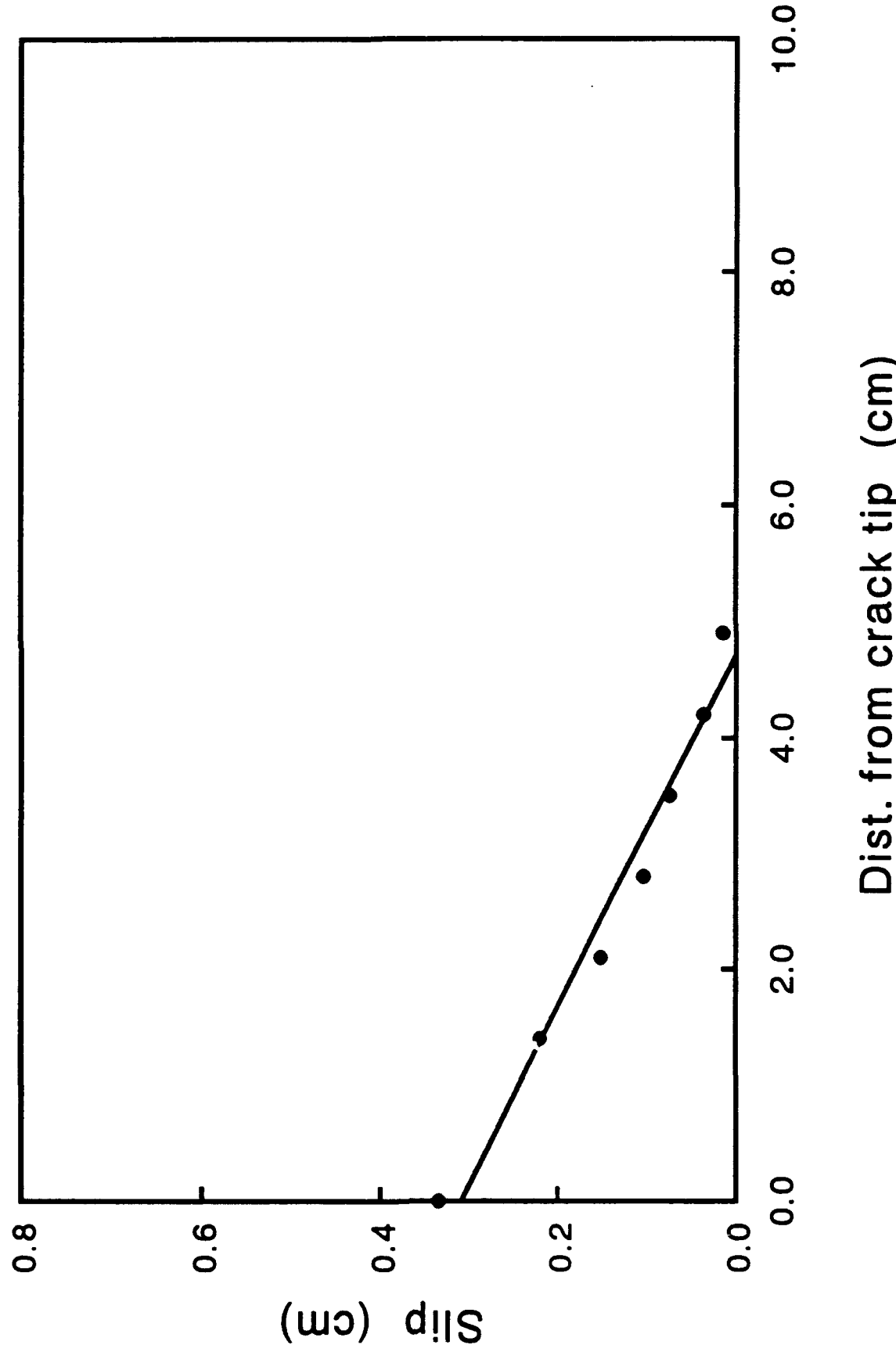


Figure 4.24 Amount of Slip Along the First Shear Band (18-1-15-91)

Slip along the first Shear Band for various levels of Rotation

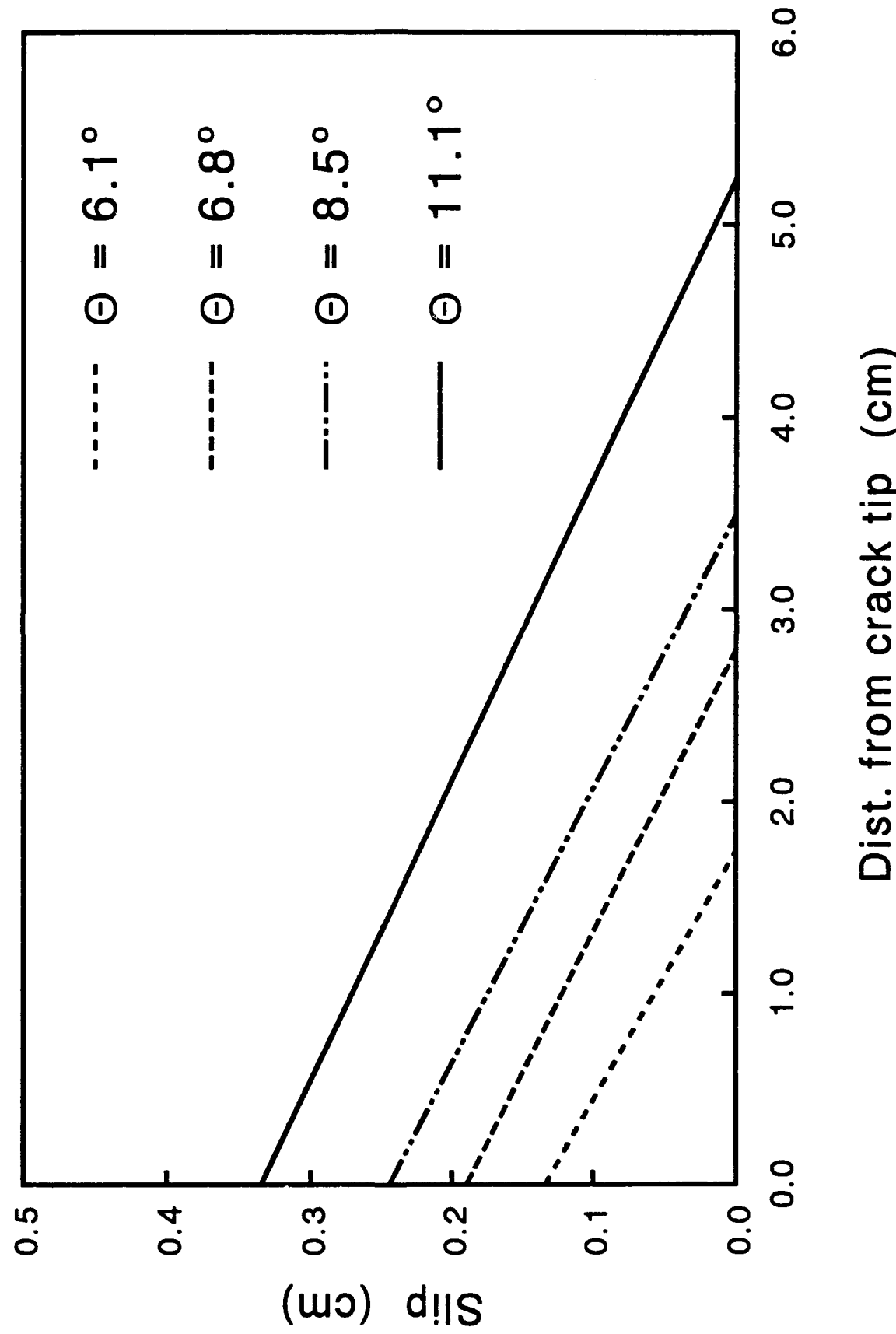


Figure 4.25 Slip Along the First Shear Band for Various Levels of Rotation
(18-1-15-91)

Length of Shear Bands for various levels of Rotation

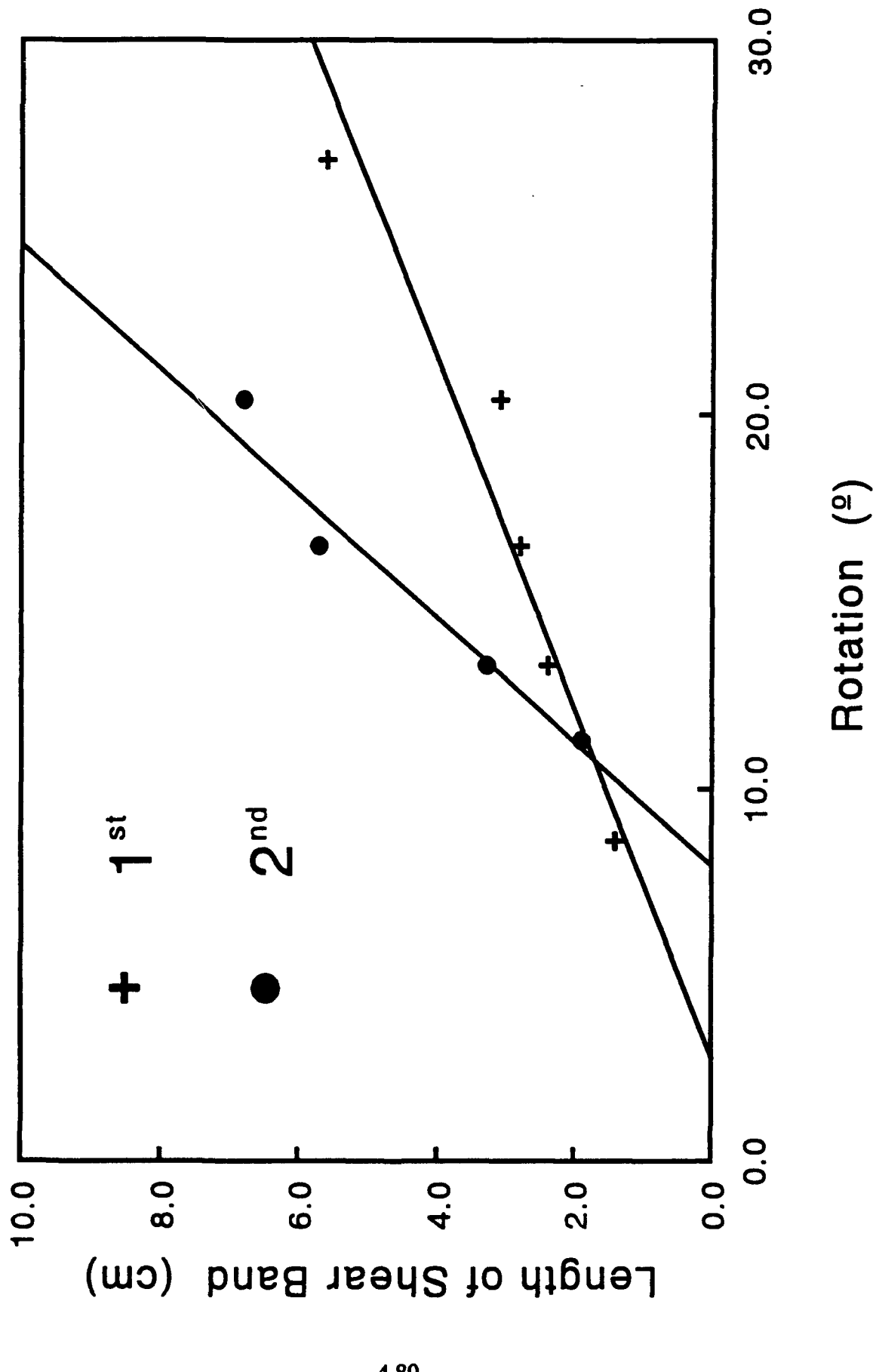


Figure 4.26 Length of Shear Bands for Various Levels of Rotation (66-5-29-91)

Slip measured along Shear Bands
at the end of the test

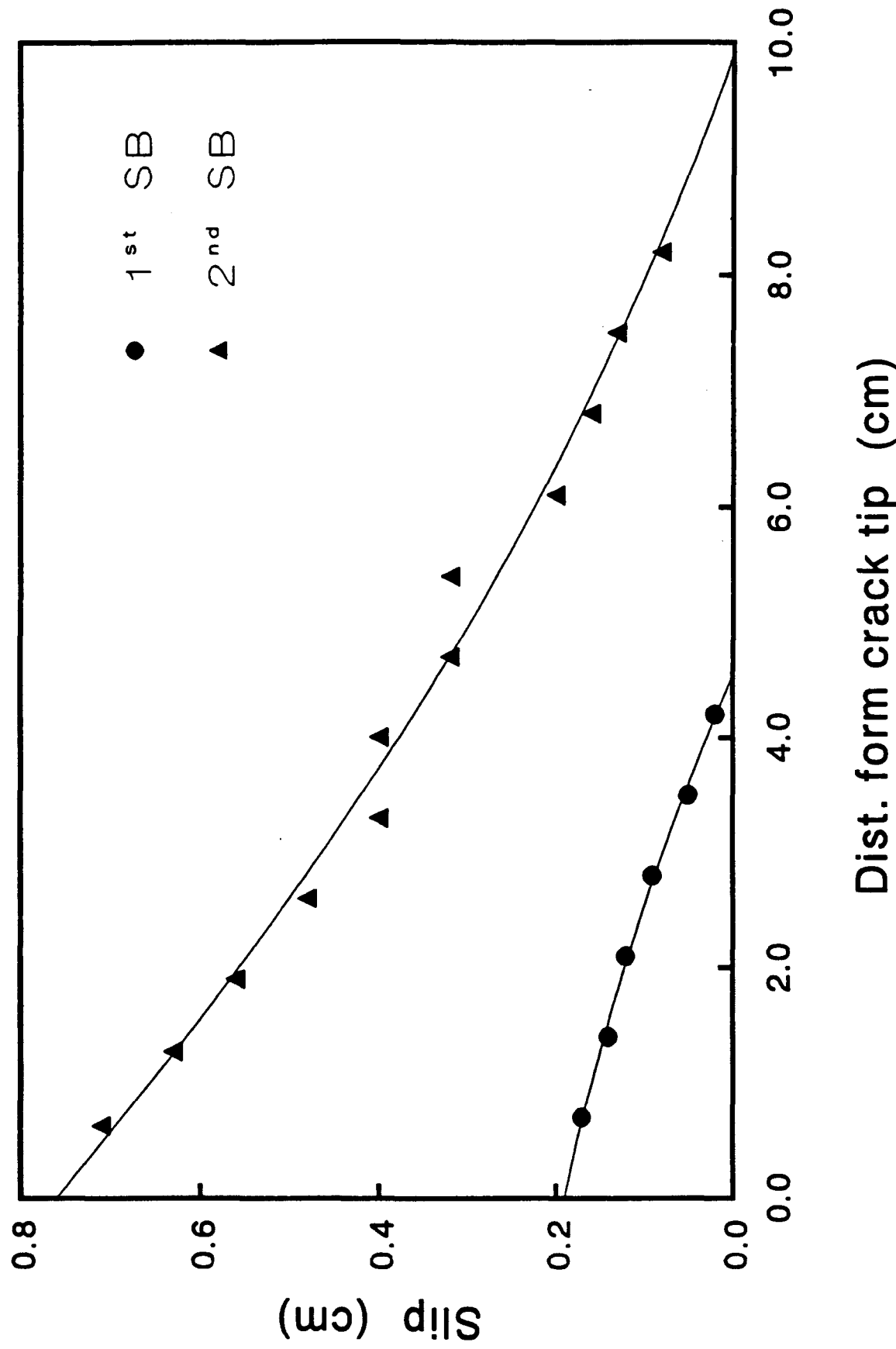


Figure 4.27 Amount of Slip Along the Shear Bands (66-5-29-91)

Length of Shear Bands for various levels of Rotation

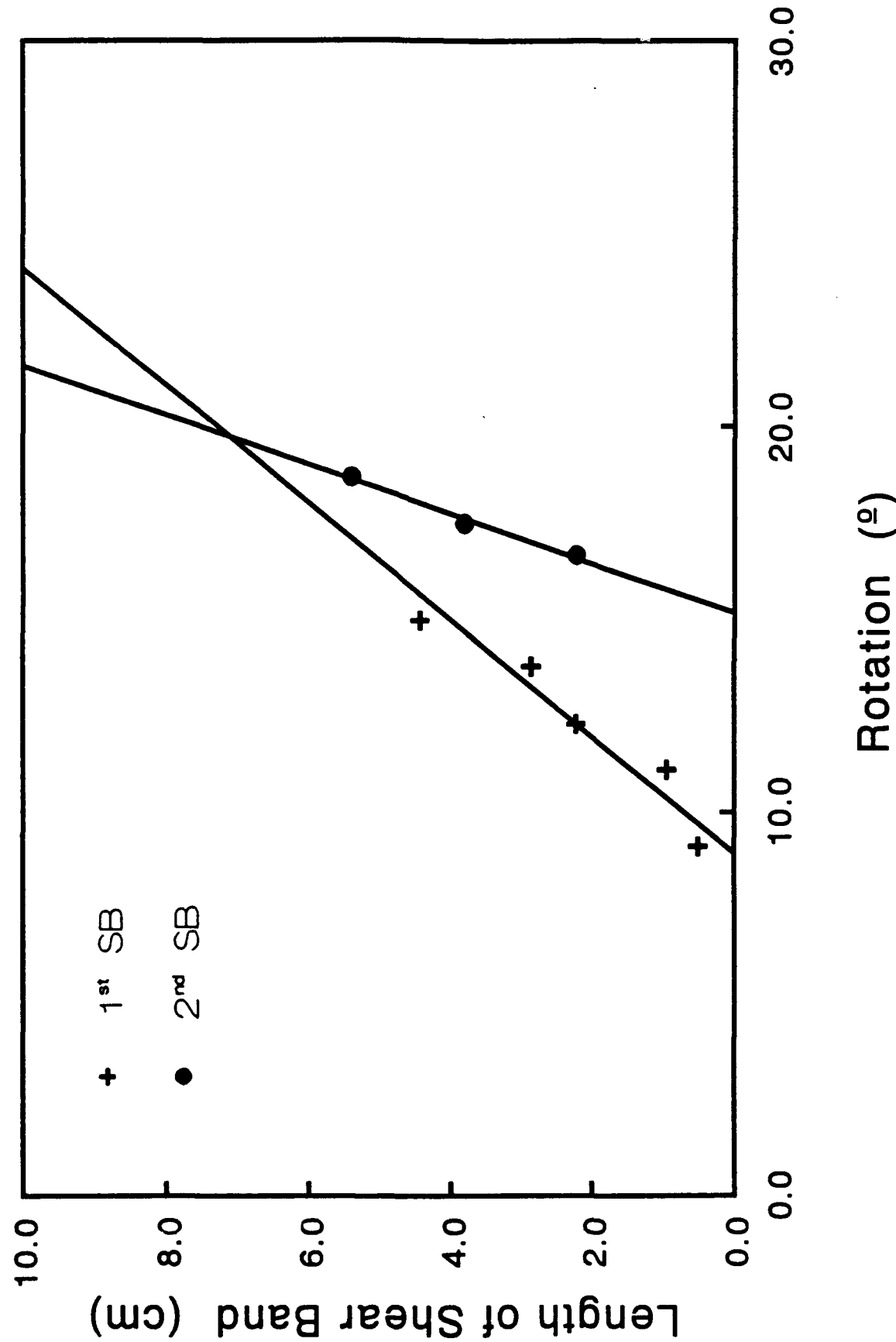


Figure 4.28 Length of Shear Bands for Various Levels of Rotation
(16-12-13-90)

**Slip measured along Shear Bands
at the end of the test**

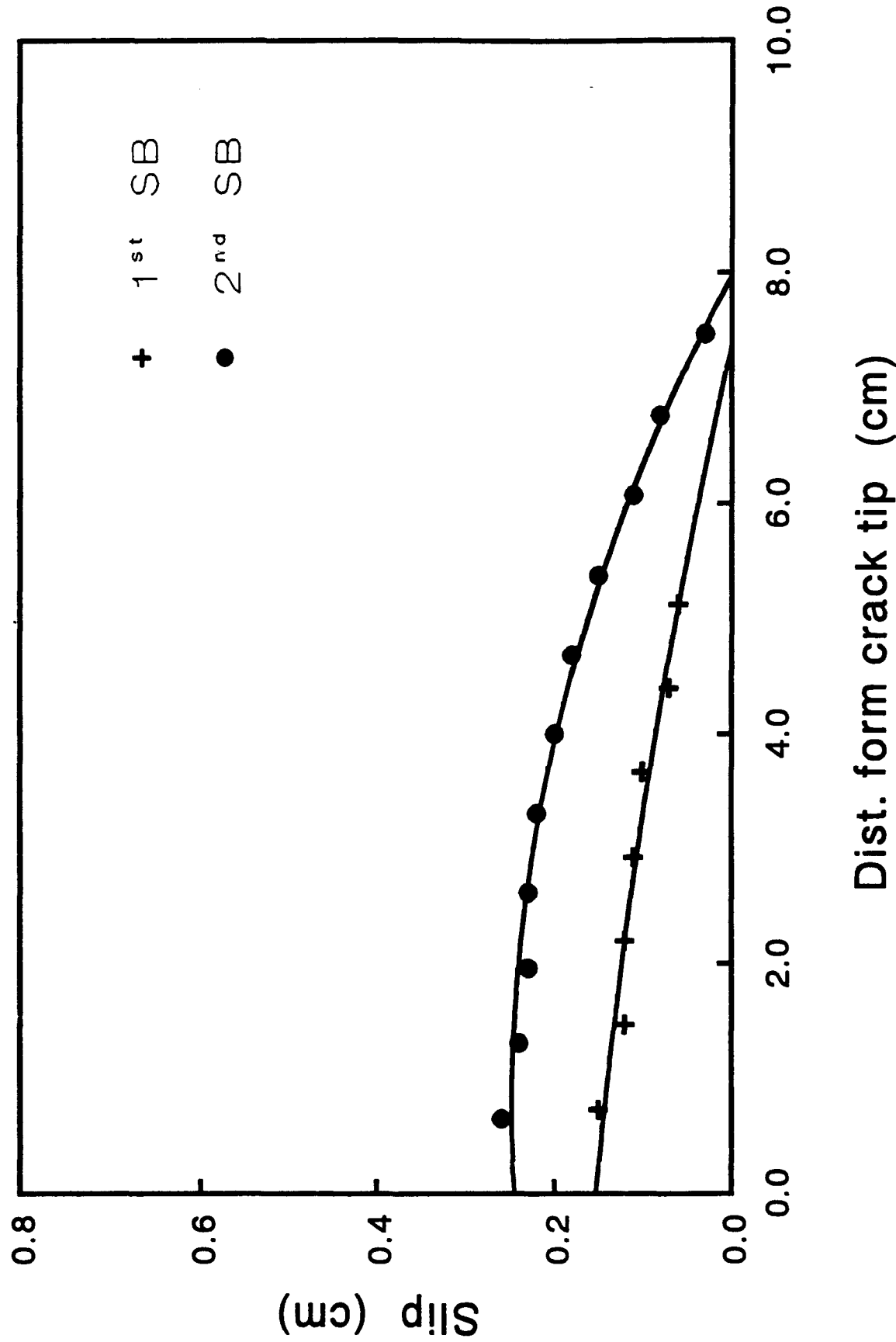


Figure 4.29 Amount of Slip Along the Shear Bands (16-12-13-90)

Length of first Shear Band for various levels of Rotation

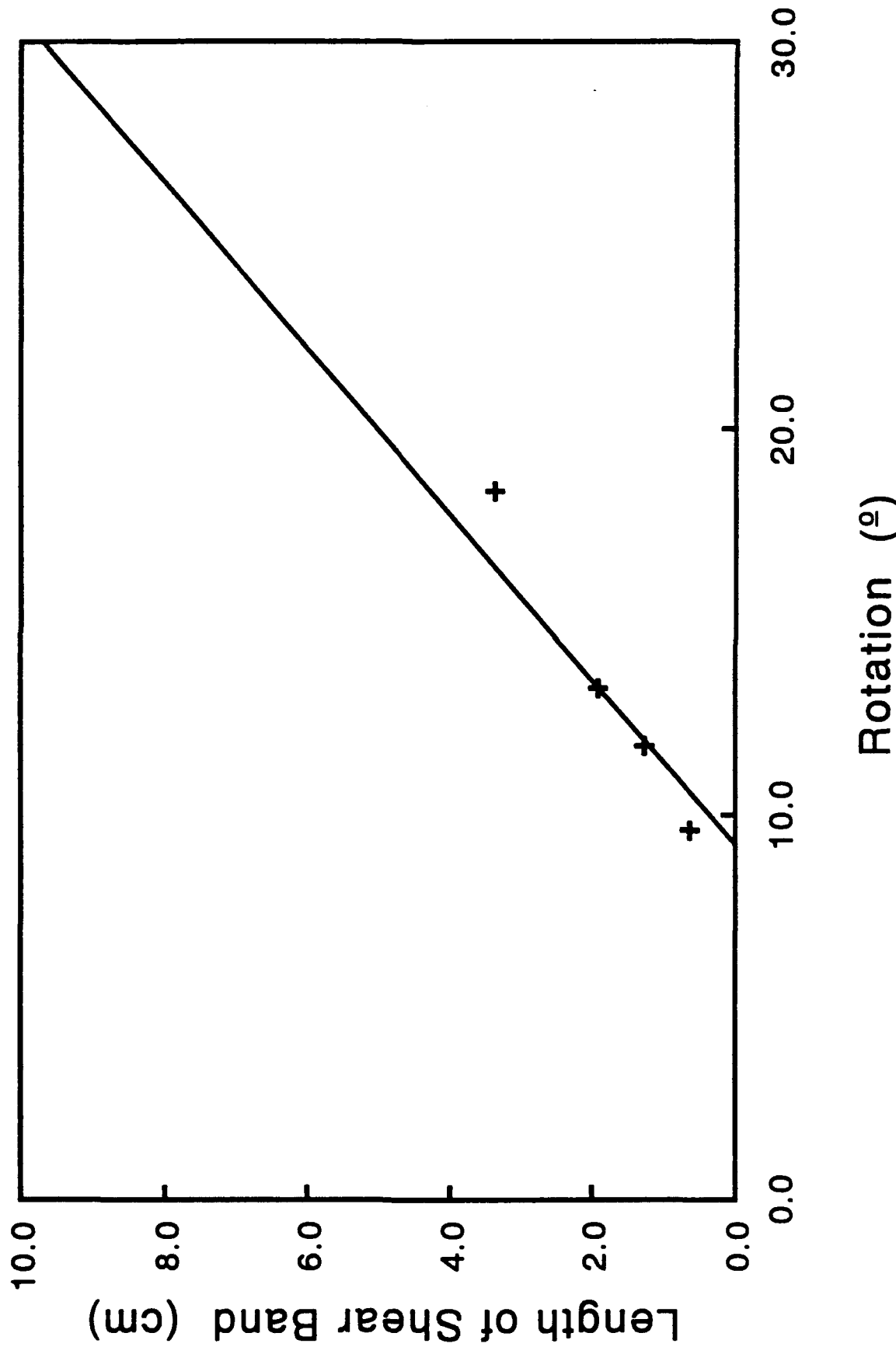


Figure 4.30 Length of First Shear Band for Various Levels of Rotation
(70-6-14-91)

**Slip measured along Shear Band
at the end of the test**

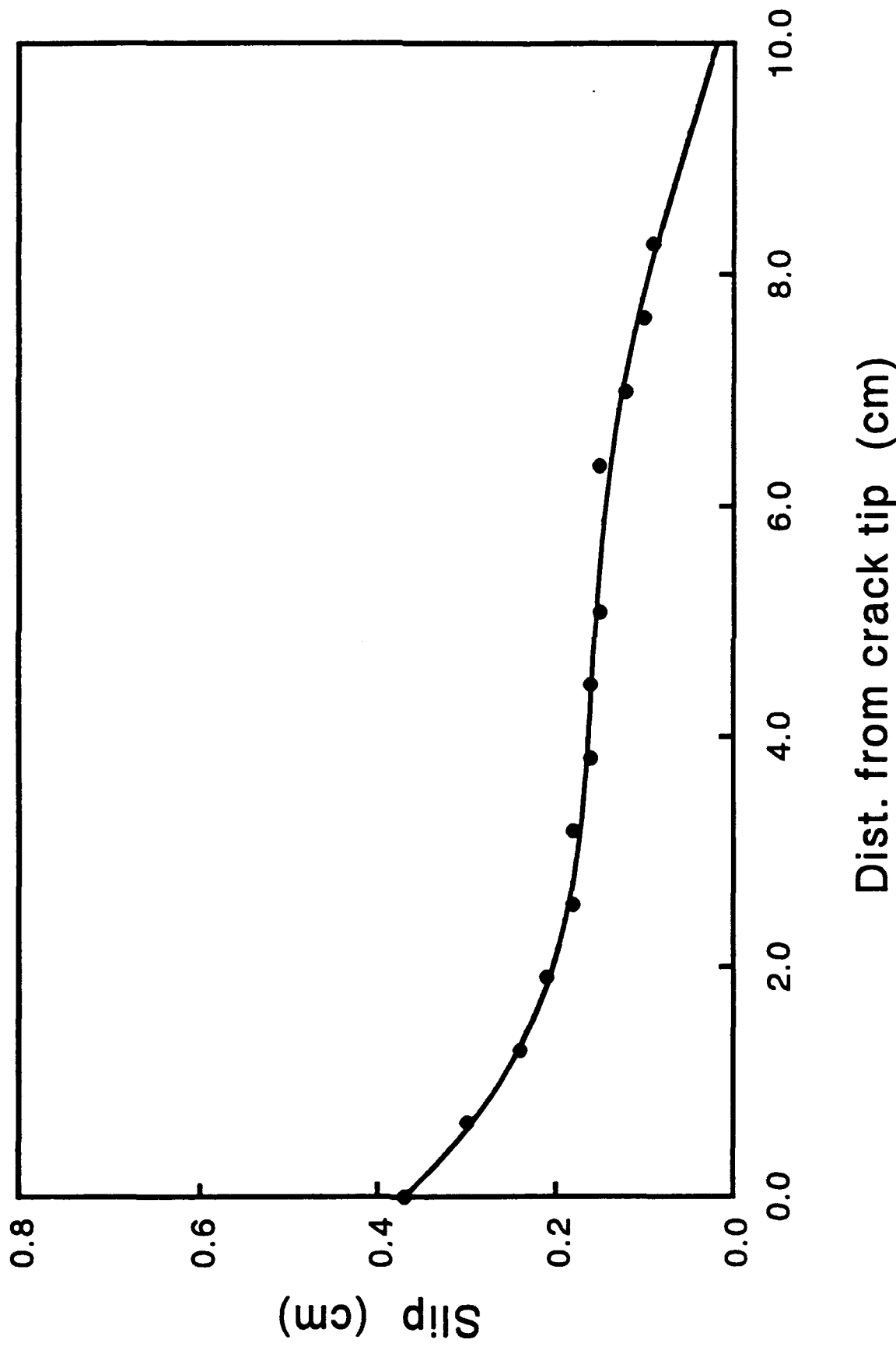


Figure 4.31 Slip Along the First Shear Band for Various Levels of Rotation (70-6-14-91)

CHAPTER 5

APPLICATION OF FRACTURE MECHANICS AND PLASTICITY THEORY

The observations made in the last two chapters indicate that neither fracture mechanics theories alone nor plasticity theories alone can describe the complete phenomenon. This was pointed out by Bazant and Mazars (1990) who suggest that the problem was one of localization of damage and stability. It is instructive however to start with the application of linear fracture mechanics and proceed from there to combining fracture mechanics and plasticity to the material at hand.

Using the results obtained from the tests conducted on specimens with cracks of various a/l ratios (Table 5) one can follow the standard procedures of linear fracture mechanics. Fig. 5.1 shows the torque versus the angle of rotation for a/l varying from 0 to 0.4. The work done is shown in Fig. 5.2 where the curves are seen to be quite close to each others specially at small angles of rotation. For ratios $a/l > 0.1$ all the curves seem to coincide indicating that the size of the crack has little effect on the energy. The J integral is shown in Fig. 5.3 and reflects the results of the two previous figures.

There is no doubt that the plasticity of the material plays an important role. Once the shear bands start forming and reach some length they control the behavior with little influence from the original size of the crack. However, stress distributions calculated using linear elasticity can be taken advantage of to explore zones of high stress concentrations in the vicinity of the crack's tip.

5.1 Stress Concentration Around Cracks Tips.

Classical solutions in terms of stress intensity factors involve approximations that restrict their use to the very close vicinity of the crack. However, Muskhelishvili (1953) gives the general expressions for the stress distribution in an infinite plate with a crack subjected to stresses N_1 & N_2 at infinity. Using a standard notation of elasticity theory. (Fig. 5.4a) we have

$$\sigma_{xx} + \sigma_{yy} = 2 (\phi(z) + \bar{\phi}(\bar{z}))$$

$$\sigma_{yy} - i\sigma_{xy} = \phi(z) + \Omega(\bar{z}) + (z - \bar{z})\bar{\phi}'(\bar{z}) \quad 5.1$$

where the complex potential $\phi(z)$ and $\Omega(z)$ are given by:

$$\phi(z) = \frac{(2\Gamma + \bar{\Gamma}')z}{2\sqrt{z^2 - a^2}} - \frac{1}{2}\bar{\Gamma}' \quad 5.2$$

$$\Omega(z) = \frac{(2\Gamma + \bar{\Gamma}')z}{2\sqrt{z^2 - a^2}} + \frac{1}{2}\bar{\Gamma}'.$$

$$\Gamma = \frac{1}{4}(N_1 + N_2) \quad 5.3$$

$$\Gamma' = -\frac{1}{2}(N_1 - N_2) e^{-2i\alpha}$$

Thus,

$$\sigma_{xx} + \sigma_{yy} = \frac{(2\Gamma + \bar{\Gamma}')z}{2\sqrt{z^2 - a^2}} + \frac{(2\bar{\Gamma} + \Gamma')\bar{z}}{2\sqrt{z^2 - a^2}} \quad 5.4$$

$$\begin{aligned} \sigma_{yy} - i\sigma_{xy} &= \frac{(2\Gamma + \bar{\Gamma}')z}{2\sqrt{z^2 - a^2}} + \frac{(2\bar{\Gamma} + \Gamma')\bar{z}}{2\sqrt{z^2 - a^2}} \\ &\quad + (z - z') \frac{2\bar{\Gamma} + \Gamma'}{2} \left[\frac{1}{\sqrt{z^2 - a^2}} - \frac{z^2}{(z^2 - a^2)^{3/2}} \right] \end{aligned}$$

For the shear conditions shown in Fig. 5.4b.

$$N_1 = \tau, N_2 = -\tau, \alpha = \frac{\pi}{4}$$
$$\Gamma = 0, \Gamma' = i\tau, \bar{\Gamma}' = -i\tau \quad 5.5$$

Thus, Eqs. 5.4 become

$$\sigma_{xx} + \sigma_{yy} = -2\tau \operatorname{Re} \frac{iz}{\sqrt{z^2 - a^2}}$$
$$\sigma_{yy} - \sigma_{xx} + 2i\sigma_{xy} = \tau \frac{ia^2 z + iz(2z^2 - 3a^2)}{(z^2 - a^2)^{3/2}} \quad 5.6$$

For a combination of axial lateral and shearing stresses superposition is used. The crack is assumed to transfer normal stresses and stress distributions due to compressions are not affected by the presence of the crack. Fig. 5.5 illustrate the superposition used in the calculations. The third dimension is ignored.

An appropriate software was used to calculate the distribution of stresses and plot contour lines of equal shearing stress σ_{xy} , normal stress σ_{xx} , normal stress σ_{yy} , minimum principal stress σ_3 , maximum principal stress σ_1 , maximum shear stress σ_{tmax} and equal mean stress σ_m . Some 3D graphs were also made to show how fast the effect of the stress concentration at the tip of the crack died down. (This effect will decrease somewhat for elastic-plastic analysis.) The 3D graphs also allow one to estimate the applicability of equations valid for the infinite medium to the case of the hollow cylinder.

Figs. 5.6a to 5.6o refer to a pure torsion test where the applied shear stress is equal to 1 kPa. On those graphs the length of the half crack is 2.54cm (2 in.)

Figs. 5.7a to 5.7o refer to combinations of tensile axial, hydrostatic and torsional stresses, namely to Test No. 52-4-9-91 in Table 3. The applied torsional shear stress is

217.1430 kPa and the applied normal stresses are 192.441 kPa axially and 375.67 kPa laterally.

Figs. 5.8a to 5.8o refer to a pure torsion test under hydrostatic conditions, namely to test No. 6v-9-26-90 in Table 3. The applied torsional shear stress is 243.225 kPa and the applied normal stresses are 336.03 kPa. This last pressure of course is the effective spherical stress acting on the specimen.

Figs. 5.9a to 5.9o refer to combinations of compression axial, hydrostatic and torsional stresses, namely to test No. 51-4-5-91 in Table 3. The applied torsional shear stress is 275.17 kPa and the applied normal stresses are 543.86 kPa axially and 302.9 kPa laterally.

Many of the graphs in Figs. 5.7 to 5.9 indicate zones of tension in spite of the reasonably high hydrostatic stress acting on the specimen. Such zones, as well as the ones exhibiting high shearing stresses would be prime areas in which the crack or the shearing bands would propagate. The graphs showing the contour lines for maximum shearing stresses should give clear indications on the direction of a shear band, should one appear at the tip of the crack; if the material were a Tresca or a Mises material in the plastic range. Indeed such directions are shown on Figs. 5.7k, 5.8k and 5.9k by a slashed line. The directions of the shear bands observed in the last chapter and shown in Figs. 4.6c, b and a show that this is not the case and point to the need for an elasto-plastic analysis taking into account the frictional nature of the material.

5.2 Finite Elements Elasto-Plastic Analysis.

The finite element code ABAQUS allows one to study the stress distribution and the propagation of the plastic zone as stresses on the specimen increase. Fig. 5.10 shows the size of the plate (developed hollow cylinder) for which the calculations were made. Notice that the crack has a blunted end to represent the thickness of the Teflon inserts. The proper size of mesh was obtained by calculating J integrals for three different mesh configurations and judging the change when passing from one mesh to the other. A mesh with eight nodes isoparametric elements was chosen. A total of 480 elements with 1626 nodes was used.

For the elasto-plastic analysis a Young's modulus of 20.7×10^4 kPa and a Poisson ratio of 0.3 were used together with either a Mises or a Drucker-Prager (DP) yield criterion. The angle for the Drucker-Prager criterion is given by (Fig. 5.11)

$$\tan\beta = \frac{6 \sin \phi'}{3 - \sin \phi'}$$

where ϕ' is the effective angle of friction chosen as 33.3 degrees. The value of

$$d = c \frac{6 \cos \phi'}{3 - \sin \phi'}$$

is chosen to correspond to a cohesion of 172.5 kPa.

Figs. 5.12 and 5.13 show the propagation of the yield zone for the Mises and DP criteria respectively. The test is a pure torsion test. Notice the direction of propagation when one changes from a non-frictional to a frictional material. As expected the Mises criterion gives a direction of propagation that is along that of the crack. On the other hand

the frictional material shows a definite inclination of the direction of the crack. This is what was observed in our experiments. Therefore, the DP criterion will be used in analyzing results obtained from tests under combined stresses.

The first step is to compare the elastic solution with the elasto-plastic one. The results of the elastic solution for the pure torsion cases are shown in Figs. 5.14a, b and c. [They compare exceedingly well with the Muskhelishvili solutions illustrated in Fig. 5.6g, i and k]. The results of the elasto-plastic solution are shown in Figs. 5.15a, b and c. Both sets of figures give lines of equal σ_1 , σ_3 and $\sigma_1 - \sigma_3$, respectively. One notices, particularly on the graphs representing σ_1 that the tension zone is much smaller for the elasto-plastic analysis than it is for the elastic analysis (see contour No. 29 along which there is tension). At a short distance from the tip, however, the two sets of contour lines are quite similar for all cases.

A better appreciation of the differences between the two analyses can be obtained from looking at Figures 5.16a and b and Figures 5.17 a and b. Figure 5.16a and b show the values of $\sigma_1 - \sigma_3$, σ_1 and σ_3 along a horizontal line starting at the tip of the crack for the elastic and the elasto-plastic analyses respectively. Figs. 5.17a and b show the same quantities along a vertical line at the tip of the crack. One notices that the distribution in the vertical direction is more affected by the type of analysis than it is along the horizontal direction. Also σ_1 seems to be the quantity that is most affected in both cases. It is compressive near the tip of the crack in Fig. 5.17b and tensile in 5.17a; in spite of the high hydrostatic pressure of nearly 340 kPa acting on the material. The plastic zone, which very

quickly appears at the tip of the crack, eliminates the high stress concentration that is seen in Fig. 5.17a.

Three tests involving combined stresses were analyzed elasto-plastically using the DP criterion. A compression-torsion test (51-4-5-91), a torsion test (6v-9-26-90) and a tension torsion test (52-4-9-91); all listed in Table 3.

Figs. 5.18a, b and c show the spread of the plastic zone for the compression-torsion test, the pure torsion test and the tension-torsion test. The loading was radial and was increased to a value of shearing stress of about 170 kPa with the axial load following proportionally. The contour lines are lines of equal equivalent plastic strain defined as

$$\epsilon_{eq}^P = \int \sqrt{\frac{2}{3} d\epsilon_{ij} d\epsilon_{ij}}$$

The evolution of the plastic zones suggest that when the material localizes it will result in shear bands having directions similar to the ones observed in Chapter 4 i.e. approximately 35° , 22° and 0° for three tests. The high concentration of contours in the upper part of the crack tip is due to the high tension existing in this region.

For the sake of completeness the contours giving σ_1 , σ_3 and $\sigma_1 - \sigma_3$ are also given in Fig. 5.19, 5.20 and 5.21 for the three tests. In those figures a, b and c refer to compression-torsion, pure torsion and tension-torsion respectively.

Tables 5.1 and 5.2 allow one to obtain the magnitudes of the stresses on the contour lines shown on Figs. 5.12 to 5.21.

TABLE 5.1 STRESS VALUES ON VARIOUS CONTOUR LINES

FIG. No.	STRESS ON CONTOUR No.1 kPa	STRESS ON CONTOUR No. 30 kPa	INCREMENT kPa
5.14a 5.15a 5.19a, b, c	1378.0	68.9	45.14
5.14b 5.15b 5.20a, b, c	-1378.0	68.9	49.89
5.14c 5.15c 5.21a, b, c	-689.0	344.5	35.64

Remark: The stress on any contour line between contours No. 2 and No. 30 is calculated as follows:

$$\text{Stress} = (\text{Contour Number}-1) \times \text{Increment} + \text{Stress on Contour No. 1}$$

**TABLE 5.2 EQUIVALENT PLASTIC STRAIN VALUES ON
VARIOUS CONTOUR LINES**

FIG. No.	STRAIN ON CONTOUR No. 1	STRAIN ON CONTOUR No.2	STRAIN ON CONTOUR No. 30	INCREMENT
5.12				
5.13				
5.18a, b, c	3.44×10^{-12}	3.44×10^{-6}	10^{-4}	3.45×10^{-6}

Remark: The equivalent plastic strain on any contour line between contours No. 2 and 30 is calculated as follows:

$$\text{Strain} = (\text{Contour Number}-2) \times \text{Increment} + \text{Strain on Contour No. 2}$$

Torque Versus Rotation

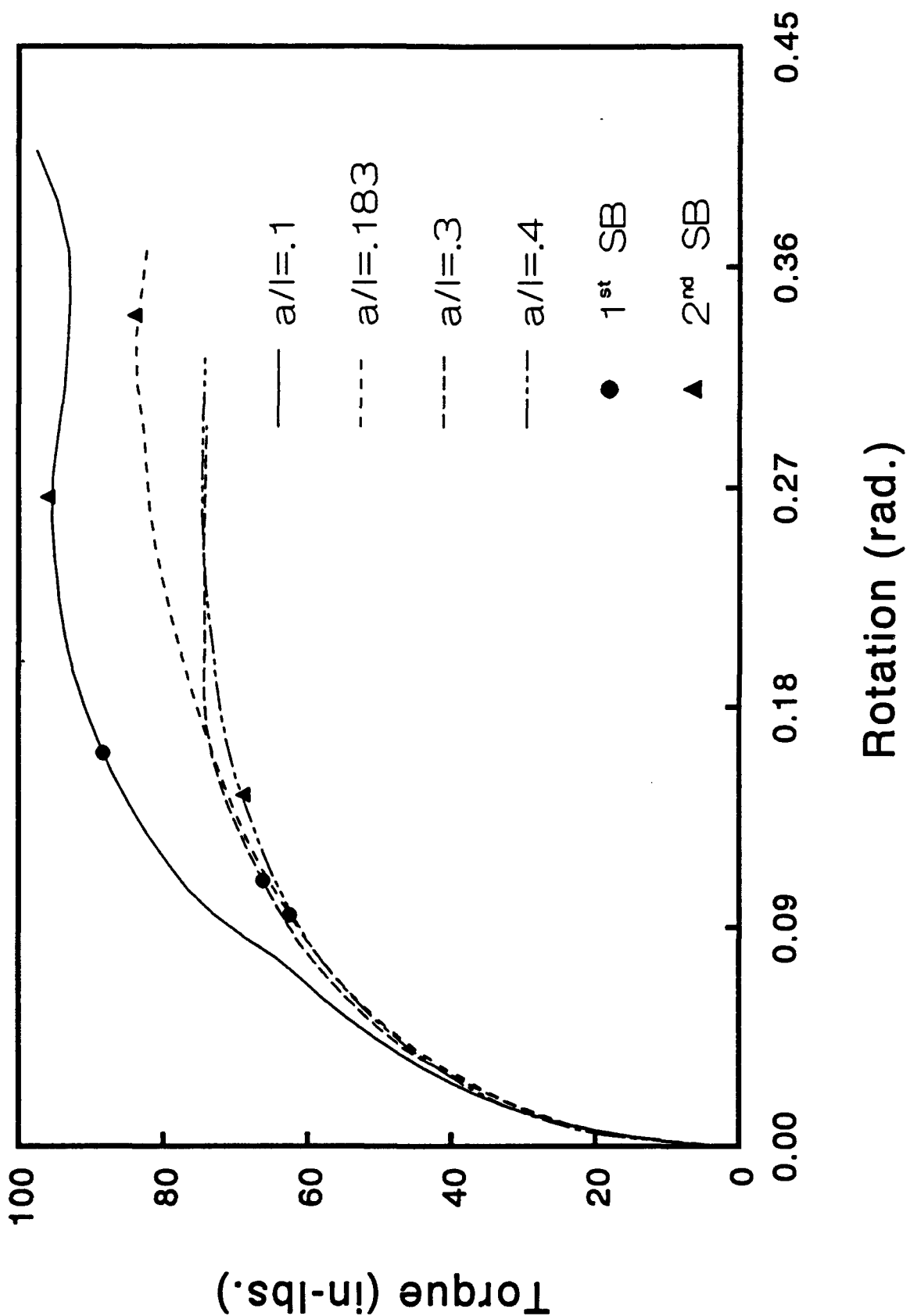


Figure 5.1 Influence of the Size of the Crack on the Strength

Torque Energy vs. Rotation

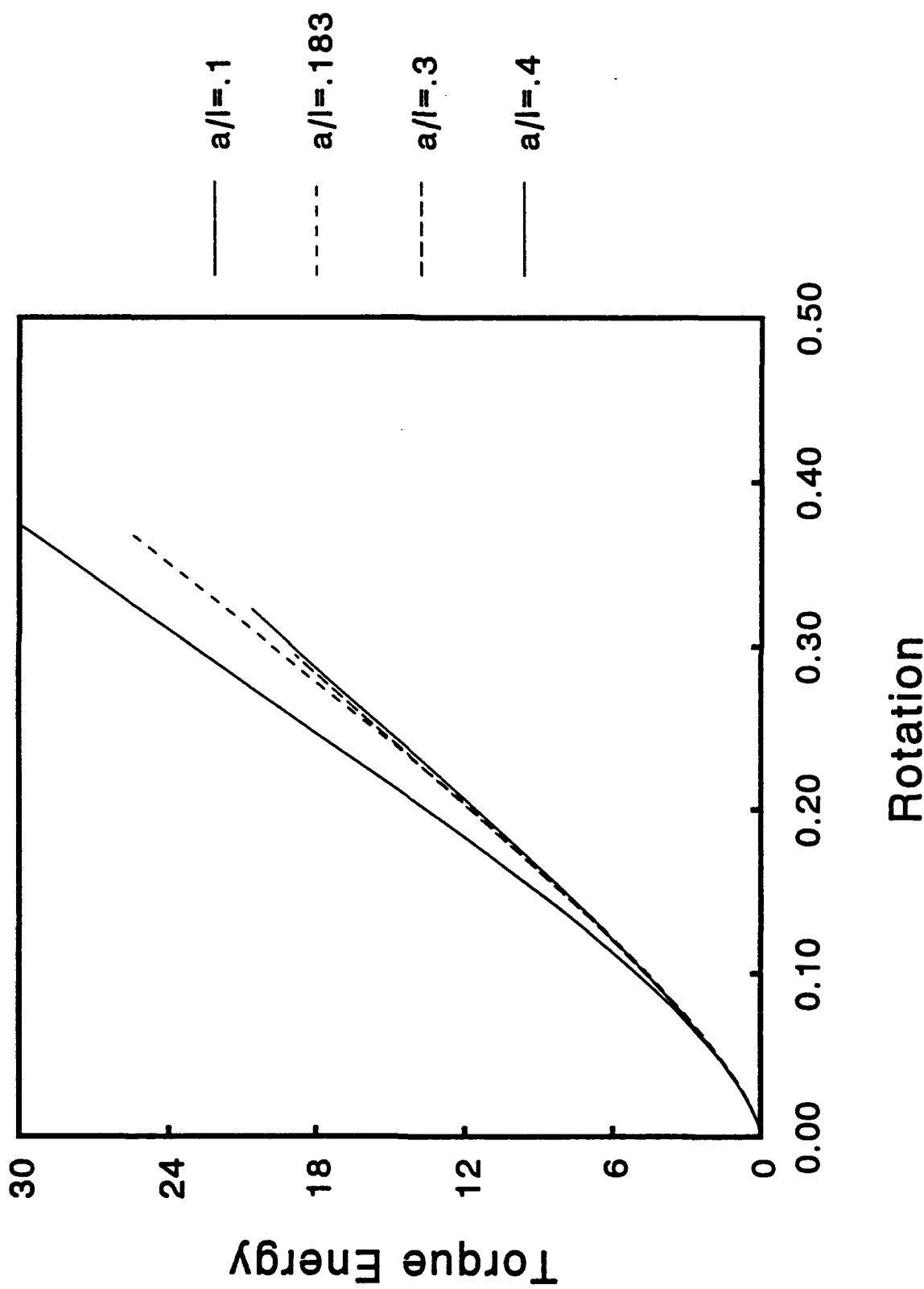


Figure 5.2 Torque Energy vs. Rotation

J-Integral vs. Rotation

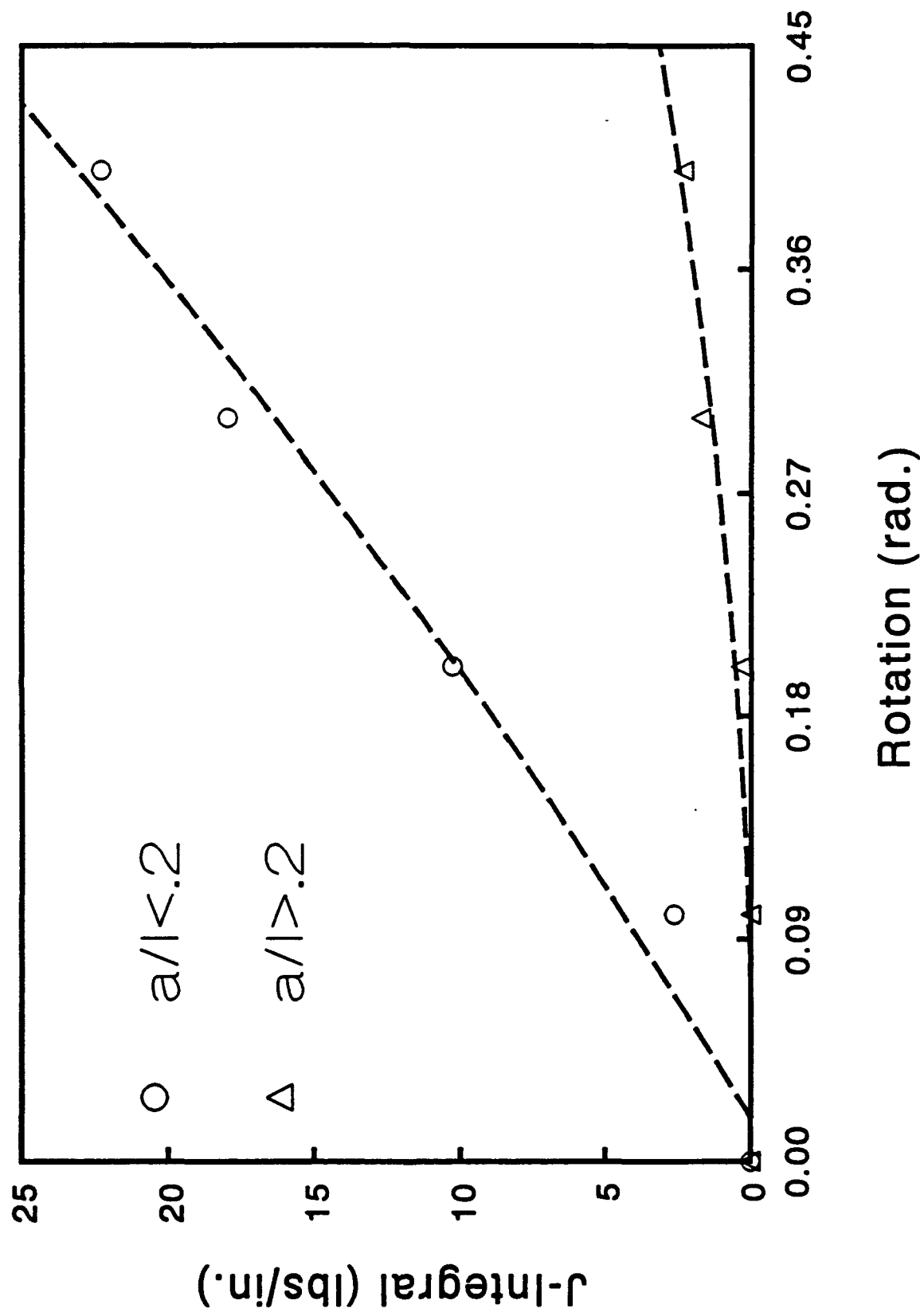


Figure 5.3 J-Integral vs. Rotation

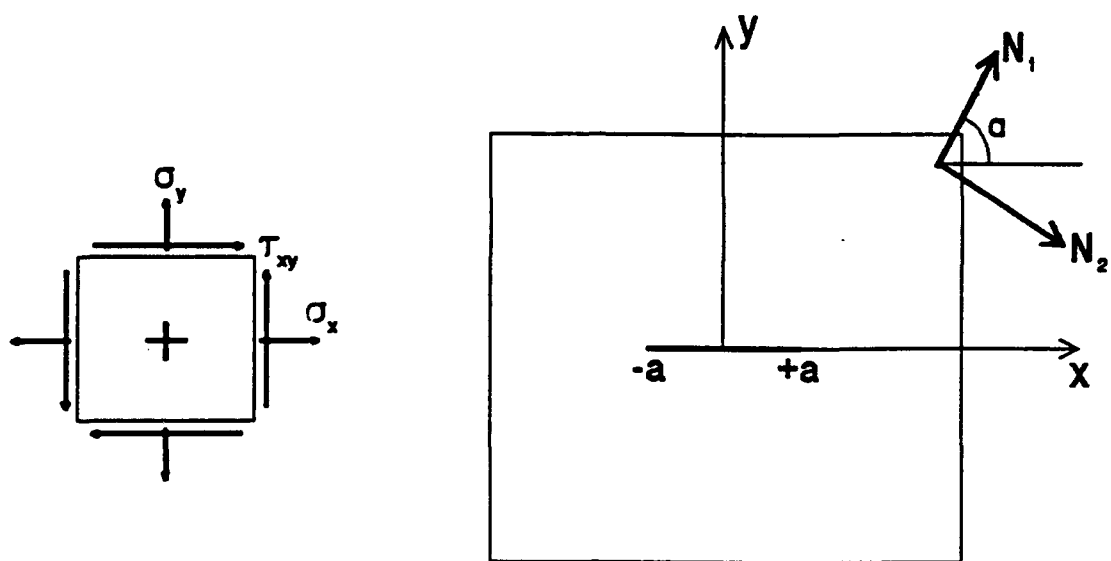


Figure 5.4a Notation

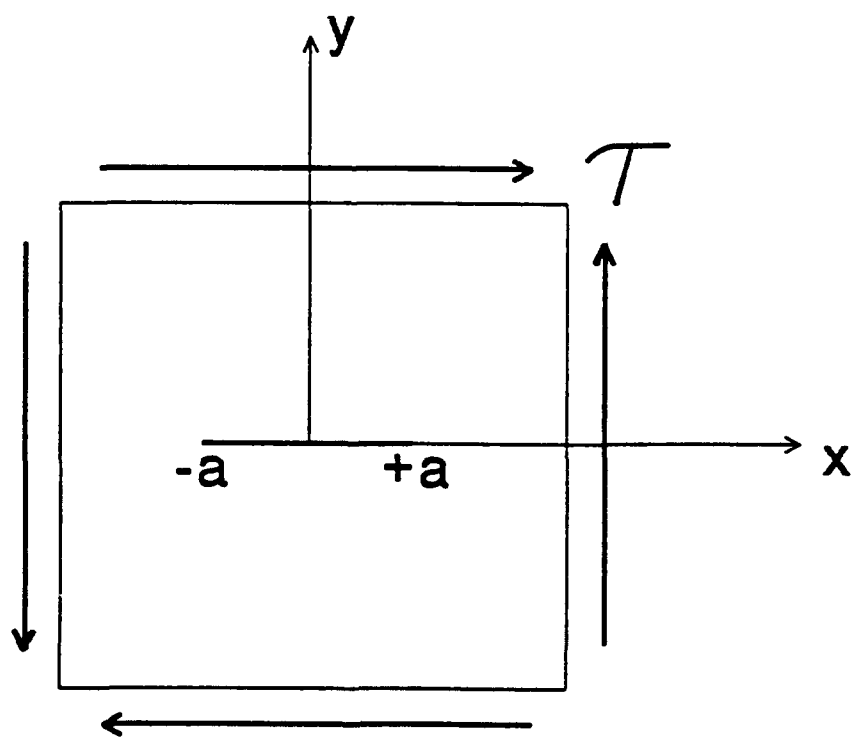


Figure 5.4b Loading Conditions
5.13

Superposition Model for Elastic Analysis

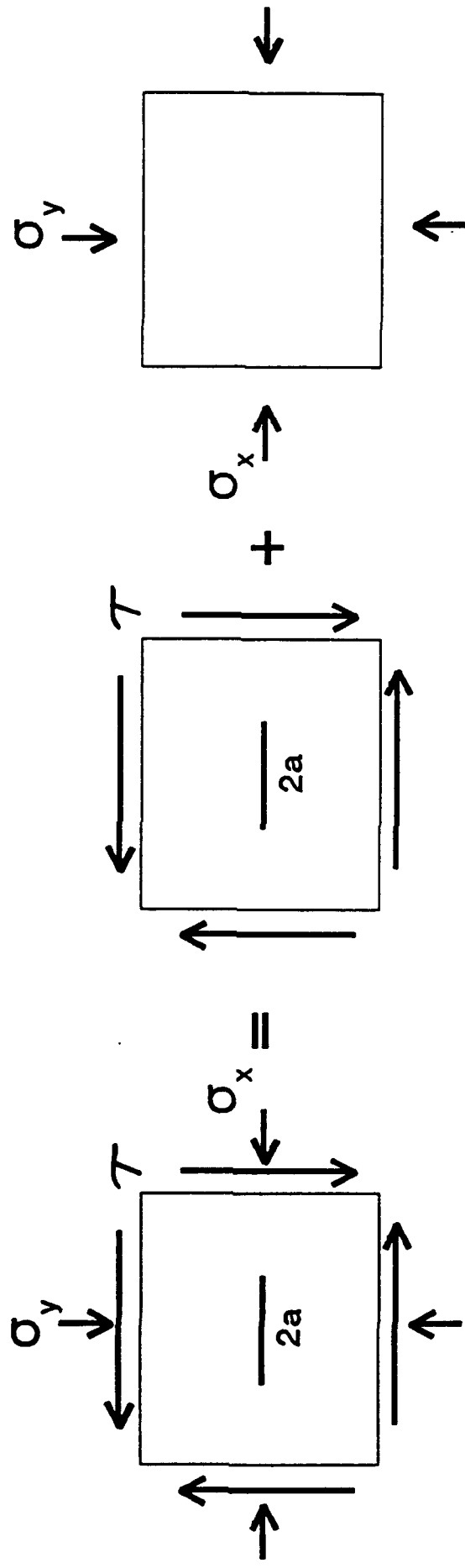


Figure 5.5 Superposition Model for Elastic Analysis

Contour of the Shear Stress σ_{xy}
 ----- Reference: Unit Shear (pure-torsion)

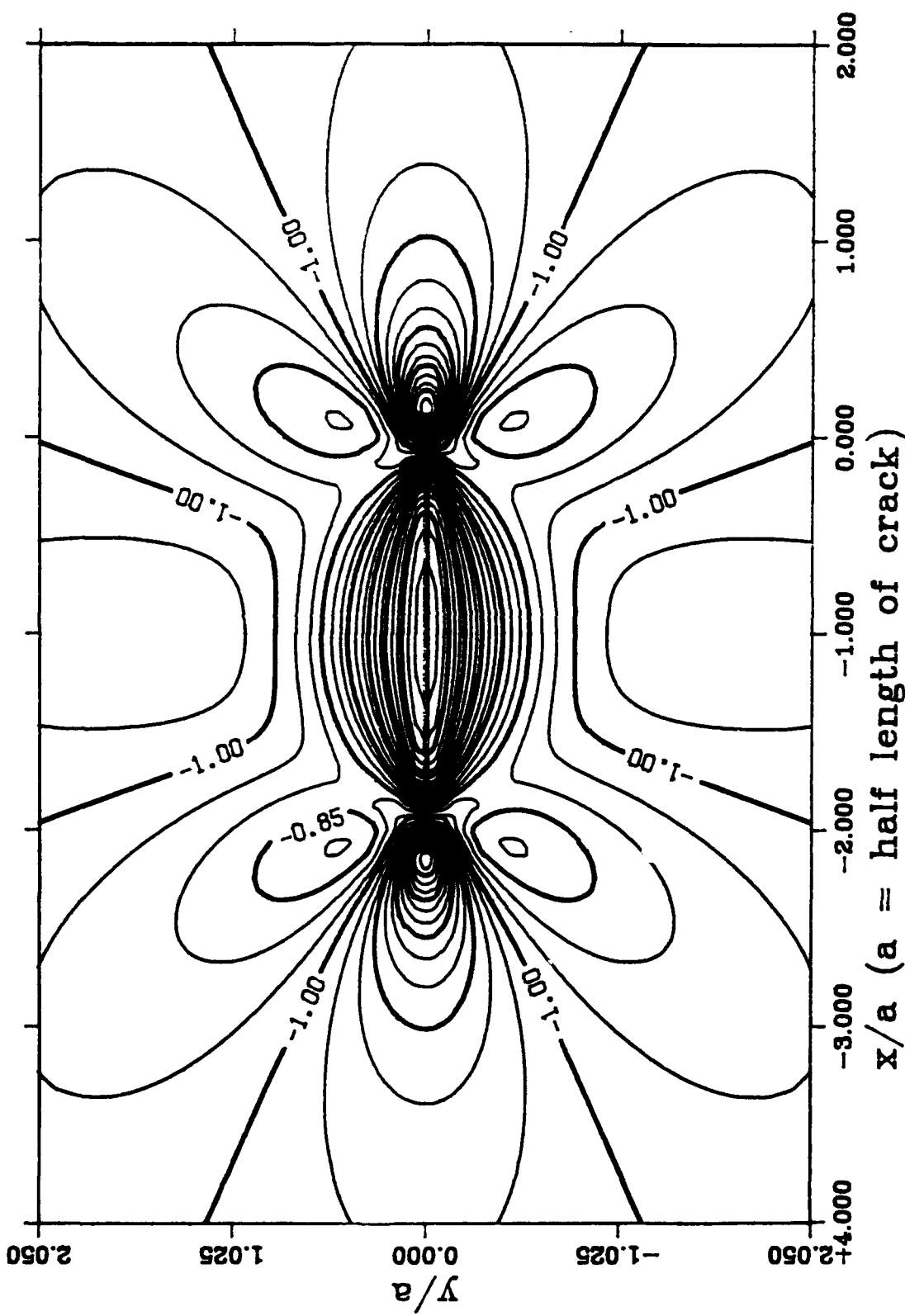
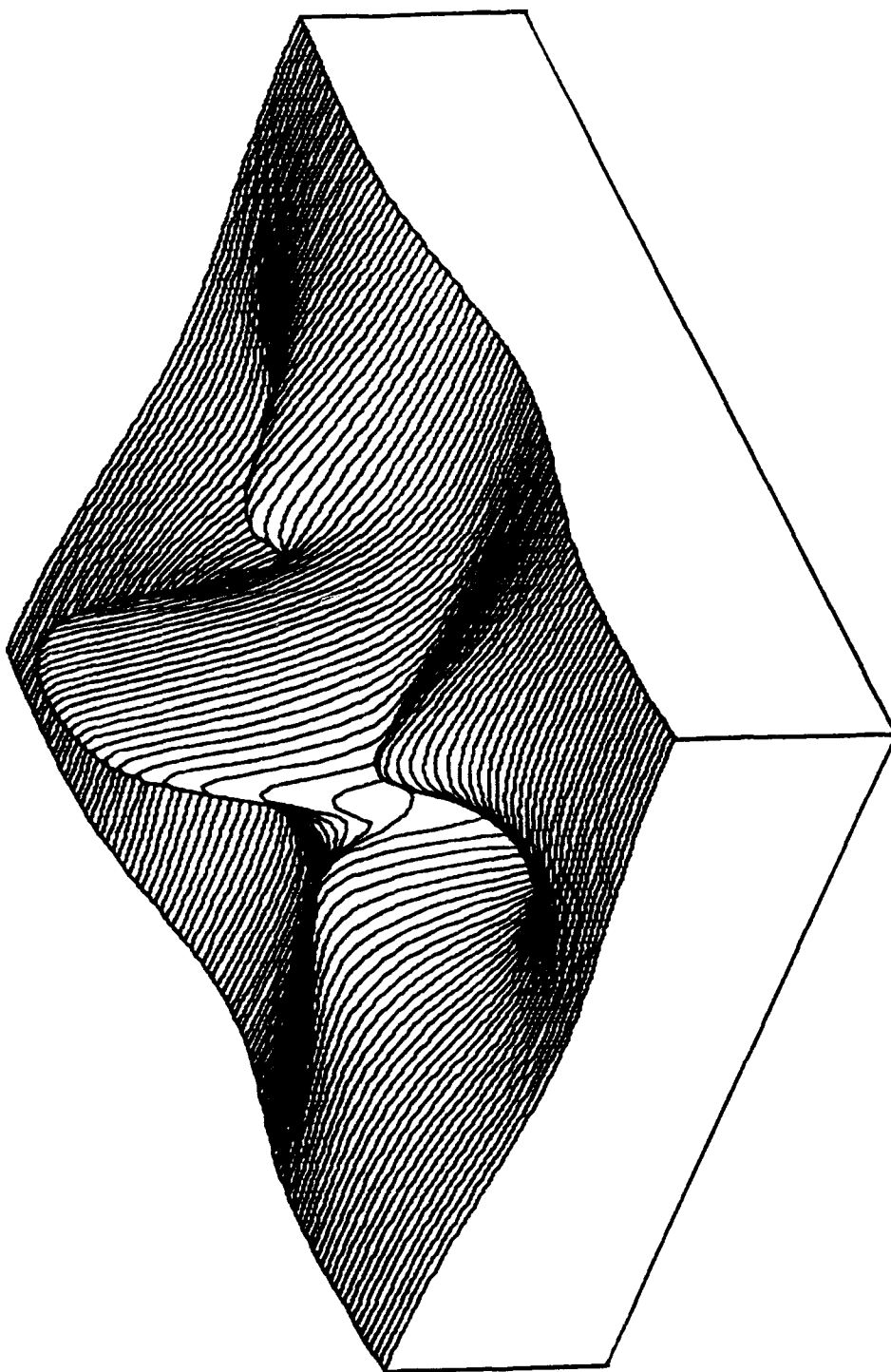


Figure 5.6a Lines of Equal Shear Stress

3-D plot for the Shear Stress σ_{xy}
--- Reference: Unit Shear (pure-torsion)



Contour of the Normal Stress σ_{xx}
 --- Reference: Unit Shear (pure-torsion)

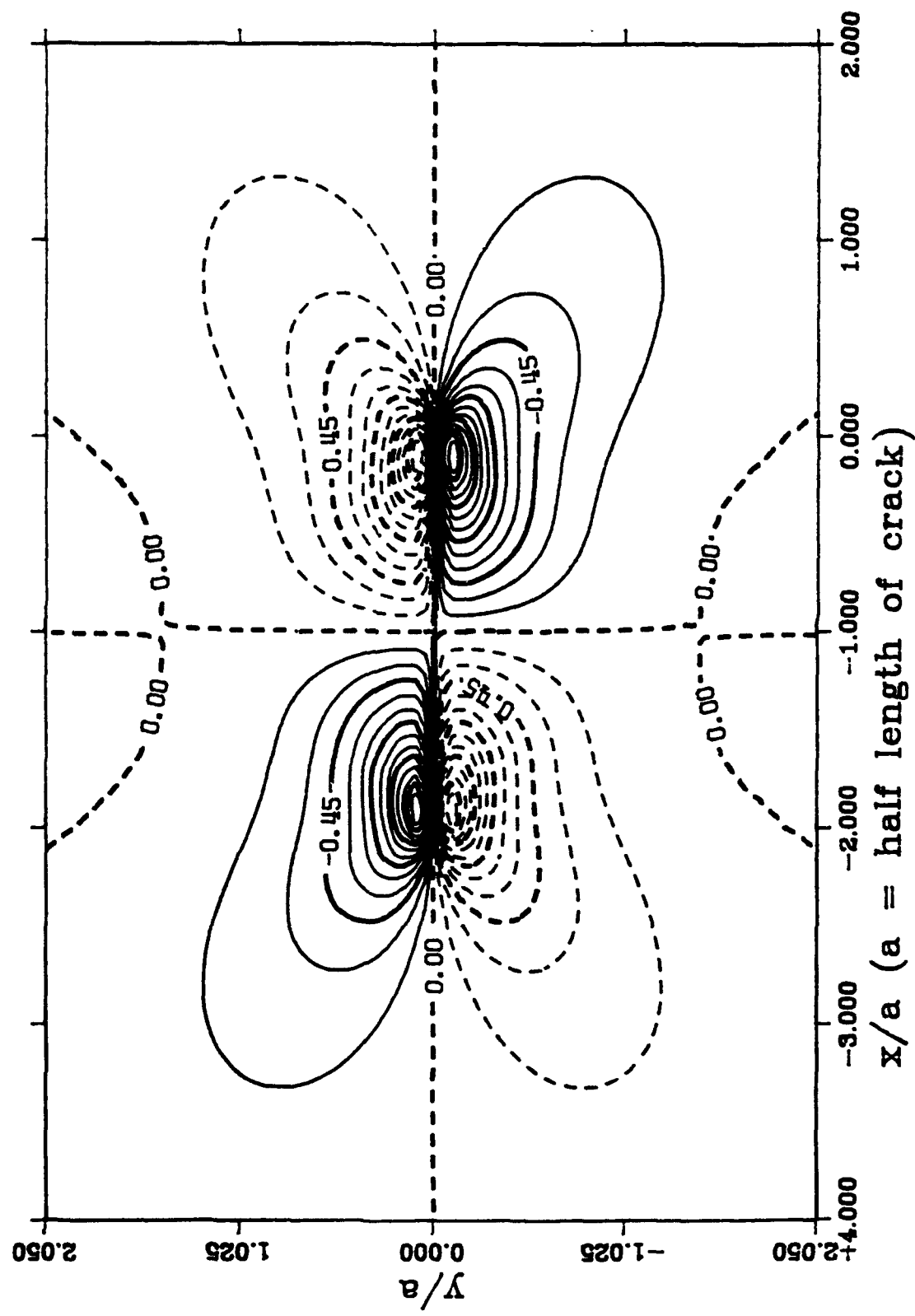


Figure 5.6c Lines of Equal Normal Stress

3-D plot for the Normal Stress σ_{xx}
----- Reference: Unit Shear (pure-torsion)

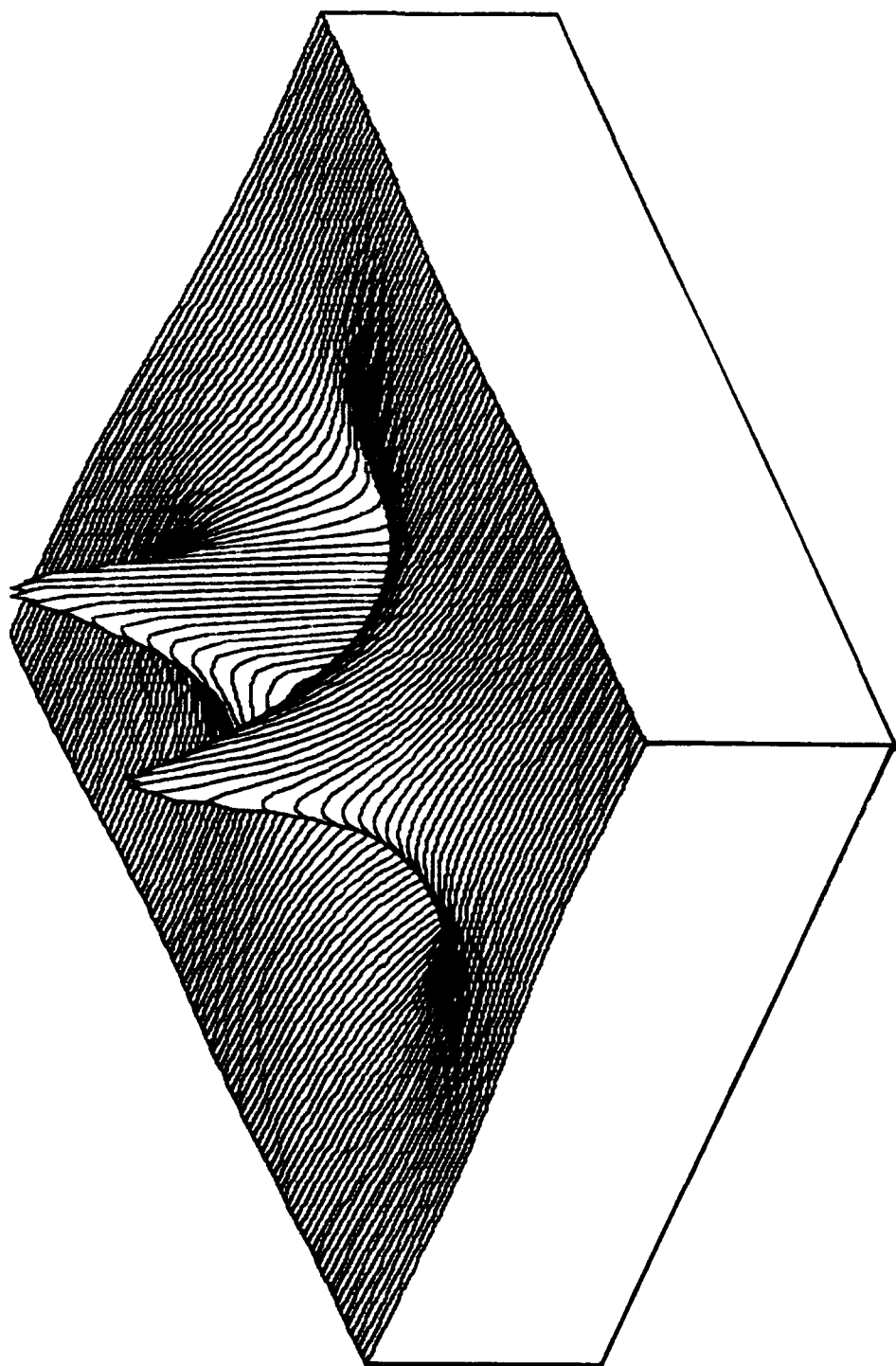


Figure 5.6d 3-D Plot of Normal Stress

Contour of the Normal Stress σ_{yy}
 --- Reference: Unit Shear (pure-torsion)

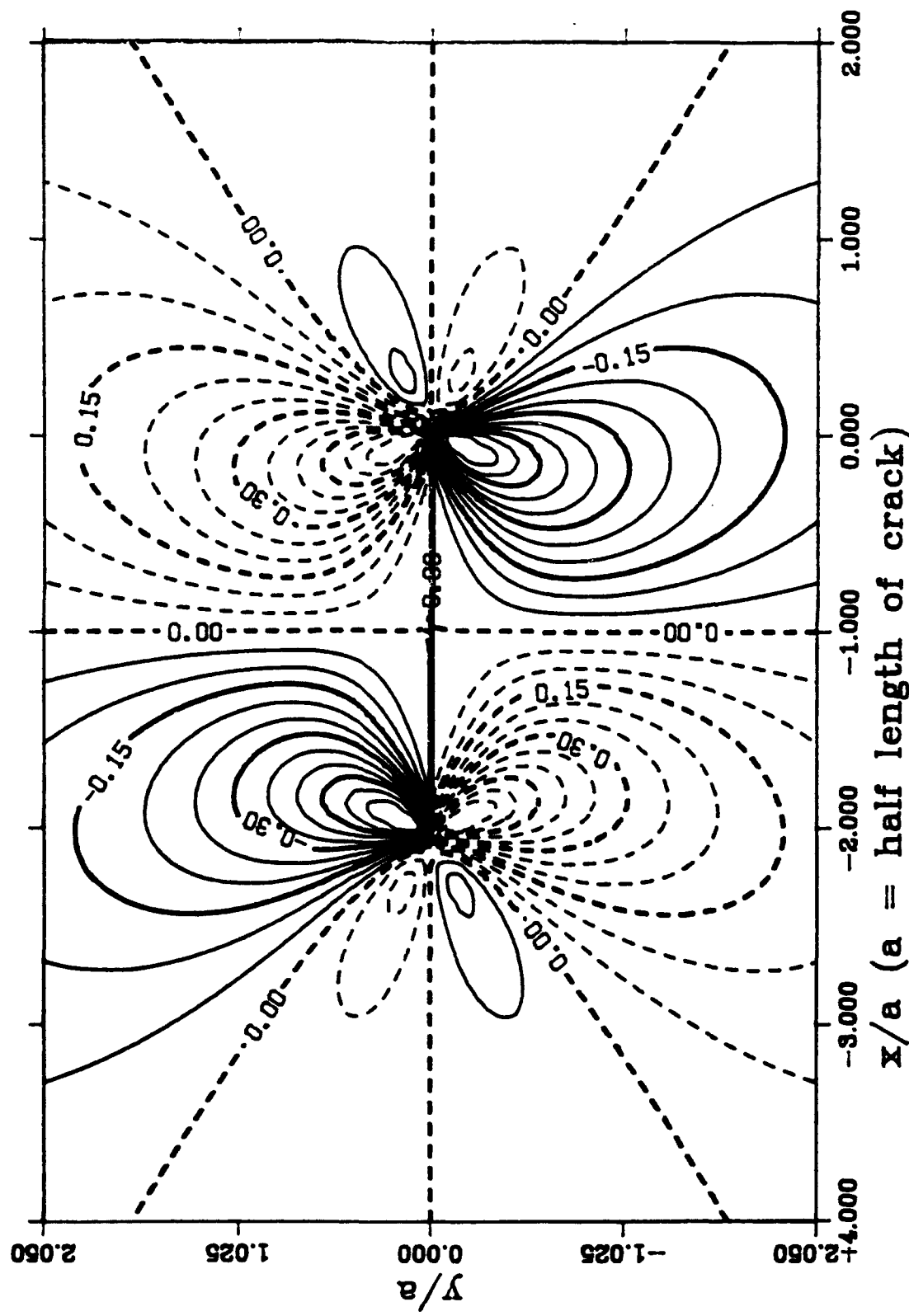


Figure 5.6e Lines of Equal Normal Stress

3-D plot for the Normal Stress σ_{yy}
Reference: Unit Shear (pure-torsion)

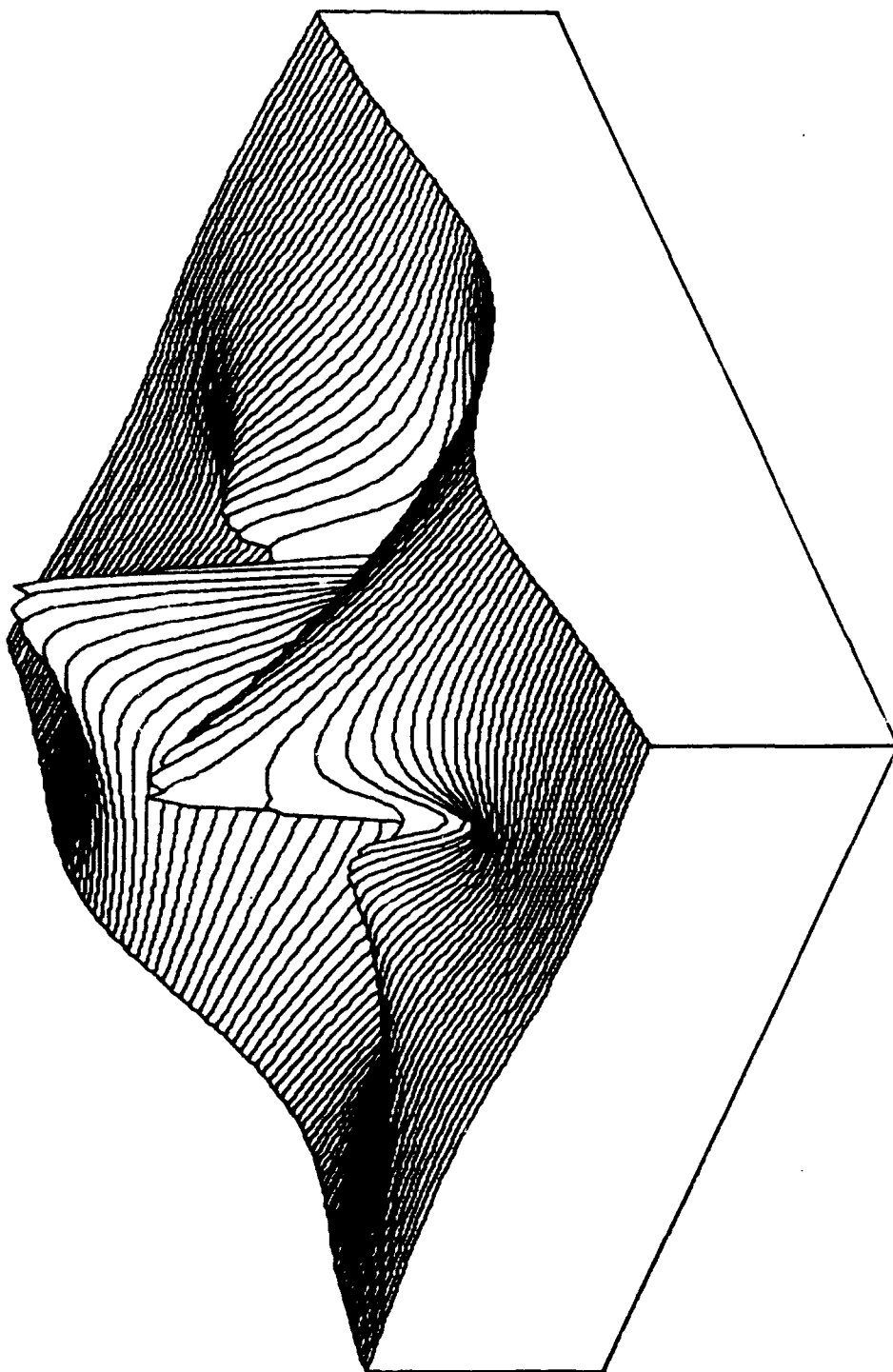


Figure 5.6f 3-D Plot of Normal Stress

Contour of the Maximum Principal Stress
--- Reference: Unit Shear (pure-torsion)

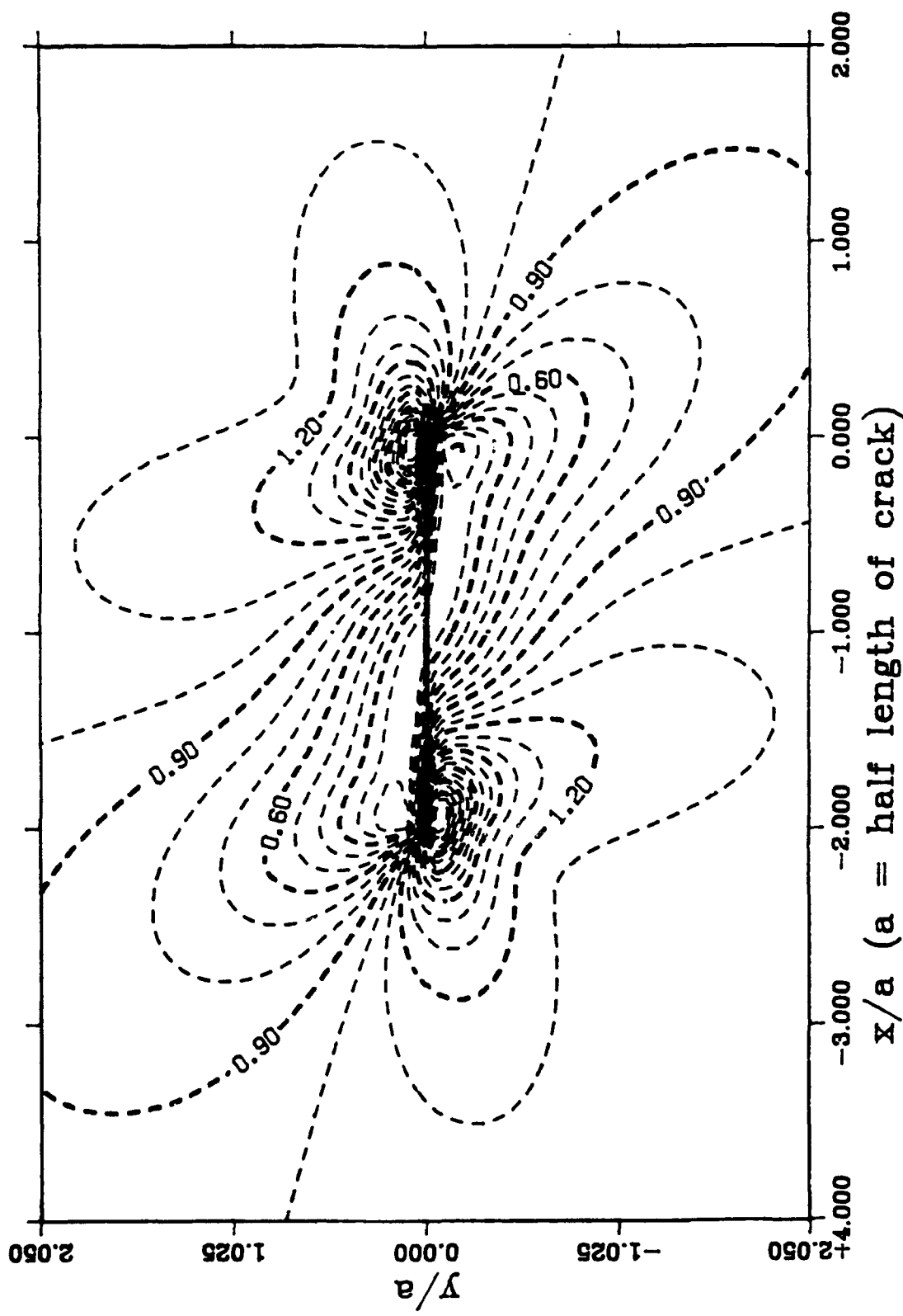


Figure 5.6g Lines of Equal Maximum Principal Stress

3-D plot for the Maximum Principal Stress
Reference: Unit Shear (pure-torsion)

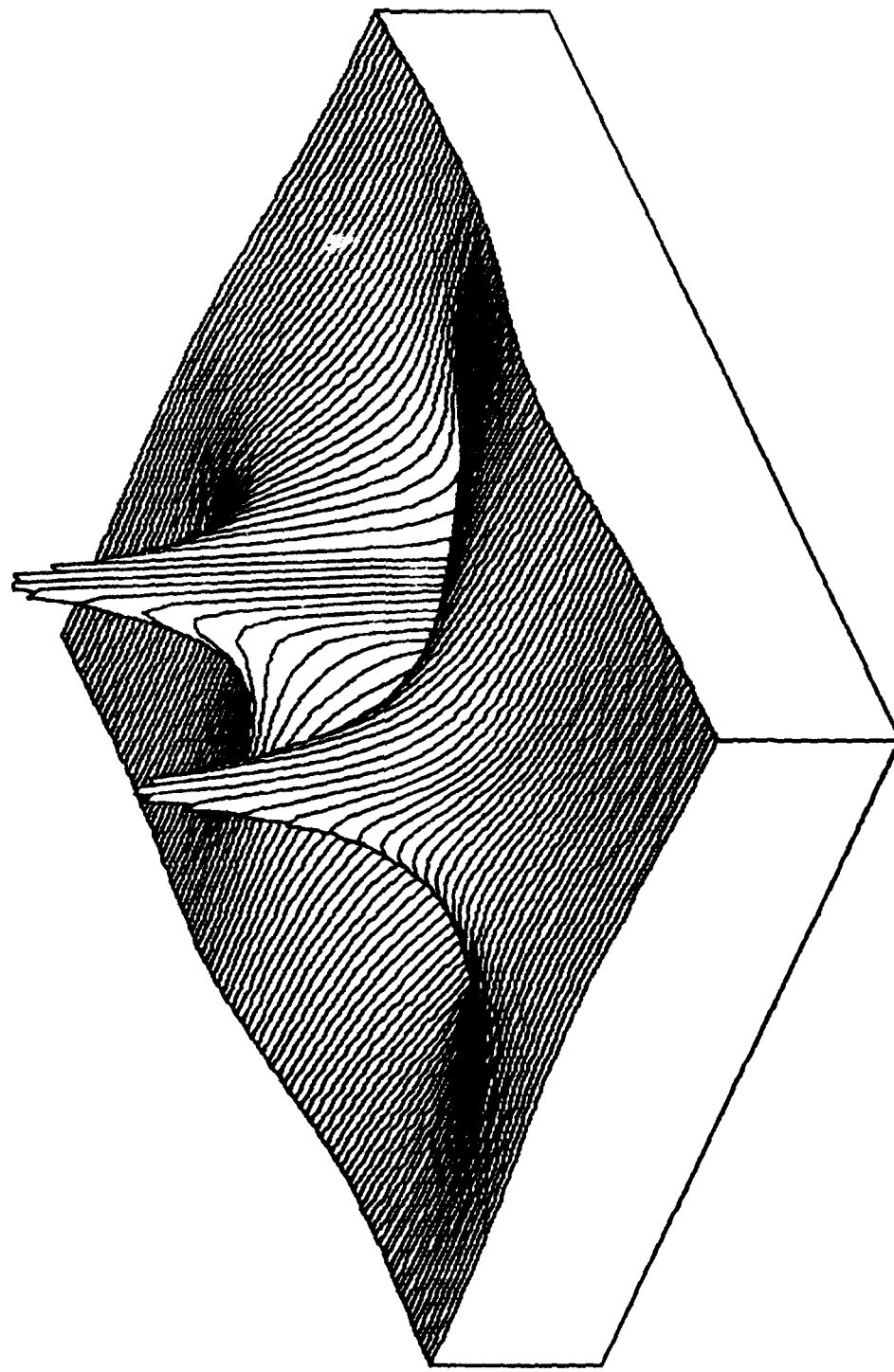


Figure 5.6h 3-D Plot of Maximum Principal Stress

Contour of the Minimum Principal Stress
 ---- Reference: Unit Shear (pure-torsion)

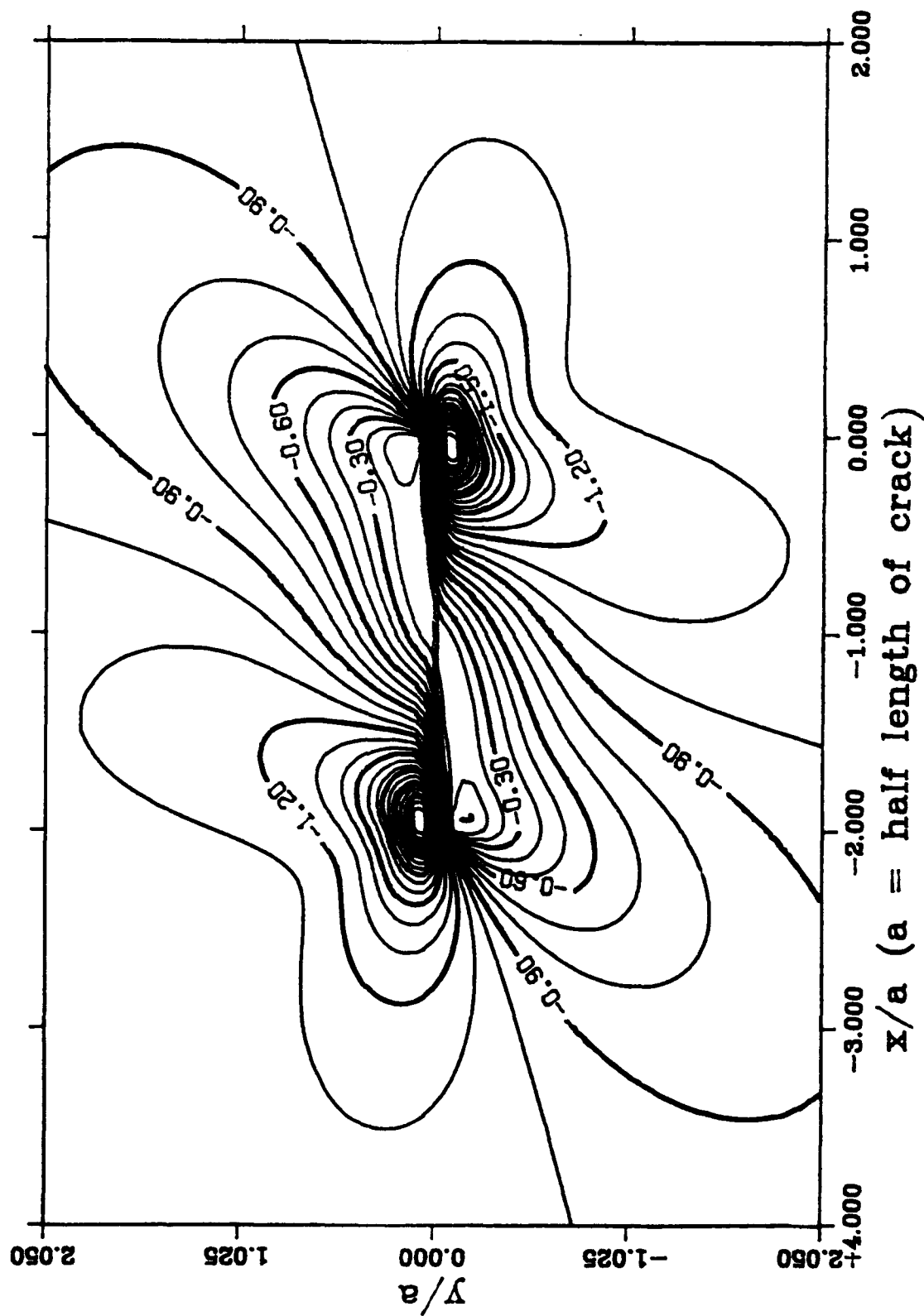


Figure 5.6i Lines of Equal Minimum Principal Stress

3-D plot for the Minimum Principal Stress
Reference: Unit Shear (pure-torsion)

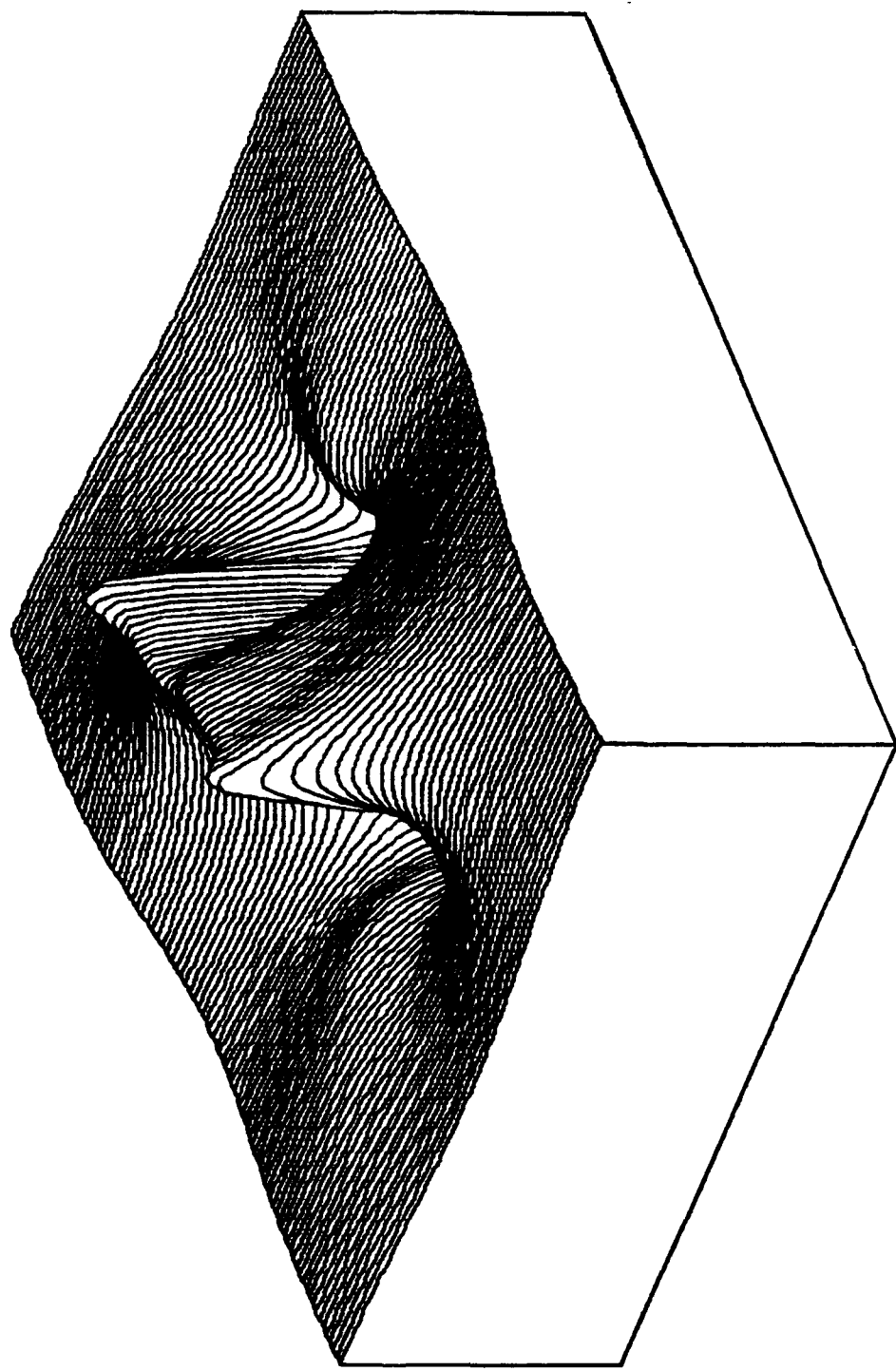


Figure 5.6j 3-D Plot of Minimum Principal Stress

Contour of the Maximum Shear Stress
 ----- Reference: Unit Shear (pure-torsion)

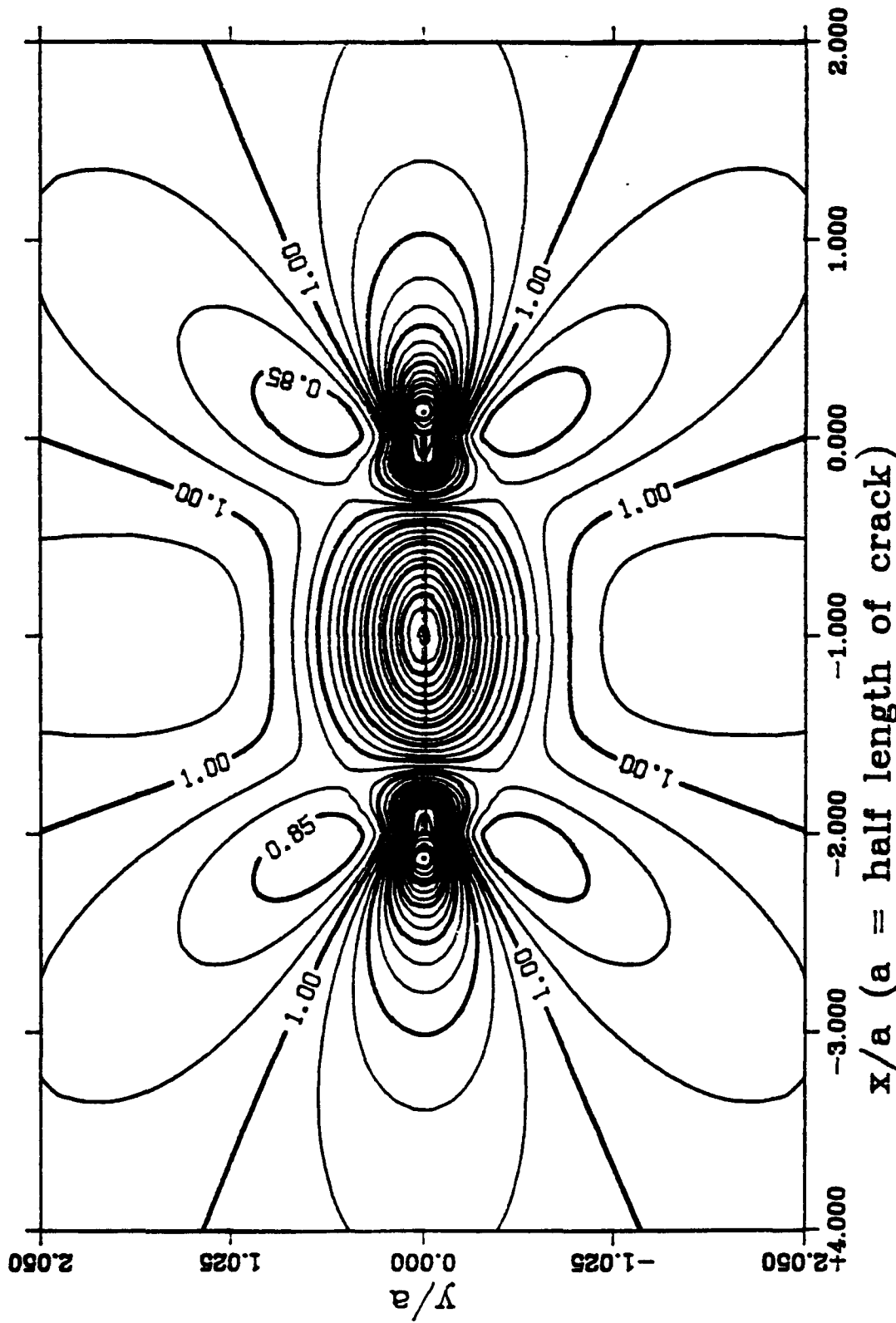


Figure 5.6k Lines of Equal Maximum Shear Stress

3-D plot for the Maximum Shear Stress
---- Reference: Unit Shear (pure-torsion)

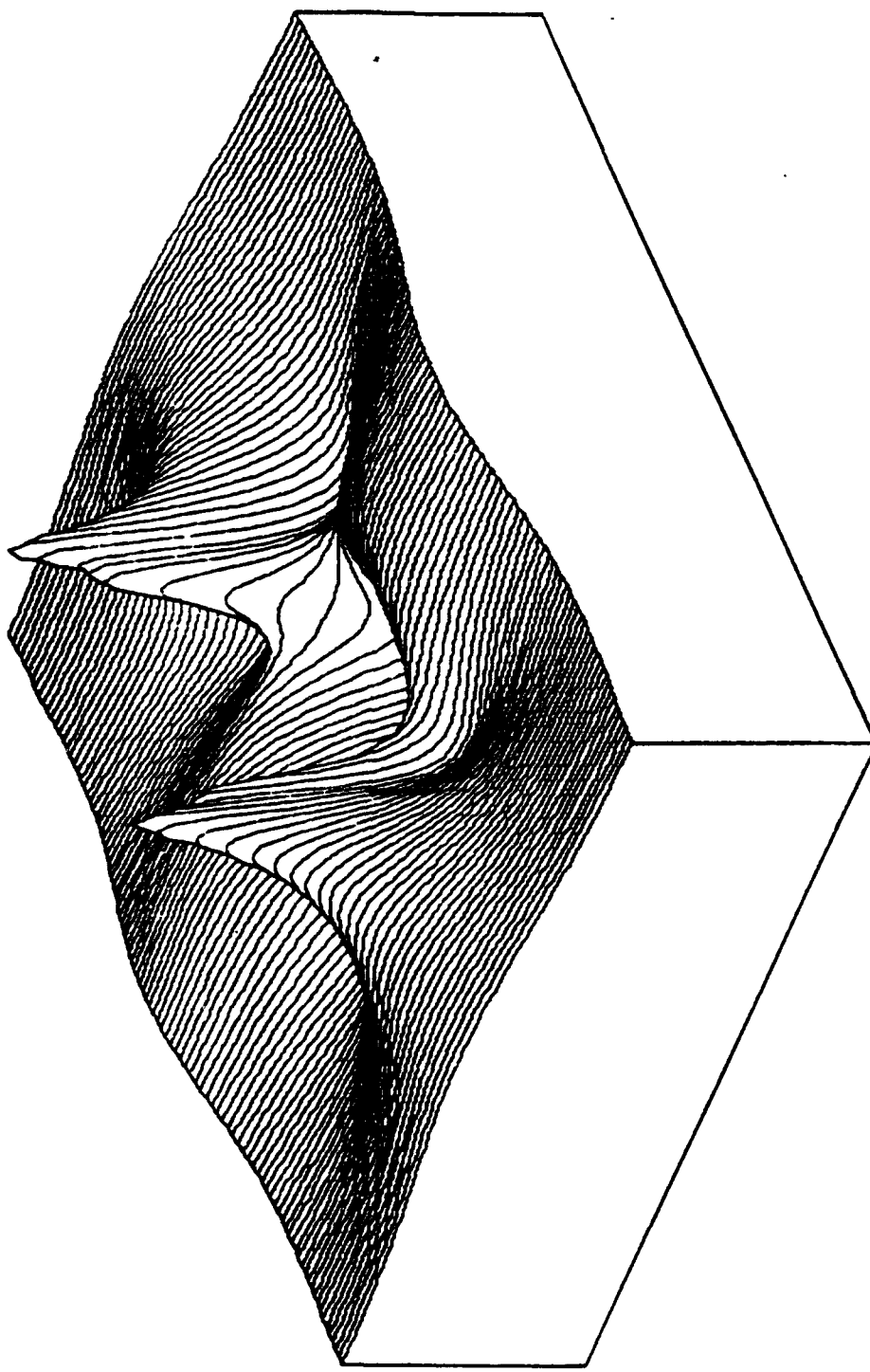


Figure 5.61 3-D Plot of Maximum Shear Stress

Contour of the Mean Stress
 ---- Reference: Unit Shear (pure-torsion)

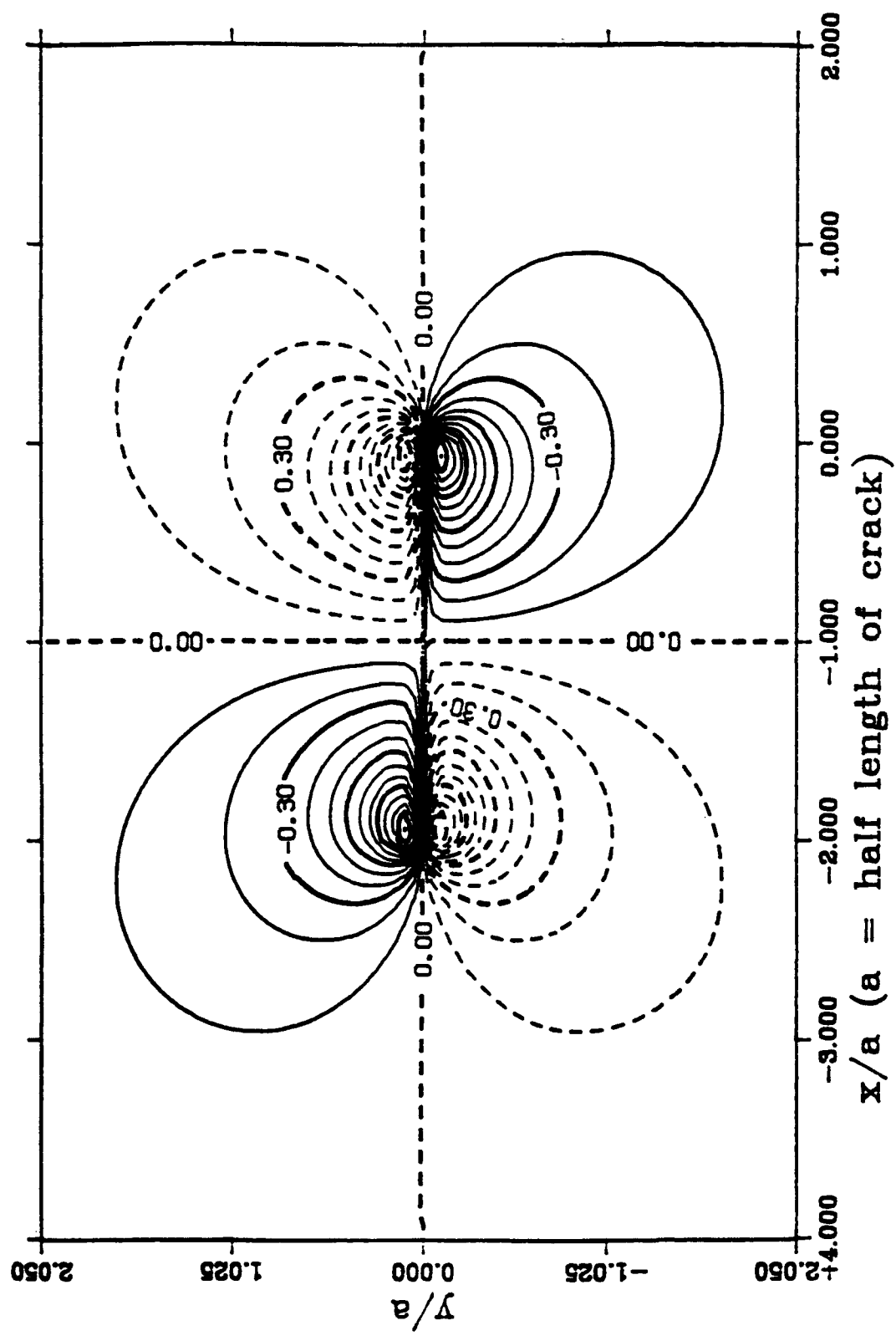


Figure 5.6m Lines of Equal Mean Stress

3-D plot for the Mean Stress
--- Reference: Unit Shear (pure-torsion)

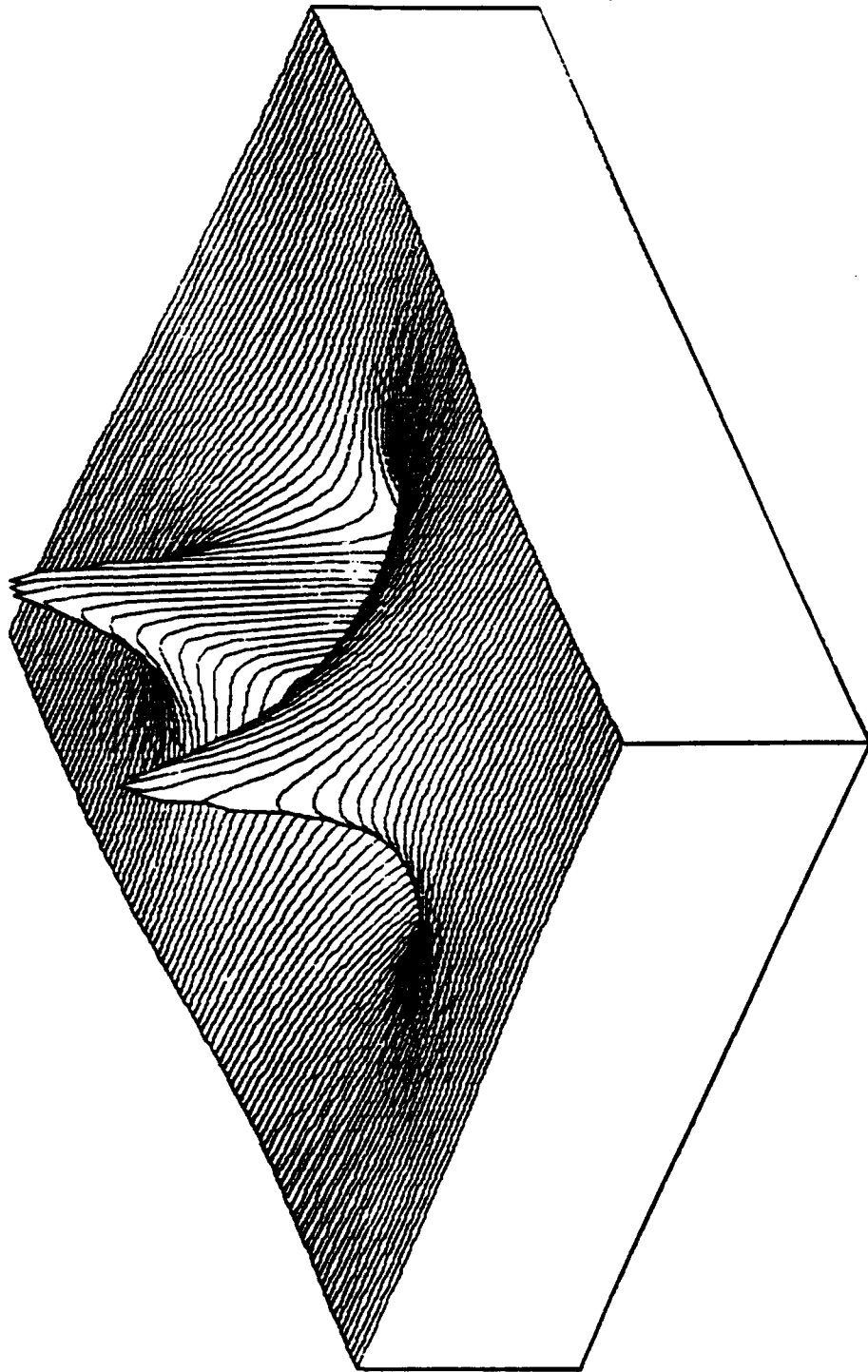


Figure 5.6n 3-D Plot of Mean Stress

Principal Stresses and Their Direction
 (Unit Shear Stress; Pure-Torsion; Scale: 1 unit = 10 kPa)

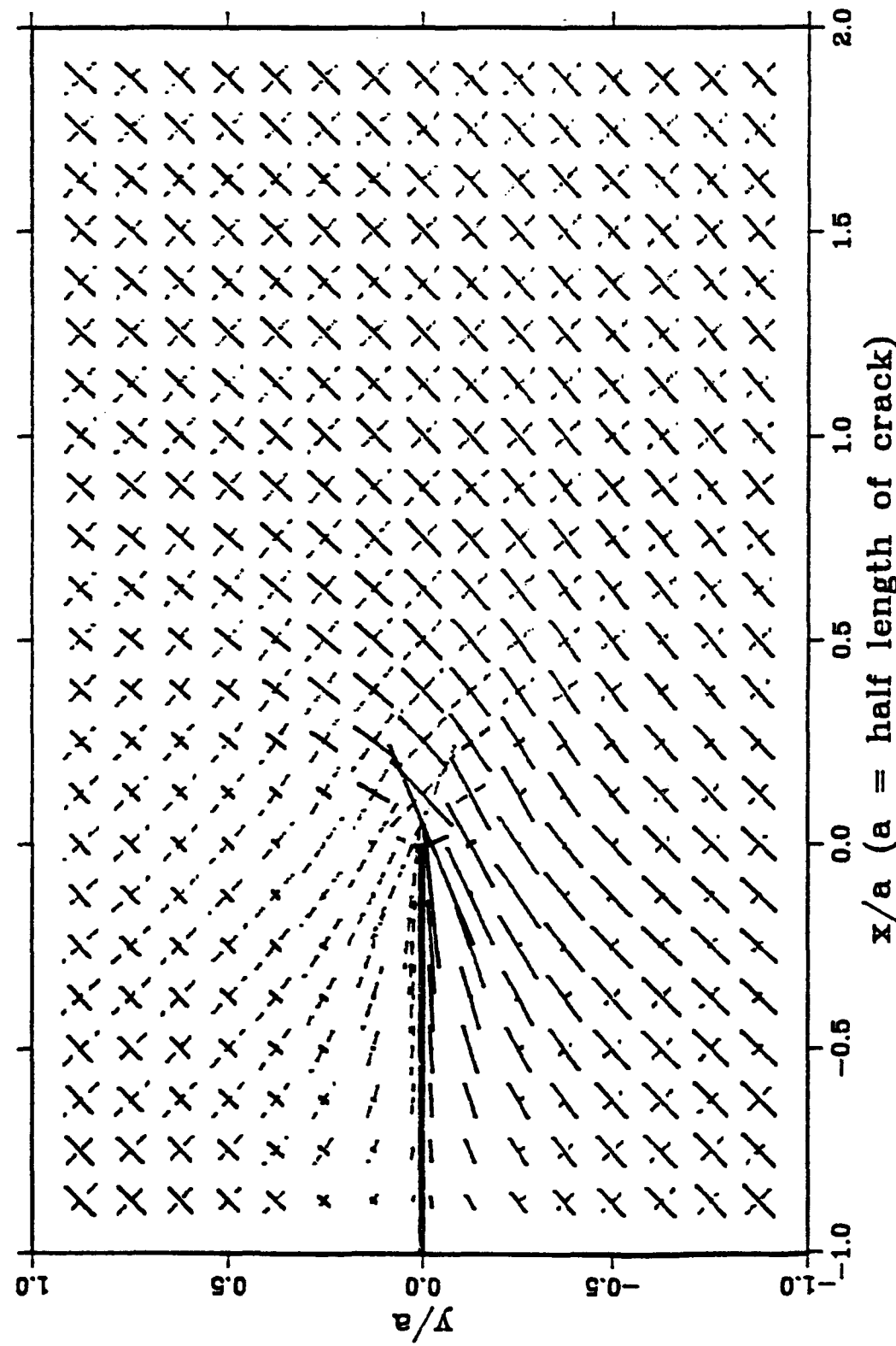


Figure 5.60 Principal Stresses and Their Directions

Stress Calculation for EPK #52: 4/9/91; Tension-Torsion
---Ko N.C.^Hor.NOTCH^a/l=0.183^F.H.^C.S.^ecp = 70-20 psi^DTR60

length of crack = 1.0000 inch

initial_x= -1.0000 stepx= 0.1000 finial_x= 2.0000
initial_y= 1.0000 stepy= -0.1000 finial_y= -1.0000

Sxy = -217.1430 Syy = -192.4410 Sxx = -374.6700 Seff = -374.6700

Contour of the Shear Stress σ_{xy}
 EPK #52-04-09-91 (tension-torsion)

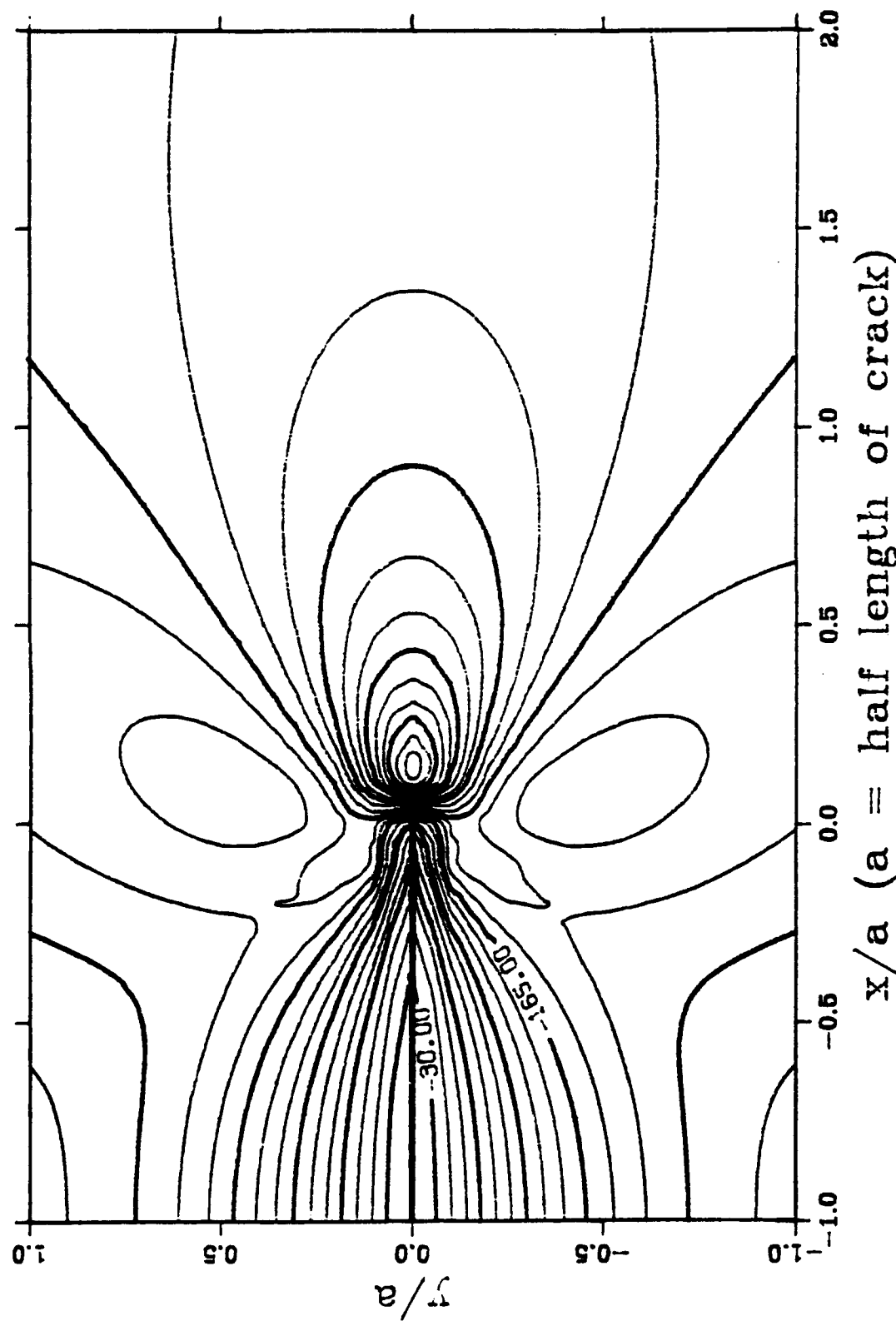


Figure 5.7a Lines of Equal Shear Stress

3-D plot for the Shear Stress σ_{xy}
--- EPK #52-04-09-91 (tension-torsion)

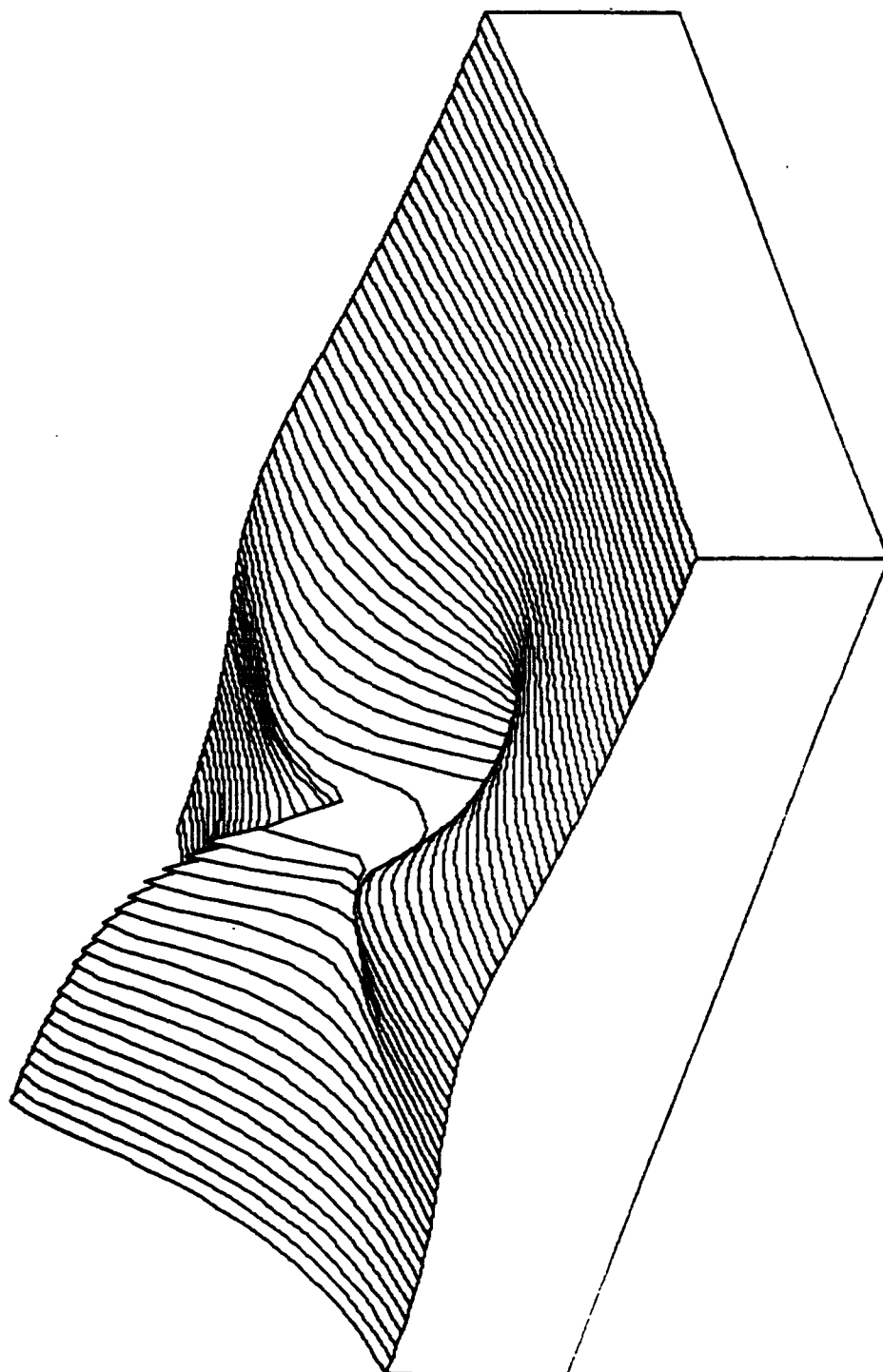


Figure 5.7b 3-D Plot of Shear Stress

Contour of the Normal Stress σ_{xx}
--- EPK #52-04-09-91 (tension-torsion)

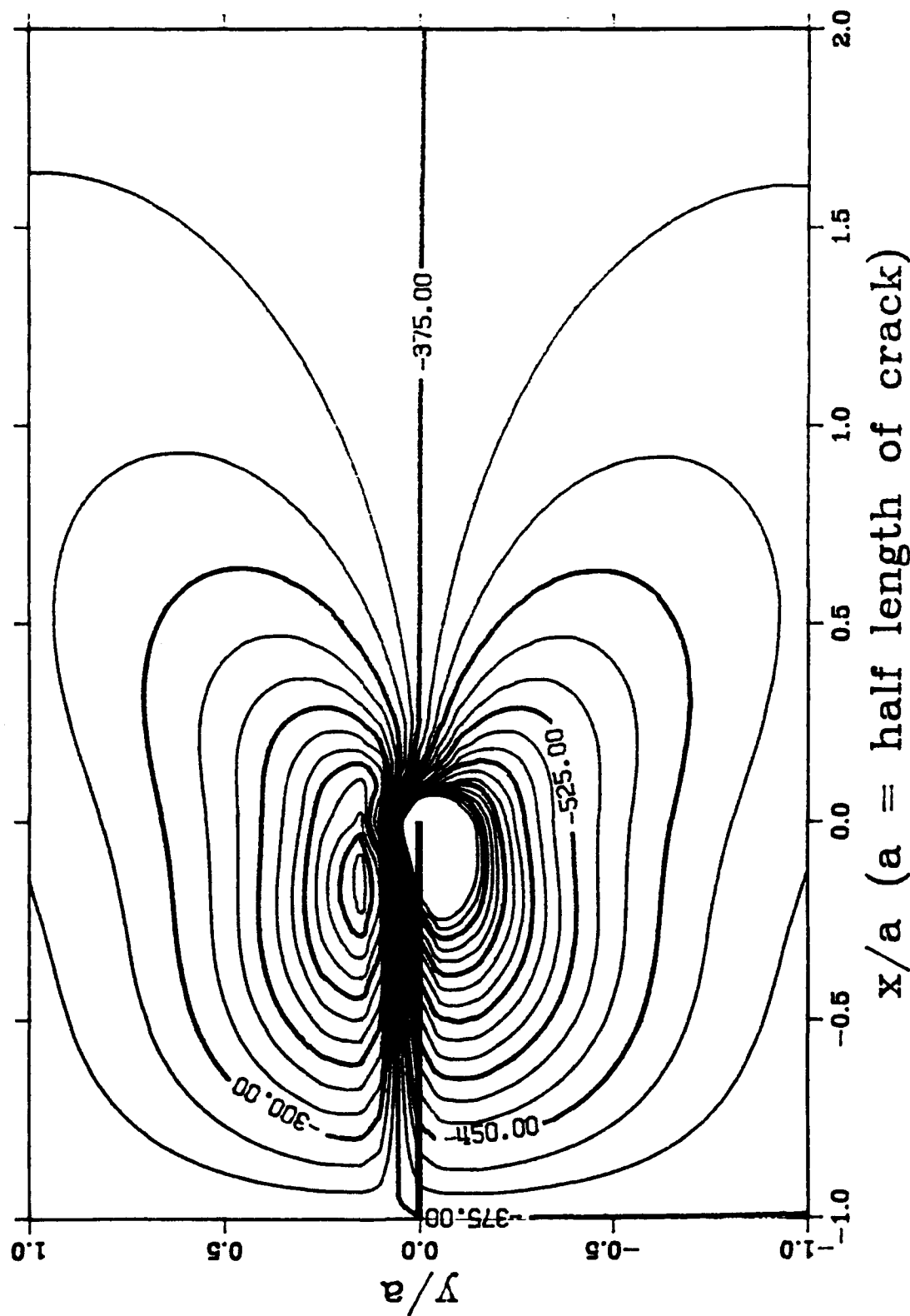


Figure 5.7c Lines of Equal Normal Stress

3-D plot for the Normal Stress σ_{xx}
--- EPK #52-04-09-91 (tension-torsion)

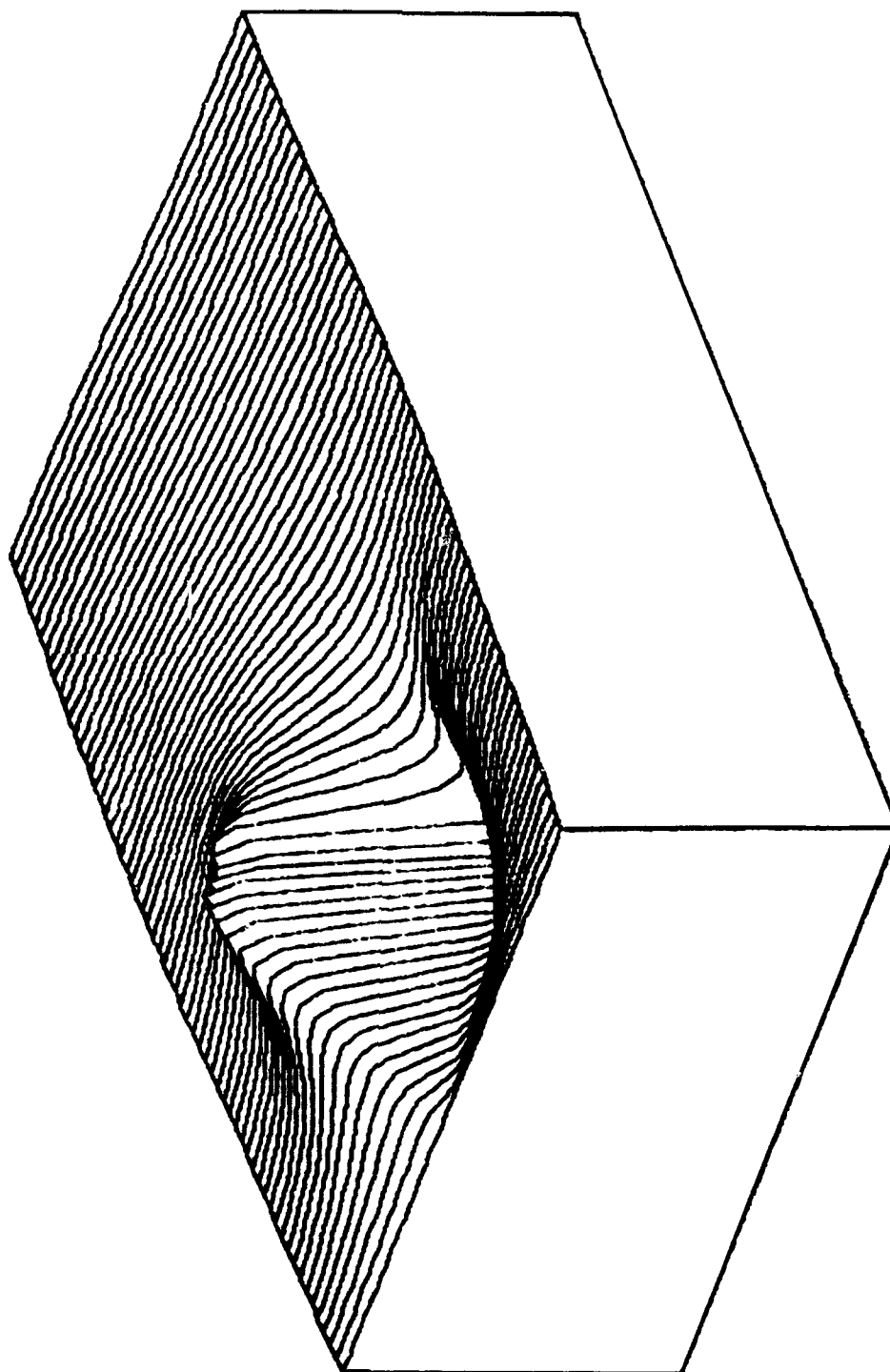


Figure 5.7d 3-D Plot of Normal Stress

Contour of the Normal Stress σ_{yy}
--- EPK #52-04-09-91 (tension-torsion)

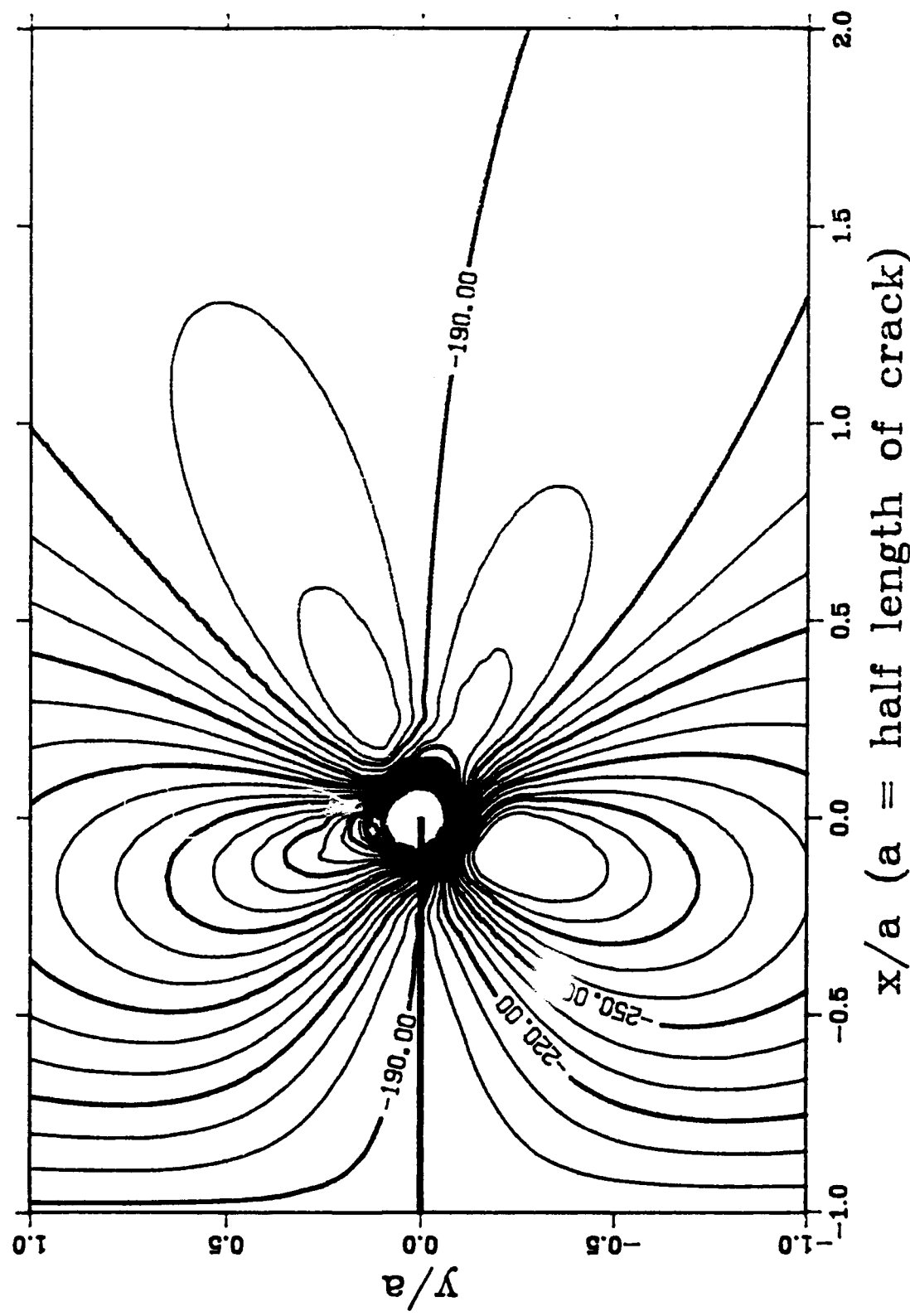


Figure 5.7e Lines of Equal Normal Stress

3-D plot for the Normal Stress σ_{yy}
--- EPK #52-04-09-91 (tension-torsion)

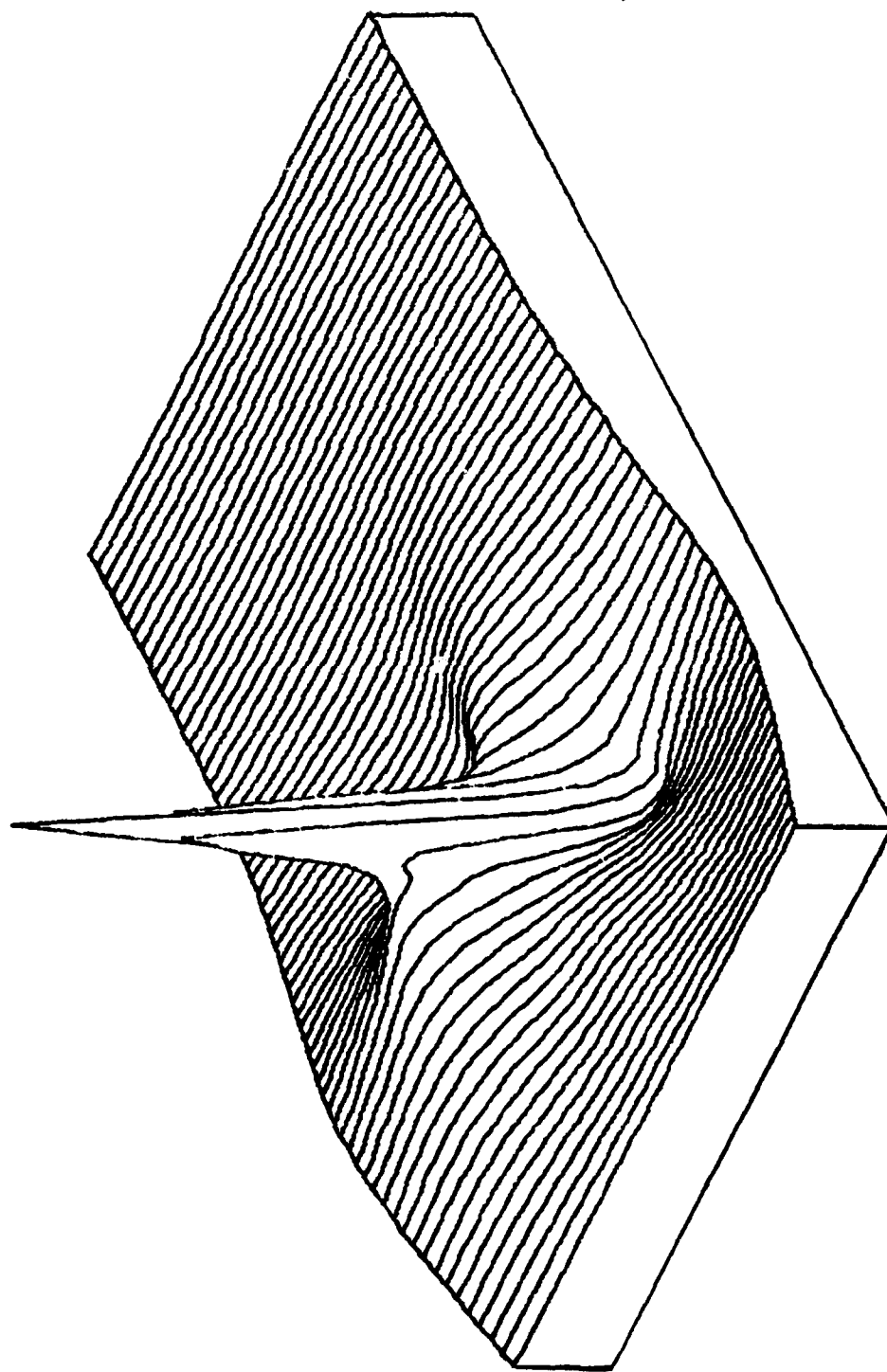


Figure 5.7f 3-D Plot of Normal Stress

Contour of the Maximum Principal Stress
--- EPK #52-04-09-91 (tension-torsion)

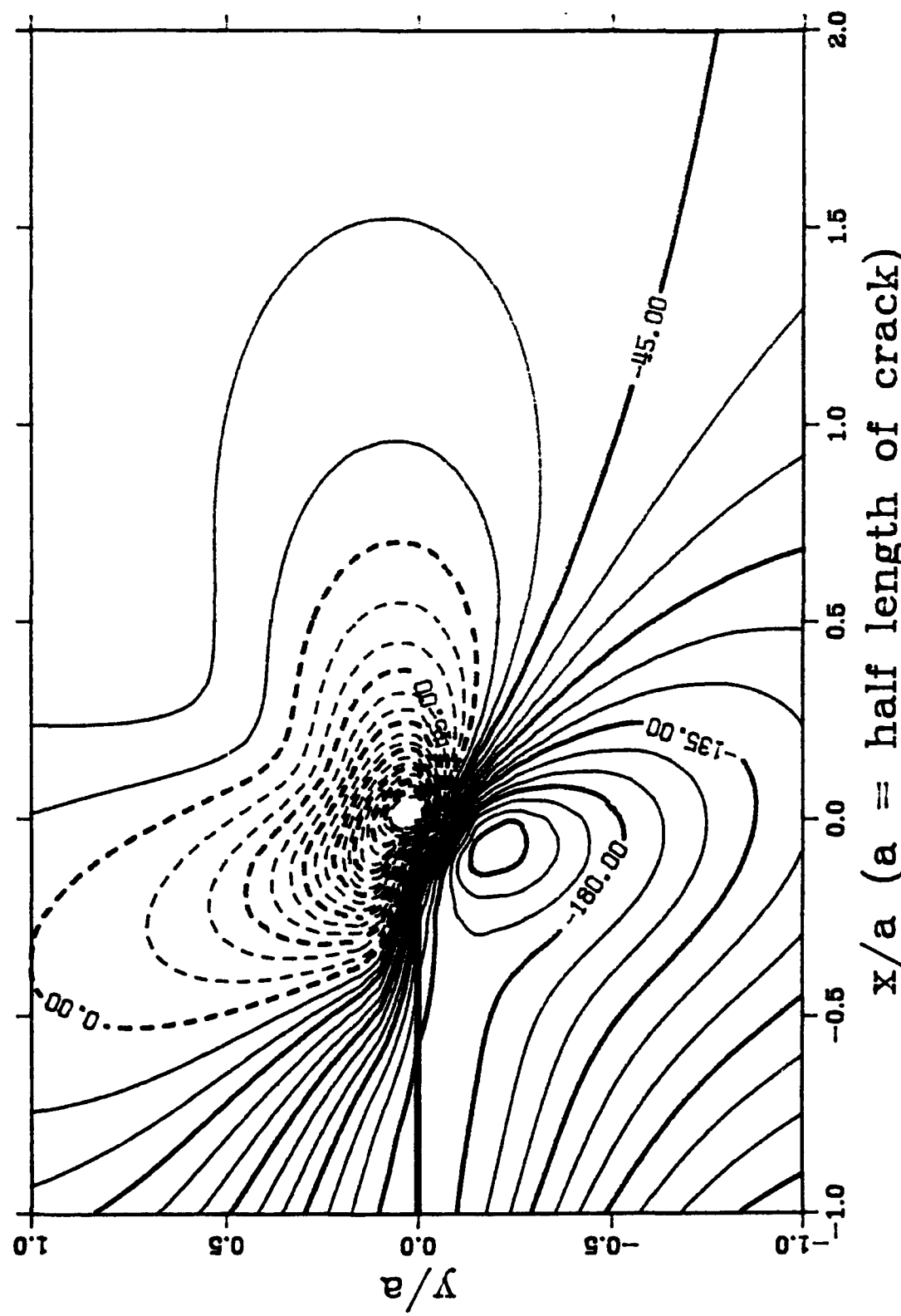


Figure 5.7g Lines of Equal Maximum Principal Stress

3-D plot for the Maximum Principal Stress
--- EPK #52-04-09-91 (tension-torsion)

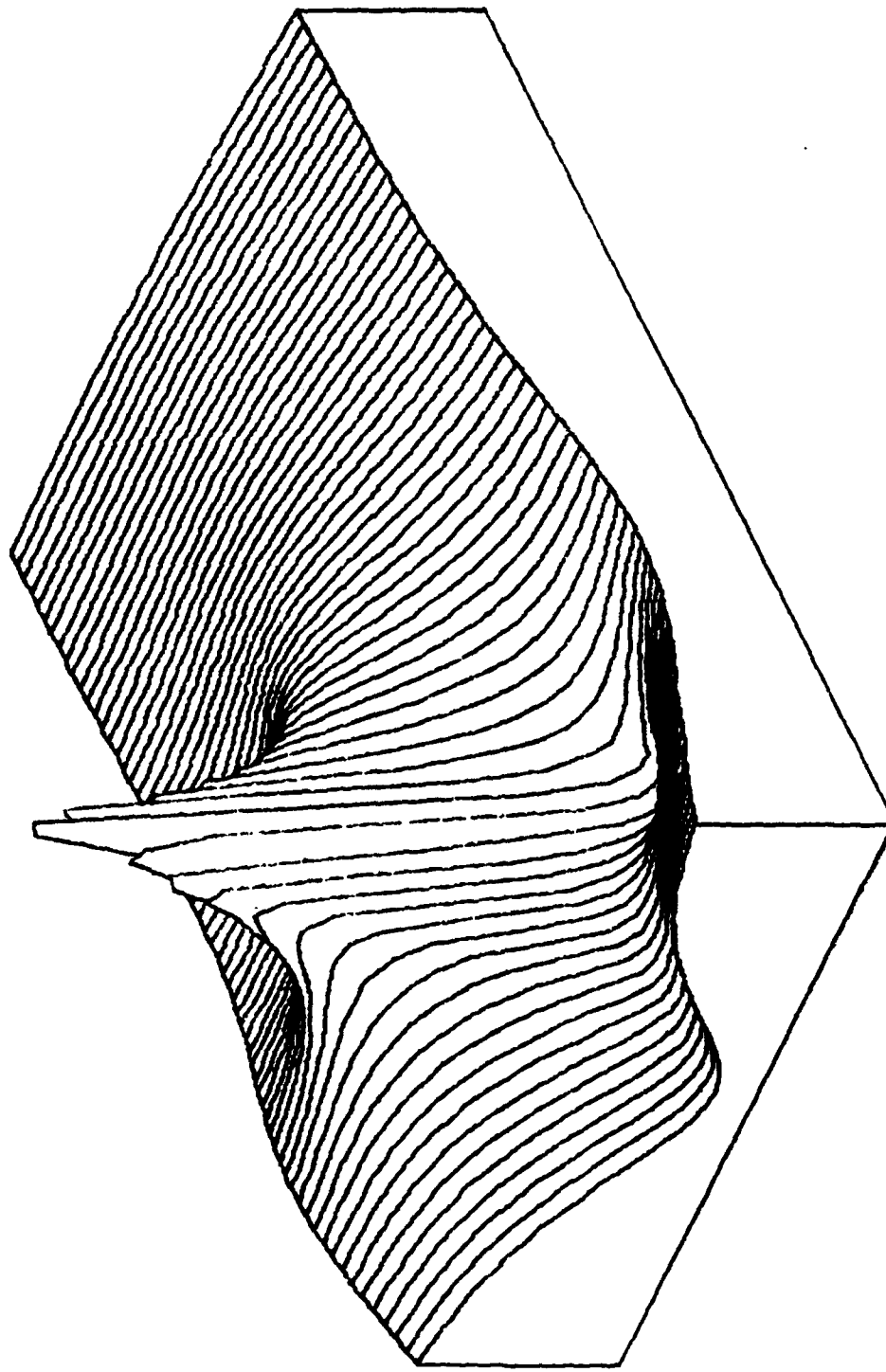


Figure 5.7h 3-D Plot of Maximum Principal Stress

Contour of the Minimum Principal Stress
----- EPK #52-04-09--91 (tension-torsion)

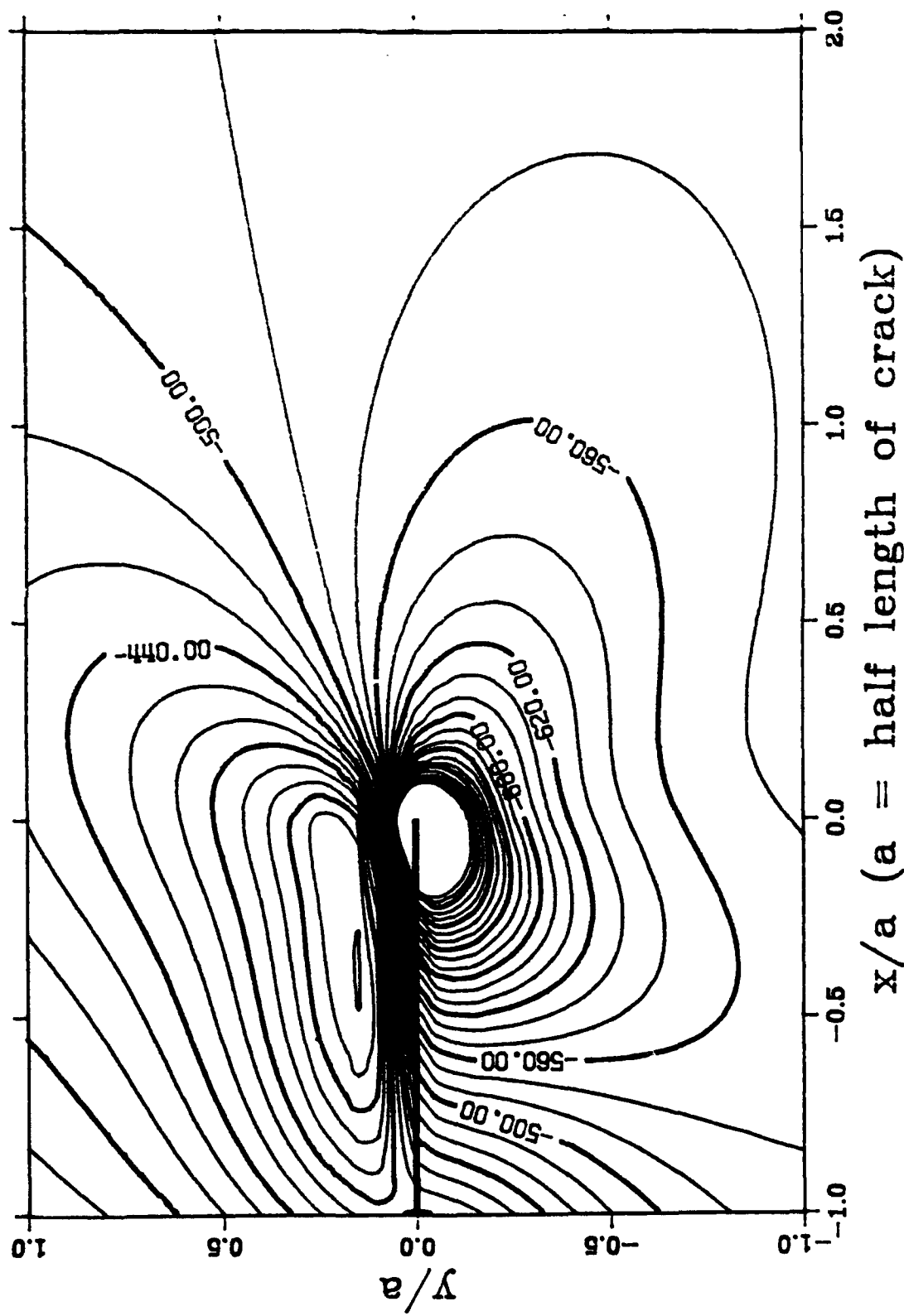


Figure 5.7i Lines of Equal Minimum Principal Stress

3-D plot for the Minimum Principal Stress
--- EPK #52-04-09-91 (tension-torsion)

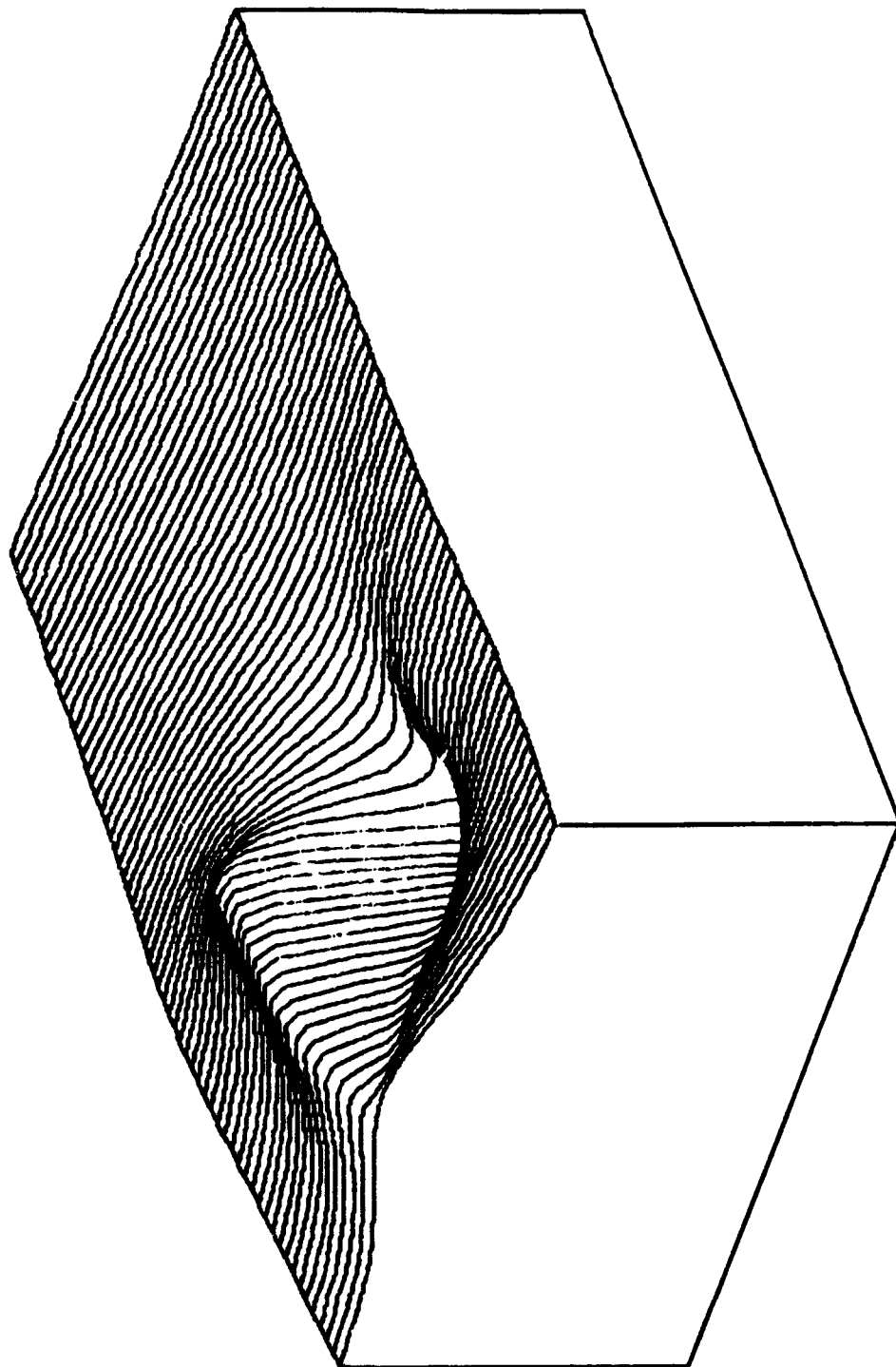


Figure 5.7j 3-D Plot of Minimum Principal Stress

Contour of the Maximum Shear Stress
--- EPK #52-04-09-91 (tension-torsion)

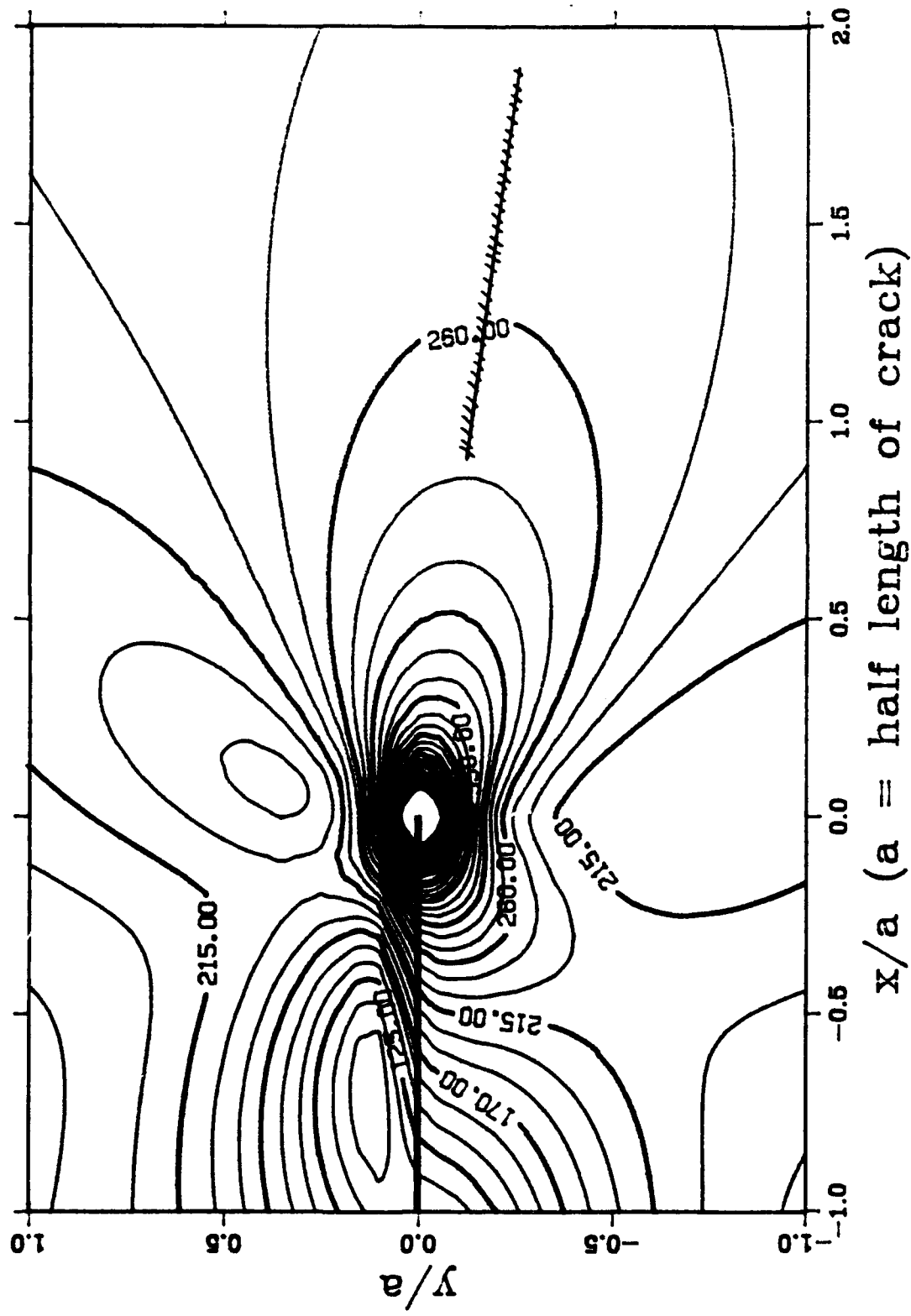


Figure 5.7k Lines of Equal Maximum Shear Stress

3-D plot for the Maximum Shear Stress
--- EPK #52-04-09-91 (tension-torsion)

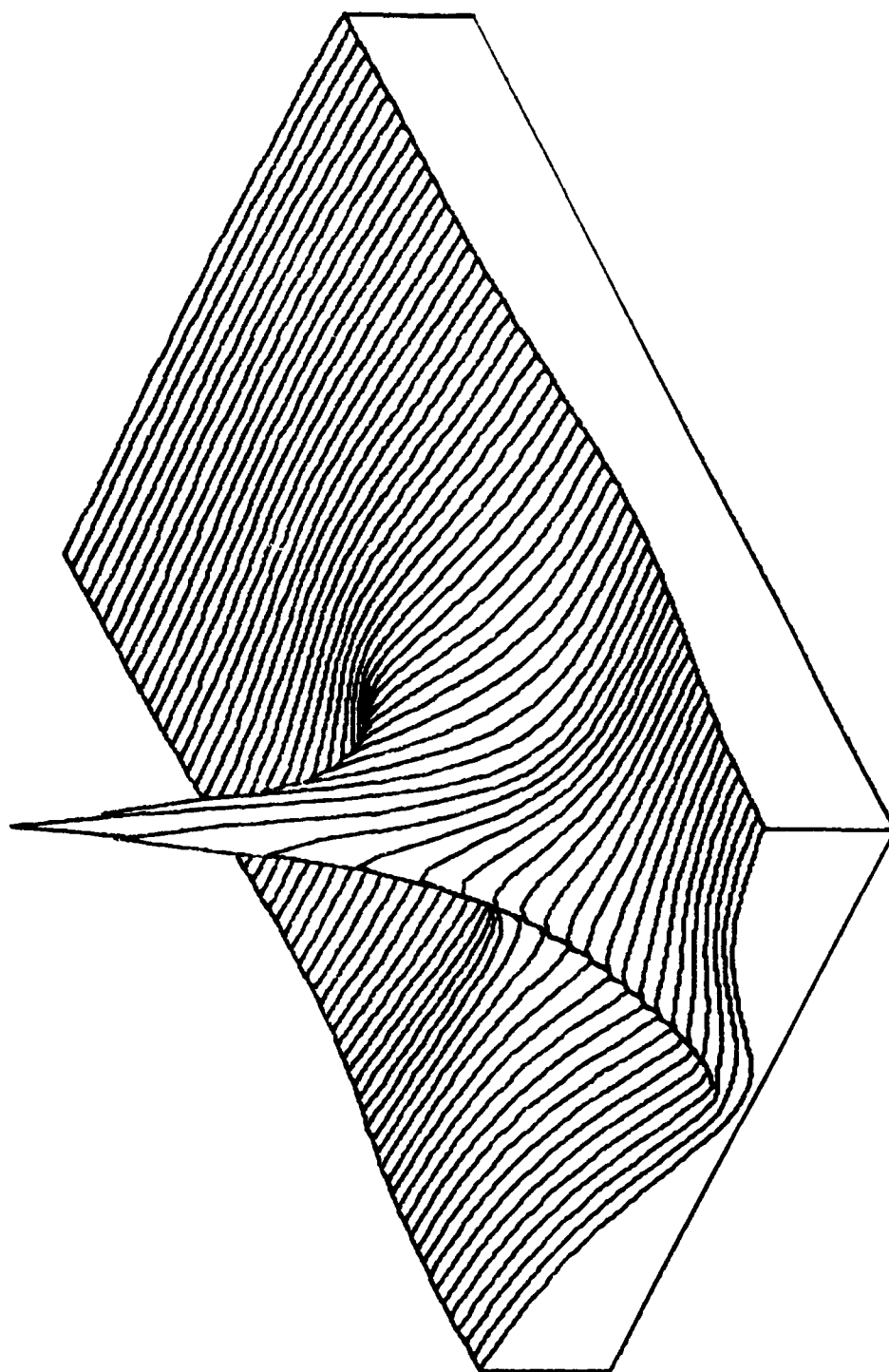


Figure 5.71 3-D Plot of Maximum Shear Stress

Contour of the Mean Stress
--- EPK #52-04-09-91 (tension-torsion)

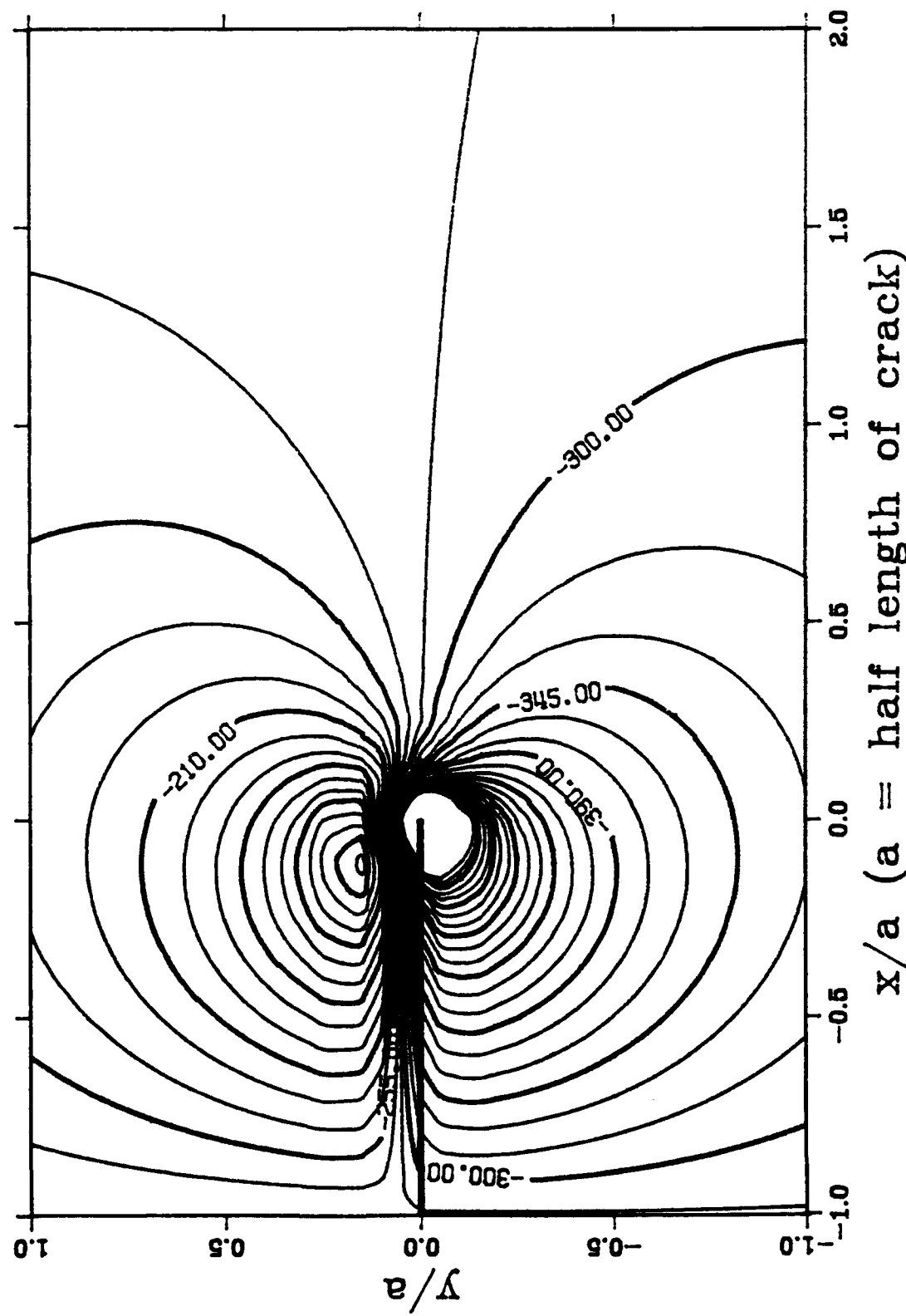
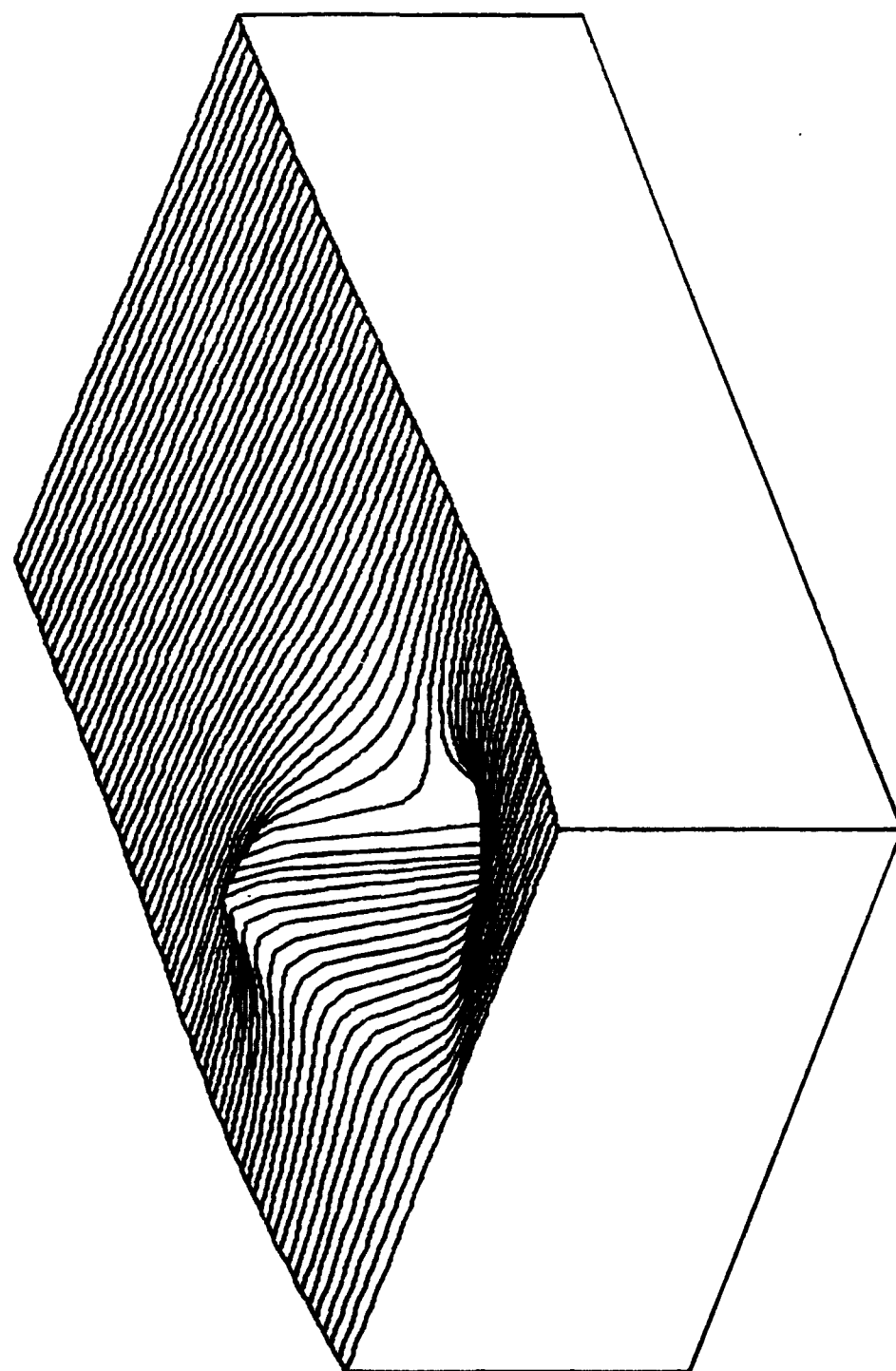


Figure 5.7m Lines of Equal Mean Stress

3-D plot for the Mean Stress
--- EPK #52-04-09-91 (tension-torsion)



Principal Stresses and Their Direction

(EPK #52-04-09-91; Tension-Torsion; Scale: 1 unit = 3500 kPa)

----- Tension —— Compression

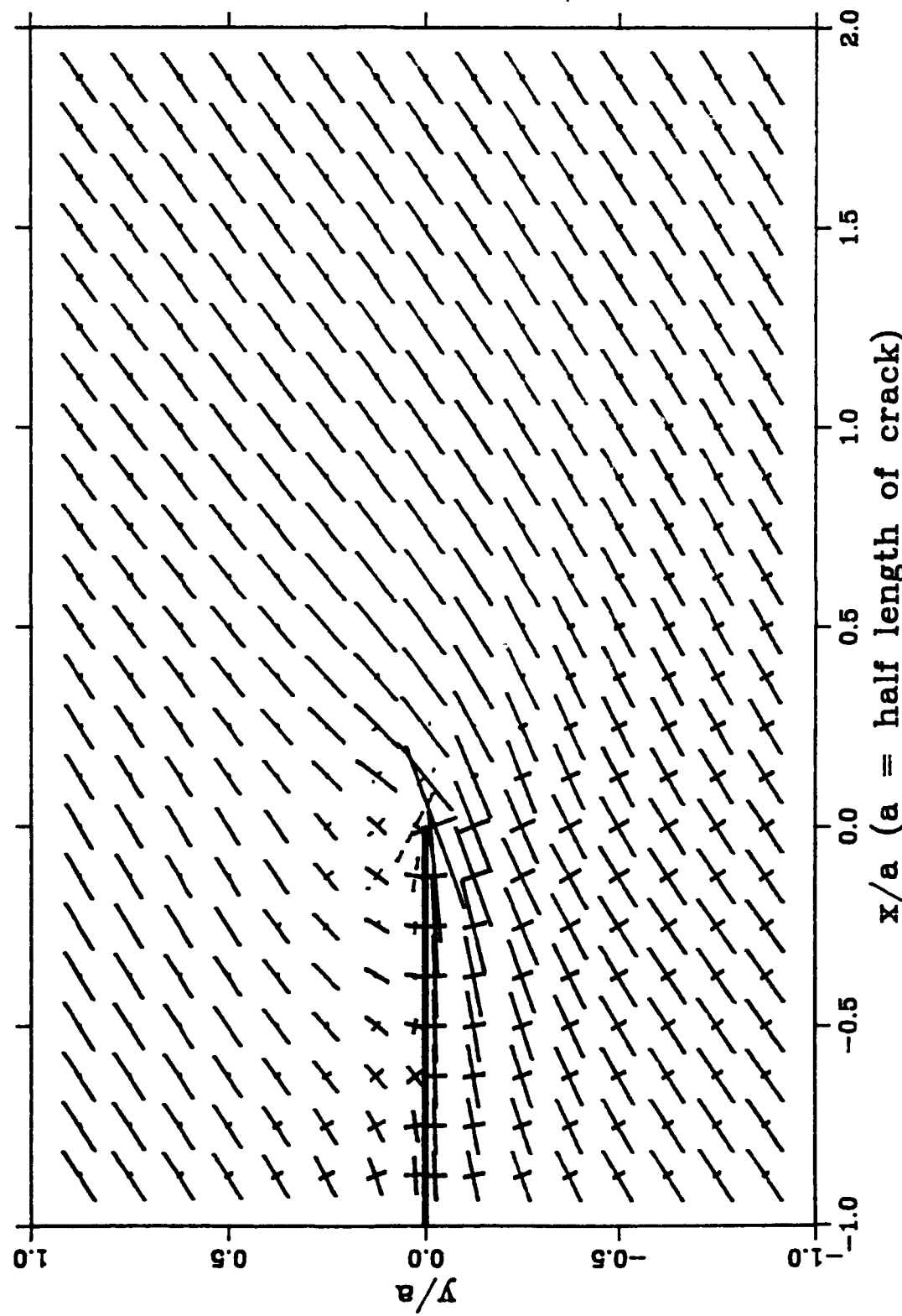


Figure 5.70 Principal Stresses and Their Directions

Stress Calculation for EPK #6v: 9/26/90; Pure-Torsion
---Ko N.C.^Hor.NOTCH^a/l=0.183^F.H.^C.D.^ecp = 70-20 psi^R45

length of crack = 1.0000 inch

initial_x= -1.0000 stepx= 0.1000 finial_x= 2.0000
initial_y= 1.0000 stepy= -0.1000 finial_y= -1.0000

Sxy = -243.2250 Syy = -336.0300 Sxx = -336.0300 Seff = -336.0300

Contour of the Shear Stress σ_{xy}
 --- FPK 6v-09-26-90 (pure-torsion)

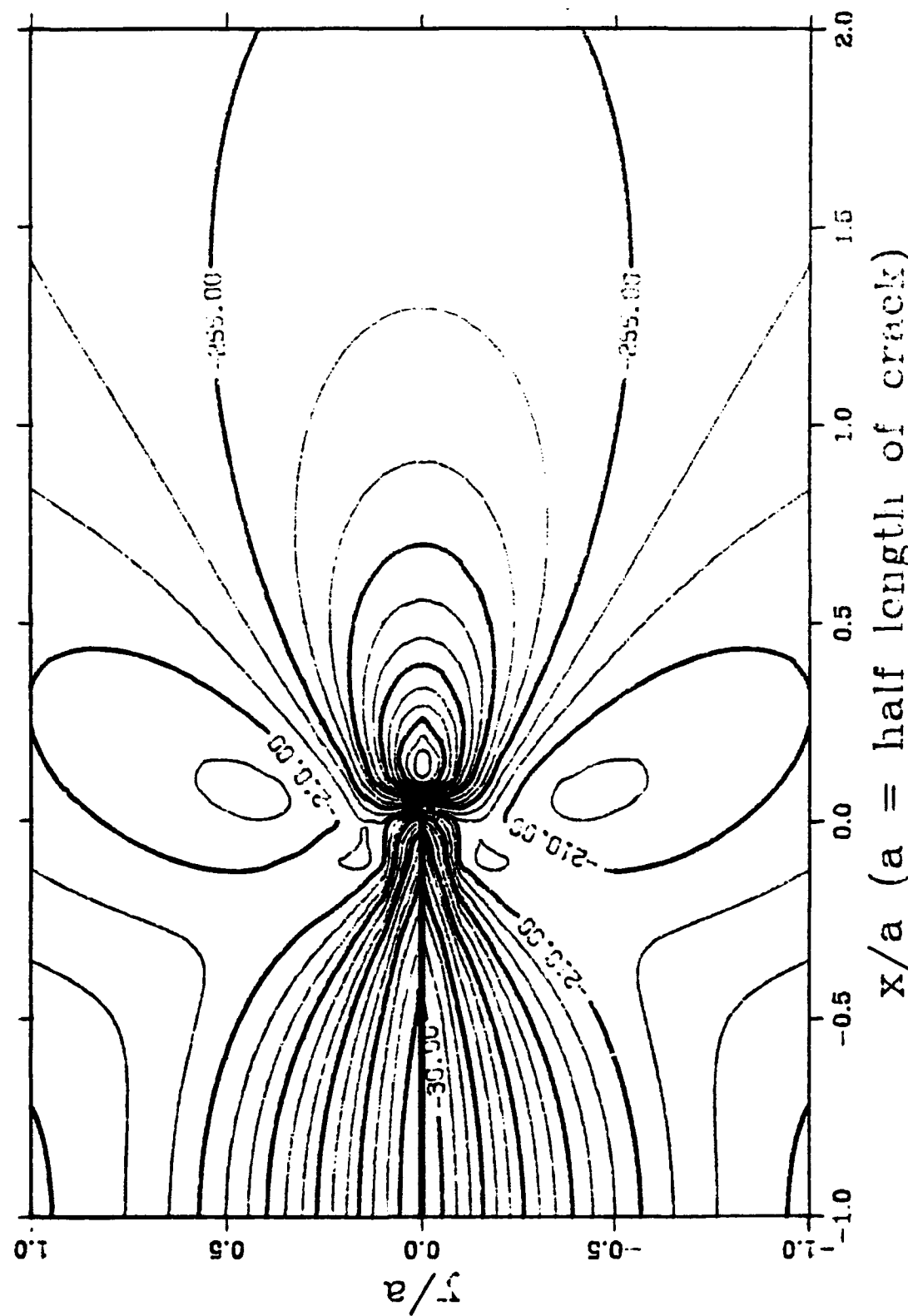


Figure 5.8a Lines of Equal Shear Stress

3-D plot for the Shear Stress σ_{xy}
--- EPK #6v-09-26-90 (pure-torsion)

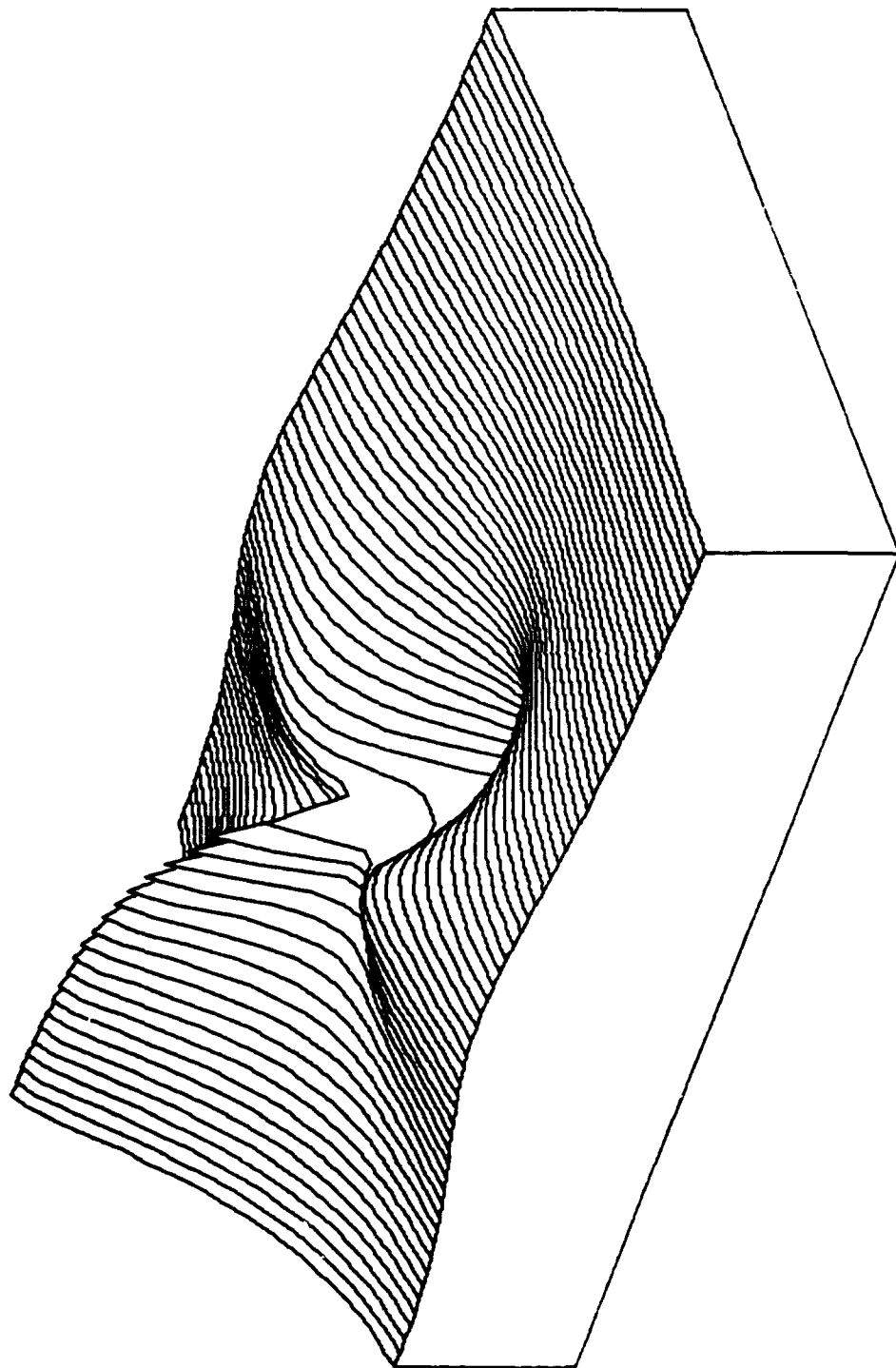


Figure 5.8b 3-D Plot of Shear Stress

Contour of the Normal Stress σ_{xx}
--- EPK #6v-09-26-90 (pure-torsion)

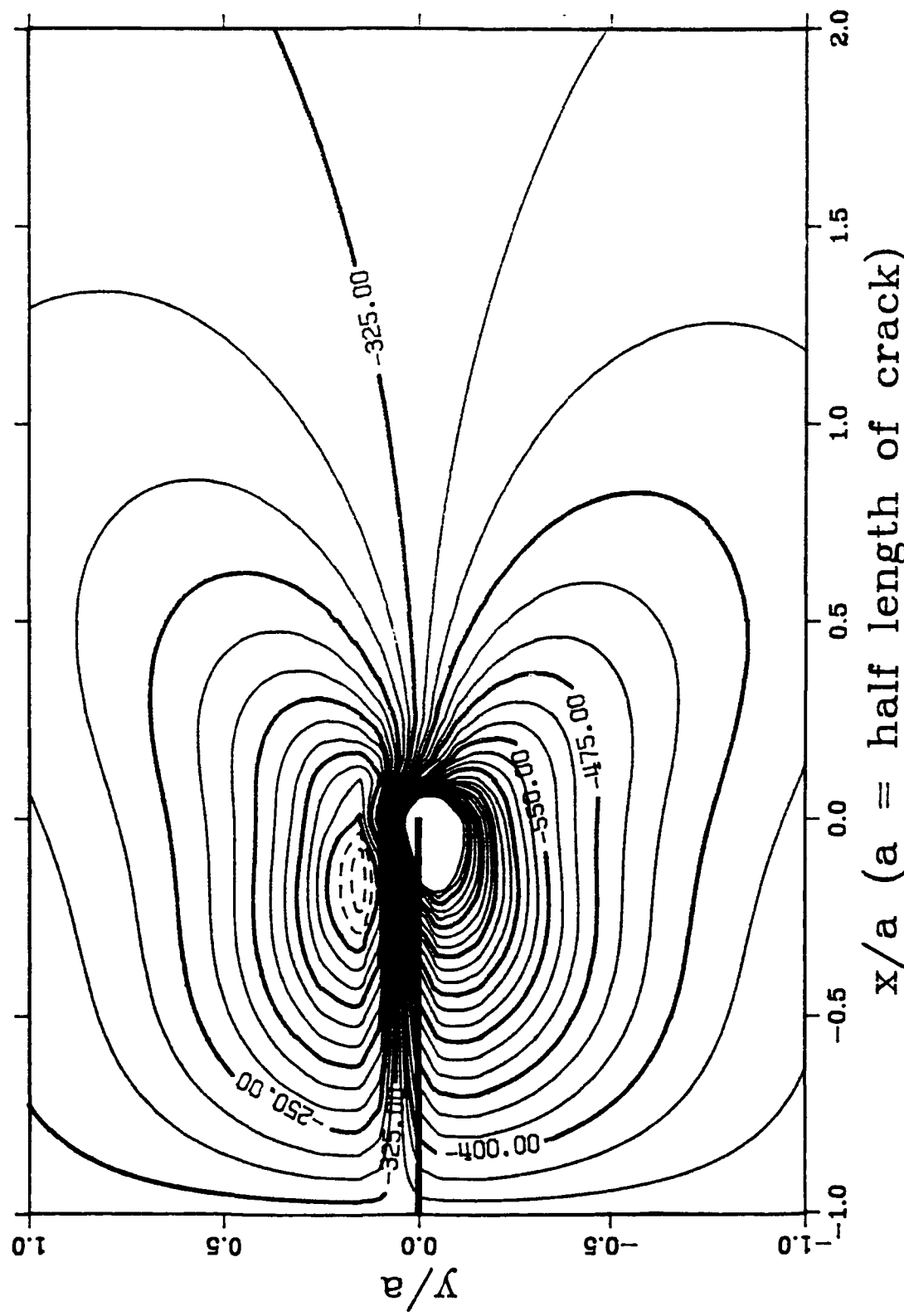


Figure 5.8c Lines of Equal Normal Stress

3-D plot for the Normal Stress σ_{xx}
--- EPK #6v-09--26-90 (pure-torsion)

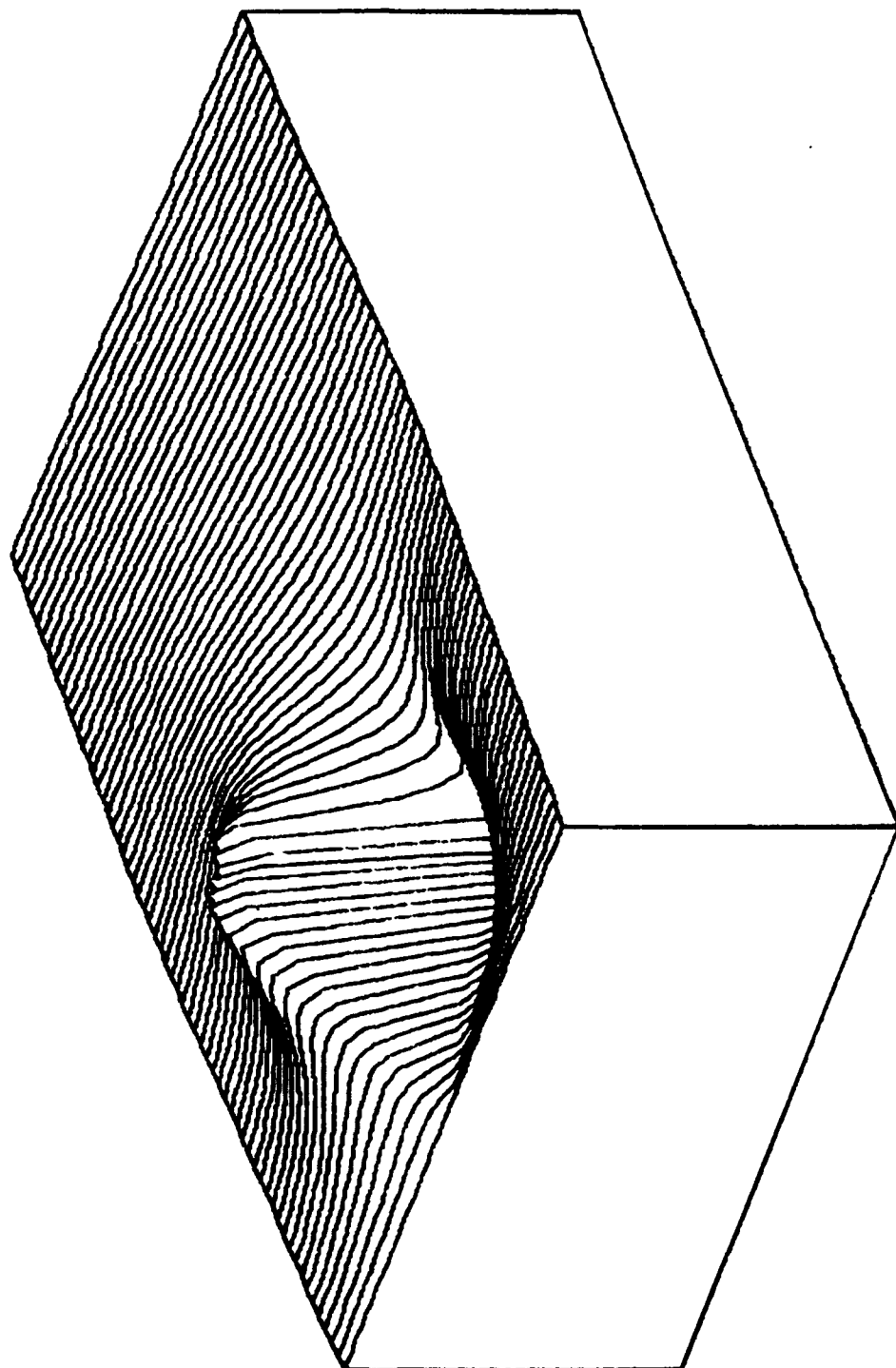


Figure 5.8d 3-D Plot of Normal Stress

Contour of the Normal Stress σ_{yy}
--- EPK #6v-09-26-90 (pure-torsion)

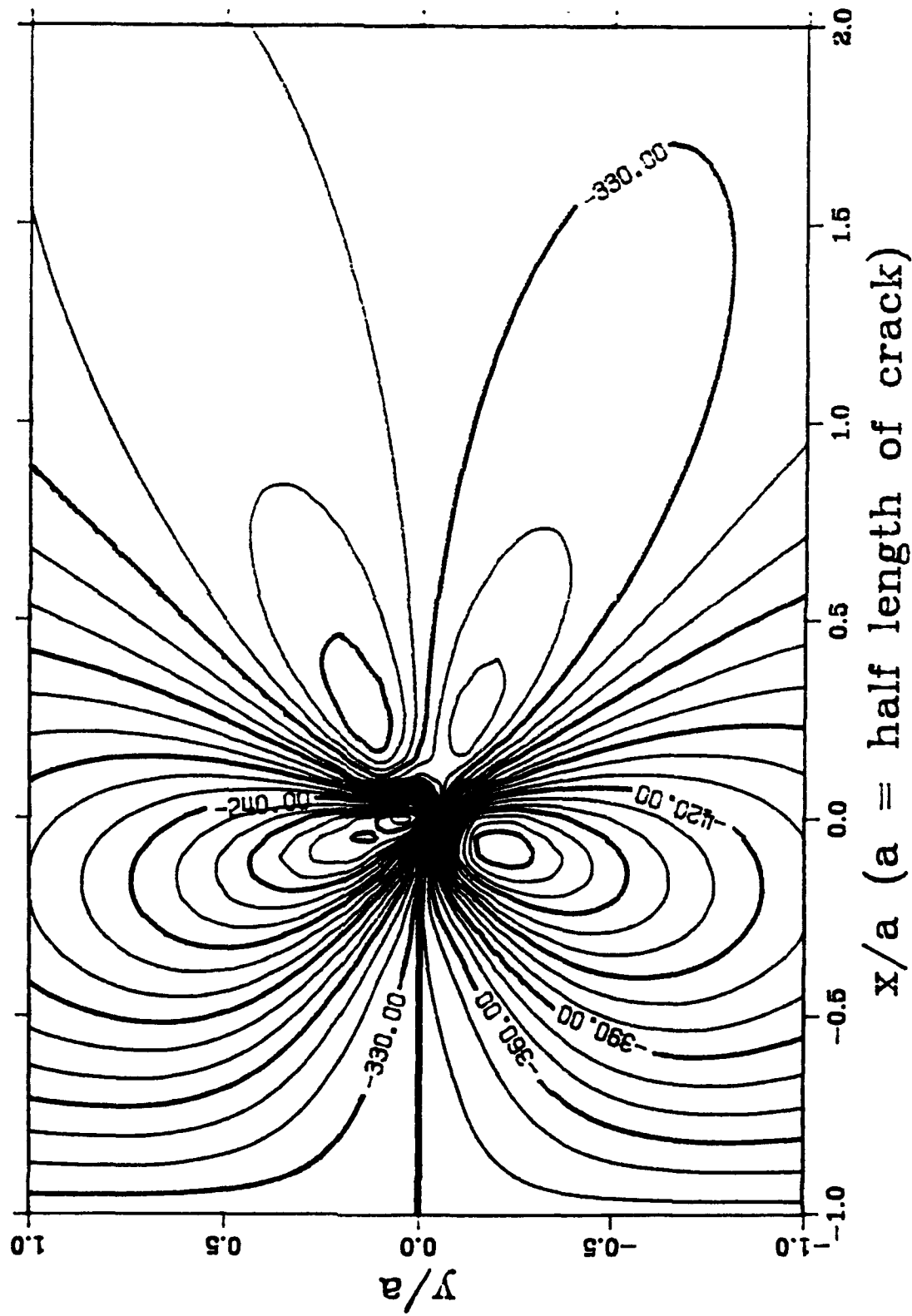


Figure 5.8e Lines of Equal Normal Stress

3-D plot for the Normal Stress σ_{yy}
--- EPK #6v--09--26--90 (pure-torsion)

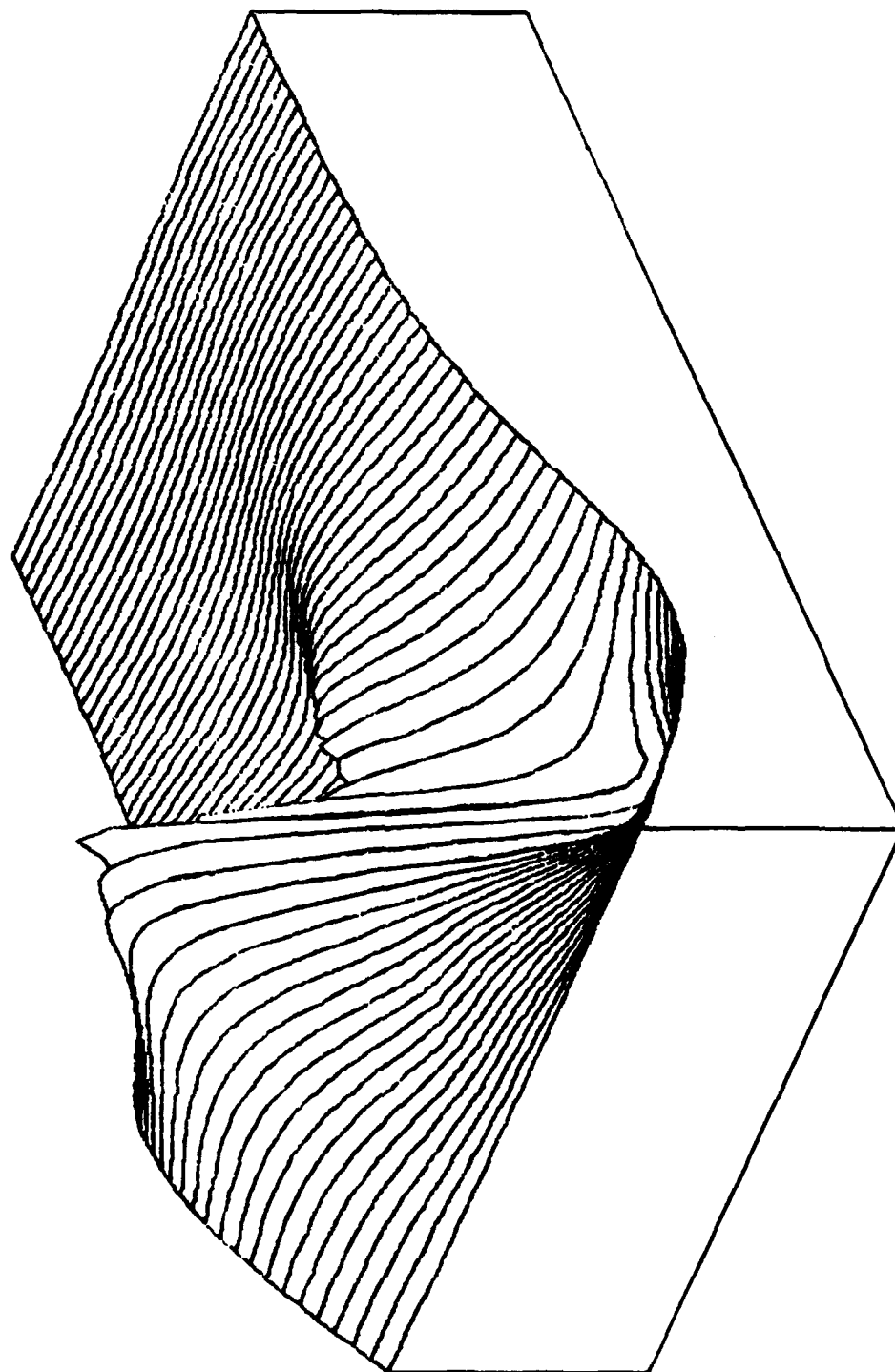


Figure 5.8f 3-D Plot of Normal Stress

Contour of the Maximum Principal Stress
--- EPK #6v--09--26--90 (pure-torsion)

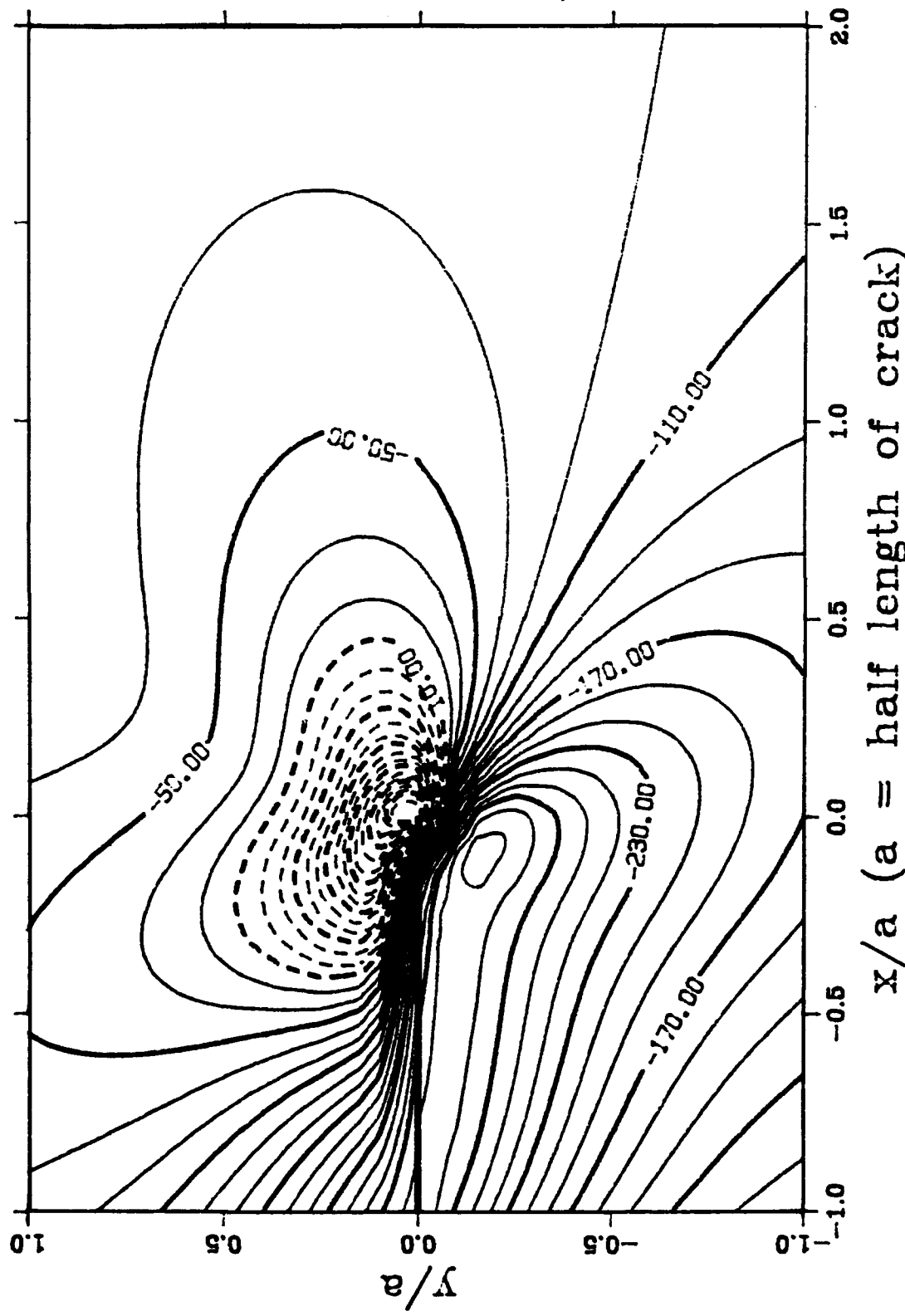


Figure 5.8g Lines of Equal Maximum Principal Stress

3-D plot for the Maximum Principal Stress
EPK #6v-09-26-90 (pure-torsion)

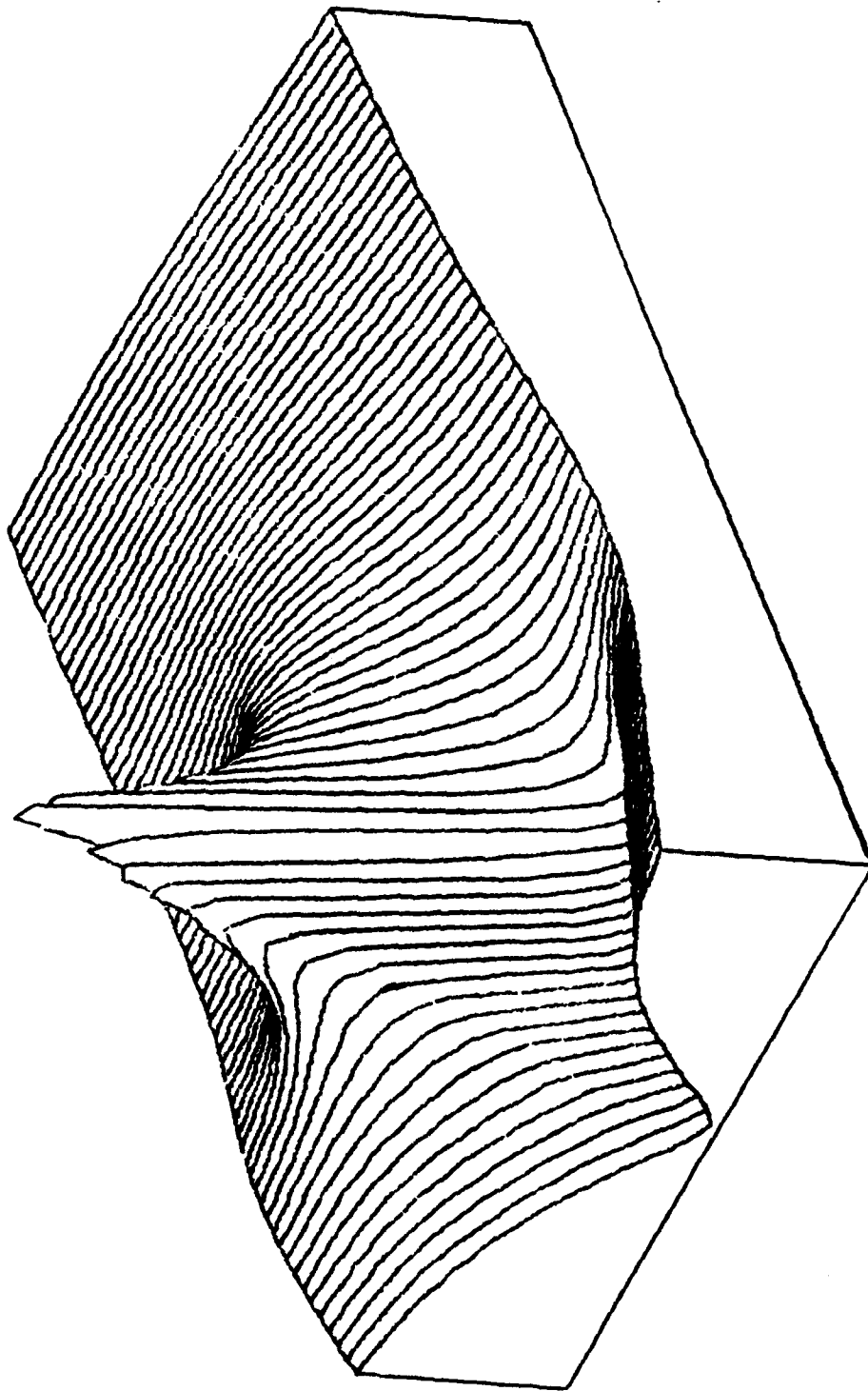


Figure 5.8h 3-D Plot of Maximum Principal Stress

Contour of the Minimum Principal Stress
--- EPK #6v-09-26-90 (pure-torsion)

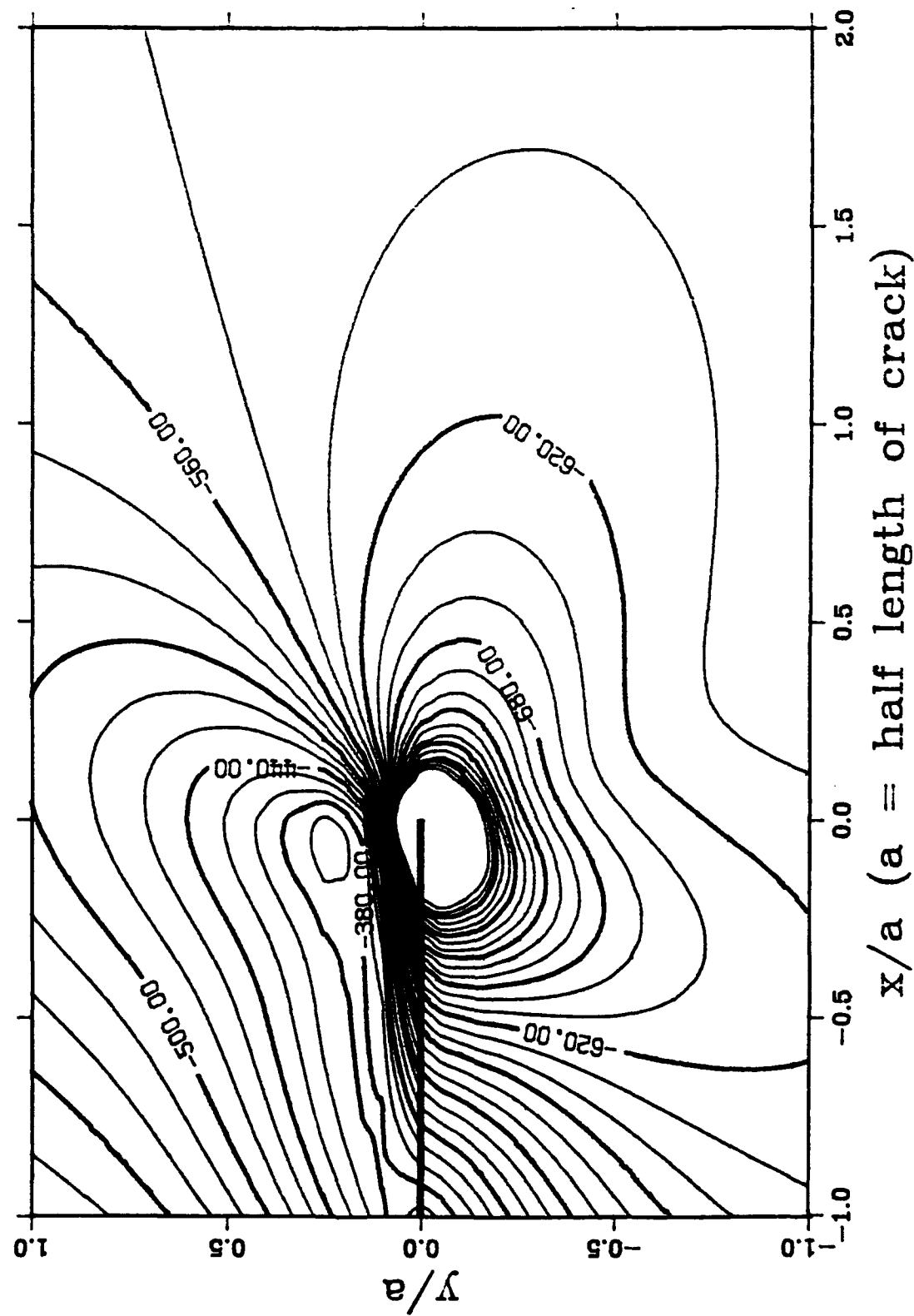


Figure 5.8i Lines of Equal Minimum Principal Stress

3-D plot for the Minimum Principal Stress
--- EPK #6v-09-26-90 (pure-torsion)

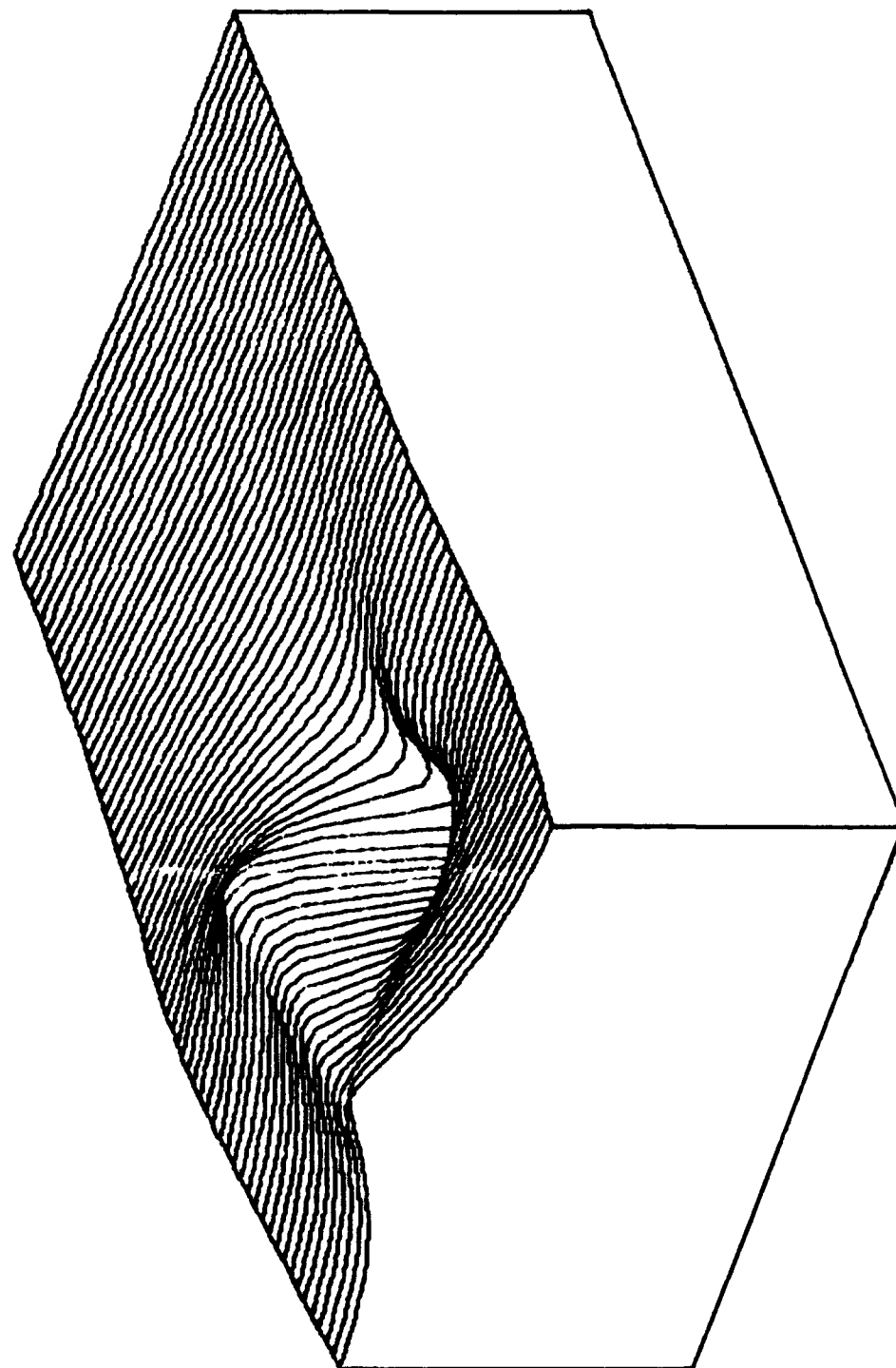


Figure 5.8j 3-D Plot of Minimum Principal Stress

Contour of the Maximum Shear Stress
--- EPK #6v-09-26-90 (pure -torsion)

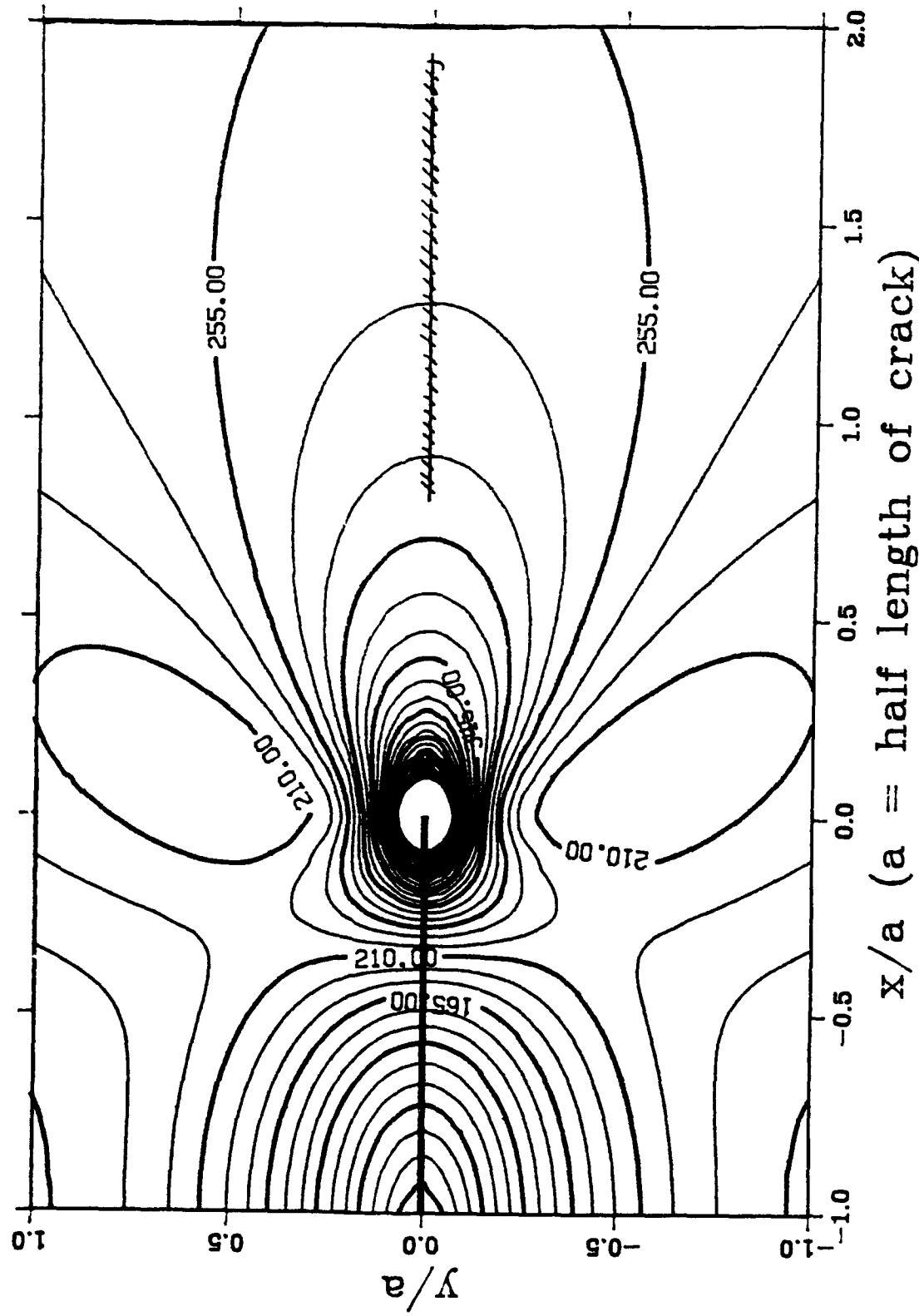


Figure 5.8k Lines of Equal Maximum Shear Stress

3-D plot for the Maximum Shear Stress
--- EPK #6v-09-26-90 (pure-torsion)

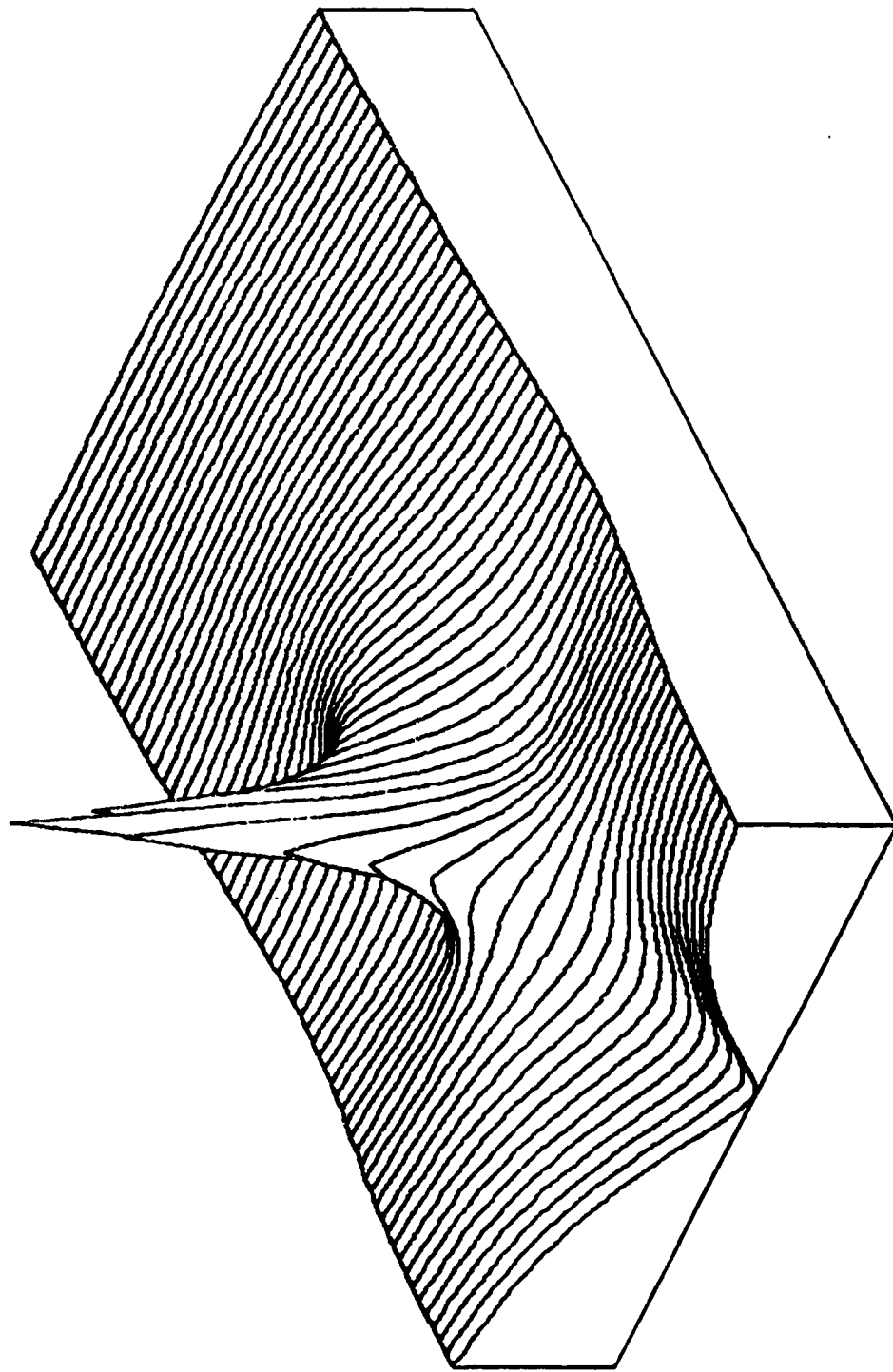


Figure 5.81 3-D Plot of Maximum Shear Stress

Contour of the Mean Stress
--- EPK #6v-09-26-90 (pure-torsion)

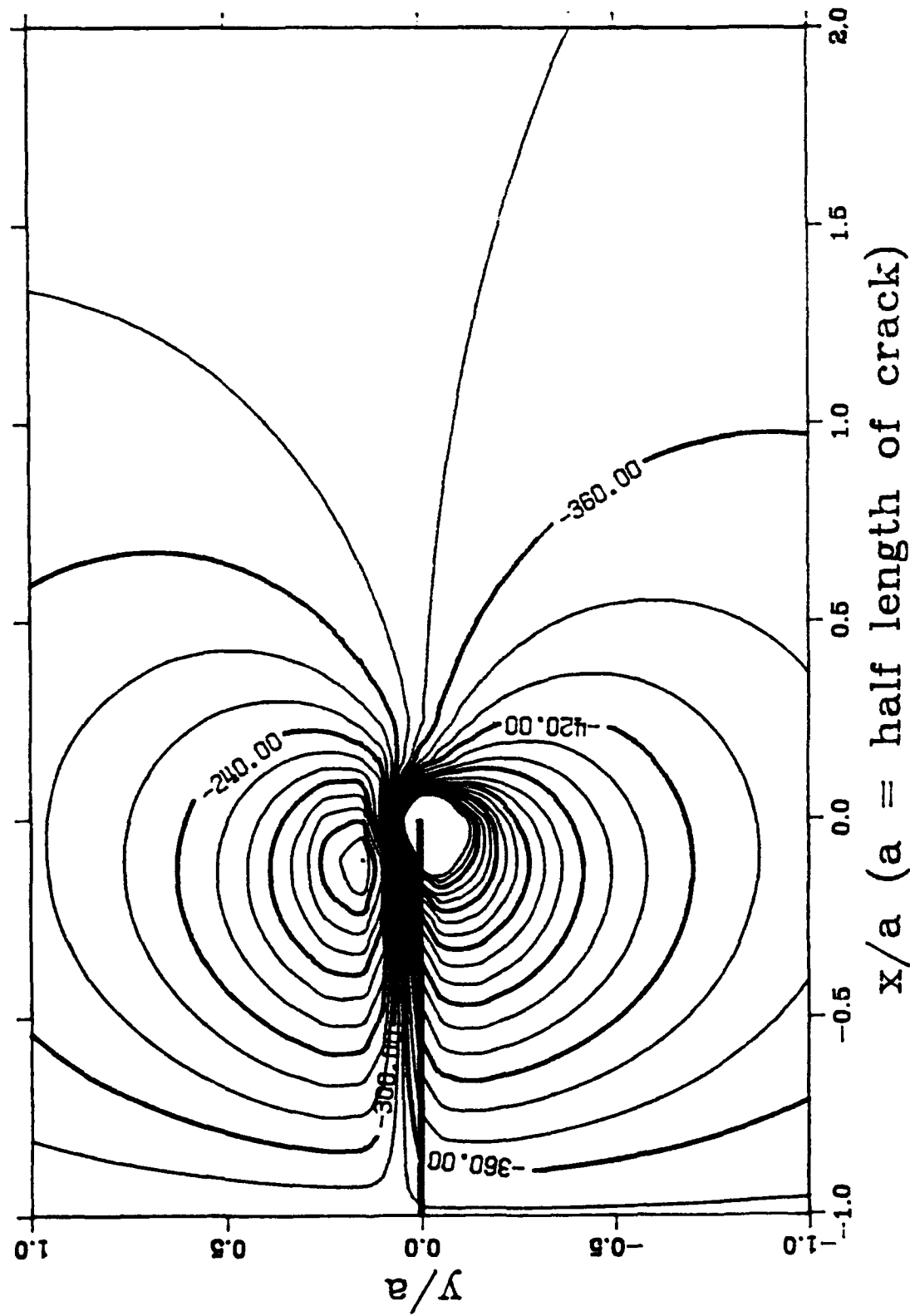


Figure 5.8m Lines of Equal Mean Stress

3-D plot for the Mean Stress
--- EPK #6v-09-26-90 (pure-torsion)

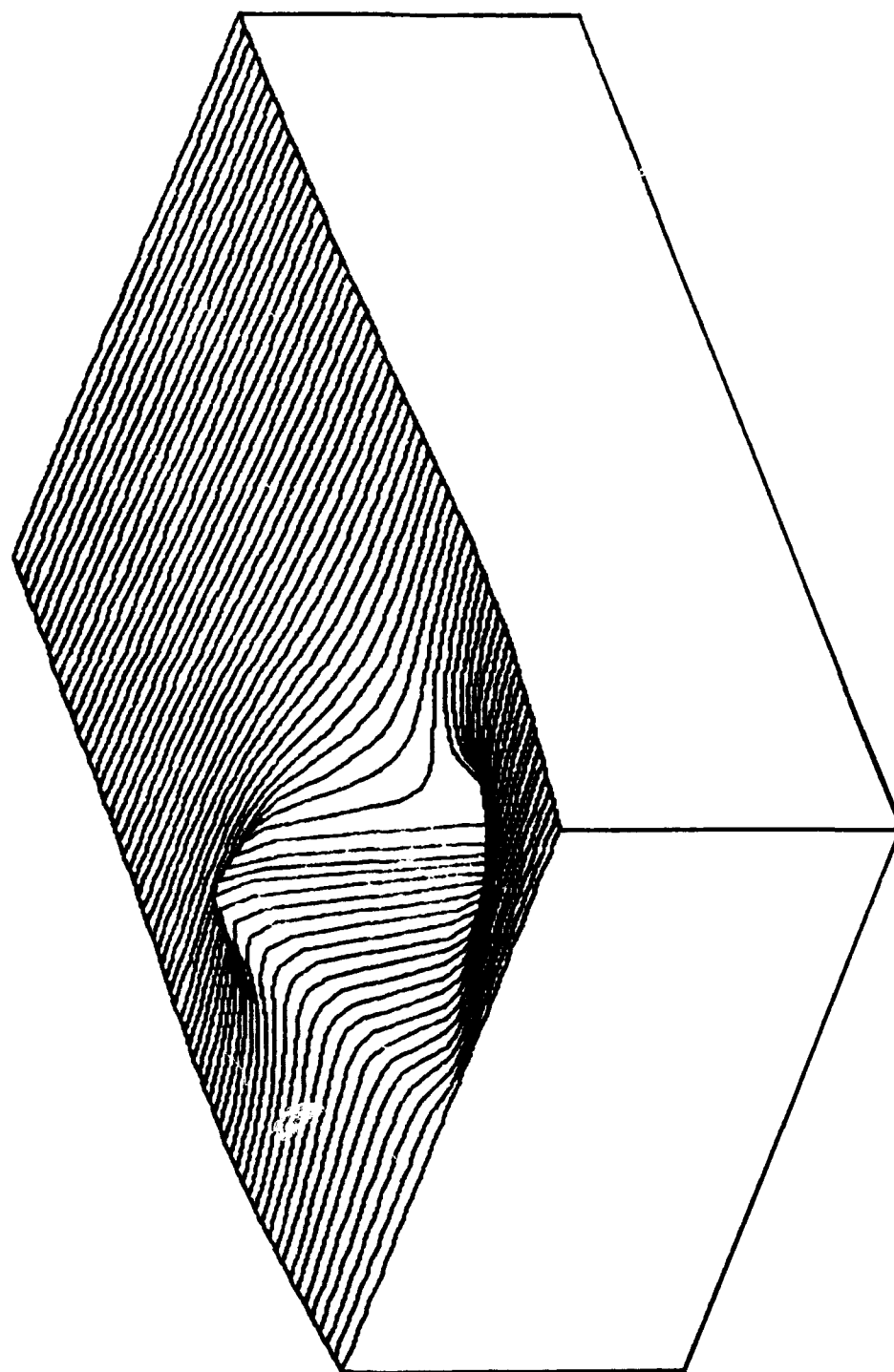


Figure 5.8n 3-D Plot of Mean Stress

Principal Stresses and Their Direction

(EPK #6v-09-26-90; Pure-Torsion; Scale: 1 unit = 4000 kPa)

----- Tension —— Compression

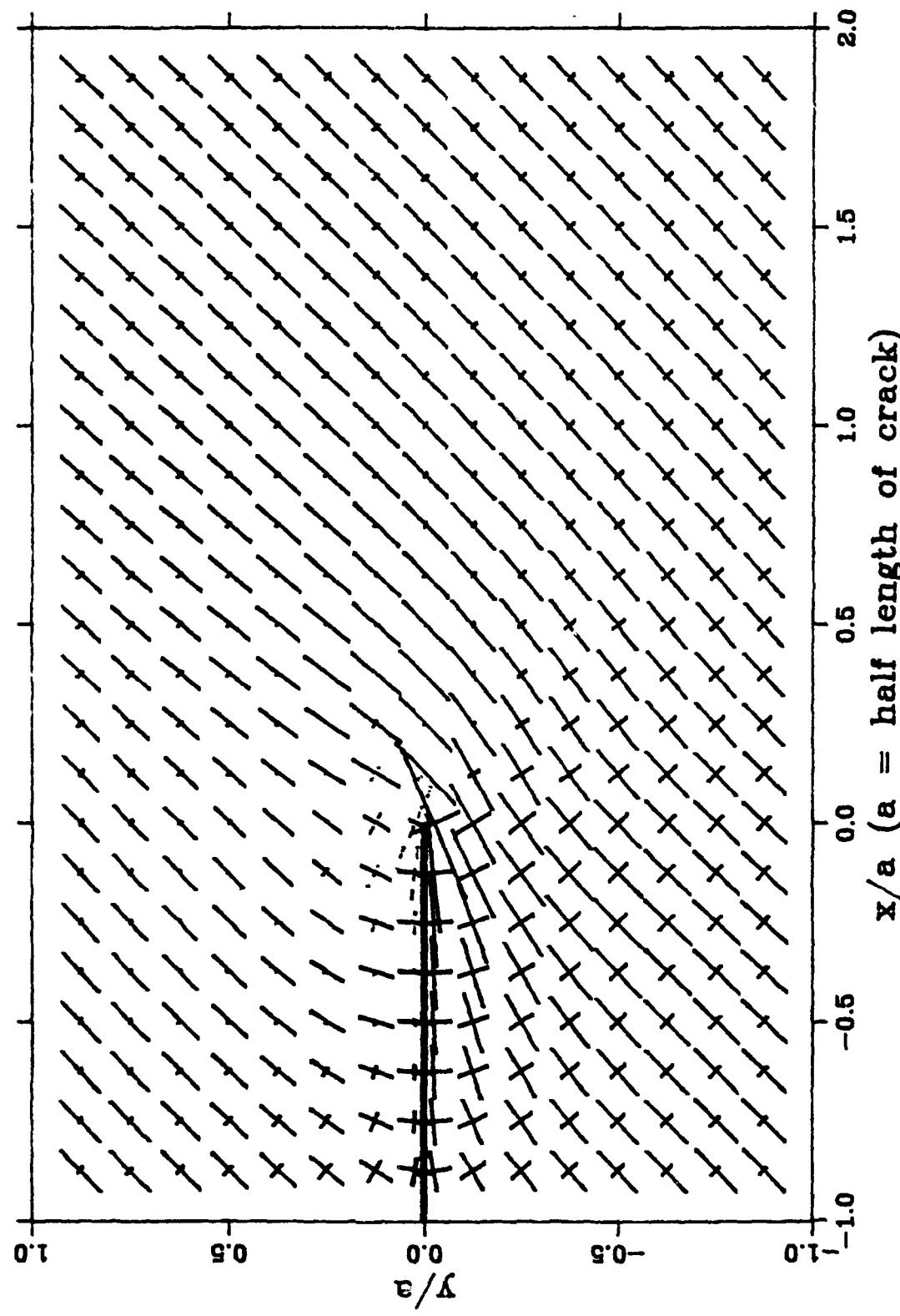


Figure 5.80 Principal Stresses and Their Directions

Stress Calculation for EPK #51; 4/5/91; Compression-Torsion
---Ko N.C.^Hor.NOTCH^a/l=0.183^F.H.^C.S.^ecp = 70-20 psi^DCR30

length of crack = 1.0000 inch

initial_x= -1.0000 stepx= 0.1000 finial_x= 2.0000
initial_y= 1.0000 stepy= -0.1000 finial_y= -1.0000

Sxy = -275.1720 Syy = -543.8580 Sxx = -302.9100 Seff = -302.9100

Contour of the Shear Stress σ_{xy}
 --- EPK #51-04-05-91 (compression-torsion)

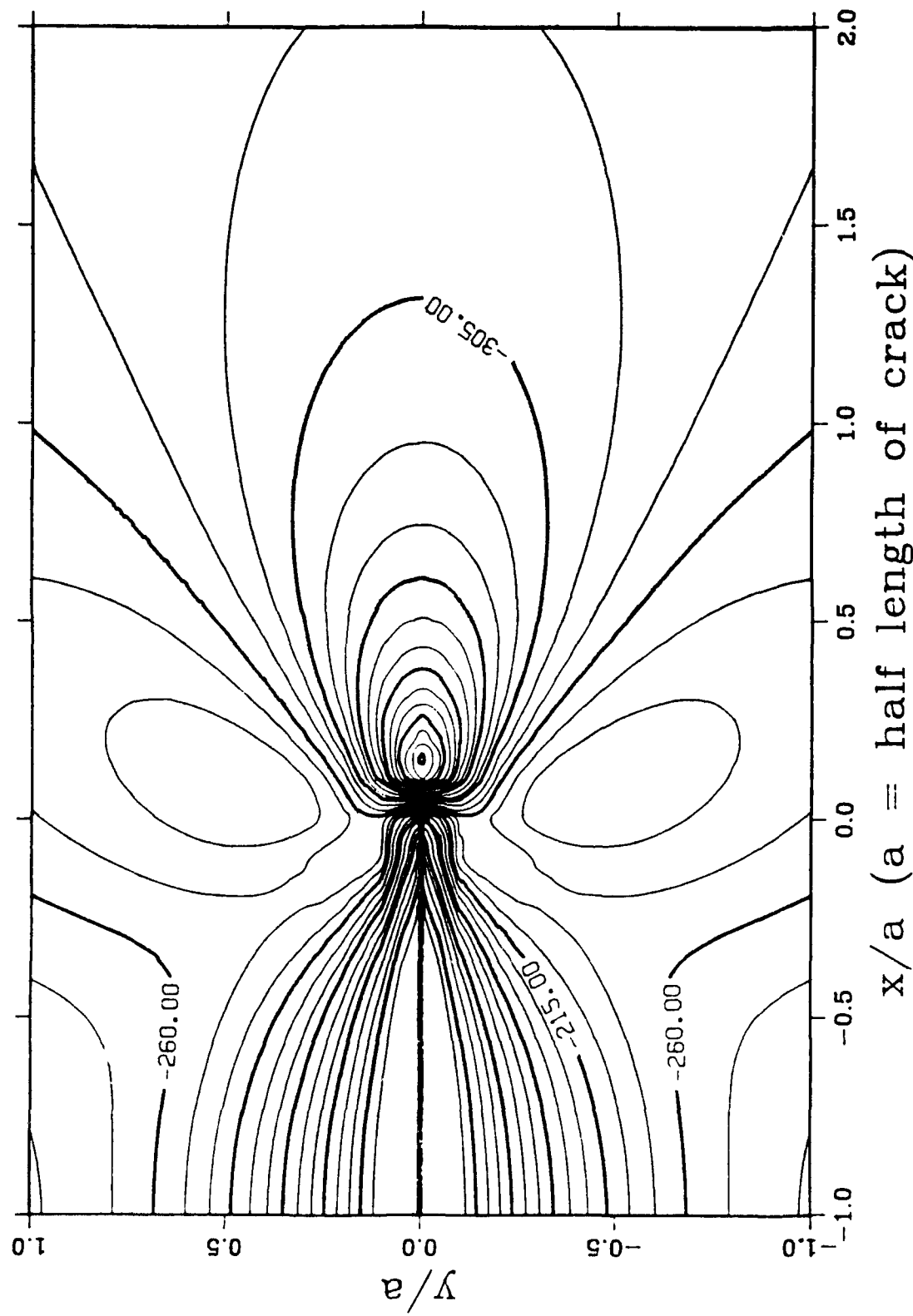


Figure 5.9a Lines of Equal Shear Stress

3-D plot for the Shear Stress σ_{xy}
--- MPK #51-04-05-91 (compression-torsion)

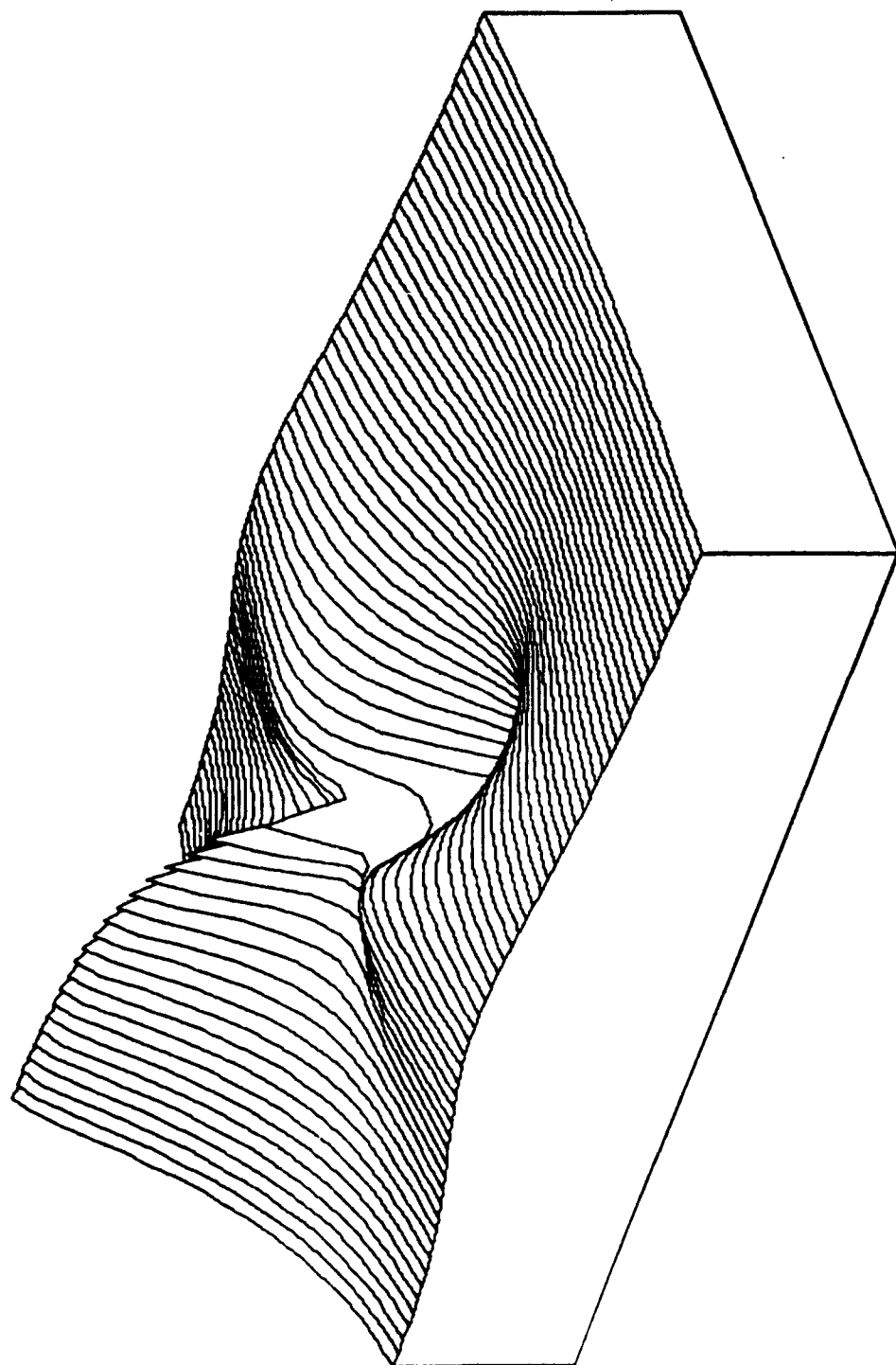


Figure 5.9b 3-D Plot of Shear Stress

Contour of the Normal Stress σ_{xx}
 FPK #51 01-05-91 (compression-torsion)

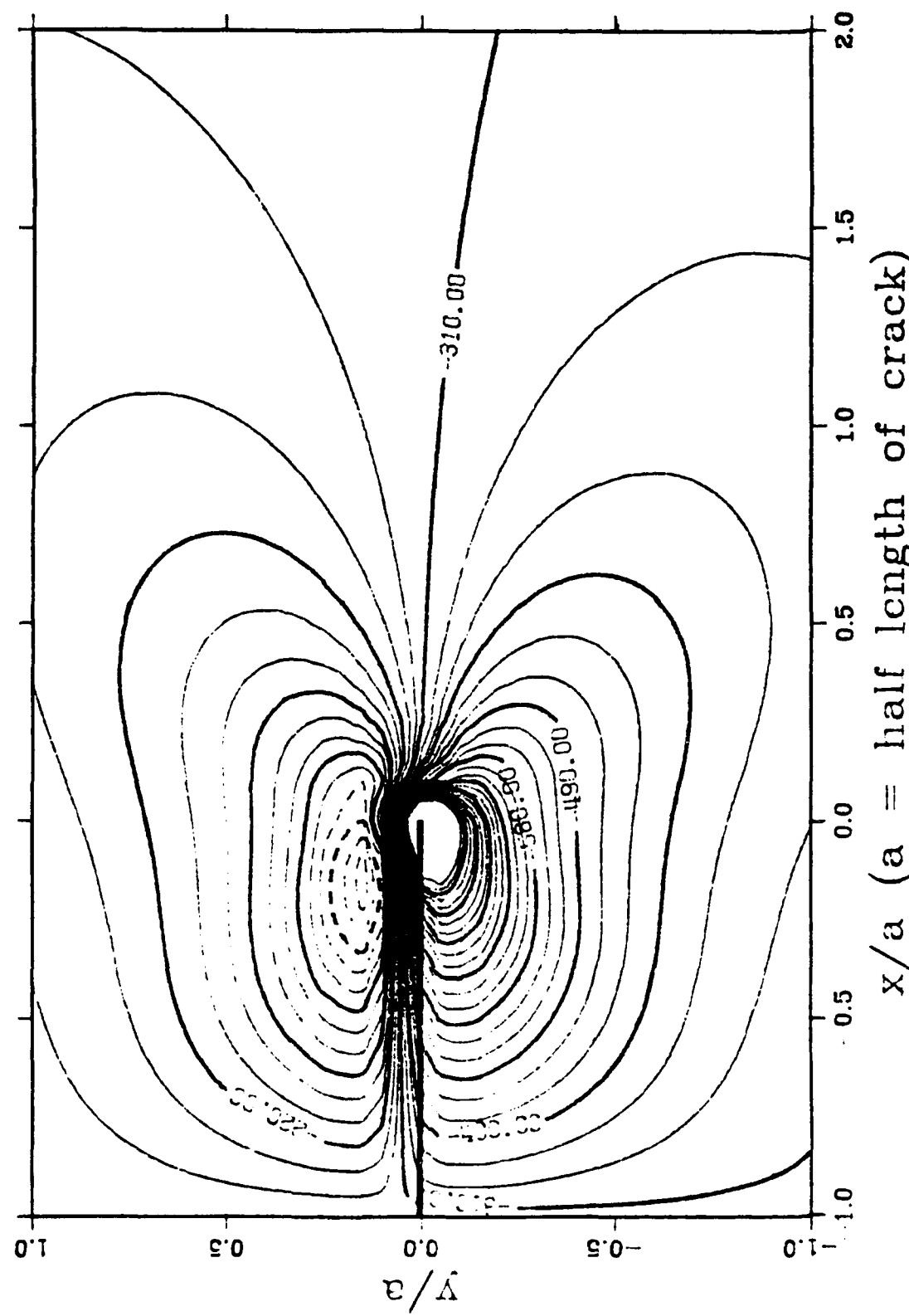
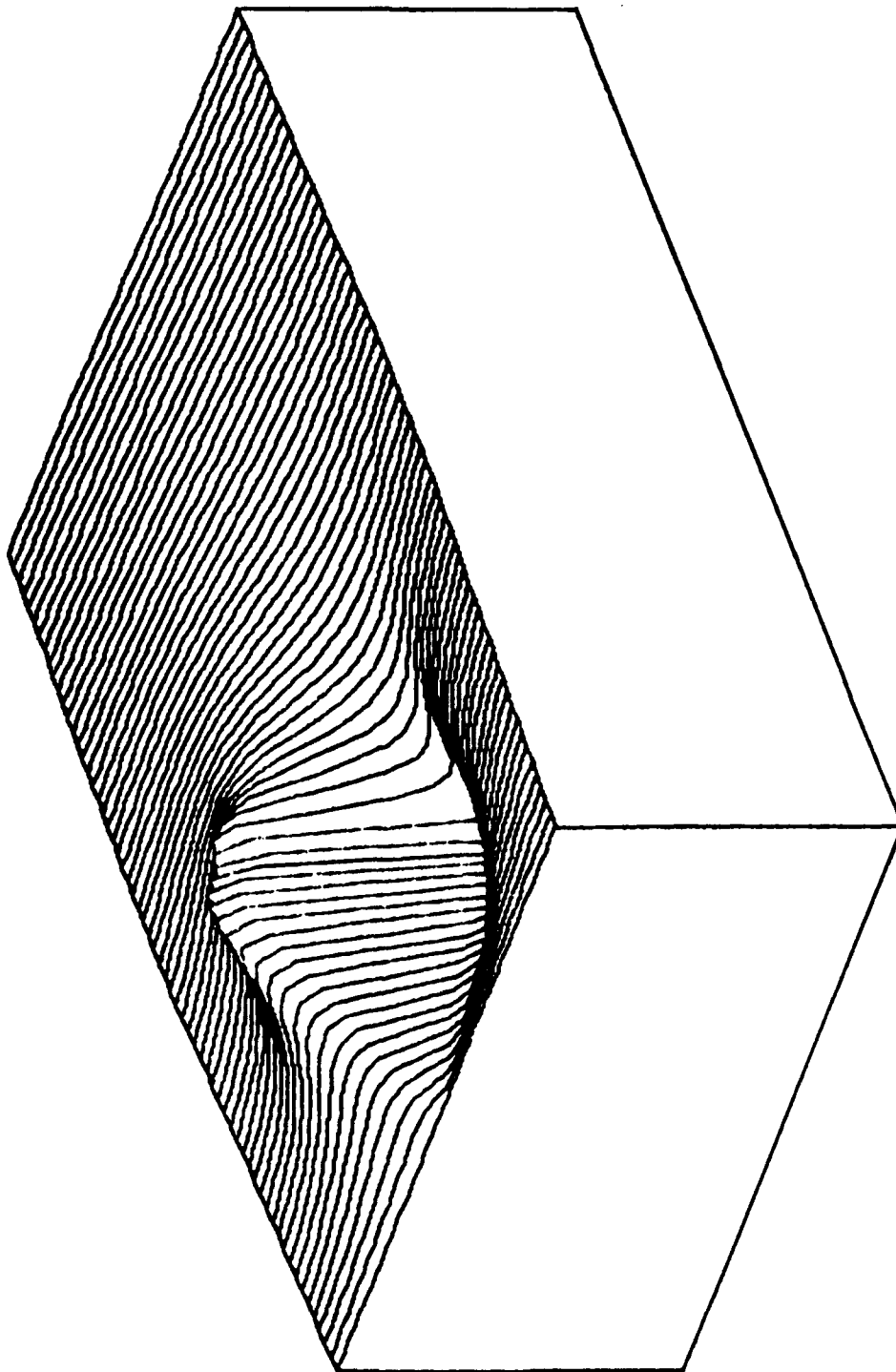


Figure 5.9c Lines of Equal Normal Stress

3-D plot for Normal Stress σ_{xx}
--- EPK #51-04-05-91 (compression-torsion)



Contour of the Normal Stress σ_{yy}
 --- MPK #51-04-05-91 (compression-torsion)

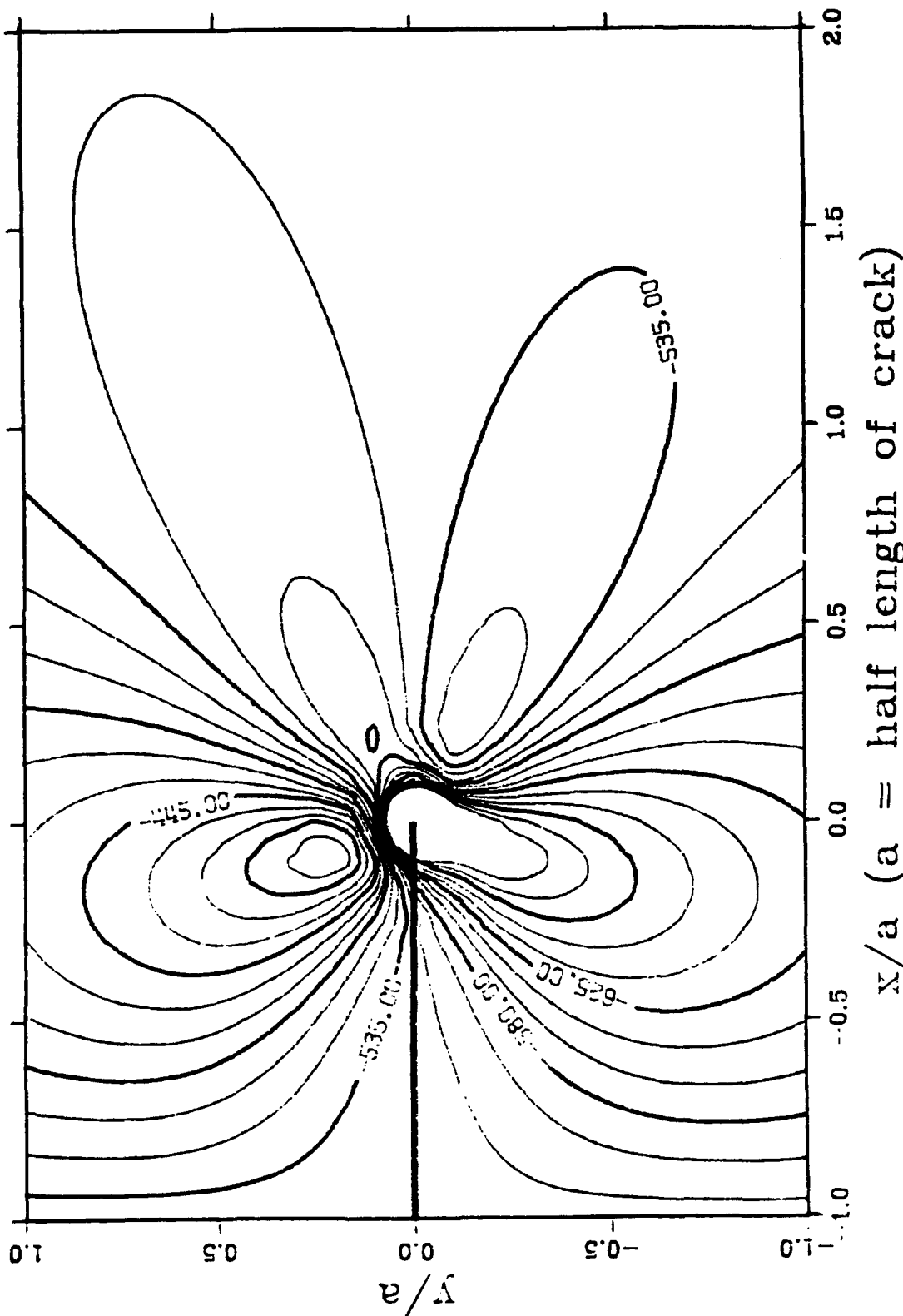


Figure 5.9e Lines of Equal Normal Stress

3-D plot for Normal Stress σ_{yy}
--- EPK #51-04-05-91 (compression-torsion)

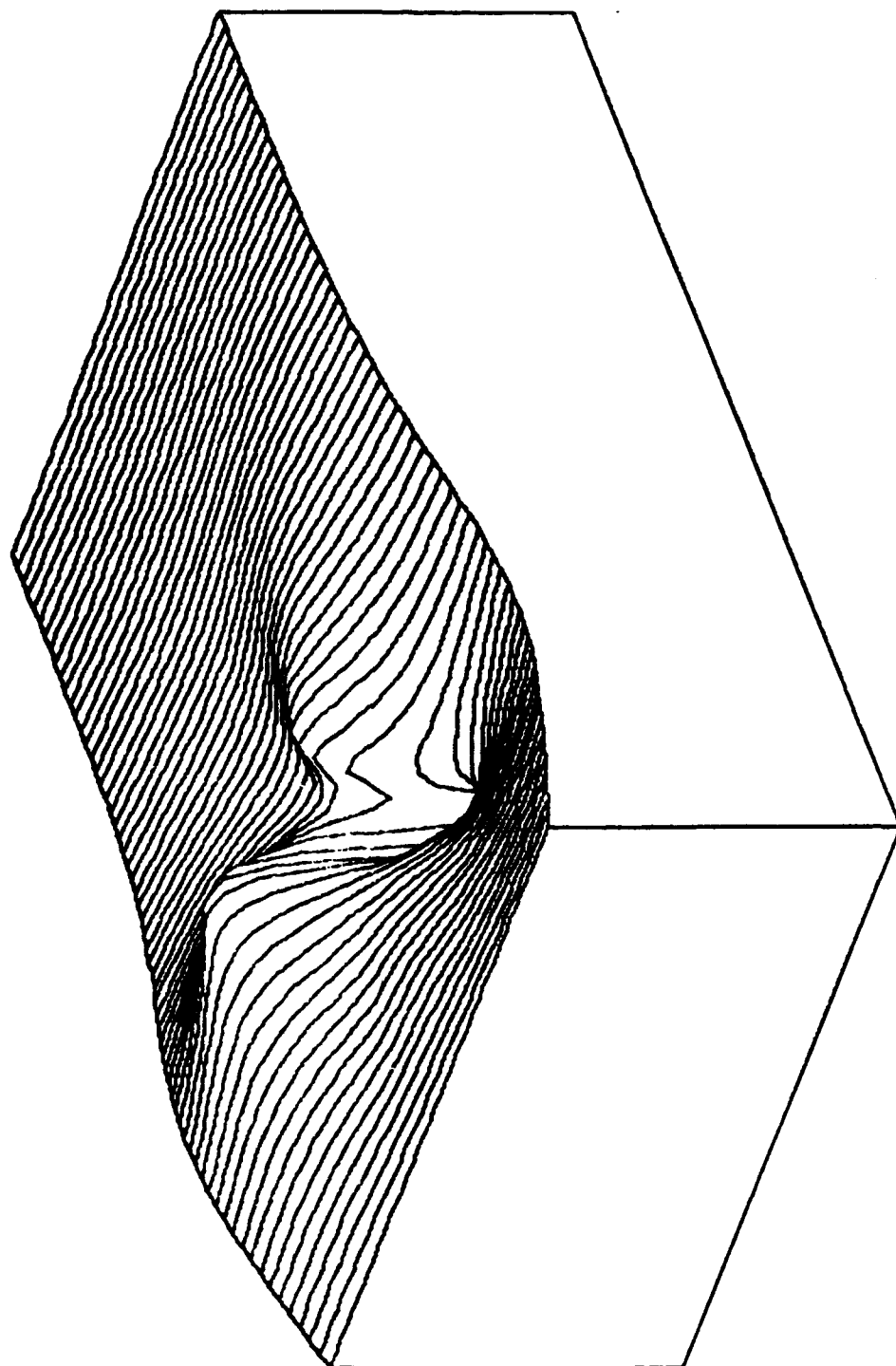


Figure 5.9f 3-D Plot of Normal Stress

Contour of the Maximum Principal Stress
--- EPK #51-04-05-91 (compression-torsion)

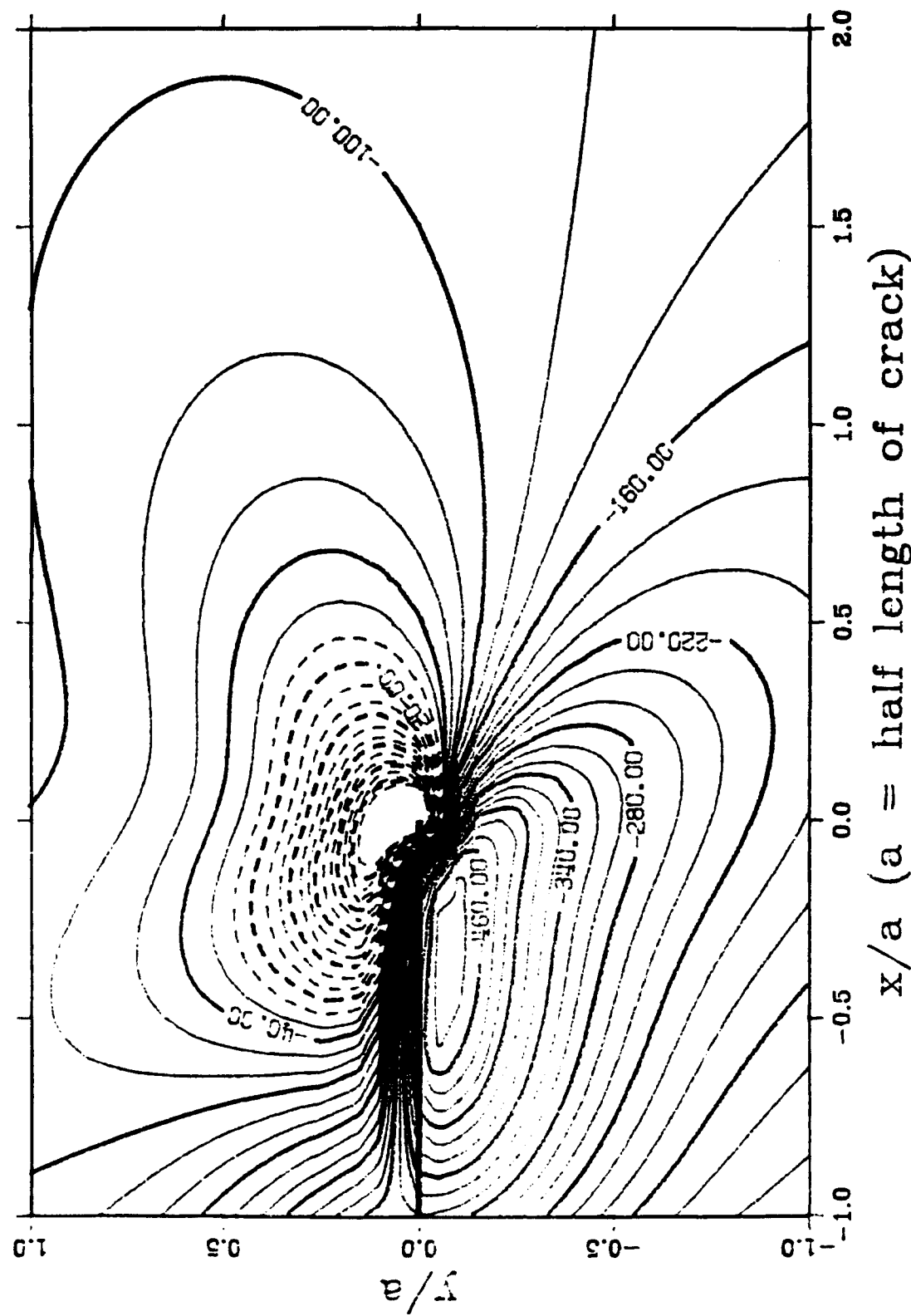


Figure 5.9g Lines of Equal Maximum Principal Stress

3-D plot for the Maximum Principal Stress
--- EPK #51-04-05-91 (compression-torsion)

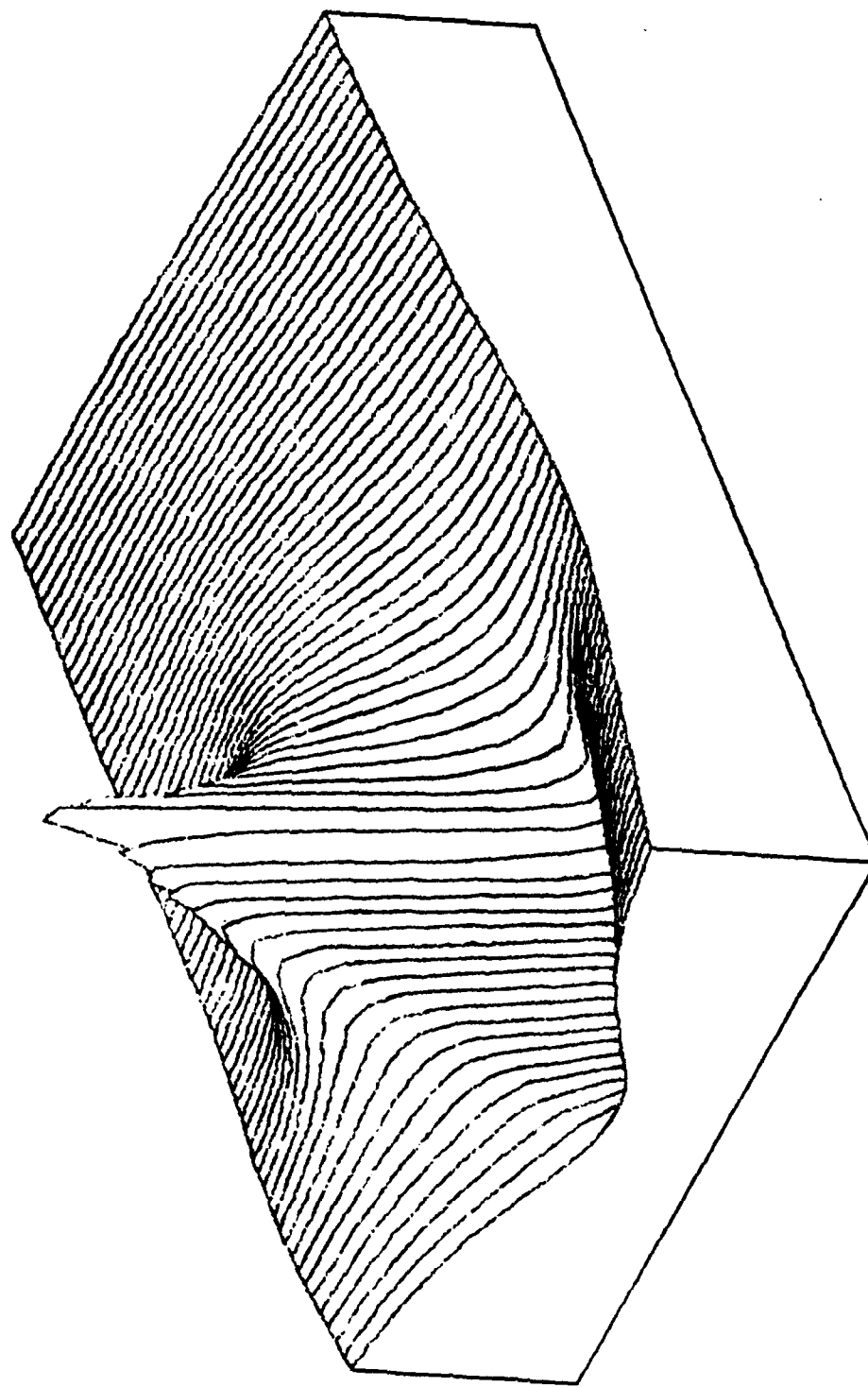


Figure 5.9h 3-D Plot of Maximum Principal Stress

Contour of the Minimum Principal Stress
--- EPK #51-04-05-91 (compression-torsion)

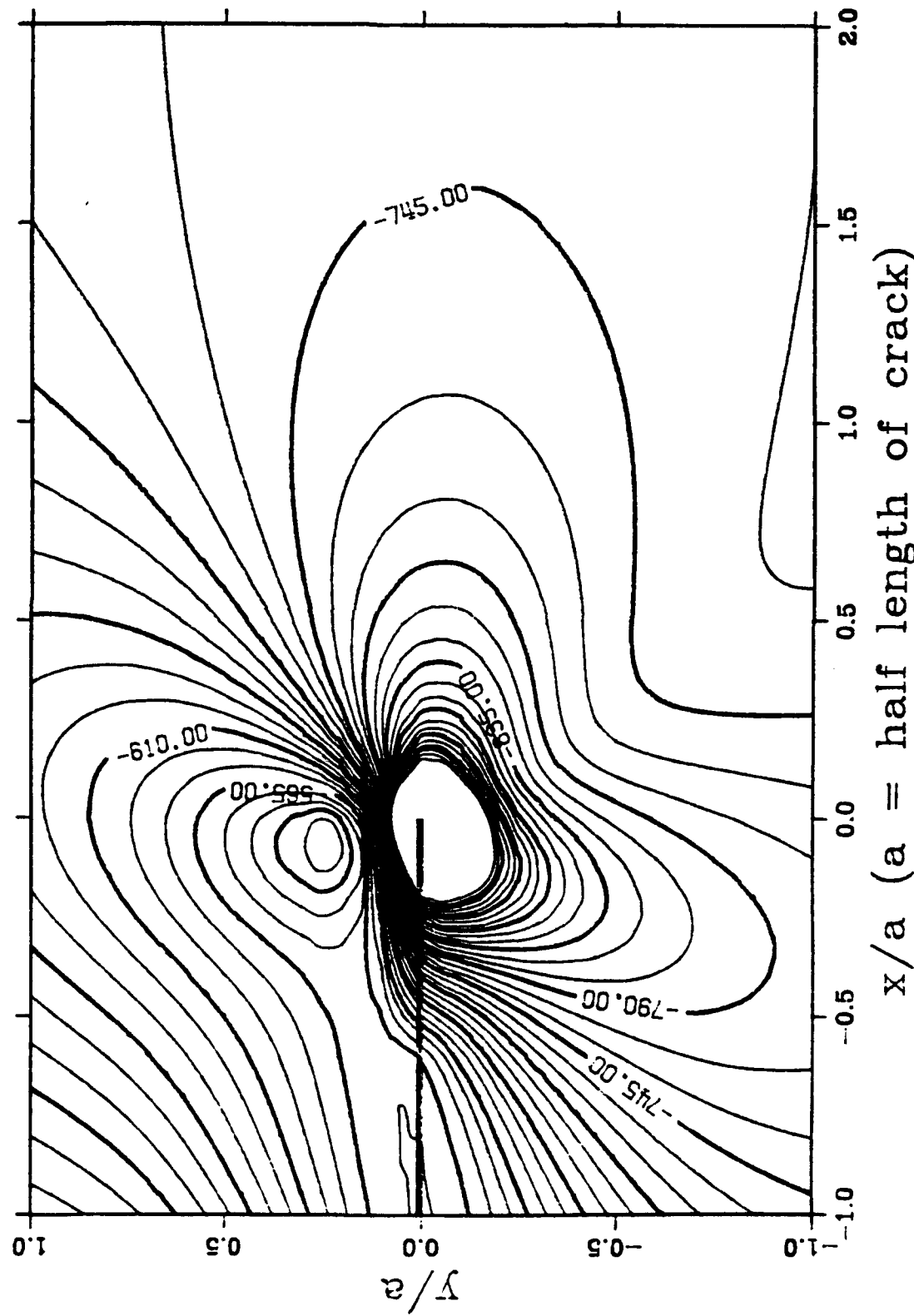


Figure 5.9i Lines of Equal Minimum Principal Stress

3-D plot for Minimum principal Stress
--- EPK #51-04-05-91 (compression-torsion)

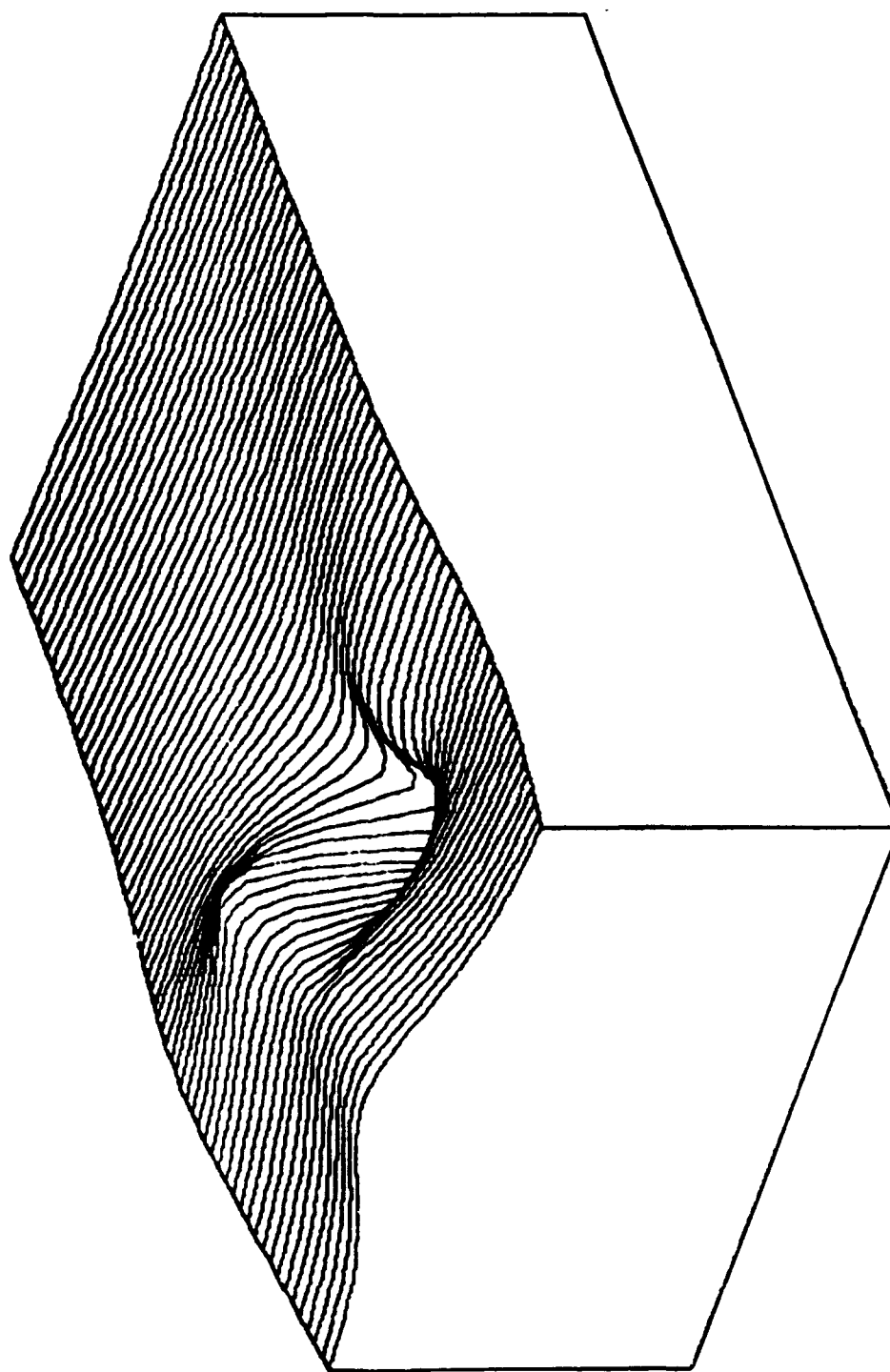


Figure 5.9j 3-D Plot of Minimum Principal Stress

Contour of the Maximum Shear Stress
--- EPK #51-04-05-91 (compression-torsion)

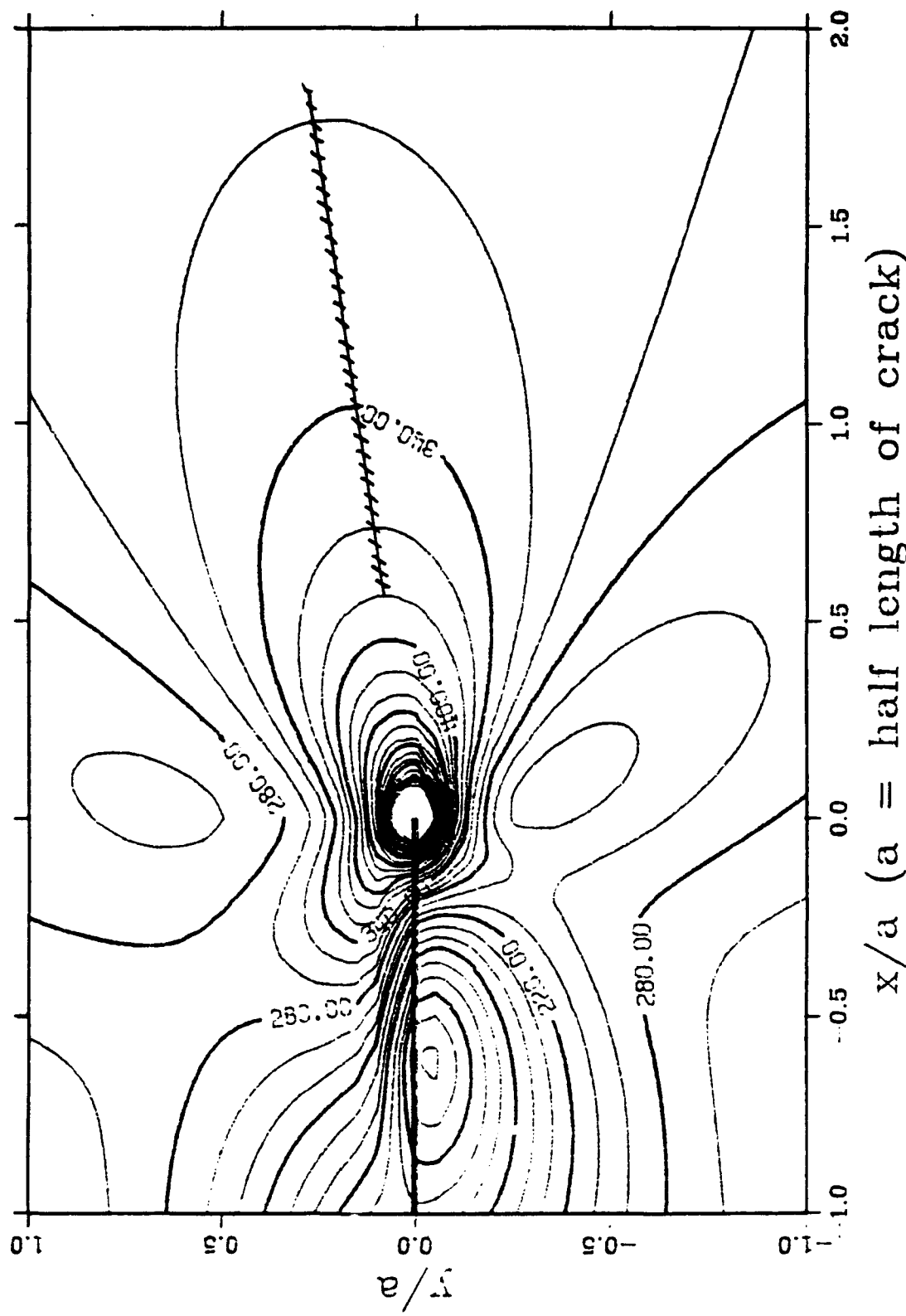


Figure 5.9k Lines of Equal Maximum Shear Stress

3-D plot for Maximum Shear Stress
--- EPK #51-04-05-91 (compression-torsion)

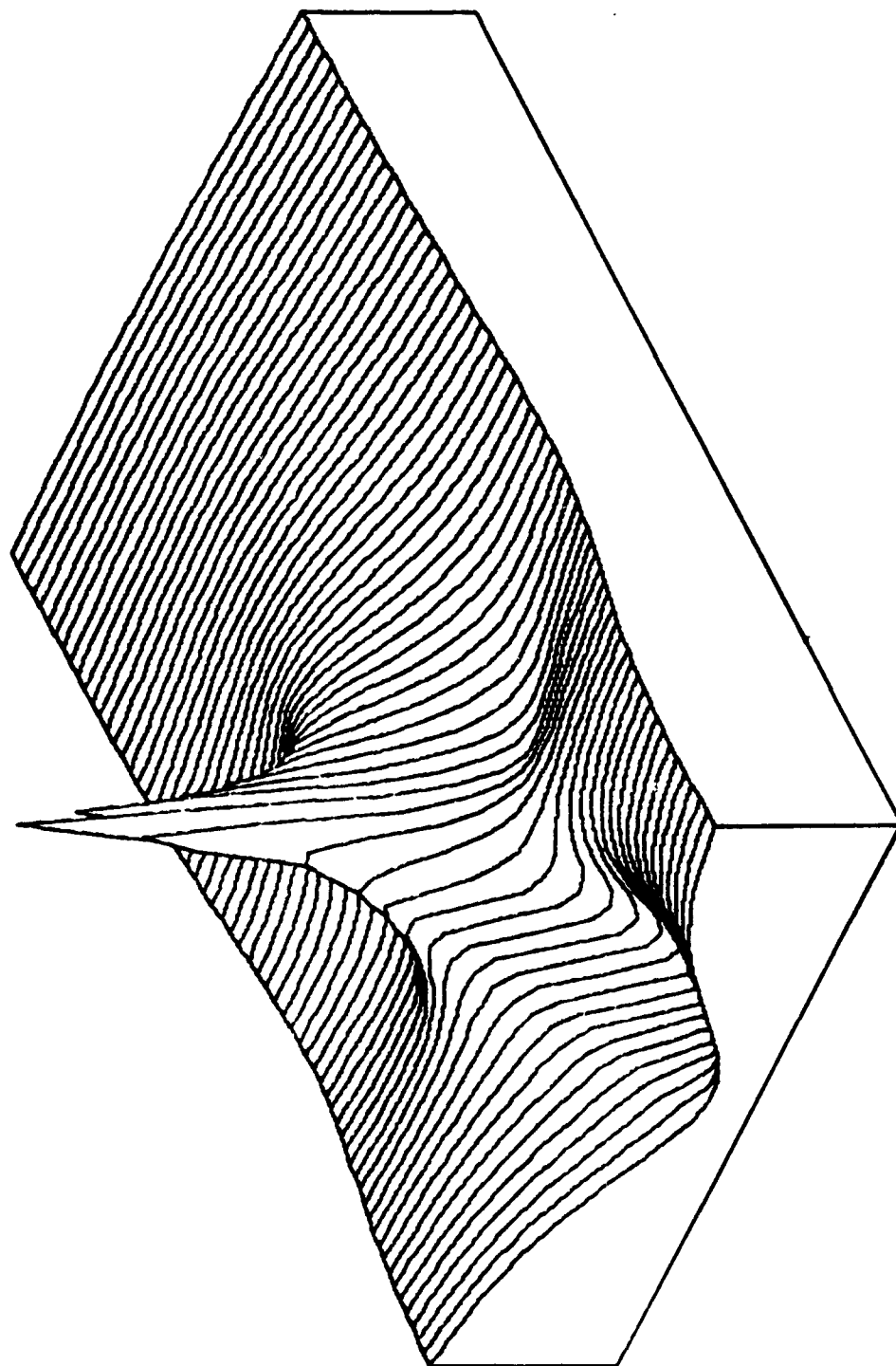


Figure 5.91 3-D Plot of Maximum Shear Stress

Contour of the Mean Stress
MPK #51-04-05-91 (compression-torsion)

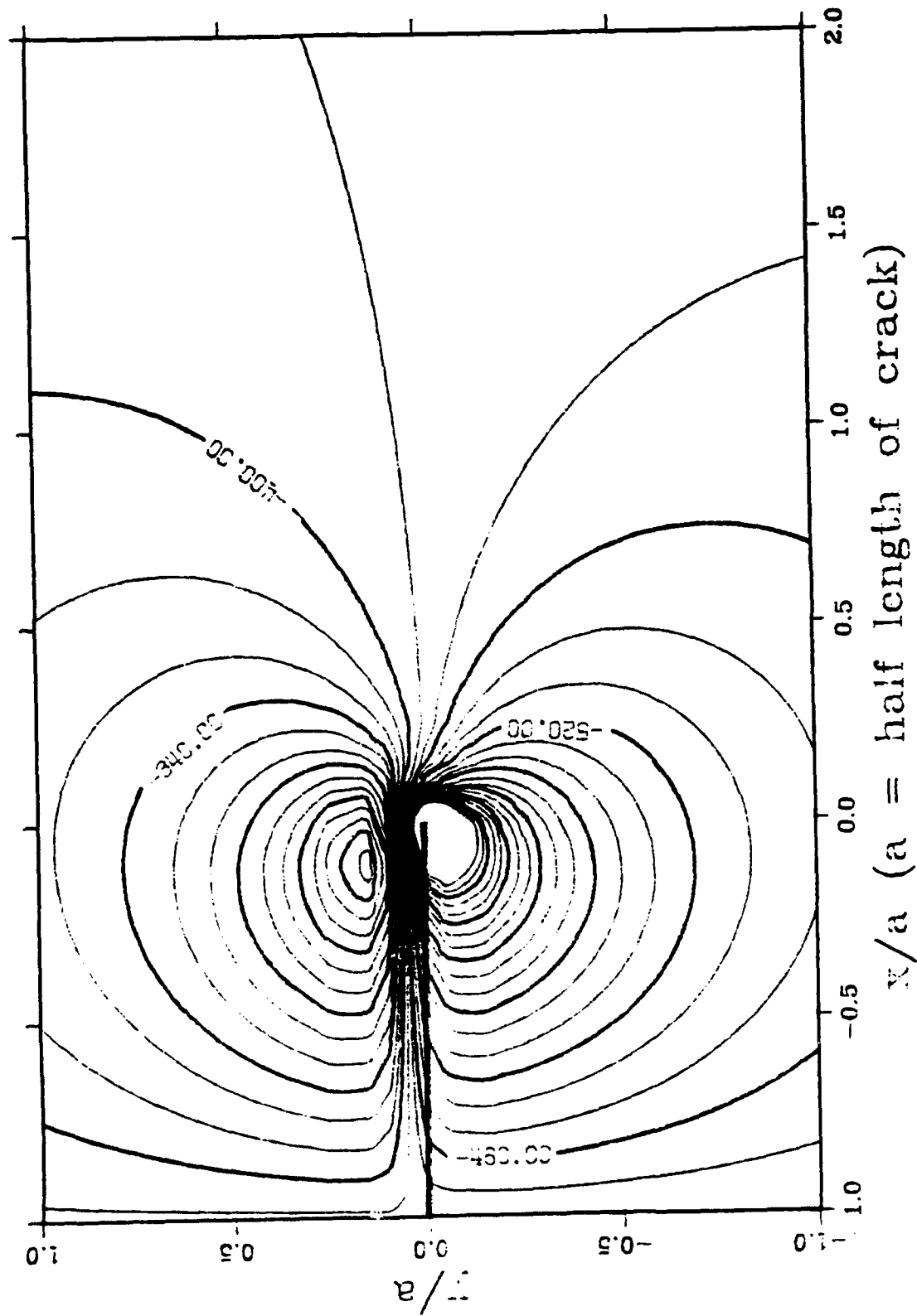


Figure 5.9m Lines of Equal Mean Stress

3-D plot for Mean Stress
--- EPK #51-04-05-91 (compression-torsion)

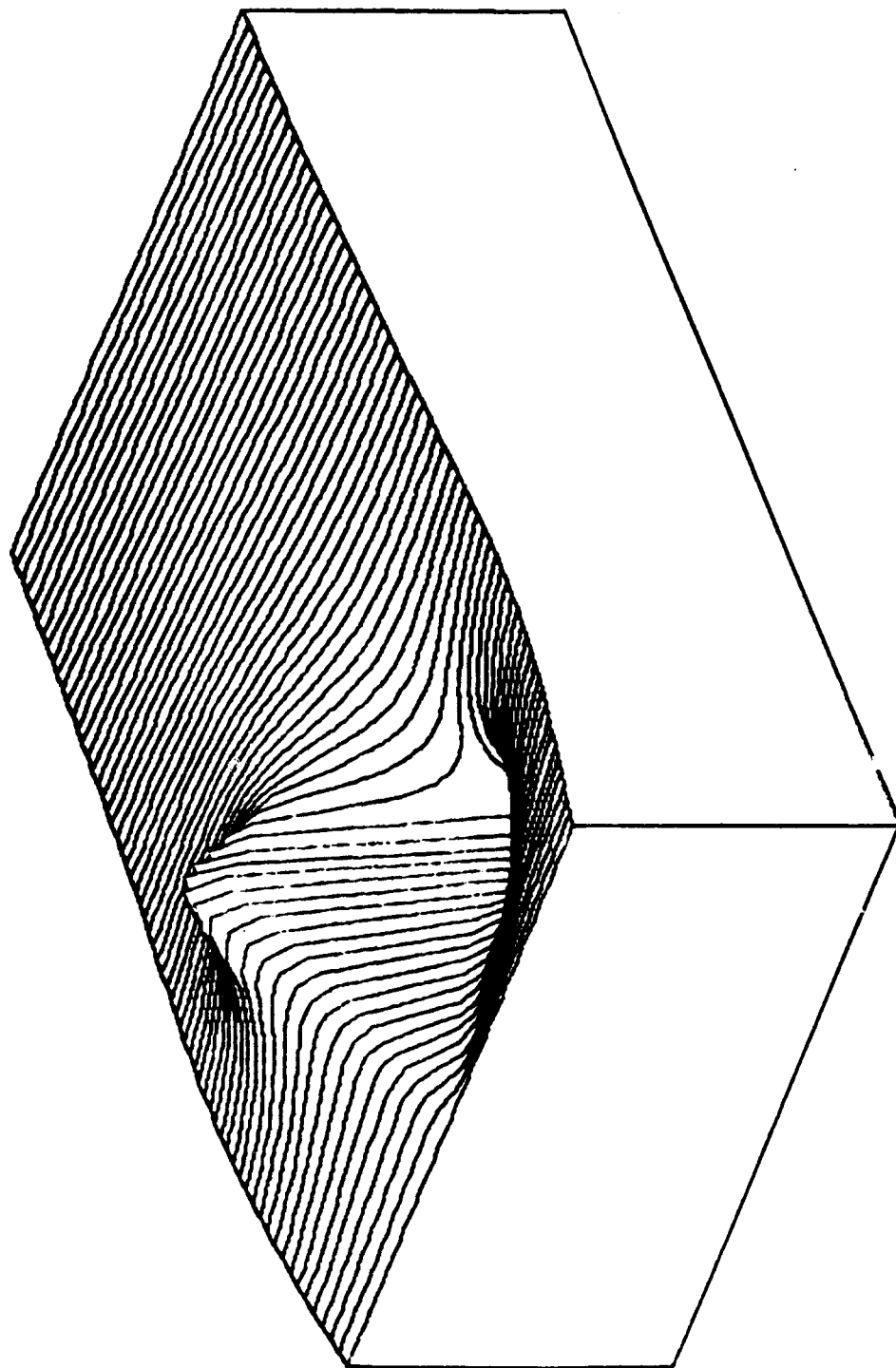


Figure 5.9n 3-D Plot of Mean Stress

Principal Stresses and Their Direction

(EPK #51-04-01-91; Compression-Torsion; Scale: 1 unit = 4500 kPa)

----- Tension —— Compression

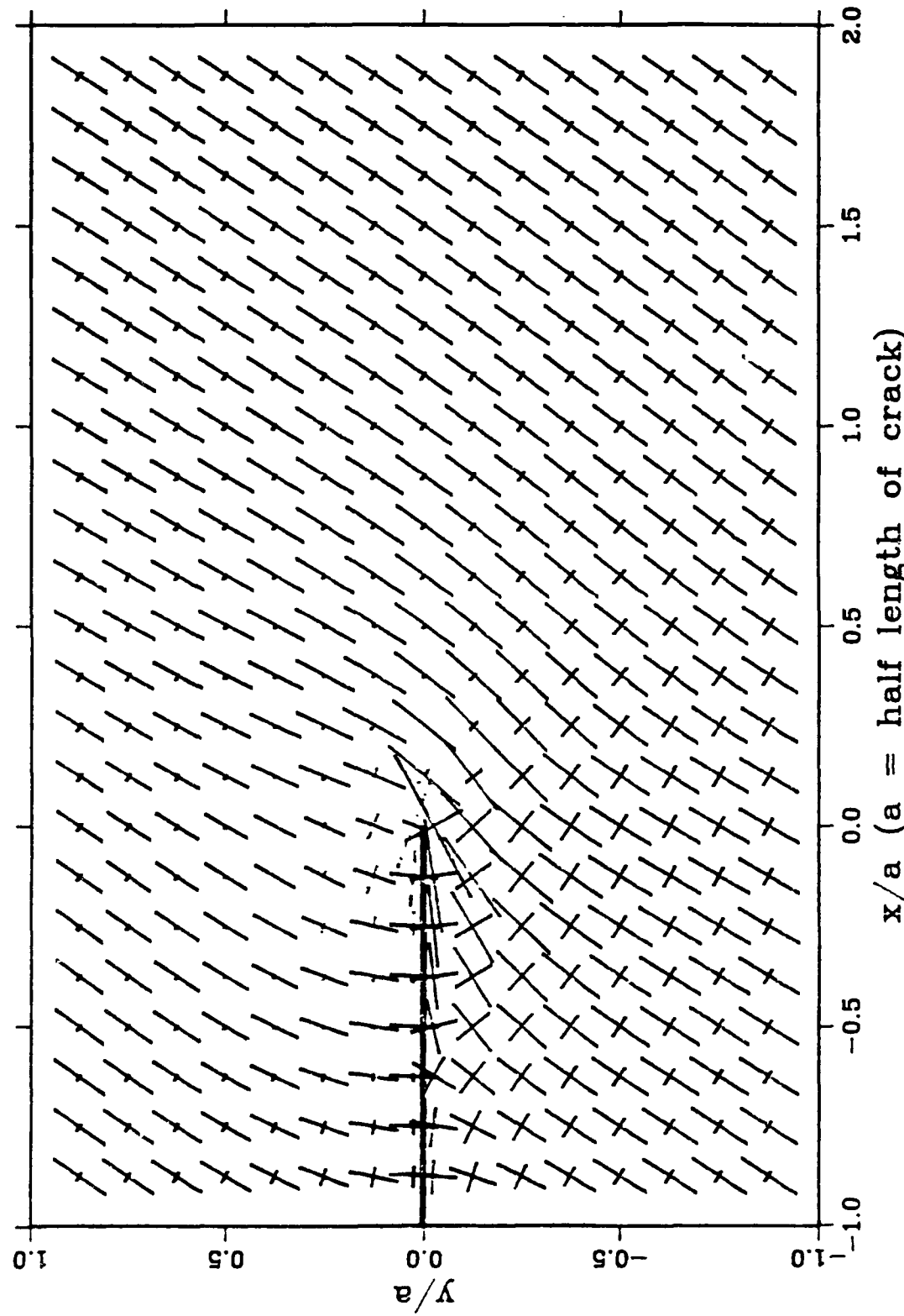


Figure 5.9o Principal Stresses and Their Directions

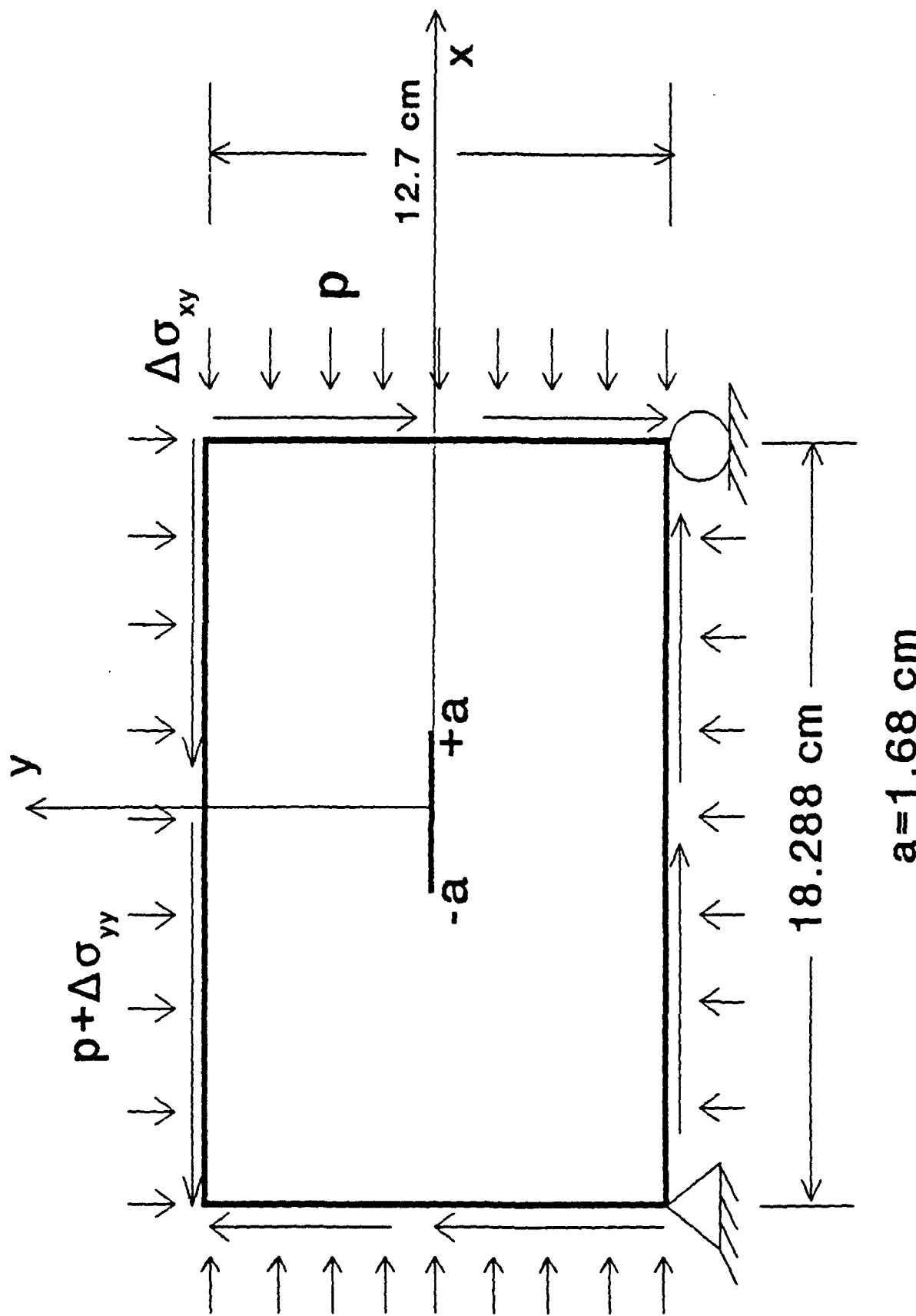
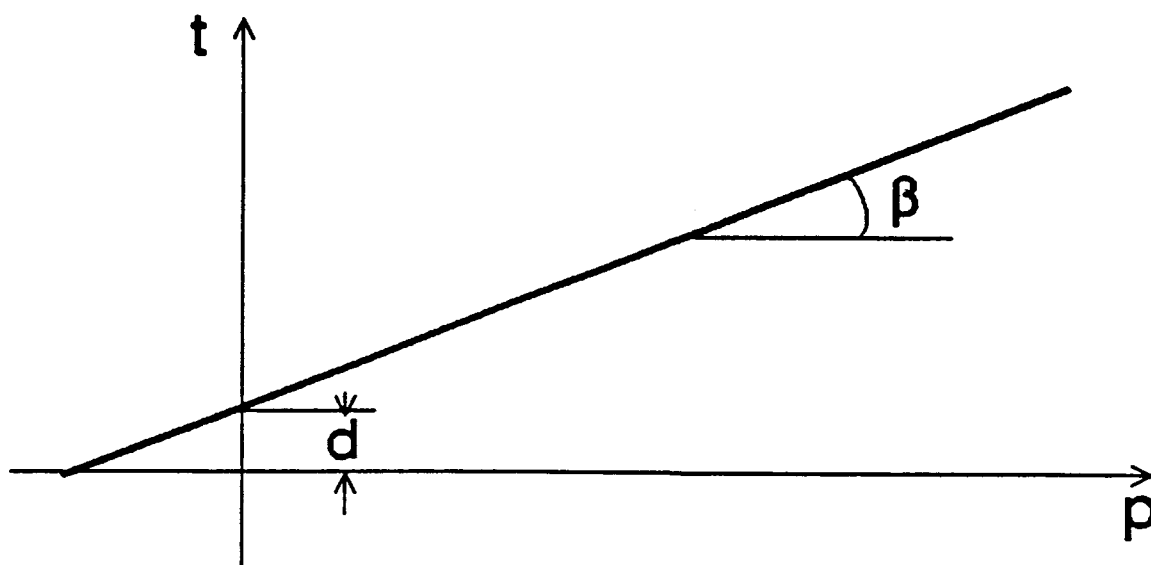


Figure 5.10 Boundary Conditions for F.E. Analysis



$$p = -\frac{1}{3} \operatorname{trace}(\sigma)$$

$$t = \frac{q}{2} \left[1 + \frac{1}{k} - \left(1 - \frac{1}{k} \right) \left(\frac{r}{q} \right)^3 \right]$$

$$r = \left(\frac{9}{2} S_{ij} S_{ji} S_{ii} \right)^{\frac{1}{3}}$$

$$q = \sqrt{\frac{3}{2} S_{ij} S_{ij}}$$

$$S_{ij} = \sigma_{ij} + p \delta_{ij}$$

Figure 5.11 Convention for the Drucker-Prager Criterion

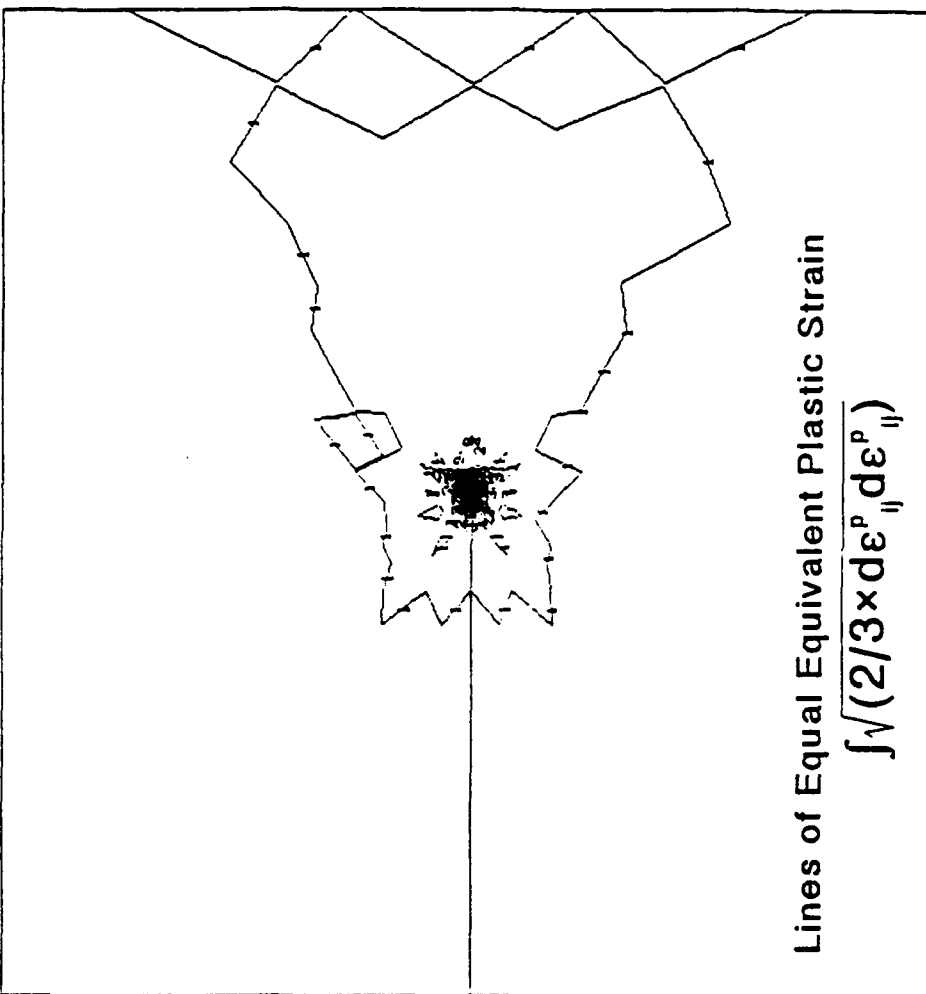


Figure 5.12 Lines of Equivalent Plastic Strain; Von Mises Model; Pure-Torsion

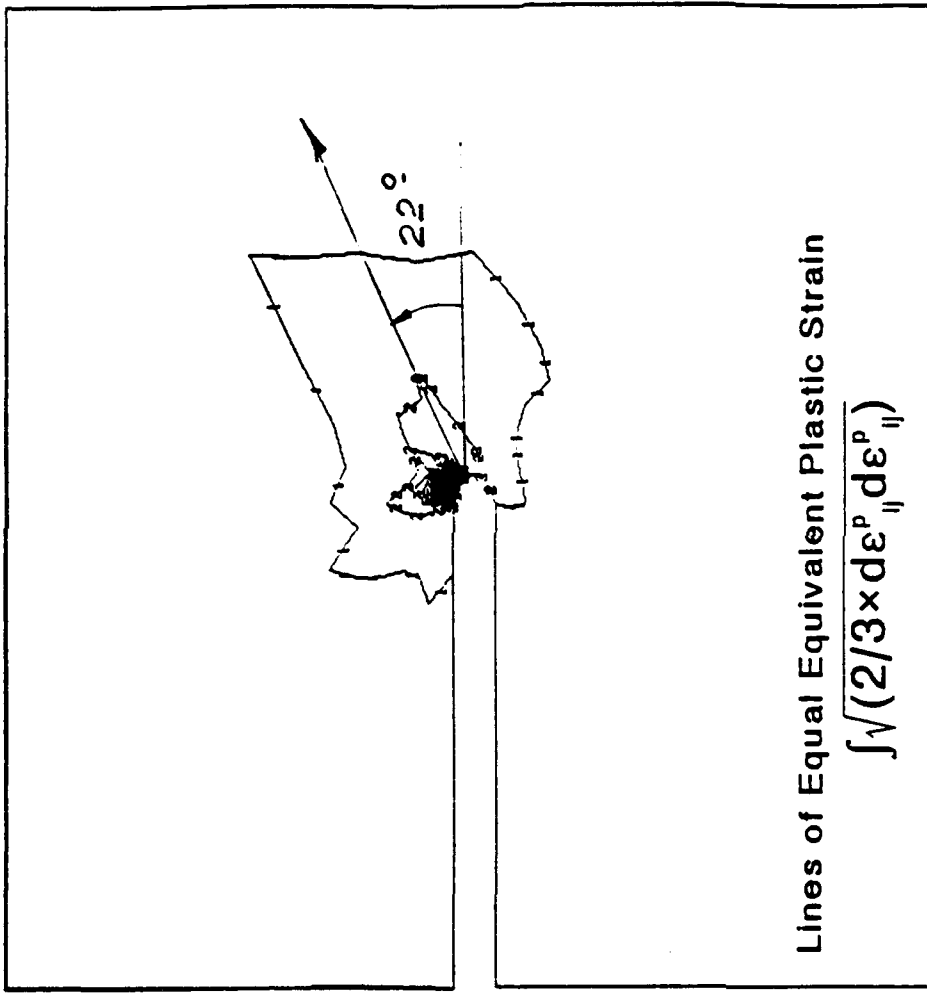


Figure 5.13 Lines of Equivalent Plastic Strain; Drucker-Prager Model; Pure-Torsion

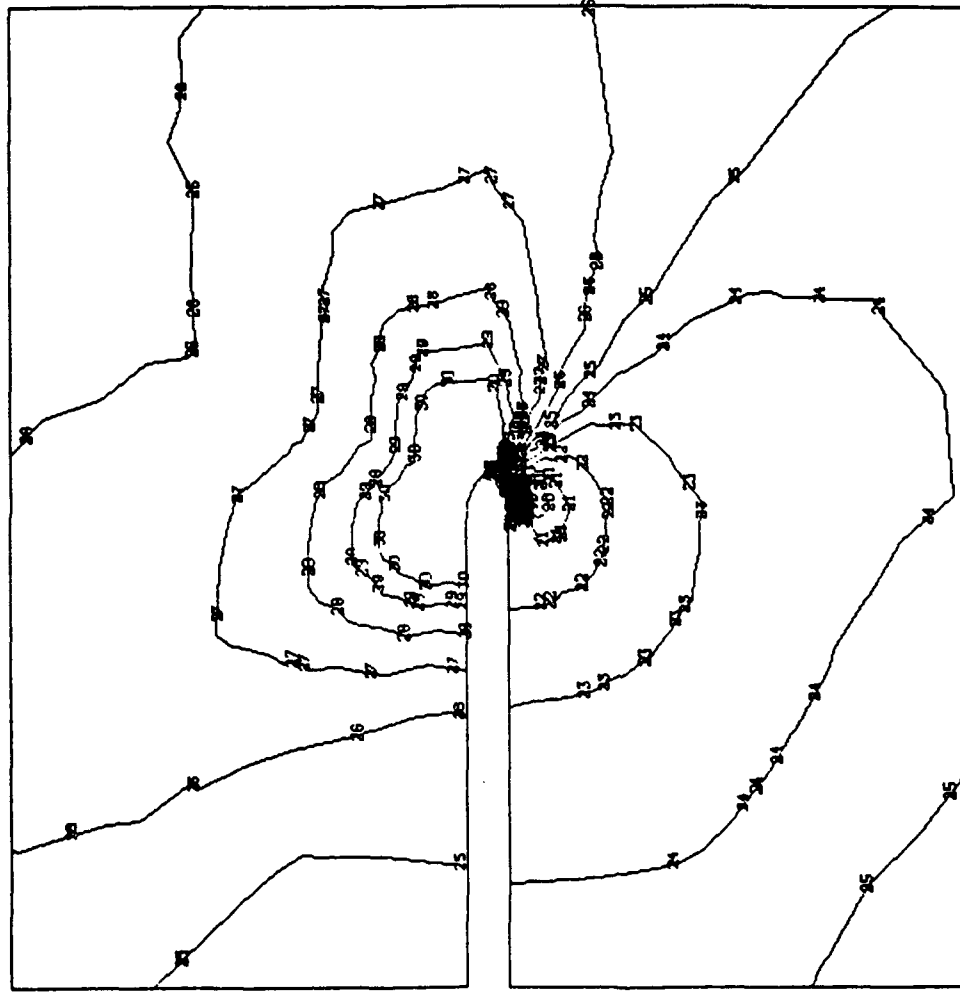
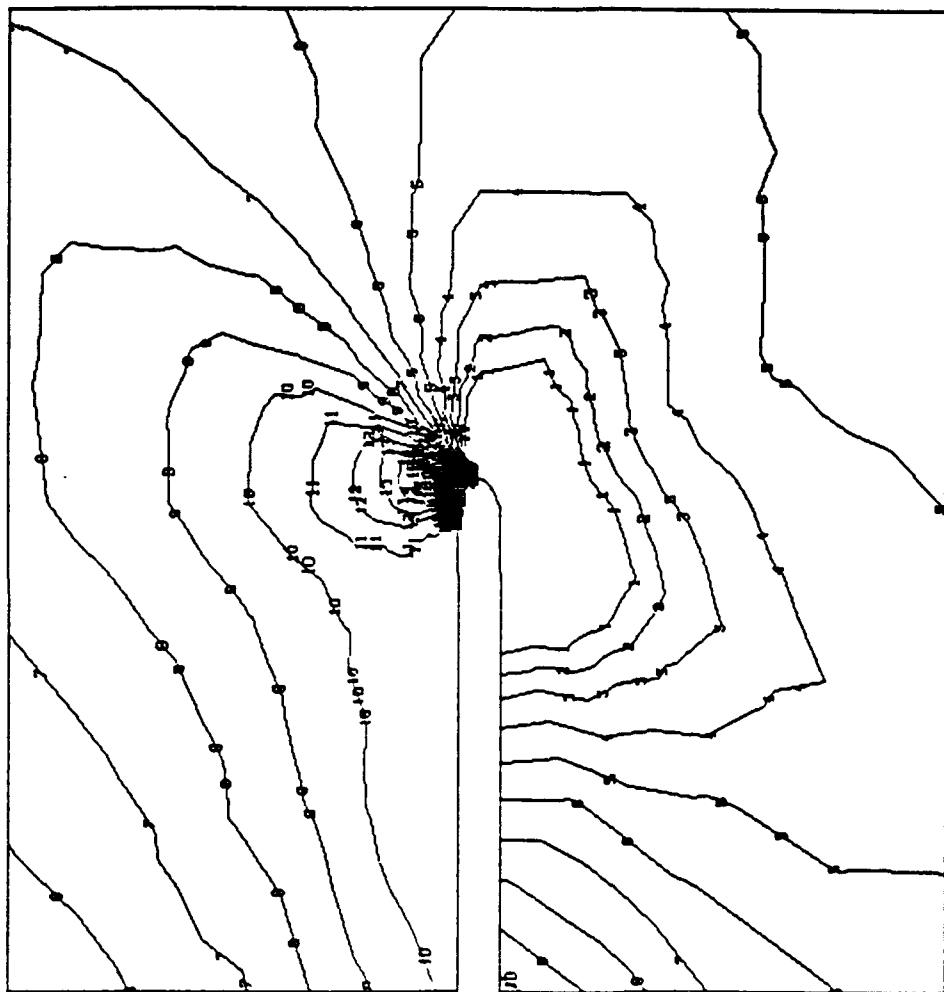


Figure 5.14a Lines of Equal Major Principal Stress; Elastic Solution; Pure-Torsion

Figure 5.14b Lines of Equal Minor Principal Stress; Elastic Solution; Pure-Torsion



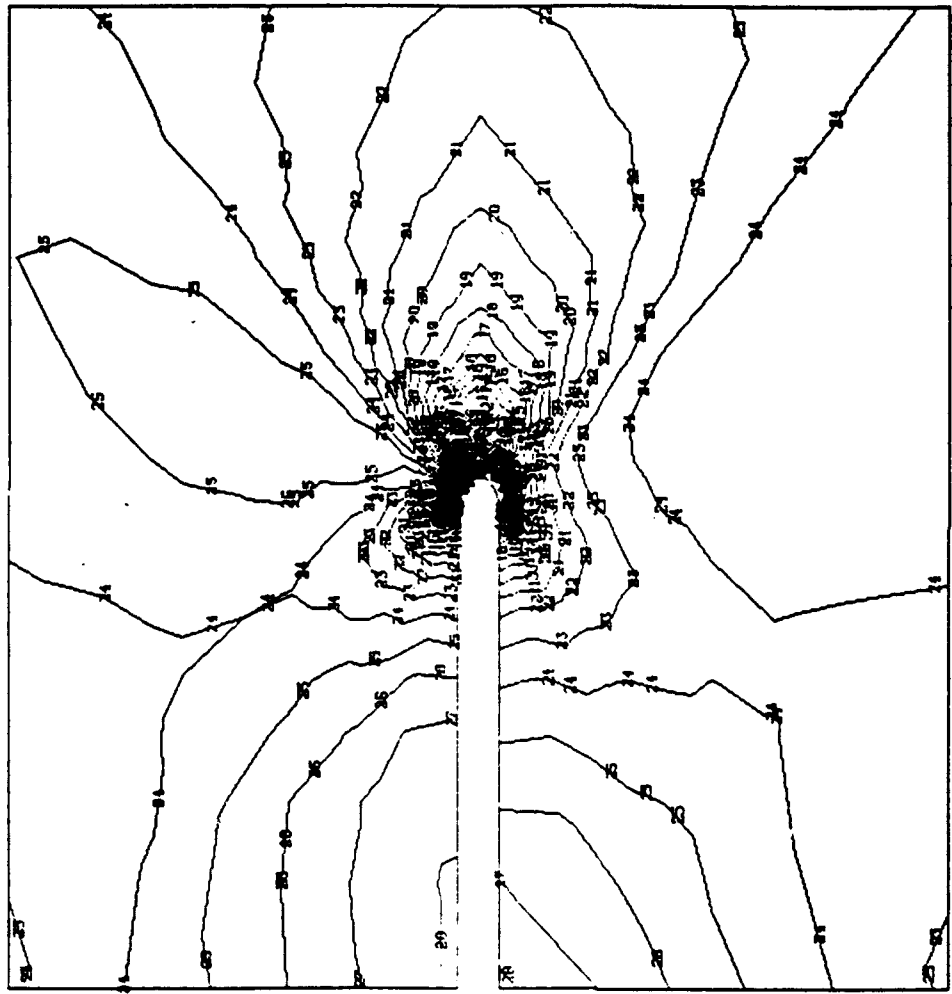


Figure 5.14c Lines of Equal Principal Stress Difference; Elastic Solution; Pure-Torsion

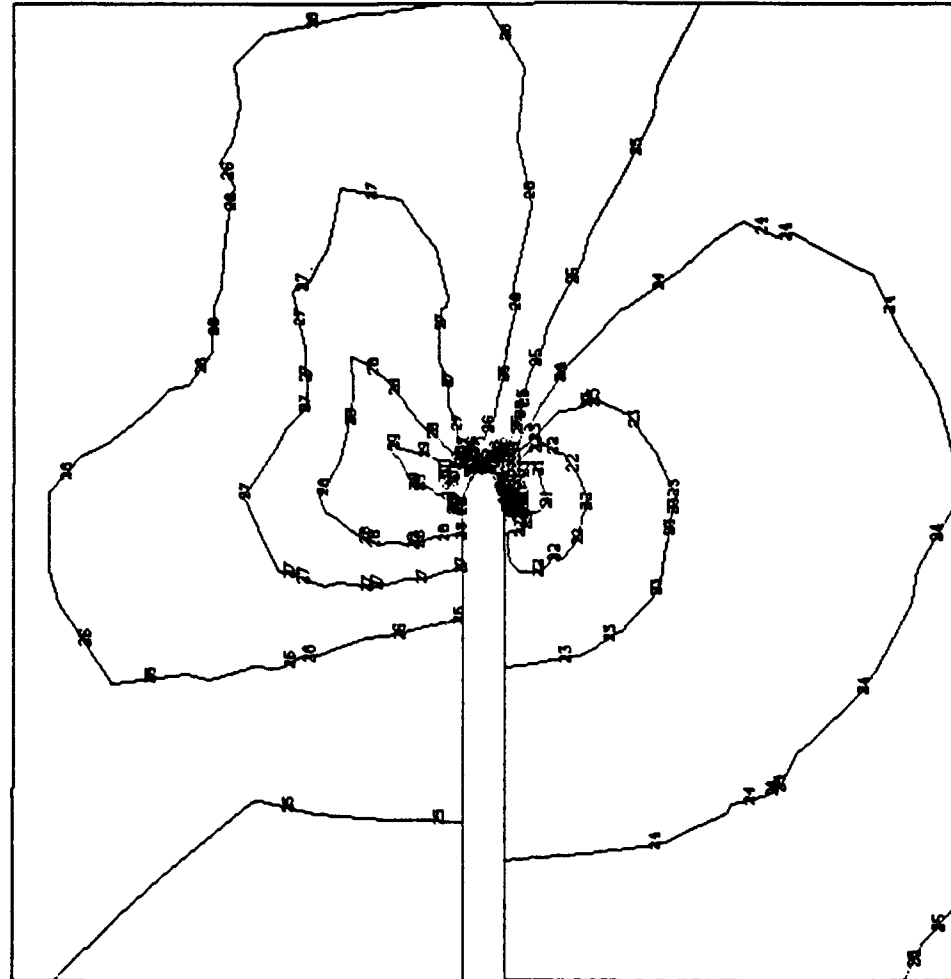


Figure 5.15a Lines of Equal Major Principal Stress; Elasto-Plastic Solution;
Pure-Torsion

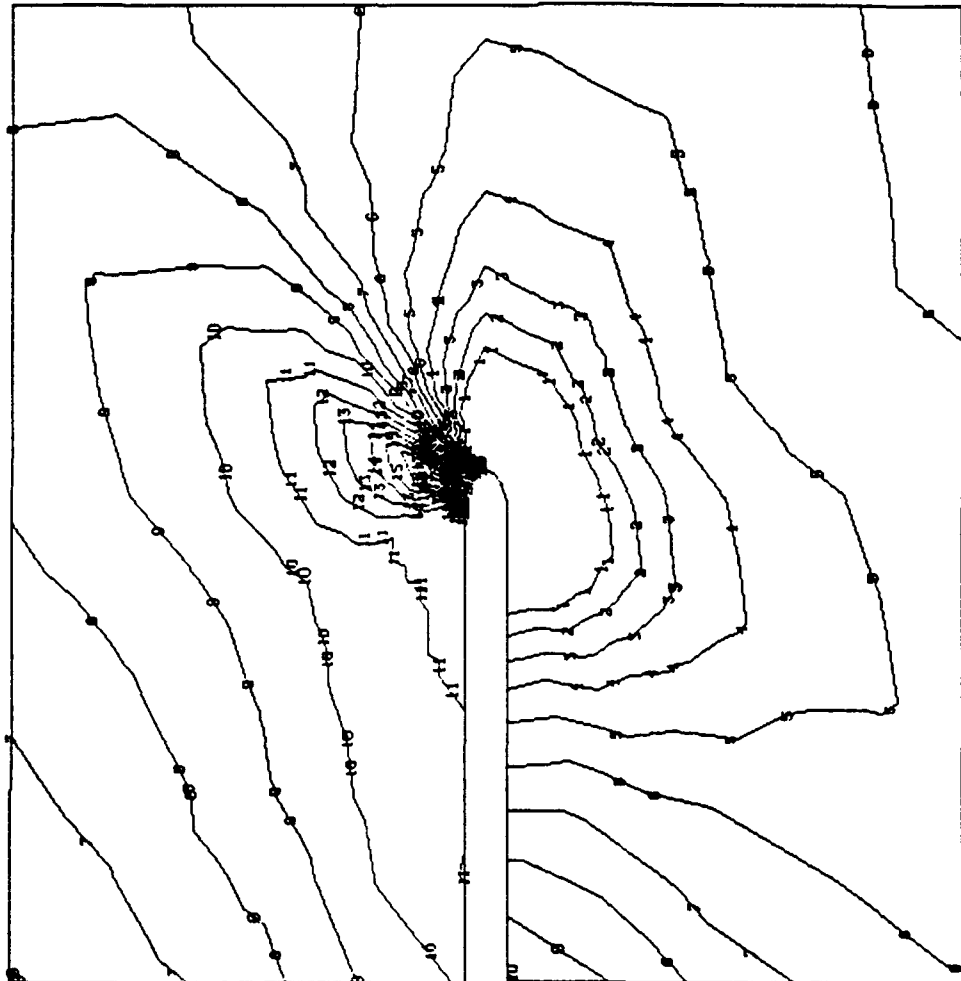
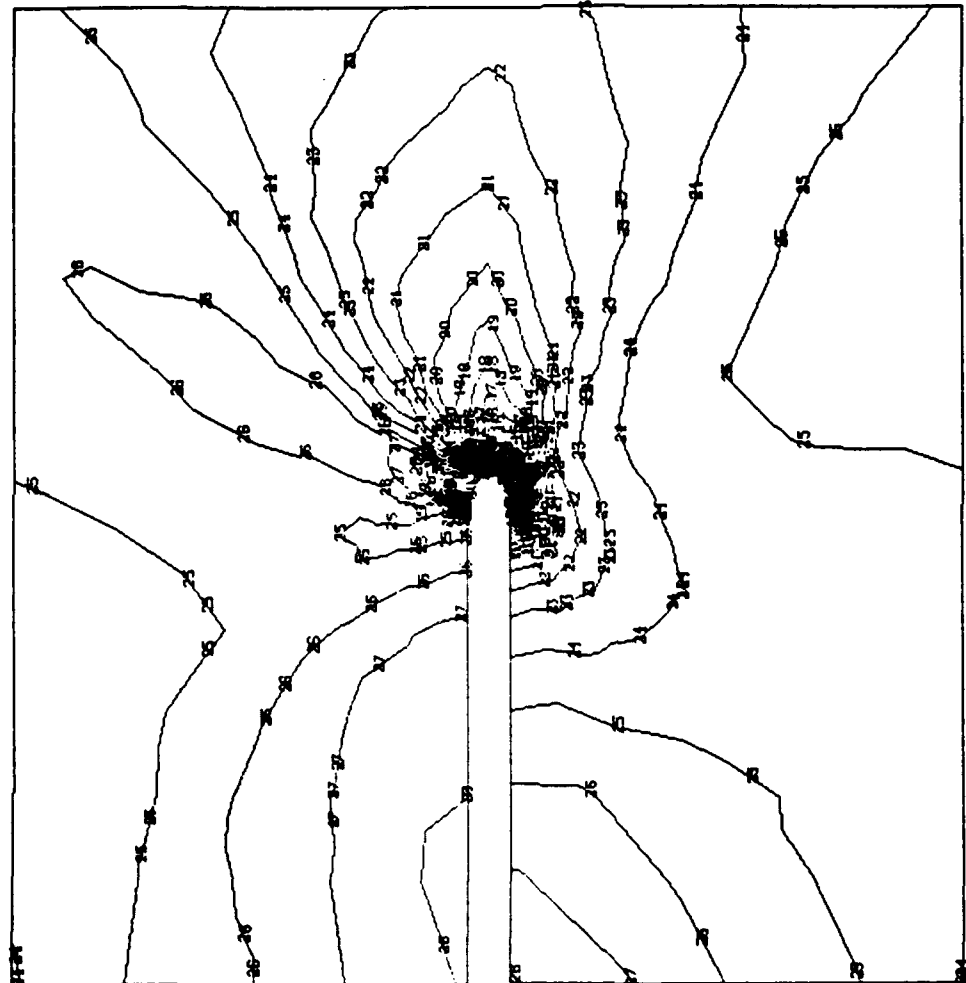


Figure 5.15b Lines of Equal Minor Principal Stress; Elasto-Plastic Solution;
Pure-Torsion

Figure 5.15c Lines of Equal Principal Stress Difference; Elasto-Plastic Solution; Pure-Torsion



Stress Distribution along OA

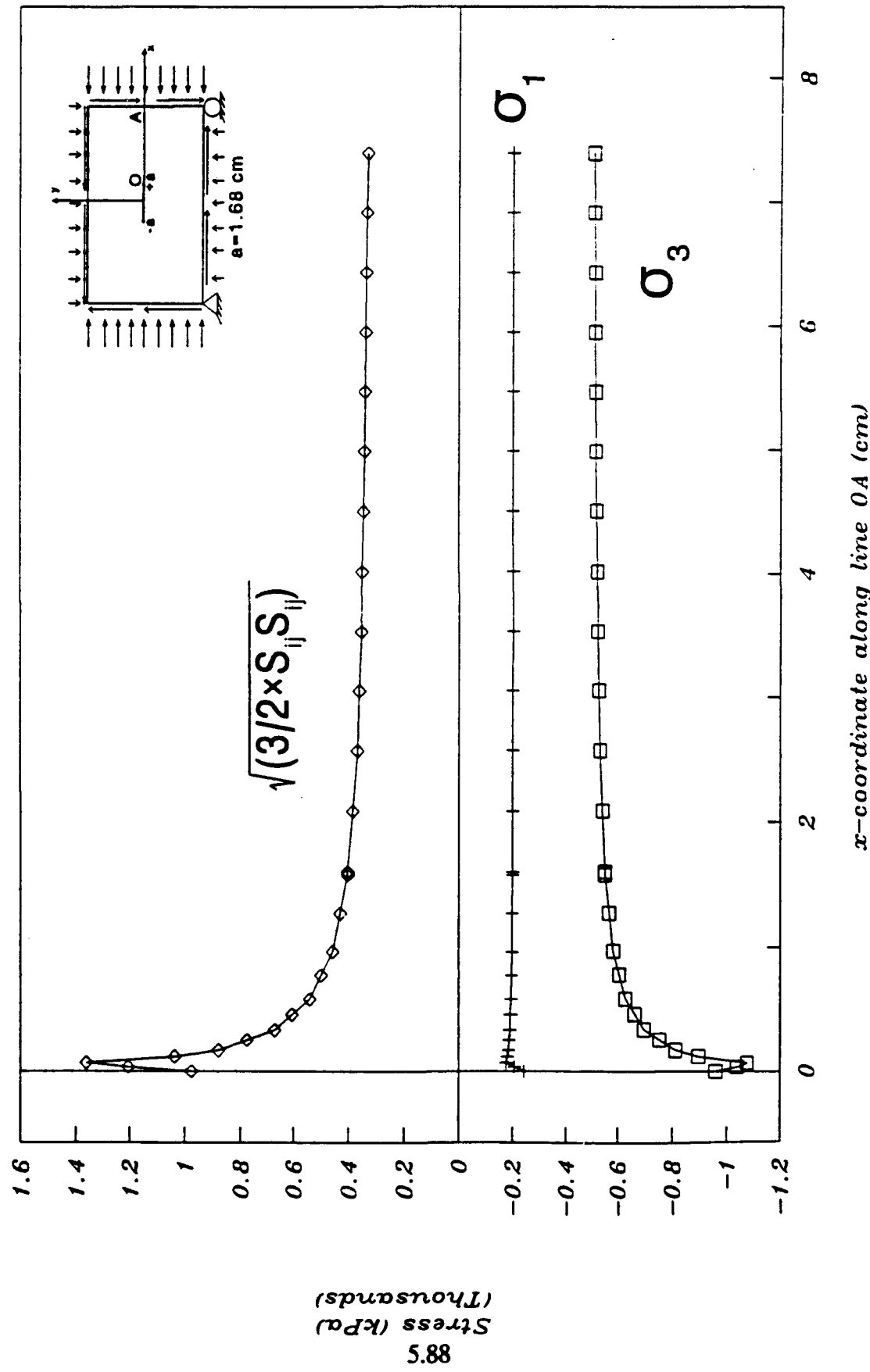


Figure 5.16a Elastic Stress Distribution along OA

Stress Distribution Along OA

(Elasto-plastic Analysis)

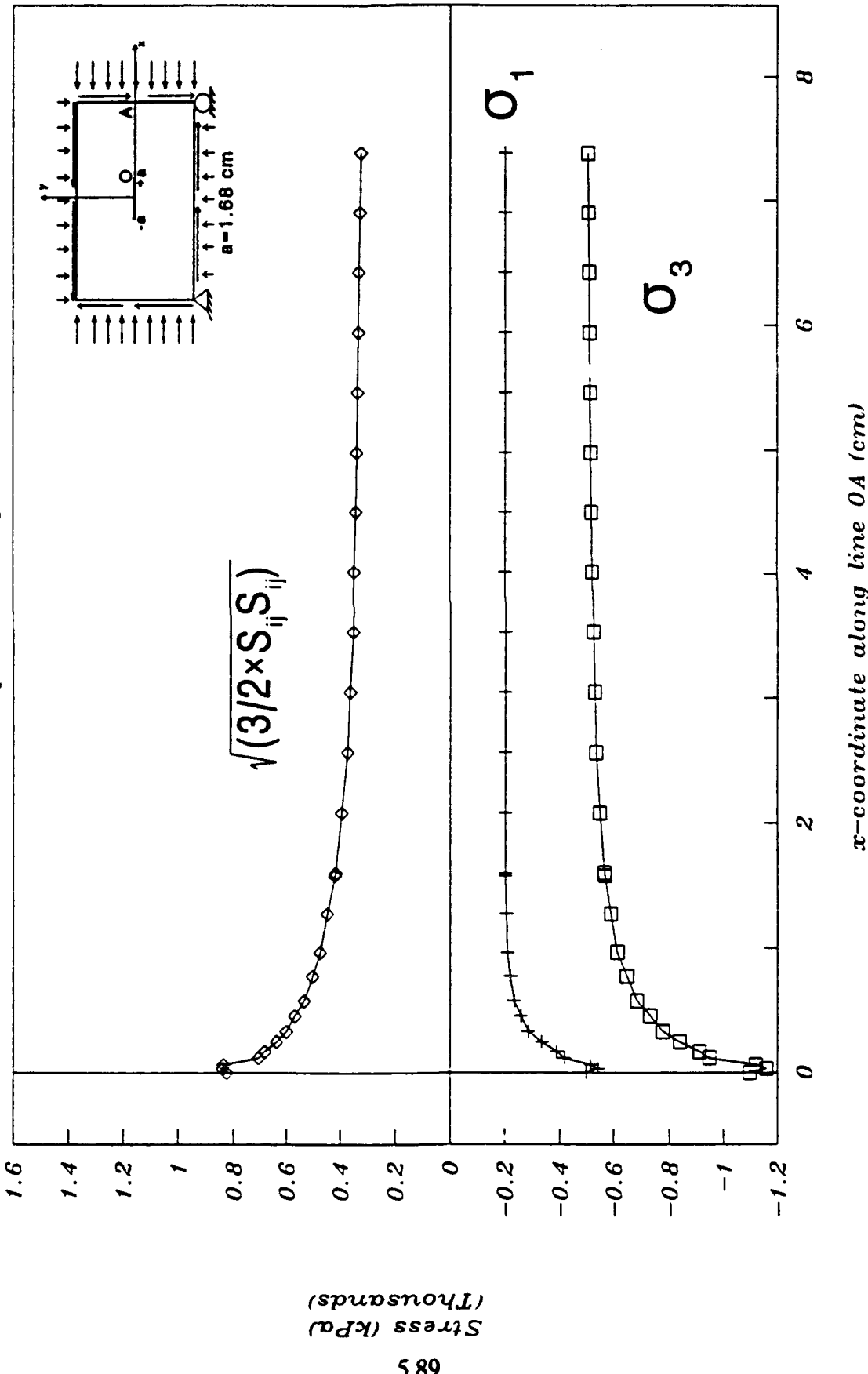


Figure 5.16b Elasto-Plastic Stress Distribution along OA

Stress Distribution along OB

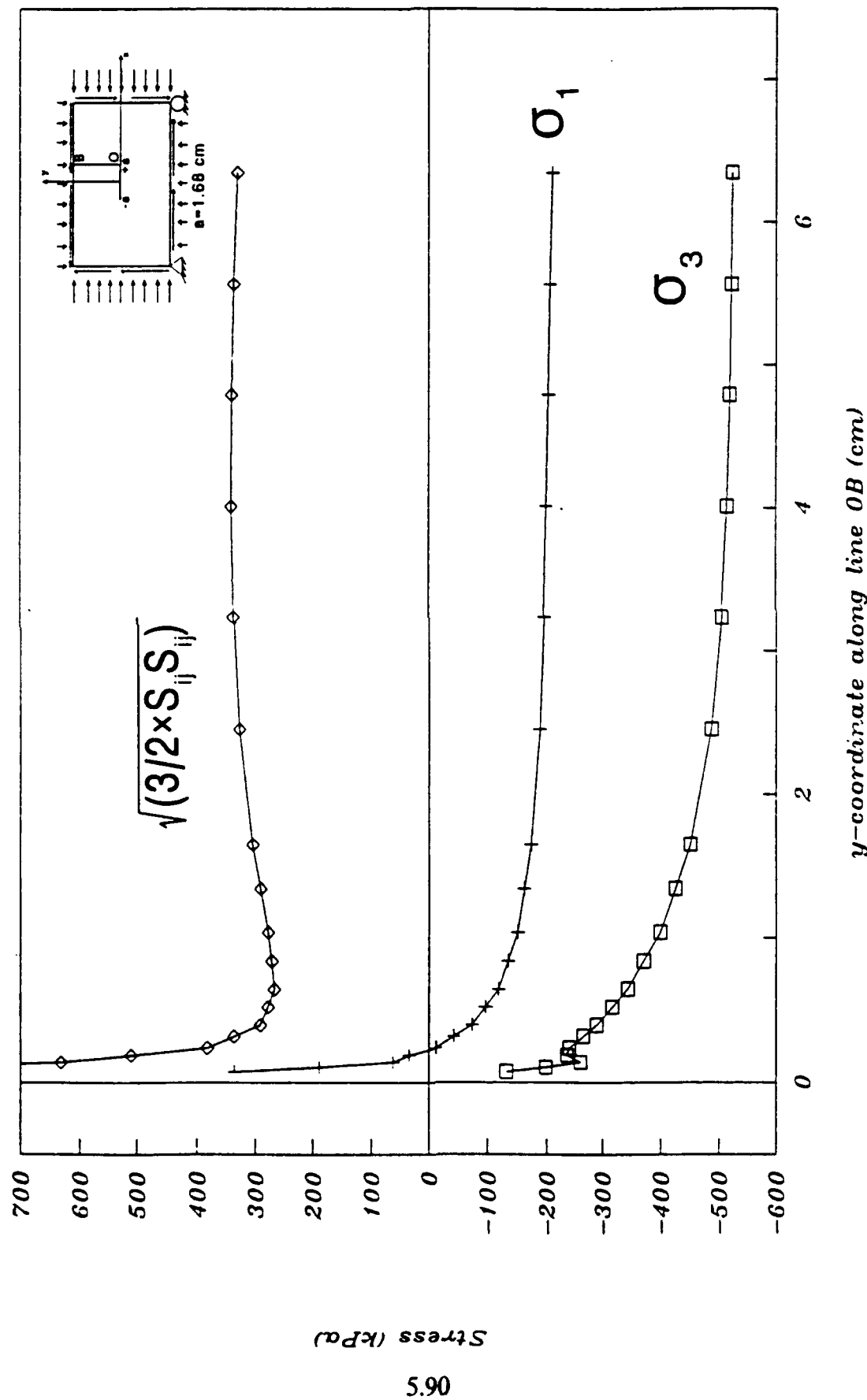


Figure 5.17a Elastic Stress Distribution along OB

Stress Distribution along OB (Elasto-plastic Analysis)

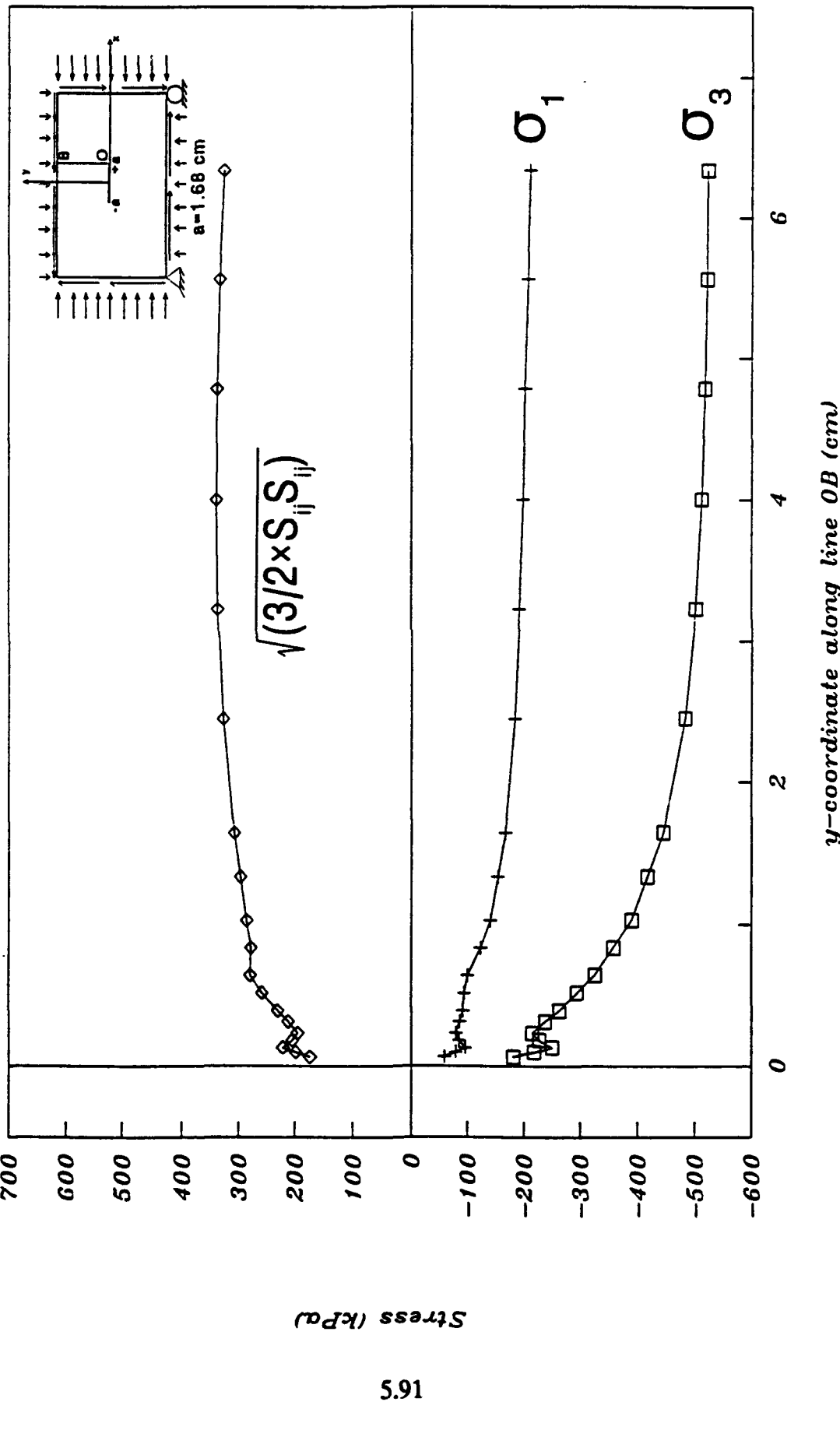


Figure 5.17b Elasto-Plastic Stress Distribution along OB

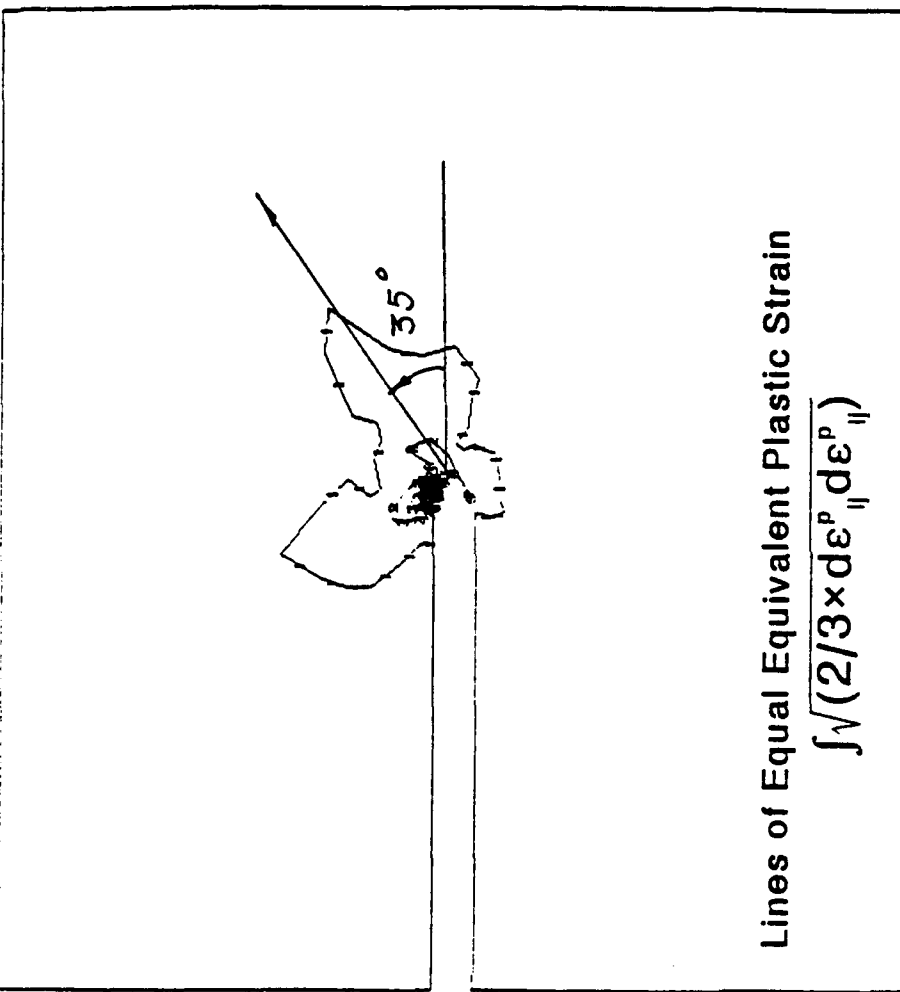


Figure 5.18a Spread of the Plastic Zone for a Compression-Torsion Test

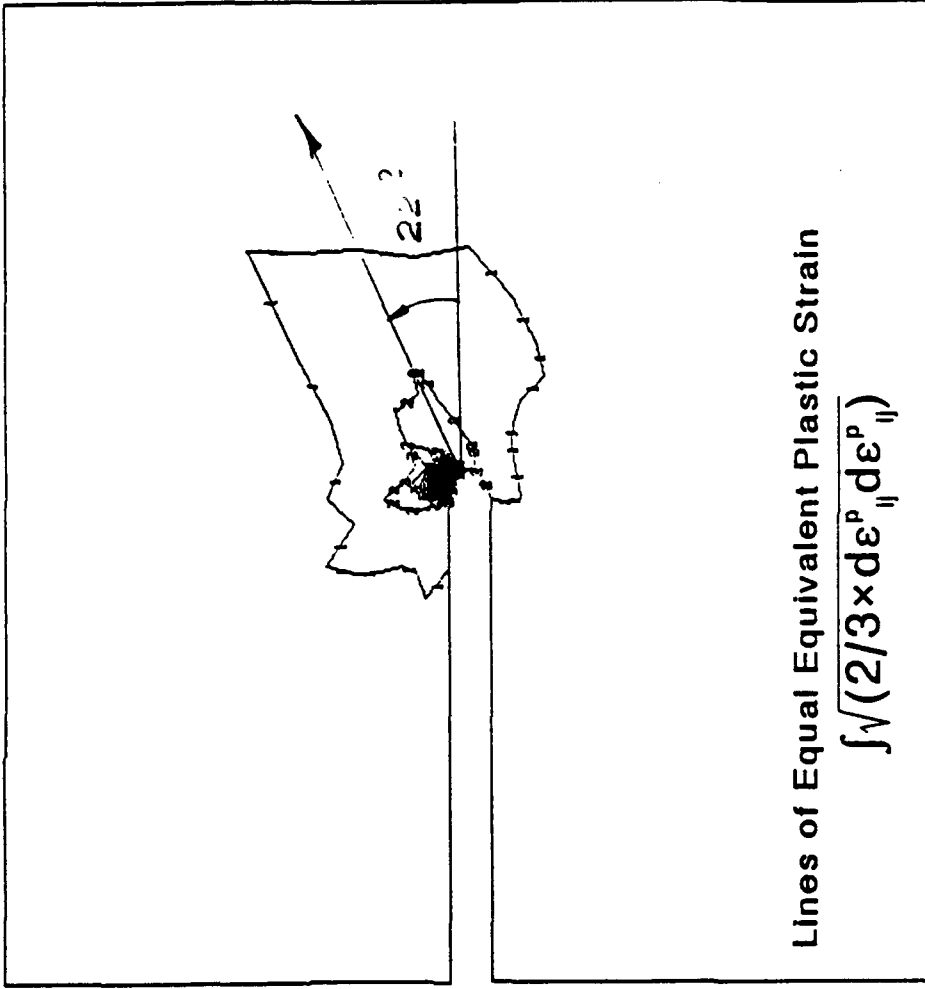


Figure 5.18b Spread of the Plastic Zone for a Pure-Torsion Test

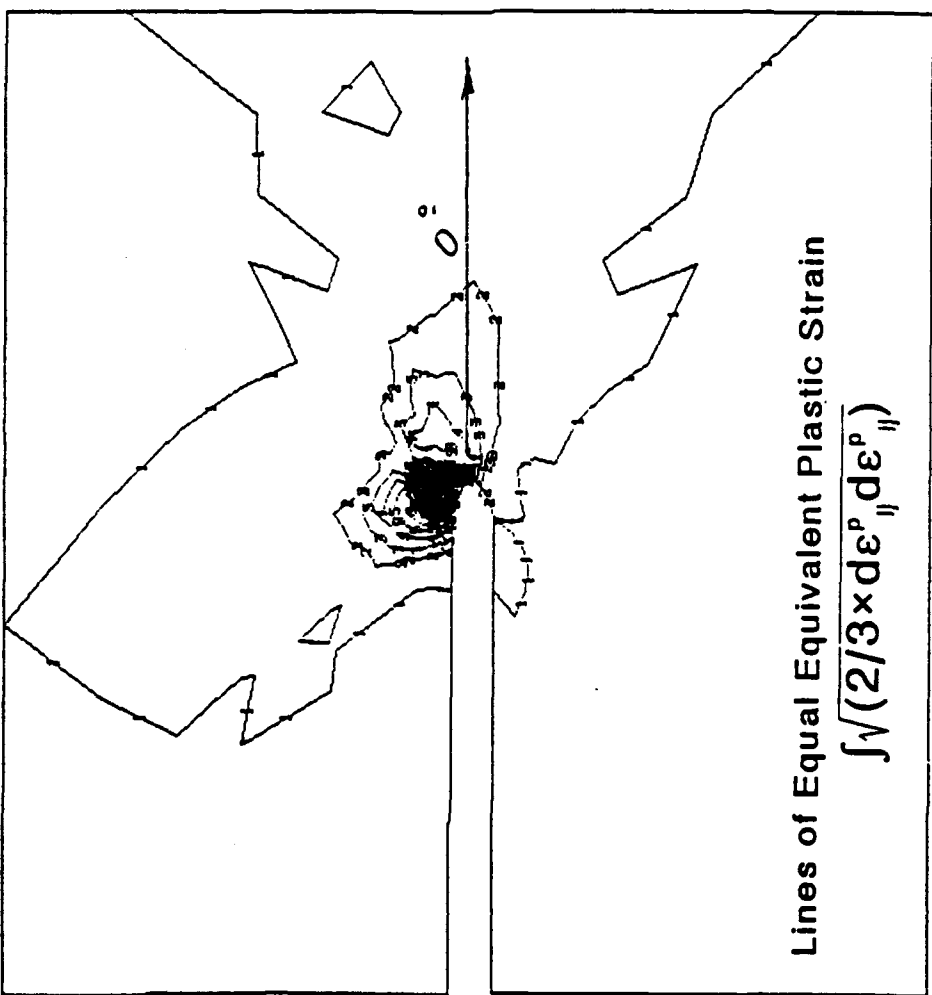


Figure 5.18c Spread of the Plastic Zone for a Tension-Torsion Test

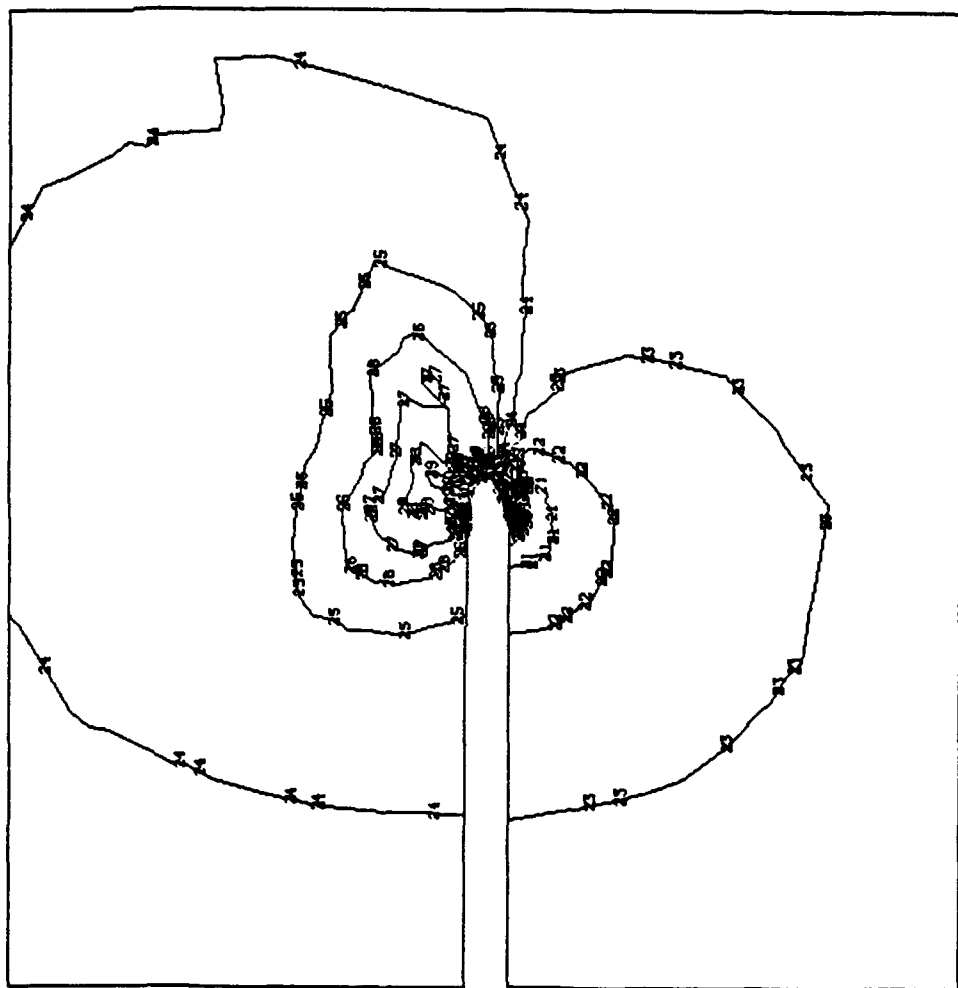


Figure 5.19a Lines of Equal Major Principal Stress; DP Model;
Compression-Torsion Test

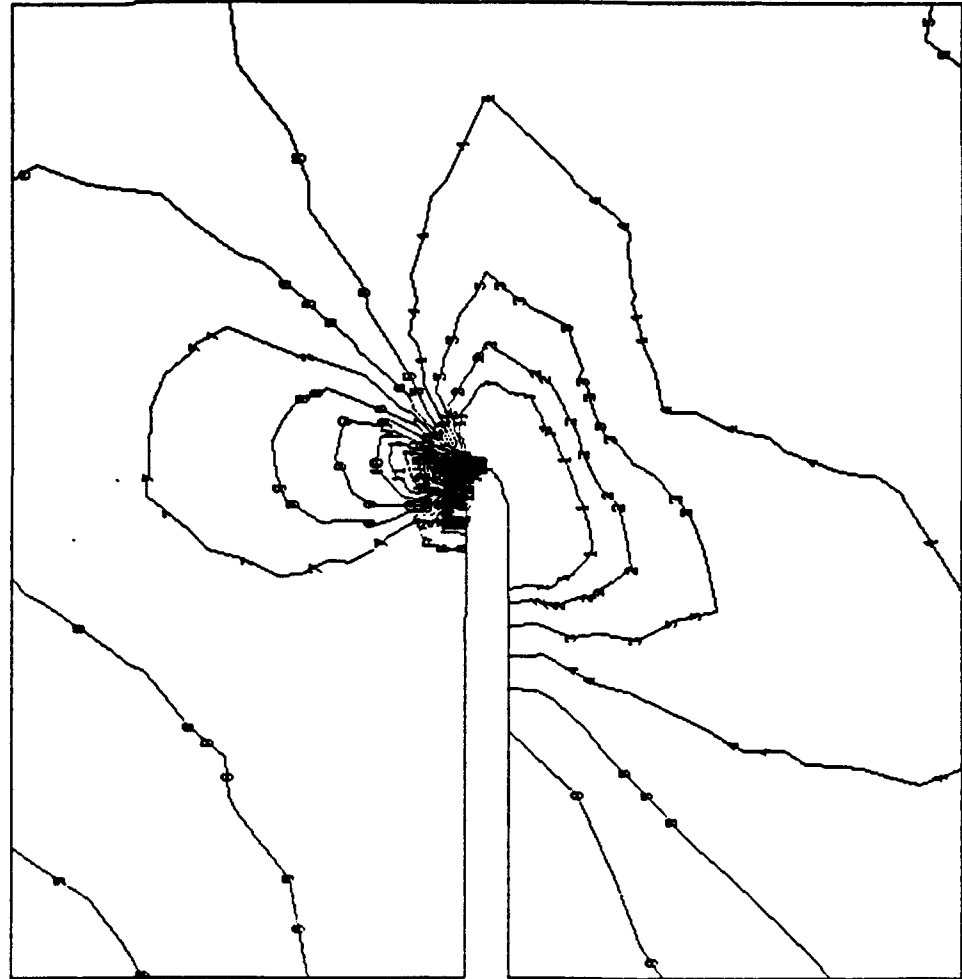


Figure 5.19b Lines of Equal Minor Principal Stress; DP Model;
Compression-Torsion Test

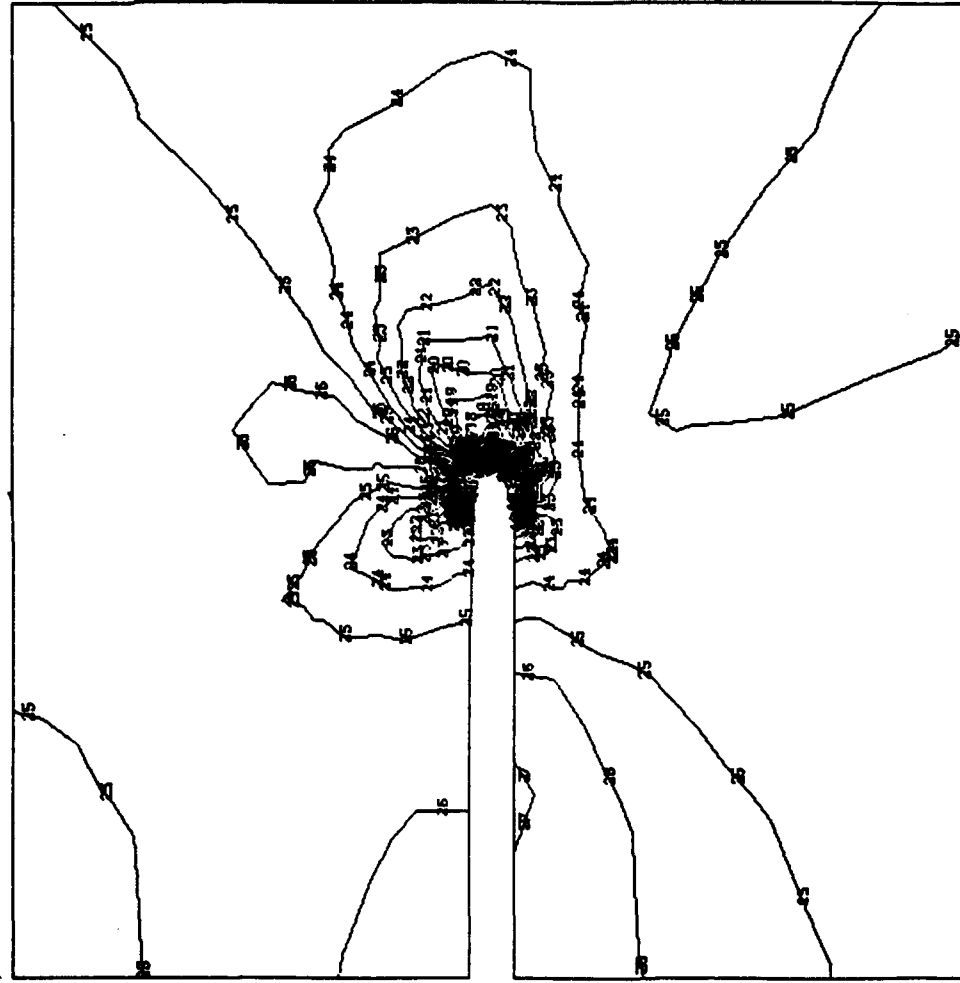


Figure 5.19c Lines of Equal Principal Stress Difference; DP Model; Compression-Torsion Test

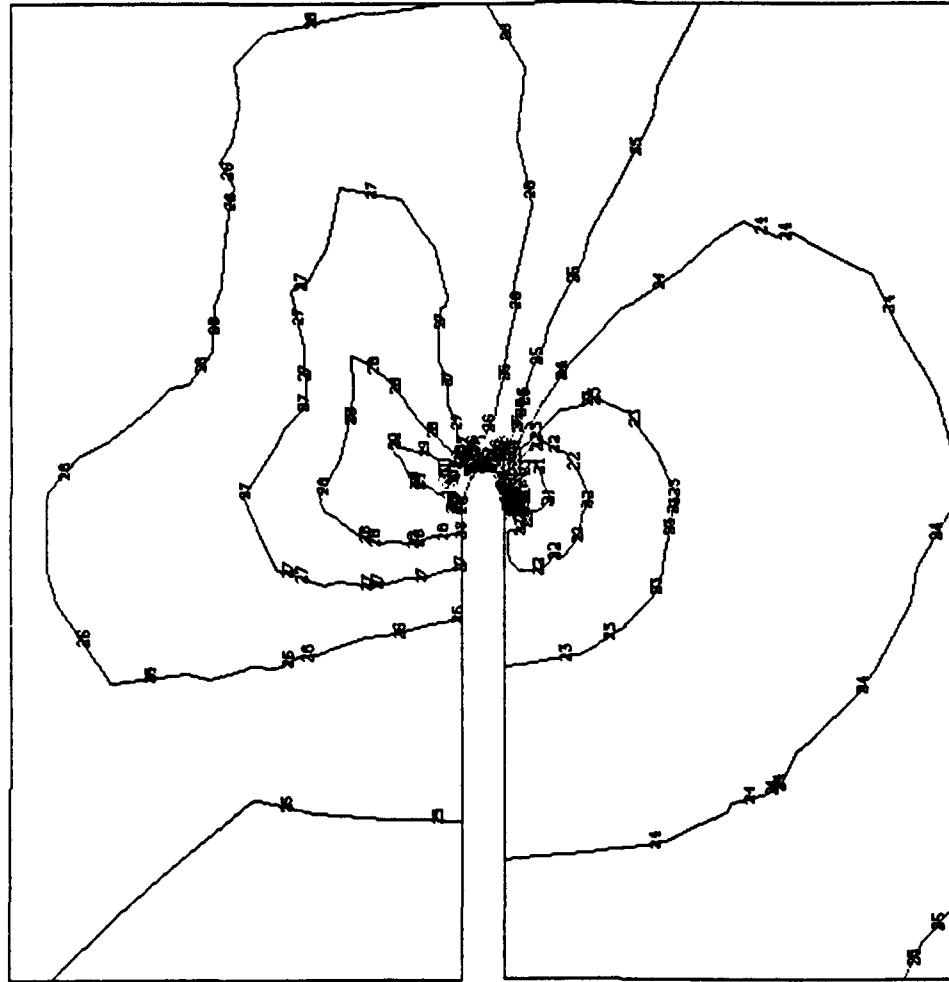


Figure 5.20a Lines of Equal Major Principal Stress; DP Model; Pure-Torsion Test

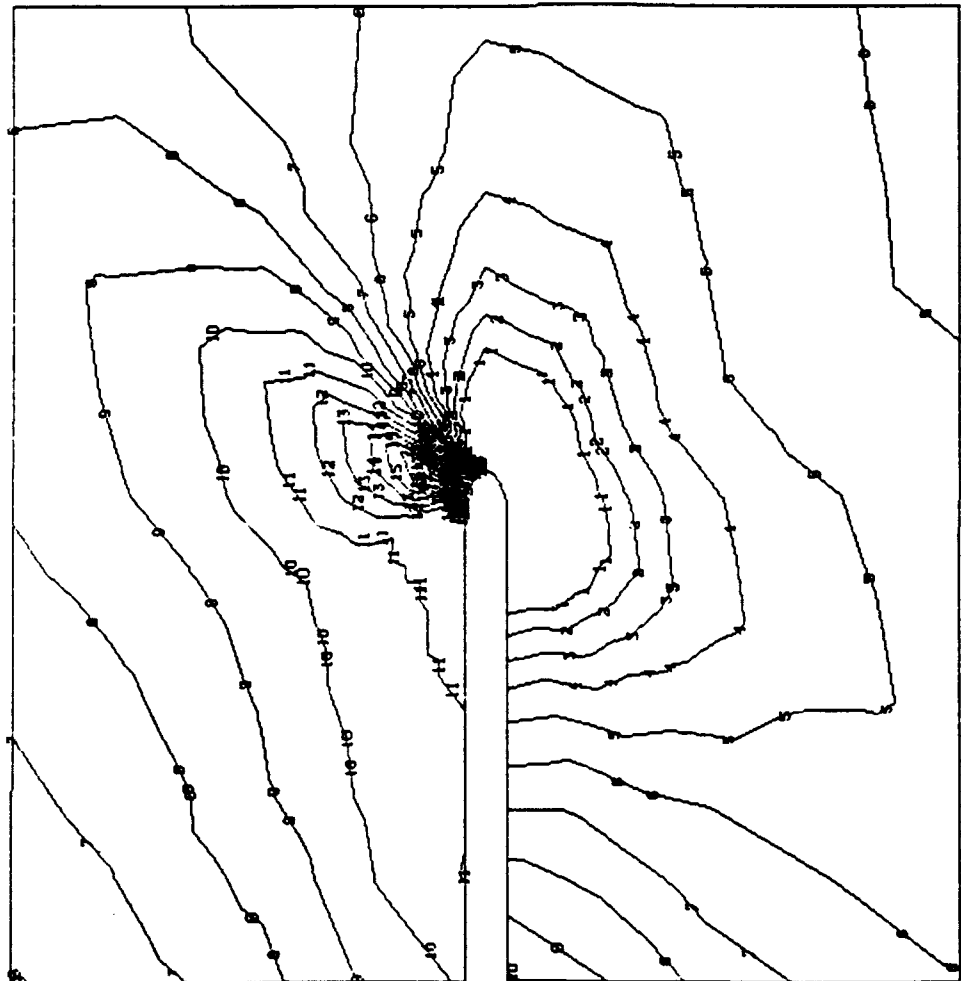
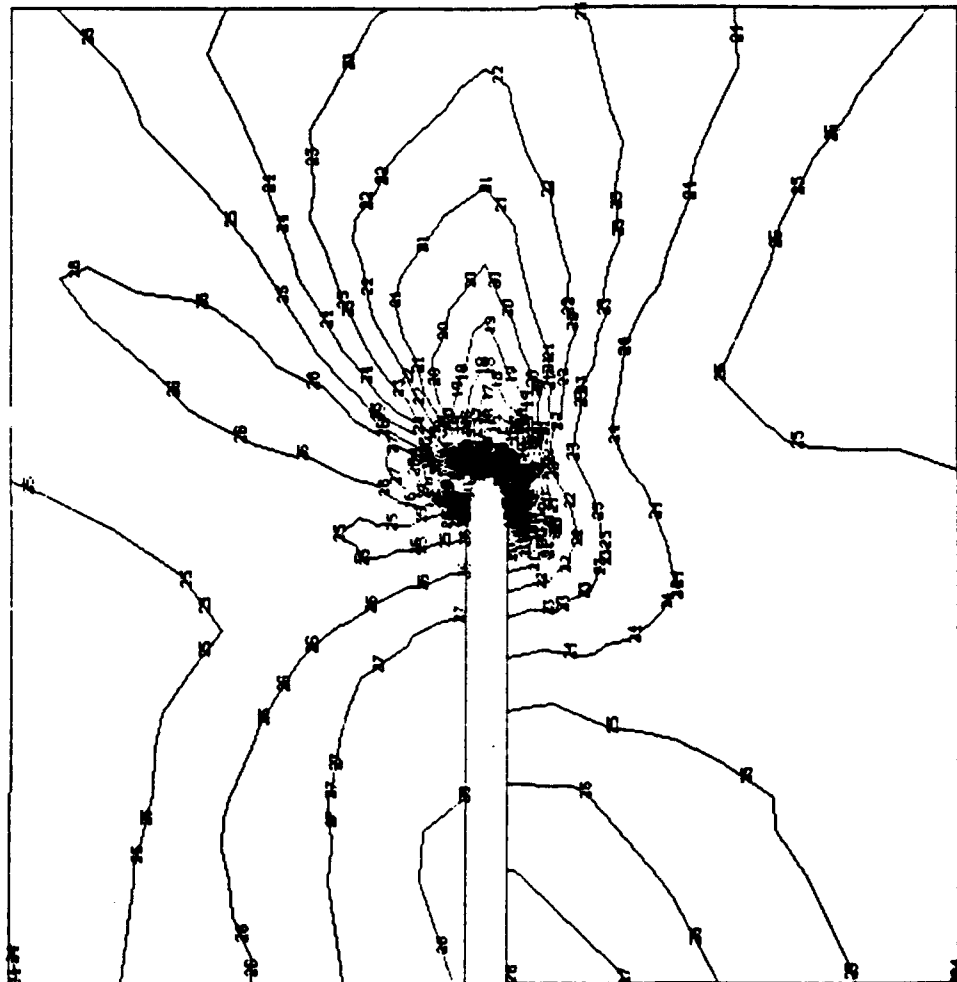


Figure 5.20b Lines of Equal Minor Principal Stress; DP Model; Pure-Torsion Test

Figure 5.20c Lines of Equal Principal Stress Difference; DP Model; Pure-Torsion Test



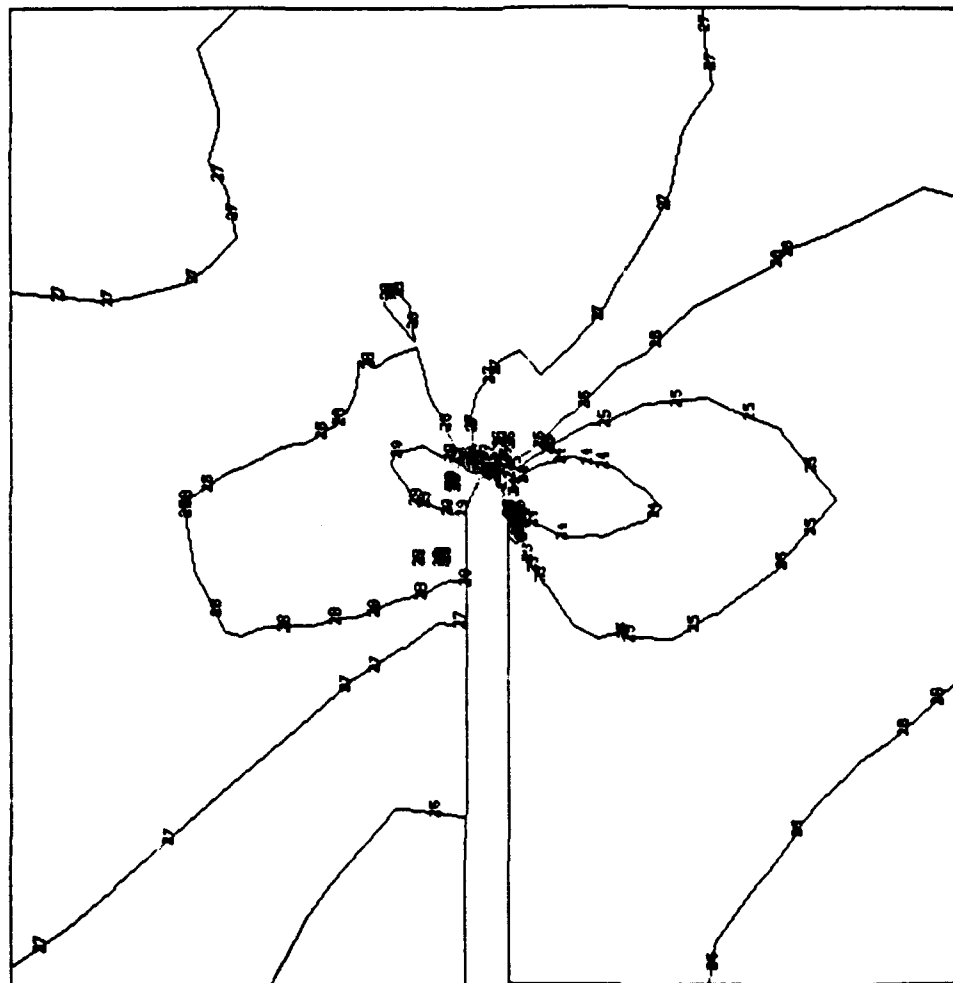


Figure 5.21a Lines of Equal Major Principal Stress; DP Model; Tension-Torsion Test

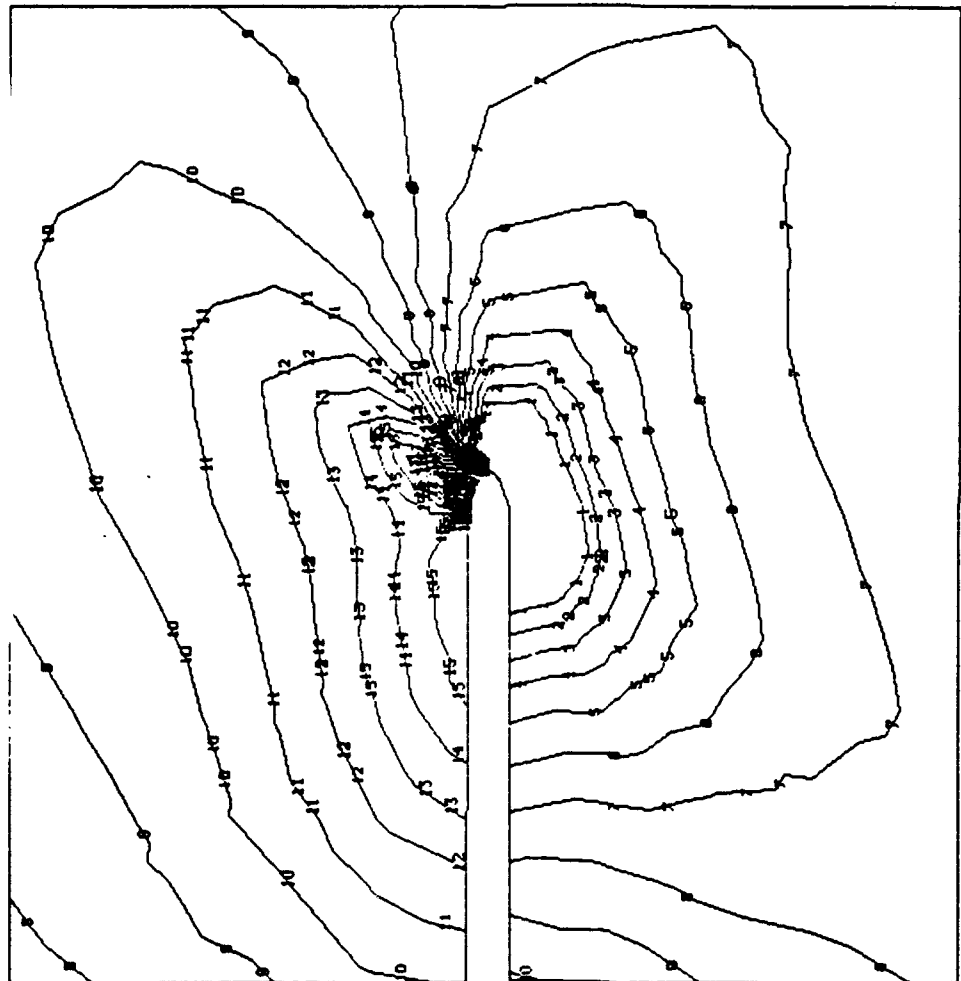


Figure 5.21b Lines of Equal Minor Principal Stress; DP Model; Tension-Torsion Test

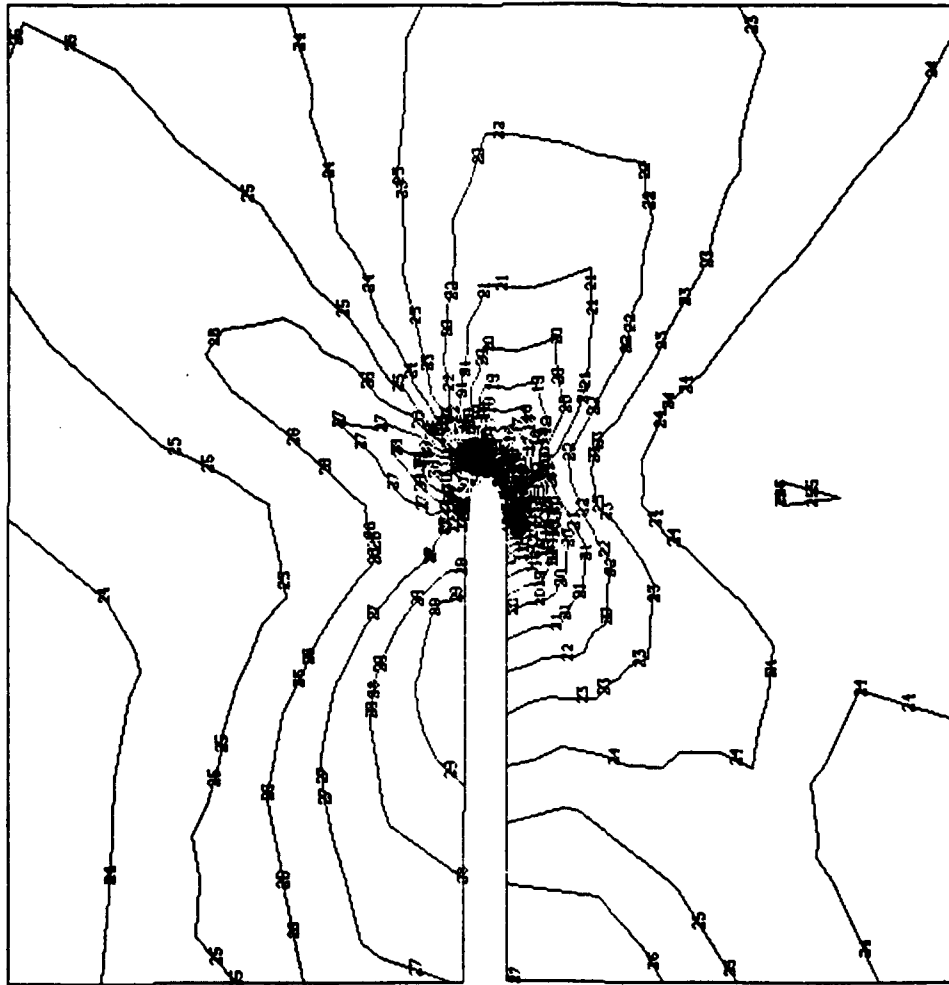


Figure 5.21c Lines of Equal Principal Stress Difference; DP Model; Tension-Torsion Test

CHAPTER VI

FABRIC CHANGE AND MICROMECHANISMS OF DEFORMATION

6.1 Macroscopic Observations.

External observation of shear band formation during static tests and damage zone propagation during dynamic tests resulted in a clear description of the kinematics of deformation of a hollow cylinder subjected to various systems of stresses. For internal examination the impregnation technique described in Chapter II was used.

Before damage can be characterized, the kaolinite must be identified in its natural state. Clay fabric has been studied among others by Yong and Warkentin (1975) and Mitchell (1976) and a scale hierarchy in the microstructure identified. Initially the clay particles (10^{-6} m) are aggregated or flocculated together in units called domains (10^{-5}). The domains, in turn, form together clusters (10^{-5} m to 10^{-4} m). Similarly, the clusters group together to form peds or larger clusters (10^{-4} m). The large clusters are large enough to be seen without a microscope.

A polished section from an untested hollow cylinder impregnation is shown in Fig. 6.1.

In this figure the kaolinite appears white and the impregnation material appear dark. The kaolinite clusters are homogeneously distributed and have a characteristic size of the order of 10^{-4} meters which compares with what has been reported by others.

Figs. 6.2 compares two radial sections cut from a cylinder of EPK clay cyclicly loaded, after impregnation; one obtained from an undamaged region and the other in front

of the tip of the crack. The undamaged section in Fig. 6.2a shows the previously reported clusters homogeneously distributed in the wax matrix. The damaged section in Fig. 6.2b indicates substantial morphological changes due to the loading condition. In this region, one notices a change in the size distribution of the clusters. A few coalesce and others split into smaller units. Also, one can see the creation of horizontal strips along which the clay clusters have agglomerated. These strip constitute surfaces within the cylinder. The process producing the surfaces has been called by Lesser (1989) "Localized Strip Densification" or LSD for short. Notice the interior fabric consisting of densified strips intermixed with clusters.

Similar results were observed with the specimens of H121 clay. The impregnation time however for this clay was quite different from that of the EPK.

6.2 Strips Characterization.

The first step in the characterization process involves making a series of radial sections through a damaged zone of an impregnated cylinder. The sections are usually equally spaced at approximately 5mm interval and start near the notch tip and continue through the entire damage zone. Each section is mounted on a slide and polished. It is then segmented into 3mm thick bands below a known reference plane as shown in Fig. 6.3. Each slide is then placed under the stereoscope and the image analyzer is used to compute the total LSD area in each band. These areas are then used to construct a histogram for each slide as illustrated in Fig. 6.4.

It was observed that the LSD area distributions are generally bell-shaped, thus a Gaussian curve is used to approximate the distribution in the axial direction. These histograms and their approximating distributions are illustrated in Fig. 6.5. Lesser (1989) gives three-dimensional plots showing the evolution of the LSD's as a function of the number of cycles.

Figs. 6.6 show the clusters and LSD's in an isotropic EPK clay. They are not very different from the ones obtained from a K_o consolidated clay.

Figs. 6.7 show undamaged and damaged regions of anisotropic H121 clay. The undamaged region shows clusters flattened by one-dimensional consolidation. This is different from what was noticed in the case of EPK clay. In the damaged zones, the LSD's although thicker do not differ significantly from their counterparts in the EPK clay.

Observations in the surface analyzer made on radial sections of impregnated specimens show no formation of LSD's to speak of in static tests. The high degree of reorientation of particles and clusters in cyclic tests is primarily due to the significant amount of energy to be dissipated by the material.

6.3 Microscopic Observations.

Impregnated specimens as well as non-impregnated ones were examined in an electron microscope in the laboratories of McGill University by Dr. R. Yong and his staff. It was found that the impregnation took place in the micropores. In addition, horizontal and vertical sections made in the undamaged parts of the K_o consolidated EPK clay and of the isotropic EPK clay showed no preferential arrangements within the clusters. The clay

particles were extremely small and randomly oriented there. The arrangement at the cluster level appears to be the main reason for the anisotropic mechanical response of this material. It is felt that the model illustrated by Yong and Warkentin on pages 86 to 88 of their treatise on Soil Properties and Behavior applies to the clay at hand and can be used to explain, at least partially, the behavior in the damage zone in front of the crack (Fig. 6.8).

Figures 6.9 and 6.10 are micrographs showing horizontal and vertical sections within the clusters in the over-consolidated anisotropic clay prior to subjecting it to cyclic loading. No preferential directions are seen indicating an isotropic or random arrangement. Remember, however, that when tested for strength this clay behaved in an anisotropic way.

Hydrite 121 was found to have much larger particles. Fig. 6.11 shows that this clay has tendencies of orientation within the clusters when the clay is one-dimensionally consolidated.

6.4 Conclusions.

The observations reported in this chapter indicate that the deformations mechanisms in a saturated clay occur primarily at the cluster level. The appearance of the LSD's during cyclic loading and the coalescence of the cluster show the potential for rearrangement at the level. The examinations in the surface analyzer and in the electron microscope both point in that direction. The model advanced by Yong and Warkentin seems to be a valid one.



Figure 6.1 Impregnated specimen of EPK

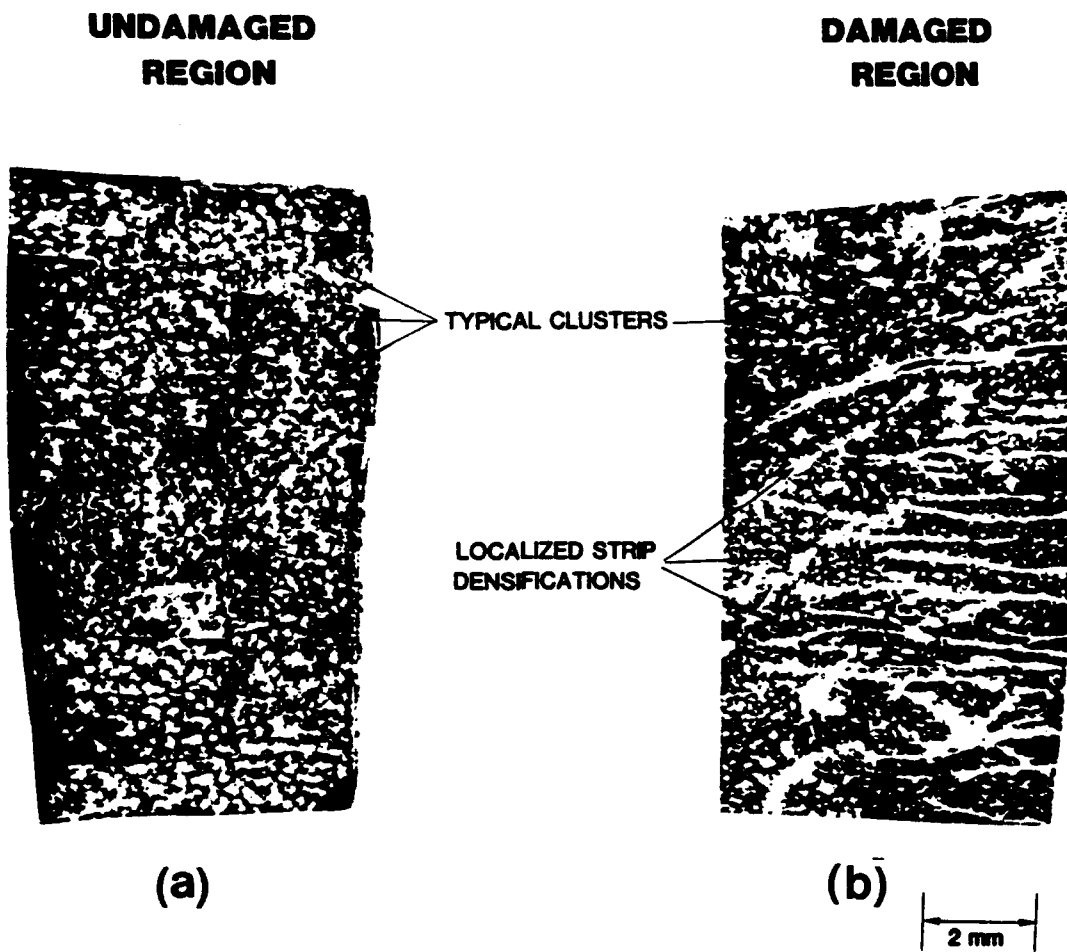


Figure 6.2 Sections of Undamaged and Damaged K_o Overconsolidated EPK

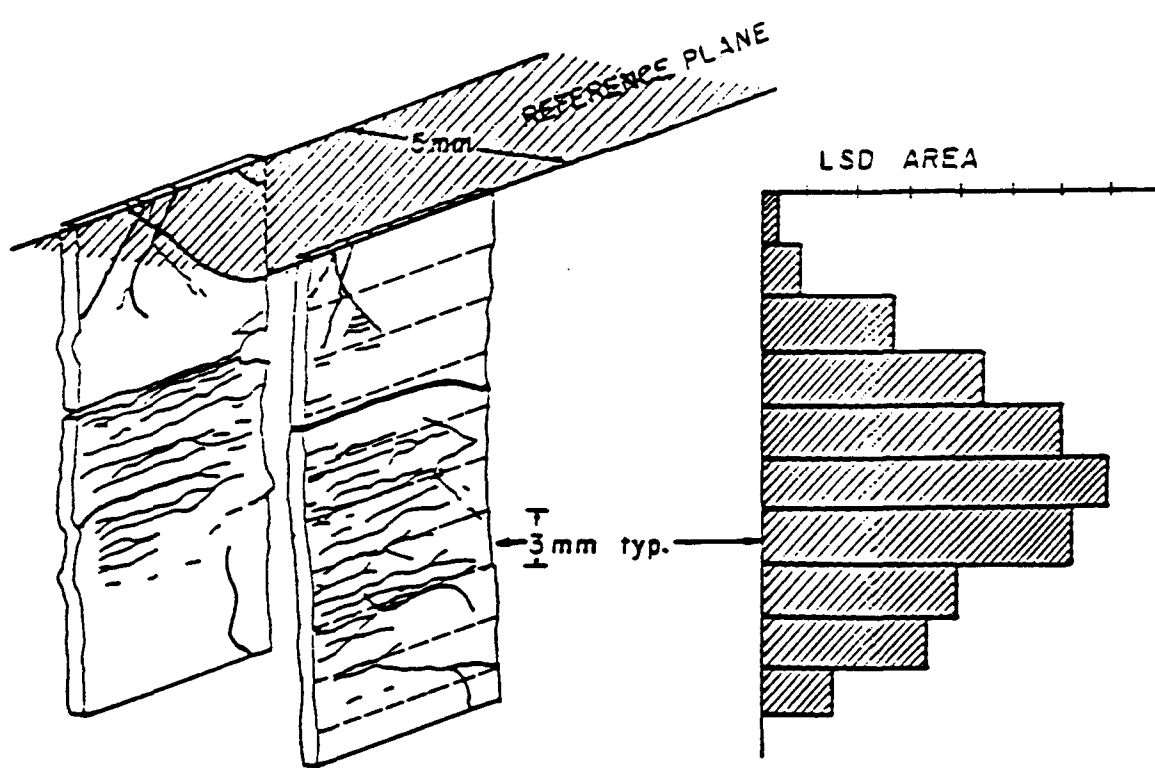


Figure 6.3 LSD Measurements Procedure

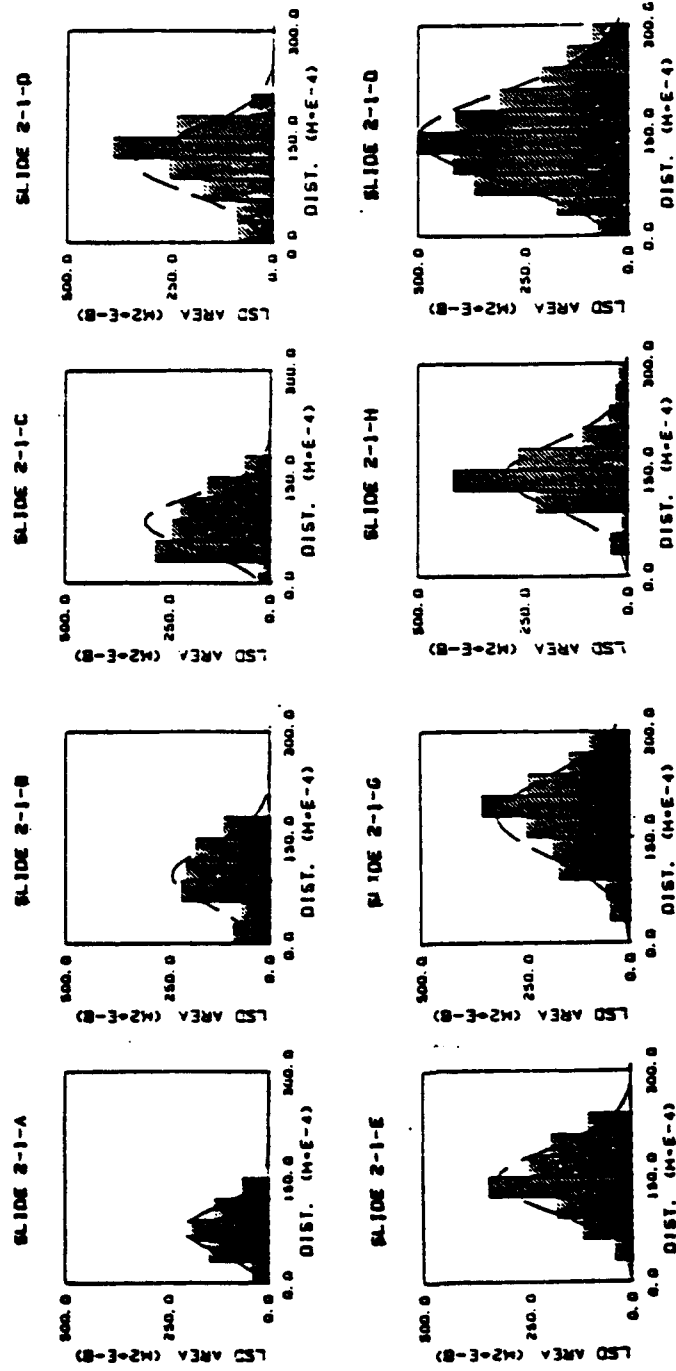


Figure 6.4 LSD Histograms at Various Locations in Front of the Crack Tip.

LOCALIZED STRIP DENSIFICATION DENSITY PLOT

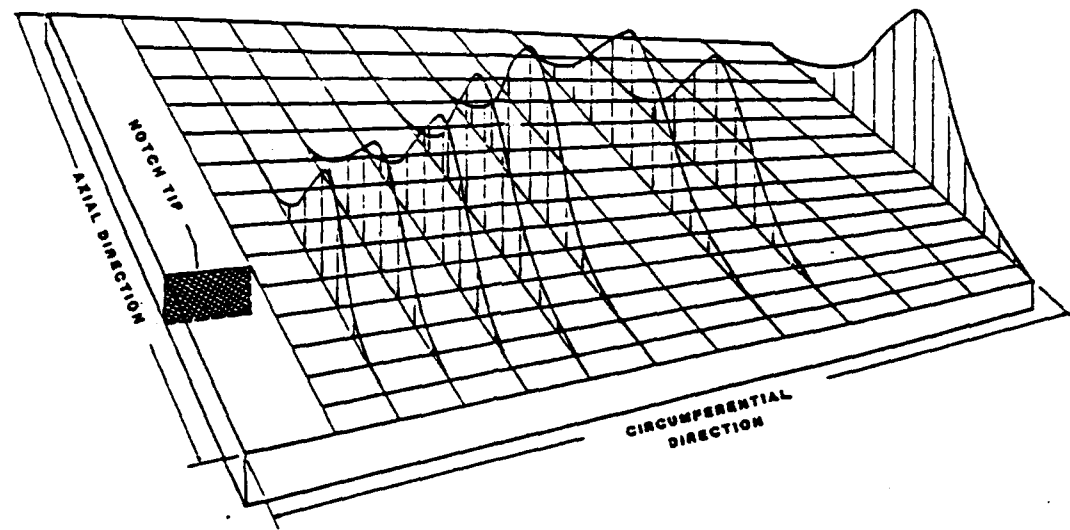


Figure 6.5 3D LSD Densification Plot

Figure 6.6 Sections of Undamaged and Damaged Isotropic EPK

(b) (a)

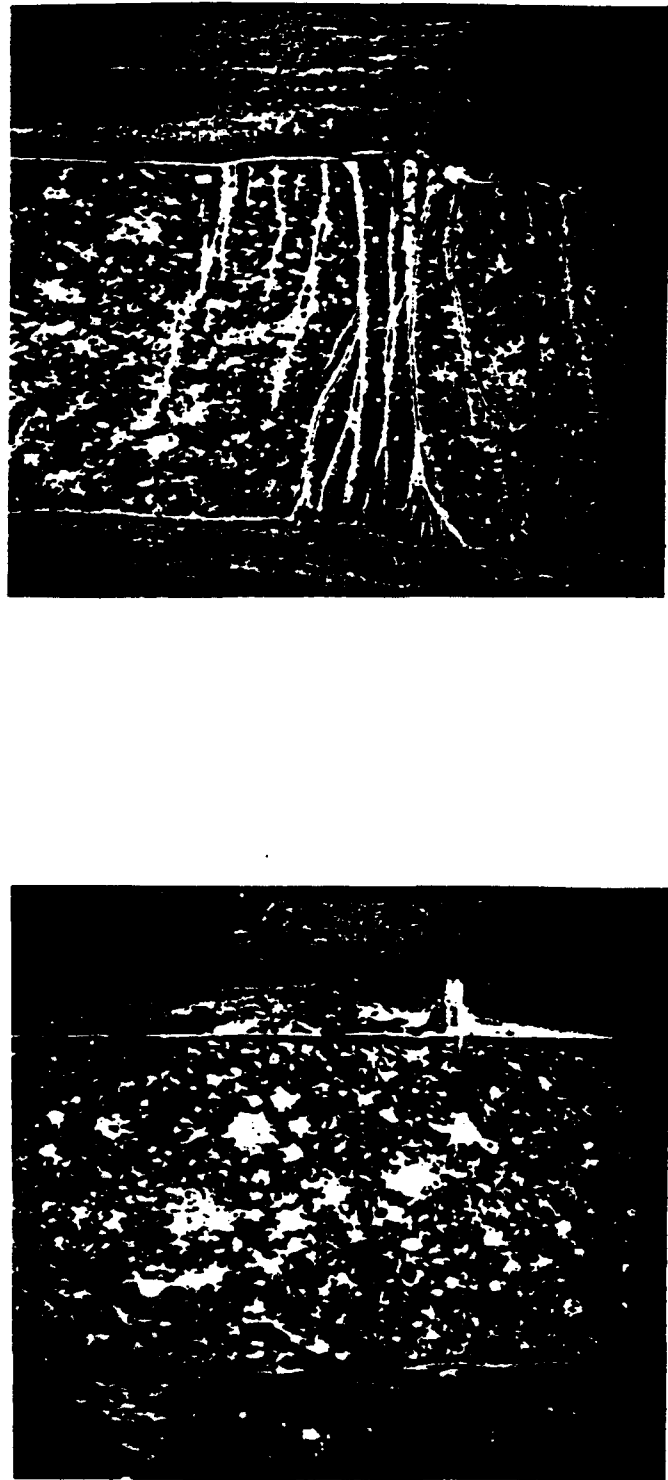
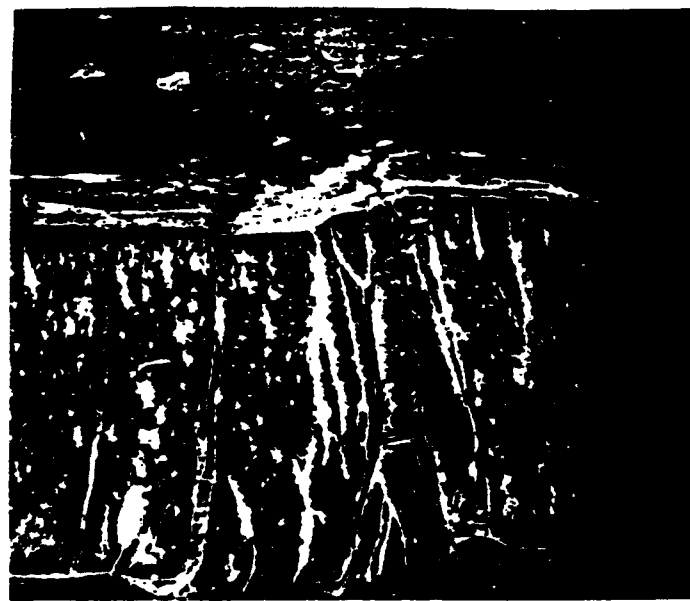
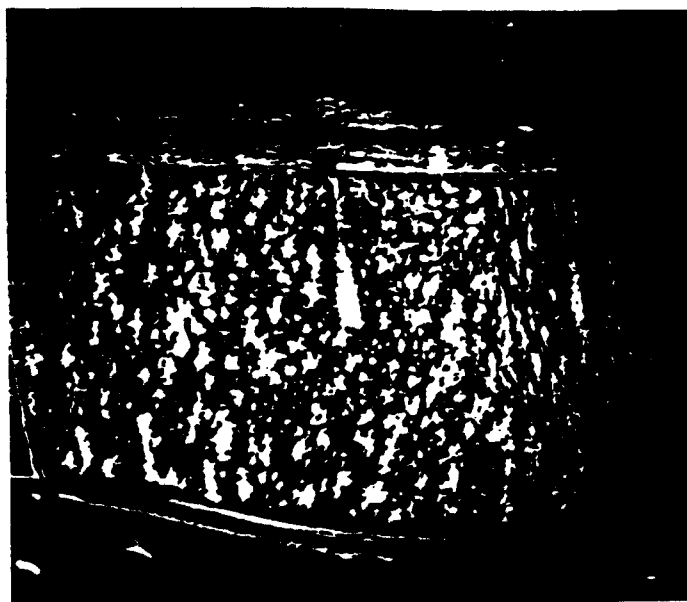


Figure 6.7 Section of Undamaged and Damaged K_o Consolidated H121

(b) (a)



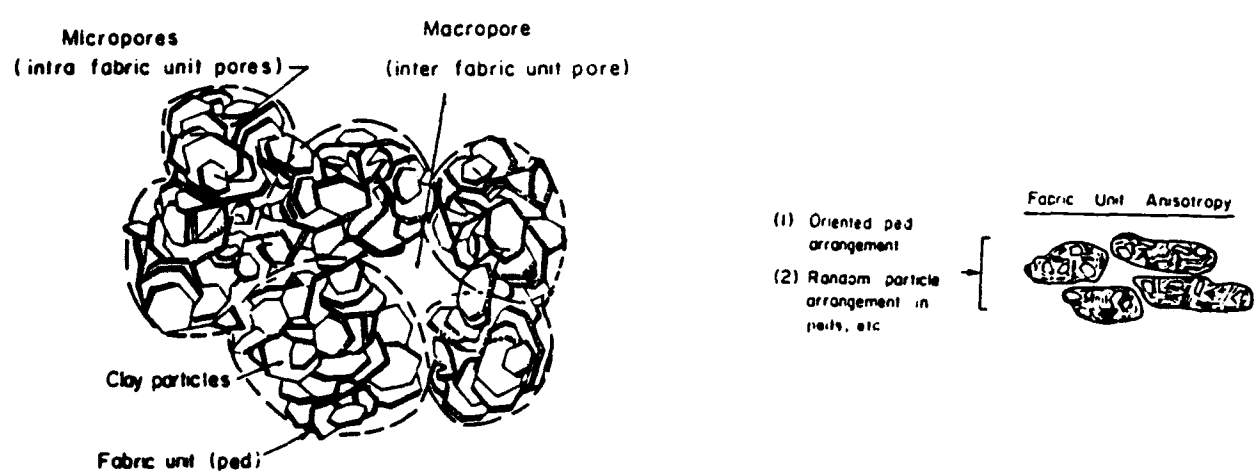


Figure 6.8 Clay Fabric Model

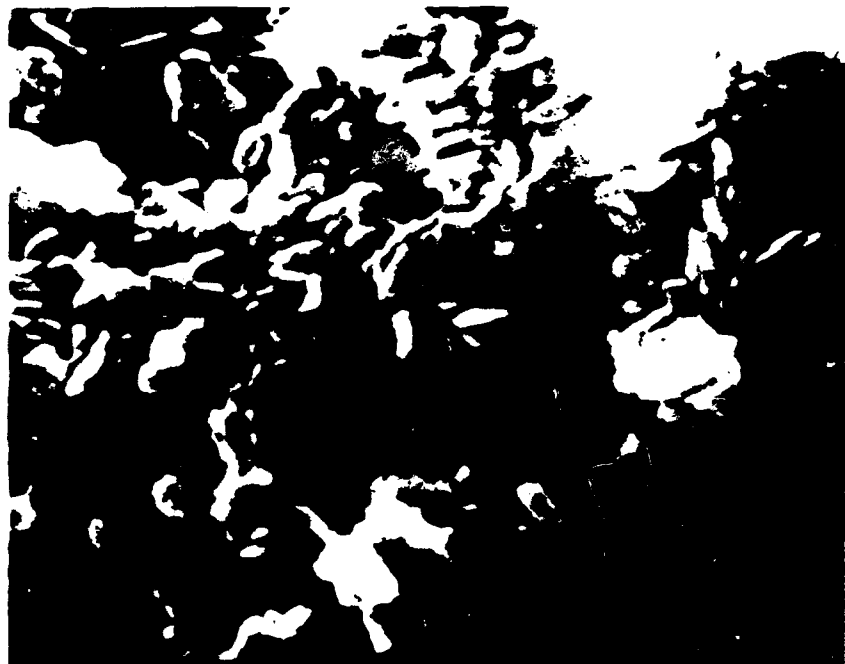
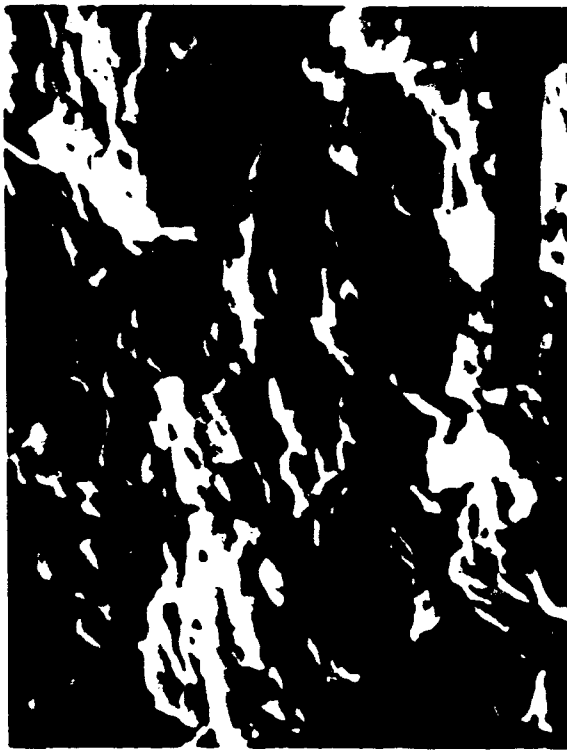


Figure 6.9 Photomicrograph of Horizontal Section; EPK

Figure 6.10 Photomicrograph of Vertical Section; EPK



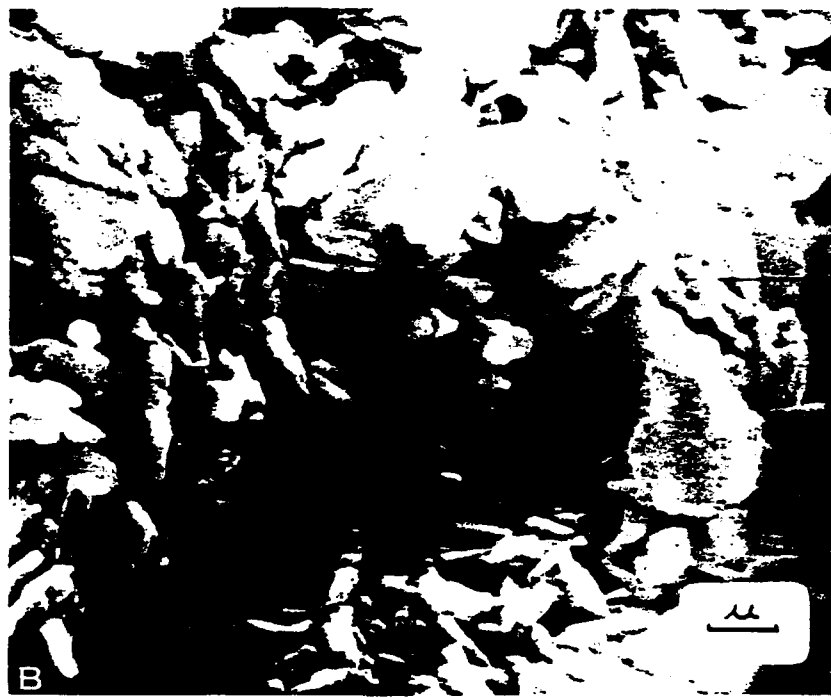


Figure 6.11 Photomicrograph of H121 (Yong & Warkentin)

CHAPTER VII

CONCLUSIONS

This research has endeavored to examine the behavior of saturated clays, in a reasonably complete way, bringing together elements of continuum mechanics, fracture mechanics and stability. Localizations, spontaneous or induced by the presence of cracks, appear as shear bands along which most of the deformations take place. Under cyclic loading they form damage zones within which clusters of clay suffer serious rearrangement.

7.1 In the Area of Strength:

It was found that for K_0 consolidated clays the response to stress was significantly influenced by the inclination of the principal stresses on the axis of symmetry of the material. Bifurcations in the form of shear bands invariably appeared near the peak stress in strength experiments. Initially well-distributed along the length of the hollow cylindrical specimens, the shear bands eventually relinquish their share of the deformation to one along which the material fails in a catastrophic way.

The presence of a crack (or notch) in a specimen did not substantially affect its overall strength. Indeed, stress-strain curves, for specimens with or without cracks, differed very little even though the observed pattern of displacement was far from being the same. The pore water pressures, which are of course measured at the specimens ends are hardly affected. One notices however a lack of smoothness in the stress-strain curves related to notched specimens; specially when the crack is oriented in the direction of the forming

shear bands. Here the bands start forming at about eighty percent of the peak value of the stress.

Under cyclic loading anisotropic clays yield an unsymmetric pattern of hysteresis loops, whether the specimen had a crack or not. The presence of an inclined crack however caused the hysteresis loop to adopt a symmetric pattern characteristic of isotropic clays.

The presence of two cracks in close proximity to each other led to interferences which depended on their relative position and on the direction of the applied shearing stresses. These interferences affected the value of the peak stress as well as the development of the shear bands. The bands were noticed at about 80 percent of the peak stress.

All our observations led us to conclude that, while cracks create local stress concentrations, the behavior of the material is dictated by its plasticity which becomes predominant at a very short distance from the tip.

7.2 In the Area of Bifurcation and Shear Band Development:

The presence of filter paper was found to hide, inhibit and direct the formation of shear bands. At failure, the slits in the filter paper have enough influence so that they dictate the final shear band pattern.

The shear bands, whether they occur near the peak in an unnotched specimen, or at 80 percent of the peak triggered by the presence of a crack, eventually take the same direction showing once more that the behavior is dictated by the plasticity of the material.

This direction was found to be fixed with respect to the direction of the major principal stress. A similar result was found by Arthur and Dunstan for sand materials.

If a specimen is subjected to further rotation, at or beyond the peak, an additional shear band develops in the vicinity of the crack tip. The first shear band, often hindered by the boundary, stops and additional deformations become primarily localized in the new shear band. The second band usually starts with a flat slope but later tends to become parallel to the first one.

The inclination of the cracks was found to act in unison with the direction of anisotropy and that of the applied shearing stress. The development of the shear bands seems to ignore the presence of an upstep crack (-ve α). Two bands will pass through the tips while others will form in other locations; some stopping while attempting to cross the crack. Stress concentrations at the tips of the crack have little or no influence. On the other hand a downstep crack (+ve α) will become a part of the shear band and this combination will tend to weaken the specimen. In particular, the crack at 22.5 degrees blended so well with the directions dictated by the plasticity of the material that only one band was seen to develop in this particular specimen to dissipate the energy.

Isotropic specimens give diffuse shear bands. It appears that the random orientation of particles and clusters inhibits the formation of the clearly defined surfaces observed when testing K_o consolidated clays. Also, the shear bands that develop in overconsolidated clays are thinner and more pronounced than their counterpart in normally consolidated clays; localization being more intense.

Most of the photographs were made at the end of the tests showing that parts of the specimens between the shear bands suffer little or no permanent deformation. This leads us to question the validity of calculated strains from measurements of deformations made on the whole specimen. However, since shear bands occur at or beyond the peak for unnotched specimens, it is only the interpretation of that part of the behavior that is in question; for notched specimens, block motions start occurring at 80 percent of the peak's value.

While there is a substantial amount of rebound that takes place upon removal of the stresses, some rebound was observed to take place in the vicinity and upon formation of the shear bands. The model of Rice and Rudnicki (1980) takes into account this possibility.

Crack propagation, shear banding and damage zones occur under symmetric cyclic loading for both normally consolidated and overconsolidated clays. The bands, in a herringbone pattern, form a damage zone on both sides and in front of a propagating crack. Isotropy tends to narrow this zone and diffuse it such that the bands are not clearly delineated. The same happens with inclined cracks in anisotropic specimens; showing the importance of fabric, direction of stress and direction of cracks.

Static and slow cyclic loading tests led to the formation of shear bands and zones where most of the deformation at failure took place, leaving the rest of the specimen "relatively" undisturbed. This is not the case for impulse loading where severe distortions occurred in all the specimen and not only in the vicinity of the crack. Viscous effects are indeed quite important and must be taken into consideration when modelling shear band formations in saturated clays.

When two cracks are present, they act independently or interact depending on their relative position and the direction of the applied stresses. In our case cracks in the downstep position acted as a single unit. The space between them could suffer instabilities without affecting the overall behavior of the specimen.

Since shear bands were found to propagate in a stable manner, measurements can be, and have been made along the crack and along the shear bands. By extrapolation, one can find with reasonable accuracy the point at which banding begins in the vicinity of a crack; its evolution can thus be studied. Such measurements are indispensable in the formulation of a bifurcation and localization model.

7.3 In the Area of Modelling:

It was found that models from linear fracture mechanics were not applicable because of the plasticity of the material. Linear elastic analyses, however, give good indications about the zones of high tensile stresses; but an elasto-plastic analysis was needed to explain the direction of the shear bands. The Drucker-Prager model was satisfactory in predicting the direction of the observed shear bands, proving once more that, even when tested undrained, saturated clays behave as frictional materials. There is no doubt that along the shear bands the dilation angle is not negligible and that water migration takes place in this zone. It is expected that, soon, local measurements of water content in the cell will be possible. A combination of measurements and finite elements analyses will be needed to investigate the physical and mechanical properties in the vicinity of shear bands and cracks.

7.4 In the Area of Fabric:

The measurements made with the surface analyzer and with the Electron Microscope indicate that the deformations occur primarily at the level of the clusters. The shear band's thickness for EPK clay was estimated to be about 0.5mm; and that is about one order of magnitude larger than the size of a cluster.

In conclusion, it is believed that this study has opened an important area of investigation for clay soils. It has shown that, with very good but not necessarily very expensive equipment one can go a long way in obtaining the information needed to characterize and model materials behavior.

REFERENCES

Ariaratnam, S.T. and Dubey, R.N. (1969). Some cases of bifurcation in Elastic-Plastic Solids in Plane Strain Quart. Appl. Math., 27, 349-358.

Arthur, J.R.F. and Dunstan, T. (1982). Rupture Layers in Granular Media. IUTAM Conference on Deformation and Failure of Granular Materials, Delft, 453-459.

Balasubramaniam, A.S. (1976). Local Strains and Displacement Patterns in Triaxial Specimens of a Saturated Clay. Soils and Foundations, Vol. 16, No. 1, 101-114.

Bardet, J. P. (1991). Orientation of Shear Bands in Frictional Soils. Proc. ASCE, Journal of Engineering Mechanics, Vol. 117, No. 7, July 1991.

Bardet, J.P. and Mortazavi, S.M. (1987). Simulation of Shear Band Formation in Overconsolidated Clay. Proc. 2nd International Conference on Constitutive Laws for Engineering Materials, Tucson, Arizona, 805-812.

Bazant, Z.P. and Mazars, J. (1990). France-U.S. Workshop on Strain Localization and Size Effect Due to Cracking and Damage. Proc., ASCE, Journal of Engineering Mechanics, Vol. 116, No. 6, 1412-1424.

Chudnovsky, A., Saada, A.S. and Lesser, A.J. (1988). Micromechanisms of Deformation in Fracture of Overconsolidated Clays. Can. Geotech. J. 25, 213-221.

Desrues, J. (1983). Localization de la Deformation Dans Les Milieux Granulaires, Thesis, presented to the University of Grenoble in partial fulfillment of the requirements for the degree of Doctor of Philosophy.

Desrues, J. and Chambon, R. (1989). Shear Band Analysis for Granular Materials: The Question of Incremental Non-Linearity. Ingenieur-Archiv, 59, 187-196.

Drescher, A. and Vardoulakis, I. (1982). Geometric Softening in Triaxial Tests on Granular Material. Geotechnique 32, No. 4, 291-303.

Hill, R. and Hutchinson, J.W. (1975). Bifurcation Phenomena in the Plane Tension. J. Mech. Phys. Solids, Vol. 23, 239-264.

Hobbs, B.E. and Ord, A. (1989). Numerical Simulation of Shear Band Formation in a Frictional-Dilatational Material. Ingenieur-Archiv. 59, 209-220.

Houlsby, G.T. and Wroth, C.P. (1980). Strain and Displacement Discontinuities in Soils. Proceedings, ASCE, Journal of Engineering Mechanics, Vol. 117, No. EMA, August 1980, 753-772.

Hsu, T.S., Peters, J.F. and Saxena, S.K., (1987) Importance of Mesh Design for Capturing Strain Localization. Proc. 2nd International Conference on Constitutive Laws for Engineering Materials, Tucson, Arizona, 857-863.

Kolymbas, D. and Rombach, G. (1989). Shear Band Formation in Generalized Hypoelasticity. *Ingenieur-Archiv*, 59, 177-186.

Ladd, C.C., Foott, R., Ishihara, K., Schlosser, F. and Poulos, H.G. (1977). Stress-Deformation and Strength Characteristics. Proceedings, 9th ICSMFE, Vol. 2, Tokyo, pp. 421-494.

Leroy, Y. and Ortiz, M. (1989). Finite Element Analysis of Strain Localization in Frictional Materials. *International Journal for Numerical and Analytical Methods in Geomechanics*, Vol. 13, 53-74.

Lesser, A.J. (1989). Theoretical and Experimental Studies of Cooperative Fracture in Overconsolidated Clays. Thesis, submitted in partial fulfillment of the requirements for the Degree of Doctor of Philosophy, Dept. of Civil Engineering, Case Western Reserve University.

Macky, T. and Saada, A.S. (1984). Dynamics of Anisotropic Clays Under Large Strains. Proc. ASCE, Journal of the Geotechnical Engineering Division, Vol. 110, No. GT4.

Mitchell, J.K. (1976). Fundamentals of Soil Behavior. John Wiley & Sons, Inc., N.Y. pp. 413.

Molenkamp, F. (1985). Comparison of Frictional Material Models with Respect to Shear Band Initiation. *Geotechnique*, 35, No. 2, 127-143.

Morgenstern, N.R. and Tchalenko, J.S. (1967). Microscopic Structures in Kaolin Subjected to Direct Shear *Geotechnique* 17, 309-327.

Muhlhaus, H.B. and Vardoulakis (1987). The Thickness of Shear Bands in Granular Materials. *Geotechnique* 37, No. 3, 271-283.

Muskhelishvili, N.I. (1953). Some Basic Problems of the Mathematical Theory of Elasticity. Translated by J.R.M. Radok, P. Noordhoff Ltd., Holland.

Needleman, A. (1979). Non-normality and Bifurcation in Plane Strain Tension and Compression. *J. Mech. Phys. Solids*, 27, 231-254.

Palmer, A.C. and Rice, J.R. (1973). The Growth of Slip Surfaces in the Progressive Failure of Overconsolidated Clay. *Proc. Roy. Soc. Lond. A*. 332, 5270548.

Potts, D.M., Dounias, G.T. and Vaughan, P.R. (1987). Finite Element Analysis of Direct Shear Box Test. *Geotechnique* 37, No. 1, 11-23.

Prevost, J.H. and Hughes, T. J.R. (1981). Finite Element Solution of Elastic-Plastic Boundary Value Problems. *Journal of Applied Mechanics*, Vol. 48, March, 69-73.

Prevost, J.H. (1984). Localization of Deformations in Elastic-Plastic Solids. *International Journal for Numerical and Analytical Methods in Geomechanics*, Vol. 8, 187-196.

Rice, J.R. (1976). The Localization of Plastic Deformation. Proc. 14th Int. Cong. Theoretical and Appl. Mech., Delft, Vol. 1, 207-220. (Edited by W.T. Koiter.)

Rice, J.R. and Rudnicki, J.W. (1980). A Note on Some Features of the Theory of Localization of Deformation. *Int. J. Solids Structures*, Vol. 16, 597-605.

Rudnicki, J.W. and Rice, J.R. (1975). Conditions for the Localization of Deformation in Pressure Sensitive Dilatant Materials. *J. Mech. Phys. Solids*, Vol. 23, 371-394.

Saada, A.S. and Bianchini, G.F. (1975). The Strength of One-Dimensionally Consolidated Clay. Proc. ASCE, Journal of the Geotechnical Engineering Division, Vol. 101, No. G%11.

Saada, A.S. and Townsend, F.C. (1981). "State of the Art: Laboratory Strength Testing of Soils." *Laboratory Shear Strength of Soils*, ASTM, STP 740, R.N. Yong and F.C. Townsend, Eds., pp. 7-77.

Saada, A.S. Chudnovsky, A. and Kennedy, M.R. (1985). "A Fracture Mechanics Study of Stiff Clays." Proc. 11th ICSMFE, Vol. 2, pp. 637-680., San Francisco.

Saada, A.S. and Macky, T. (1985). Integrated Testing and Analysis of a Gulf of Mexico Clay. *Strength Testing of Marine Sediments:Laboratory and In-Situ Measurements*, ASTM, STP 883, R.C. Chaney and K.R. Demars, Eds., pp. 363-380.

Saada, A.S. and Townsend, F.C. (1981). "State of the Art: Laboratory Strength Testing of Soils." *Laboratory Shear Strength of Soils*, ASTM, STP 740, R.N. Yong and F.C. Townsend, Eds., pp. 7-77.

Scarpelli, G. and Wood, D.M. (1982). Experimental Observations of Shear Band Pattern in Direct Shear Tests. *IUTAM Conference on Deformation and Failure of Granular Materials*, Delft, 473-484.

Shuttle, D.A. and Smith, I.M. (1988). Numerical Simulation of Shear Band Formation in Soils. *International Journal for Numerical and Analytical Methods in Geomechanics*, Vol. 12, 611-626.

Vallejo, L.E. (1987). The Influence of Fissures in a Stiff Clay Subjected to Direct Shear. *Geotechnique*, 37, No. 1, 69-82.

Vallejo, L.E., (1988). The Brittle and Ductile Behavior of Clay Samples Containing a Crack Under Mixed Mode Loading. *Theoretical and Applied Fracture Mechanics*, 10, 73-78.

Vallejo, L.E. (1989). Fissure Parameters in Stiff Clays Under Compression. Proc., ASCE, *Journal of Geotechnical Engineering*, Vol. 115, No. 9, 1303-1317.

Vardoulakis, I., Goldscheider, M. and Gudehus, G. (1978). Formation of Shear Bands in Sand Bodies as a Bifurcation Problem. *International Journal for Numerical and Analytical Methods in Geomechanics*, Vol. 2, 99-128.

Vardoulakis, I. (1980). Shear Band Inclination and Shear Modulus of Sand in Biaxial Tests. *International Journal for Numerical and Analytical Methods in Geomechanics*, Vol. 4, 103-119.

Vardoulakis, I. (1982). Stability and Bifurcation of Soil Samples. Results of the International Workshop on Constitutive Relations for Soils, Grenoble, Sept. 1982, 477-483.

Vardoulakis, I. and Graf, B. (1982). Imperfection Sensitivity of the Biaxial Test on Dry Sand. *IUTAM Conference on Deformation and Failure of Granular Materials*, Delft, 485-491.

Vardoulakis, I. (1983). Rigid Granular Plasticity Model and Bifurcation in the Triaxial Test. *Acta Mechanica*, Vol. 49, 57-79.

Vardoulakis, I. and Hetter, A. (1984). Behavior of Dry Sand Tested in a Large Triaxial Apparatus. *Geotechnique* 34, No. 2, 183-198.

Vardoulakis, I. (1985). Stability and Bifurcation of Undrained, Plane Rectilinear Deformations on Water-Saturated Granular Soils. *International Journal for Numerical and Analytical Methods in Geomechanics*, Vol. 9, 399-414.

Vermeer, P.A. (1982). A Simple Shear Band Analysis. *IUTAM Conference of Deformation and Failure of Granular Materials*, Delft, 493-499.

Yong, R.N. and Warkentin, B.P. (1975). *Soil Properties and Behavior* Elsevier Scientific Publishing Co., N.Y. pp. 449.

Young, N.J.B. (1976). Bifurcation Phenomena in the Plane Compression Test. *J. Mech. Phys. Solids*, Vol. 24, 77-91.